GEOMAR REPORT

# FS/RV SONNE
# FAHRTBERICHT SO163
# CRUISE REPORT SO163
# SUBDUCTION I

MULTI-SYSTEM ANALYSIS OF FLUID RECYCLING AND GEODYNAMICS
AT THE CONTINETAL MARGIN OFF COSTA RICA

SO163-1
BALBOA - CALDERA, MARCH 13 - APRIL 20, 2002
SO163-2
CALDERA - BALBOA, APRIL 21 - MAY 21, 2002

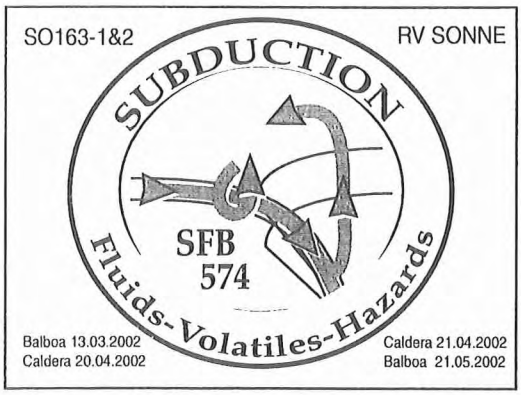


# 106

GEOMAR REPORT

doi: 10.3289/geomar_rep_106_2002

# FS/RV SONNE
# FAHRTBERICHT SO163
# CRUISE REPORT SO163
# SUBDUCTION I

MULTI-SYSTEM ANALYSIS OF FLUID RECYCLING AND GEODYNAMICS
AT THE CONTINENTAL MARGIN OFF COSTA RICA

SO163-1
BALBOA - CALDERA. MARCH 13 - APRIL 20, 2002

SO163-2
CALDERA - BALBOA. APRIL 21 - MAY 21, 2002

**Edited by**
**Wilhelm Weinrebe and Ernst Flüh**
**with contributions of cruise participants**

**Investigations in the frame of SFB 574**
**"Volatiles and Fluids in Subduction Zones:**
**Climate Feedback and Trigger Mechanisms for Natural Disasters"**

**Contribution No. 14 of SFB 574**

**GEOMAR**
Forschungszentrum
für marine Geowissenschaften
der Christian-Albrechts-Universität
zu Kiel

**KIEL 2002**

**GEOMAR REPORT 106**

**GEOMAR**
Research Center
for Marine Geosciences
Christian Albrechts University
in Kiel

Redaktion dieses Reports:
Wilhelm Weinrebe und Ernst Flüh

Umschlag und Titelei: Gerhard Haass

GEOMAR REPORT
ISSN 0936 - 5788

**GEOMAR**
Forschungszentrum
für marine Geowissenschaften
Wischhofstr. 1-3
D - 24148 Kiel
Tel. (0431) 600-2555, 600-2505

Editors of this issue:
Wilhelm Weinrebe and Ernst Flüh

Cover and prelims: Gerhard Haass

GEOMAR REPORT
ISSN 0936 - 5788

**GEOMAR**
Research Center
for Marine Geosciences
Wischhofstr. 1-3
D - 24148 Kiel
Tel. (49) 431 / 600-2555, 600-2505

Table of Contents

## 1. Summary

During cruise SO163 (13. March to 20. Mai 2002, Balboa to Balboa) the Pacific continental margin off Cost Rica was surveyed using a variety of tools. These investigations follow several previous cruises and are part of the new research initiative (Sonderforschungsbereich) SFB574:"Volatiles and Fluids in Subduction Zones: Climate Feedback and Trigger mechanisms for Natural Desasters". Several other cruises will follow in 2002 and 2003.
The cruise was split into two legs with an intermediate port call on April 20 in Caldera., Costa Rica.

Leg 1 was set about to investigate the material input, mobilisation, and return flow of volatiles in the subduction zone off Costa Rica. During leg 1 a comprehensive study of the area of investigation was carried out, applying a whole set of different mapping tools with different resolution. The results comprise an important database for all forthcoming expeditions and will be an invaluable help in finding appropriate target areas for future sampling work. The investigations during leg 1 also aimed in quantifying the processes in the material cycle which directly affect the seafloor and its morphology, such as sediment deposition, erosion, submarine landslides as well as manifestations of fluid venting. In particular deep-towed systems were used. The TOBI system of the Southampton Oceanography Centre was used for a reconnaissance survey to detect places of active mud diapirism and mass wasting. In total, this system was used for 315 hours to map an area of about 8000 km_ with a resolution on the order of around 10 metres. Together with the results of the TOBI survey during the SO-144 cruise in 1999, nearly a complete coverage of the whole continental margin from Santa Elena Peninsula in the northwest to the Cocos Ridge in the southeast was achieved. In order to image parts of the surveyed area with greater resolution, the newly acquired GEOMAR DTS-1 deep-towed sidescan sonar system was used to map five key areas. In total an area of about 650 km was mapped in 175 hours with a resolution of less than one metre. As a further step to even greater resolution and ground truthing, direct observations of the seafloor by TV-sled OFOS was carried out at 24 deployment sites. The survey was completed with sampling the seafloor by the TV-guided grab at nine positions.

During leg 2 numerous seismic and seismological experiments and a water sampling programme dominated the work carried out. The active seismic work focussed on three areas. The Megalens structure, being interpreted as a key factor for erosional processes, the decollement reflection and the BSR occurences off Nicoya. In all three areas numerous wide angle data sets were collected using ocean bottom hydrophones (OBH) and seismometers (OBS), The Megalens reflections are not easily identified in the records processed onboard. The profiles collected on the decollement reflection show a pronounced lateral variability of the interface, and surprisingly several deep penetrating faults that cut the subducting oceanic plate have been identified on preliminarily processed sections. Off Nicoya several profiles were shot to collect three component data in areas were a strong BSR reflection had been observed before. These three component data should allow to identify shear waves and be used for receiver transfer function methods to investigate the shear wave velocity of gas hydrate bearing sediment. Numerous records were collected where p-s conversions observed at about the time expected for a conversion at the BSR.
Two seismological network were operated. The first one comprising ten instruments was placed on and around an active vent site and was operational for about 40 days. Preliminary analysis of the data showed a special kind of events , termed hongo events, which could be localised at the vent site. These events consist of an approximate 1 sec long monochromatic (36 Hz) burst with increasing amplitudes, followed by a two second long monochromatic (20 Hz) arrival of lower frequency. These events are most probably related to the hydrologic system in the vent site. A second network was installed around Jaco Scar. This network comprises 28 stations (5 of them are actually centered on the near by Quepos mound) and shall be operational until October 2002. It is

further augmented by an 15 element land array. In addition, two tiltmeters were deployed in this network to monitor long term slope changes.
In total, the seismic programme comprised 212 OBH/S deployments, with 184 successful recoveries and 28 instruments left on the seafloor for monitoring. More than 800 nm of seismic profiles were collected, with a total of about 25000 airgun shots fired.
The water column sampling program comprised a total of 24 stations and had two main objectives. (a) The investigation of the general oxygen and methane distribution off Costa Rica. Two sections with 6 CTD/rosette stations spread over 100 nm were sampled in the northern and southern part of the working area. The results will provide information about the production of methane within the upper 600m of the water column due to the geostrophical upwelling along the western coast of Middle America (Costa Rica Dome), and will define the methane background for the detection of venting-related methane-rich plumes in bottom-near waters. (b) Detailed surveys of the methane distribution at potential vent sites in order to quantify the release of $CH_4$ to the water column and to define targets for a detailed geochemical program during expeditions later this year. Multiple CTD casts were deployed in the Jaco Scarp area as well as at Quepos Mound and Mound Culebra. The results revealed evidence for active venting of methane rich fluids in all 3 areas. The water column program was accompanied by a small sediment sampling program, which lead to first data on the geochemical composition of the non-vent-influenced upper sediment in the SFB target area.

The Simrad system of Sonne was operated continuously, and magnetic data were collected along 4 profiles extending over more than 200nm.

## 2. Introduction
## 2.1 Objectives of the cruise SO-163/1&2

SO-163/1 continues the series of cruises with RV SONNE to the Pacific convergent continental margin off Costa Rica and Nicaragua, which started with SO-76 in 1991. That cruise was followed by SO-81 in 1993, SO-107 in 1996 and SO-144 with 6 legs in 1999. Moreover, this area was also investigated by several cruises of other institutions with different research vessels (RV EWING, ROGER REVELLE), and in addition, probed by drilling with JOIDES RESOLUTION. Furthermore, more cruises with RV SONNE and RV METEOR are already scheduled for 2002 and 2003. Why is this section of the margins of the Pacific plates so in the focus of current geoscientific research?

The segment of the Central American continental margin off Costa Rica and Nicaragua provide along a relatively short distance a spectrum of quite different subduction styles and scenarios. The differences are: Age and source of subducted oceanic crusts, subduction angle, depth of melting zone and earthquake focal depths. Characteristic features are also the seamount province parallel to the Cocos Ridge, which is subducted under Costa Rica, or the heavily fragmented plate segment cut by numerous normal faults, subducted off Nicaragua. As such, the segment off Costa Rica and Nicaragua is a natural laboratory to investigate causes, consequences, and relationships between these different parameters.

Volatiles and fluids play a major role in the global geological material budget. At subduction zones, material from the oceanic plate (the oceanic crust and its overlying sediments) is brought to great depth. Sediments from the continental margin transported downslope by mass wasting, add to the subducted material. These processes extract considerable amounts of carbon, sulphur, water, and halogenes out of the exosphere. Inside the subduction zone, the downgoing material is remobilized, fractionated, and forms new reservoirs with different volatile compositions. A portion of the subducted and remobilized material is partly fed back into the exosphere through different transport pathways and mechanisms, partly subducted into the lower mantle. The return flow is accomplished through three distinct pathways:

- fluid venting at the deformation front
- mud diapirism and gas hydrate dynamics at the margin
- magmatism and exhalations at the volcanic arc

The long-term development of the Earth's climate, the geochemical evolution of the hydrosphere and atmosphere, and the causes of natural disasters (earthquakes, volcanic eruptions, submarine landslides, tsunamis) are all connected with the return flow and impact of volatiles and fluids from subduction zones. To understand and quantify these processes and relationships is the main objective of the new research initiative (Sonderforschungsbereich) SFB 574: "Volatiles and Fluids in Subduction Zones: Climate Feedback and Trigger Mechanisms for Natural Disasters". SO-163 is the first cruise carried out in the framework of this SFB.

The SFB 574 addresses its objectives in three overarching themes:

A. Material input and tectonic behaviour during plate subduction
B. Formation and role of gas hydrates and mud diapirs as exotic volatile reservoirs
C. Devolatilization through magma and metamorphic processes

This first cruise in the framework of the SFB 574 focuses on the processes, which directly affect the seafloor by changing its topography, nature, and compositional characteristics, such as:

- deposition of sediments
- erosion
- downslope transport by mass wasting
- gas and fluid expulsion due to tectonic activity and dewatering of the lower slope wedge.

Because of convergent movements of several centimetres per year and resulting erosional and accretional processes, subduction zones are dynamic areas that are subject to rapid changes. Among other parameters, the kind of mechanic coupling between upper and lower plate, trench fill volume, geological history and the formation and decomposition of gas hydrates all play a major role. Convergent plate boundaries are areas of the earth's greatest topographic relief and are characterised by their morphological variation.

Due to rapid accumulation of sediments high fluid pressure build up within the tectonic compression setting of a subduction zone. The mixture of materials, e.g. pelagic mud with high water content and silt/sand containing less water but being more permeable, allows an overpressurization of the sediment water mixture. For the pressure to be released, fluid pathways will open towards the surface and fluids and volatiles move upwards. On the seafloor, manifestations of fluid venting should appear.

At convergent margins, gravitational downslope mass transport takes place in varying dimensions. Submarine landslides occur as large megaslumps of several hundreds to thousands of $km^3$, but also as a sequence of individual slumps, generated by oversteepened submarine slopes. Major slides are often attributed to high sedimentation rates leading to overpressuring. Earthquakes are considered the likely immediate triggers for failure along the continental margins, yet compelling evidence for these causal factors is inconclusive. In the Costa Rica area, special downslope transport is associated to seamount subduction (Ranero and von Huene, 2000; von Huene et al., 2000).

The formation of gas hydrates may increase the shear strength of sediments immediately below the seafloor, and thus may play an important role in stabilizing the continental margins (Mienert et al., 1998). Decomposition of gas hydrates consequently results in weak zones, where failure could be triggered by gravitational loading or seismic disturbances and hence submarine landslides would result. The slides may generate large tsunamis, possibly larger than those generated by earthquakes alone. Numerous large landslides occur in areas where gas hydrates have been documented by geophysical investigations. Furthermore, there is abundant evidence for the presence of fluid and gas escape structures in these areas. Therefore, a causal relationship between gas hydrates and slides has been proposed, but direct proof is missing.

All these processes shape and change the seafloor. Cruise SO-163/1 is set about to map in detail the surface of the continental margin off Costa Rica in a multiscale approach, applying a whole set of different mapping tools with different resolution. High resolution surveys will aim to identify local features such as tectonic structures, slides, and fluid-venting related manifestations on the seafloor. To assist interpretation, direct observations and detailed optical imaging of the seafloor by TV-sled are necessary. Simultaneously, the results of this investigations constitute the most important basis for sample site selections for most other subprojects of the SFB 574.

In the following leg, SO-163/2, a variety of geophysical, mainly seismic experiments are planned, in addition to the installation of a temporary (6 month) local seismic network, with is further augmented by an onshore array. These experiments focus on target reflections that can help to better understand the erosion process along the margin, the nature of vent sites and gashydrates.

A second topic of high priority during this leg are water column and upper sediment core sampling. Fluid flow associated with subduction leads to the upward transport of reduced, energy-rich compounds, which can be either consumed within the upper sediment column and at the sediment water interface, or be injected into the water column. Both processes are complimentary and need to be assessed to close the carbon budget at seep sites. In addition, methane plumes within the lower water column are an unquestionable sign for active venting, and the results will help to define targets for the extensive geochemical field work planned for this summer.

## 2.2 Tectonic Setting and Previous Studies

(César R. Ranero)

The Pacific convergent margin of Middle America, particularly along Costa Rica and Nicaragua has become a classical example of forearc tectonics driven by the variable character of the subducting ocean plate [Corrigan and Mann, 1990; Fisher et al., 1998; Ranero and von Huene, 2000; von Huene et al., 1995; von Huene et al., 2000]. The subducting ocean plate has a variable character because it was formed in two different spreading centers (East Pacific Rise and Cocos-Nazca spreading center) and has also been modified by the volcanism of the Galapagos hot spot (Barckhausen et al., 2001). The Galapagos hot spot has created the Cocos Ridge and flanking seamounts (Werner et al., 1999) and has thickened the preexisting crust in some areas. The different types of ocean plate are well displayed in the bathymetry. Opposite SE Costa Rica the Cocos Ridge stands 2.5 km shallower than the surrounding seafloor due to a ~ 20 km thick crust. Offshore Central Costa Rica subducts a seamount province with large conical seamounts and elongated ridges (e.g. Quepos Ridge). Facing Nicoya Peninsula there is a smooth ocean plate. A small linear ridge that subducts offshore middle Nicoya Peninsula separates the previous 3 areas formed at the Cocos-Nazca spreading center from the lithosphere located to the NW formed at the East Pacific Rise. The plate formed at the East Pacific Rise exhibits a rather different morphology, characterised by pervasive normal faulting that forms a rough terrain approaching the trench.

The differences in character of the ocean plate are probably caused by a combination of variations in crustal thickness and age of the subducting plate and lead to dramatic differences along the trench in the behaviour of the incoming plate entering the subduction zone. Other subduction parameters like convergence rate or sediment input vary little along the research area and thus the effects on forearc tectonics of subducting segmented plate can be isolated.

The subduction of the buoyant Cocos Ridge shows little bending into the subduction zone. The underthrusted portion of the Cocos Ridge has uplifted Osa Peninsula at the front of the margin and also the volcanic arc forming the Talamanca Cordillera (deBoer et a., 1995). In that area, subduction related volcanism ceased at ~7 Ma, perhaps associated to the arrival of Cocos Ridge type of crust, but the age of the impact of Cocos Ridge in to the margin of Costa Rica is a matter of debate, ranging from ~ 1 Ma (Lonsdale & Klitgord, 1978) to ~ 5 Ma (Graeffe, 1998). Offshore central Costa Rica, the subduction of the large conical seamounts and ridges has produced large embayments in the continental slope (*von Huene et al.*, 2000). The subduction of the smooth ocean plate offshore Nicoya Peninsula is paralleled by the most stable morphology of the continental slope. The subduction of the lithosphere formed at the East Pacific Rise, located to the NW, and pervasively faulted is related to the deepest trench and a steep continental slope.

The nature of the rocks units forming the overriding upper plate in the area has been a matter of considerable recent research and the concepts of the origin and structure of onshore and offshore rock bodies have dramatically changed in the last decade.

Onshore, the basic igneous complexes cropping out along much of Pacific Costa Rica were previously interpreted as ophiolites resulting from accretion of several oceanic crust nappes. However, recent studies show that they are part of the large Caribbean Flood Basalt province. This province formed possibly at the Galapagos Hot Spot, between 74 and 94 Ma, intruding older lithosphere (Hauff et al., 1997; Hauff, 1998; Sinton et al., 1997; Sinton et al., 1998). Also, those studies find that some of the smaller igneous rocks bodies of oceanic origin cropping out along Middle America are younger accreted seamounts and aseismic ridges.

Offshore, near-vertical and wide-angle seismic data (Ye et al., 1996; Ranero and von Huene, 2000; Walther et al., 2000) indicate a basic structural configuration of the frontal ~60 km of the continental margin from the Costa Rica to Nicaragua. It consists of a wedge shaped body of relatively high velocity rock comprising the bulk of the continental margin (the so-called margin wedge) covered by 1-2 km of slope sediment, underthrust by trench sediment, and fronted by a

small (3-10 km wide) sediment prism. The origin of the margin wedge has been long debated. Some data sets were interpreted as representing a large, active accretionary prism that grows through frontal accretion and underplating of the sediment overlying the ocean plate (e.g. Silver et al., 1985; Moore and Shipley, 1988; Shipley et al., 1992). Alternatively, it was also interpreted as formed by the offshore extension of the igneous complexes observed onshore (von Huene and Flueh., 1994; Ye et al., 1996). Drilling offshore Nicoya Peninsula, during ODP leg 170 demonstrated that basically all sediment of the ocean plate is underthrusted past the frontal sediment prism and that accretion is not an important process at the margin (Kimura et al., 1997). The frontal sediment prism is formed by reworked slope sediment at the location of the ODP 170, although may locally involved small amount of accretion elsewhere along the margin (von Huene et al., 2000). In addition, drilling during leg 170 also supported that the bulk of the margin is formed by the seaward extension of the igneous complexes outcropping along Pacific Costa Rica.

More recently geophysical data sets along the Nicaraguan (Ranero et al., 2000a) and Costa Rican (Ranero and von Huene, 2000; von Huene et al., 2000) segments of the margin have shown evidence for widespread extension and long-term subsidence of the margin that can best be explained as produced by subduction erosional processes. Further independent evidence has come from the study of samples from the unconformity separating the margin wedge from the slope sediment collected during ODP 170 drilling. The evidence for erosion comes from the identification of beach rock overlying the unconformity (Vannucchi et al, 2001). The unconformity, cut by wave surf, is currently ~ 4 km deep at the lower slope and has subsided since early-middle Miocene time implying a continental slope retreat of ~50 km.

Submersible and deep towed camera investigations have revealed a widespread cold venting system along the margin. The main evidence for vents is the presence of chemoautotrophic communities and carbonate mounds observed at several localities (Bohrmann et al, 2002, Kahn et al, 1996) and mapped along much of the margin with swath bathymetry, sidescan data and seismic reflection images (Shipley et al., 1990; Shipley et al., 1992; Bialas et al., 1999; Ranero et al., 2000b). The areas where venting might be the most vigorous are areas of rapid tectonic activity related to seamount subduction (headwalls of slides and uplifted regions ) and at the carbonate mounds (Bohrmann et al, 2002). Submersible investigations on the lower continental slope indicate non-localized diffuse flow to be the dominant process there (McAdoo et al, 1996).

Samples from Leg 170 from the decollement yielded freshened water containing thermogenic methane. Samples from the upper plate sediment revealed fresh water from dissociated gas hydrate in addition to freshened water with thermogenic methane (Silver et al., 2000). A different hydrological system seems to exist beneath the decollement. There, water has a near seawater salinity. Measured temperatures are insufficient generate mineral dehydration and thermogenic methane, implying a fluid flow from ~ 15 km depth in the subduction zone (Kimura et al, 1997).

On the incoming ocean plate heat flux measurements near the trench axis offshore Nicoya Peninsula yielded very low values that were interpreted as indication of fluid flow into the ocean basement (Langseth and Silver, 1996). More recently, new measurements at several locations of the ocean plate opposite Nicoya Peninsula, have confirmed previous results near the trench (Fisher et al., 2001). Also, the measurements collected in areas away from the trench show a complex pattern that suggests active fluid flow into the ocean igneous crust. The robust evidence for fluid flow is very significative because those measurements have been obtained in the area where the ocean plate displays the least deformation associated to the bending approaching the trench. The segments of the ocean plate located to the NW and to the SE, where faulting is more pervasively developed and fault offsets are larger, leading to the exposure of ocean basement to the seawater, awaits as an exciting area for further investigations.

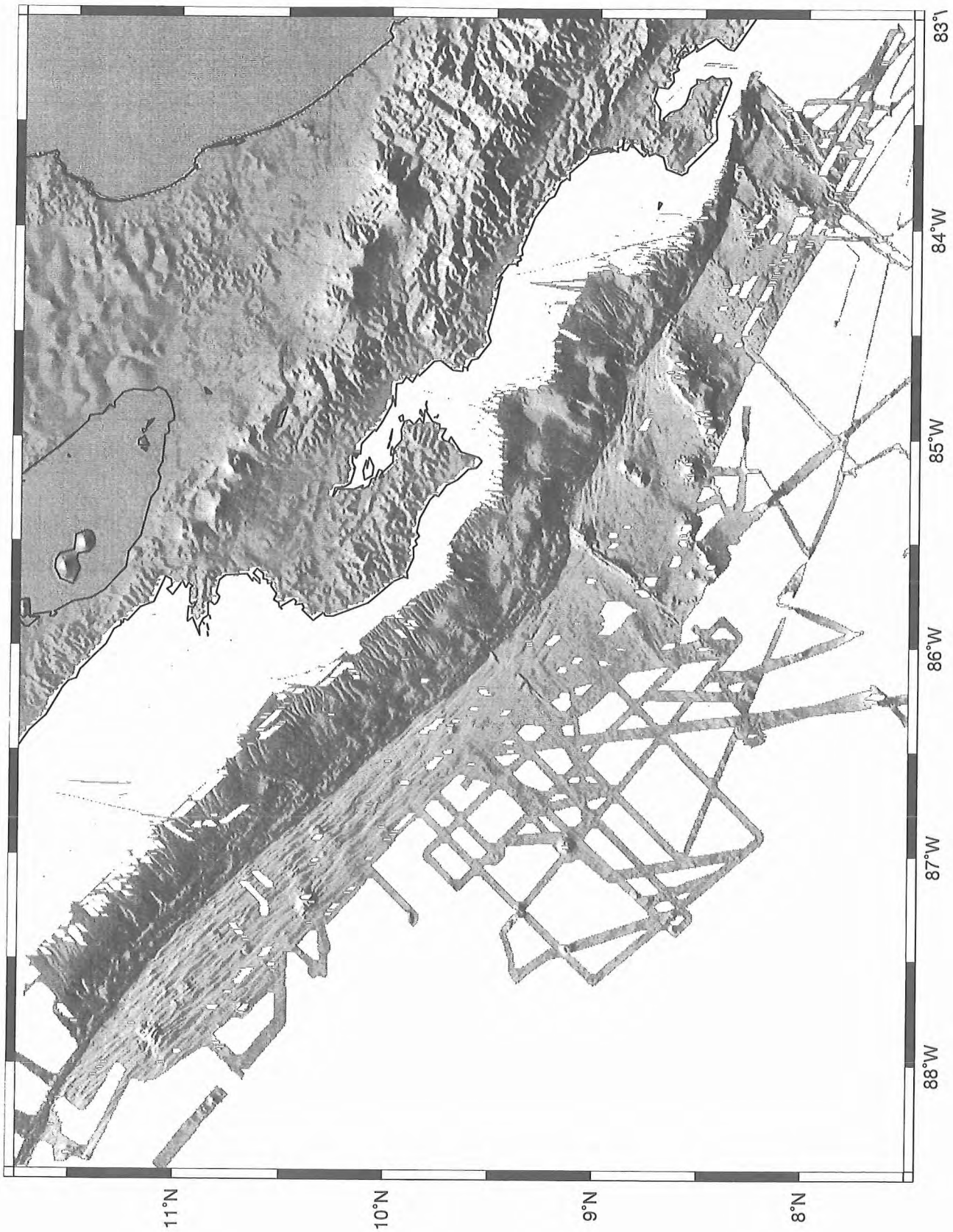


*Figure 2.2.1* *Bathymetric compilation along the Middle American trench showing the different morphological provinces of the ocean plate and the continental slope (SONNE 76, 81, 107, 144, 150, 163-1 and EWING 0005, 0104 cruises).*

## 3. Participants

### 3.1 Scientists

#### 3.1.1 Scientists - SO 163-Leg 1

| | |
|---|---|
| Dr. Wilhelm Weinrebe | GEOMAR, chief scientist |
| Frank Eichelhardt | SFB 574 |
| Rolf Hamann | SFB 574 |
| Christian Hartmann | SFB 574 |
| Dr. Caroline Huguen | SFB 574 |
| Veit Hühnerbach | SOC |
| Dr. Ingo Klaucke | GEOMAR |
| Dr. Douglas Masson | SOC |
| Duncan Matthew | SOC |
| Thomas Nadler | SFB 574 |
| Dr. Cesar Ranero | GEOMAR |
| Ian Rouse | SOC |
| Dr. Heiko Sahling | SFB 574 |
| Thorsten Schott | Octopus |
| Dirk Schwerdtfeger | SFB 574 |
| Peter Oliver Thierer | GEOMAR |

#### 3.1.2 Scientists - SO 163-Leg 2

| | |
|---|---|
| Prof. Dr. Ernst R. Flüh | GEOMAR, chief scientist |
| Ivonne Arroyo | ICE |
| Arnim Berhorst | GEOMAR |
| Ileana Boschini | ICE |
| Guido Calvo | ICE |
| Denise De Nil | SFB 574 |
| Noemi Fekete | SFB 574 |
| Dr. Jürgen Goßler | SFB 574 |
| Dr. Sibylle Grandel | SFB 574 |
| Rolf Hamann | SFB 574 |
| Dr. Heidrun Kopp | GEOMAR |
| Susan Mau | SFB 574 |
| Virginie Pierre | GEOMAR |
| Lars Planert | GEOMAR |
| Dr. Gregor Rehder | GEOMAR |
| Michael Schnabel | SFB 574 |
| Karen Stange | SFB 574 |
| Klaus-Peter Steffen | KUM |
| Peter Oliver Thierer | GEOMAR |
| Tanja Woronowicz | GEOMAR |

### 3.2 Crew

#### 3.2.1 Crew - SO 163-Leg1

| | |
|---|---|
| Henning Papenhagen | Master |
| Jörn Löffler | Chief Mate |
| Walter Bascheck | 1st Mate |
| Frank Göldner | Radio Officer |
| Anke Walther | Surgeon |
| Volker Hartig | Chief Engineer |
| Norman Lindhorst | 2nd Engineer |
| Andreas Rex | 2nd Engineer |

| | |
|---|---|
| Uwe Rieper | Electrician |
| Hilmar Hoffmann | Chief Electronic Engineer |
| Jörg Leppin | Electronic Engineer |
| Paul Wintersteller | System Operator |
| Matthias Großmann | System Operator |
| Herrmann Rademacher | Fitter |
| Christian Kunze | Motorman |
| Rene Brendel | Motorman |
| Heinrich Riedler | Motorman |
| Rudolf Prammer | Chief Cook |
| Volkhard Falk | 2nd Cook |
| Andreas Wege | Chief Steward |
| Anja Baumgärtel | 2nd Steward |
| Justine Hasler | 2nd Steward |
| Karl-Heinz Lohmüller | Boatswain |
| Ulrich-Bruno Hampel | A. B. |
| Andreas Woltmann | A. B. |
| Peter Rosin | A. B. |
| Norbert Bosselmann | A. B. |
| Dirk Schachel | A. B. |
| Karsten Bosselmann | A. B. |

### 3.2.2 Crew - SO 163-Leg 2

| | |
|---|---|
| Hartmut Andresen | Master |
| Jörn Löffler | Chief Mate |
| Nils-Arne Aden | 1st Mate |
| Frank Göldner | Radio Officer |
| Anke Walther | Surgeon |
| Volker Hartig | Chief Engineer |
| Normann Lindhorst | 2nd Engineer |
| Andreas Rex | 2nd Engineer |
| Thorsten Dammann | Electrician |
| Jörg Leppin | Chief Electronic Engineer |
| Kurt Stammer | Electronic Engineer |
| Paul Wintersteller | System Operator |
| Matthias Großmann | System Operator |
| Jochen Stenzler | Fitter |
| Rene Brendel | Motorman |
| Christian Kunze | Motorman |
| Klaus Parschow | Motorman |
| Heinrich Riedler | Motorman |
| Rudolf Prammer | Chief Cook |
| Volkhard Falk | 2nd Cook |
| Andreas Wege | Chief Steward |
| Justine Hasler | 2nd Steward |
| Anja Baumgärtel | 2nd Steward |
| Norbert Bosselmann | Boatswain |
| Dirk Schachel | A.B. |
| Torsten Bierstedt | A.B. |
| Andreas Woltmann | A.B. |
| Karl-Michael Braasch | A.B. |
| Jörn Dettmer | A.B. |
| Peter Rosin | A.B. |

### 3.3 Addresses of Participating Institutions


**GEOMAR:** GEOMAR Forschungszentrum für marine Geowissenschaften
der Christian-Albrechts-Universität zu Kiel
Wischhofstr. 1-3
24148 Kiel
Germany
Tel.: +49 - 431 - 600 - 2972
Fax: +49 - 431 - 600 - 2922
eMail: Iname@geomar.de
Internet: www.geomar.de

**SFB 574:** Sonderforschungsbereich 574
Christian-Albrechts-Universität zu Kiel
c/o GEOMAR Forschungszentrum
Wischhofstr. 1-3
24148 Kiel
Germany
Tel.: +49 – 431 – 600 - 2972
Fax: +49 – 431 – 600 – 2922
eMail: Iname@geomar.de
Internet: www.geomar.de

**SOC:** Southampton Oceanography Centre
Empress Dock
Dock Gate 4
Southampton, SO14 3ZH
United Kingdom
Tel.: +43-1703-596568
Fax.: +43-1703-596554
eMail: d.masson@soc.soton.ac.uk

**Oktopus:** OKTOPUS
Gesellschaft für angewandte Wissenschaft
Innovative Technologien und Service in der Meerestechnik mbH
Wischhofstr. 1-3, Geb. D5
24148 Kiel
Germany
Tel.: +49 - 431 - 7209 - 350
Fax: +49 - 431 - 7209 - 356

**ICE:** Insituto Costaricense de Electricidad
C.S. Exploratió Subterránea, Sabana Norte
Apartado 10032 San José, Costa Rica
Tel.: 00506-220-6394
00506-695-6522
Fax: 00506-220-8212
e-mail: igarroyo@cariari.ucr.ac.cr

**KUM:** K.U.M. Umwelt- und Meerestechnik Kiel GmbH
Wischhofstraße 1-3, Geb. D5
24148 Kiel, Germany
Tel.: 0049-431-7209-220
Fax: 0049-431-7209-244
e-mail: KUM.Umweltsmeersestechnik@t-online.de

*Figure 3.1* *Cruise participants of SO-163/1*

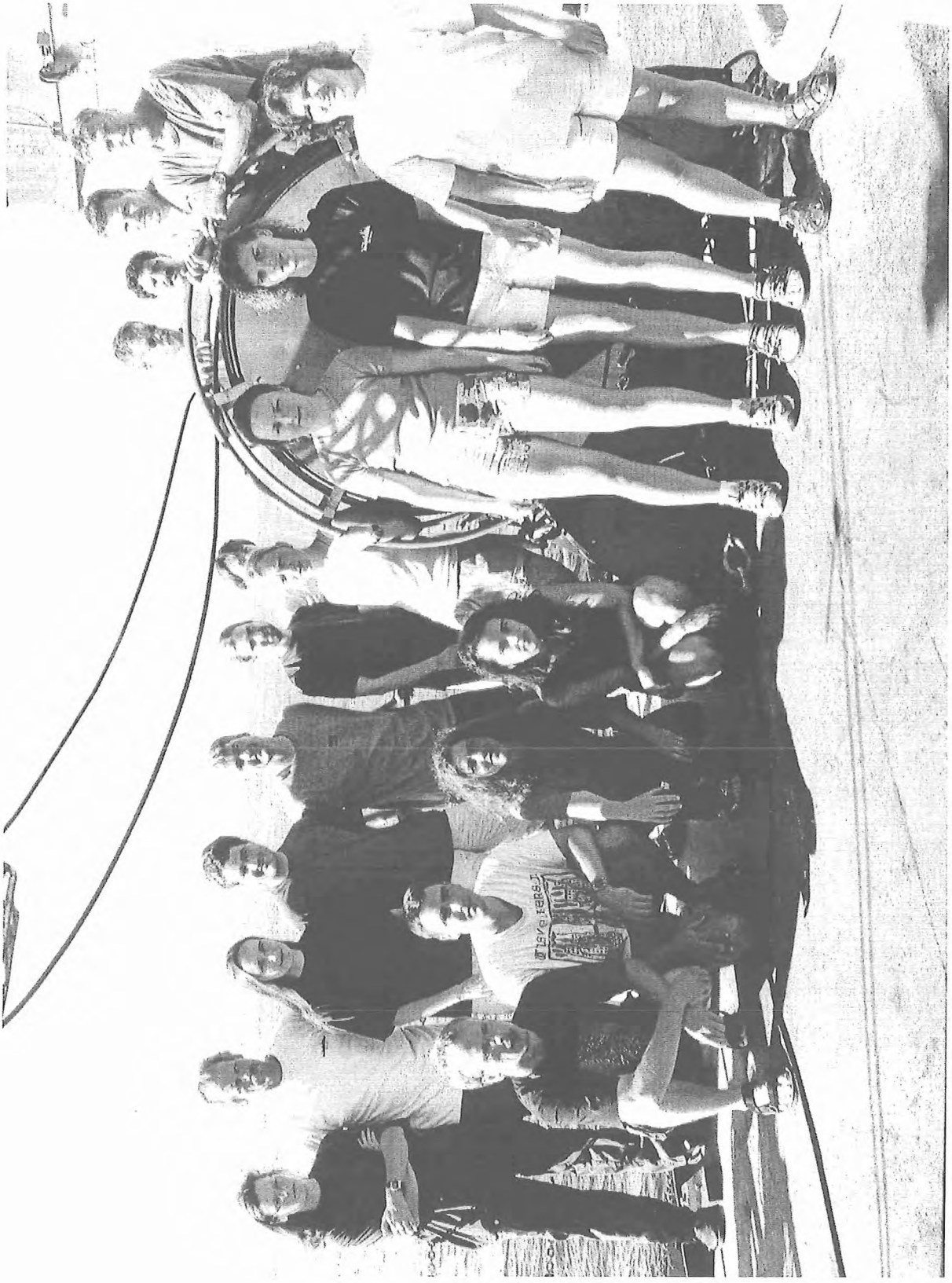

**Figure 3.1.2.:** Scientists of SO 163-2

## 4.1 Agenda of the cruise SO163-1

(W. Weinrebe)

Cruise SO 163 „SUBDUCTION I" started on March 13, 2002, in Balboa, Panama. 13 scientists embarked on RV SONNE in Balboa, whereas 3 participants of cruise SO 162 stayed onboard and completed the international group of scientists from Great Britain, France, Spain, and Germany. Although most of the scientific equipment was already set up onboard since the previous cruise, additional work was necessary to load and install the TOBI system of our colleagues from Southampton.

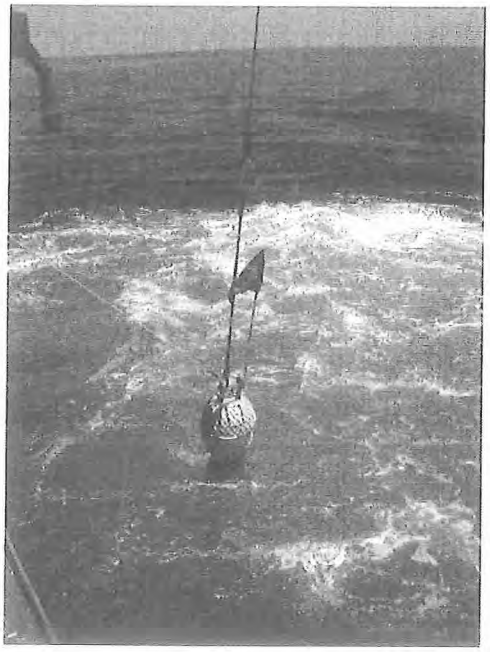

*Figure 4.1.1 Deployment of OBH*

At 11:00 in the morning of March 14 SONNE left the port of Balboa and steamed towards the research area offshore Pacific Costa Rica. The first target was an area west of Nicoya Peninsula, where several mud volcanoes had been found on previous cruises. It was planned to deploy a seismological network comprising 10 ocean bottom hydrophones (OBH) on top and around a mud volcano. These OBH will be recovered during the subsequent leg. During the transit to the working area the Simrad multibeam system was used to map several small areas in order to fill gaps in the existing bathymetric coverage.

Before starting to deploy the OBHs, a releaser test was carried out successfully in a water depth of 1,750 m. The deployment of the 10 OBHs was accomplished in 4 hours in the morning of March 16. After running a CTD down to a depth of 1,900 m to determine the water sound velocity profile, the calibration procedure for the new POSIDONIA USBL-system was started in the afternoon. Unfortunately this calibration failed due to a system error. As the first launch of TOBI was determined to take place in daylight, an additional mapping with Simrad EM120 multibeam, Parasound, and a magnetometer was carried out during the night.

TOBI with a weight of 2 tons as well as the depressor of around 650 kg were launched smoothly in 45 minutes in the morning of march 17. For this first deployment 8 profiles each of 40 nm in length and spaced 5 km apart were planned, adding up to a total time of around 6 days. First data from the upper continental margin showed many incised, probably active canyons and gullies.

Unfortunately, due to a faulty connection between umbilical- and deep sea cable, data transfer was interrupted. The first profile was abandoned incomplete and TOBI was recovered in daylight in the morning of March 18. The time span for repairs was used for additional bathymetric and magnetic mapping, before TOBI could be relaunched again successfully in the afternoon of the same day.

*Figure 4.1.2 Deployment of TOBI*

TOBI started surveying at the beginning of the second profile and operated well for more than three and a half days. Many steeply incised canyons and gullies could be seen. The upper slope is dominantly characterised by mass wasting processes. Very few circular features, interpreted as mud diapirs, were imaged, though many more of these structures show up in the bathymetry data, Obviously, just these few still seem to be active, as derived by their higher backscattering strength.

As on the lower slope no more manifestations of fluid venting were detected, TOBI was recovered on the morning of March 22 before finishing profile 6. It was decided to investigate the most prominent mud volcano seen so far at 10°17.85' N, 86°18.36' W with the TV-sled OFOS. Due to strong winds and currents OFOS runs could only be carried out in a distinct direction. Two missions with OFOS in the afternoon of the same day revealed considerable amount of carbonate crusts and vent fauna (vesicomyid clams and pogonophora tube worms). Thus it seemed worth to sample this location with a TV-grab. Two deployments were carried out. Both grabs felt over during the closing of the jaws, however, we retrieved some pieces of rocks, sediment with sulfide odour and shell fragments. The calcareous cemented sediments are probably formed in the course of methane venting.

Mapping work was continued southwards with an additional survey with TOBI from March 23 to March 25. This survey area includeded the characteristic mud volcano field seaward of Central Nicoya Peninsula locally studied during cruise SO-144 in 1999. The work during the following days was concentrated in that area.

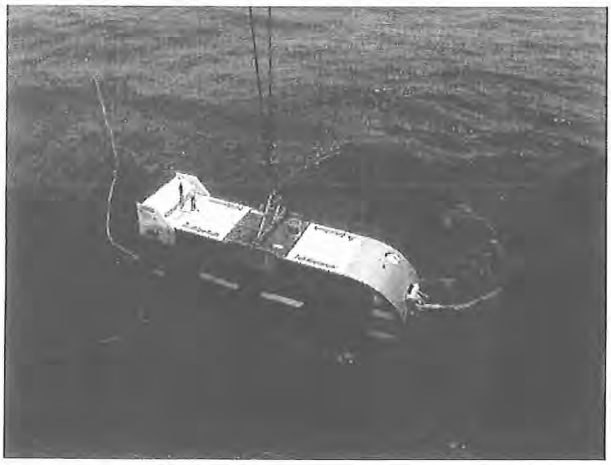

*Figure 4.1.3 Deployment of DTS-1*

A deployment of the DTS-1 deep-towed side-scan sonar system followed the TOBI survey. This system operates with higher frequencies (75 kHz, 410 kHz) than TOBI (30 kHz), and is therefore capable of mapping the seafloor with a much higher resolution but also with a considerably smaller range. The two systems are complementary.

After the new USBL underwater positioning system POSIDONIA had been calibrated, DTS-1 was launched in the evening of March 25 for a 36 hours survey around the mud volcano area at 9°36' N, 85°50' W. Later on, this survey was completed by five missions with the TV-sled OFOS. in order to acquire more detailed information.

So far, target areas for OFOS deployments concentrated on features interpreted as mud-volcanoes. These structures are small circular features, several hundred meters in diameter, some showing a central crater, which can be well detected in the bathymetry, and display high backscatter in TOBI images. During the OFOS surveys it became evident that these structures are actually related to fluid venting. At the top or the flanks of the mounds we found massive chemoherm-like carbonates, and at some of these structures, vesicomyid clams and pogonophoran tubeworms. However, we found no geological evidence for active fluid expulsion.

The next working area was located on the oceanic plate, whereas all other targets so far were situated on the continental plate. A recent cruise with RV EWING found an area with local anomalously high heat flux. This area occurs at the inception of the trench parallel flexural faults created by the bending of the oceanic lithosphere into the subduction zone. The anomalous heat flux and the faulting point towards fluid flow in the area, and we looked for venting activity and specific fauna. Due to the limited length of the deep-sea cable on RV SONNE (around 7,000 m), the success of a survey of this area with the DTS-1 is at least highly questionable. An operation of the deep-towed vehicle at a depth of 3,300 m requires a longer cable. Based on experience, a cable length 2.5 to 3.5 times the towing depth is necessary. Therefore we used the Simrad EM120 multibeam system for a detailed survey switching the beams focused in the center, and the ship's speed adjusted in order to obtain a dense coverage along-track. We processed and displayed the „sidescan" information of the system to obtain the backscattering properties. The area of high heat-flux is characterised by a gentle high and marked by higher backscatter. However, two missions with OFOS failed to find typical vent fauna.

Following this survey towards the end of the third week, an area just downslope of the headwall of the prominent Nicoya Slide was surveyed with DTS-1. The TOBI images of this region, acquired during SO-144 cruise in 1999, show spots of high backscatter not justified by seafloor topography. This area was mapped with DTS-1 75 kHz side-scan and subbottom profiler on five parallel lines.

Work continued on April 2 offshore Central Costa Rica in the area of the upper plate opposite the seamount province of the oceanic plate. The margin here is sculptured by the furrows of seamounts subducting with the lower plate. First target was the Christmas Ridge. OFOS observations revealed massive outcropping carbonates at the whole top area of this local high (1 mile in diameter). Neither at the top nor at the western flanks we found sufficient recent venting activity that would have justified further investigations.

The next target was the uplift landward of Jaco Scarp, caused by a subducting seamount. The top of the structure, the area of highest uplift, is characterised by numerous faults. We ran two OFOS missions across these areas characterised by high backscatter in TOBI images. OFOS 10 revealed a seafloor either paved by carbonates, or covered by fragmented and donut-shaped carbonates. In the whole area we observed scattered bivalve shells. OFOS 11 verified that most of the lineated high backscatter areas are caused by faults indicated by small depressions with depths on the order of 5 to 15 m. Only at the rim of the depressions talus boulders were found. The top of the uplifted area is structured by massive chemoherm-like carbonates. A dense field of vesicomyid clams were observed at a place, where the massive chemoherm complex were probably cut by fractures.

Generally, all OFOS deployments had to cope with relatively strong currents. Planning the tracks often had to follow operational rather than geological requirements.

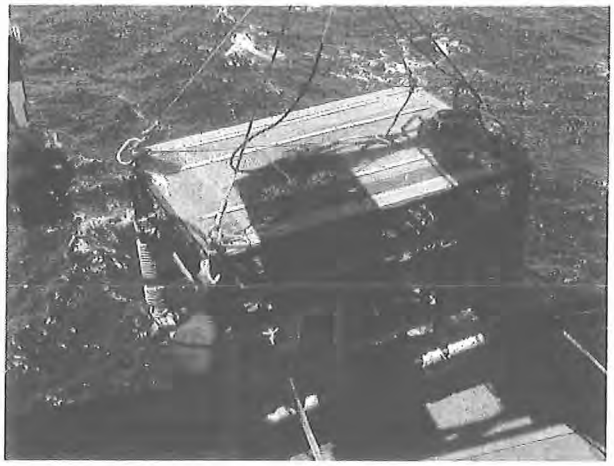

*Figure 4.1.4 Deployment of OFOS*

Starting on April 3 in the morning, we continued to survey the uplifted and faulted area upslope Jaco Scarp with the side-scan sonar and the subbottom profiler of the DTS-1. Gaining more and more experience after several launch and recovery operations, the deployment was carried out smoothly in less than 15 minutes. The whole uplifted area with the pronounced fault pattern was imaged with 8 parallel profiles each around 10 miles in length. The northeastern flank of the uplifted area, showing a steady slope in the bathymetric data, turned out to be a series of rather steep, staircase like precipicies. As the DTS-1 vehicle is towed at a height of just 100 m above the seafloor, steaming uphill required total attention of the DTS-1 watchkeepers. The survey across the uphill area of Jaco Scarp was completed with a track operating the DTS-1 system in the high-frequency mode. The faults and cracks on top of the structure, and the headwall of Jaco Scarp were imaged in great detail.

Work continued in the morning of April 5 with a TV-grab in order to sample donut-shaped carbonates observed by OFOS 10 two days ago. The grab felt over again, yet it yielded eroded carbonate chimneys and calcitic cemented sediments forming partly rounded boulders. In addition, more than 90 specimen of the seep-typical bivalve Acharax (Solemyidae) were extracted from the sediment indicating a weak venting activity at this site.

The mosaic of the processed TOBI data recorded during SO-144 in 1999 show a small area with striking high backscatter between Jaco und Parrita Scarp. This structure was investigated with an OFOS mission on

the afternoon of the same day. Beside very infrequent clamshells in soft sediment along the whole track we observed no changes in the sediment texture or lithology which could explain the high backscatter patterns.

In the evening of the same day, following the OFOS survey, TOBI was again launched for a more than 4 days mapping of the lower part of the margin and the deformation front. Three parallel profiles, each about 80 miles in length, extend the investigated area southward until Osa Peninsula. The structures of the middle slope and the frontal prism were mapped in great detail. In the area between Quepos Plateau and Cocos Ridge, we observed several small indentations of the deformation front, scars of seamounts currently impacting the margin. Close to the western crest of the Cocos Ridge a circular cone showing extremely high backscatter, surrounded by several concentric rings, was imaged.

The TOBI survey stopped on wednesday, April 10, near Cocos Ridge in order to run several OFOS missions in between wednesday morning and thursday afternoon, aimed at ground truthing the structures with high backscatter in the TOBI images.

In the afternoon of April 11, TOBI was relaunched again for a mission to map the area landward of Quepos Plateau up to the upper slope. This area, characterised by the large Quepos Slide, was surveyed during cruise SO-144 with an OFOS (OFOS-4). The observations then showed considerable indications for fluid venting. The 40 hours TOBI survey mapped this part completely. TOBI data showed several mounds with high backscatter as well as small bands of slightly increased backscatter, downwards of these mounds. TOBI was recovered on saturday, April 14 in the late afternoon.

During the last week of the cruise, there were some highlights as a reward for the efforts made in the course of the preceding weeks. The results obtained from OFOS, used twice in the area of the Quepos-slide, confirmed that bacteria mats cover a large surface at the basis of the landslide edge, as had been observed on cruise SO-144. Using the TV-guided grab, samples were taken from this area. Although no bacteria mat was found in the TV-G, the sediment, containing large amounts of sulphide, allows the conclusion that anaerobic methane oxidation is the predominant geochemical process.

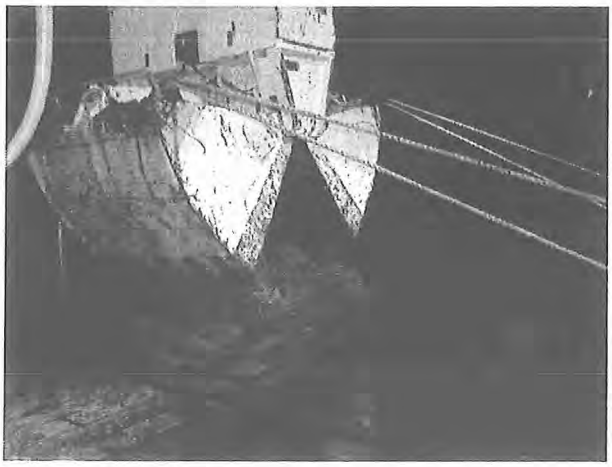

*Figure 4.1.4 TV-grab on deck*

Work continued on April 15 and 16 with a deployment of the DTS-1 sidescan sonar above Parrita Scarp. The faults caused by the uplift could be mapped well. Then OFOS was again deployed several times north of the Parrita Scarp. A small mound of about 30 m height showed clear signs of active fluid-venting. Here, the same species occur as had been found previously, however, throughout a considerably larger surface. In an area of about 150 m carbonates occur massively. Gaps between carbonate surfaces are covered with shells and pogonophoran tubeworms. This gigantic seep area is excellently suitable for future investigations. On Wednesday, we spontaneously decided to operate DTS-1 for high-resolution mapping in 410 kHz mode to record the aerial extent of this structure. Due to the limited time only one profile could be recorded since a ship's turn to obtain another profile would have taken too long. Owing to the joint efforts of the work groups and the Captain's bridge the mound could be measured successfully.

Work continued during April 17 and 18 with several OFOS and TV-grab operations at Jaco Scarp. Bathymetric measurements with the Simrad EM-120 multibeam system on the passage to Caldera terminated the scientific programme at 2.00 h a.m. of 19 April. In the morning of 19 April at 09:15 h RV SONNE moored at pier 3 in port of Caldera, Costa Rica. Thus, the first leg of cruise SO-163 ended after 37 days at sea.

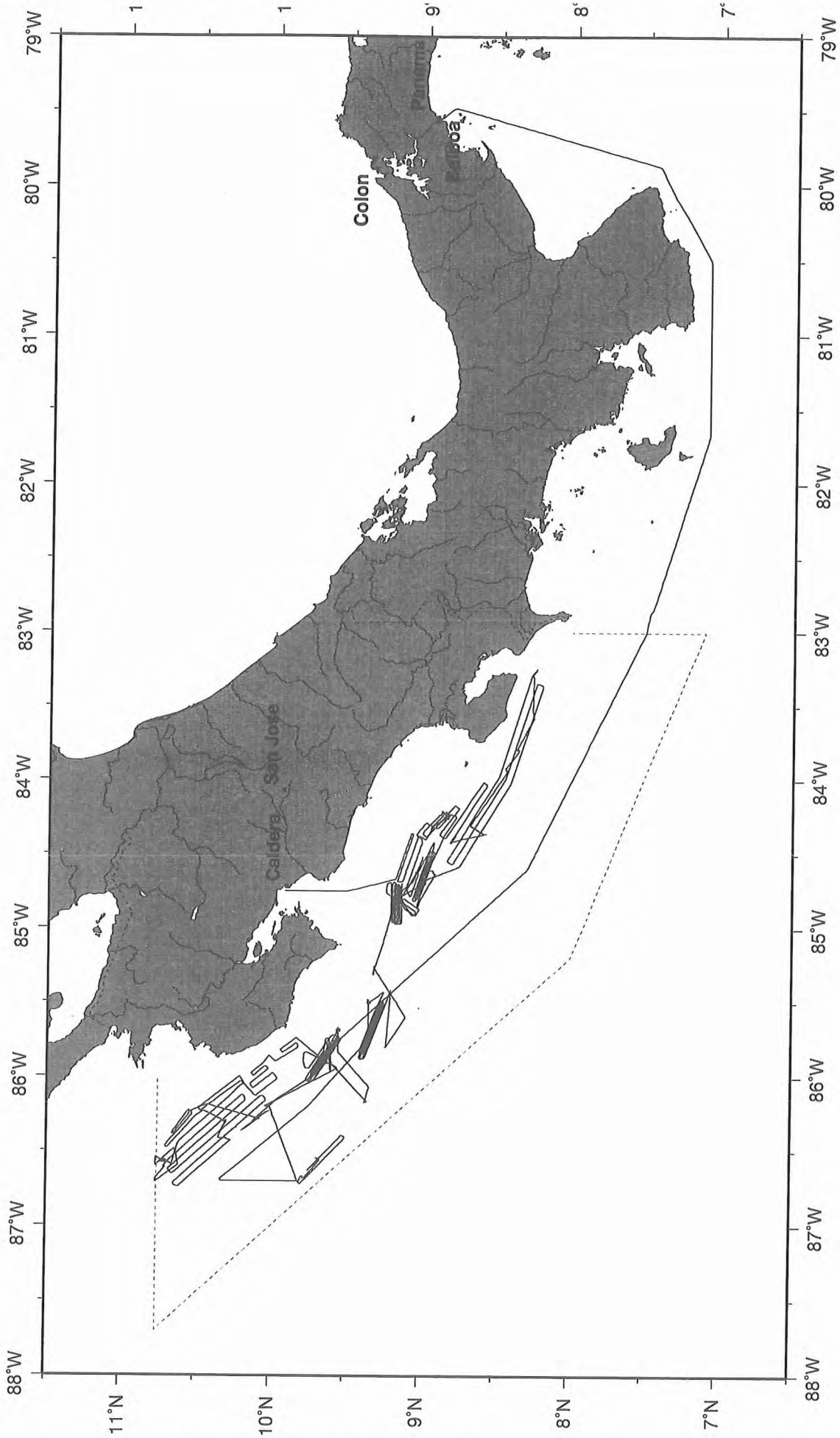


*Figure 4.1.6 Total track of the cruise SO163 Leg 1*

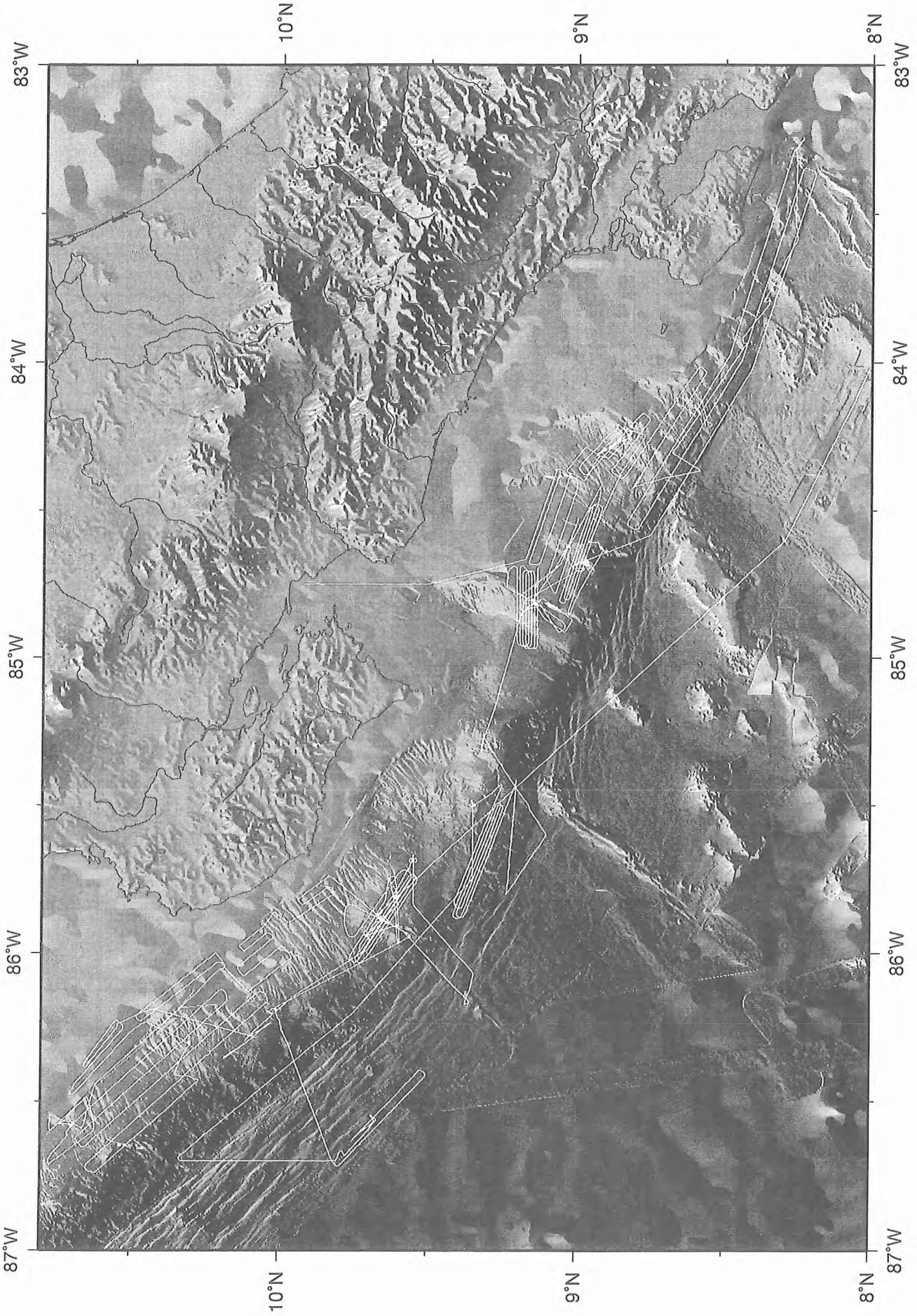


*Figure 4.1.7 Cruisel track of the cruise SO163 Leg 1 in the area off Costa Rica*

## 4.2 Agenda of the cruise SO163-2

Cruise SO 163 "SUBDUCTION I-Leg 2" started when leaving the pier of Puerto Caldera on 22. April at 10:40. Four containers with scientific equipment had been loaded and installed before, and the computer network needed for the seismic data processing remained onboard from the two previous cruises.After a short transit of only 3 hours we reached the Jaco Scar area, where a seismological network was to be installed for several month (to be picked up during cruise M54/3B in october 2002). Three instrument were ready for imedeate deployment, before the remaining acoustic releases were tested using W6 winch at a waterdepth of 3000 m. Then four more instruments and a new tiltmeter were also installed.

We then headed northwest to an active vent site, where during the previous leg a local seismic array comprising 10 instruments had ben installed. We first added two more instruments and shot sic short airgun profiles across the array, thereby varying the gun depth from 3.5 to 14 m to monitor the far field signal. Only two of the instruments were recovered, bevor we started a regional transect of CTD/water sampling/multicorer investigations.In between stations CDT02 and 03 the magnetometer was deployed during the transit.

On 25. April two more profiles, now using the g-gun clusters, were shot across the array before all instruments were safely recovered at 09:00 25.04.

Next we deployed 12 OBS/H on the Nicoya slide and shot into them along two long lines (profiles P9 and P10). While shooting on the oceanic plate, two more magnetic profiles were collected.

After the recovery of three instruments two more were deployed (amongst them a new OBS design) and several short cross lines were shot using different airgun configurations. All instruments were recovered by 17:00 27.04.

CDT05 and 06 completed the northern regional transect and Sonne returned to the Jaco Scar area. Here the tiltmeter was recovered, 5 instruments were deployed for the seismic network and a CTD was run in the center of Jaco Scar.

On 29. April 17 instruments (OBH43 to 59) were deployed on the margin above a previuosly identified reflection, that is interpreted to indicate upper plate erosion through the detachment of megalense type structures. Shooting across this ca 40 nm long linear array was done twice, again using different airgun configurations(P15 and16). Amongst the 17 instruments was a new OBS design (OBS2002), with failed to return to the surface upon interrogation. The release command was acknowledged, but the instrument did not pop up. Since the waterdepth was only 200 m, an attempt to dredge the instrument was made but failed due to problems with the cable.

Following two more CTD stations (CTD08 and09) another attempt to dredge the instrument was finally successfull.

In the evening of 01. Mai two tiltmeterstations (OBT60 and 61) were deployed on Quepos plateau, and after CDT10 a 30 nm long cross line on the megalense structure was coverd with 14 OBS/H (OBH62 to 75), shooting was done twice (P17,18) across the array. All instruments were safely recovered 03. Mai in the morning.

Two more CTD stations (CDT11 and 12) were run on Quepos mound, using the Sonne USBl positioning system attached to the instrument, so samples could be taken along profiles across the mound.

A second strike line across the megalense structure was made after the depployment of a 15 instrument linear Array (OBH76 to 90). This profiles was shot four times unsing different airgun configurations (P18, 20, 21, and 22), and a short reflection profile (P19) was included across Quepos mound, using a high frequency airgun array and a shot interval of only 10 sec. All instruments were recovered 05. May, followed by two CTD-stations on Quepos mound (CTD13 and 14). The last profile on the megalense was collected parrallel to Profiles 15 and 16, with 15 instruments (OBH92 to 106) deployed. Again, this line was shot using two different airgun configurations (P24 and 25). This work was completed in the morning of 07. May.

A regional CTD-transect off southern Costa Rica comprising 6 stations was started with the first two measurements (CTD15 and 16) in the afternoon of 7 may.

The next seismic work focussed on the detachment reflection south of Quepos Plateau. In Total 15 instruments (OBH107 to 121) were deployed in the evening of 07 May, the first and the last

instruments were deployed with a 1000 m long cable such that the far field signature of the guns could be monitored without interference from the sea floor reflection. Shooting along this 8.5 nm long profile was made at a minimum speed of 2 kn with different airguns and trigger rates (profiles P 26,27,28), and was followed by a series of testshots using various combinations throughout the G-Gun cluster (P29). All instruments were successfully recovered 08. May in the evening, before two more CTD stations were made on the southern regional transect (CTD17 and 18).
On May 09 the two tiltmeters and the 7 instruments from the first deployment (OBS14 to 21) were all recovered, followed by a transit to the outermost two CDT stations of the southern transect (CTD 19 and 20).
Two parallel strike lines on the detachment reflection were collected May 10 and 11 (profiles P30 and 31), and three more instruments (OBH 139 to 141) were deployed in the Jaco Scar seismological network, where another CTD (21) was deployed on Jaco Scar.
On May 12 20 instruments were deployed on a regional profile across the Culebra Mound, including a short strike line and a densely sample line (Profile 33) across Culebra Mound. Here also two CTD deployment were made, and subsequently two attempts to dredge rocks from this mound unfortunately failed.
On the transit back to Nicoya slide a high resolution bathymetric profile including Parasound echosounding was collected around the planned ODP-leg 205 drilling.
On the Nicoya slide another 20 instruments were deployed, and a regional line plus two short strike lines were collected May 15 and 16.
Finally, 20 additional instruments (OBH192 to 212) were all deployed in the Jaco Scar seismological network, and three profiles (P38 to P40) were shot into the then 28 instruments deployed in the network. Shooting terminated at 06:00 on May 18, and following a last CDT deployment at Jaco Scar (CTD 24) sonne set course to Balboa, Panama. The transit through Costa Rican waters was chosen such that an hithero unsurveyed part of the oceanic plate could be mapped with the Simrad system, and we also deployed the magnetometer (magnetic profile M04). Upon reaching Panamenian waters at 83°W the Simrad system was shut down and the magnetometer was recovered at 04:00 on 19. May, which terminated the scientific work.
Sonne finally reached the pilot station in Balboa at 06:00 May 20 after cruising a total of 4000 nm within 28 days at sea. A trackplot of leg SO163-2 is shown inFigure 4.2.1.

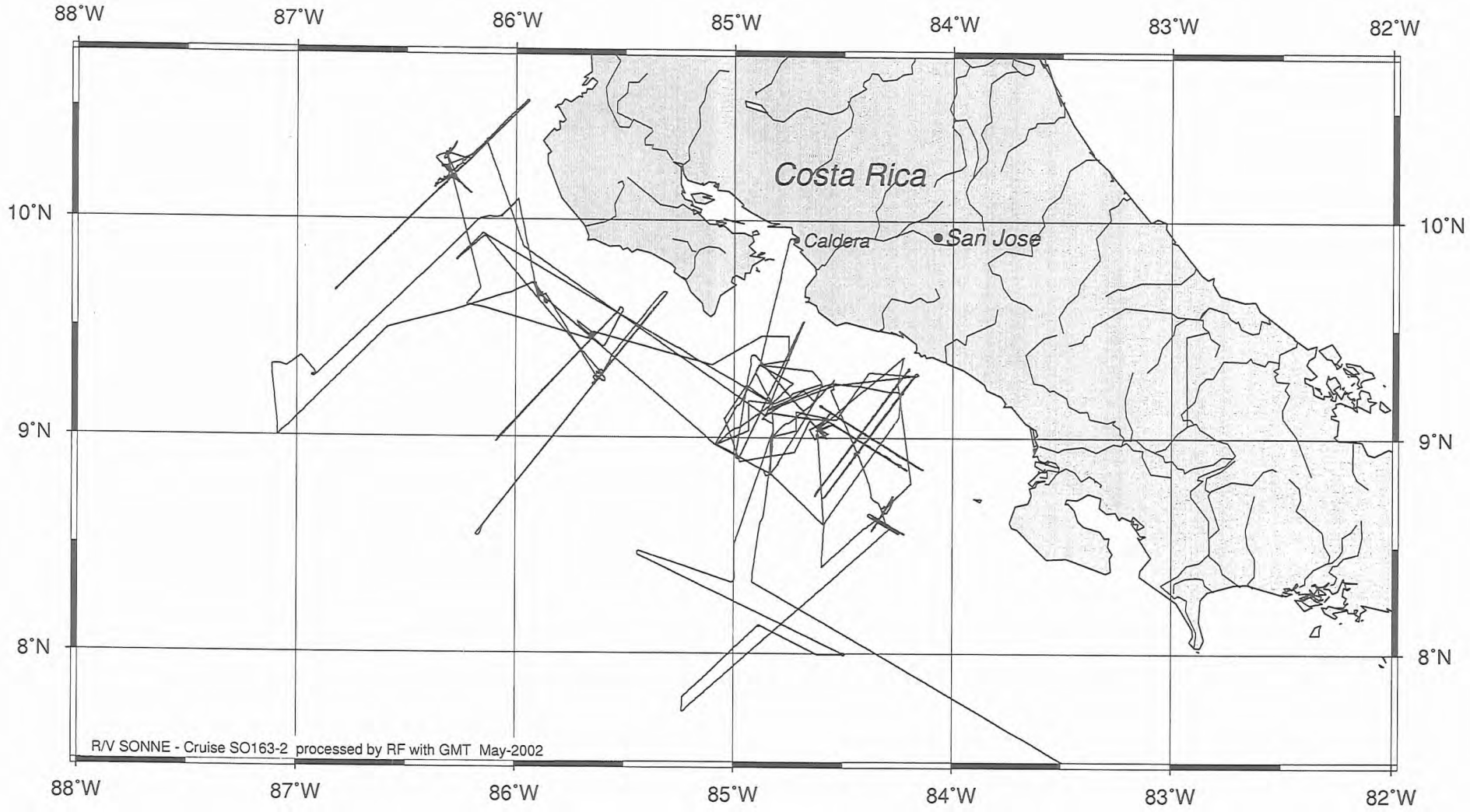


**SUBDUCTION Fluid-Volatiles-Hazards**
**Caldera 21.04.2002 - Balboa 21.05.2002**

**GEOMAR Kiel / SFB 574**

Figure 4.21: Cruise Track of 163-2

Scale 1:3.000.000
Mercator Projection (WGS 84)

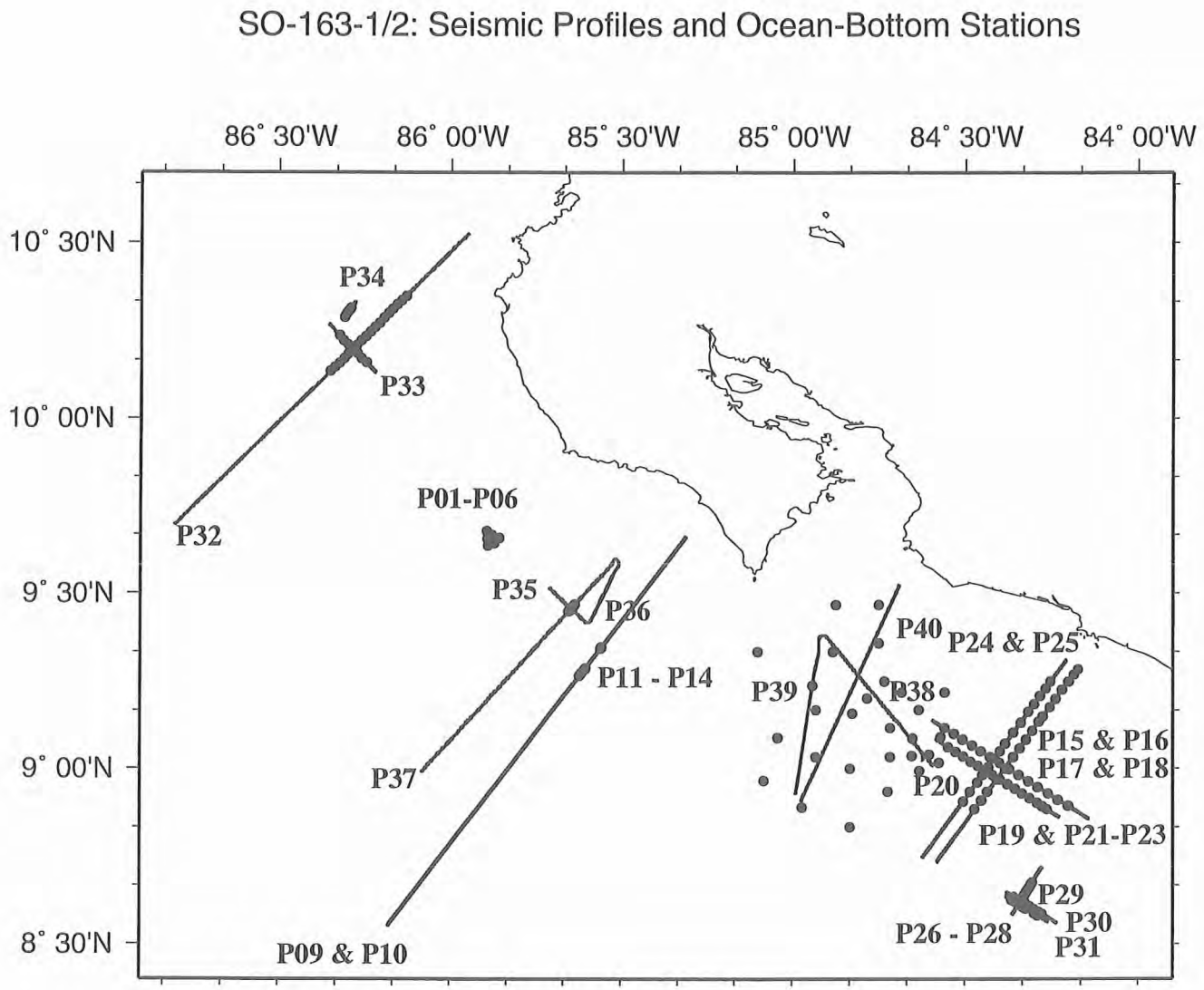


**Figure 4.2.2:** Location map of profiles P01-P40 and stations OBH1-OBH212.

### 5.1.1 Navigation

(W. Weinrebe)

A crucial prerequisite for all kinds of marine surveys is the precise knowledge of position information (latitude, longitude, altitude above/below a reference level). Since 1993 the global positioning system (GPS) is commercially available and widely used for marine surveys. It operates 24 satellites in synchronous orbits, thus at least 3 satellites are visible anywhere at any moment (Seeber, 1996). The full precision of this originally military service yields positioning accuracies of a few meters. In the past this was restricted to military forces and unaccessible to commercial users (Blondel and Murton, 1997). Since about two years the full resolution is generally available.

The resolution of GPS can be enhanced with the Differential GPS (D-GPS) scheme (Blondel and Murton, 1997, Knickmeyer, 1996). Using several reference stations the determination of the ship's position can be corrected in real time and enhanced to a 1 m to 5 m accuracy. Since the cruise SO-109 (1996) D-GPS service is available onboard R/V SONNE. The ships ASHTEC system provides a validated accuracy better than 5 - 10 m in the area off Costa Rica.

D-GPS-values as well as most other cruise parameters are continuously stored in the navigation database, and are distributed via the DVS- („data distribution system") on the ship's network.

Unfortunately, the precision of the position information does not correspond to the accuracy of the time base in the navigation database, as the navigation processing unit Atlas ANP 2000 does not copy the precise GPS-time values, but adds time stamps of its internal unsynchronized clock.

### 5.1.2 Simrad EM120 Multibeam System

(C. Huguen)

The EM120 system is a multibeam echosounder (with 191 beams) providing accurate bathymetric mapping up to depths higher than 11000 m. This system is composed of two transducer arrays fixed on the hull of the ship, which send successive frequency coded acoustic signals (11.25 to 12.6 kHz). Data acquisition is based on successive emission-reception cycles of this signal. The emission beam is 150° wide across track, and 2° along track direction (Fig. 5.1.2.1). The reception is obtained from 191 overlapping beams, with widths of 2° across track and 20° along it (Fig. 1). The beam spacing can be defined as equidistant or equiangular, and the maximum seafloor coverage fixed or not. The echoes from the intersection area (2°*2°) between transmission and reception patterns (Fig. 5.1.2.1), produce a signal from which depth and reflectivity are extracted.

For depth measurements, 191 isolated depth values are obtained perpendicular to the track for each signal. Using the 2-way-travel-time and the beam angle known for each beam, and taking into account the ray bending due to refraction in the water column by sound speed variations, depth is estimated for each beam. A combination of phase (for the central beams) and amplitude (lateral beams) is used to provide a measurement accuracy practicaly independant of the beam pointing angle. The raw depth datas need then to be processed to obtain depth-contour maps. In the first step, the data are merged with navigation files to compute their geographic position, and the depth values are plotted on a regular grid to obtain a digital terrain model (*DTM*). In the last stage, the grid is interpolated, and finally smoothed to obtain a better graphic representation. Together with depth measurements, the acoustic signal is sampled each 3.2ms and processed to obtain a cartographic representation, commonly named mosaic, where grey levels are representative of backscatter amplitudes. These data provide thus informations on the sea-floor nature and texture; it can be simply said that a smooth and soft seabed will backscatter little energy, whereas a rough and hard relief will return a stronger echo.

During the SO 163 cruise, the Simrad EM 120 Multibeam echosoundeur, available on R/V SONNE since June 2001, was used continuously. Bathymetric data were processed routinely onboard during the survey, using the NEPTUNE software from Simrad, available on board and the academic software MB-System from Lamont-Doherty Earth Observatory.

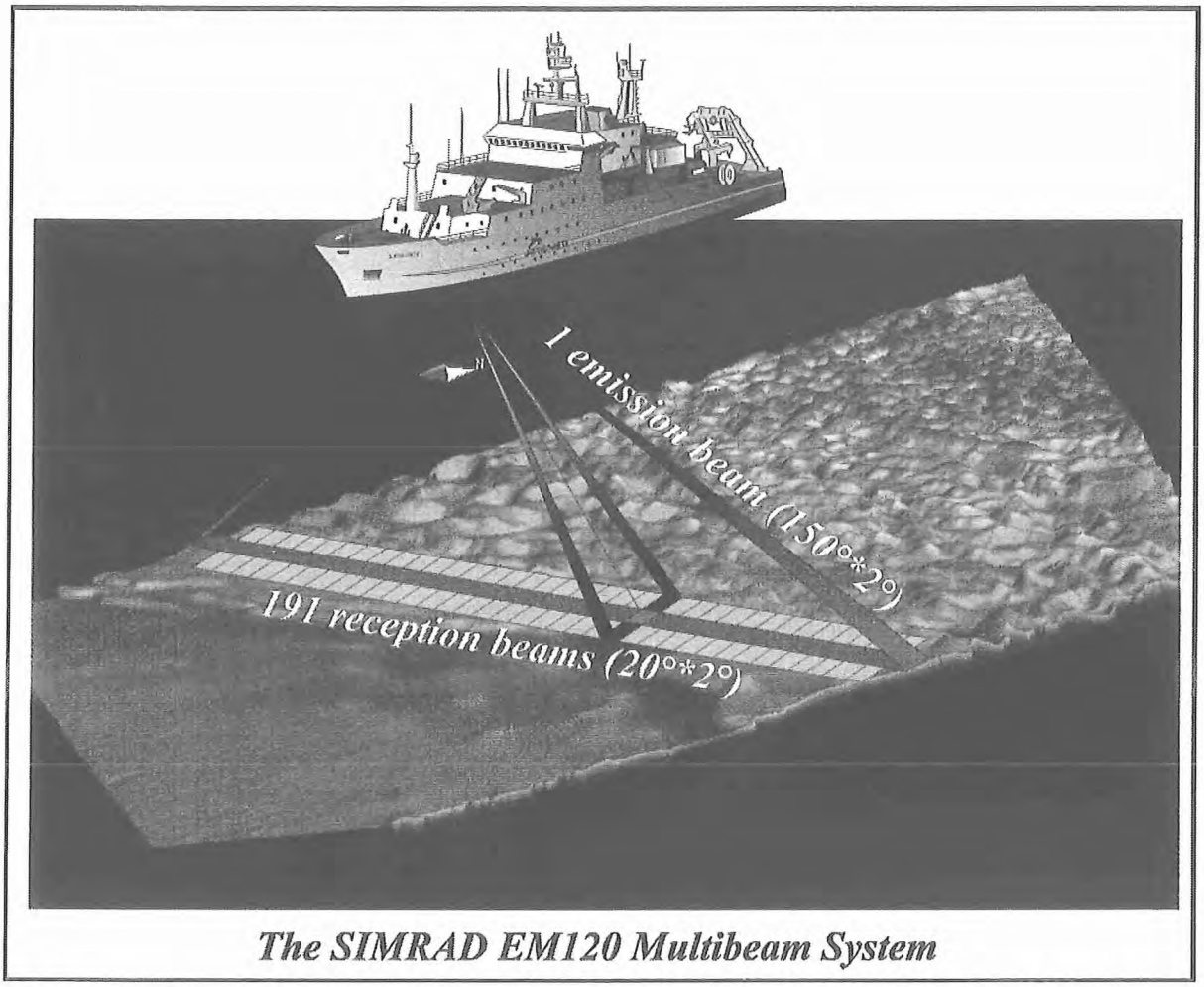


*Figure 5.1.1 Acquisition method for bathymetric and backscatter data from the Simrad EM120 system (crossed beams technique)*

### 5.1.3 PARASOUND

(T. Nadler)

The PARASOUND system works both as a low-frequency sediment echosounder and as a high-frequency narrow beam sounder to determine the water depth. It utilizes the parametric effect, which produces additional frequencies through nonlinear acoustic interaction of finite amplitude waves. If two sound waves of similar frequencies (here 18 kHz and e.g. 22 kHz) are emitted simultaneously, a signal of the difference frequency (e.g. 4 kHz) is generated for sufficiently high primary amplitudes. The new component travels within the emission cone of the original high frequency waves, which are limited to an angle of only 4° for the equipment used. Therefore, the footprint size of 7% of the water depth is much smaller than for conventional systems and both vertical and lateral resolution are significantly improved.

The PARASOUND system is permanently installed on the ship. The hull-mounted transducer array has 128 elements within an area of 1 m2. It requires up to 70 kW of electric power due to the low degree of efficiency of the parametric effect. In 2 electronic cabinets, beam formation, signal generation and the separation of the primary (18, 22 kHz) and secondary frequencies (4 kHz) is carried out. Using the third electronic cabinet located in the echosounder control room, the system is operated on a 24 hour watch schedule.

Since the two-way travel time in the deep sea is long compared to the length of the reception window of up to 266 ms, the PARASOUND System sends out a burst of pulses at 400 ms intervals, until the first echo returns. The coverage in this discontinuous mode is dependent on the water depth and also produces non-equidistant shot distances between bursts.

The main tasks of the operators are system and quality control and to adjust the start of the reception window. Because of the limited penetration of the echosounding signal into the sediment, only a short time window close to the sea floor is recorded.

In addition to the analog recording features with the b/w DESO 25 device, the PARASOUND System is equipped with the digital data acquisition system ParaDigMA, developed at the University of Bremen. The data is stored on removable hard disks using the standard, industry-compatible SEGY-format. The 486-processor based PC allows for buffering, transfer and storage of the digital seismograms at very high repetition rates. Of the emitted series of pulses, usually only every second pulse can be digitized and stored, resulting in recording intervals of 800 ms for a given pulse sequence. The seismograms were sampled at a frequency of 40 kHz, with a typical registration length of 266 ms for a depth window of ~200 m. The source signal was a band limited, 2-6 kHz sinusoidal wavelet with a dominant frequency of 4 kHz and duration of 1 period (250 µs total length). Data was stored on DAT-tapes using Windows NT backup software.

### 5.1.4 Ocean Floor Observation System (OFOS) and TV-guided grab (TVG)

(H. Sahling, T. Nadler)

OFOS

The OFOS system on board RV Sonne is a most sophisticated camera sled, which has been specifically adapted to completely satisfy all scientific requirements. OFOS is equipped with following instruments: two video cameras (colour camera: Deep Sea Power and Light, black and white camera: Photosea), a stereo still camera system (Photosea), various xenon and halogen lights (Deep Sea Power and Light), CTD (Seabird), a compass, pitch and roll sensor, and a Simrad SSBL responder.

The sled is towed behind the ship at a speed of about 0.8 knots (kn). The distance of about 1.5 m to the seafloor is manually adjusted by the winch operator. For that, a weight is hanging on a rope of 2 m length below the sled. Two laser pointer can be used to scale the video image and the still camera images. Two laser pointer are parallel and 20 cm apart, while a third one points in an oblique angel. The still camera is loaded with a slide film (Kodak Ectachrom 200) allowing a maximum of 800 shots. After using an aperture of 5.6 (camera A) and 8 (camera B) during OFOS 1 & 2, which resulted in too-dark seafloor images an aperture of 4 resulted in a satisfactory illumination. The images were taken manually or at regular time intervals. On the video signal and on the images the date and time (UTC) is overlaid. The ships data, the SSBL position and some OFOS data were recorded in the database of the ship. These data were downloaded and stored in the database Access referenced by the UTC time. Additionally, the system operators downloaded the raw data of the CTD mounted on OFOS (sampling rate 0.5 sec.). These data were recalculated to the time of deployment and integrated also into the database.

During SO 163 cruise we were confronted with peculiarities of the investigation area that influenced the deployments of OFOS considerably. Strong currents and, at some times winds made navigation difficult. Thus, most tracks were planed in arrangement with the bridge. Furthermore, OFOS should be preferential towed downslope. As a result the directions of survey lines were strongly controlled by these factors rather than solely on scientific targets, which we wanted to image.
There are a few improvements concerning OFOS we would like to mention. The data of the CTD, which is mounted on OFOS, are not stored in the ships database. That would be most important in the future. The front end for OFOS Bottom travel should include the SSBL position, too.

TVG
The TV-guided grab (TVG) is a heavy tool to collect sediment, rock or biological samples from the seafloor. Its lits can be closed hydraulically. It is powered by deep-sea batteries allowing closing and opening it about three times. The opening of the grab is about 1.8 m2. For the deployments the grab was equipped with the black-and-white camera and the colour camera used in OFOS. Accurate position can be acquired by a SSBL responder, which is tied on the fiberoptic cable 50 m above the tool.

### 5.1.5 CTD

(H. Sahling)

A CTD was deployed during SO 163-1 cruise in order to acquire a sound velocity profile through the water column. This profile was then used to calibrate the echosounding systems (Simrad, Posidonia).
The CTD/rosette aboard Sonne consists of a deck unit (SBE 11 plus), which supports the underwater unit of the CTD (SBE 9 plus) and the SBE 32 carousel water sampler equipped with 24 * 10 l Niskin bottles. The used CTD system supplies a modular temperature sensor (SBE 3 plus), a conductivity sensor (SBE 4), a Digiquartz pressure sensor, and an oxygen sensor (SBE 13). An external pump (SBE 5) maintains an optimum and constant water flushing speed for temperature, conductivity and oxygen sensors via a TC Duct, thus guaranteeing that all sensors measure the same water.
The deck unit provides DC power to the sea cable, decodes the serial data stream arriving from the underwater unit and passes the data to a companion computer. Binary data from the sensors are transmitted serially 24 times a second. The deck unit has a separate communication channel for controlling the Seabird carousel and an audible bottom contact alarm. Acquired data are placed on the computer where postprocessing is achieved with the software provided by Seabird. The data were averaged and bottle files were produced.

## 5.2 Computer facilities for bathymetry, magnetic, and seismic data processing

(W. Weinrebe)

The experiments and investigations during SO163 required special computing facilities in addition to the existing shipboard systems. For programming of ocean bottom stations, processing and interpretation of seismic data and analysis of magnetics several workstations and a dedicated PC-laptop were installed by the wide angle and seismology groups of GEOMAR. Due to the large amount of data transfer GEOMAR installed a workstation cluster onboard comprising the following systems:

| | | | | | |
|---|---|---|---|---|---|
| 1 | "moho" | SUN Sparc20<br>2 CPU | 256 MB<br>memory | 20 GB disks<br>DAT, CD | Sun<br>Solaris 5.8 |
| 2 | "devonia" | SUN Ultra 60<br>2 CPU | 1 GB<br>1 GB | 150 GB disks<br>1x DLT8000<br>2x DAT<br>2x Exabyte | Sun<br>Solaris 5.6 |
| 3 | "hotblack" | SUN Ultra 1<br>1 CPU | 128 MB<br>memory | 36 GB disks<br>CD | Sun<br>Solaris 5.8 |
| 4 | "galicia" | SUN Sparc 10<br>1 CPU | 96 MB<br>memory | 12 GB disks<br>DAT | Sun<br>O.S.4.1.4 |
| 5 | "crimea" | AMD<br>DURON<br>700 MHz | 128 MB<br>memory | 68 GB disks<br>6x PCMCIA | Windows2000 |
| 6 | „pinta" | AMD<br>DURON<br>700 MHz | 128 MB<br>memory | 68 GB disks<br>6x PCMCIA | Windows2000 |

In addition to these computers, several laptops were used. For plotting and printing two HP Postscript Laserprinters (papersize A3 and A4) as well as the shipboard color plotters were available.

The workstation cluster was placed in the Magnetiklabor and the Reinlabor where it was set up according to a "client-server" model, with "moho" being the server. All important file systems from the main server at GEOMAR were duplicated onto the "moho"-disks. Using NFS-, NIS-, and automounter services the computing environment was nearly identical to that at GEOMAR, so every user found his/her familiar user interface. The convenience of network mounted file systems has to be paid for with a heavy network load, particularly during playback of OBH-data (c.f. SO123 cruise report, Flueh et al., 1997). This required a high-performance network, which was accomplished by a switched twisted-pair ethernet. A 12-port ethernet switching-hub (3COM-SuperstackII 1000) with an uplink connection of 100 Mbps to the server "moho" and dedicated 10 Mbps ports for the client workstations maintained the necessary network performance. In order to keep the shipboard network undisturbed by the workstation cluster, but to allow for communication between them, the server "moho" was equipped with two network interfaces and served as a router. This provided the additional benefit of a simplified network configuration. Considerable setup work was dedicated to "moho", while the other workstations used the same IP-addresses and network configuration as at GEOMAR. In addition, „hotblack" was set up as an redundant server, so in case „moho" would have failed, „hotblack" could easily switched to replace „moho" as a server.

This network setup showed a reliable and stable performance, and no breakdowns were observed.

## 5.3 Seismic Instrumentation

### The Ocean Bottom Hydrophone

The first GEOMAR Ocean Bottom Hydrophone was built in 1991 and tested at sea in January 1992. This type of instrument has proved to have a high reliability; in fact during this cruise we celebrated the 2000 successful deployment. A total of 20 OBH and 9 OBS instruments were available for SO163. Altogether 212 sites were occupied during the SO163 cruise.

The principle design of the instrument is shown in Figure 5.3.1, and a photograph showing the instrument upon deployment can be seen in Figure 5.3.2. The design is described in detail by Flueh and Bialas (1996).

The system components are mounted on a steel pipe which holds the buoyancy body on its top. The buoyancy is made of syntactic foam and is rated, as are all other components of the system, for a water depth of 6000 m, except for the pressure cylinders holding the recording electronics. Here, various models are available for variable depths (2500 m, 3000 m, and 6000 m). Attached to the buoyant body are a radio beacon, a flash light, a flag and a swimming line for retrieving from aboard the vessel. The hydrophone for the acoustic release is also mounted here. The release transponder is a model *RT661CE* made by *MORS Technology*. Communication with the instrument is possible through the ship's transducer system, and even at maximum speed and ranges of 4 to 5 miles release and range commands are successful. For anchors, we use pieces of railway tracks weighing about 40 kg each. The anchors are suspended 2 to 3 m below the instrument. The sensor is an *E-2PD* hydrophone from *OAS Inc.*, or the HTI-01-PCA hydrophone from *HIGH TECH INC.* and the recording device is a *MBS* recorder of *SEND GmbH*, which is contained in its own pressure tube and mounted below the buoyant body opposite the release transponder (see Figures 5.3.1 and 5.3.2).

### The Ocean Bottom Seismometer

The Ocean Bottom Seismometer (OBS) construction (Bialas and Flueh, 1999; Fig. 5.3.3) is based on the experiences with the GEOMAR OBH. For system compatibility the acoustic release, pressure tubes, and the hydrophone are identical to those used for the OBH. Syntactic foam was used as floatation again but of larger diameter due to the increased payload. In contrast to the OBH the OBS has three legs around a center post to which the anchor weight is attached (Fig. 5.3.4). While the OBH is floating about 1 m above the sea bottom, the OBS is positioned on the sea bottom to avoid collisions between the the seismometer cable and the anchor. The sensible seismometer is deployed about 1 m to the side of the system once the OBS lands on the sea floor. The three component seismometer ist housed in a titanium tube, modified from a package build by Tim Owen (Cambridge) earlier. Geophones of 4.5 or 30 Hz natural frequency are available. During descent to the ocean bottom, the footplate of the seismometer release lever is about one meter below the base of the anchor and therefore hits the seafloor first. At touch down the baseplate forces an upward movement of the lever which lays out the seismometer hook until the seismometer anchor is about 0.5 m above the seafloor. At about 45 degrees to the vertical the seismometer is released from its hook and falls to the sea floor from about 1 m height, ensuring coupling between the seismometer and the sea floor. At this time the only connection from the seismometer to the instrument is a cable and an attached wire which retracts the seismometer during ascent to the sea surface. An oscillation of the instrument caused by possible currents is therefore not transmitted mechanically to the seismometer. All three channels are preamplified within the seismometer housing and recorded by the standard Methusalem recorder as used in the OBH units. Parallel to these three channels the standard hydrophone is recorded on the fourth channel. A self-levelling seismometer with 4.5 Hz geophones was also successfully used during SO163. The levelling of the three component geophone (termed LG01) is done at a preset time by unlocking springs that clamp the geophone package against the titanium housing.

Beside the standard OBS type used for active seismic recording broadband seismometer were available and routinely deployed within the profiles. Two different types of sensors can be attached to the

to 4 storage cards may be used. Currently, up to 640 MB per card are available. Data compression allows allows to increase this capacity. Recently technical specifications of flashdisks (disk drives of PCMCIA technology) have been modified to operate below 10 °C, therefore 2 GB drives are now available for data storage. After recording the flashcards need to be copied to a PC workstation. During this transcription the data are decompressed and data files from a maximum of four flash memory are combined into one data set and formatted according to the PASSCAL data scheme used by the *Methusalem* system. This enables full compatibility with the established processing system. While the *Methusalem* system did provide 16 bit integer data, the 18 bit data resolution of the *MBS* can be fully utilized using a 32 bit data format.

**The Marine Longtime Seismograph**

For the purpose of low frequent recordings such as seismological observations of earthquakes during long term deployments of about one year time a new data logger, the Marine Longtime Seismograph (MLS) was developped by *SEND GmbH* with support from GEOMAR.

The MLS is again a four channel data logger whose input channels have been optimized for 3-component seismometers and one hydrophone channel. The modular design of the analogue front end allows to adopt for different seismometers and hydrophones or pressure sensors. Currently front ends for the Spahr Webb, PMD and Guralp seismometers as well as for a differential pressure gauge (DPG) and the OAS hydrophone are available. With these sensors we are able to record events between 50 Hz and 120 s. The very low power consumption of 250 mW during recording together with a high precision internal clock (0.05 ppm drift) allows data acquisition for one year. Data storage is done on up to 12 PCMCIA type II flashcards. The instrument can be parameterized and programmed via a RS232 interface. After low pass filtering the signals of the input channels are digitized using Sigma-Delta A/D converters. A final decimating sharp digital low-pass filter is realized in software by a Digital Signal Processor. The effective signal resolution depends on the sample rate and varies between 18.5 bit at 20 ms and 22 bits at 1 s. Playback of the data is done under the same scheme as described for the MBS above. After playback and decompression the data is provided in PASSCAL format from where it could be easily transformed into standard seismological data formats.

**Towed Streamer**

In addition to the ocean bottom seismic recorders also a mini-streamer was used during seismic profiling. This streamer was manufactored by *SIG (Service et Instruments de Geophysique, France)* The system comprises several parts: four 50 m long active sections with 20 hydrophones spaced at 2.50 m, two 2.50 m long lead in sections seperating the depth transducer (Philips P30) in the tail and the depth transducer and preamplifier in the head from the active sections.The lead-in cable is 150 m, and a 50 m long deck cable can be laid out to connect the winch to the lab. The individual hydrophones are omnidirectional and have a flat frequency responce from 10 to 1000 Hz. The sensitivity is –90db, re 1V/µbar, +-1 db. The hydrophones are mounted in an oilfilled polyurethane pipe of 34 mm diameter, with a nominal density of 1.12 gr/cm3. The lead-in cable can be trimmed to the required depth using air and seawater. A control unit provides power to the preamplifier, displays the depths of the head and tail depth transducers and provides the anologue signals of the four channels. The depth readings are also available on RS232 interfaces for storage on a PC.

The signals recorded by the streamer were stored on a four-channel MBS recorder, identical to those used in the ocean bottom seismic recorders. The streamer winch was placed midships about 8 m away from the aft of the vessel.

instrument. The "Spahr Webb" type seismometer is based on *Mark-L4* sensors which are operated with a feedback loop to enable recordings of frequencies as low as about 60 sec. As the sensors are sensitive to horizontal or vertical adjustment the complete construction is fully gimbaled. Tilt is measured at selected intervals and two electric motors are used to adjust and fix for a proper positioning. The second sensor is a *PMD-113* which has a flat frequency responce curve from 95 sec. up to 30 Hz. This sensor type operates on the base of measuring levels within electrolytical tubes. This principle is less sensitive to ist horizontal adjustment. The sensor is fixed like a pendulum while ist lower third is surrounded by a viscose oil filling that gives freedom to very slow movements (within a circle of 18°) and could be assumed to be solid within the measured frequency range. Both systems are mounted within a 17" glas sphere with an additional weight at the bottom (20 kg weight in water) which should ensure a good coupling to the ground. The above discribed lever system was not able to handle this size of sensor and therefore a slide system was designed (Fig. 5.3.5 and 5.3.6) which allows to deploy the sensor about three meters to the side of the instrument carrier. A clock controled burning wire is used first as release of the slide. Then the sensor is pulled by an elastic rope along the slide until he falls off at the end of the boom. Secondly the clock releases the sledge itself to enable deployment of the sensor even if it does not drop off the slide for any reason. Both sensors are recorded by use of the *Marine Longtime Recorder (MLS)* which is manufactured by *SEND GmbH* and specially designed for longtime recordings of low frequency bands. Together with the broadband sensors the fourth channel record a Differential Pressure Gauge (DPG) as described by Cox et al (1984).

During cruise SO163 a prototype of a new instrument design was tested. This design, termed OBS2002, is characterized by a very shallow design, which should potentially decrease current induced noise. Also, the mechanical design is such that only a few pieces of hardware are needed, which potentially will reduce the price of manufactoring. In addition, the instrument can be disassembled rapidly and can be packed in a rather dense fashion, such that up to 50 instruments could be stored in a single container. A picture of the instrument is shown in Figure 5.3.7. All sensors and operational devices remain identical to those described above

**Marine Broadband Seismic Recorder (MBS)**

The so-called *Marine Broadband Seismic recorder (MBS;* Bialas and Flueh, 1999*)*, manufactured by *SEND GmbH*, was developed based upon experience with the DAT based recording unit Methusalem (Flueh and Bialas, 1996) over the last few years. This new recorder avoids a mechanically driven recording media, and the PCMCIA technology enables static flash memory cards to be used as unpowered storage media. Read/write errors due to failure in tape handling operations should not occur with this system. In addition, a data compression algorithm is implemented to increase data capacity. Redesign of the electronic layout enables a decreased power consumption (1.5 W) of about 25% compared to the *Methusalem* system. Depending on the sampling rate, data output could be in 16 to 18 bit signed data. Based on digital decimation filtering, the system was developed to serve a variety of seismic recording requirements. Therefore, the bandwidth reaches from 0.1 Hz for seismological observations to the 50 Hz range for refraction seismic experiments and up to 10 kHz for high resolution seismic surveys. The basic system is adapted to the required frequency range by setting up the appropriate analog front module. Alternatively, 1, 2, 3 or 4 analogue input channels may be processed. Operational handling of the recording unit is similar to the *Methusalem* system or by loading a file via command or automatically after power-on. The time base is based on a DTCXO with a 0.05 ppm accuracy over temperature. Setting and synchronizing the time as well as monitoring the drift is carried out automatically by synchronization signals (DCF77 format) from a GPS-based coded time signal generator. Clock synchronization and drift are checked after recovery and compared with the original GPS units. After software preamplification the signals are low-pass filtered using a 5-pole Bessel filter with a -3 dB corner frequency of 10 kHz. Then each channel is digitised using a sigma-delta A/D converter at a resolution of 22 bits producing 32-bit signed digital data. After delta modulation and Huffman coding the samples are saved on PCMCIA storage cards together with timing information. Up

## Tiltmeter

Research and surveying in risk areas such as the vicinity of volcanoes and earthquake-prone areas have been supported on land by tiltmeters for years ( e.g. Decker and Decker, 1981). Small-scale as well as integral, large-scale surveys are carried out - i.e. gauges with short (ca. 2 m) as well as long (several tens to hundreds of m) base lines are being used. These systems have been successfully deployed especially in areas with tunnels and mining. The combination of tiltmeters with seismic surveys yielded good results in the field of short-term forecasts of eruptions (Dzurisin et al., 1982). Tiltmeters for marine usage have been successfully used only recently (e.g. Dünnebier and Harris, 1996; Anderson et al., 1997). Many of the systems employed up to now have been developed and constructed in academia (Simamura and Kazanawa, 1988; Wyatt et al., 1984 and 1996; Anderson et al., 1997). Short baseline systems constituted the majority among these. They are less expensive to develop, their deployment is less complicated and they can be mounted onto a variety of different platforms.

As the electronics of the referenced marine tiltmeters are all in house developments that have not been designed to be used and operated by a wide community we decided to complete a new easy-to-use instrument for the SFB574 making use of existing components as far as possible. Based on the experiences with marine long baseline instruments published by Anderson et al. (1997) we favored a short baseline solution. Future operation should then result into a larger number of instruments distributed over the area of investigation to allow minimization of station effects by an overall integration of (parts of) the deployed systems. Restricting to short baseline enables the use of the GEOMAR OBS (Bialas and Flueh, 1999) as a system carrier further using the available periphery of support (e.g. release system, relocation tools, etc.). Internet recherché and personal discussion with other long term users of tiltmeters led to the decision of selecting the type 501 and 900-45 tiltmeters from Applied Geomechanics. The company had already been involved in marine tiltmeter developments with other customers. In general tilt values should be expected to be in the range of a few 2.5 urad to 200 urad (Wyatt et al, 1996; Tolstoy et al., 1998; a.o.) which could be easily resolved by the type 510 (+/- 1400 urad, < 10 nrad resolution). From earlier developments of a marine tiltmeter Applied Geomechanics could offer a gimbaled system based on freezing Jojoba oil. Repetitive leveling would not be possible with this solution and therefore we decided to use a motor driven leveling. The basic type 510 tiltmeter was developed for drill hole deployments and could therefore compensate for a small amount of tilt only. To adopt for sea floor applications and possible larger angles of tilt caused by the slope of the sea floor the leveling system was extended to +/- 30 degrees for the GEOMAR sensor. The type 900-45 clinometer can be operated over a range of +/- 50 degrees with a resolution of 0.02 degrees. It is used to give an overall impression about the large scale tilt variations throughout the deployment. As the complete system is designed to free fall to the seafloor a C-100 compass from KVH Industries is implemented within the tiltmeter housing to allow later orientation of the tilt axis. It is well known from earlier studies that such high precision instruments are sensitive against temperature changes which requires continuous recording of this value. For data recording the easiest solution was to modify two of the long time operated MLS type seismic data loggers (Bialas et al., 2002) from SEND. X- and Y-axis of the 510 tiltmeter and temperature are permanently recorded with 1 s sample interval while the 900-45 and the magnetic compass are read after each leveling operation.

## Seismic Sources
## 32 l BOLT Airgun

A Model 800 CT *BOLT* airguns was used during the cruise; a photo of the guns is shown in Figure 5.3.8. The gun has a volume of 32 liters (2000 $inch^3$), and generates a signal with a main frequency centered around 6 to 8 Hz and including higher harmonics. The gun was deployed and towed from the assistant winch and beam normally used for the piston corer recovery. Trigger cables and airhoses were deployed manually. The gun was suspended on two floats with an additional float attached to the supply lines to prevent contact between the gun and the towing wire. The gun weas towed 60 m behind the vessel and operated at 145 bar in 7 to 8 m depth. Due to good weather conditions the handling of the gun was smooth all the time.

During cruise SO162 the gun was used twice. The total operation time was about 10 hours, with more than 1500 shots being fired, either at a 20 s or a 15 s shot interval The ship's compressor system worked smoothly and caused no delays or interruptions.

**G-Gun-Cluster**

During this cruise two G-Gun clusters were available as a loan from Sodera, France. Each G-gun cluster comprises two identical guns mounted in a fixed frame. This assembly garantees an interaction between the bubbles, and thus increases peak to bubble (P/B) ratio compared to a single gun. One cluster consisted of G-Gun 520 cu. in. each, the other one G-Gun 380 cu. in.. The P/B ratio should be between 16 and 17 according to the manufactorers specifications, being slightly higher for the smaller gun.

The clusters were towed over the A-frame of Sonne using the anchor winches and worked without any problem. In Figure 5.3.9 one of the clusters is shown upon deployment.

The G-Guns can ans should be operated at a pressure of 3000 psi, unfortunately the Sonne compressor only provides a maximum pressure of 2000 psi.

**Prakla –Array**

In addition to the high and low frequency guns, a small airgun array was set up using the airgun slide at port aft of R/V Sonne. The array comprised of 7 Prakla VLA and VLF type guns, with volumes of 2.0 l, 1.2 l, 2 x 0.65 l, and 3 x 0.33l (Fig. 5.3.10). Parts of the array were provided on loan from the Institut für Geowissenschaften, Sektion Geophysik, Universität Kiel. Compared to trials undertaken during earlier cruises with R/V Sonne, some modifications in terms of single chamber volume, gun spacing and towing depth were done. As a consequence the frequency content of the array signal could be enhanced and the bubble period could be further suppressed. Single gun volumes and separations are shown on Fig. 5.3.11. Towing depth of the array was 2.5 m when three fenders were used as floatation buoys to carry the array. Shooting of the array was synchronized using a LongShot source controller with two FourShot power supplies. Two ports of the power supplies were reconfigured to operate the GI-gun, while the remaining 6 ports were used for the Prakla array. As a consequence, one of the 7 guns was always deployed as a spare. The source controler read the sensor signals submitted from each gun at shot release to synchronize the individual shot delays to the same aiming point with an accuracy of 1 ms. The array was operated at a pressure of 140 bar and a shot interval of 10 s. Despite problems with irregular sensor signals, all guns operated without major failures.

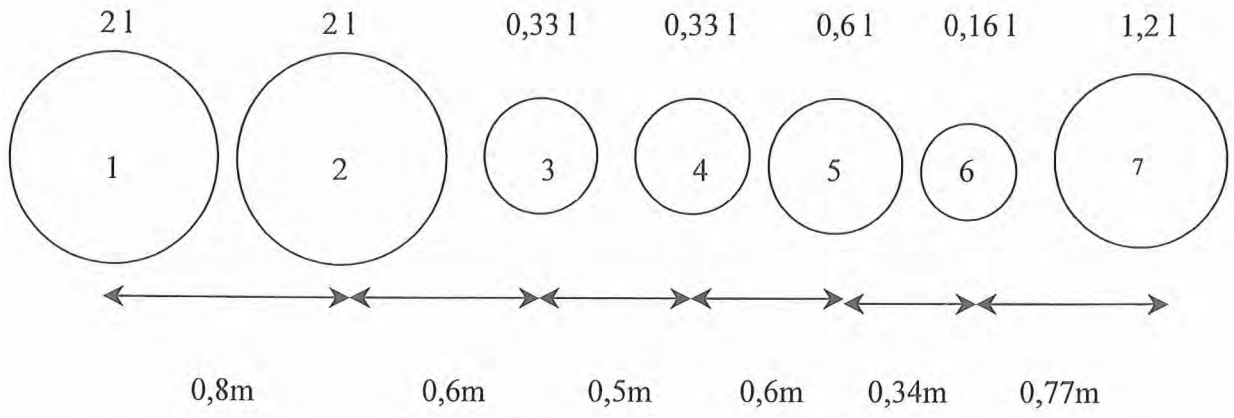


**Fig. 5.3.10:** Configuration for Prakla Type Airgun Array
Guns were towed at 2,5m depth

**External Trigger**

The trigger signal was supplied from the ships *Ashtech* GG24 GPS/Glonass receiver, and was available in the Geology Lab and the Seismic Lab. The receiver can provide a one millisecond long 5 V-TTL pulse at intervals between 0.2 and 999 s. The impulse should be stable to within the accuracy of the GPS Time, which is 70 nanoseconds. The impulse was delivered to the *Longshot* trigger box, which can handle different guns (G-gun, GI-Gun, Bolt abd Prakla guns). The shotbreaks, necessary for subsequent data processing and instrument location, were stored on a MBS recorder and displayed in real time to double check. For this process the same time basis was used that is used for the OBH (see chapter 4.4) and the trigger signal was converted into a 5 V TTL pulse of 250 ms length by a circuit provided from the ships technical support staff (WTD). Exact position calculation for the shot time should be done by later post-processing using shot time and UTC time values stored with DGPS coordinates in the ship's data base. As kwon from earlier cruises the coordinates stored within the data base were provided by the *Atlas ANP 2000* system, which does not copy the exact GPS time values but adds time stamps of its internal uncontrolled clock to the high precision coordinates of the DGPS system. Accuracy of the time values mainly depends on the operators skills by manually setting the ANP clock to GPS time. This is clearly a somewhat conservative method compared to the efforts of precise positioning. To enable the most accurate GPS related time stamps within the ANP system prior to each seismic survey the system operates were informed to reset the ANP.

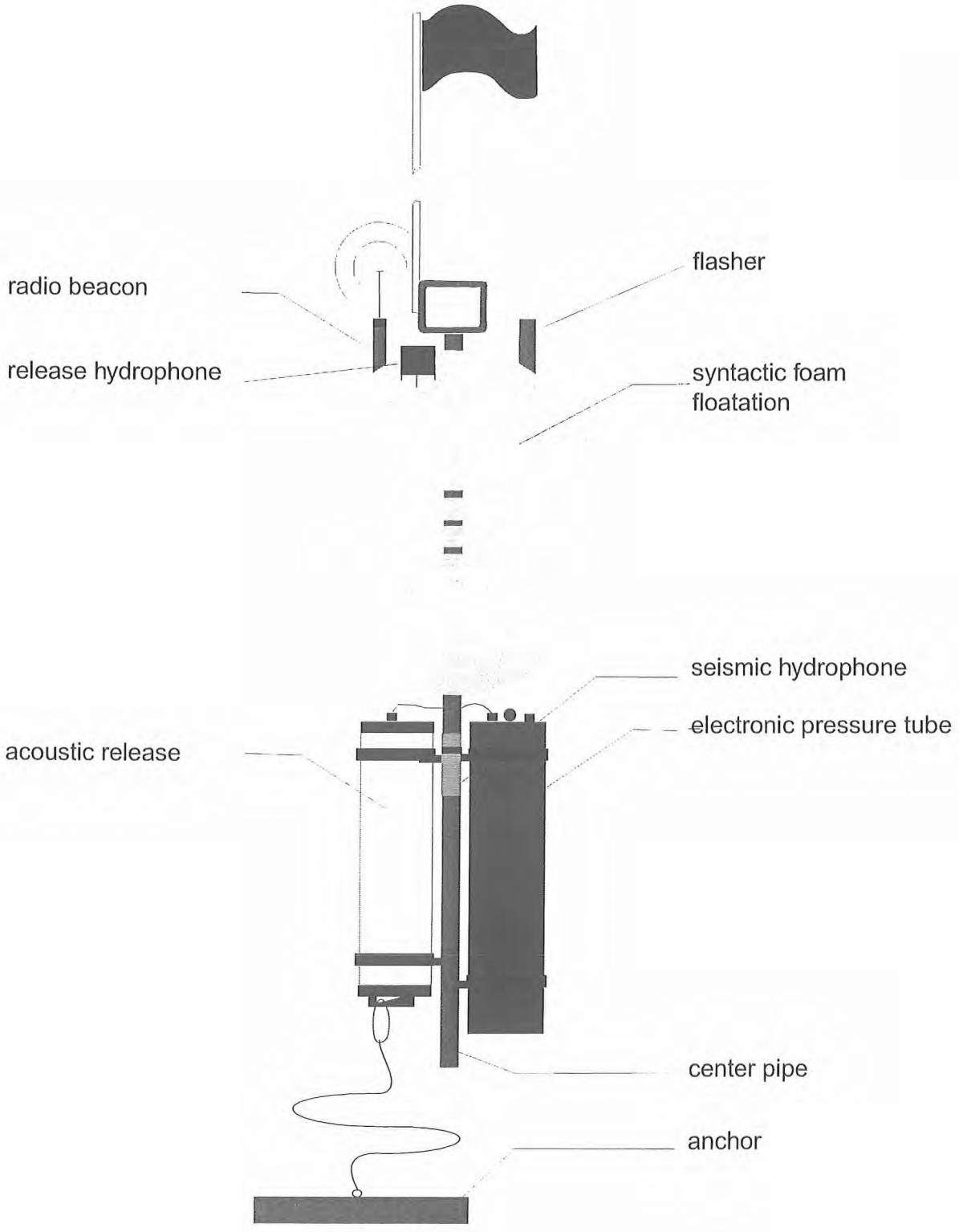


Figure 5.3.1: Principle design of the GEOMAR OBH (after Flueh and Bialas, 1996)

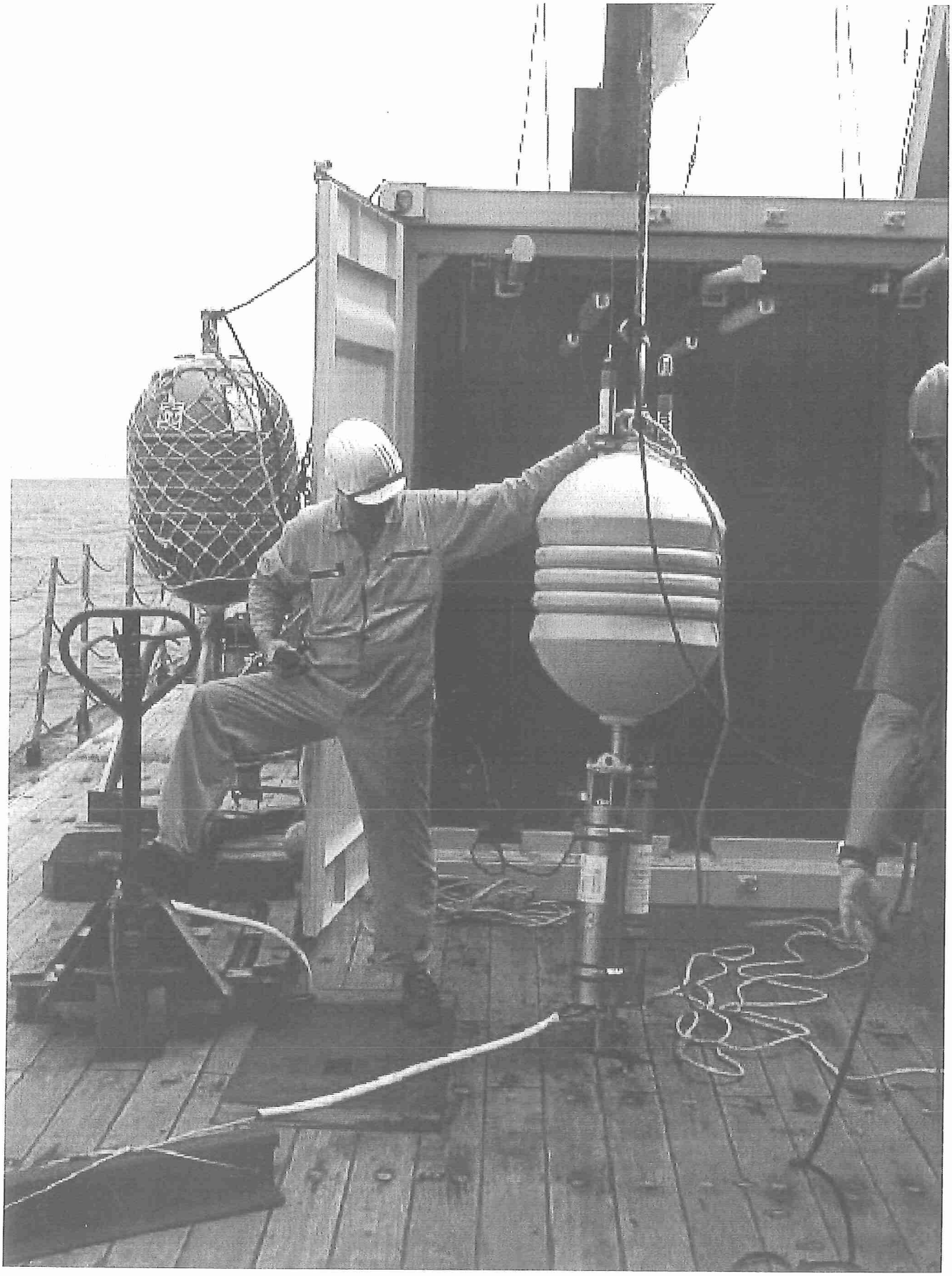

Figure 5.3.2 : The GEOMAR OBH ready for deployment
Background left: GEOMAR OBS
Background right: OBH container

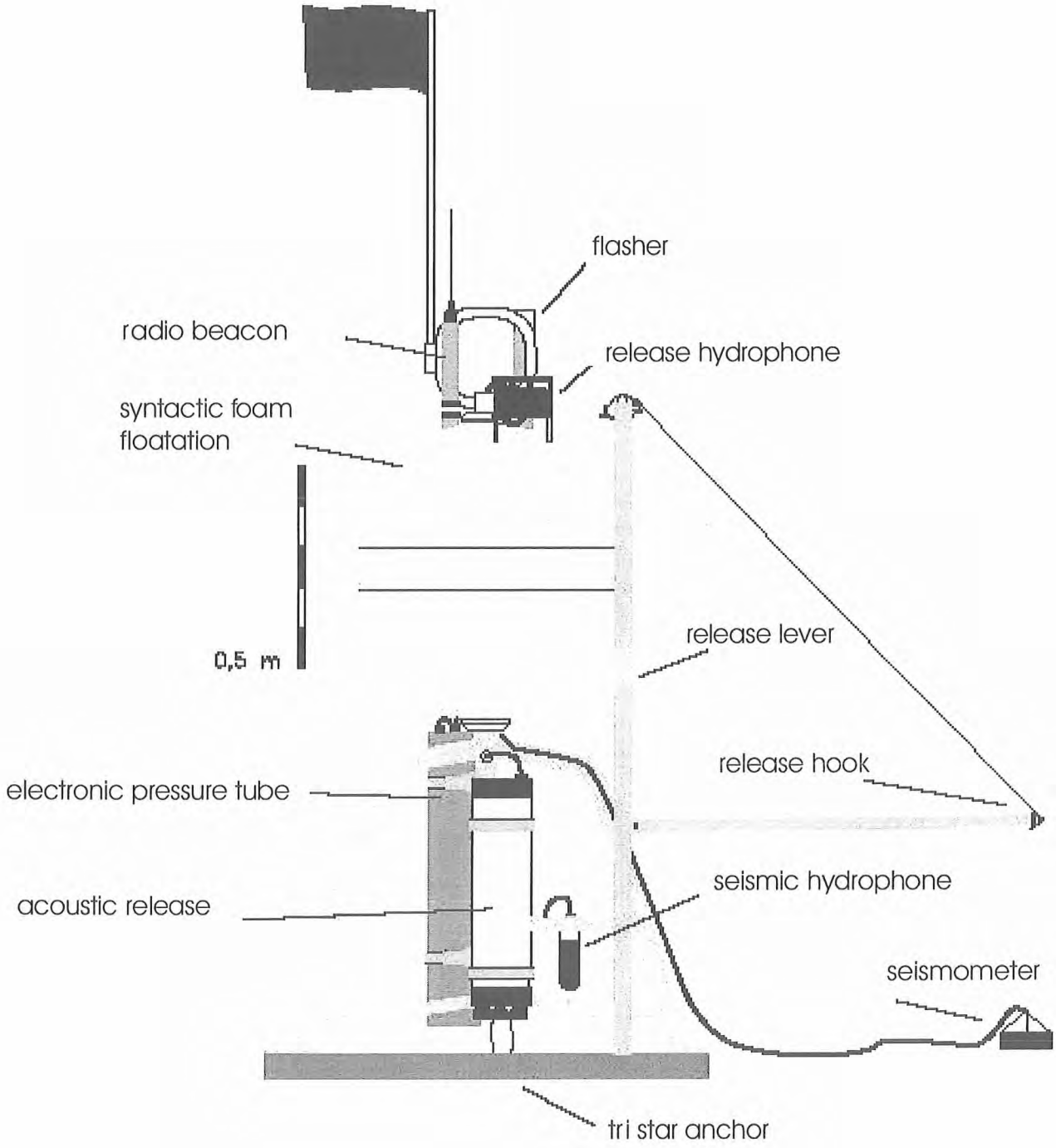


Figure 5.3.3: Pr inciple of the GEOMAR OBS (after Bialas and Flueh, 1999)

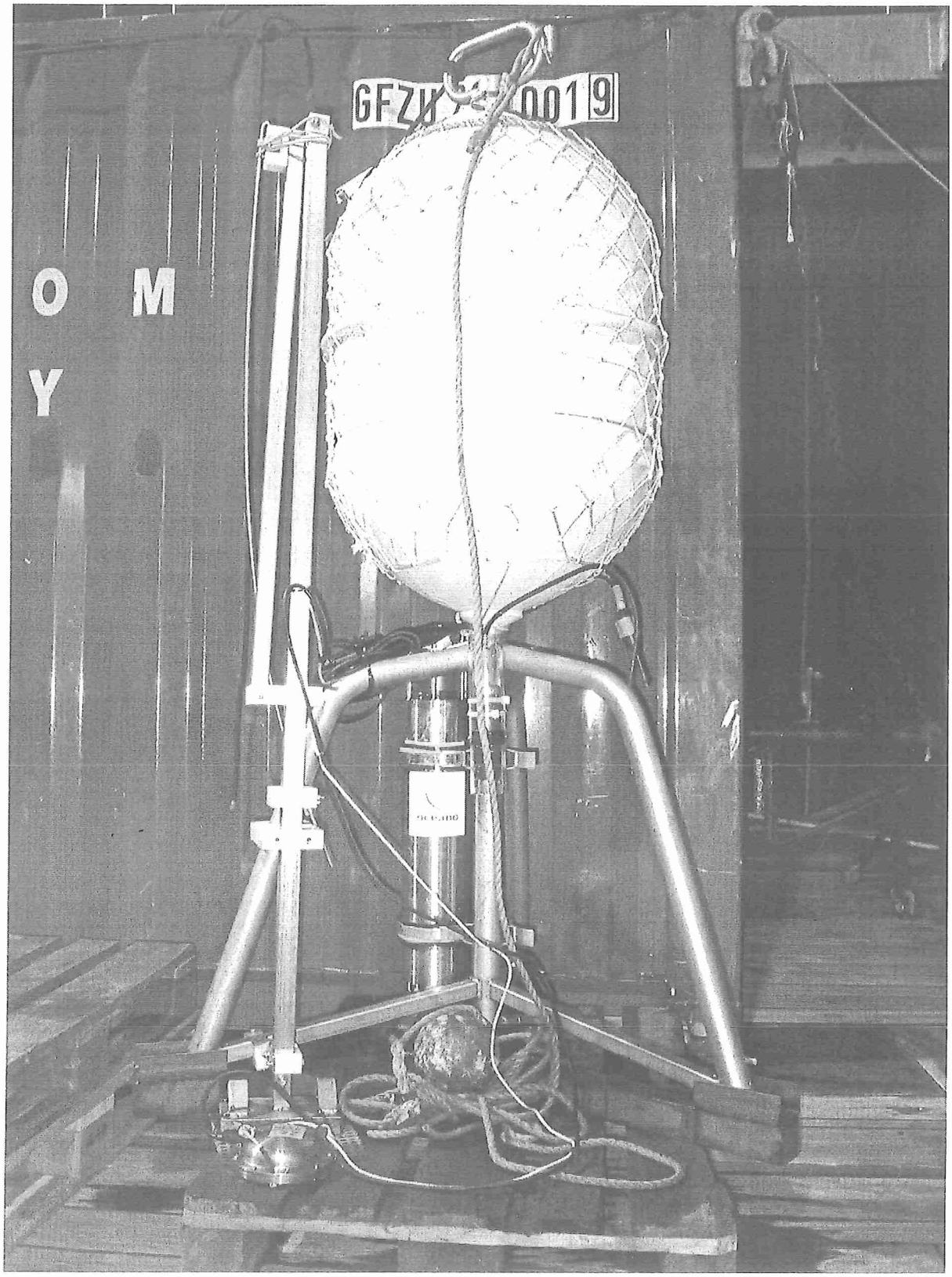


**Figure 5.3.4:** The GEOMAR OBS

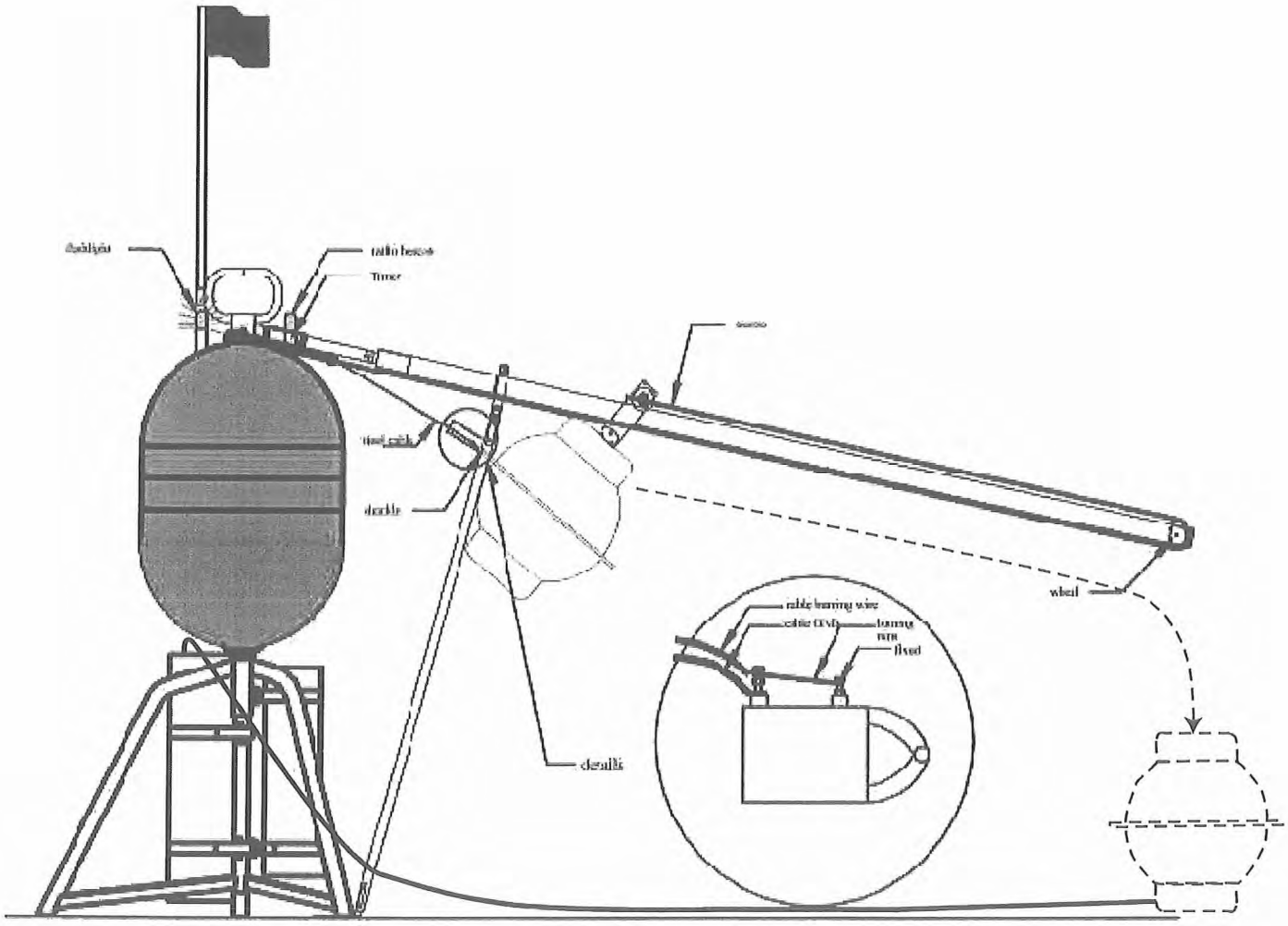


Figure 5.3.5: Scetch of GEOMAR broadband seismometer
dashed lines indicate deployment of the external broadband sensor at the seafloor

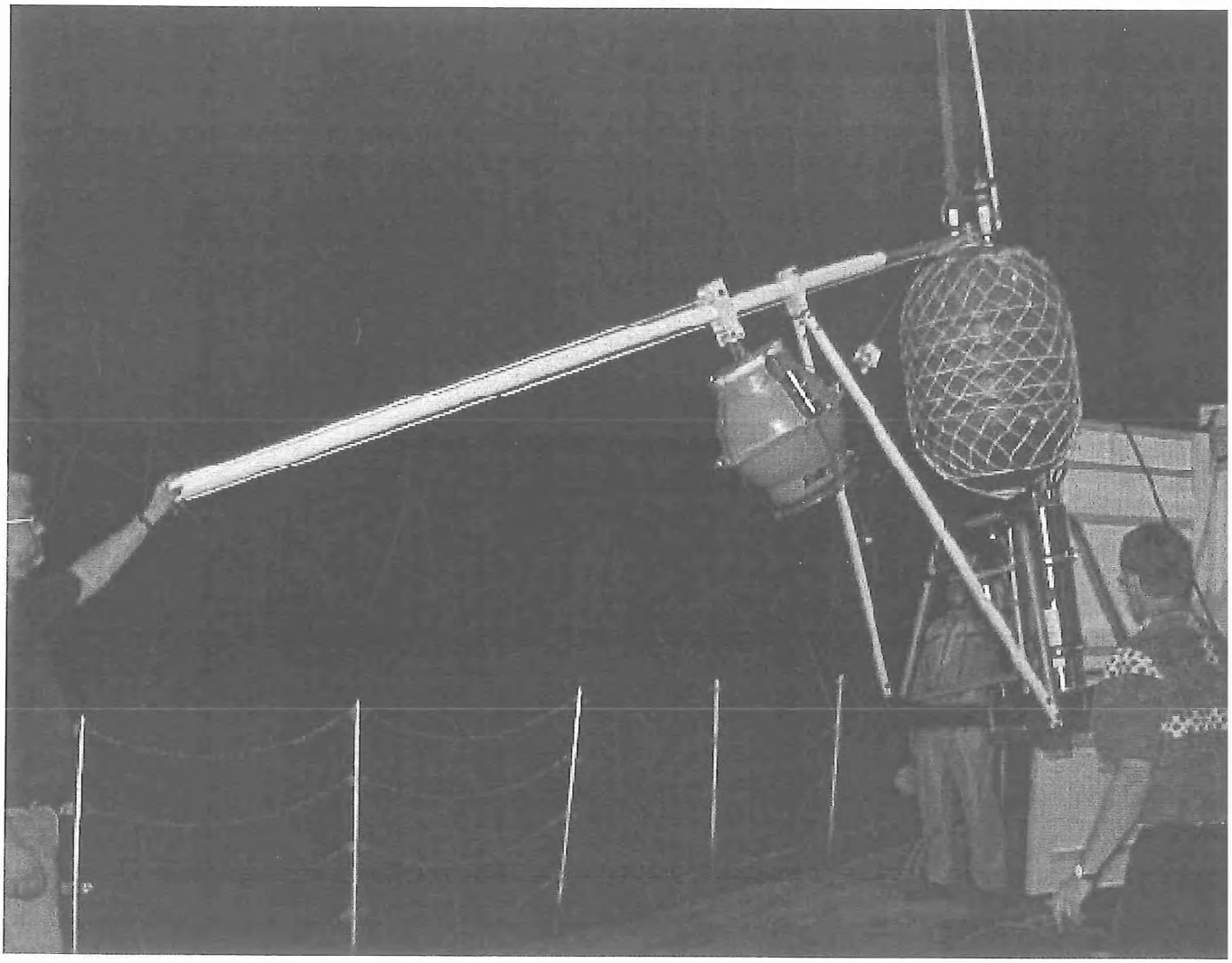

**Figure 5.3.6**: The GEOMAR broadband seismometer equipped withWebb seismometer at deployment

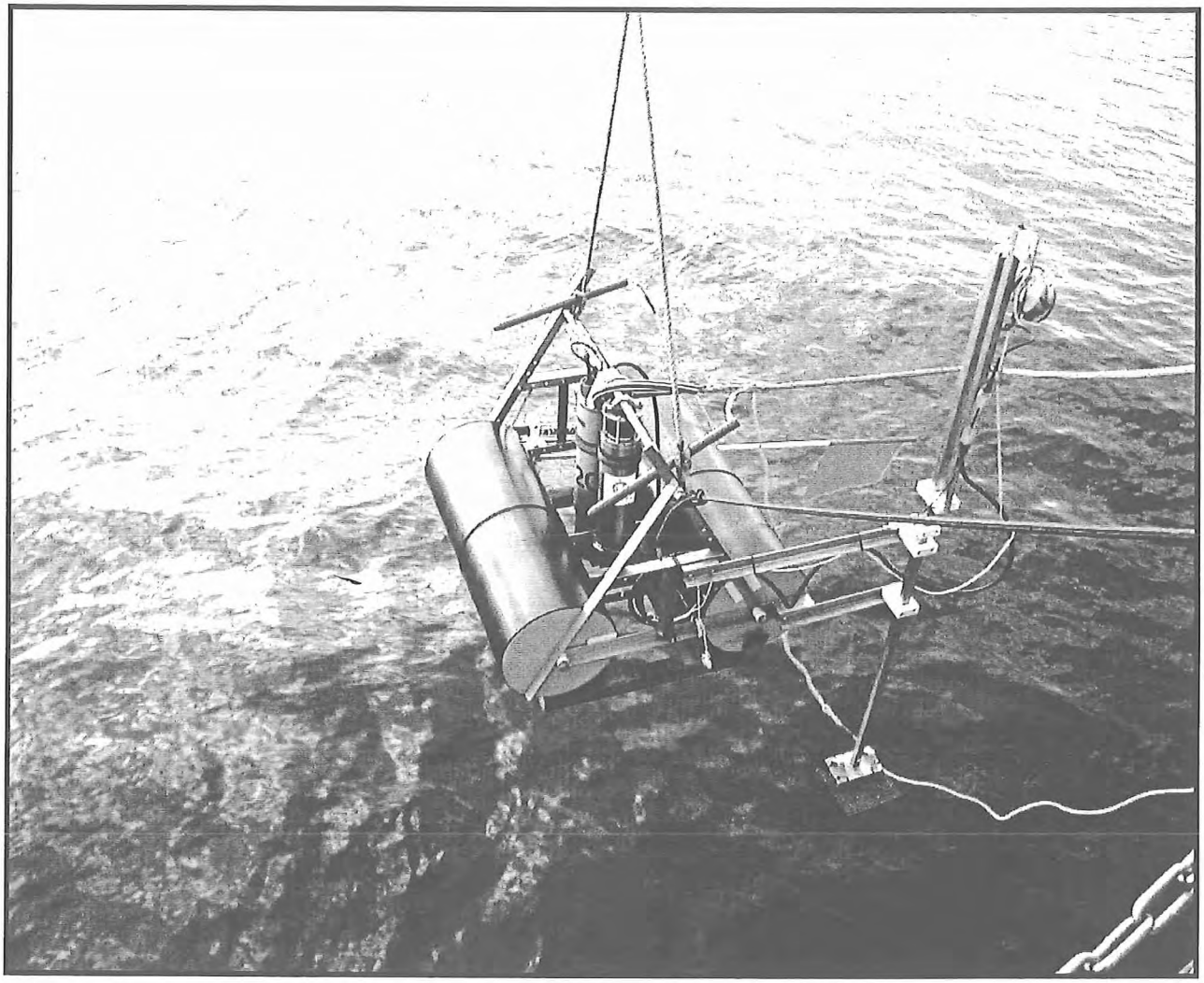

Figure 5.3.7: OBS 2002 upon deployment

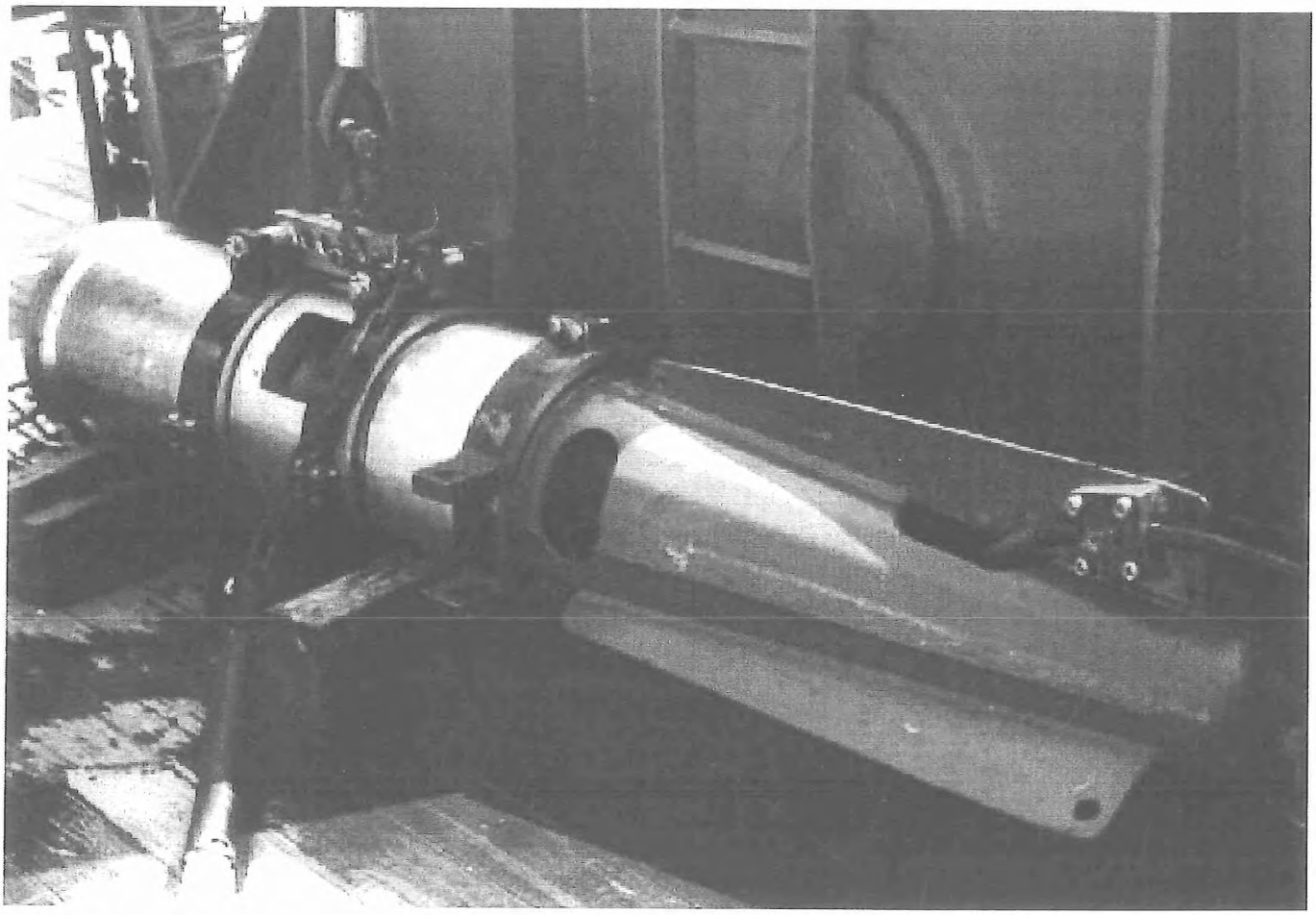

Figure 5.3.8: Photograph of a Bolt PAR 800 CT airgun with 32 l chamber

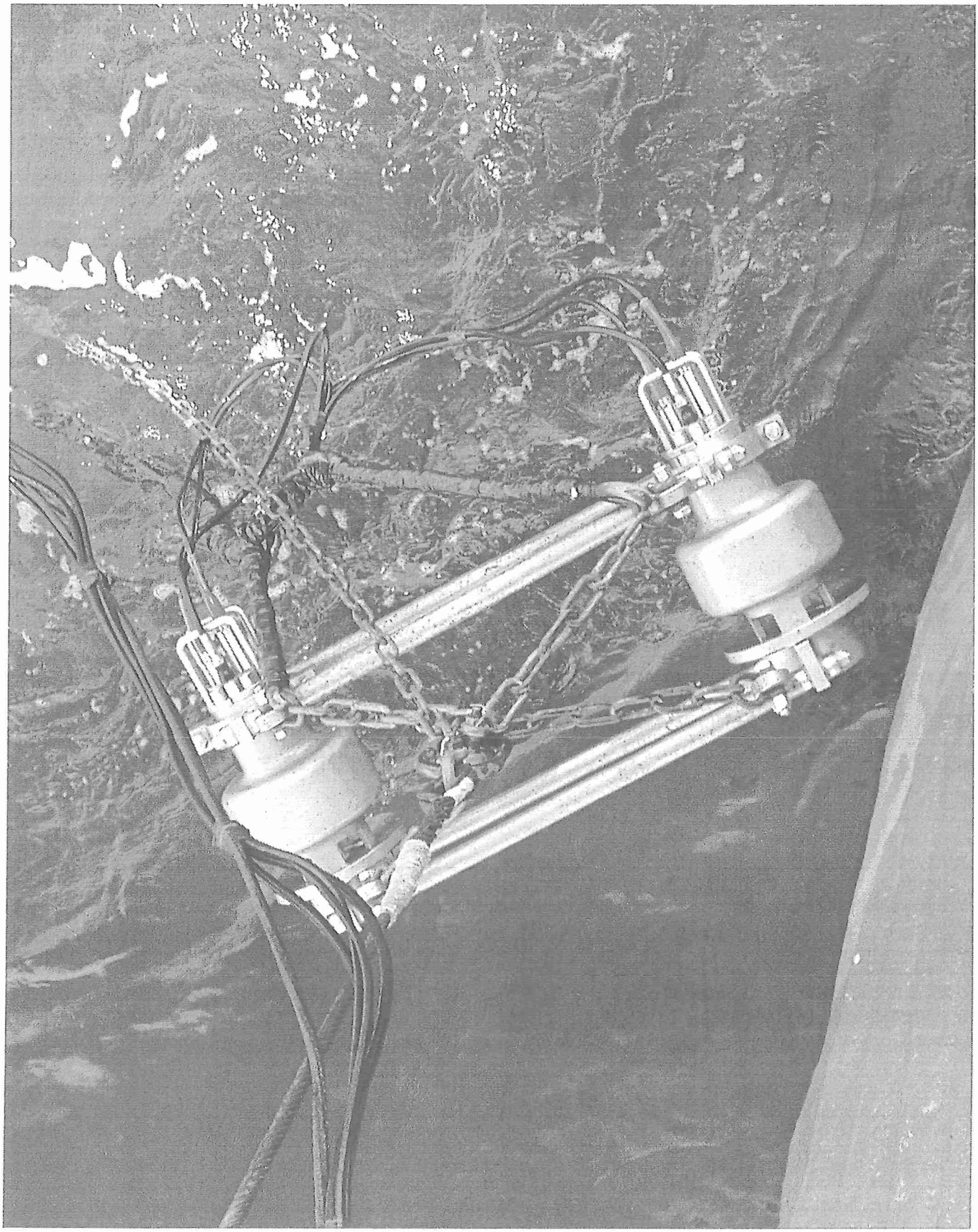

Figure 5.3.9: The G-Gun Cluster.

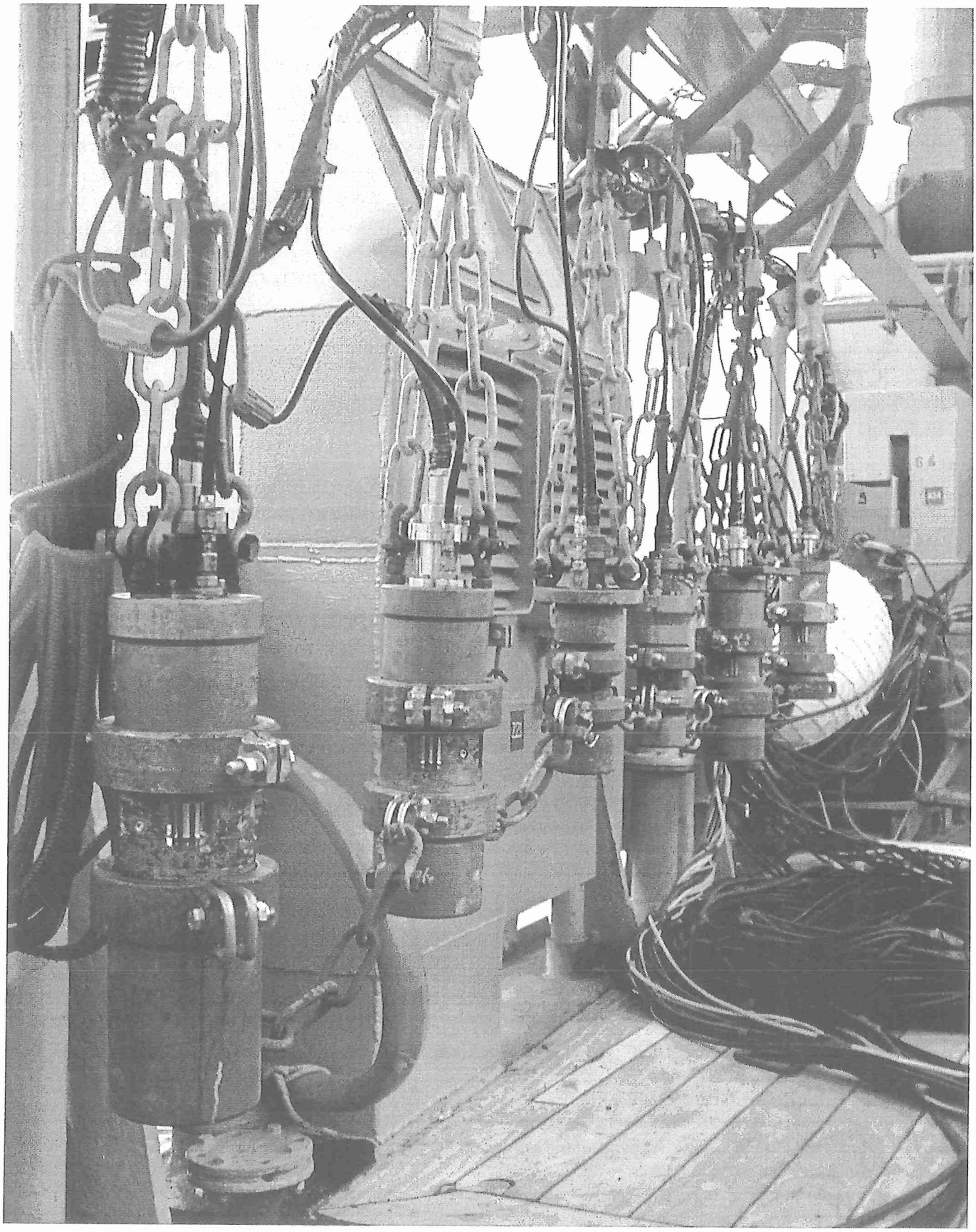

Figure 5.3.11: The Prakla Array, consisting of seven air guns of different volume.

## 5.4 The Magnetometer

(P. O. Thierer)

During cruise SO163-1 we used a GeoMetrics G801/3 Marine Proton Magnetometer. This unit uses a gasoline-filled sensor with 350 m marine cable and a control unit. During a polarisation cycle an electric current generates a strong magnetic field in the coil and forces the magnetic moments of the protons to be aligned for a short time parallel to the existing field. During the following measuring cycle, i.e. when the electric current is turned off, the previously excited field is removed and the protons "try" to realign themselves with the Earth's magnetic field. According to the moment preservation law, this happens by precession of the protons with a certain frequency, which is directly proportional to the intensity of the Earth's magnetic field. Basically, this frequency is measured as AC electric current created by magnetic induction in the coil, amplified, counted and transformed to the magnetic field intensity values (measuring unit: 10-9 Tesla = 1 nT), which are recorded.

In order to minimize the influence of the ship's hull, the sensor of the Magnetometer is towed 180 m behind the ship. This distance of the sensor from the ship was long enough, so that the magnetic influence of the vessel could not produce any disturbances in the recorded magnetic field, so we achieved a resolution of about 5 nT.

On board of RV SONNE, the winch was placed on the port back deck and the sensor was towed to the port side of the vessel. A boom leads the cable about 7 m to the side of the ship in order to prevent it from being tangled with the ship. After having some minor problems at the beginning, the system worked well throughout the trip.

The measured values of the total intensity magnetic field were displayed on a console and written as digital output coded in BCD values. The system was set to deliver one data value every 3 seconds via digital multiport interface to a PC, where a special software was used to store the data together with UTC-time in ASCII tables.

After data backup the files were transferred to a SUN workstation. GPS coordinates and time were taken from the ship's navigation system and assigned to each magnetic stamp on the basis of the recorded time. The magnetic and the navigation data were resampled to 10 s interval. After optional median filtering they were displayed using GMT plot routines (Wessel and Smith, 1995).

## 5.5 USBL Underwater positioning

(I. Klaucke, C. Huguen)

During cruise SO163/1 the ship was equipped with a POSIDONIA deployable acoustic array for underwater navigation from OCEANO Technologies (figure 5.5.1). This system is based on a bi-directional exchange of submarine acoustic signals between one or several acoustic transponders and the acoustic array consisting of 1 transmission transducer and two pairs of hydrophones. The acoustic transponders are interrogated by an acoustic signal and will send a 25ms M-FSK (multi-frequency shift keying) reply. The 25ms M-FSK signal is a succession of ten monochromatic pulses (each 2.5ms long) of ten different frequencies ranging from 14.5 to 17.5 kHz. The order of frequencies during the pulse is determined by the M-FSK code. For best detection of the signal with Posidonia, codes 22 or 23 should

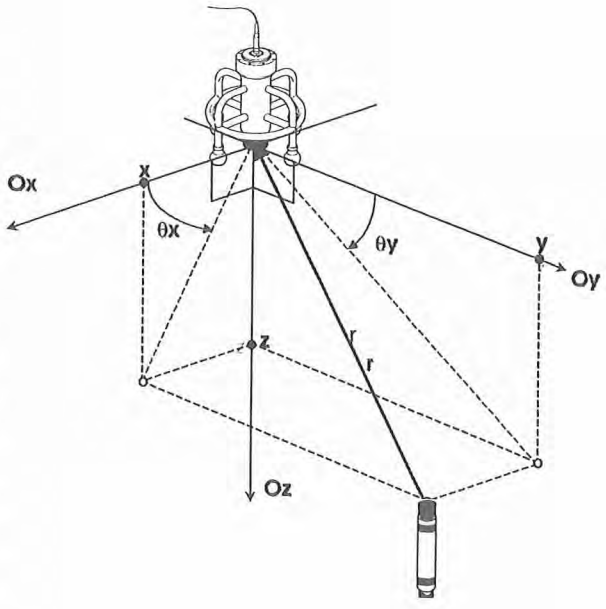


*Figure 5.5.1 USBL Positioning principle*

be selected. The four reception hydrophones of the array receive this signal that is then transmitted to the processing unit, which measure the phases of the signals and the time between interrogation and reply in order to deduce the relative position of the transponder and calculate its geographical position. The Posidonia positioning system runs in two different modes: the free mode and the towed-fish mode. In the free mode all four hydrophones are used to calculate the position of the transponder. In the towed-fish mode only the hydrophones aligned with the towed vehicle are used together with depth information provided by a built-in depth sensor. The free mode should be used when the transponder is located in a cone of 60 degrees underneath the ship, but this mode will work fine up to an angle of 120 degrees. Beyond this angle the towed-fish mode should be used.

The Posidonia array is deployed in the moon pool onboard FS Sonne. Although tightly fitted when locked, the antenna will not be in exactly the same position after each deployment. Following each deployment of the Posidonia antenna a calibration run for the Posidonia system is necessary. For this calibration a transponder of the ET/RT 8x1 series has to be deployed on the seafloor in 1000-2000 m of water depth (Fig. 5.5.2). Following deployment of the transducer, the ship will run a figure of eight above the transducer location in order to allow for communication between the antenna and the transducer from all sides of the ship and from all directions. A minimum total number of 400 data points should be registered during this calibration run. A special programme of the Posidonia system POSICAL will then allow to eliminate obviously erroneous data points and to calculate values for the bias on yaw, pitch and roll of the vessel.

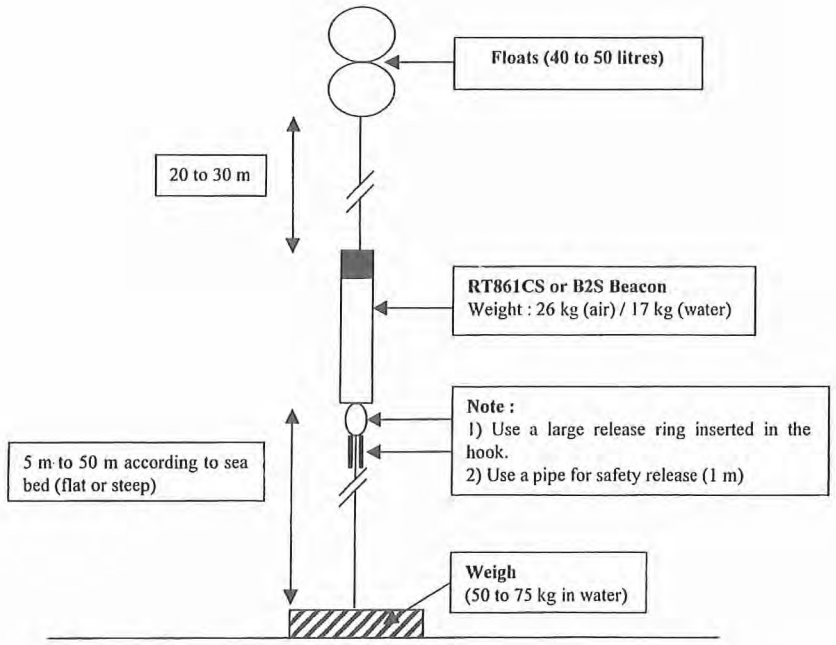


*Figure 5.5.2 Mooring used for calibration*

## 5.6 TOBI (Towed Ocean Bottom Instrument)

(D. Masson, I. Rouse, D. Matthew, V. Huehnerbach)

### System Description

TOBI - Towed Ocean Bottom Instrument - is Southampton Oceanography Centre's deep towed vehicle. It is capable of operating in 6000 m of water (Fig. 5.6.1). The maximum water depth encountered during the TOBI surveys during this cruise was around 3000 m.

Although TOBI is primarily a sidescan sonar vehicle a number of other instruments are fitted to make use of the stable platform TOBI provides. For this cruise the instrument complement was:

1. 30 kHz sidescan sonar (Built by IOSDL)
2. 6-10 kHz chirp profiler sonar (Built by IOSDL/SOC)
3. Three-axis fluxgate magnetometer. (Ultra Electronics Magnetics Division MB5L)
4. CTD (Falmouth Scientific Instruments Micro-CTD)
5. Swath bathymetry capability
6. Light backscattering sensor (WET Labs Inc LBSS)
7. Pitch & Roll sensor (G + G Technics ag SSY0091)

A full specification of the TOBI instrumentation is given in **table 5.6.1**.

The TOBI system uses a two-bodied tow system to provide a highly stable platform for the on-board sonars (Fig. 5.6.2). The vehicle weighs two and a half tonnes in air but is made neutrally buoyant in water by using syntactic foam blocks. A neutrally buoyant umbilical connects the vehicle to the 600 kg depressor weight. This in turn is connected to the main armoured coaxial tow cable. All signals and power pass through this single conductor.

The deck electronic systems and the logging and monitoring systems were set up along the port side of the aft geophysical laboratory, giving both watchkeepers and scientists a clear view of the incoming data.

### TOBI Deployment

The Sonne is equipped with a stern mounted hydraulic 'A' frame but it is too narrow to allow normal athwartships launch and recovery so the vehicle had to be launched in a fore-aft orientation. The main sheave was used for deploying and recovering both the TOBI vehicle and the depressor weight as well as towing during the survey. Launch and umbilical winches were supplied by SOC and mounted on the afterdeck using a custom designed bed plate originally built for Sonne 144 leg 2. The winches were run from a self-contained electrically-powered hydraulic power pack.

### TOBI Watchkeeping

TOBI watchkeeping was split into three, four-hour watches repeating every 12 hours. Watchkeepers kept the TOBI vehicle flying at a height of ideally 350 to 400 m above the seabed by varying wire out and/or ship speed. Ship speed was usually kept at 2.5 kt over the ground with fine adjustments if the TOBI vehicle depth carried out by using the winch. As well as flying the vehicle and monitoring the instruments, watchkeepers also kept track of disk changes and course alterations.

The bathymetry charts of the work area were found to be very accurate which helped immensely when flying the vehicle. The ship's EM120 multibeam system provided a real time display of bathymetry.

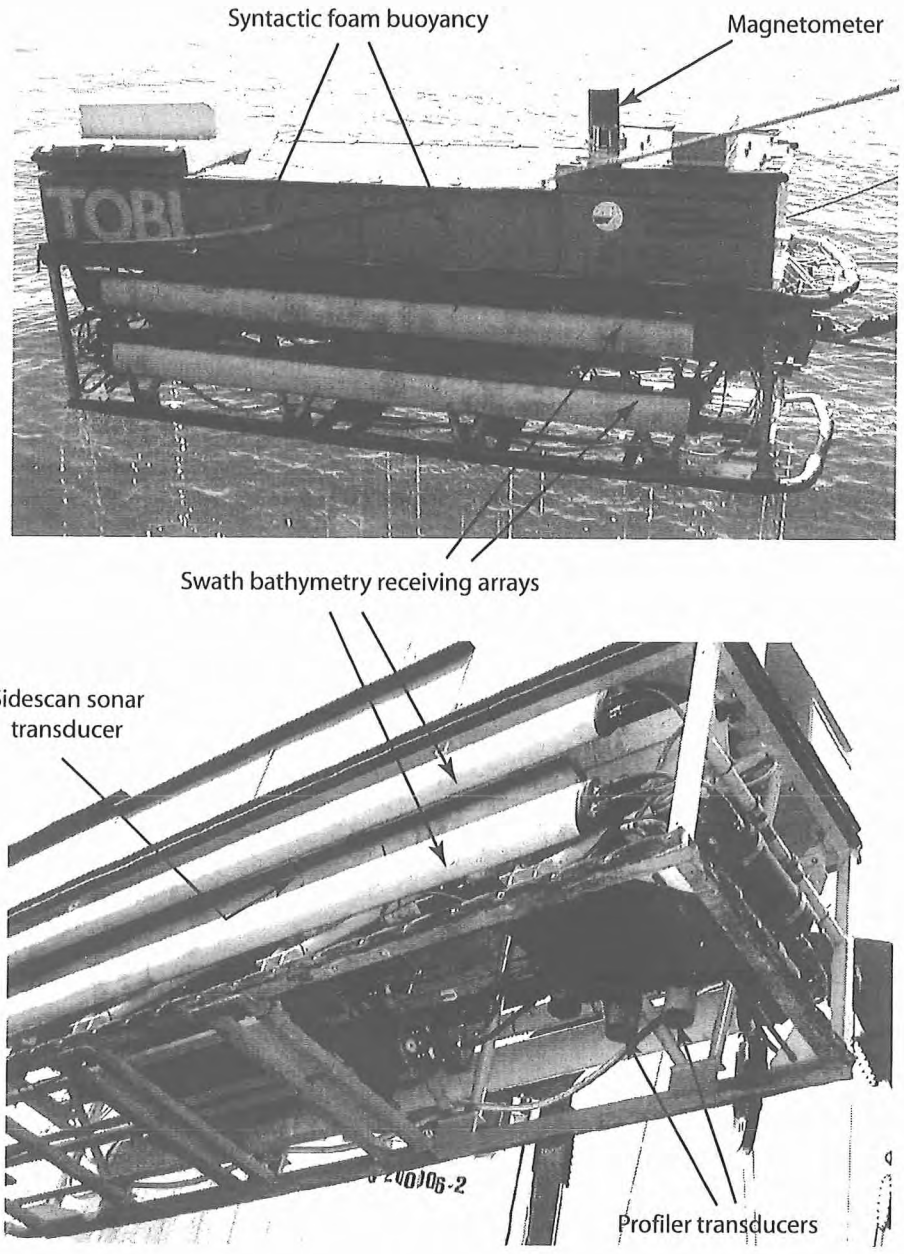


*Figure 5.6.1 (top)*

*Figure 5.6.2 (bottom)*

### 5.6.1. TOBI: Technical Specification

| | |
|---|---|
| **Mechanical** | |
| Towing method | Two bodied tow system using neutrally buoyant vehicle and 600kg depressor weight. |
| Size | 4.5 m long, 1.5 m wide, 1.1 m high |
| Weight | 2500 kg in air. |
| Tow cable | Up to 10 km armoured coax. |
| Umbilical | 200 m long x 50 mm diameter, slightly buoyant. |
| Tow speed | 1.5 to 3 knots (dependent on tow length). |
| **Sonar Systems** | |
| **Sidescan Sonar** | |
| Frequency | 30.37 kHz (starboard) 32.15 kHz (port). |
| Pulse Length | 2.8 ms. |
| Ouput Power | 600 W each side. |
| Range | 3000 m each side. |
| Beam Pattern | 0.8 x 45 degree fan. |
| **Bathymetry Sonar** | |
| Transmitter | Uses sidescan sonar. |
| Receiver | 6 hydrophone arrays in 2 housings for each side. |
| Detection | Single and multi-phase. |
| Range | Up to 3000 m each side. |
| **Profiler Sonar** | |
| Frequency | 6 to 10 kHz Chirp. |
| Pulse Length | 26 ms. |
| Output Power | 1000 W |
| Range | >50 ms penetration over soft sediment. |
| Resolution | 0.25 ms |
| Beam Pattern | 25 degree cone. |
| **STANDARD INSTRUMENTATION** | |
| **Magnetometer** | Ultra Electronics Magnetics Division MB5L. |
| Range | +/- 100,000 nT on each axis. |
| Resolution | 0.2 nT. |
| Noise | +/- 0.4 nT. |
| **CTD** | Falmouth Scientific Instruments, Micro CTD. |
| Conductivity | |
| Range | 0 to 65 mmho/cm. |
| Resolution | 0.0002 mmho/cm. |
| Accuracy | +/- 0.005 mmho/cm. |
| Temperature | |
| Range | -2 to 32° C. |
| Resolution | 0.0001° C. |
| Accuracy | +/- 0.005° C. |
| Depth | |
| Range | 0 to 7000 dbar. |
| Resolution | 0.02 dbar. |
| Accuracy | +/-0.12% F.S. |

| | |
|---|---|
| **Extra Depth Sensor** | AML Pressure Smart Sensor |
| Range | 0 to 6000 dbar. |
| Resolution | 0.1 dbar. |
| Accuracy | +/-0.05% F.S. |
| | |
| **Light backscattering sensor** | WET Labs Inc LBSS |
| Source | 880 nm LEDS source and solar blind light detector |
| Range | 0-10 $\mu g\ l^{-1}$ suspended particle concentration detection range |
| Resolution | 0.01% FSD at 1 $\mu gl^{-1}$ resolution |
| | |
| **Heading** | S.G. Brown SGB 1000U gyrocompass. |
| Resolution | 0.1 degrees. |
| Accuracy | Better than 1°, latitude < 70°. |
| Pitch/Roll | Dual Axis Electrolytic Inclinometer. |
| Range | +/- 20 degrees. |
| Resolution | 0.2 degrees. |
| | |
| **Altitude** | Taken from profiler sonar. |
| Range | 1000 m. |
| Resolution | 1 m. |

### 5.6.2 TOBI Image Processing

Onboard processing equipment during this cruise consisted of a UNIX workstation (SUN ULTRA 10) with 36 Gb of disk space. Final maps containing side-scan sonar imagery were plotted on an A0 plotter. All data were also archived using CD-ROM (via a networked PC).

The ships navigation was recorded online on a UNIX server on the ship. The data was transferred on a daily basis and then tested for time continuity and abnormal speed values. Good navigation data is essential for processing, because the vehicle position is calculated from it. The winch data (wireout) were also recorded online and stored with the sidescan raw data. Errors in wireout values were corrected manually. The TOBI imagery was downloaded from the CD-ROM using a subsample and average factor of 8. This gives the pixel resolution of 6 m and a signal-to-noise ratio improvement by a factor of nearly three.

Each survey area was divided into smaller map blocks to facilitate processing. The approximate size of the blocks was 0.25° by 0.25°. As each area was completed the imagery was processed using the PRISM (v3.1) and ERDAS Imagine (v8.3) software suites to produce geographically registered imagery which can then be composed onto a series of mapsheets.

The processing of TOBI imagery has two main phases: Pre-processing and Mosaicing. The pre-processing stage is the correcting of the side-scan sonar characteristics, removal of sonar specific artefacts and geographical registration of each individual ping. This stage is solely composed of PRISM programs and runs from a graphical user interface.

For the pre-processing stage, the PRISM software uses a modular approach to 'correct' the imagery which is predefined by the user in a 'commands.cfg' file. For this data it was defined as:

```
suppress_tobi -i %1 -o %0
tobtvg -i %1 -o %0 -a
mrgnav_inertia -i %1 -o %0 -t -u 260 -n navfile.veh_nav
tobtvg -i %1 -o %0 -h -l 50
```

```
tobslr -i %1 -o %0 -r res , res
edge16 -i %1 -o %0 -m
drpout -i %1 -o %0 -u -f -p -k 201
drpout -i %1 -o %0 -u -f -p -k 51
shade_tobi -i %1 -o %0 -tl,4095
```

To explain this in sonar terms (in order):

- `suppress_tobi -i %1 -o %0`

Removal of any surface reflection (i.e. from TOBI to the sea surface and back) - only a problem in water depths <3000 m, where a bright stripe or line is seen semi-parallel to the ship's track. Removal is only done when the imagery is unambiguous, where the line is true artefact and not an actual seafloor feature. The result can sometimes be seen on the final imagery as a faint dark line.

- `tobtvg -i %1 -o %0 -a`

Smoothing of the altitude of the vehicle above the seafloor. The altimeter sometimes cannot locate the seafloor, possibly due to very soft sediment reducing the strength of the profiler signal. Smoothing is done by a median filter of the given values, comparing this with the first return seen on the port and starboard sides, and applying a maximum threshold for altitude change if first return and altitude value differ. Generally first return values are used as that value will be used in the slant-range correction.

- `mrgnav_inertia -i %1 -o %0 -t -u 260 -n navfile.veh_nav`

Merging of ship navigation and cable data with the imagery and calculation of the TOBI position using an inertial navigation algorithm. The 'navfile.veh_nav' file contains ship position and cable values and an umbilical length of 200 m is assumed (default) plus an additional 60 m for the distance between the GPS receiver and the point where the cable enters the water. The recorded cable values in the TOBI data are used. Various defaults are assumed: the cable is assumed to be straight, the cable value is assumed to be accurate, and zero cable is set when the depressor enters the water.

- `tobtvg -i %1 -o %0 -h -l 50`

Replaces the TOBI compass heading with the track heading calculated from the navigation data. A smoothing filter is applied. The heading values are used in the geographic registration process to angle each ping relative to the TOBI position.

- `tobslr -i %1 -o %0 -r res , res`

Slant-range correction assuming a flat bottom. This is a simple Pythagoras calculation assuming that the seafloor is horizontal across track and sound velocity is 1500 $ms^{-1}$. Each pixel is 8 ms and generally equates to 6 m resolution; any pixel gaps on the output file are filled by pixel replication.

- `edge16 -i %1 -o %0 -m`

Median filter to remove any high or bright speckle noise. A threshold is defined for the maximum deviation for adjoining pixels over a small area above which the pixel is replaced by a median value.

- `drpout -i %1 -o %0 -u -f -p -k 201`

Dropout removal. When the vehicle yaws excessively, it is possible for the 'transmit' and 'receive' phase of each ping to be angled apart. If this exceeds the beam sensitivity value (0.8°) little or no signal is received, creating a dark line on the imagery. The program detects the dropout lines and interpolates new pixel values. If more than 7 dropouts are present concurrently (time = 28 s) no interpolation is done.

- `drpout -i %1 -o %0 -u -f -p -k 51`

More dropout removal, but for smaller, partial line dropouts. If more than 7 partial dropouts are present concurrently (28 s) no interpolation is done.

- `shade_tobi -i %1 -o %0 -tl,4095`

Across-track equalisation of illumination on an equal range basis. This assumes that the backscatter from a particular range should average a given amount for each piece of data. The near-range pixels and far-range pixels are generally darker than mid-range pixels. This is due to the transducer's beam pattern and differences in seafloor backscatter response in terms of angle of incidence. This procedure typically amplifies the near and far-range pixels by about 1.5 and reduces the mid-range pixels by 0.8.

Once this has been done for a piece of data the individual pings are placed on a geographic map. To emulate beamspreading the pixels are smeared over a small angle (0.8°) if no other data is present in the area of those pixels. As survey tracks are designed to overlap the imagery at far range, any overlapping data pieces are placed on separate layers of the same map. This allows user intervention to define the join where one piece touches the other. If small pixel gaps are visible between the geographically mosaiced pings, these are filled with an interpolated value plus a random amount of noise (but having the same variance as the surrounding data pixels).

The second phase (mosaicing) allows the user to view all the 'layers' of data for an area. The software used is a commercial package named ERDAS Imagine (v8.3). Within this software the different layers can be displayed in different colours to distinguish the layers with data that overlaps. In order to merge the different layers and their data together polygons (Areas of Interest -or AOI) are drawn by the user to define the join lines between layers and then applied to create a single layer final image map. This procedure can also be used to remove shadow zones and areas of no data. The program that merges all data within selected AOIs into the final single layer image is called 'addstencil'. Several of these final images can then be mosaiced together into an overall image from which maps can be created in different projections and spheroids, including scales, co-ordinates and text. Also annotation such as ship track, vehicle track and dates and times can be added to the map. The map can than be plotted on the A0 plotter and/or converted into other format e.g. TIFF, JPEG, generic postscript etc. to be used for further analysis on PC, Macintosh or UNIX workstations.

## 5.7 DTS-1 deep-towed sidescan sonar

(I. Klaucke, C. Huguen, T. Schott, W. Weinrebe)

The GEOMAR DTS-1 deep-tow sidescan sonar (Fig. 5.7.1) was used during cruise SO163/1 in order to provide detailed acoustic imagery of the seafloor of a number of target selected on the basis of TOBI mid-range sidescan sonar data. Sidescan sonar mapping is a well established technique and a thorough summary of its theory and principles would be too long for this report. For more detailed information about sidescan sonar principles and data processing, please refer to Blondel and Murton (1998). The instrument used here allows imaging the backscatter intensity of the seafloor at high resolution due to 75 and 410 kHz sidescan transducers. This surface information can be integrated with very high-resolution subbottom information of the uppermost sedimentary layer, therefore allowing volume estimates of sedimentary units at the seafloor. During cruise SO163/1 a number of targets including zones of active mud volcanism, faulting, fluid venting and mass wasting have been investigated in detail.

### 5.7.1 Technical description of the instrument

#### 5.7.1.1 Underwater set-up

The DTS-1 sidescan sonar (Fig. 5.7.1) is a EdgeTech Full-Spectrum (FS-DW) dual-frequency, chirp sidescan sonar working with 75 and 410 kHz centre frequencies. The 410 kHz sidescan sonar emits a pulse of 40 kHz bandwidth and 2.4 ms duration (giving a range resolution of 1.8 cm) and the 75 kHz sidescan sonar provides a choice between two pulses of 7.5 and 2 kHz bandwidth and 14 and 50 ms pulse length, respectively. They provide a maximum resolution of 10 cm. In addition to the sidescan sonar sensors, the DTS-1 contains a 2-16 kHz , chirp subbottom penetrator providing a choice of three different pulses of 20 ms pulse length each: a 2-10 kHz pulse, a 2-12 kHz pulse and a 2-15 kHz pulse giving nominal vertical resolution between 6 and 10 cm. The sidescan sonars and the subbottom penetrator can be run with different trigger modes: internal, external, coupled and gated triggers. Coupled and gated trigger modes also allow to specify trigger delays. The sonar electronics provide four serial ports (RS232) in order to attach up to four additional sensors. One of these ports is used for a Honeywell attitude sensor providing information on heading, roll and pitch. Finally, there is the possibility of recording data directly in the underwater unit through a mass-storage option with a total storage capacity of 2 x 30 Gbyte.

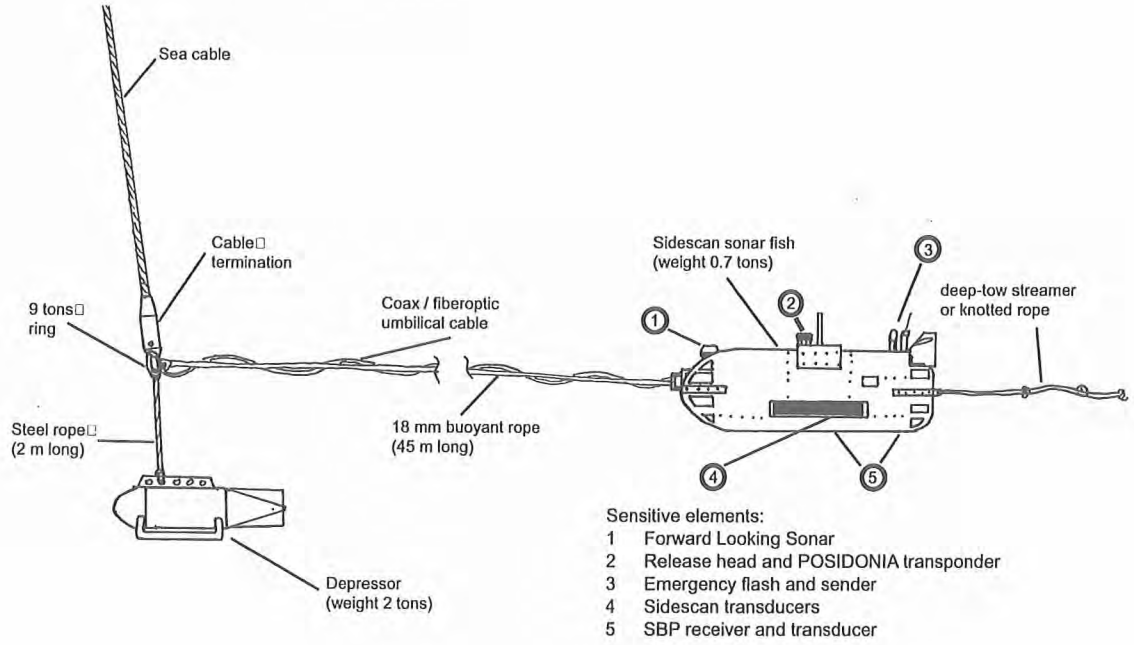


*Figure 5.7.1 The DTS-1 towing configuration*

The sonar electronic is housed in a titanium pressure vessel mounted on a towfish of 2.8m x 0.8m x 0.9m in dimension. The towfish houses a second titanium pressure vessel containing the wet-end of the SEND DSC-Link telemetry system and the bottom PC of the seismic streamer data acquisition system (see also section on deep-tow streamer). In addition, a Posidonia capable OCEANO releaser with separate receiver head and a NOVATECH emergency flash and sender are included in the towfish. Additional syntactic foam has also been placed in the front of the towfish in order to improve the fish's towing behaviour. For the same reason, the towfish has been fitted with a deflector at the rear . This deflector has five positions from 0 to –5 and is designed to reduce the pitch of the towfish.
The towfish is connected to the sea cable via the depressor (2 tons weight) through a 40 m long umbilical cable. The umbilical cable is tied to a buoyant rope that takes up the actual towing forces. An additional rope has been taped to the buoyant rope and serves to pull in the instrument.

### 5.7.1.2 Laboratory set-up

The laboratory set-up consists of four elements: the dry-end of the SEND DSC-Link telemetry, the topside PC of the streamer acquisition system, the Edgetech surface interface unit FS-IU and the topside unit running ELAC Hydrostar Online software (Fig. 5.7.2). In the basence of the deep-towed seismic streamer, the only function of the bottom and topside PC of the streamer acquisition system is to provide a serial link between the OCEANO releaser operating in responder mode and the Posidonia topside unit. Hydrostar Online allows general running of the sidescan sonar and subbottom penetrator operations as well as onscreen display of a subset of the acquired data. Unfortunately some additional settings such as the trigger mode or data window size can only be changed by accessing the underwater electronics directly via the FS-IU. The FS-IU also runs JStar, a diagnostic software tool, that also allows running some basic data acquisition and data display functions.

### 5.7.1.3 Software

The main operations of the DTS-1 sidescan sonar are essentially run using Hydrostar Online, a multibeam bathymetry software developed by ELAC Nautik GmbH and recently adapted to the acquisition of EdgeTech sidescan sonar data. For cruise SO-163 a new version of HydroStar Online (version 3.3.3) with improved

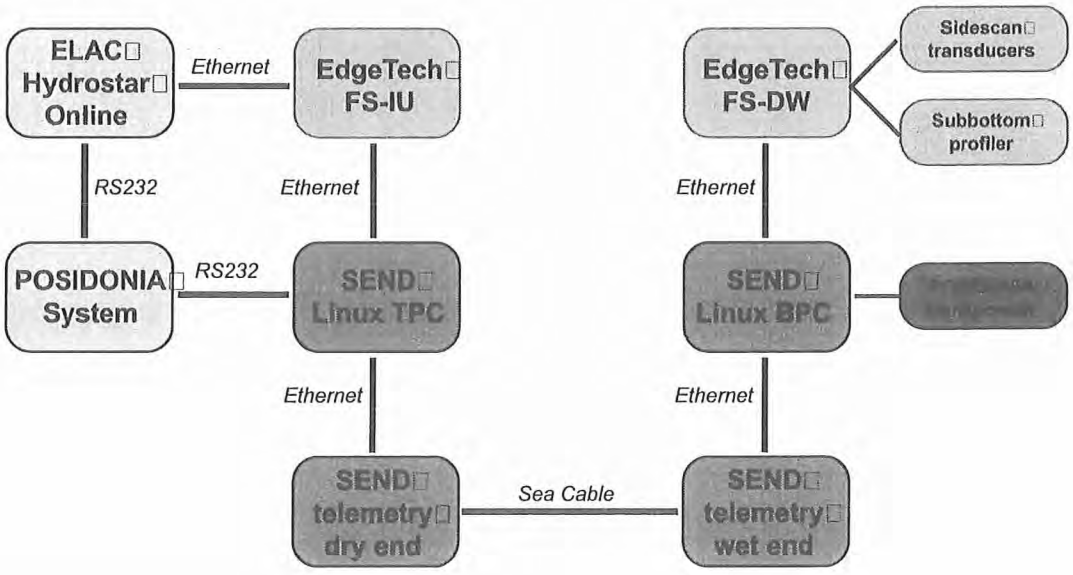


*Figure 5.7.2 The DTS-1 electronics configuration*

onscreen data representation and time synchronisation has been available. This software package allows onscreen representation of the data, of the fish's attitude, and of the towfish's navigation. It also allows setting some principle parameters of the sonar electronics, such as the selected pulse, the range, the power output, the gain, the ping rate, and the range of registered data. However, this version does not allow to set the trigger mode or the master subsystem in coupled trigger mode. HydroStar Online also allows to start and stop data storage either in XSE-format on the HydroStar Online computer on in JSF-format on the FS-DW. Simultaneous storage in both XSE and JSF-formats is also possible. HydroStar Online creates a new XSE-file when a file size of 10 Mb is reached, while a new JSF-file is created every 20 Mb. How fast this file size is reached depends on the amount of data generated, which in turn essentially depends on the use or not use of the high-frequency sidescan sonar. The amount of data generated is also a function of the sidescan sonar and subbottom pulses and of the data window that is specified in the sonar.ini file on the FS-DW. The data window specifies the range over which data are sampled. Proper selection of this parameter strongly depends on the selected range of the sidescan sonar systems in order to avoid good data to be cut-off, or to prevent too large amounts of unuseful data using up storage space.
Further handling of the data is still problematic as neither the XSE nor the JSF data format can be read directly by our sidescan sonar and seismic (for the subbottom penetrator) processing software, which require NetCDF and SEG-Y formats, respectively. Major efforts to achieve data conversion into formats for use with either PRISM of MB Systems are still going on onshore and will soon allow proper processing of the sidescan sonar data.

#### 5.7.1.4 Deployment and recovery procedures

Operations for deployment and recovery of the sidescan sonar are a bit demanding and require relatively calm sea for handling that is safe for both crew and instrument. During cruise SO163-1 three seamen, the boatswain, the sidescan sonar technician and the responsible scientist were on deck for the operations. The sidescan sonar instrument should ideally be towed via the A-frame. With no speed made by the ship the kite tail is first thrown into the water and let to drift away. Then the sidescan towfish is heaved into the water (Fig. 5.7.3) and released with a special hook allowing to detach the crane cable. The sidescan fish then also drifts astern with minimal speed made by the ship. Meanwhile, the buoyant rope is secured. Then the depressor

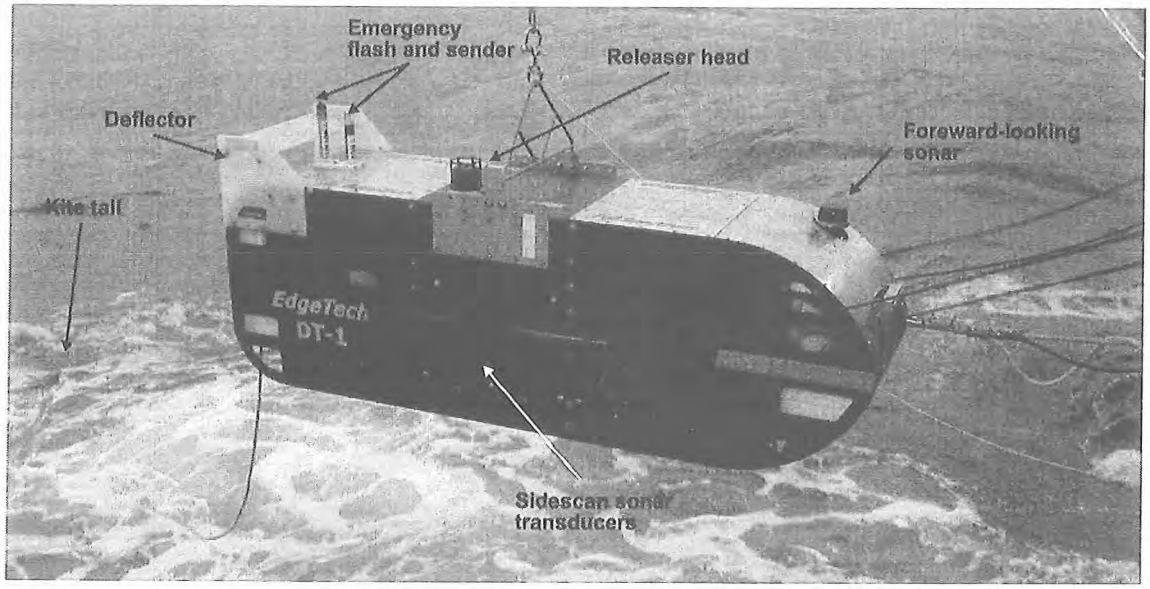


*Figure 5.7.3 Picture of the DTS-1 towfish during deployment*

## 5.8 Mini corer (MIC)

(S. Grandel)

Sediment samples were taken by means of a mini corer, which is a smaller version of the multiple-corer (Fig. 5.8) . The device is equipped with four sampling cores of about 50cm length, and was deployed together with the CTD-rosette unit, hanging approximately 20m beneath. Bottom contact was recorded by a pinger, and penetration of the cores into the sediment is controlled by deployment speed and weight of the device. While lifting the device, cores are closed by lids on the top and bottom. Collected sediment cores were approximately 25cm long, overlain by a clear bottom water column, indicating a sediment surface virtually undisturbed by sampling procedures (Barnett et al., 1984).

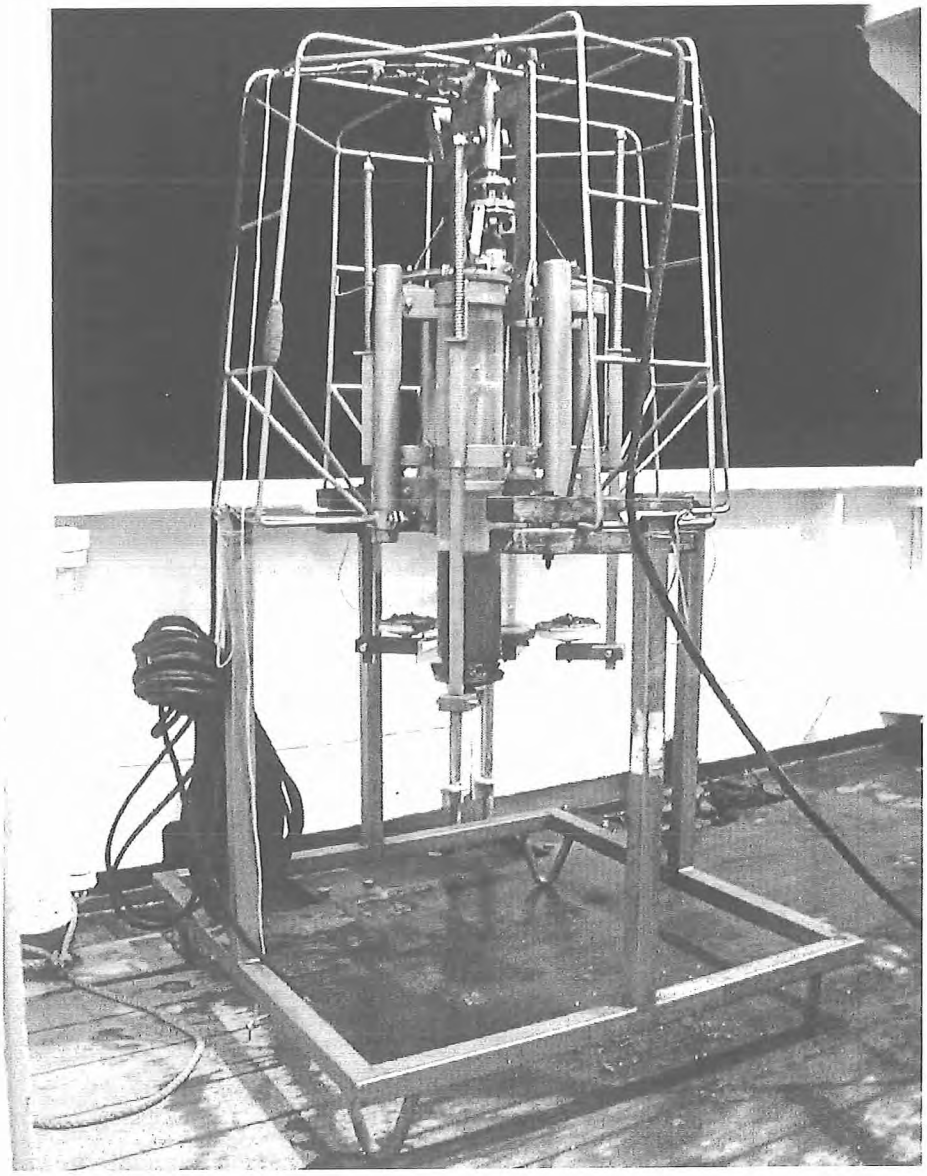

**Figure 5.8:** Mini corer used for the sampling of the upper sediment column.

## 6.1 Multibeam bathymetry

### 6.1.1 Multibeam bathymetry results from Sonne 163 leg 1

(C. R. Ranero, P. O. Thierer and watchstanders)

During Sonne 163 leg 1 multibeam bathymetry was collected during the entire leg in parallel with dedicated surveys for Tobi, DTS and OFOS. Time dedicated for the collection of only bathymetry was mainly available during down time of Tobi surveys for reparation of the instruments and some transits and therefore most of the bathymetric data are located in areas where there was existing bathymetric coverage. The only area not previously surveyed is west of the Nicoya Peninsula where bathymetric soundings filled some existing data gaps in the upper slope during Tobi repairs. In spite of covering areas with existing data the high performance of the new Simrad system produced high quality data that improved notably the resolution of the bathymetric coverage. The Simrad system, used for the first time in this margin where previously existing data had been collected with the hydrosweep system of R/V Sonne and R/V M. Ewing greatly outperforms the capabilities of the older systems and some of the detail surveys carried out during this leg have produced a brand new topographic map of areas that were previously mapped at lower resolution. Some of the description in this section will be dedicated to compare the results from the new system with older maps and to try to strengthen the great potential of the system if used in properly planned, dedicated surveys.

By the end of leg 1, the large majority of the bathymetric soundings had been cleaned using MBsystem version 5beta12 (Caress and Chayes, 1996) and only cleaned data were used for the illustrations in this section.

In the next points we will show a series of areas where bathymetric coverage with Simrad data has brought some interesting new results. The areas that will be discussed are indicated by the boxes in figure 6.1.1.1.

6.1.1.1 Mapping the ocean plate.

We run a small survey in an area of the ocean plate that had been previously covered with hydrosweep bathymetry. The difference between the results produced by both systems can be observed in figure 6.1.1.2. The purpose of the survey was to produce a detailed map to use for planning an OFOS study of the area where a cruise by R/V M. Ewing had found anomalously high heat flow values and indications of anomalous composition of fluids collected by piston coring. Those observations seem to point to vigorous deep penetrating fluid flow in the ocean lithosphere (Fisher et al., 2001).

Figure 6.1.1.2a shows the data collected with the Simrad system in a survey with two parallel tracks run at 5 knots and with a narrow aperture of the beams (4 km on either side) in order to obtain high quality data and a suitable coverage to grid the data at ~ 50 m in the area of interest. Figure 6.1.1.2b shows the compilation of soundings from previous cruises that could only be gridded at ~ 100 m to avoid spatial aliasing. The comparison of the images shows some straightforward differences. The hydrosweep data displays a considerable amount of noise that masks much of the fine scale topography of the plate. The noise of each individual track is particularly clear in this area because the seafloor topography is rather subdued. In contrast, the map constructed wit the Simrad data shows a detailed image of a number of morphological features not observed in the other map. The new bathymetry shows that the heat flux measurements were carried out in an area where the ocean plate begins to be pervasively faulted due to bending as it approaches the trench. The faults run with a NW-SE strike with the hangingwall to the NE. In addition, a small graben structure about 200 meter wide is conspicuous in the SE of the surveyed area. The fault offsets, of the order of 50 meter (Figure 6.1.1.2c), and associated half grabens, are well displayed in the Simrad bathymetry, whereas only the graben is clearly visible in the SE part of the hydrosweep map. Although a more fair comparison could be done by removing some of the worse tracks (or beams) from the hydrosweep compilation, a detailed map like that of the Simrad system could most likely not be achieved.

The heat flux survey carried out with R/V M. Ewing is in between to main lineaments of faulting. The faults to the west of the measurements area smaller offset that to the east, where a SE striking fault with ~ 100 m throw is visible at the NE edge of the coverage. The faults have formed depressions (half grabens) that are filled in the deepest parts with a few tens of meters of strata (Figure 6.1.1.2d) that discordantly onlaps the basins and probably represent recent turbidites. The basal layers of the infilling strata are tilted forming wedge like geometries against the fault scarps indicating a syntectonic deposition.

All the above observations indicate that the heat flux data were collected in an extensional environment of currently tectonically active normal faults related to the bending of the ocean lithosphere. This could indicate that the anomalous fluid flow might be related to the extensional faulting. The lateral variability in the heat flux measurements (Figure 6.1.1.a) might indicate areas of inflow in the ocean plate (low values) and of outflow (local high values).

6.1.1.2 Ridge subduction and middle slope normal faulting and chemoherm mounds

An example of the middle slope structure offshore Nicoya peninsula is shown in Figure 6.1.1.3a. Much of area in the figure was covered during a DTS survey and parts during transit tracks. The area covered during the DTS survey is most of the center of the figure and can be easily identified because it shows smoother morphology lacking high frequency noise. The areas covered during transits are located to the SE and SW-W of the figure and two overlapping tracks leaving the area towards the NE. All those areas display high frequency noise that partially masks the real morphology and is close to aliasing at the ~ 50 m grid in the figure. A perspective view of the area is shown in figure 6.1.1.3b where the noise is also displayed.

Well above the noise level are a series of real morphological structures. In the SW of the images occurs a landslide with a concave up geometry and a clear semicircular headwall. The slide is in line with a small linear ridge in the ocean plate (figure 6.1.1.1) that is subducting beneath the upper plate (von Huene et al 2000). A seismic profile landward of the slide indicates that the ridge continues beneath the middle slope (Barckhausen et al., 2001) and the slide has probably been formed by the effect of the subducting ridge. The morphology within the slide is rougher than in the surrounding areas indicating blocks of slided material and a recently detached semicircular block is visible downslope of the headwall. Normal faults immediately upslope of the headwall and striking oblique to other faults in the areas probably are created by uplift due to the subducting ridge. In addition, two other sets of prominent structures are visible in the diagrams.

A series of roughly margin parallel offsets in the seafloor are the surface expression of normal faults. The faults are widespread in the area and have been mapped with bathymetry in other areas of the margin (e.g. Ranero et al., 2000b). Normal faults in other areas of the margin have been observed in seismic reflection records cutting deep into the slope sediment section and some of them possibly into the basement (McIntosh et al., 1993; Ranero and von Huene, 2000). Faults upslope of the slide and to the W seem to downthrow downslope, whereas some of the faults observed to the NE of the slide downthrow upslope.

A swath of mounds, few hundred meters to ~1 km wide and some tens to 100-200 meter high, spreads across the middle slope. These structures, initially interpreted as mud volcanoes (e.g. Shipley et al., 1990, Shipley et al., 1992) seem to be mounds formed essentially by carbonate chemoherms with abundant indications of active fluid flow (see OFOS chapter for a detail description; Kahn et al., 1996; Borhmann et al., in press). Although they cluster in a swath in the middle slope, two others occur upslope at the edge of the area of figures 6.1.1.3a and 6.1.1.3b (@ 85° 50'/ 9° 44.5'). Is it interesting to note that the swath of carbonate mounds occurs in the area where, with the current resolution, also occurs the inception of widespread normal faulting. A more detailed image of the relationships between faulting and carbonate mounds is shown in the perspective diagrams of figures 6.1.1.3c and 6.1.1.3d that encompass the area of the detailed DTS survey where the coverage is the best allowing gridding at ~ 25 meter. A small portion of the area downslope in the figures is covered by transit tracks and aliasing has produced a poor quality image compared

to the ~50 meter grids of figures 6.1.1.3a and 6.1.1.3b. A preliminary interpretation of the images is that the carbonate mounds grow associated to fluids expelled along the faults, perhaps related to methane coming from deep in the sediment section. The sediment cover in this area is 1.5-2 km thick and bottom simulating reflections (indicating gas hydrates) occurring at ~400 m depth are widespread (Pecher et al., 1998; von Huene et al., 2000). Fluids either from sediment compaction or perhaps from greater depths may rise along the faults and locally disassociate hydrates releasing methane that will rise along faults. This might explain the spatial occurrence of most mounds and the inception of widespread faulting. Normal faulting may also occur upslope of our observations (e.g. McIntosh et al, 1993) where a few other mounds also occur but they might be below the resolution of our images. This in turn may indicate that faults in the middle slope are more frequently active favouring a more continuous fluid supply.

The fate of the mounds may also be governed by normal faulting. Faults offset is larger in the faults located downslope of the mound swath, and that may indicate that fault grow leads to the destruction of the mounds. Some of the mounds at base of the swath seem to be cut by the faults (e.g. @ -85° 58'/ 9° 43') and no mounds are observed towards the lower slope (although our resolution is worse in that area, mounds several hundred meters wide should be visible). If this preliminary model were correct it would imply that the carbonate mounds develop for long periods of time. There is no age information on the faulting, but it is probably related to the collapse of the margin produced by basal tectonic erosion (Ranero and von Huene, 2000). This process leads to progressive subsidence of the margin in which the upper slope will eventually become a middle slope and even a lower slope at the end of the process in such a model, before being tectonically eroded away. The rates of erosion and subsidence are currently poorly constrained but it certainly implies millions of years. The top of the basement drilled in the ODP leg 170 (Kimura et al., 1997) was a beach rock about 17 Ma and it is currently beneath the lowermost slope (Vannuchhi et al., 2001).

### 6.1.1.3 Upper slope canyons, middle slope normal faulting and chemoherm mounds

A second area showing the relationships between faulting and carbonate mounds has been chosen to illustrate the great improvement obtained with the Simrad system. In addition, a spatial relationships among upper slope canyons, normal faulting and carbonate mounds is also starting to emerge from the new data (Figure 6.1.1.4). Much of figure 6.1.1.4 is in an area that had been previously surveyed with hydrosweep bathymetry, usually collected at speeds ranging from 8 to 12 knots. The quality of the previous data set can be appreciated in the lower left area of the figure where gridding at ~ 50 meter has yielded a poor image of the morphology and numerous small gaps in the coverage. In contrast, the rest of the figure shows a fairly new image of the slope morphology, in spite of the gaps among tracks in the uppermost slope. Much of the Simrad data in the figure was collected during a Tobi survey with speed of ~ 2.5 knots, but parts of the data were also collected at ~ 8 knots yielding comparably good data.

A complex pattern of canyons occurs in the upper slope running roughly downslope and with numerous tributary gullies that form a "herring bone" texture. At the mouth of the main canyons two areas show a fairly smooth morphology probably indicating recent sediment deposition and that the canyons are active (around -86° 20' / 10° 20' and –86° 18' / 10° 06'). Around these areas, numerous slope-parallel scarps break the seafloor indicating active faulting. The fact that the mouth of the canyons is associated to smoother topography may indicate that sediment supply is high enough to mask fault offsets. Most faults seems to occur downslope of the canyons but a few cut transverse across the them (e.g. @ -86° 15' / 10° 12').

Several mounds appear clearly displayed in the bathymetry. A cluster of 4-5 mounds occurs at –86° 24.5' / 10° 22' and an isolated large mound about 1 km wide and 200 m high occurs at –86° 18.5' / 10° 18' (surveyed with OFOS). Another cluster of mounds occurs at –86° 12' / 10° 1'. All those large mounds occur in the area of widespread extensional faulting inception, similarly to the mounds described in the previous section.

### 6.1.1.3 Uplift and slope failure related to seamount subduction: the Jaco scarp and uplift

Another example of the unprecedent resolution and a wealth of structural information obtained with Simrad multibeam bathymetry in the margin is the area of the Jaco scarp and uplift (Figure 6.1.1.4a and 6.1.1.4b). The uplift is produced by a subducting seamount (von Huene et al., 2000). The subducting seamount has uplifted the upper plate and produced numerous fractures that ofsset the seafloor and probably allow fluid flow (Ranero and von Huene, 2000). Large subducting seamounts, like those currently underthrusting central Costa Rica and causing the Jaco uplift break the entire upper plate where the plate thickness is less that ~ 10 km and may allow fluids from even the plate boundary to rise along the fractures (Ranero and von Huene, 2000).

In the wake of a subducting seamount forms a furrow parallel to the convergence vector (Figure 6.1.1.1; von Huene et al., 2000) . The furrows indicate that material from the upper plate is removed during the seamount subduction process, and seismic images document that basal erosion along the underside of the upper plate is responsible for much of the material missing (Ranero and von Huene, 2000).

The new bathymetric data show that downslope from the edge of the scarp there is a terrace very similar to the seafloor surface of the uplift area (Figure 6.1.1.5c). This terrace probably corresponds to the last slided block that has moved a few hundred meters downslope as a coherent block. The block is dissected by several faults perpendicular to its strike and that seem to be the continuation of the faults observed in the uplift area. The fact that an elongated block, dissected by several faults, remains coherent after several hundred meters of displacement along the detachment plane might indicate creeping rather that a single catastrophic movement.

The edge of the uplifted area shows the largest amount of deformation with a network of fractures that break the upper plate in blocks similar to the block forming the terrace downslope of the scarp edge. The faults forming the lateral walls of the furrow seem to penetrate into the uplift area and crosscutting roughly perpendicular fractures dissect the terrain in blocks that later will slide down the scarp (Figure 6.1.1.5c). The area of maximum uplift, where faults have the largest offsets is located about 2 km upslope from the scarp and may indicate the position of the top of the seamount.

### 6.1.1.4 Summary

Bathymetric data collected with the new Simrad system and carefully cleaned with the Mbsystem has yielded a new, detailed image of the structure of the margin in areas where previous bathymetric sounding had a lower resolution. The use of dedicated surveys planned taking into account water depth and desired grid cell size to calculate ping aperture, and ship speed (ping rate) can produce high quality terrain data for maps of unpreceded high resolution.

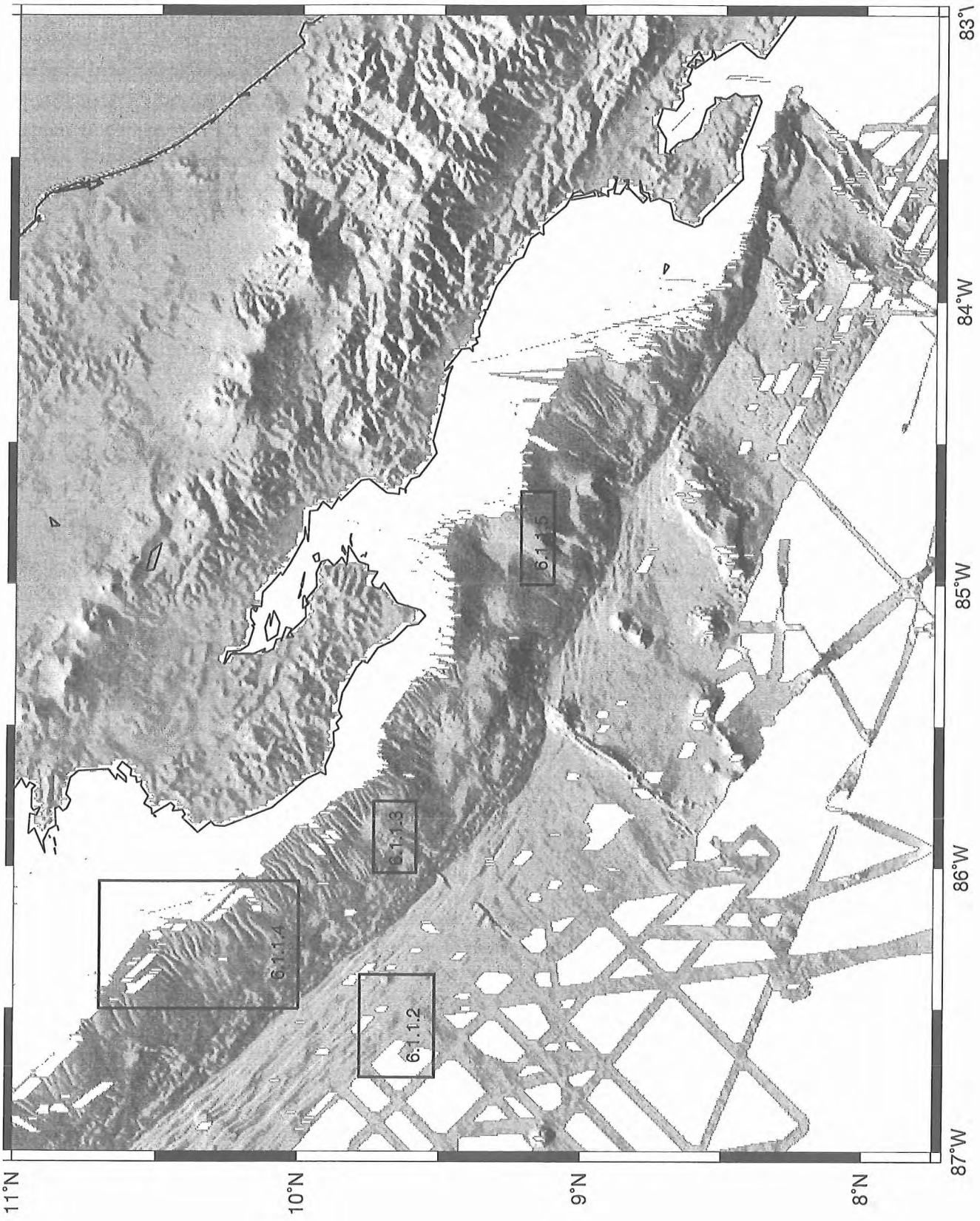


***Figure 6.1.1.1.*** *Compilation of multibeam bathymetry along the area studied during SONNE 163 leg 1. Boxes indicate location of areas discussed in detail in this chapter and numbers refer to figures.*

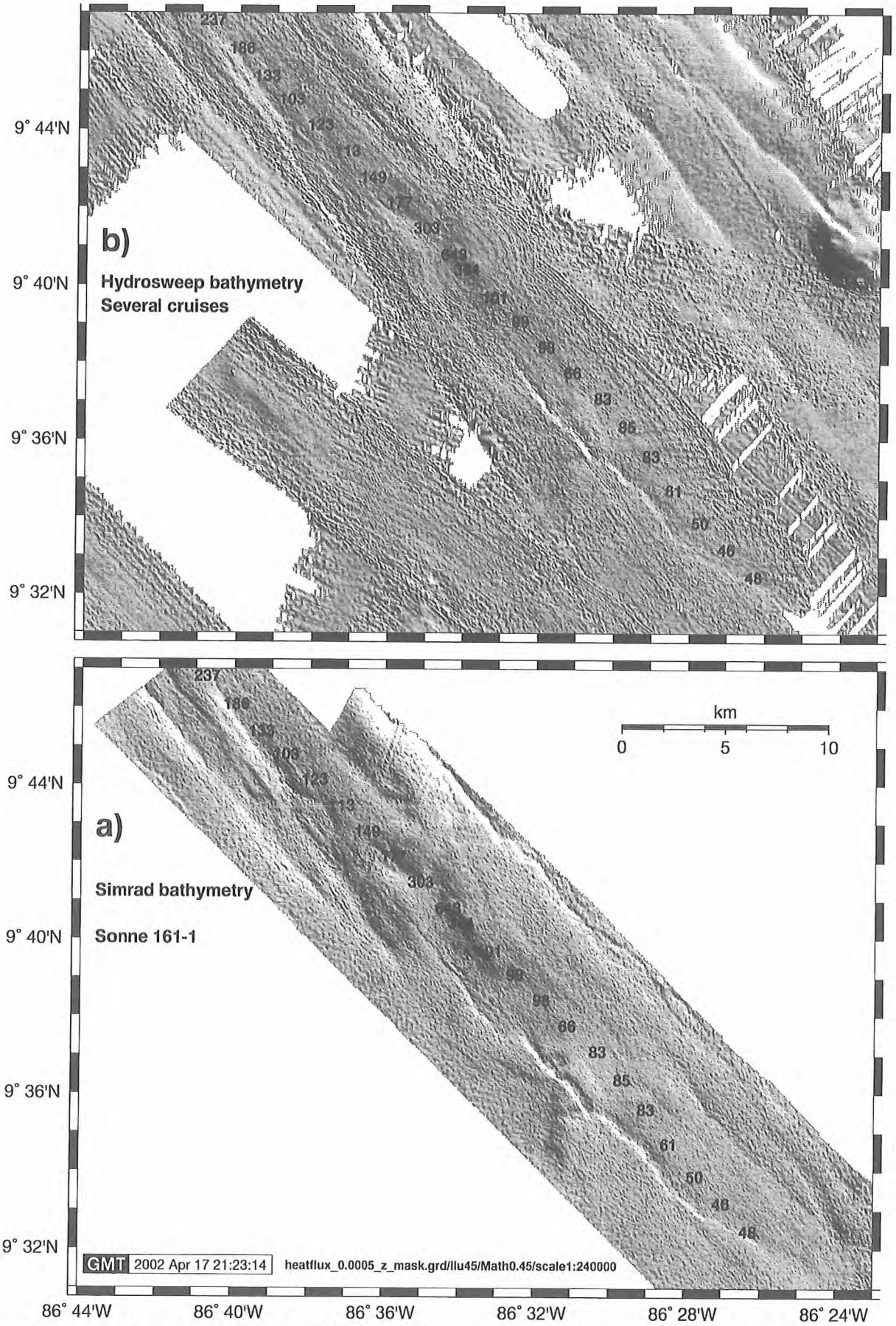


***Figure 6.1.1.2. a)*** *Shaded relief map of Simrad bathymetry on the ocean plate. Grid size is ~ 50 meter. Numbers along the bathymetric swath are heat flux values from Fisher et al. (2001) collected with R/V M. Ewing cruise 0104. Note some anomalously high values (303, 364, 643, 2370).* ***b)*** *Compilation of hydroweep bathymetry from several cruises in the same area. Note the better resolution of Simrad data. Location on figure 6.1.1.1.*

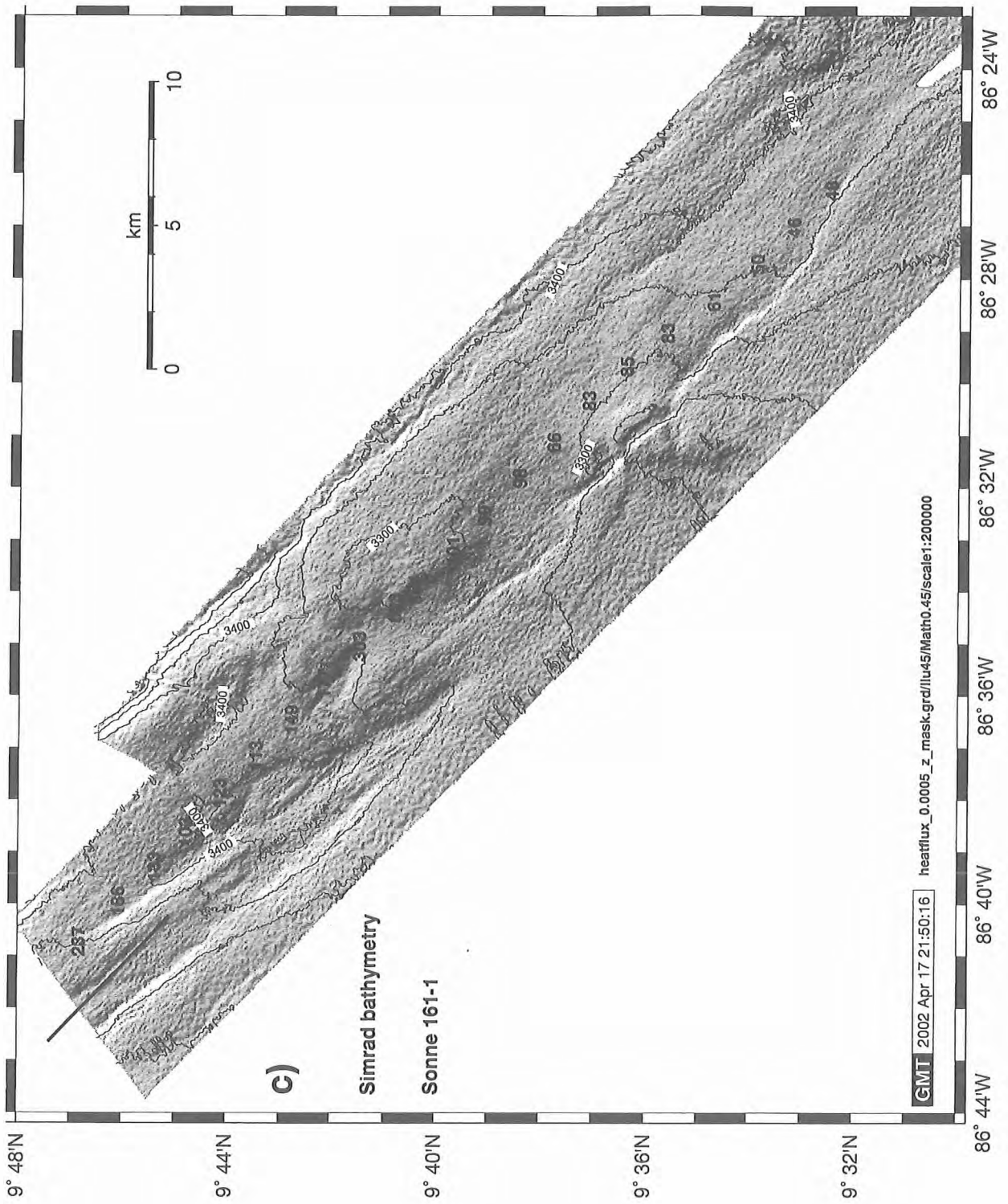


***Figure 6.1.1.2. c)*** *Shaded relief map of high resolution Simrad survey on the ocean plate. Grid size is ~ 50 meter. Illumination is from 45° and contours are every 50 meters. Numbers along the bathymetric swath are heat flux values from Fisher et al. (2001) collected with R/V M. Ewing cruise 0104. The black line is the parasound track of Figure 6.1.1.2d. Location on figure 6.1.1.1.*

***Figure 6.1.1.2. d)*** *Parasound profile in the ocean plate showing tilting of deepest strata in the center of the figure and filling of basin with probably recent turbidites. Tilting and wedge shape units may indicate syntectonic deposit of some of the turbidites, although the geometry of the profile, parallel to the main faults, is inadequate for imaging of the true geometrical relationship between faults and sediment units. The location of the profile is shown in figure 6.1.1.2c.*

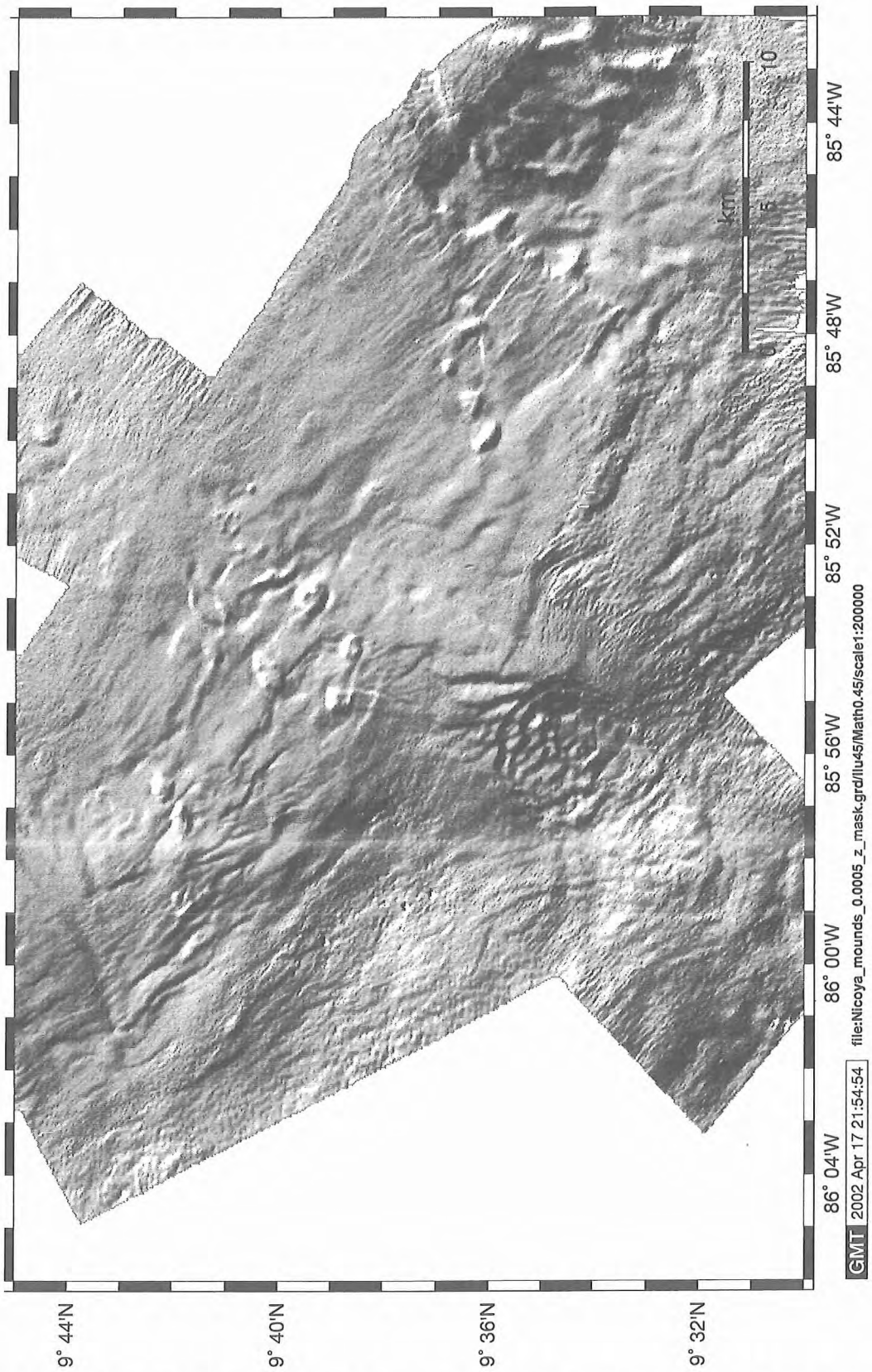


***Figure 6.1.1.3. a)*** *Shaded relief map of Simrad survey in the middle continental slope offshore Nicoya (see location in figure 6.1.1.1). The data are gridded at ~ 50 meters. The grid includes data collected during a detailed DTS survey in the center of the figure, with track spacing of ~ 1km, where the resolution is highest. Data to the S, SW and W on the figure and two tracks leaving the area to the NE were collected during transit lines and the faster ship speed of ~ 8-10 knots resulted in higher levels of noise. A large slide with a rough seafloor morphology produced by failed slope sediment is visible at ~ 85° 56'/ 9Ú°34'. A swath of mounds runs along the middle slope. Linear, slope-parallel features are surface expresion of normal faults.*

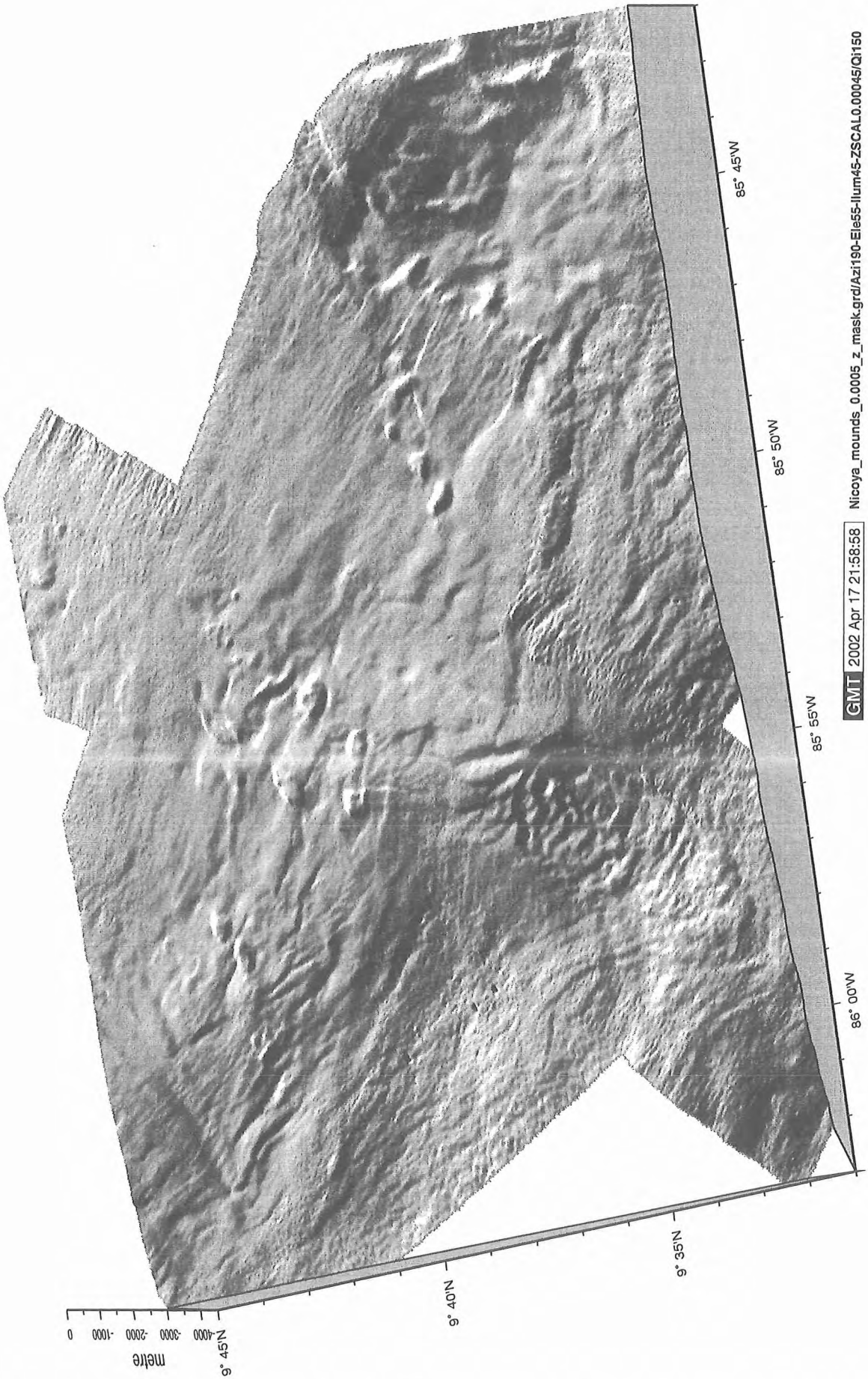


***Figure 6.1.1.3. b)*** *Shaded relief perspective view of Simrad survey in the middle continental slope offshore Nicoya (location in figure 6.1.1.1). See figure 6.1.1.3a for explanation and text for discussion.*

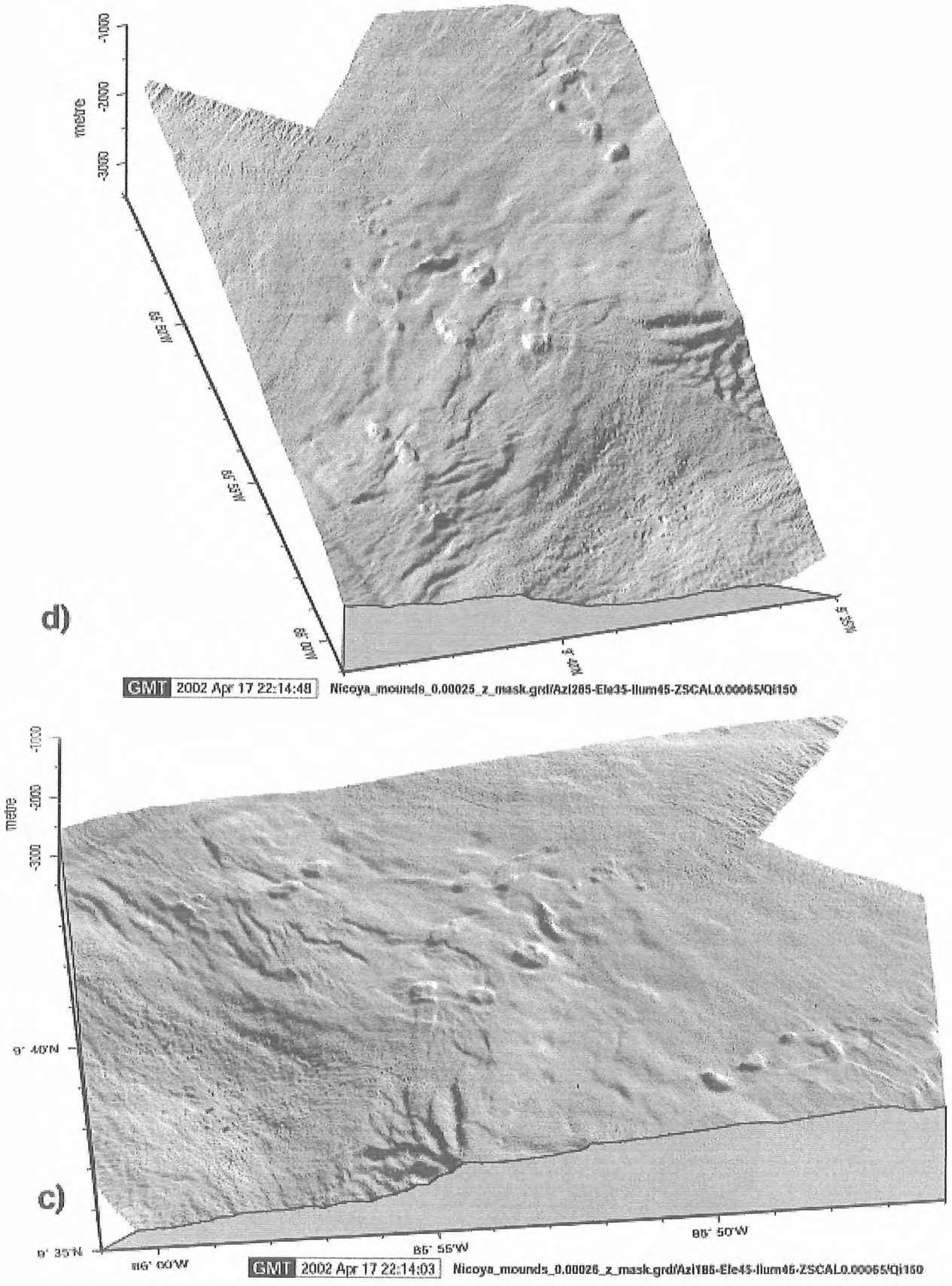


***Figure 6.1.1.3. c)*** *and* ***d)*** *Shaded relief perspective views of Simrad survey in the middle continental slope offshore Nicoya (location in figure 6.1.1.1). The grids were created using mainly the data of a detail DTS survey (see caption of Figure 6.1.1.3a) allowing gridding at ~ 25 meter. The two perspectives show the relathionship between mounds and normal faulting. See text for discussion.*

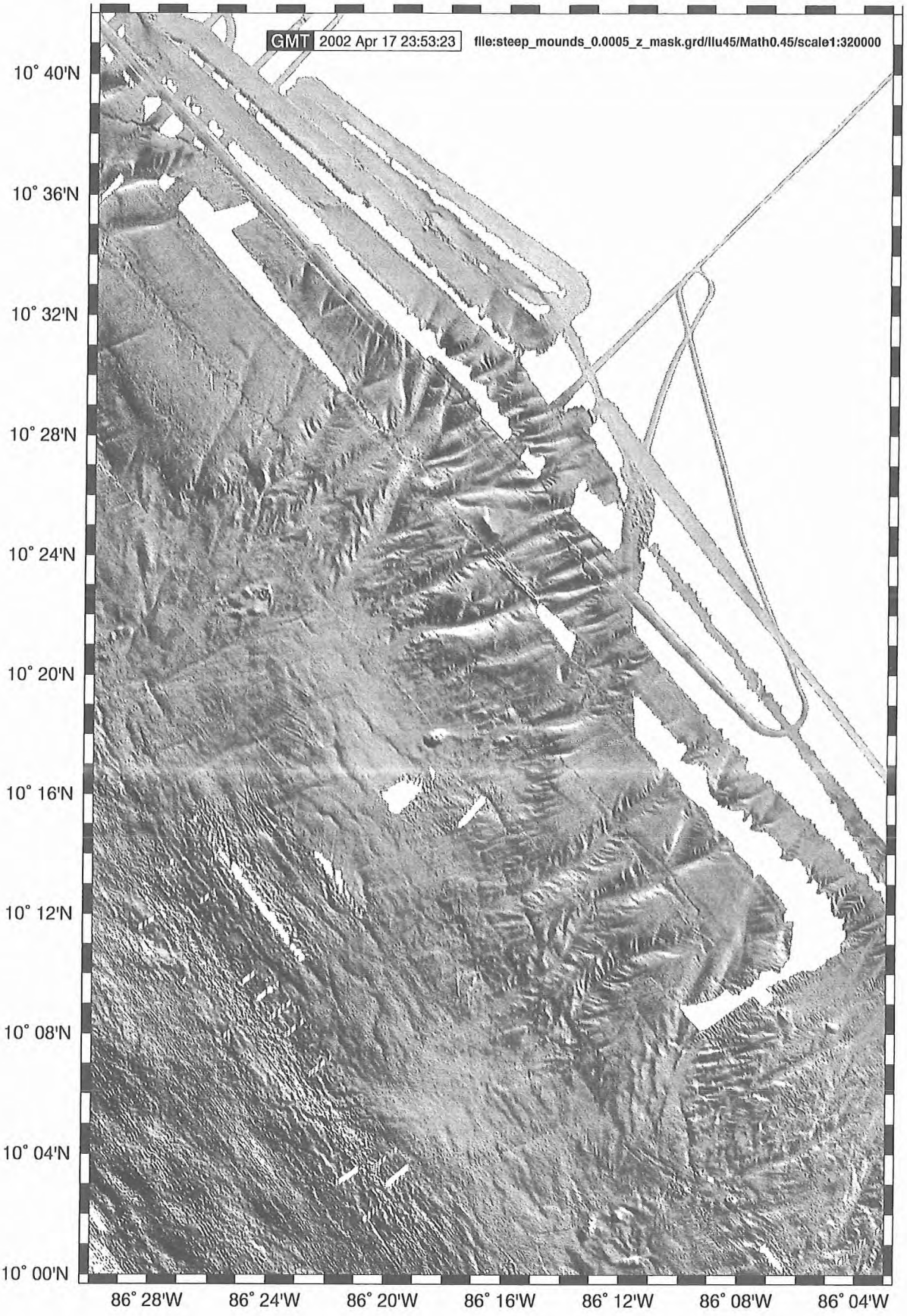


***Figure 6.1.1.4.*** *Shaded relief map of the compilation of Simrad data from So163 leg 1 and hydrosweep data from previous cruises. The area with no Simrad coverage is clearly visible in the SW corner of the figure where noise and data gaps largely obscure the morphology. The image shows the relationships among canyons in the upper slope, faulting and mounds in the middle slope. See text for discussion. Location in figure 6.1.1.1.*

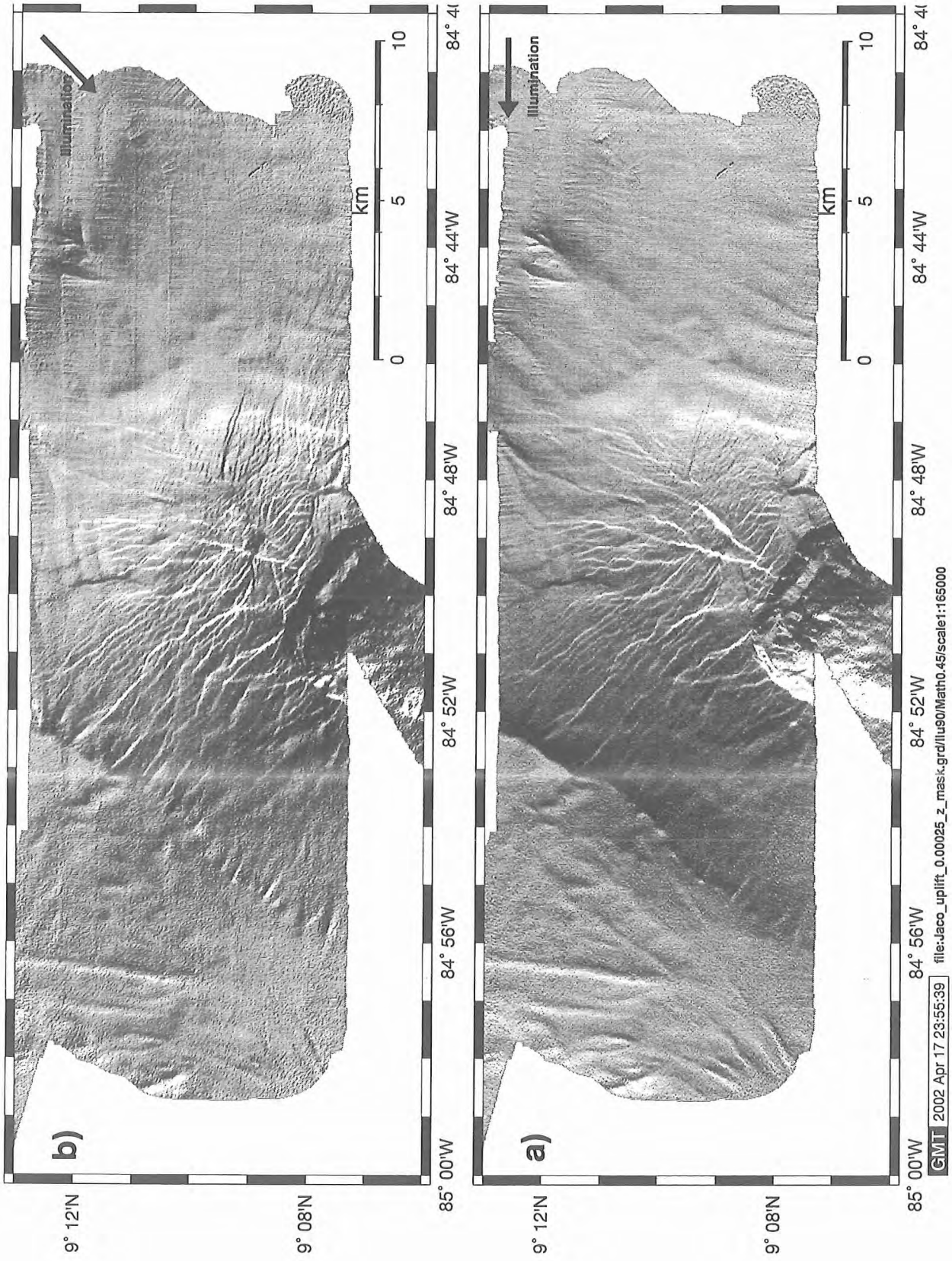


***Figure 6.1.1.5.*** *Shaded relief map of Simrad survey across the Jaco uplift and scarp. The uplift is produced by a subducting seamount in the ocean plate. The data were collected during a DTS survey allowing gridding at ~ 25 m.* ***a)*** *Data illuminated from 90° highligthing radial faults and headwall of the slide.* ***b)*** *Data illuminated from 45° highligthing faults roughly perpendicular to the convergence vector. Location in figure 6.1.1.1.*

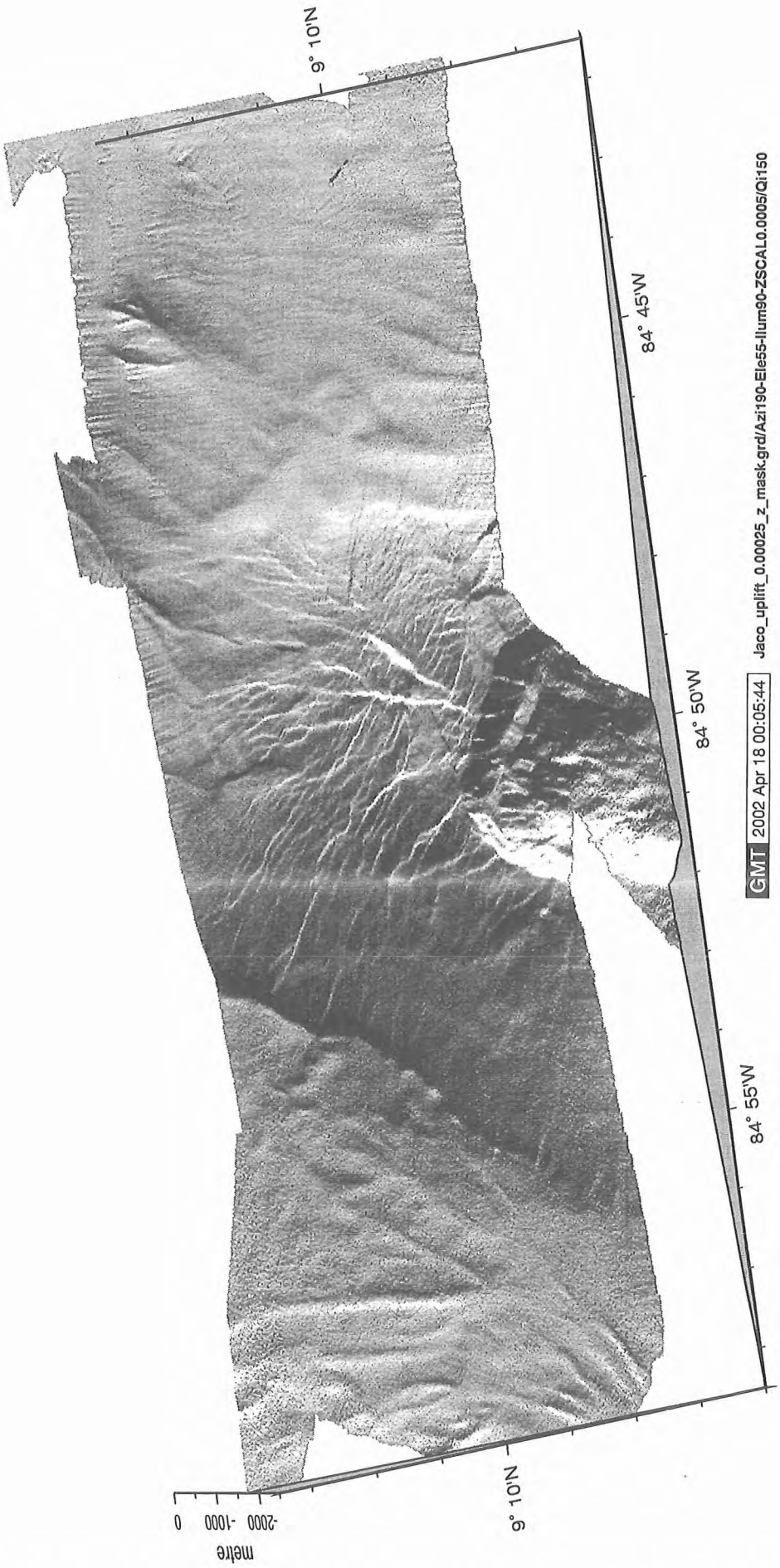


***Figure 6.1.1.5. c)*** *Shaded relief perspective view of Simrad survey across the Jaco uplift and upper scarp. Note that faults extend from the center of the uplift area laterally to the edge of the uplift region. Note terrace in headwall area from last slided block. Location in figure 6.1.1.1.*

## 6.2. TOBI operation and initial data interpretation

(D.G. Masson, I.P. Rouse, V. Hühnerbach and D. Matthew)

### 6.2.1. Summary of TOBI operations

Operational Procedure

Mobilisation

The SOC TOBI system was transported to the Sonne in two 20' containers. One hardtop container was for electronics, computers, tools and spares, and one soft-top for the vehicle, winches, bedplate and depressor weight.

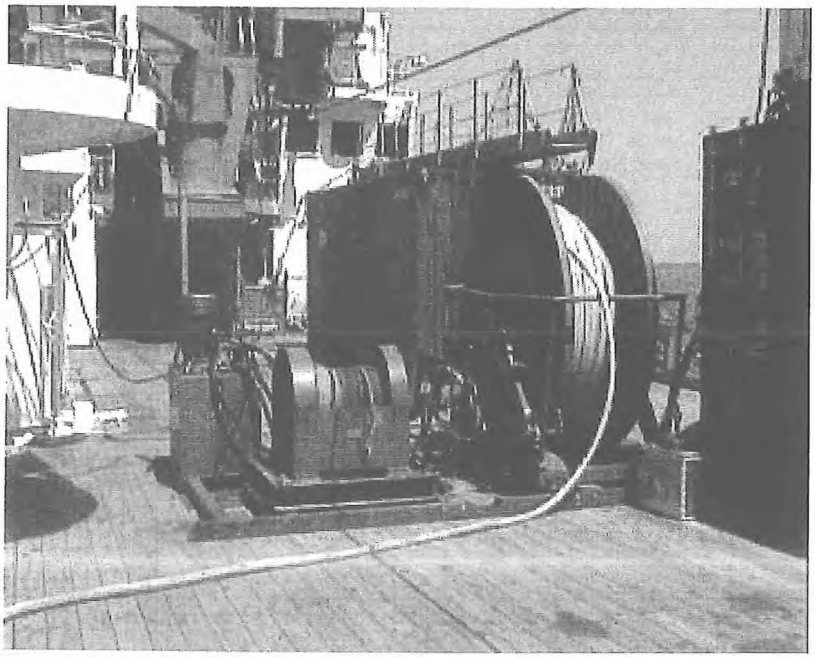

*Figure 6.2.1 TOBI winch system. From left to right, power pack, launch winch, umbilical winch.*

As TOBI had previously been installed on the Sonne for SO-144, the mobilisation was quickly undertaken. The bedplate was assembled on the deck and bolted into position as before. The launch and umbilical winches and the power pack were bolted to the bedplate (Fig. 6.2.1). The power pack was connected to a 3-phase 15kW supply in the gun control shack aft of the geology laboratory.

The deck electronics systems were set up in the geology laboratory on the port side of the main deck. 8' x 4' x 18 mm plywood sheets were used to extend the bench space available on the middle benches in the laboratory. The electronics racks plus the TOBI replay system were mounted on these. It was found that the provision of electrical supply sockets above the benches provided a very neat installation (Fig. 6.2.2).

*Figure 6.2.2 TOBI laboratory set-up.*

The GPS receiving aerial was mounted on a pole on the port side of the main deck. Experience on SO-144 showed that this position gave good reception and was conveniently close to the geology laboratory.

Approximately 1.5 days were spent setting up the equipment prior to the first test of the TOBI system on deck.

Pre-launch

Prior to the first launch of TOBI a number of essential tasks were carried out. The launch/recovery wire was wound onto the launch winch. A special link that had been manufactured in Southampton to connect the depressor weight to the main tow cable was offered up for fitting. It was found that it was too wide for the shackles that it was to fit and had to be machined down. The vehicle was rigged with four steadying lines plus the main recovery line for a fore-aft launch (Fig. 6.2.3). The launch wire was run through the main block and connected to the lifting strops on TOBI with the launch pin. The umbilical was connected to the vehicle and the emergency release mechanism cocked.

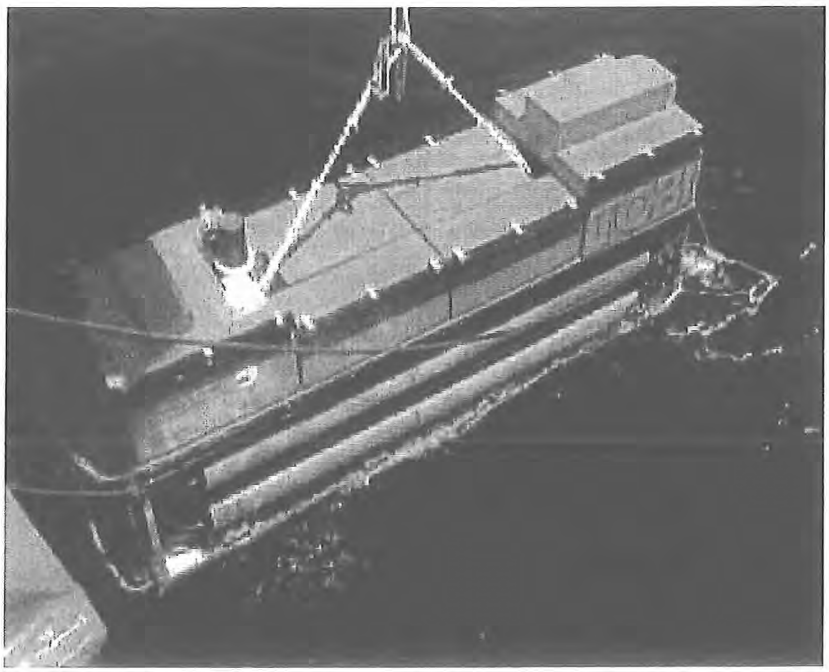

*Figure 6.2.3 TOBI on recovery – note lifting strops and steadying lines.*

A deck lead was run out to the vehicle for test purposes. The vehicle was powered up and all systems apart from the swath receivers worked. The problems with the swath system were worked on at length and although progress was made, it was clear that with the necessary hardware changes that had to be made to the system, that it was unlikely for it to be operation during the cruise.

A final check of the vehicle running the power through the umbilical revealed a short circuit. The umbilical was swapped for the spare prior to the first launch. The spare umbilical was found to have a crushed connector that had to be replaced.

Launch procedure

The TOBI vehicle is launched in a fore-aft position rather than the more preferred athwart ships position on the Sonne due to the narrow 'A' frame. The vehicle is lifted off the deck with the launch winch while being steadied by two lines to the fore of the vehicle. The 'A' frame is then extended over the stern of the ship and the launch winch paid out until the vehicle is in the water. The steadying lines are then let go, pulled back aboard and the launch pin pulled to release the vehicle. As the umbilical is being paid out the depressor weight is brought round under the 'A' frame and the main tow cable fed through the main block. The cable is mechanically connected to the depressor. The electrical termination bottles are attached to the main cable using clamps and cable ties. At the end of the umbilical a loop enables it to be tied off so that the free end can be mechanically connected to the depressor weight and electrically to the main cable. The vehicle is then powered up to check correct operation. If all is OK then the depressor is lifted into the water and survey commenced.

Recovery procedure

Recovery of the TOBI system commences with the recovery of the depressor weight. Making sure that the power to the vehicle is switched off, the depressor is swung aboard and landed in its cradle. The loop in the umbilical is grabbed and made fast to a cleat or eye with a rope. The umbilical is then disconnected from the depressor weight and main cable. The free end is attached to the rope pennant on the umbilical winch and is slowly recovered. During this time the depressor is disconnected from the main cable, and the main cable is replaced through the main block with the launch wire. When the vehicle is in boat hook range (approx 10 m) the recovery hoop is grabbed and the steady and recovery lines brought aboard. These are carefully

sorted out with the vehicle just astern of the ship. The recovery line is attached to the launch wire and once the steady lines are in position – two fore inside the 'A' frame, two aft outside the 'A' frame – the vehicle is brought out of the water (Fig. 6.2.3). Once clear of the stern, the 'A' frame is brought in and the vehicle landed on the deck.

Survey guidelines

As a general rule the survey speed for TOBI should not exceed 3 kts. Above this speed the stability of the vehicle is reduced, the wire out will become excessive and the along track resolution becomes large compared to that across track. During the cruise the tow speed was between 2.0 and 2.5 kts dependant on the wire out. It was only necessary to slow below 2.5 kts when surveying in water depths of 2,500 m or more.

TOBI is kept to between 350 and 400 m above the sea floor except on turns. Due to the amount of wire deployed it is essential that the ship does not make any sharp turns or speed fluctuations. A sharp turn or loss of speed will send TOBI plummeting whereas a rise in speed will take the vehicle above the most favourable altitude. A turn rate of 2° per minute has been found to be optimal for survey line spacing of 5 km and a ship speed of 2.5 kts. A maximum veer rate of 0.5 m $s^{-1}$ and a maximum haul rate of 0.7 m $s^{-1}$ are recommended so that no damage is done to the vehicle or cable due to too high a tension or too much slack wire causing instability.

TOBI Deployments

Run 1

The depressor was put into the water around 1810/076 GMT 12:10 local. Initially all look fine. Some speckle noise was observed on the starboard sidescan. Both sidescan channels seemed to be low on gain. The profiler was giving weak returns and the bottom-tracking algorithm couldn't lock onto the signal so hand altitude values had to be entered most of the time. The starboard sidescan suddenly increased in gain at around 2355/076 GMT and remained until 0335/077 GMT when it returned to its previous value. The digital data telemetry started giving corrupt readings at around 2025/076 GMT although the trigger and frame sync pulses were still being correctly detected. Substituting a spare card interface card in the display computer eventually cured the problem at around 2130/076 GMT. However the magnetometer didn't give reliable readings for the remainder of the run. At around 0530/077 GMT the system suffered a cable failure. The depressor weight was recovered at first light and the problem traced to the cable between the main tow cable termination and the TOBI connector bottle. This cable had rubbed through against the main cable. A test of the vehicle showed that there were no sonar transmissions so that a recovery had to be effected.

The lack of sonar transmissions was traced to a blown MOSFET in the sidescan power amplifier caused by the power cycling originated by the bad cable. This and a resistor were replaced. Also replaced was the magnetometer cable. A test on the sonar arrays showed that one of the port transducers was low in impedance (~20 Mohms under test). A spare transducer replaced this. The vehicle was re-rigged ready for deployment.

Run 2

The depressor was put into the water around 2300/077 GMT. The starboard sidescan channel exhibited a low gain compared to the port channel. The magnetometer worked until a depth of 300 m was reached. All digital telemetry then gave corrupt data but again the trigger and frame sync pulses were unaffected. Eventually the digital data returned at 0230/078 at a depth of 430 m and subsequently the magnetometer started to work at a depth of 640 m at 0650/078. The magnetometer stayed correct until a depth of 420 m at 1550/078 when it stopped for the remainder of the run. The profiler was again giving weak returns and also lost its trigger intermittently. This improved with increasing depth and was solid for the remainder of the run. At 0330/078 the logging system was stopped to reset the day number. This had been incorrectly set before the first run. The run ended with the vehicle on deck at around 1500/081 GMT. The recovery was not good and the vehicle ran underneath the ship. This caused damage to the magnetometer mounting and to the rubber bumpers on the syntactic foam buoyancy blocks.

On deck the sidescan electronics was investigated and an intermittent contact was found on the starboard match pad. The whole of the starboard match pad was secured with heavy gauge wire to ensure connectivity. Also it was found that the port and starboard pre-amplifiers had been switched around. This was corrected and both match pad arrays checked for tuning. 21 dB of gain was added to the profiler receiver before the correlator. Repairs were done to the magnetometer mounts and the bumper fixings. The magnetometer was removed from its housing and two packages of silica gel added to try and combat any residual dampness. The vehicle was re-rigged ready for deployment.

Run 3

The depressor was put into the water at around 2015/082 GMT. A short on the cable became apparent almost immediately. The depressor was recovered and the fault traced to a connector. This was replaced with the vehicle still deployed and the depressor was re-launched. The sidescan and profiler sonar systems both gave excellent signals. After a brief spell during the descent the magnetometer worked throughout the run. Bursts of noise were observed on the sidescan but did not prove obtrusive. The vehicle was recovered at around 1630/084 GMT.

On deck all electronics cards were treated with conformal coating to improve their resistance to dampness. An extra 10dB of gain was added to the profiler. The swath pre-amp tube was isolated using blanking plugs to stop any possibility of it causing any noise. The vehicle was re-rigged ready for launch.

Run 4

The depressor was put into the water around 0130/096 GMT. Again a short period of corrupt digital data was observed during the descent. Also the magnetometer gave bad readings for a short period. These problems resolved themselves quickly at a depth of 630 m. Apart from some periods of low gain on both the sidescan and profiler all instruments worked fine throughout the run. Even on the lower gain the profiler gave a large enough signal for the bottom tracking to work correctly. The vehicle was recovered at around 1430/100 GMT.

On deck the cable connecting the hydro tube to the sidescan tube was replaced with the cable previously used on the swath pre-amps. The vehicle was re-rigged ready for launch.

Run 5

The depressor was put into the water at around 0048/102 GMT. All looked fine at the surface but at 0105/ 102 GMT the sonar systems stopped transmitting. The vehicle was recovered at around 0225/102 GMT. The problem was traced to the cable that had just been replaced. A spare was quickly installed and the vehicle re-rigged for deployment.

Run 6

The depressor was put into the water at around 0338/102 GMT. Apart from the magnetometers now obligatory funny five minutes on the descent all instruments worked well. Only in shallow water - less than 300 m on the rise and 400 m on the descent - did the magnetometer give corrupt readings. This points to a plug/cable problem. The light backscattering sensor failed at 1520/102 GMT. This was an instrument failure rather than a cable problem. The vehicle was recovered at around 2130/103 GMT.

Run Summary

The above detailed descriptions concentrate on the problems that were encountered during the TOBI surveys. This does not give a balanced picture as the system performed exceedingly well for the majority of the time deployed. The mosaics produced bear testament to this. The vehicle was deployed for a total of 12 days 14 hours and 32 minutes during the cruise. The only significant downtimes came as a result of the cable shorts during runs 1, 3 and 5. This totalled just over 8 hours or approximately 2.5% of the total time.

| Deployment | Start time/day | End time/day | Comments |
|---|---|---|---|
| 1 | 1810/076 | 1200/077 | Short on cable. |
| 2 | 2300/077 | 1500/081 | Second run. |
| 3 | 2015/082 | 1630/084 | Third run. |
| 4 | 0130/096 | 1430/100 | Fourth run. |
| 5 | 0048/102 | 0225/102 | Aborted due to bad cable. |
| 6 | 0338/102 | 2130/103 | Sixth run. |

TOBI Watchkeeping

TOBI watchkeeping was split into three, four-hour watches repeating every 12 hours.
Watchkeepers kept the TOBI vehicle flying at a height of ideally 350 to 400 m above the seabed by varying wire out and/or ship speed. Ship speed was usually kept at 2.5 kts over the ground with fine adjustments carried out by using the winch. In deeper water – greater than 2500 m – the speed was reduced to 2.0 kts to reduce the scope of wire deployed. As well as flying the vehicle and monitoring the instruments watchkeepers also kept track of disk changes and course alterations.

Data Management

Data from the TOBI vehicle is recorded onto 1.2 Gbyte magneto-optical (M-O) disks. One side of each disk gives approximately 16 hours 9 minutes of recording time. All data from the vehicle is recorded along with the ship position taken from the GPS receiver. Data was recorded using TOBI programme LOG. Data recorded on the M-O disks were copied onto CD-ROMs for archive and for importation into the on board image processing system.

As well as recording sidescan and digital telemetry data LOG displays real-time slant range corrected sidescan and logging system data, and outputs the sidescan to a Raytheon TDU850 thermal recorder. PROFDISP displays the chirp profiler signals and outputs them to a Raytheon TDU850. DIGIO9 displays the real-time telemetry from the vehicle – magnetometer, CTD, pitch and roll – plus derived data such as sound speed, heading, depth, vertical rate and salinity. LOG, PROFDISP and DIGIO9 are all run on separate computers, each having its own dedicated interface systems.

A program called HITSCOPY was used to strip off magnetic and attitude data from the raw TOBI data files and store it in ASCII format for direct importation into a spreadsheet.

The details of the times of the logged part of each TOBI run are given in Table 6.2.1

Instrument Performance

Most of the problems with individual instruments have been covered above in the details of each run. The relatively minor problems with the sonar systems were mostly easily fixed in the processing of the data. Whilst the individual instruments themselves performed exceedingly well the same cannot be said for the underwater connectors and cables. These were the source of almost all the problems encountered and it must be emphasised that these items must be regularly maintained and replaced if high reliability is to be ensured in the future.

| M-O Number | File Name | Time/ Day START | Time/ Day STOP | Comments / Run # |
|---|---|---|---|---|
| 830 | TOBIB.DAT | 1813/076 | 0523/077 | Run 1 curtailed due to cable short. Day number corrected. |
| 831 | TOBI.DAT<br>TOBIB.DAT<br>TOBIC.DAT | 2310/077<br>0334/078<br>0339/078 | 0329/078<br>0337/078<br>1526/078 | Run 2 Day number corrected<br><br>Day number correct |
| 832 | TOBI.DAT | 1526/078 | 0733/079 | |
| 833 | TOBI.DAT | 0733/079 | 2340/079 | |
| 834 | TOBI.DAT | 2340/079 | 1548/080 | |
| 835 | TOBI.DAT | 1548/080 | 0755/081 | |
| 836 | TOBI.DAT | 0755/081 | 1419/081 | End of run 2 |
| 837 | TOBI.DAT | 2120/082 | 1323/083 | Start of run 3 |
| 838 | TOBI.DAT | 1323/083 | 0535/084 | |
| 839 | TOBI.DAT | 0535/084 | 1558/084 | End of run 3 |
| 840 | TOBI.DAT | 0145/096 | 1752/096 | Start of run 4 |
| 841 | TOBI.DAT | 1752/096 | 1000/097 | |
| 842 | TOBI.DAT | 1000/097 | 0207/098 | |
| 843 | TOBI.DAT | 0207/098 | 1815/098 | |
| 844 | TOBI.DAT | 1815/098 | 1022/099 | |
| 845 | TOBI.DAT | 1022/099 | 0229/100 | |
| 846 | TOBI.DAT | 0229/100 | 1355/100 | End of run 4 |
| 847 | TOBI.DAT<br>TOBIA.DAT<br>TOBIB.DAT | 0052/102<br>0340/102<br>1016/102 | 0156/102<br>1014/102<br>1846/102 | Run 5<br>Start of run 6<br>Reboot logging |
| 848 | TOBI.DAT | 1846/102 | 1053/103 | |
| 849 | TOBI.DAT | 1053/103 | 2103/103 | End of run 6 |

*Table 6.2.1 Summary of logged TOBI data*

Sonar artefacts

During the cruise a number of interesting artefacts appeared within the TOBI sidescan images from sources other than the direct sea floor. These are naturally occurring phenomena and are included here to enable users of TOBI imagery to recognise them.

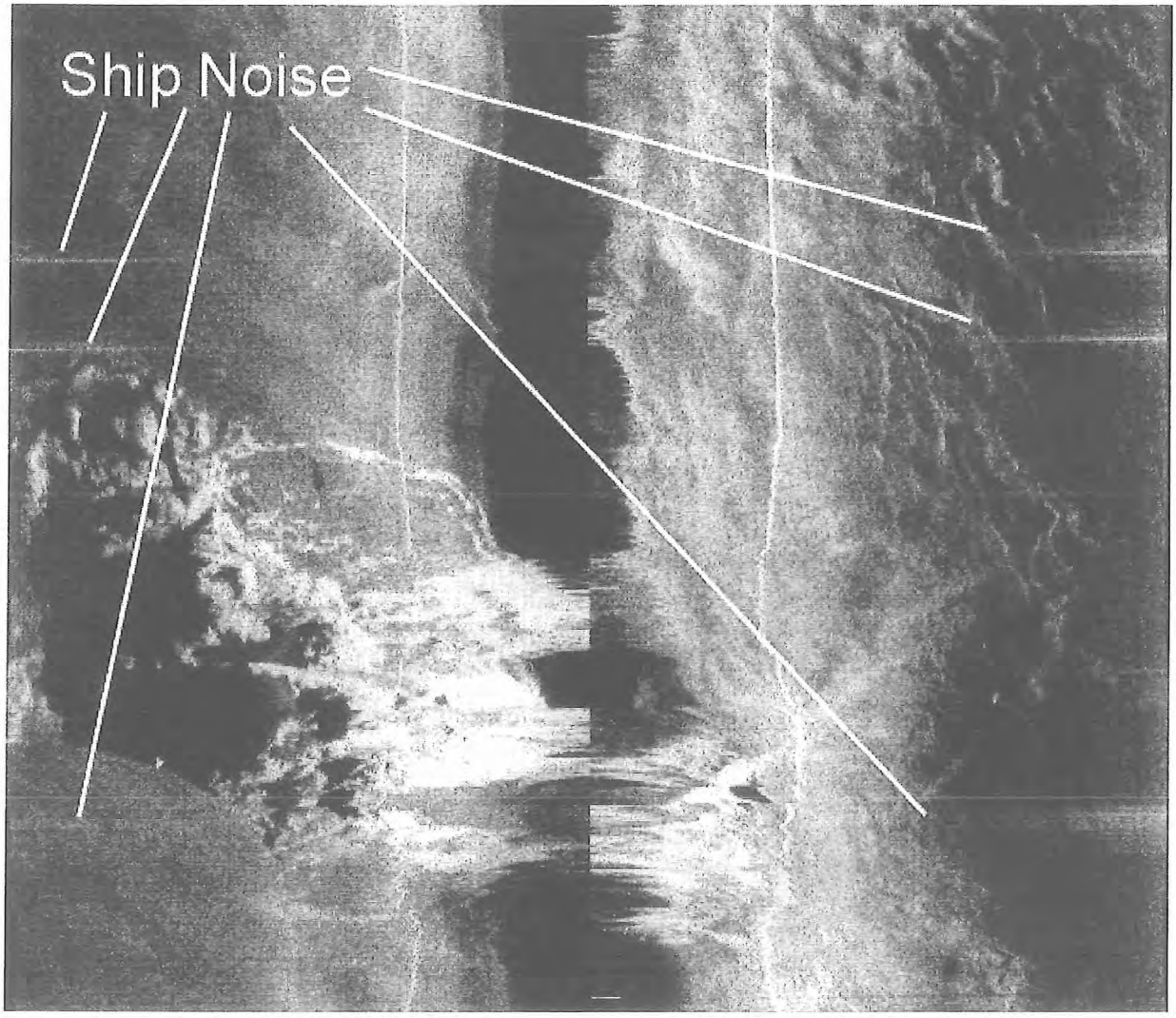


*Figure 6.2.4 Passing ship noise on the TOBI sidescan record.*

Ship noise (Fig 6.2.4) is usually seen when a passing ship is abeam of the TOBI vehicle position. Bubbles produced by the ship's propeller collapsing cause the noise that is quite intense but usually short-lived, a few minutes at the most. A look out of the porthole or radar is enough to identify the source.

Rain noise (Fig 6.2.5) is similar in appearance to ship noise. However it is not usually as intense and is longer lived, maybe over an hour. The heavy rainstorms experienced on the cruise were easily detected with TOBI as these usually give strong signals.

False sonar (Fig 6.2.6) occurs in shallow water, when TOBI is being flown at depths above the local sound speed minimum. This is especially true if the water is highly stratified. The acoustic impedance mismatches between the various layers or bodies of water are enough to create a sonar reflection. These images can look surprisingly like real geology so great care must be taken when interpreting images from these regions.

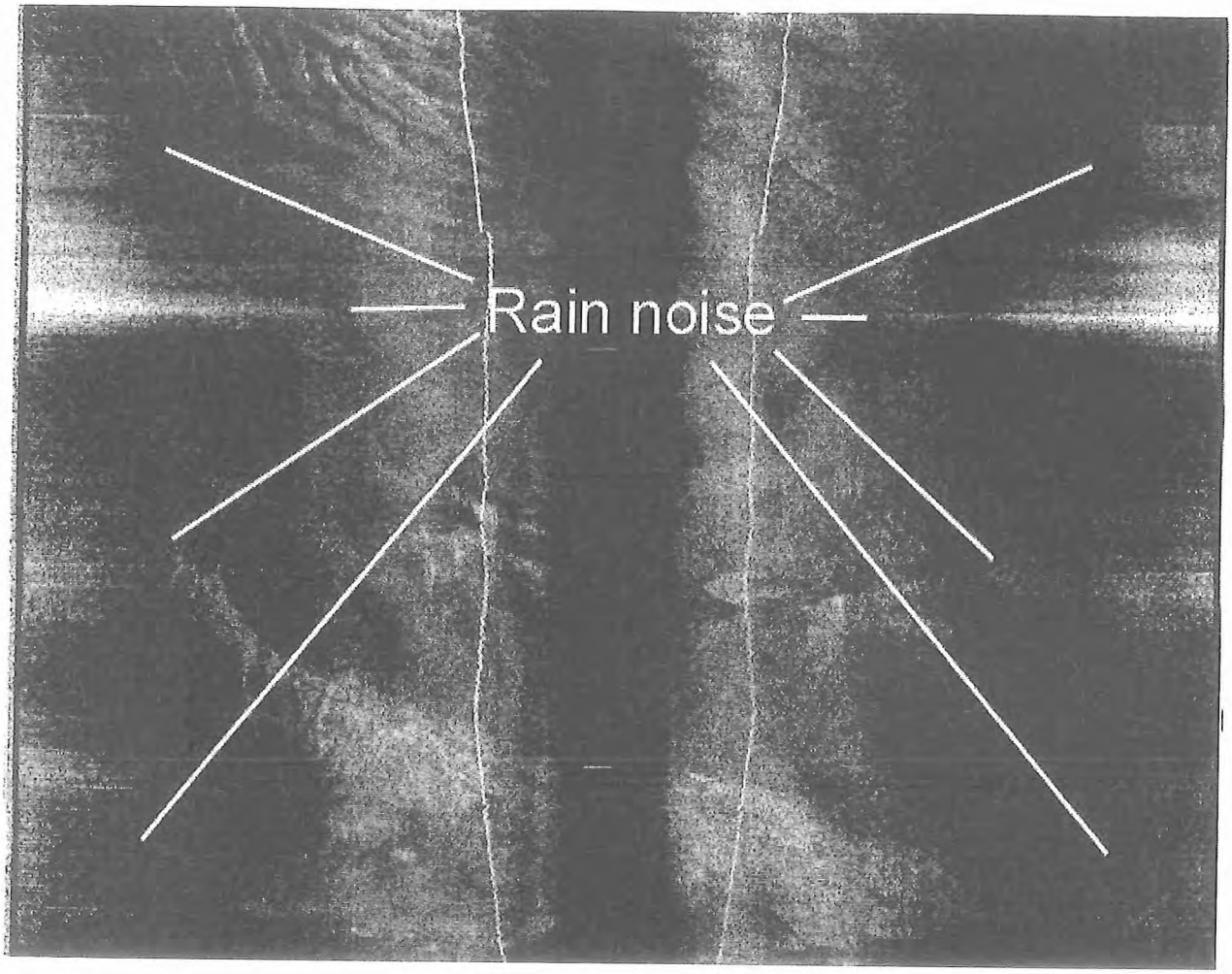


*Figure 6.2.5 Rain noise on the TOBI sidescan record.*

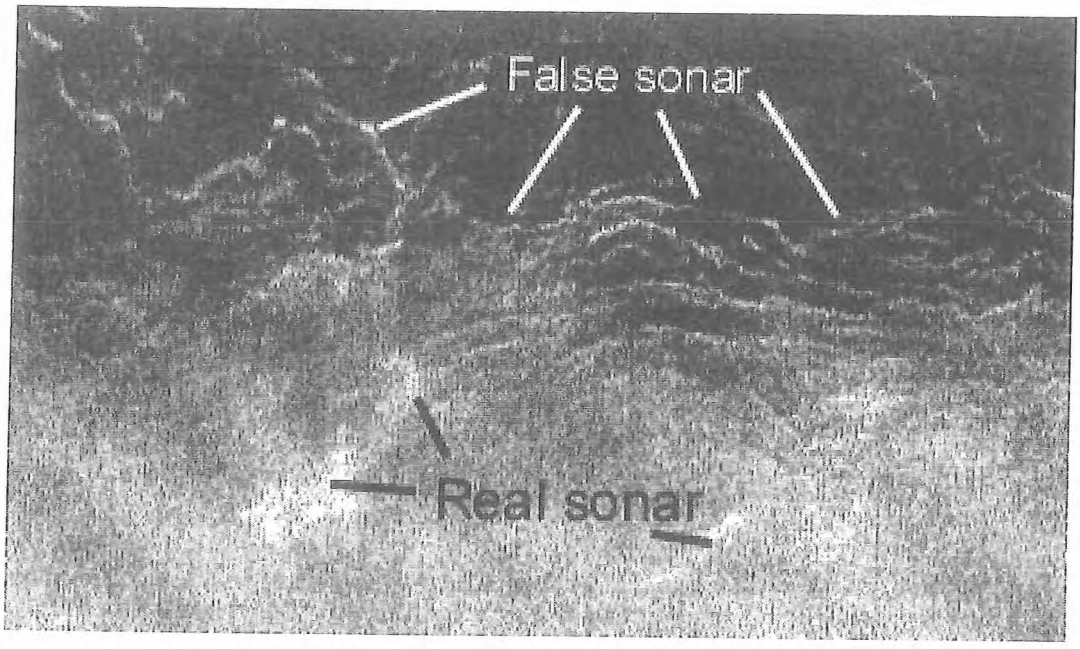


*Figure 6.2.6 False sonar echoes on the TOBI sidescan record.*

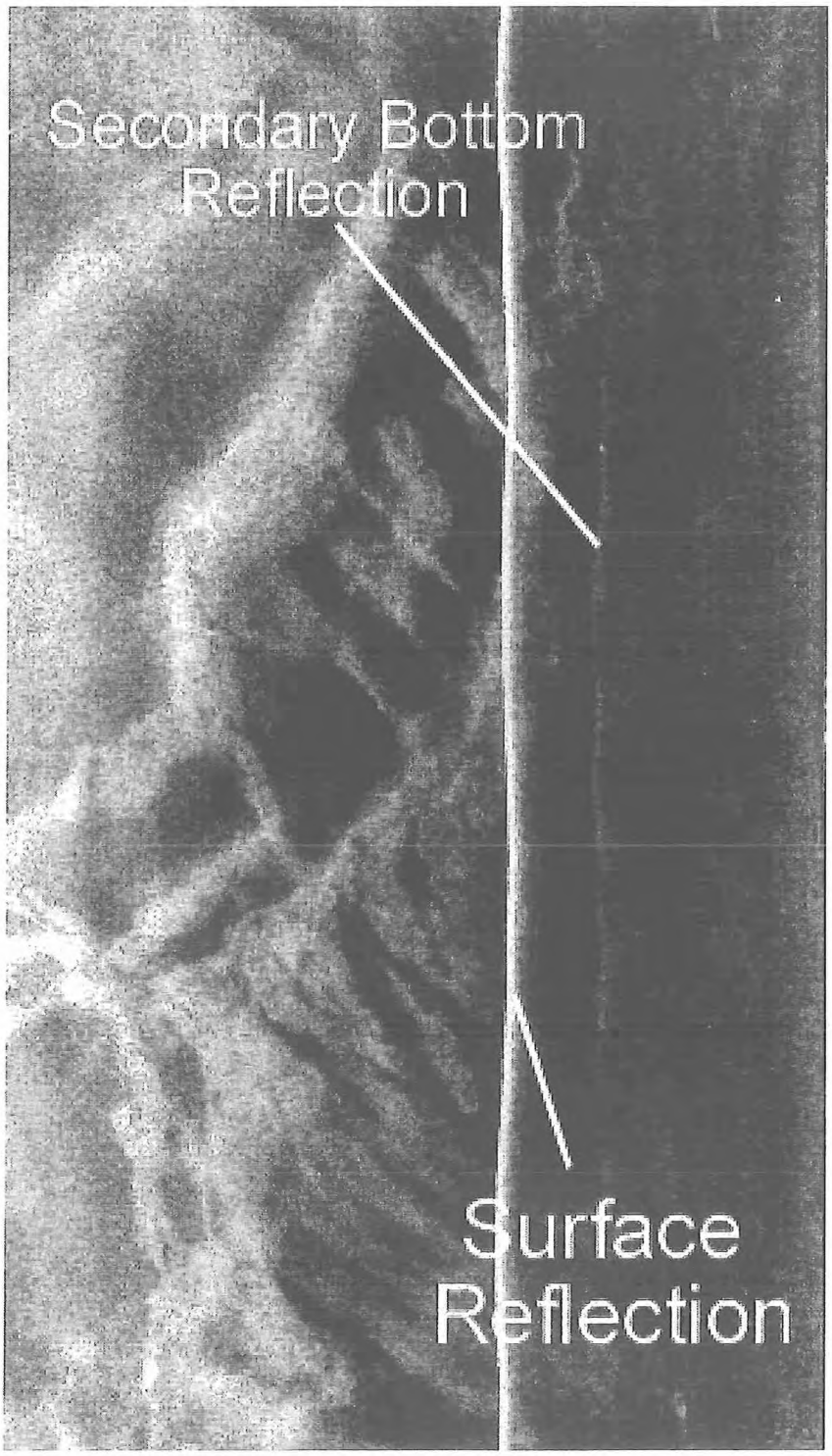


*Figure 6.2.7 Secondary bottom reflection on the TOBI sidescan record.*

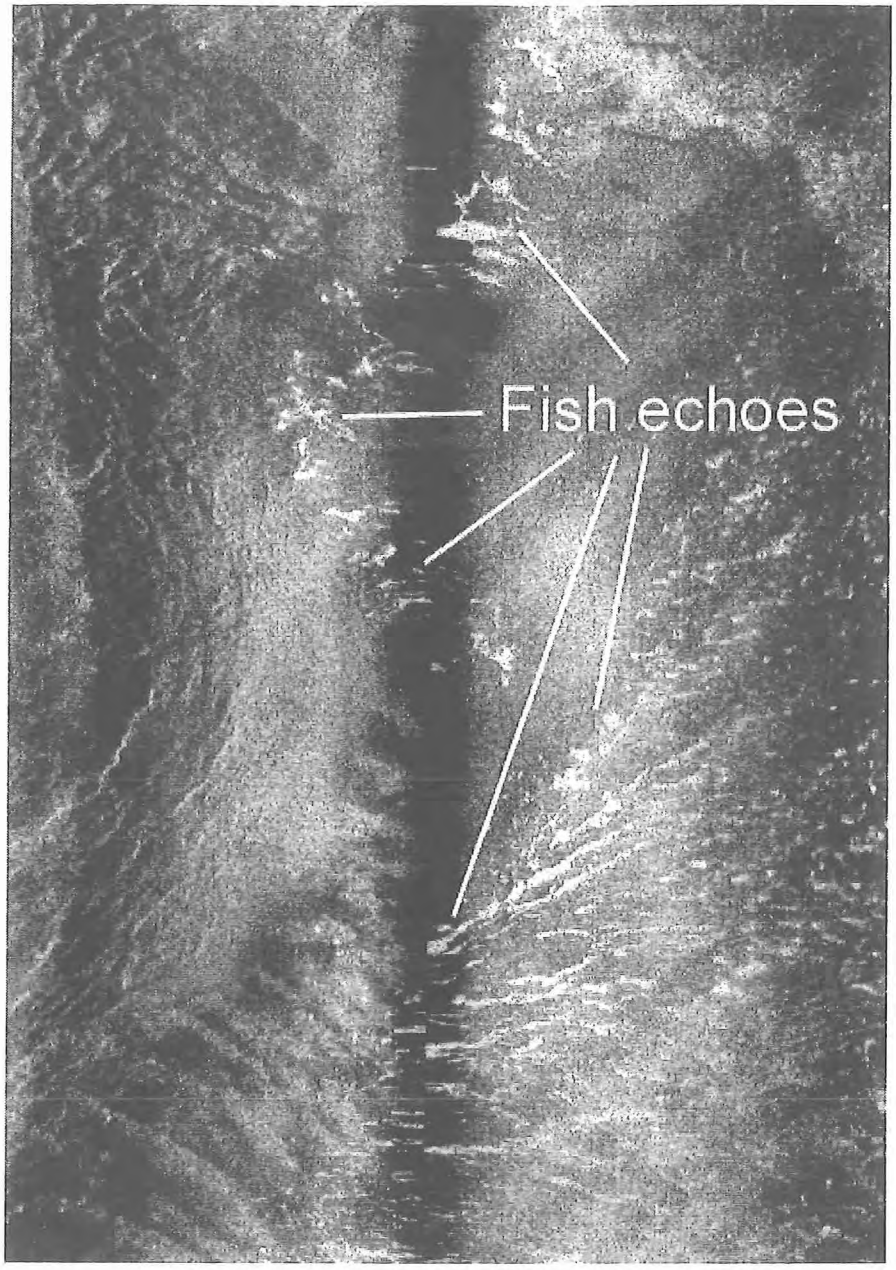


*Figure 6.2.8 Echoes from shoals of fish on the TOBI sidescan record.*

Secondary bottom (Fig 6.2.7) is where there is a strong reflector beneath the TOBI vehicle. Energy from the sonar is not only reflected back from the sea floor to the vehicle directly but also via the sea surface. This gives a second image of the sea floor at a distance of the water depth away from the original image. The secondary image is very weak compared to the direct image and is only seen over hard, rocky sea floor terrains. The secondary image disappears when the water depth exceeds 3 km due to the 4-second sweep rate of the TOBI vehicle.

Fish (Fig 6.2.8.) can generate sonar targets due to the air in their swim bladders. Shoals of fish can make quite large targets that can be imaged by TOBI. This was especially evident in one area where there seemed to be large shoals of fish over a shallow bottom during run 6.

### 6.2.2. Preliminary interpretation of TOBI sidescan sonar and profiler data

Two main areas were mapped with TOBI during Sonne 163. The first covered the middle and upper slope between 86° 06' and 86° 45' W and part of the middle slope between 85° 42' and 86° 06' W (Fig. 6.2.9). The main aim of this survey was to detect and characterise any mound –like structures or backscatter anomalies that could be related to fluid venting. The second area extends along the margin from 83° 15' to 84° 40' W. In the east, off the Osa Peninsula where the slope is very narrow, this survey covered the entire slope. Further west, it covered the middle and lower slope, including the deformation front at the base of the slope, with a limited area of coverage of the upper slope in the area of the Quepos landslide. The main aim of this survey was to examine the processes associated with the collision of seamounts and ridges, for example the Quepos plateau and a series of unnamed ridges on the Cocos plate, with the margin. As with the more western area, we also hoped to detect features associated with fluid venting.

<u>The Costa Rican margin between 85° 42' and 86° 45' W (the 'western' TOBI survey area)</u>

The main features seen on the TOBI images from this area include:

(i) extensive submarine canyons
(ii) seafloor mounds up to 1 km across and 100 m high
(iii) complex patterns of faults which offset the present day seafloor
(iv) erosional scars related to seamount and ridge subduction

*Submarine canyons*
Submarine canyons are the dominant seafloor feature along the entire upper slope area imaged with TOBI, between 86° 07' and 86° 45' W (Fig. 6.2.10). Typically they extend from the shelf edge to about 2500 m water depth, but die out further downslope. On the sidescan images, individual canyons have a typical 'fish bone' appearance, with the canyon floor imaged as a narrow, high-backscatter stripe and the canyon walls characterised by closely-spaced gullies which trend almost perpendicular to the main canyon axis (Fig. 6.2.10). Overall, the larger canyons tend to coalesce downslope in a dendritic pattern, so that only a few large canyons reach the middle slope at 2000 to 2500 m water depth. TOBI profile data confirm that the canyons usually have a maximum depth of <100 m (Fig. 6.2.11).

*Seafloor mounds*
A large number of seafloor mounds were identified using a combination of TOBI sidescan sonar images and Simrad EM120 bathymetry maps. Mounds are circular to elongate features a few hundred metres to 1 km in diameter and a few tens of metres high. On the sidescan images, mound relief is often severe enough to produce a clear shadow behind each mound (Fig. 6.2.12). Many mounds are characterised by high to very high backscatter, which may cover all or part of the mound (for further detailed mound images see section 6.4). The mound summits are often marked by small-scale rough topography, which can only just be resolved by the TOBI sidescan. Mounds often occur in groups. A series of OFOS transects across mounds established that, in general, the high backscatter corresponds to areas of carbonate or rocks outcropping at the seabed. Lower backscatter areas on the mounds are usually sediment covered. For further images and discussion of the mounds, see section 6.4.

*Faults*
Faults appear on the TOBI sidescan sonar images as distinct linear targets or shadows, dependent on whether they downthrow towards or away from the sonar (Fig. 6.2.13). Individual faults can rarely be traced for more than a few km, although zones of faulting can be traced for 10 km or more. Most faults are sub-parallel to the regional contours, except in the vicinity of seamount subduction scarps where more arcuate fault zones can occur (see below). Faults outcropping at the seabed are particularly common on the middle part of the slope in 2000 to 2500 m water depth. On the upper to mid-slope, faults predominantly downthrow in an upslope direction (Fig. 6.2.13). On the steeper lower slope, however, large faults which downthrow downslope become more common.

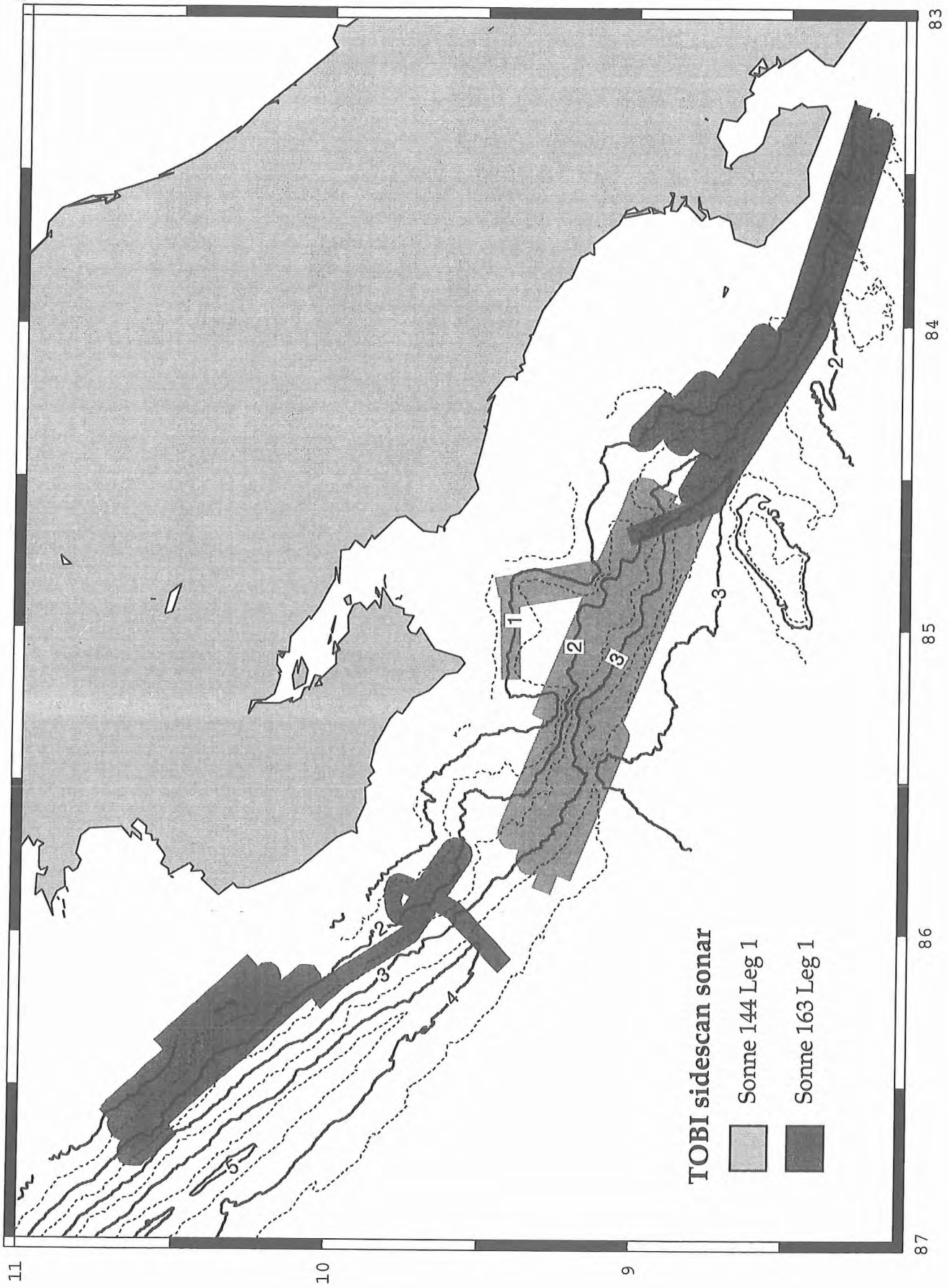


*Figure 6.2.9 Map showing TOBI sidescan coverage obtained during S0 144 and 163. Contour interval 500 m.*

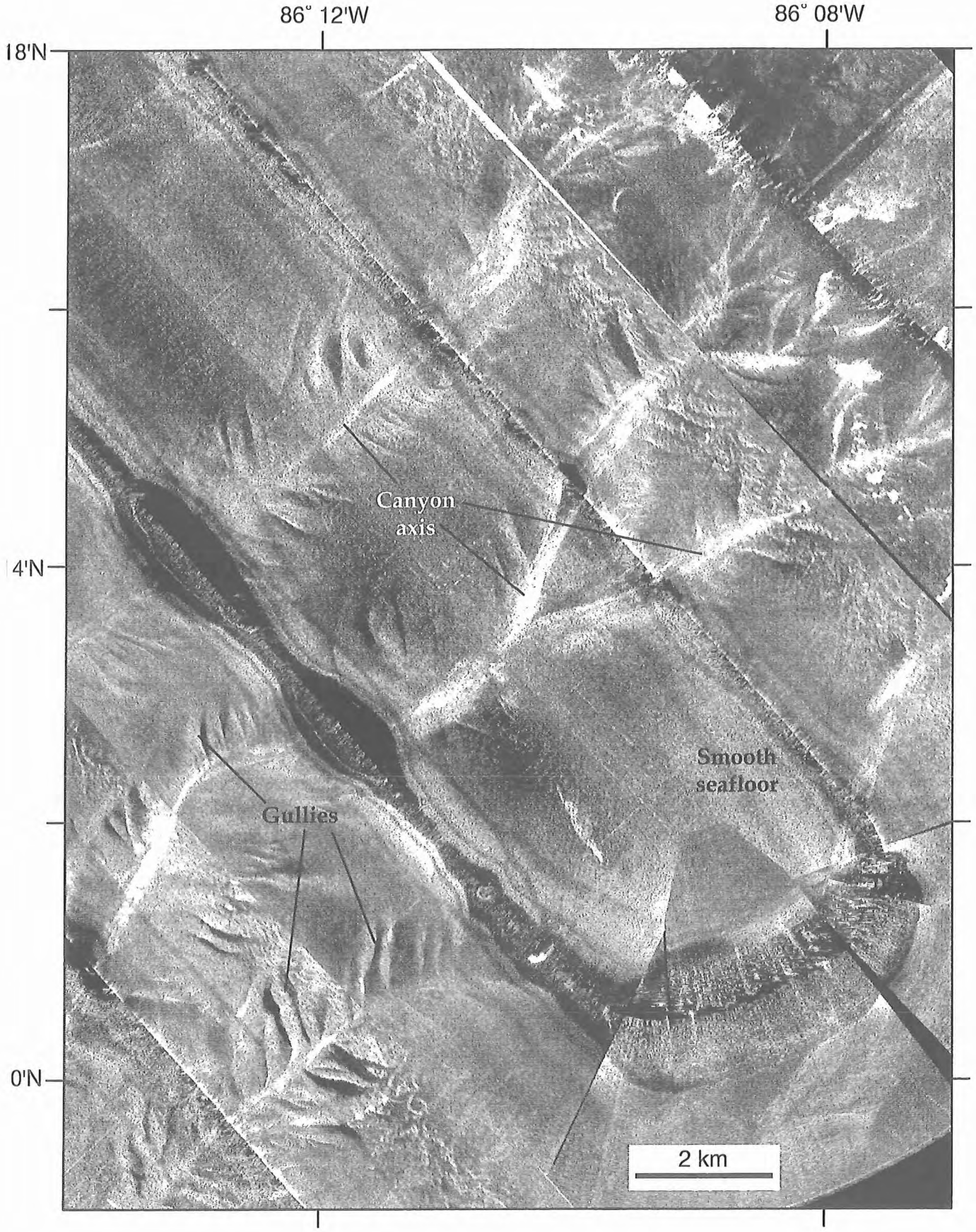


*Figure 6.2.10 Sidescan sonar image of a dendritic canyon system in the western part of the survey area. Canyon axis are imaged a high backscatter stripes (white). Note the 'fish bone' pattern of the gullies on the walls of each canyon.*

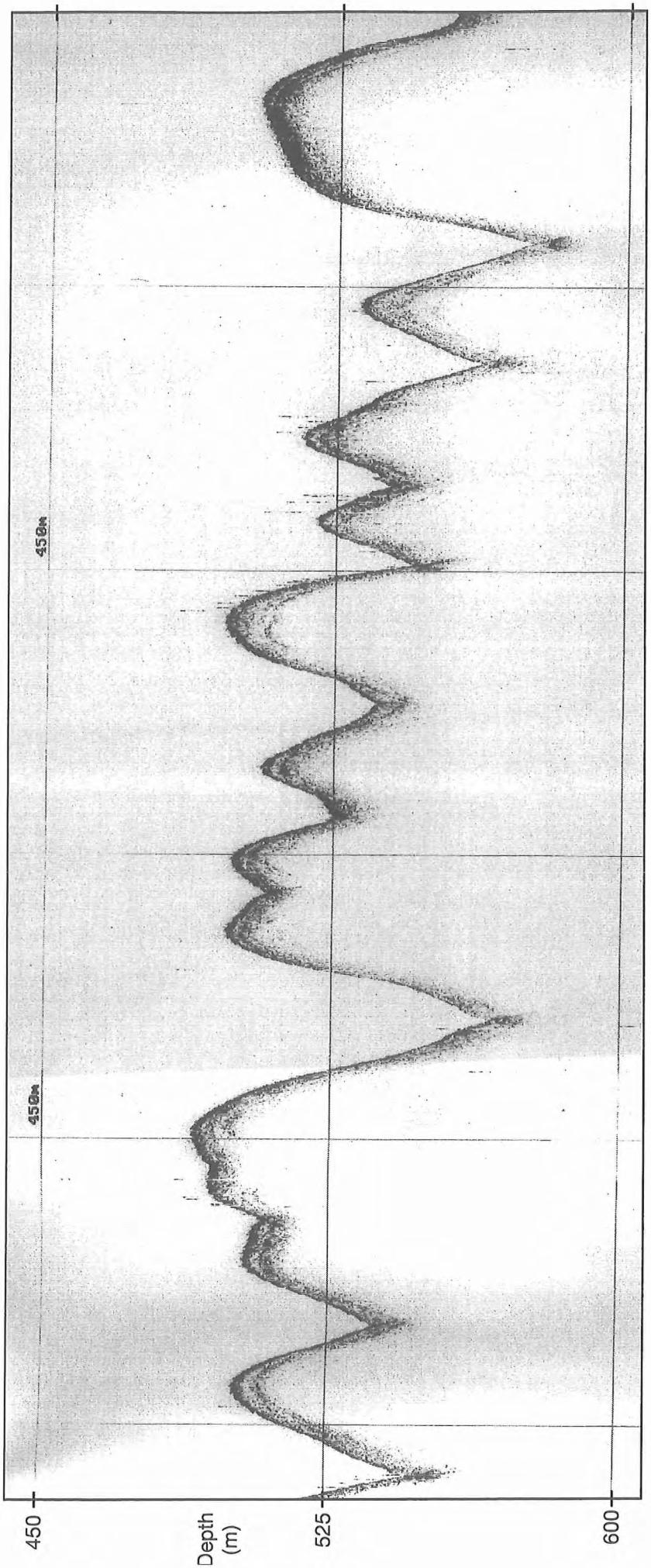
450
Depth
(m)
525
600
450m
450m

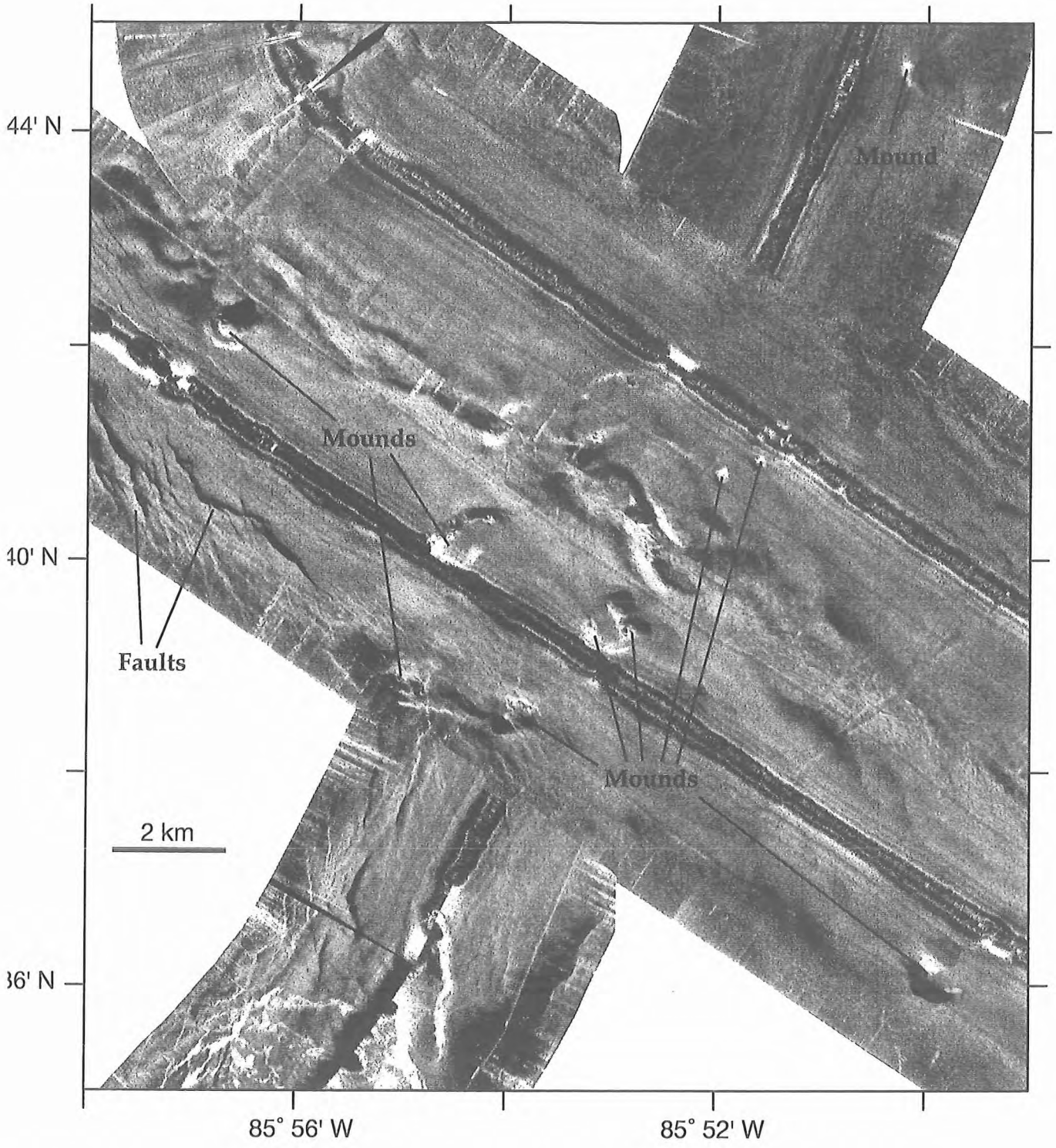


*Figure 6.2.12 Sidescan sonar image of mounds in the western part of the survey area. For further detailed images of mounds see section 6.4.*

*Figure 6.2.11 (previous page): TOBI 7 kHz profile across the canyons on the upper slope in the western n part of the survey area. Maximum canyon depth is this area is usually less than 100 m. Some sediment deposition can be seen on the interfluves between canyons.*

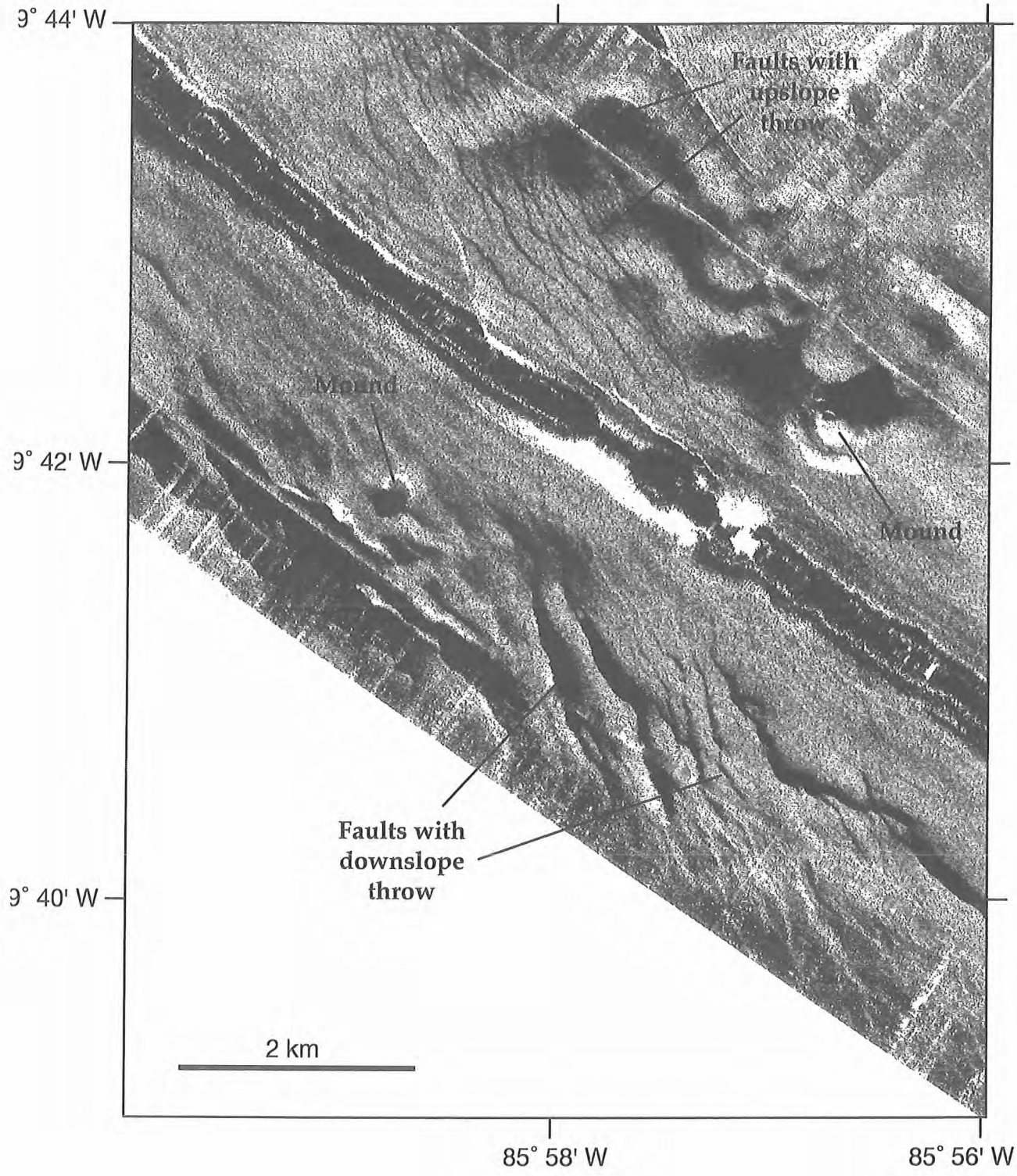


*Figure 6.2.13 Sidescan sonar image showing the complexity of fault systems that are developed on some parts of the slope.*

*Seamount and ridge subduction*

In the western survey area, a single example of an erosional scar related to seamount subduction was imaged (in part only) in the extreme northwest part of the area surveyed with TOBI. Toward the southeast limit of the western area, a single large oceanic basement ridge is subducted beneath the margin (Fig. 6.2.14). On the upper plate, the scar in the upper plate extends some 15 km landward of the deformation front. The material that partially fills the scar appears severely deformed, and probably consists largely of landslide debris. The headwall of the scar is marked by a pronounced scarp and several large arcuate faults

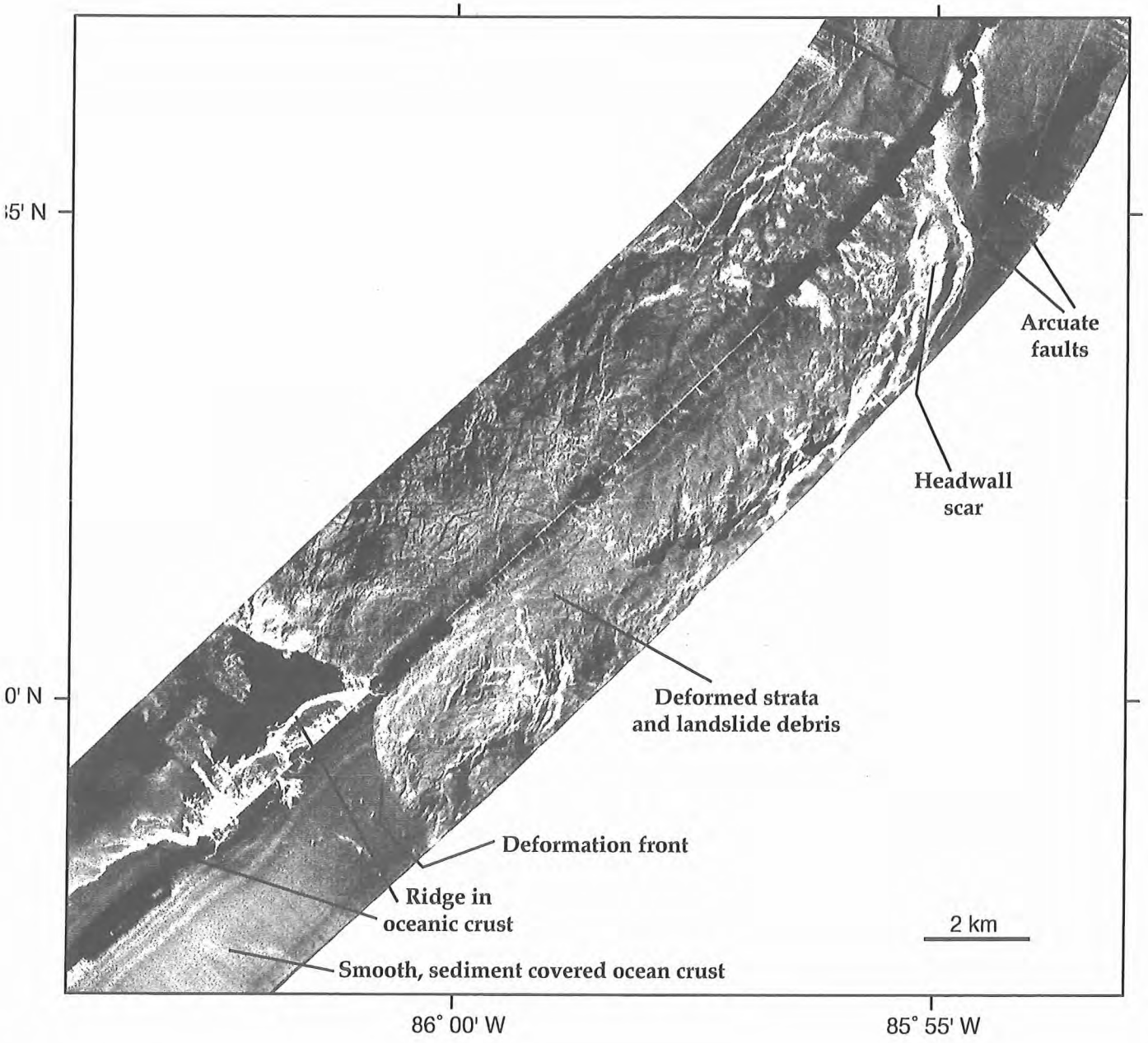


*Figure 6.2.14 Sidescan sonar image showing an area where an oceanic basement ridge is being subducted.*

The Costa Rican margin between 83° 15' and 84° 40' W

The main features seen on the TOBI images from this area include:

(i) the deformation front between the subducting oceanic plate and the overriding continental margin
(ii) several ridges and seamounts at various stages of subduction
(iii) submarine canyons
(iv) a variety of landslides
(v) seafloor mounds

*The deformation front*

The deformation front, marking the outcrop of the plate boundary at the seabed, was imaged between 83° 20' and 84° 37' W. Except where it is affected by subducting seamounts and ridges, it forms a gently lobate feature separating smooth sediment covered ocean crust to the southwest from faulted and folded continental margin strata to the northeast (Fig. 6.2.15). On the basis of the sidescan imagery, we would suggest that very little sediment accretion occurs along this deformation front. Where accretion is suggested by the margin morphology, the accretionary wedge is rarely more than a few hundred metres wide (Fig. 6.2.15). The trend of normal faults in the ocean crust, which is slightly oblique to the deformation front, can be seen to extend into the overriding plate in several places, indicating that the subduction of 'steps' in the ocean crust can significantly modify the deformation front. There is some suggestion that accretion may occur primarily in the wake of such subducting steps, as the deformation front seeks to establish a new equilibrium profile. There is little evidence of significant sediment accumulation in the trench, with the exception of a few flat basins of limited extent that show low backscatter on the sidescan images; these are interpreted as ponded turbidites.

*Seamounts and ridges*

The deformation front is indented by several subducted seamounts and ridges of oceanic crust (Figs. 6.2.16, 6.2.17, 6.2.18). A small seamount that was been subducted at 83° 56'W is currently interpreted, on the basis of an uplift in the margin topography, to lie some 6 km landward of the deformation front (Fig. 6.2.16). Seaward of the uplift, a very steep scarp, generated by collapse of the uplift and landsliding as the support of the seamount progresses landward, is partially filled with debris avalanche material. The uplift itself is intensely fractured by arcuate faults, most of which throw downslope. This faulting extends well to the east of the scar cut by the seamount, and this, added to a second indentation of the deformation front at 83° 54' W, suggests that a second seamount may also have been subducted there (Fig. 6.2.16.). Between 83°43' and 83° 48' W, three circular seamounts, each 2-3 km across at the base, are currently positioned adjacent to the deformation front (Fig. 6.2.17). One, at 83° 47' W, has just started to indent the deformation front; here, using OFOS, a small landslide scar was observed on the oversteepened slope. The other two seamounts have not yet collided with the margin, but they are of interest because of the unusual circular patterns which characterise their surfaces. Subducting ridges, such as that seen at 83° 42' W, create a high level of deformation in the overriding plate (Fig. 6.2.18). They drive deep re-entrants into the deformation front; these may migrate along the margin where the ridge is not exactly parallel to the convergence direction. Large fields of debris may be found at the base of slope and on the ocean plate where collapse of the oversteepened margin occurs as a result of ridge subduction (Fig. 6.2.18).

*Submarine canyons*

Submarine canyons occur in limited areas of the western part of the eastern survey area, where the slope is less steep than to the east. In contrast to the western area, canyons tend to be short, straight features of very limits length; dendritic systems are not seen (Fig. 6.2.19).

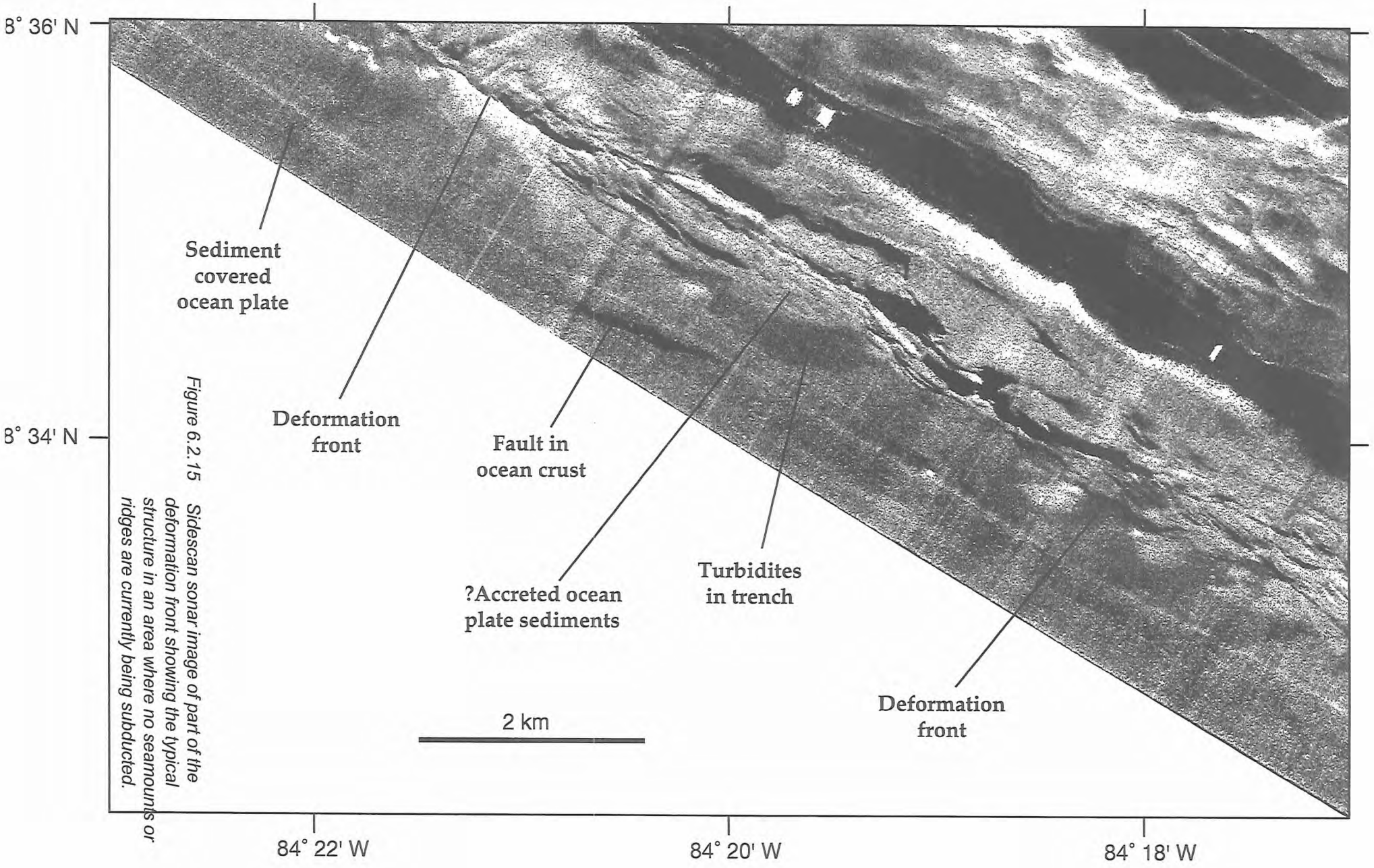


*Figure 6.2.15 Sidescan sonar image of part of the deformation front showing the typical structure in an area where no seamounts or ridges are currently being subducted.*

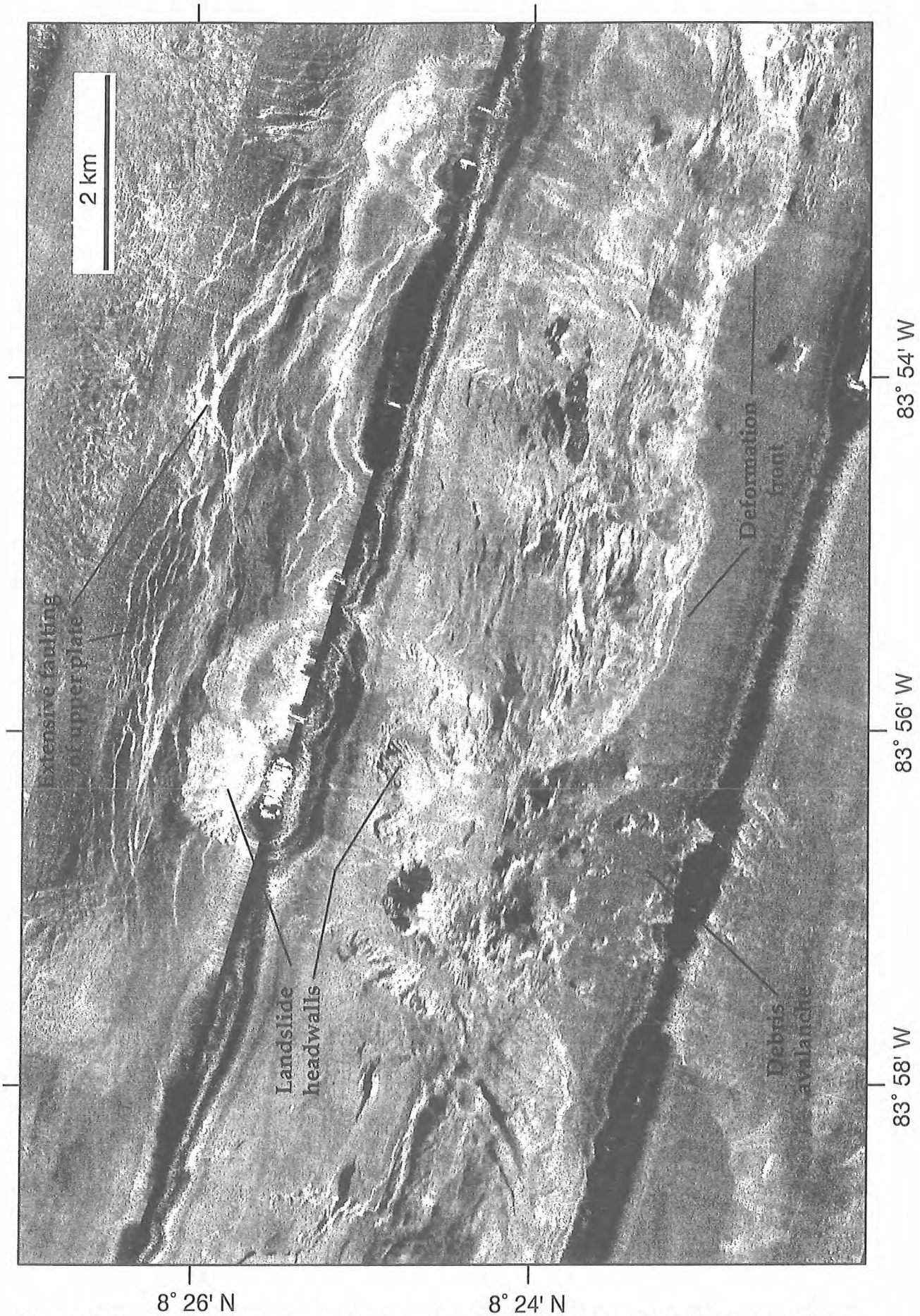


*Figure 6.2.16* *Sidescan sonar image showing an area where one (or possibly two) seamounts have been subducted. One scar, at 83° 56' W, is clearly defined by uplift and faulting of the upper plate above a scar cut through the plate by the seamount subduction process. A re-entrant is seen in the deformation front, and a large field of debris, derived from collapse of the steep headwall of the scar, covers the adjacent ocean plate. A second possible scar, at 83° 54' W, is marked by a small re-entrant and uplift and faulting of the upper plate, but*

*Figure 6.2.17 Sidescan sonar image showing three seamounts, defined by very high backscatter (white) which currently lie at or are approaching the deformation front.*

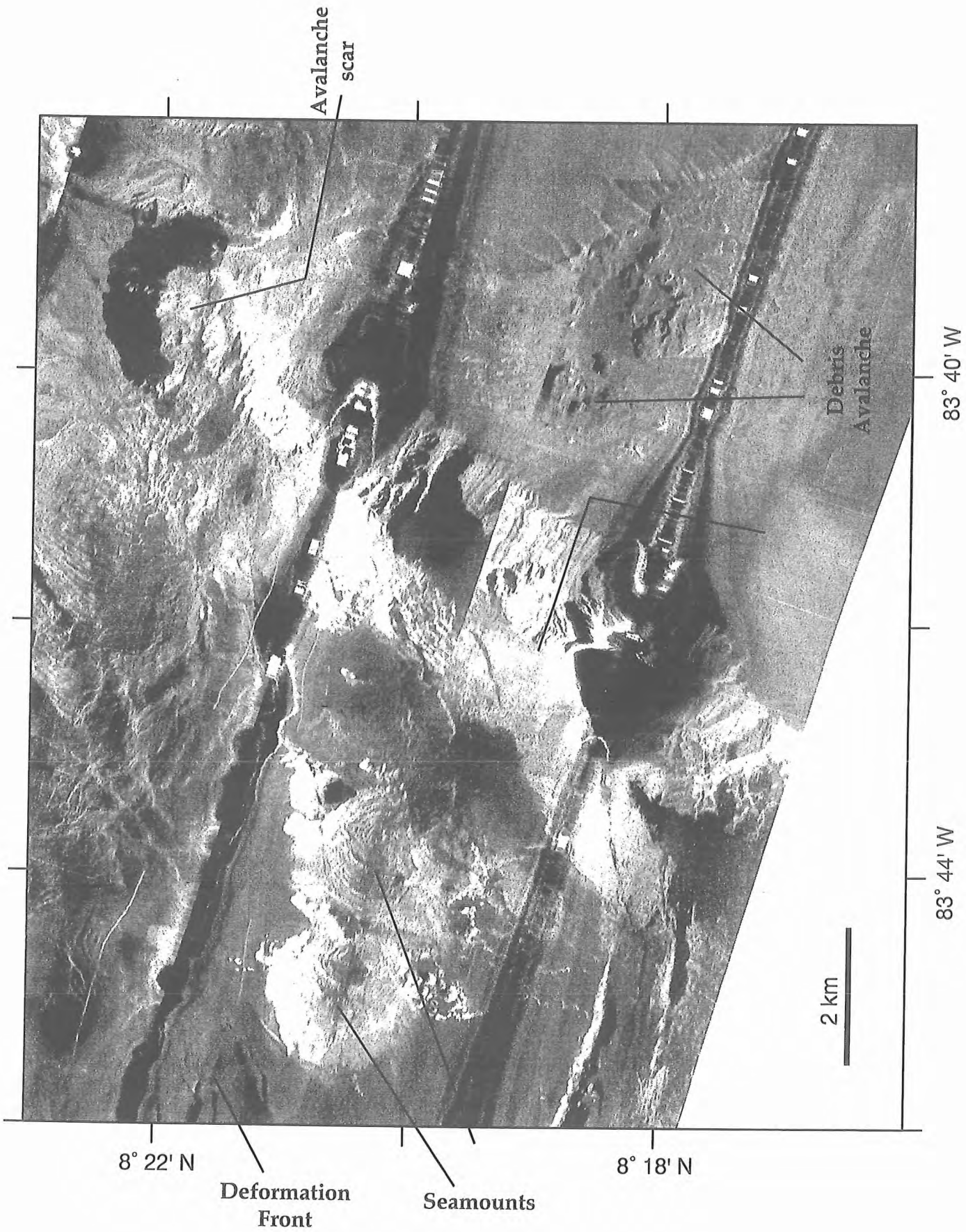


*Figure 6.2.18* *(above) Sidescan sonar image showing a large subducting ridge which indents the margin. Note the large field of debris derived from collapse of the oversteepened margin.*

*Figure 6.2.19* *(next page) Sidescan sonar image of the typical submarine canyon morphology found in the eastern survey area.*

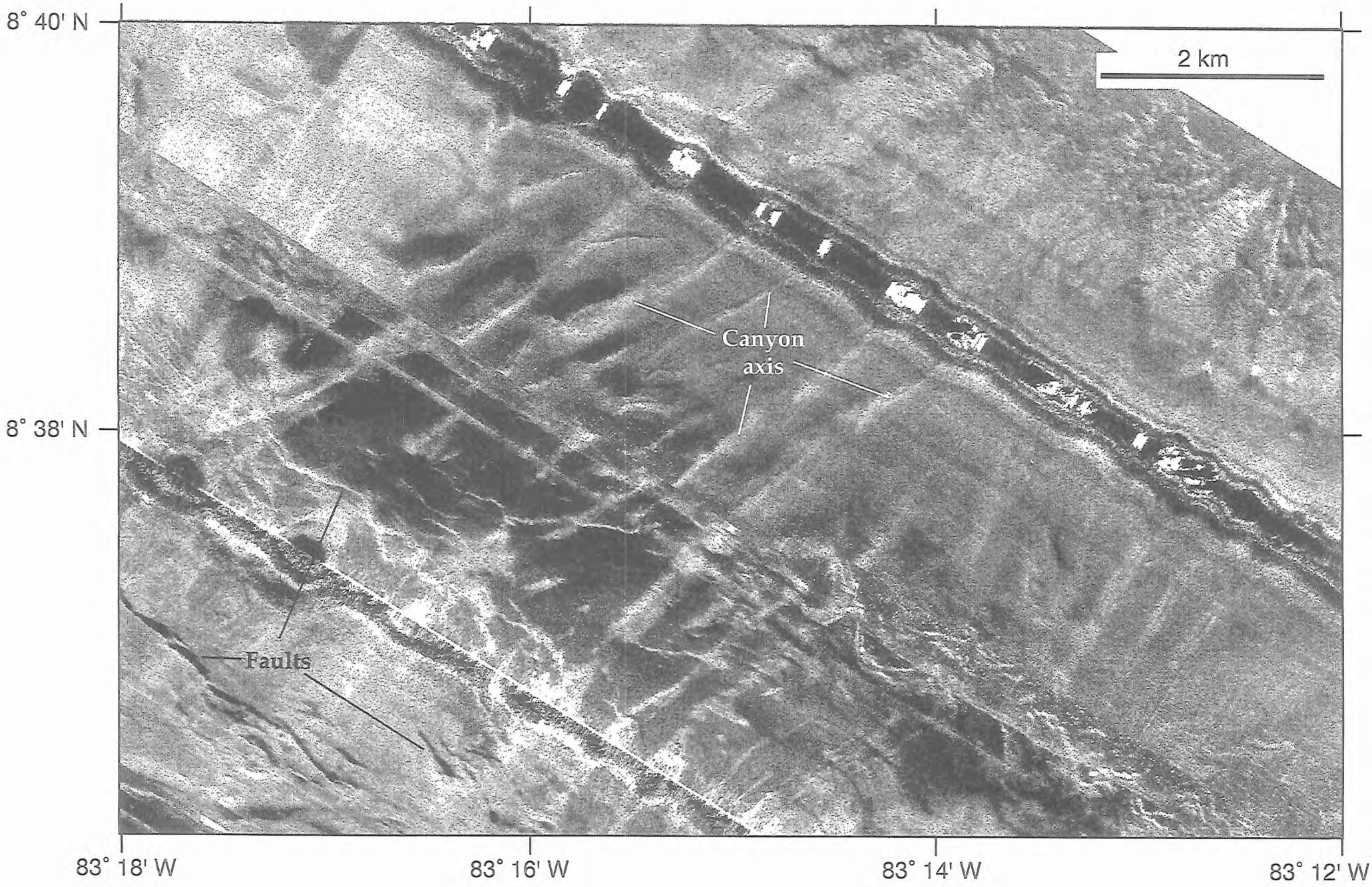
8° 40' N
8° 38' N
2 km
Canyon
axis
Faults
83° 18' W
83° 16' W
83° 14' W
83° 12' W

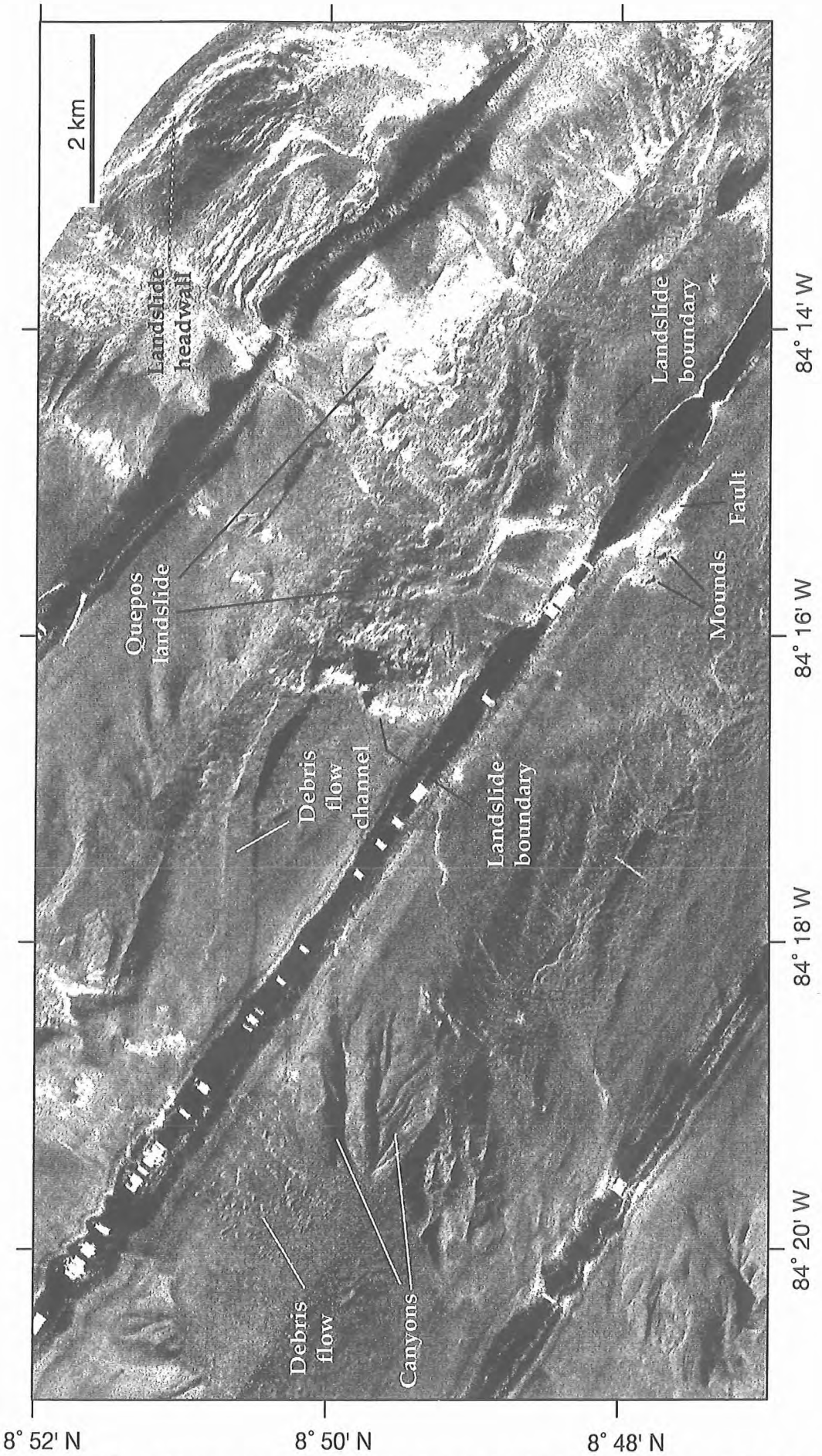


*Figure 6.2.20 Sidescan sonar image of the Quepos landslide. The blocky and ridged topography suggests that slumping was the main process involved, with little disaggregation of the landslide material. Note the secondary debris flow channel and accumulation of debris to the west of the main landslide.*


*Figure 6.2.21 Sidescan sonar image of a linear group of mounds in the eastern survey area.*

*Landslides*

A variety of landslide processes were observed in this area. As noted above, debris avalanches have occurred at several sites of seamount and ridge subduction (Figs. 6.2.16, 6.2.18). These contain angular blocks up to several hundred metres across. Near 8° 50' N, 83° 14' W, the Quepos landslide affects an area of some 8 x 4 km (Fig. 6.2.20). The morphology of this landslide suggests a slump and perhaps partial debris flow process. Immediately west of Quepos landslide, a broad, flat-floored channel or chute leads down to a accumulation of debris which fills a deeper valley. This is interpreted as a secondary debris flow triggered by the Quepos landslide.

*Seafloor mounds*

Mounds were less commonly observed in the eastern areas than either in the western area surveyed during Sonne 163 or the central area surveyed during Sonne 144 (see Fig. 6.2.9). A single group of four mounds, forming a linear chain, was discovered near 8° 56' N, 84°18' W. This suggests that they are fault controlled. OFOS observations suggest that these were among the most active mounds examined in the area.

## 6.3 DTS1 operation and initial data interpretation

(C. Huguen, I. Klaucke)

Deep-towed side scan sonar deployments have been conducted during SO163-1 within the framework of subproject A1 of SFB 574. Subproject A1 is dedicated to continental margins processes and related changes in seafloor morphology. The EDGE-Tech DTS1 was deployed in the Central America subduction zone, offshore Costa Rica, to provide detailed surface (75 and 410 kHz side scan sonar) and subsurface (sub-bottom profiler) imaging of the continental slope. This deep-towed system has unfortunately not been operated in deep waters (oceanic plate) due to the length of the cable available on R/V SONNE. As a result, the survey areas focused on the continental slope (Fig. 6.3.1). They were chosen to assess a better understanding of both mud and fluid expulsions (DTS1-01, DTS1-02 and DTS1-05), as well as fault patterns and destabilisations related to seamount subduction (DTS1-03 and DTS1-04).

The GEOMAR deep-towed side scan sonar DTS1 has been successfully deployed five times during SO163-1 (Fig. 6.3.1), providing a total of **550** km of low frequency side scan sonar (75 kHz) and **25.9** km of high frequency (410 kHz) records. Both were run together with a 2-16 kHz sub-bottom profiler for **575.9** km of high resolution seismic records. Details about the deployments are available on table 6.3.1.

| Deploy-ment | Average water depth | Track length | Mapped area | Time on sea-floor | Deployment | Recovering | Total |
|---|---|---|---|---|---|---|---|
| 1 | 1300-2400 | 141.0 km | 162.2 km² | 37 h | 1 h 40 | 2 h | 40 h 40 |
| 2 | 2500-3200 | 134.0 km | 145.0 km² | 44 h | 2 h 30 | 2 h 50 | 49 h 20 |
| 3 | 400-1900 | 172.4 km | 175.2 km² | 44 h | 35 min | 2h | 46 h 30 |
| 4 | 900-2000 | 120.4 km | 161.0 km² | 30 h | 2 h | 2 h | 34 h |
| 5 | 1300-1500 | 9.0 km | 1.8 km² | 2h | 55 min | 1h 05 | 4h |

The *POSIDONIA* positioning system, installed on R/V SONNE during SO162 (*see 5.5*) was used to follow the position of the tow fish during deployments and to provide an accurate positioning on the sea floor. All data collected have been recorded by both *Hydrostar Online* (xse format) and the FS-DW unit directly (jsf format). Two backups of the xse files and one of the jsf were made on CD-ROM for the five deployments.

### 6.3.1 Deployment 1 (DTS1-01)

The first deployment of DTS1 during SO163 was conducted between 26.03.02, 6h16 and 27.03.02, 19h10, on an area of the continental slope, NW of Nicoya peninsula (Fig. 6.3.1). Here, small mound-like, circular features have been identified and initially interpreted as probable mud domes based on the multibeam bathymetry data (see 6.1.1) and the first TOBI deployment during SO163-1, which illustrates clear evidences of high backscatter patches (Fig. 6.3.2). During deployment 1 of DTS, 7 NW-SE trending parallel profiles have been run with a 1100 m track-spacing (Fig. 6.3.3), using the 75 kHz side scan sonar and the sub-bottom profiler. 162.2 km2 of the sea surface have been mapped and 141 km of high resolution sub-bottom profiler data recorded over several of the inferred mud domes. A cross-cutting 10.4 km long track has been run with the high resolution (410 kHz) side scan sonar, along an E-W direction, over a small circular mud dome, located at 9°36 N - 85°49 W.

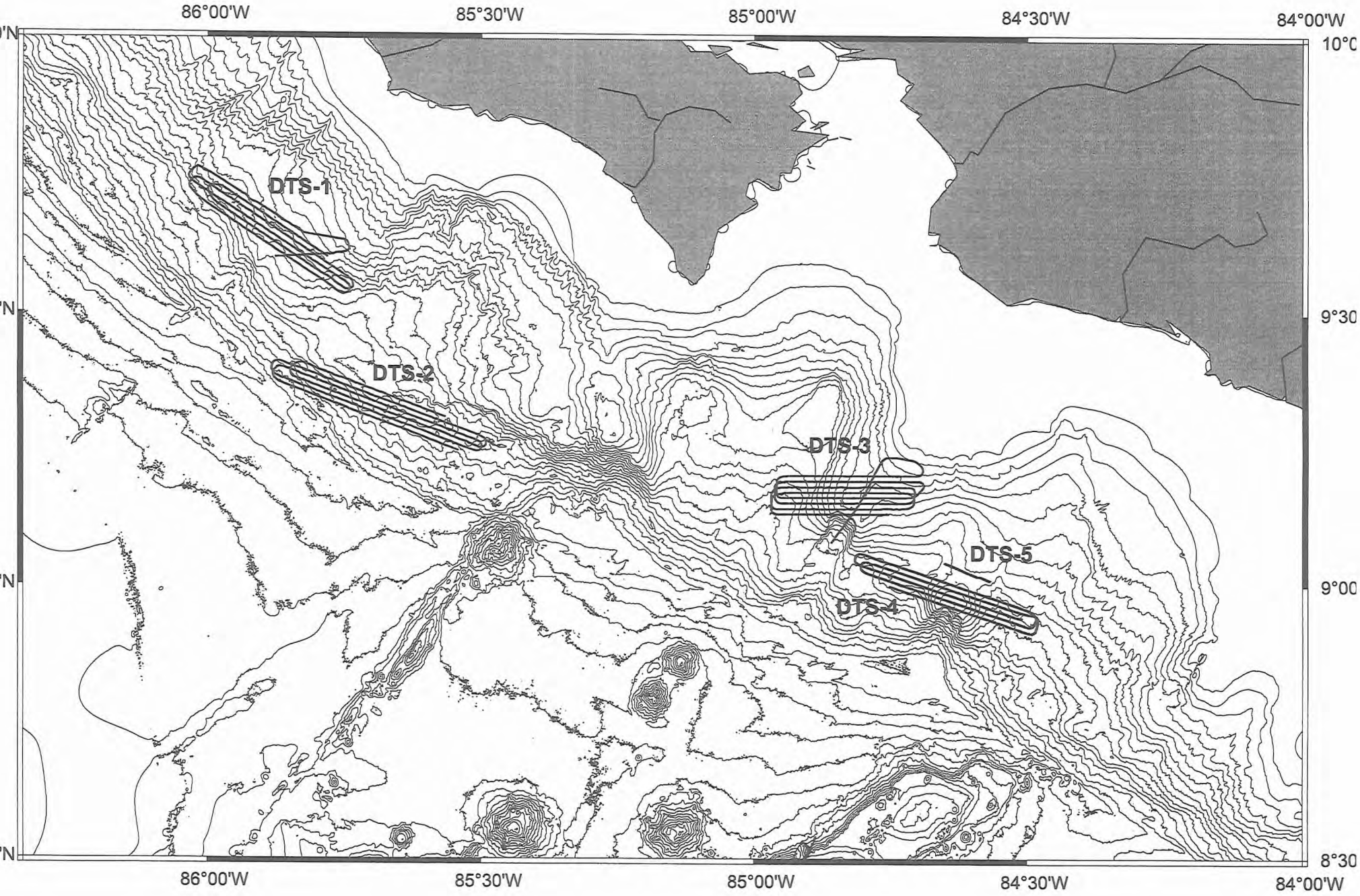


Figure 6.2.1. Map showing the ship's tracks for the five SO163-1 DTS deployments on a 100 m

During deployment 1 the range of the 75 kHz side scan sonar was set to 1500 m (0.49 Hz ping rate) and the data window size fixed to 26000 samples. The data window for the 2-10 kHz sub-bottom profiler, with its ping rate coupled to the 75 kHz side scan sonar, was set to 6000 samples, which corresponds to an average depth window of 250 m. For the last high resolution side scan sonar profile, the recording window size of the 410 kHz side scan sonar was fixed to 16000 samples corresponding to 100 m per side. The survey speed varied around 3.5 knots during all deployment. It was slightly increased during the turns (4.5 to 5 knots), in order to reduce them to less than 3 hours. During turns, enough cable was pulled in to keep the towed fish at a safe distance from the sea bottom.

Special remarks for deployment 1

1 - All signals were lost on *Hydrostar Online* for a few minutes between 12h58 and 13h16, on 26.03.02, and the winch stopped for safety reasons, while waiting for the signals to return.
2 - No response from the *Posidonia* fish transponder for more than 20 minutes between 13h17 and 14h39 on 26.03.02.
3 - Shortly after that, problems have been observed to find again the connection between Posidonia and the *DTS* acquisition system.
4 - *DVS* export data were not recorded between 15h55 and 19h54.
5 - *DTS* was crashed on a small mud mound, while using the high resolution side scan sonar (27.03.02, 19h05). The *DTS* frontal protection was slightly damaged during this crash, but the sensors were not affected.
6 - After recovering, the *DTS* titanium ring between the fish releaser and the umbilical cable (+ buoyant and pull in ropes) was broken. For the following deployments it has been replaced by a larger one for safer recovery.

### 6.3.2 Deployment 2 (DTS1-02)

The second DTS deployment during SO163-1 focused on an area downslope of the headwall of the prominent Nicoya slide (Fig. 6.3.1), where TOBI data recorded during SO 144-1 revealed scattered high reflectivity patches of yet unknown origin (Fig. 6.3.4).
This deployment lasted from 31.03.02, 10h34 to 02.04.02, 11h49. It consists of 6 WNW-ESE parallel lines (Fig. 6.3.5) along which the low resolution side scan sonar (75 kHz) and the sub-bottom profiler were run together, for a total length of 134 km and a 145 km2 surveyed area. As during deployment 1, the range of the 75 kHz side scan sonar and sub-bottom profiler, was set to 1500 m (data window size 26000 samples) and 250 m (6000 samples), respectively. The ship's speed was kept at 3.5 knots and reduced to less than 3 knots when reaching 3000 m of water depth, in order to reduce the cable length and keep the tow fish within range of the sea-floor.

Special remarks for deployment 2

1 - The side scan sonar system worked properly during the whole deployment, except a 20 min break down on 02.04.03, between 22h32 and 22h53. The whole DTS acquisition system had to be restarted and the connection with *Posidonia* underwater navigation was lost after the restart of the DTS logging system.
2 - Two important *Posidonia* crashs also occured during this deployment. A first one on 31.03.02 between 18h24 and 20h16, after 1818 cycles, and a second one on 01.04.02, between 9h16 and 12h51. No real explanations have been found for both crashs. Communication problems between the ship's information (*DGPS, VHRU*) and the *Posidonia* system have been suspected. Moreover, both communications losses between the antenna and the fish's transponder occurred in water depths between 2500 and 3000 m and could be related to large cable length (more than 6000m).

*Figure 6.3.2: Positions of the first DTS deployment profiles superposed to TOBI imagery from SO163-1 (see 6.2).*

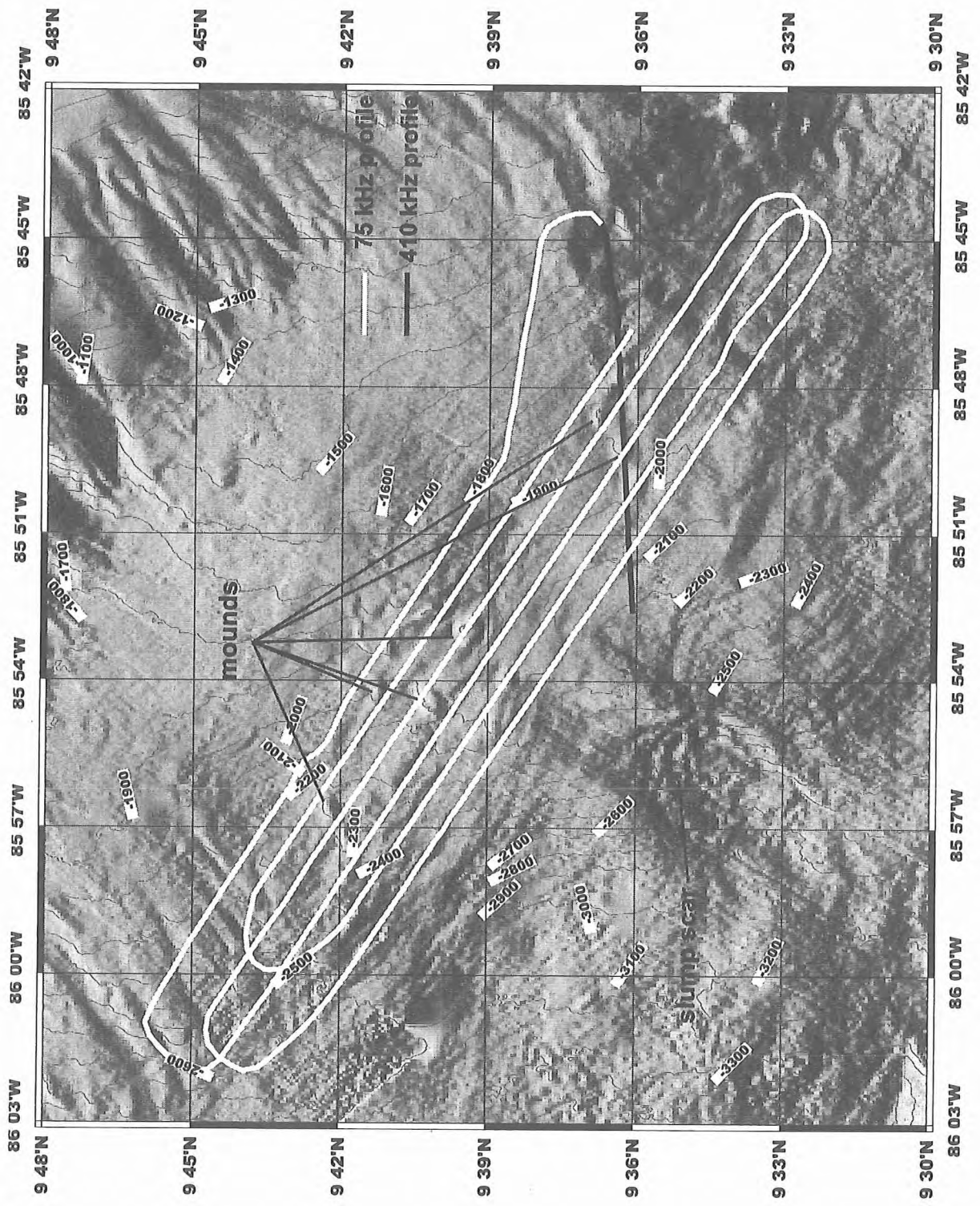


*Figure 6.3.3: Map showing the ship's tracks during the first DTS deployment (DTS1-01) on the continental slope NW of Nicoya Peninsula.*

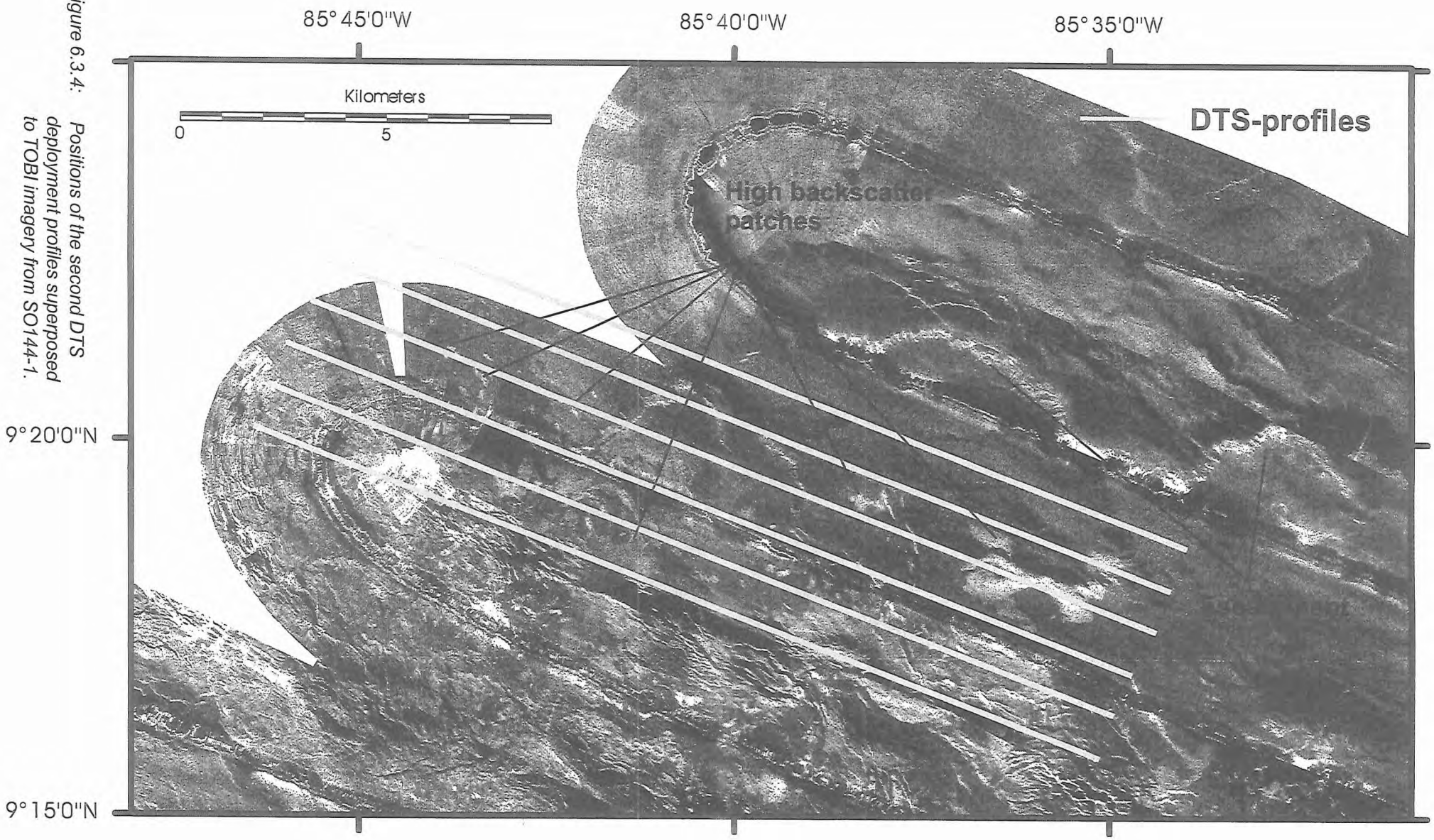


*Figure 6.3.4: Positions of the second DTS deployment profiles superposed to TOBI imagery from SO144-1.*

### 6.3.3 Deployment 3 (DTS1-03)

The third deployment of DTS1 was focused on the uplifted and faulted area upslope of Jaco Scar (Fig. 6.3.1) that was already surveyed with TOBI during SO144-1 (Fig. 6.3.6) and lasted for 46h30 between 03.04.02, 15h39 and 05.03.02, 13h54.
It consisted of 8 E-W trending parallel profiles upslope of Jaco Scar and a cross-cutting NE-SW profile ending at the base of Jaco escarpment (Fig. 6.3.7). A total of 44h of DTS records has been collected including 165.8 km of low resolution side scan sonar and sub-bottom profiler data covering 173.9 km2 of the seafloor. In addition, a 6.52 km long high resolution side scan sonar profile was run, covering 1.3 km2 of the seafloor . Starting with the same settings than for the two previous deployments the ranges have been switched to 750 m for the 75 kHz side scan sonar (0.98 Hz frequency) and 100 m for the high resolution side scan sonar from 05.04.02, 7h15 in order to optimise the along-track resolution. The ship speed was also held around 3.5 knots for most of the deployment and reduced to 2.8 knots during the high resolution profile for an improved along-track resolution.

Special remarks for deployment 3

1 - The contact with the sonar has been lost for 120 pings on 03.04.02, around 17h32 (no xse data recoded by *Hydrostar online)*.

2 - Strong noise due to a sports fishing boat closeby has been observed on the sub-bottom profiler at 21h02 on 04.04.02. The sub-bottom profiler signals were strongly disturbed during more than 15 min, but the same noise has not been observed on the side scan sonar records. The DTS side scan sonar and profiler records have also been disturbed with some noise generated from another boat on 05.04.02, around 4h18.

3 - The *Posidonia* positioning system worked well during deployment 3. No crash or loss of connection with the fish's transponder have been observed. This probably results from smaller water depth and cable length.

4 - The connection with the *FS-DW* data disks has been lost on 05.04.02, 5h48. The fish storage disks D and E remained still not visible after reboot of the *FS-DW* unit. As a consequence, jsf data were not recorded until the end of the deployment. The *DTS* data were only recorded in xse format on the *Hydrostar Online* computer. After recovery of the system both storage disks were checked and they both worked properly. Therefore a faulty connector has been suspected as the cause of the problem. The connection between *Hydrostar Online* and the *FS-DW* unit was checked with DTS1 on deck before deployment 4. Both storage disks were visible and the jsf files recorded properly on the hard disk.

### 6.3.4 Deployment 4 (DTS1-04)

The fourth deployment of the DTS1 side scan sonar during SO163-1 focused on the area upslope the Parrita scar, located SW of the Jaco scar investigated during deployment 3 (Fig. 6.3.1). TOBI records available from SO144-1 (Fig. 6.3.8) at the front of the Parrita seamount, showed both intense faulting and large highly reflective patches, generating a complex morphostructural pattern.
This deployment lasted from 15.04.02, 17h14 to 17.04.02, 00h42 and consisted of 5 WNW-ESE parallel lines. As for all other deployments track-spacing was 1100 m (Fig. 6.3.9). As during deployment 2 only the 75 kHz and the sub-bottom profiler (2-10 kHz) were used along a total distance of 120.4 km providing 161 km2 of total seafloor coverage. On the basis of the good quality data recorded during deployment 3 after the range modification, the same 750 m range (0.98 Hz frequency) has been been conserved for the 75 kHz side scan sonar during deployment 4. The ship speed averaged 3.5 knots during the whole deployment and had to be increased to 4.5 knots when crossing the major fault scarps, in order to maintain the fish at a safe distance from the seafloor. With some escarpments being over 700 m high, it proved important to keep cable length

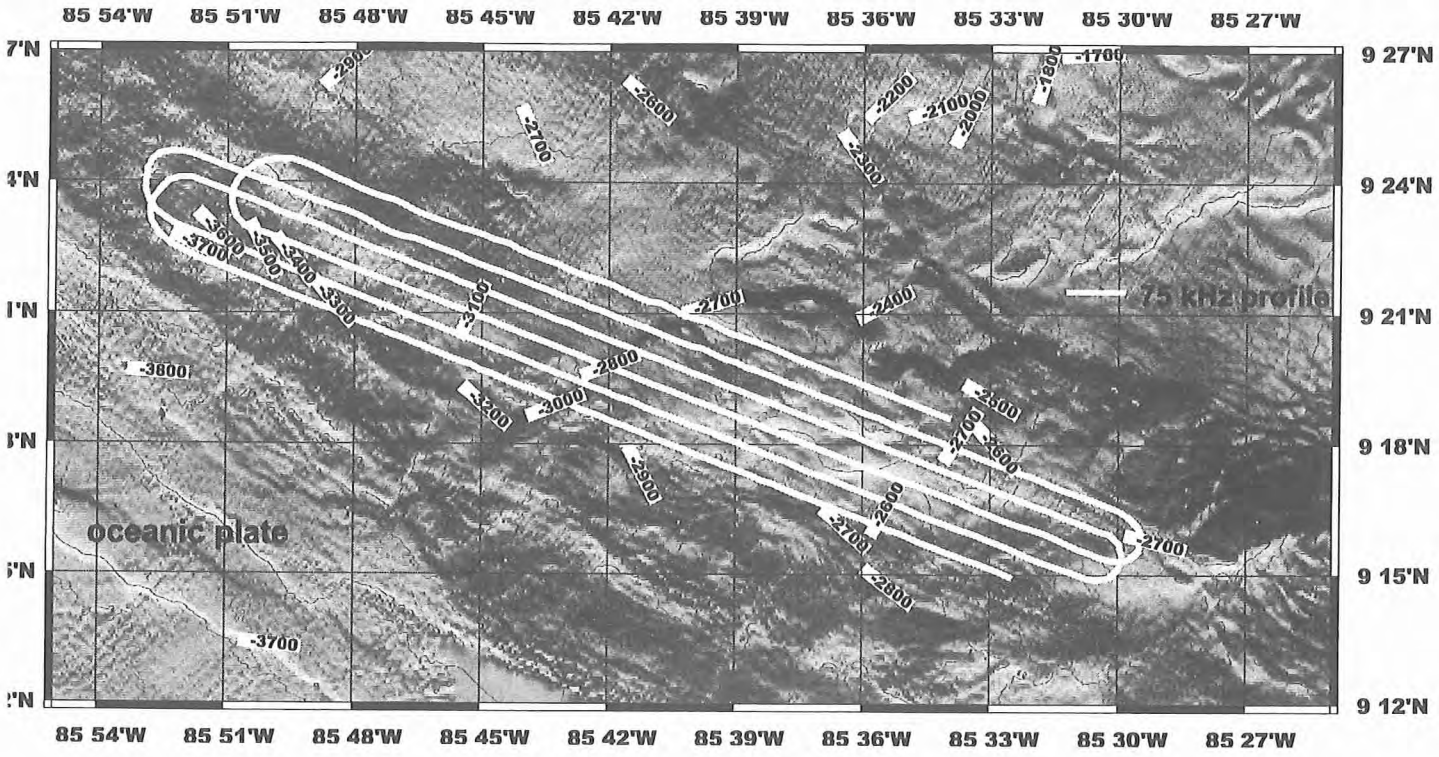


*Figure 6.3.5: Map showing the ship's tracks during the second DTS deployment (DTS1-02) downslope of the headwall of the Nicoya slide.*

at a minimum while approaching the escarpments. Reduced ship's speed of 3.0 knots allowed to have a shorter cable at the foot of the escarpment. Still, hauling at winch speeds of 1.0 m/s was necessary to keep the side scan fish off the seafloor.

Special remarks for deployment 4

1 - During this deployment the fiber optic cable has been used for the first time. After a first test with DTS on deck, the fiber optic modem initially set to a *low energy mode* was changed to the *high energy mode*, more appropriate for the 7 km long cable available on R/V SONNE. With such a configuration, the data and power signals are not modulated together as with the coaxial cable. As a consequence, significantly less noise was observed on the side scan sonar records during deployment 4.

2 - During deployment 4 serious problems have been observed with the *Posidonia* positioning system. Almost no position values were obtained from sensor H2 during the whole deployment and the calculated positions of the fish are strongly scattered around the ship. In some cases the fish's position had even been located ahead the ship... The only useful data available from the *Posidonia* system during this deployment are the depth sensor information. After recovering the *DTS*, the *Posidonia* acoustic array mounted below the ship hull has been checked and no real problem has been found. One possible explanation could be the presence of a fishing line around one of the sensors, lost when stopping the ship before pulling in the antenna or while pulling in the antenna. In any case, during the next deployment (DTS1-05), the *Posidonia* positioning system worked without problems.

*Figure 6.3.6: Positions of the third DTS deployment profiles superposed to TOBI imagery from SO144-1.*

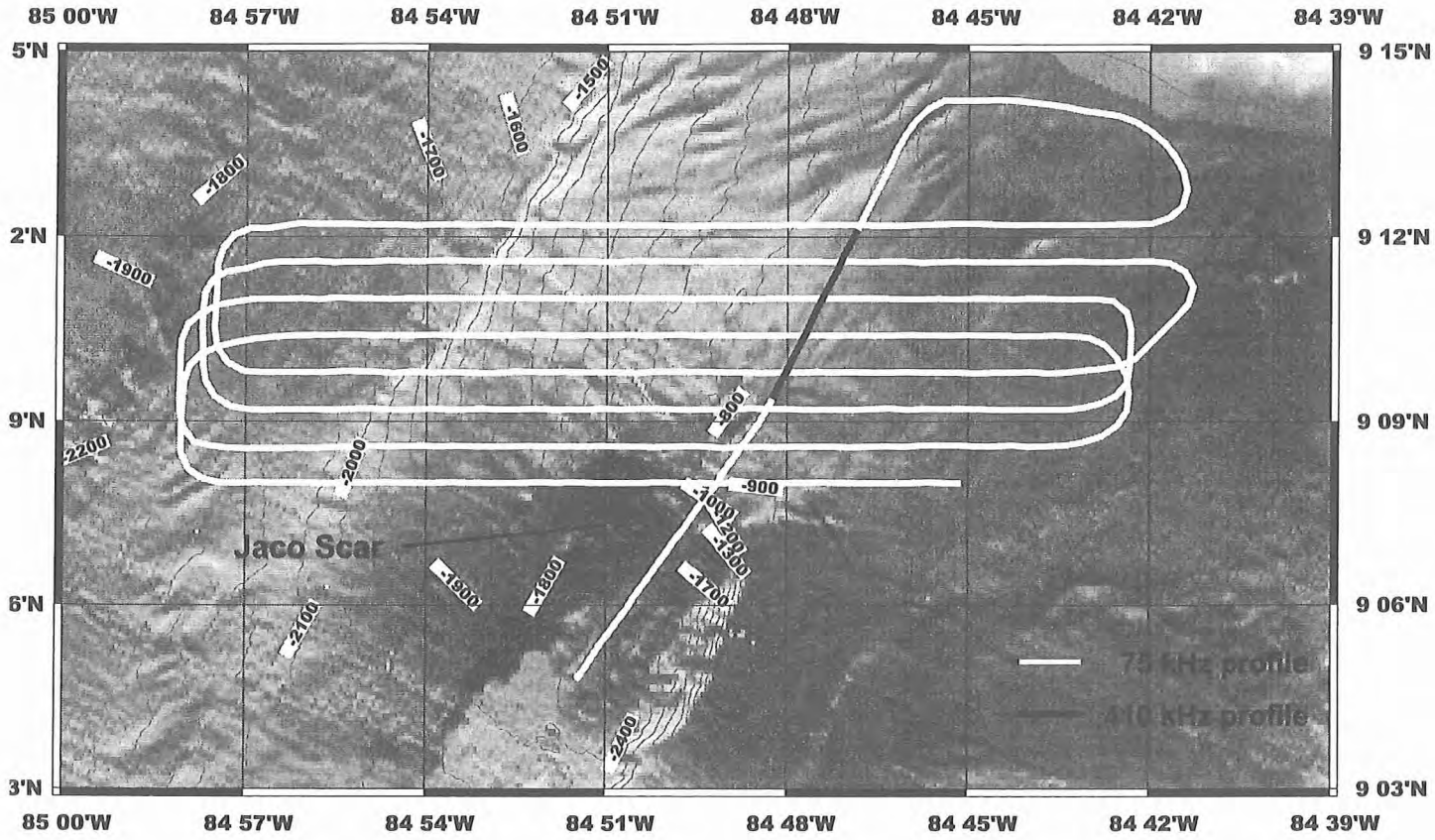


*Figure 6.3.7: Map showing the ship's tracks during the third DTS deployment (DTS1-03) upslope of the Jaco Scar.*

### 6.3.5 Deployment 5 (DTS1-05)

The fifth and last deployment of the DTS1 side scan sonar during SO163-1 was rather short on 17.04.02 between 18h10 and 22h20. It consisted of one high resolution (410 kHz) side scan sonar profile, located upslope Parrita scar, just north of the DTS1-04 low resolution profiles (Fig. 6.3.1, 6.3.8 and 6.3.9). This 9 km long profile has been run on the basis of the OFOS profiles obtained earlier this day over a small mound north of the Parrita scar (see 6.4), where intense activity has been observed.
During this deployment, the data window size was set to 10000 samples for the high resolution side scan sonar, which was run together with the 75 kHz side scan sonar (range 750 m, 26000 samples) and the sub-bottom profiler (range 250 m, 6000 samples). As during deployment 4 the fiber optic cable was used. The ship speed was kept around 2.5 knots in order to reduce the cable length for a more safe operation of the high resolution side scan sonar and to improve along-track resolution of the side scan sonar.

Special remarks for deployment 5

1- The connection to the fish was lost twice during deployment 5, for 1 or 2 minutes at 19h51 and for 100 pings at 20h27. No xse data have been recorded by *Hydrostar Online* during this time.
2- The quality of the sub-bottom profiler records was relatively poor during most of the profile, due to the relatively low speed of the ship resulting in a constantly important pitch for the fish. A slightly better display has been reached when the gain was reduced to values of 8.
3- The main objective of this deployment was to map a relatively small structure (no more than 200 m in diameter) which can easily be missed with the high resolution side scan sonar having a range of 100 m. The *Posidonia* positions were used to calculate the necessary offset of the ship to keep the fish exactly along the line and the structure was perfectly mapped.

*Figure 6.3.8: Positions of the fourth and fifth DTS deployments profiles superposed to TOBI imagery from SO144-1.*

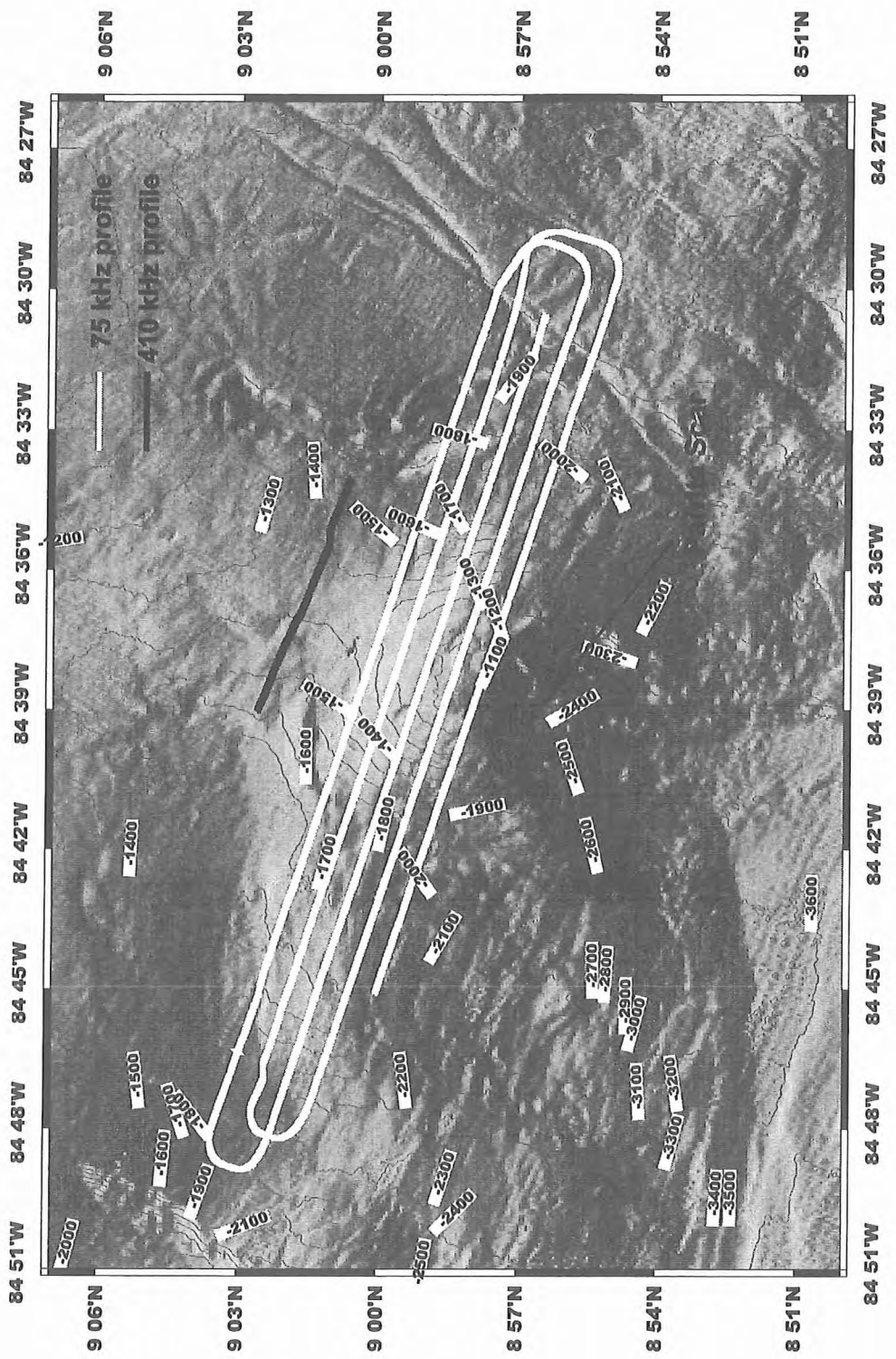


*Figure 6.3.9: Map showing the ship's tracks during the fourth and fifth DTS deployments (DTS1-04 and DTS1-05) upslope of the Parrita Scar.*

4- The *Posidonia* positioning system was run during this deployment without prior calibration after the *Posidonia* array had been pulled in after deployment 4. Yet, *Posidonia* underwater navigation data seemed to be sufficiently accurate to hit a small target.

### 6.3.6 General Remarks

a- Different types of noise observed

- During all deployments, regular interferences related to the Posidonia pinging sequence (5s pinging rate) has been clearly evidenced on the low resolution side scan sonar records and on the sub-bottom profiler.
- Some interference has been observed when running the high resolution side scan sonar (410 kHz) related to the sub-bottom profiler.
- Proximity of other boats always results in strong noise either on the side scan sonar or the sub-bottom profiler.
- Strong noise has also been observed at the beginning of all deployments on the low resolution side scan sonar. This noise decreases progressively during the first 30 minutes of DTS deployment and then completely disappears. This might be related to internal gain settings of the side scan data. As long as no bottom return is registered the gain is very high and amplifies noise. An alternative explanation might be that parasite energy level resulting from the start up sequence need some time to dissipate.
- Every day, between 20h03 and 21h50 UTC, a weak noise has been observed on the DTS data. All scientists involved agree to attribute this noise to some daily internal operations in the tow fish. The automatic backups done by the *Bottom PC* of the seismic streamer acquisition system that is housed in the telemetry pressure housing, has been switched off after deployment 3 and this noise completely disappeared.

b- A good bathymetry for safe deployments

- One of the most important remarks following those five deployments is the real need of a detailed bathymetric map for safe flying of the tow-fish, especially when running the high resolution mode with the fish only 20 m above the seafloor. A detailed bathymetry also helps to anticipate seafloor escarpments or other strong changes in relief and to keep the tow fish at a safe distance from the bottom by hauling in enough cable prior to bathymetric escarpments. During SO163, the available bathymetry was only a 100m grid and most of the fault scarps along the DTS profiles were not clearly shown. The result was two *emergency* situations during deployments 3 and 4 when cutting across the fault scarps upslope the Jaco and Parrita seamounts. Cable had to be pulled in at 1.0 m/s with ship speed increased from 3.5 to 4 knots during deployment 3 and at 1.5 m/s with a ship speed increased to 4.5 knots during deployment 3, in order to avoid bottom contact.

### 6.3.7 Preliminary observations and scientific results

Even though significant progress been in understanding and reading the *DTS* data format (thanks to W. Weinrebe during this cruise), we are still not yet able to process the side scan sonar data. Both subbottom profiler records and side scan sonar images are not georeferenced and corrected for towfish altitude variations, and we still have to find a way to properly filter and use the *Posidonia* underwater navigation.
As a result, we are not able to provide accurate scientific results or preliminary interpretations, but some interesting points can still be pointed out based on the online observation of the raw data during the deployments.

a- Structures related to mud and fluid escapes

One of the main interests of the DTS backscatter images is to provide information concerning the seafloor topography and lithology. An anomalous high backscatter signal could for example be tentatively interpreted as an evidence for a recent mud flow or a fluid escape structure. This information were obviously of high interest during DTS deployments 1, 2 and 5, focused on 3 areas where mud and fluid escape were supposed to take place.

- **DTS1-01:** During the first DTS deployment small bathymetric mounds have been investigated on the continental slope NW of the Nicoya Peninsula. The DTS low resolution side scan images illustrates two different types of anomalous high backscatter patches. **(1)** Some large highly reflective accumulations over several hundreds of meters, correlated with an echo-free surficial layer on the subbottom profiler which might correspond to mud accumulations. Some of them show scattered domains characterised by a more chaotic acoustic pattern, which could be interpreted as the acoustic expression of localised encrusted areas, covered by thick carbonate crusts. Clear relationships have been observed with tectonic features for several of these inferred mud flows. They could be observed on side scan images with small scale sigmoidal features like tension gashes or linear faults followed over hundreds of meters and clearly imaged on the subbottom profiler records when crossed by the fish. **(2)** Numerous small bright spots have been observed along all the lines. They might correspond to isolated fluid or gas escape centers like pockmarks structures. No special relationships with tectonic features have been observed so far.

- **DTS1-02:** During this deployment, several small reflective mounds which might correspond to mud diapirs have been observed, but no large highly reflective mud flow could be evidenced. The data quality of the subbottom profiler was really good during this deployment and illustrates a complex tectonic pattern with faults and tilted blocks clearly evidences on the profiles. This intense fracturation could constitute possible pathways for fluids and mud from depth to the surface.

- **DTS1-05:** The high resolution side scan sonar run during deployment five provides a very good quality backscatter image over a subcircular feature of about 200 m in diameter. Both the morphology and the backscatter strength of this topographic relief seems to indicate a mud construction. Moreover, some concentric circular rims have been clearly evidenced over the whole structure and could be the result of two different emplacement processes: **(a)** a progressive construction of the dome by successive flows, if an "extrusive" emplacement mode is evoqued, or **(b)** some circular cracks generated by a diapir-like "intrusive" emplacement. Some localised chaotic acoustic patterns have also been identified, and could be explained by the presence of carbonate crusts on top of the structure. Therefore, this relief could correspond to a relatively old structure and the circular rims be the result of a late subsidence of the whole structure, after the fluid escape activity has decreased.
During SO163-1 OFOS has been deployed on most of these possible mud structures (see 6.4) and provides the necessary ground-truthing for a meaningful interpretation of the DTS reflectivity data. Further detailed correlation between OFOS and DTS are definitely required to better understand the real signification of the acoustic patterns.

b- Fault patterns upslope Jaco and Parrita scars

Jaco and Parrita scars areas are well known since the SO144 expedition as complex tectonic features related to seamount subduction beneath the overriding plate, SE of the Nicoya Peninsula. The bathymetric highs observed upslope of both scars as well as their lateral walls are characterised by a complex morphostructural pattern shaped by crosscutting faults.
DTS deployments 3 and 4 have been run upslope Jaco and Parrita scars, respectively. During both deployments, the backscatter images from the low resolution side scan sonar clearly illustrates two main sets of faults: **(1)** radial normal faults, probably related to the seafloor uplift due to the seamount subduction and **(2)** linear faults trending perpendicular to the direction of subduction (N130-N140) over several kilometers. An well expressed surface deformation, mainly characterised by elongated short wavelength folding has been observed

on both structures and could be related to the combination of compressive stresses in front of the subducting seamounts and strike-slip motion on the lateral walls.
The different purposes of these two deployments were to understand the evolution and chronology of faulting, but also to image some possible fluid escape structures related to seamount subduction. Some noticeable differences have been observed between both scars. The radial normal faults seem much more developed upslope of Jaco scar and many sigmoidal structures might reveal strike-slip motions. The Parrita scar is mainly controlled upslope by folding and linear N140 faults. A large number of small scale highly reflective patches have been observed in both cases and could be attributed either to encrusted areas related to fluid escapes or to mud flows injected through the crosscutting faults which appears as the easiest way for fluid ascension. The compressive stresses at the front of the subducting seamounts would then provide the necessary overpressure to allow mud and fluid ascensions.
Several preliminary hypotheses could be proposed to explain the differences observed between both structures. **(1)** Parrita scar only 6 km upslope from the deformation front is a more recently subducted seamount covered by a thinner sedimentary sequence than Jaco scar. This could explain why Parrita scar shows less important uplift and brittle deformation. **(2)** The Parrita seamount could also be a smaller seamount more easily subducted. Both hypotheses also account for the presence of a larger amount of reflective patches around Jaco scar, where compressive tectonics seem to be more important. A further detailed analysis and interpretation of the side scan sonar mosaics and subbottom profiler lines should allow to better understand the tectonic mechanisms and associated fluid venting related to seamount subduction, as well as the evolution through time of these processes.

## 6.4 Results and discussion of OFOS and TVG deployments

(H. Sahling, T. Nadler, D. Masson, V. Hühnerbach, C. Ranero)

A major target of this cruise was to discover and sample seafloor areas that are influenced by venting of methane-rich fluids. It is generally accepted that the microbial-mediated process of anaerobic methane oxidation occurs, when these fluids come in contact with sulfate-rich waters at shallow sediment depths. This biogeochemical process causes, firstly, the precipitation of (chemoherm) carbonate and, secondly, the production of sulfide, that is then used by chemoautotrophic organisms. Carbonates and chemoautotrophic organisms are, thus, indicators of methane venting. One goal during this cruise was to collect these (geological and biological) indicators in order to confirm their methane-dependent origin.

It is generally thought that tectonic and mass wasting processes control fluid venting. Therefore, we concentrated our investigations on prominent geological structures; these are mounds (originally described as mud volcanoes), subducted seamounts and ridges, the accretionary wedge, and landslides. In addition, we surveyed a site on the oceanic plate that has revealed unusual high heatflux values and hydrothermally influenced porewater geochemistry.

A prerequisite for successful OFOS and TVG investigations are seafloor images based on multibeam echosoundings and sidescan sonar mapping. Wide areas were mapped during previous cruises or have been mapped during this cruise (compare SIMRAD and TOBI chapters). These images are shown in this chapter in order to draw a comprehensive picture of the seafloor processes.

During this cruise 26 OFOS deployments and 9 TVG deployments were successfully accomplished (Fig 6.4.1, Fig. 6.4.2, Tab. 6.4.1).

### 6.4.1 Mounds

Circular structures tens of meters high that were originally described as mud volcanoes, occur along the Costa Rican continental margin (Shipley et al., 1992). At these structures luxuriant chemosynthetic communities as well as chemoherm-like carbonates were observed by DSS Alvin and OFOS (Bohrmann et al., in press; Kahn et al., 1996). During the first OFOS deployments it became evident that these structures are indeed fluid venting related: at the top or the flanks of the mounds we found massive chemoherm-like carbonates outcropping and, at some of these structures, vesicomyid, mytilid or solemyid bivalves and pogonophoran tubeworms occur. However, there was no evidence for mud expulsion. Furthermore, at the top of some of these mounds, described in detail below, massive carbonate crop out, suggesting that these structures constitute partly, if not entirely, of carbonate. These structures may be mounds build up by chemoherm-like carbonates. This is further corroborated by the occurrence of chemosynthetic communities on top and on the flanks of the mounds, which indicate fluid flow at present.

Along the continental margin of Costa Rica several mounds were discovered using TOBI. Most mounds are characterised by high backscatter relative to the surrounding sediment covered slope. This can be attributed mainly to the occurrence of carbonate (or carbonate-cemented sediment?) although mound topography may also contribute to elevated backscatter levels on slopes facing the sidescan. Backscatter levels show some variability both within and between mounds, probably reflecting variation in sediment cover on the mound. Most mounds are readily identified in the bathymetric map. For clarity, numbers were given for each mound that were surveyed with OFOS during this cruise (Tab. 6.4.1.1, Fig. 6.4.1.1).

Mound # 1 (Mound Culebra) OFOS 1 & 2, TVG 1 & 2

Mound # 1 is located at 1600-m water depth and is recognisable in the bathymetry. It is a circular structure of about 0.8 nautical miles in diameter and rises about 100 m above the surrounding seafloor. The mound was surveyed by two TOBI lines, which showed high reflectivity throughout the mound (Fig. 6.4.1.2). Due to ocean currents and wind direction we were forced to tow OFOS from west to east (Fig. 6.4.1.3). To avoid going up the steep western slope we deployed both OFOS close to the top and surveyed the highest parts and the flanks on the E and NE side. "Bumps" about 30 m high largely structure the top of the mud volcano (Fig. 6.4.1.4); these can also be seen on the TOBI image. On top of these "bumps" massive carbonate is exposed. Carbonate also outcrops at the flanks suggesting that the whole structure is cemented. We found no evidence

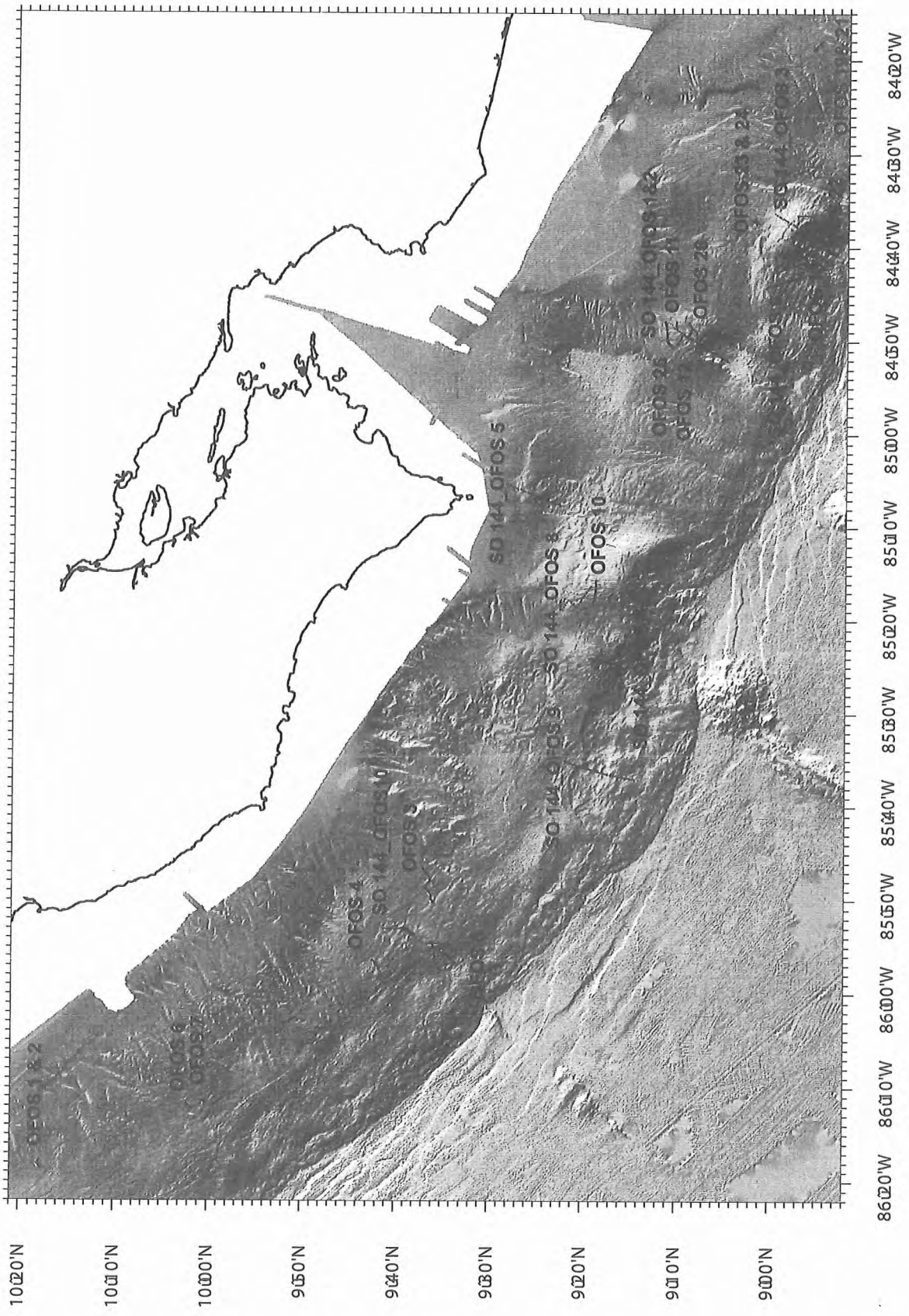


*Figure 6.4.1: Overview of all OFOS deployments during SO 163 and SO 144 on the Western continental margin off Costa Rica.*

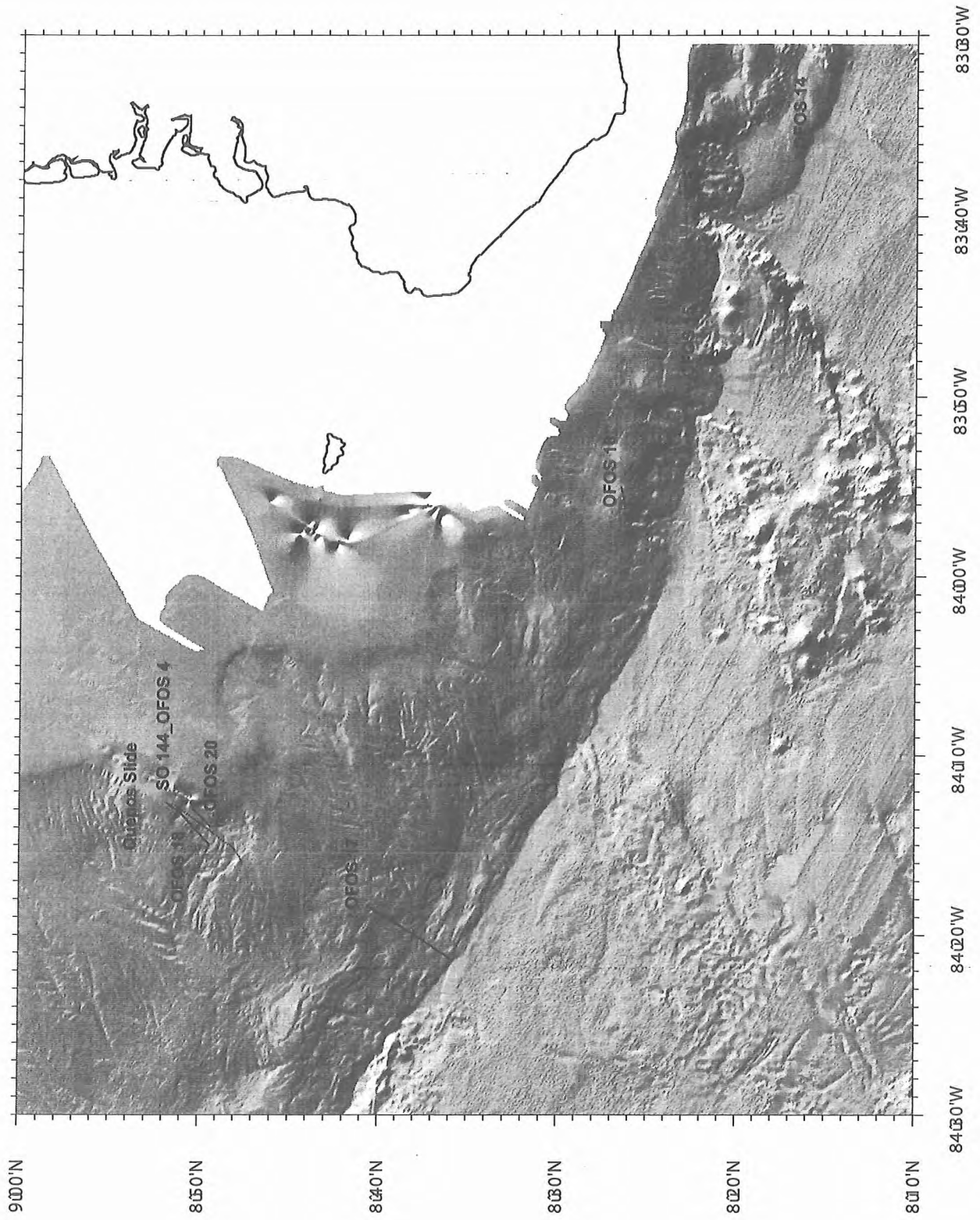


*Figure 6.4.2: Overview of OFOS deployments during SO 163 on the Eastern Costa Rican margin.*

Tab. 6.4.1: Summary of OFOS and TVG deployments during SO 163-1.

| Station | Area | Date | at seafloor Time | Lat | Long | Depth | off seafloor / grab location Time | Lat | Long | Depth | Observation / recovery |
|---|---|---|---|---|---|---|---|---|---|---|---|
| **Mounds** | | | | | | | | | | | |
| OFOS 1 | Mound # 1 | 22.03.2002 | 17:41:48 | 10° 17.86 | 86° 18.37 | 1540 | 19:41:49 | 10° 18.01 | 86° 17.99 | 1570 | Carbonates, clams and pogonophorans, No SSBL Position |
| OFOS 2 | Mound # 1 | 22.03.2002 | 21:29:10 | 10° 17.84 | 86° 18.56 | 1510 | 23:21:10 | 10° 18.14 | 86° 18.07 | 1550 | Carbonates, clams and pogonophorans, SSBL 50 m above OFOS |
| TVG 1 | Mound # 1 | 23.03.2002 | 01:59:50 | 10° 17.88 | 86° 18.40 | 1500 | 02:07:00 | 10° 17.923 | 86° 18.32 | 1516 | 2 carbonate pieces on top of grab |
| TVG 2 | Mound # 1 | 23.03.2002 | 03:26:00 | 10° 17.93 | 86° 18.33 | 1490 | 03:36:00 | 10° 17.987 | 86° 18.29 | 1473 | Several carbonate pieces and clamshell fragments |
| OFOS 3 | Mound # 2-6 | 28.03.2002 | 00:10:30 | 9° 37.12 | 85° 46.53 | 1588 | 08:25:26 | 9° 35.95 | 85° 50.15 | 1989 | Crossed 4 mounts from NE to SW, some with carbonates, pogonophorans, clams; Camera B problems |
| OFOS 4 | Mound # 7, 8 | 18.03.2002 | 11:32:36 | 9° 42.53 | 85° 56.30 | 2203 | 15:17:14 | 9° 41.98 | 85° 56.90 | 2240 | Small aera with carbonates, pogonophorans and clams |
| OFOS 6 | Mound # 9 | 29.03.2002 | 05:01:30 | 10° 02.16 | 86° 11.80 | 2240 | 07:24:10 | 10° 01.56 | 86° 12.23 | 2342 | No seep indication |
| OFOS 7 | Mound # 10 | 29.03.2002 | 09:24:10 | 10° 00.73 | 86° 11.35 | 2305 | 11:36:10 | 10° 00.65 | 86° 11.50 | 2341 | Abundant vent indication; clams, pogonophorans, carbonate |
| OFOS 13 | "Bright Spot W of Parrita" | 05.04.2002 | 20:19:50 | 9° 59.70 | 84° 42.50 | | 23:35:00 | 8° 58.00 | 84° 41.65 | | Beside scattered clamshells no seep indications |
| OFOS 19 | Mound # 11, 12 | 14.04.2002 | 05:44:20 | 8° 54.94 | 84° 17.91 | 1023 | 08:14:32 | 8° 55.95 | 84° 18.83 | 1005 | Extensive carbonates, clams, mussels and pogonophorans |
| OFOS 21 | Mound # 12 | 14.04.2002 | 15:09:30 | 8° 55.94 | 84° 18.53 | 998 | 18:40:16 | 8° 55.73 | 84° 18.95 | 1013 | Extensive carbonates, clams, mussels and pogonophorans; Video on 16:32 |
| TVG 4 | Mound # 12 | 14.04.2002 | 22:29:35 | 8° 55.79 | 84° 18.74 | 1002 | 23:14:45 | 8° 55.81 | 84° 18.62 | 992 | Piece of outcropping carbonate |
| TVG 5 | Mound # 12 | 15.04.2002 | 00:16:50 | 8° 55.79 | 84° 18.75 | 1002 | 00:41:00 | 8° 55.80 | 84° 18.74 | 1005 | Complete seep ecosystem: Acharax, Bathymodiolus, Lamellibrachia, galatheid crabs and carbonates |
| OFOS 23 | Mound # 13 | 17.04.2002 | 05:12:40 | 9° 02.20 | 84° 37.24 | 1451 | 12:28:39 | 9° 01.78 | 84° 37.06 | 1403 | Most extensive field of carbonates, pogonophorans, bivalves |
| OFOS 24 | Mound # 13 | 17.04.2002 | 14:27:44 | 9° 01.95 | 84° 37.22 | 1406 | 16:41:50 | 9° 01.95 | 84° 37.13 | 1397 | Mapping most extensive seep area |
| TVG 8 | Mound # 13 | 18.04.2002 | 16:55:10 | 9° 01.96 | 84° 37.22 | 1408 | 17:06:40 | 9° 01.97 | 84° 37.22 | 1408 | Carbonates |
| TVG 9 | Mound # 13 | 18.04.2002 | 18:44:15 | 9° 01.96 | 84° 37.25 | 1408 | 18:47:35 | 9°0 1.96 | 84° 37.24 | 1408 | Vent fauna, carbonates |

| | | | at seafloor | | | | off seafloor / grab location | | | | |
|---|---|---|---|---|---|---|---|---|---|---|---|
| Station | Area | Date | Time | Lat | Long | Depth | Time | Lat | Long | Depth | Observation / recovery |
| **High heatflow area** | | | | | | | | | | | |
| OFOS 8 | Basement hight | 30.03.2002 | 04:43:17 | 9° 40.25 | 86° 33.76 | 3275 | 08:20:00 | 9° 41.01 | 86° 33.17 | 3267 | No indication for hydrothermal venting |
| OFOS 9 | Fault | 30.03.2002 | 10:58:04 | 9° 46.48 | 86° 40.78 | 3315 | 13:40:51 | 9° 46.89 | 86° 40.41 | 3346 | No indication for hydrothermal venting |
| **seamount scars** | | | | | | | | | | | |
| OFOS 5 | Scarp of fracture ridge trace | 28.03.2002 | 17:42:39 | 9° 36.31 | 85° 54.28 | 2194 | 23:00:40 | 9° 33.94 | 85° 56.53 | 3145 | very few seep indication or other geological structures |
| OFOS 10 | Rio Bongo Scarp | 02.04.2002 | 18:39:39 | 9° 18.86 | 85° 15.54 | 470 | 23:27:30 | 9° 19.16 | 85° 18.31 | 772 | Carbonated top, few vent fauna |
| OFOS 11 | Jaco Scarp | 03.04.2002 | 04:52:39 | 9° 10.43 | 84° 47.75 | 731 | 07:16:42 | 9° 10.40 | 84° 48.66 | 779 | Carbonates, bivalve shells |
| OFOS 12 | Jaco Scarp | 03.04.2002 | 09:03:40 | 9° 10.40 | 84° 50.34 | 928 | 13:15:33 | 9° 08.74 | 84° 48.69 | 865 | Chemoherm-like carbonates, vesicomyid clamfield |
| TVG 3 | Jaco Scarp | 05.04.2002 | 15:44:10 | 9° 10.42 | 84° 48.25 | 763 | 15:50:57 | 9° 10.43 | 84° 48.24 | 763 | Chemoherm-like carbonates, living solemyid bivalves, bivalve shells |
| OFOS 25 | Jaco Scarp | 18.04.2002 | 00:09:48 | 9° 11.60 | 84° 47.80 | 774 | 05:03:20 | 9° 10.78 | 84° 50.62 | 996 | No vent indication |
| OFOS 26 | Jaco Scarp | 18.04.2002 | 06:22:55 | 9° 08.24 | 84° 49.64 | 953 | 09:08:31 | 9° 09.14 | 84° 48.04 | 810 | No vent indication |
| TVG 7 | Jaco Scarp | 18.04.2002 | 14:01:32 | 9° 09.03 | 84° 49.18 | 834 | 14:32:00 | 9° 09.01 | 84° 49.13 | 824 | Carbonates |
| OFOS 15 | "Frontal collision" | 11.04.2002 | 00:02:00 | 8° 22.20 | 83° 47.684 | 1260 | 02:52:24 | 8° 21.182 | 83° 48.013 | 1633 | Steep morphology, beside clamshells no seep indication |
| OFOS 16 | "Small seamount scarp" | 11.04.2002 | 05:05:00 | 8° 26.48 | 83° 54.981 | 701 | 07:48:14 | 8° 25.893 | 83° 56.002 | 1095 | No vent indication |
| OFOS 22 | Parrita | 15.04.2002 | 09:15:58 | 8° 57.55 | 84° 36.51 | 1228 | 14:12:57 | 8° 55.17 | 84° 37.89 | 2338 | Beside scattered clamshells no seep indications |

| | | | at seafloor | | | | off seafloor / grab location | | | | |
|---|---|---|---|---|---|---|---|---|---|---|---|
| Station | Area | Date | Time | Lat | Long | Depth | Time | Lat | Long | Depth | Observation / recovery |
| **Accretionary wedge** | | | | | | | | | | | |
| OFOS 14 | "Creast of Cocos Ridge" | 10.04.2002 | 19:21:24 | 8° 15.572 | 83° 34.185 | 1710 | 20:41:58 | 8° 15.343 | 83° 34.803 | 1902 | No seep indication |
| OFOS 17 | "Seismic Line SO 81 #5" | 11.04.2002 | 12:34:30 | 8° 40.56 | 84° 18.35 | 2000 | 20:57:25 | 8° 35.93 | 84° 21.30 | 2500 | No seep indication |
| **Landslide** | | | | | | | | | | | |
| OFOS 18 | Quepos Lanslide | 13.04.2002 | 22:56:41 | 8° 51.87 | 84° 12.60 | 179 | 03:48:43 | 8° 49.50 | 84° 15.51 | 831 | Larg bacterial mats at headwall, few seep indications in slide mass |
| OFOS 20 | Quepos Lanslide | 14.04.2002 | 10:16:00 | 8° 50.30 | 84° 13.00 | 438 | 13:06:00 | 8° 48.61 | 84° 13.90 | 740 | Beside one bacterial mat no seep indication at slide mass |

*Tab. 6.4.1.1: List of mounds surveyed during SO 163 cruise along the Cost Rican continental margin.*

| Mound No. | Latitude | Longitude | Depth | DTS | SO 163 | Results |
|---|---|---|---|---|---|---|
| | | | | | | |
| 1 | 10°17.90 N | 86°18.40 W | 1600 | -- | OFOS 1, 2; TVG 1, 2 | carbonates, clams and pogonophorans |
| 2 | 9°36.50 N | 85°47.40 W | 1760 | 75 kHz | OFOS 3 | sediment covered |
| 3 | 9°36.40 N | 85°47.80 W | 1760 | 75 kHz | OFOS 3 | carbonates, clamshells |
| 4 | 9°36.80 N | 85°48.60 W | 1800 | 75 kHz | OFOS 3 | carbonates, clamshells |
| 5 | 9°36.30 N | 85°49.30 W | 1800 | 75 kHz | OFOS 3 | few carbonates, largely sediment covered |
| 6 | 9°36.10 N | 85°50.00 W | 1950 | 75 kHz | OFOS 3 | sediment covered |
| 7 | 9°42.20 N | 85°56.60 W | 2200 | 75 kHz | OFOS 4 | no seep indication |
| 8 | 9°41.90 N | 85°57.10 W | 2200 | 75 kHz | OFOS 4 | small area with carbonates, pogonophorans and clams |
| 9 | 10°02.00 N | 86°12.00 W | 2300 | 75 kHz | OFOS 6 | no seep indication |
| 10 | 10°00.40 N | 86°11.50 W | 2300 | 75 kHz | OFOS 7 | abundant vent indication; clams, pogonophorans, carbonate |
| 11 | 8°55.33 N | 84°18.26 W | 1000 | -- | OFOS 19 | carbonates |
| 12 | 8°55.80 N | 84°18.70 W | 980 | -- | OFOS 19, 21; TVG 4, 5 | extensive field of carbonates, clams, mussels and pogonophorans |
| 13 | 9°01.90 N | 84°37.23 W | 1400 | 410 kHz | OFOS 23, 24 | most extensive field of carbonates, pogonophorans, bivalves |

of mudflows. At the top of the mound chemoautotrophic species, vesicomyid clams and pogonophoran tubeworms indicate that venting still occurs. We deployed two TVG in order to sample the carbonates. Both grabs felt over during the closing of the jaws. However, we retrieved some pieces of rocks, sediment with sulfide odour and shell fragments. The calcareous cemented sediments are probably formed in the course of methane venting.

Mound # 2-6 OFOS 3

With OFOS 3 we surveyed fault-like structures and 5 mounds that were imaged by TOBI (Fig. 6.4.1.5). The OFOS survey revealed that the spotted backscatter on the slope between the beginning and a (OFOS-CTD) depth of 1750 m correspond to hardground that is hardly covered by soft sediment. At a depth of 1730 m big slabs of several m indicate tectonic activity that is probably linked to a fault imaged by TOBI. Mound # 2 was completely sediment covered, and only a few single clamshells were observed. The track crossed Mound # 3 and followed the southern slope, crossed the eastern flank of Mound # 4, where the direction of the sled turned so that it crossed, then, the top of Mound # 4 (Fig. 6.4.1.6, Fig. 6.4.1.7). At the summits of both mounds as well as the steep S flanks massive carbonate crops out. At the top of Mound # 3 the carbonate appears chemoherm-like and indicates venting activity. Additionally, clamshells were observed at the top that further confirms venting processes at present. The origin of the outcrops on the flanks is unknown, although we speculate that the entire mounds are made of carbonate originating from methane venting. In the following we have crossed the top area of Mound # 5 twice. This mound as well as Mound # 6 is largely sediment covered. The area Northeast of Mound # 6 is characterised by lower backscatter than the surrounding seafloor. The OFOS depth profile indicates an apparently flat seafloor (area 8'- 9'), suggesting a sediment filled depression.

In general, methane venting in this area appears to be largely inactive. The massive carbonate outcrops indicate considerable methane venting in the past.

*Future investigation:* To gain better understanding of the origin of carbonate we suggest dredge deployments in this area.

*Additional note:* Around 6:51 h (UTC) OFOS passed through a cloud of bentho-pelagic animals of very high densities. These may have been juvenile crustaceans.

Mound # 7, 8 OFOS 4

OFOS 4 covered two mounds that are largely sediment covered (Fig. 6.4.1.8, Fig. 6.4.1.9, Fig. 6.4.1.10). On top of Mound # 8 several boulders of unweathered chemoherm carbonates, a few bushes of vestimentiferan tubeworms and vesicomyid clam clusters are present in a very small area, which we crossed twice with OFOS. Due to the small extension of venting this area may not be a high priority target for future investigations.

Mound # 9 OFOS 6

This mound was completely sediment covered and does not show any signs of carbonates, or biological communities associated with fluid venting (Fig. 6.4.1.11, Fig. 6.4.1.12, Fig. 6.4.1.13).

Additional note: A dense aggregation of several dozens large spider crabs occurred at the beginning of the track.

Mound # 10 OFOS 7 and OFOS 6

This mound is associated with crosscutting, fault patterns that are clearly seen upslope of the mound on the TOBI image. We found abundant vent indications in the top area and the on the higher northern flank. Here, unweathered chemoherm carbonate boulders, vestimentiferan tubeworms and vesicomyid clam occur. Clamshells are scattered over wide areas but only a few clusters of living clams were seen. However, one clam cluster several meters wide and very long suggests, firstly, venting at present and, secondly, that faults control their distribution. Again, we found no evidence for mudflows. Due to the extensive vent areas this site should be a subject for future geochemical investigations.

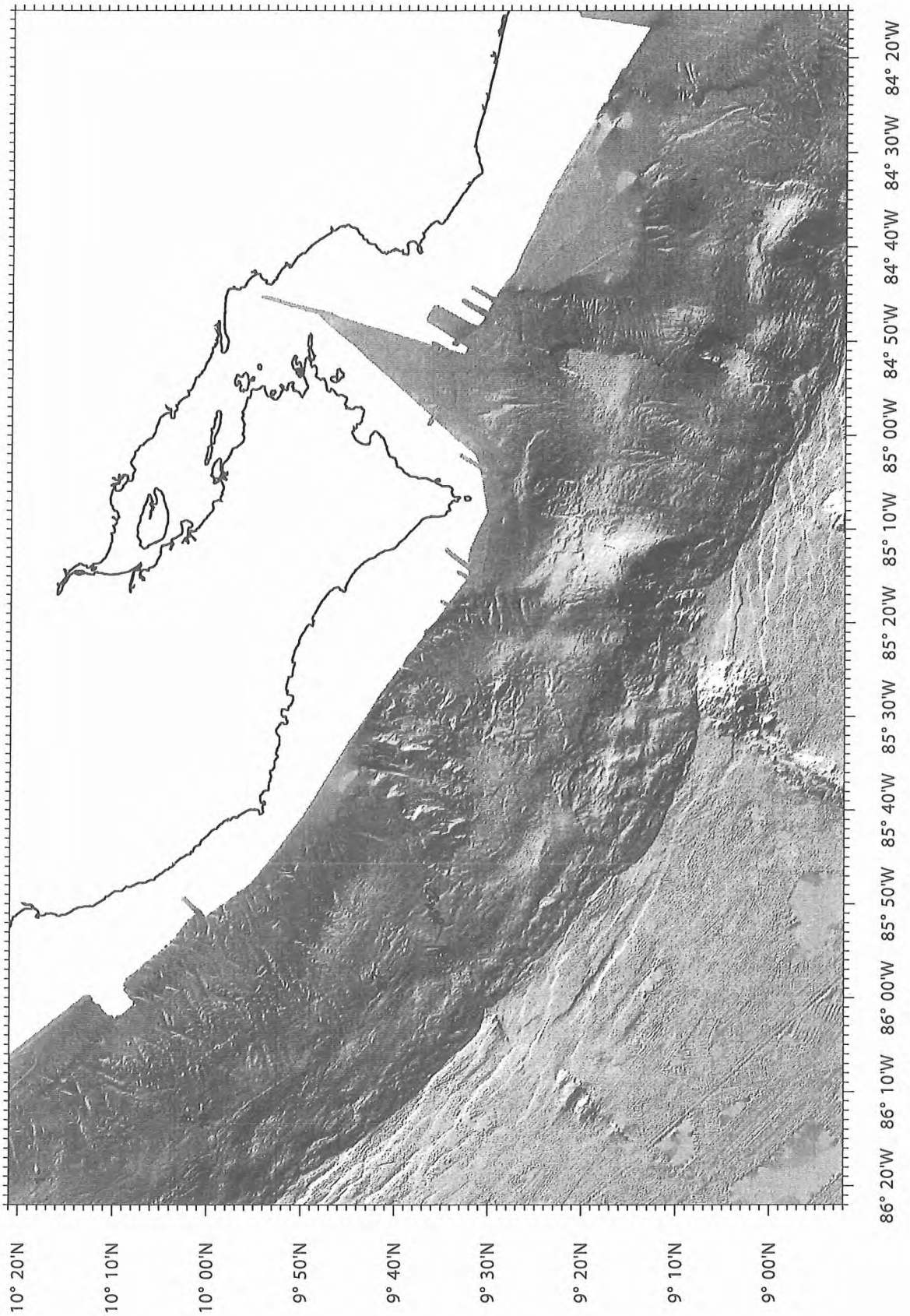


*Figure 6.4.1.1: Location of mounds surveyed during SO 163 cruise along the continental margin off Costa Rica. The numbers indicate mounds listed in Tab. 6.4.1.1.*

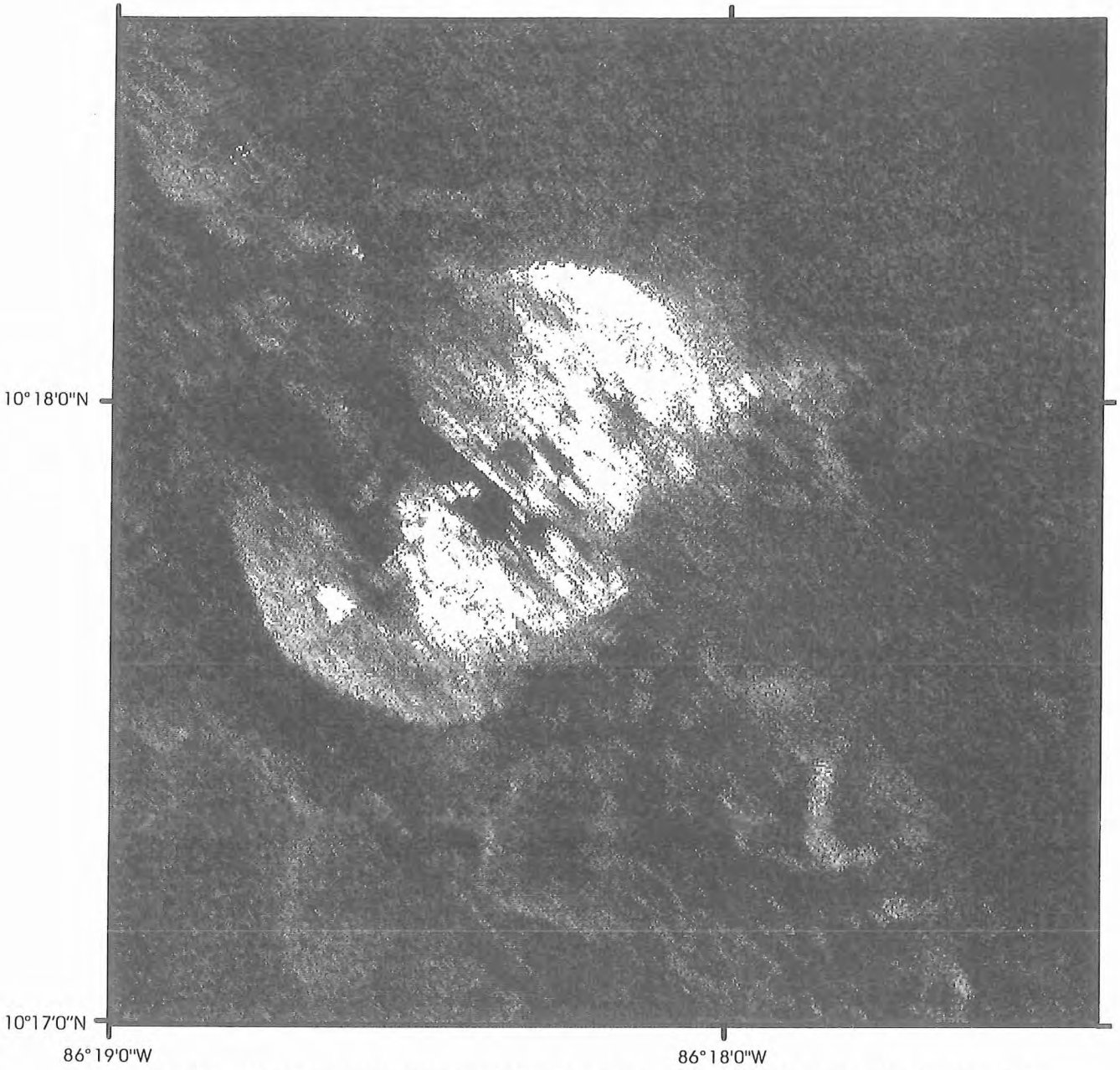


*Figure 6.4.1.2: TOBI backscatter image of Mound # 1. White = high backscatter, black = shadows. Rough areas on the mound crest correlate with elevated carbonate outcrops seen on the OFOS transact.*

Mound # 11, 12 OFOS 19, 21, TVG 4, 5

Mound # 11 and 12 were imaged by TOBI (see Fig. 6.2.21). With OFOS 19 we surveyed both mounds (Fig. 6.4.1.14). At Mound # 11 outcrops were seen, at Mound # 12 outcropping chemoherm-like carbonates and, in addition, abundant seep fauna. With OFOS 21 we surveyed on a very small scale the distribution of carbonates and organisms (Fig. 6.4.1.15). The abundance and diversity of pogonophorans and bivalves were high. At some sites the sediment between carbonates appeared blackish and very thin white bacterial mats occur. We found an area at which the mytilid bivalve *Bathymodiolus* occurs in cluster of up to about 5 meter in diameter. Although we do not know the relation between geochemical processes and the occurrence of seep organisms, we speculate that the high abundance of bivalves indicate the sites of most active methane seepage. With TVG 4 we cut a piece of outcropping carbonate, that has brecciated appearance. With TVG 5 we sampled a whole small ecosystem, that consisted of a living pogonophoran tubeworms (cf. *Lamellibrachia* sp.) and mytilid bivalves (*Bathymodiolus* sp.) in addition to chemoherm-like carbonates.

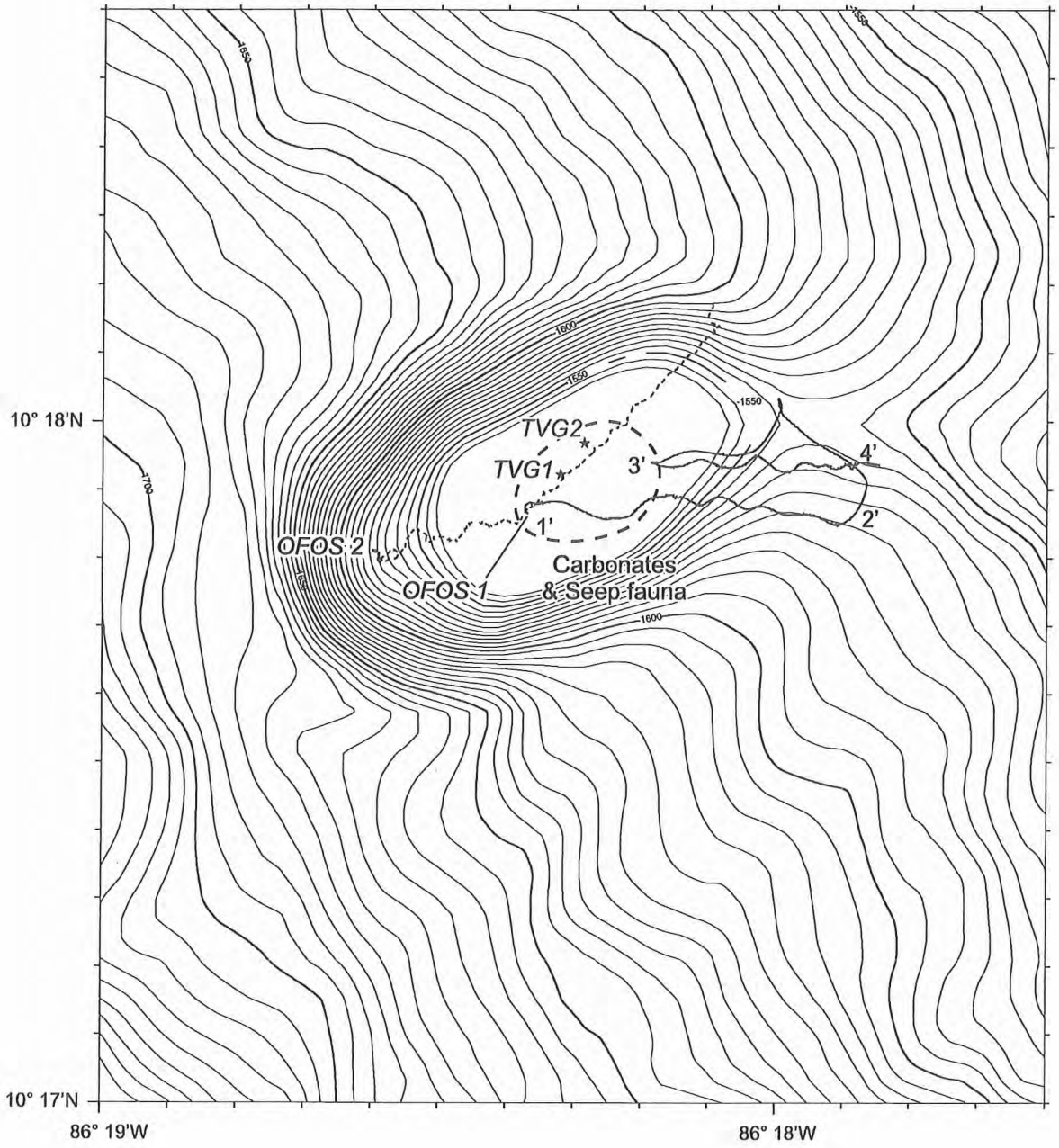


*Figure 6.4.1.3: OFOS and TVG deployments at Mound # 1 (Mound Culebra). Tracks indicate OFOS 1, TVG 2 (ship position), OFOS 2, TVG 1 (SSBL positions). The bathymetry is based on Simrad multibeam obtained during this cruise. The position of major areas with outcropping carbonates and seep fauna is indicated.*

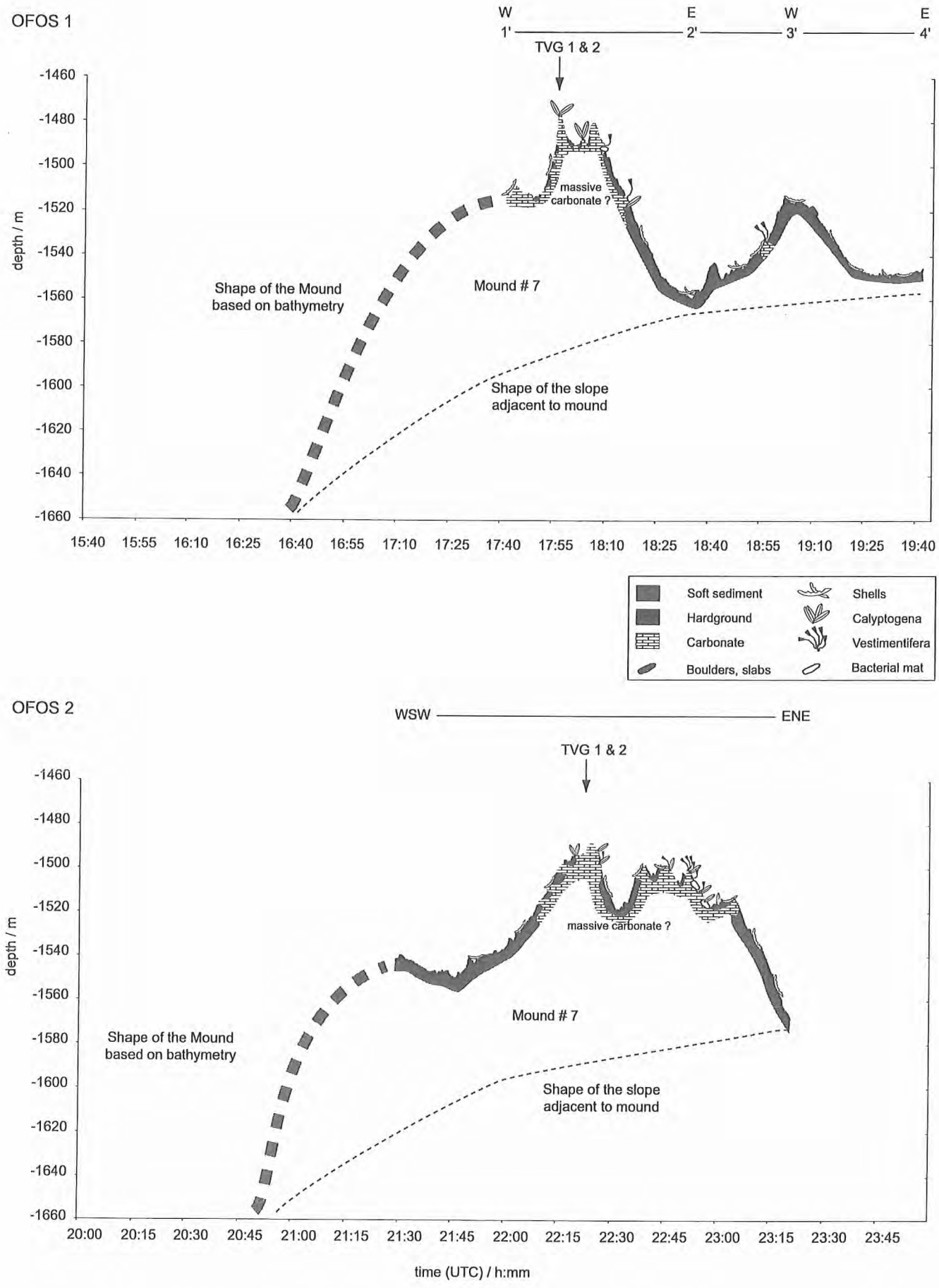


*Figure 6.4.1.4: OFOS depth profiles at Mound # 1. The outcropping carbonates at the top and on the flanks of the mound suggest that the whole summit, if not the entire mound, consist of carbonate.*

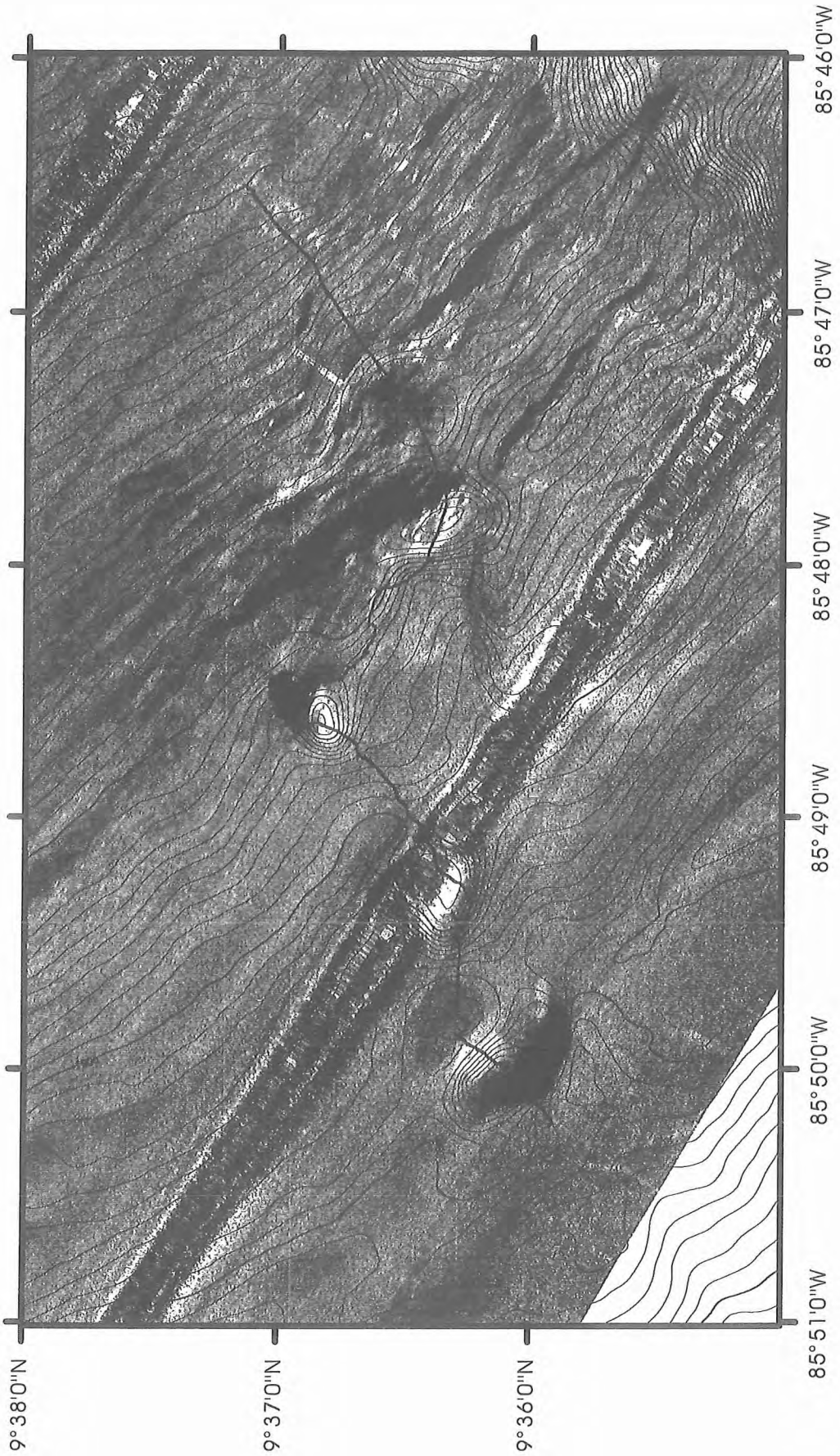


*Figure 6.4.1.5: TOBI image with overlaid bathymetry and the track of OFOS 3 in the area of Mound # 2-6. This map is on the same scale as Figure 6.4.1.6 . High backscatter (white) is found at mounds. Linear high and low backscatter features to the east of the two central mounds are interpreted as outcropping faults.*

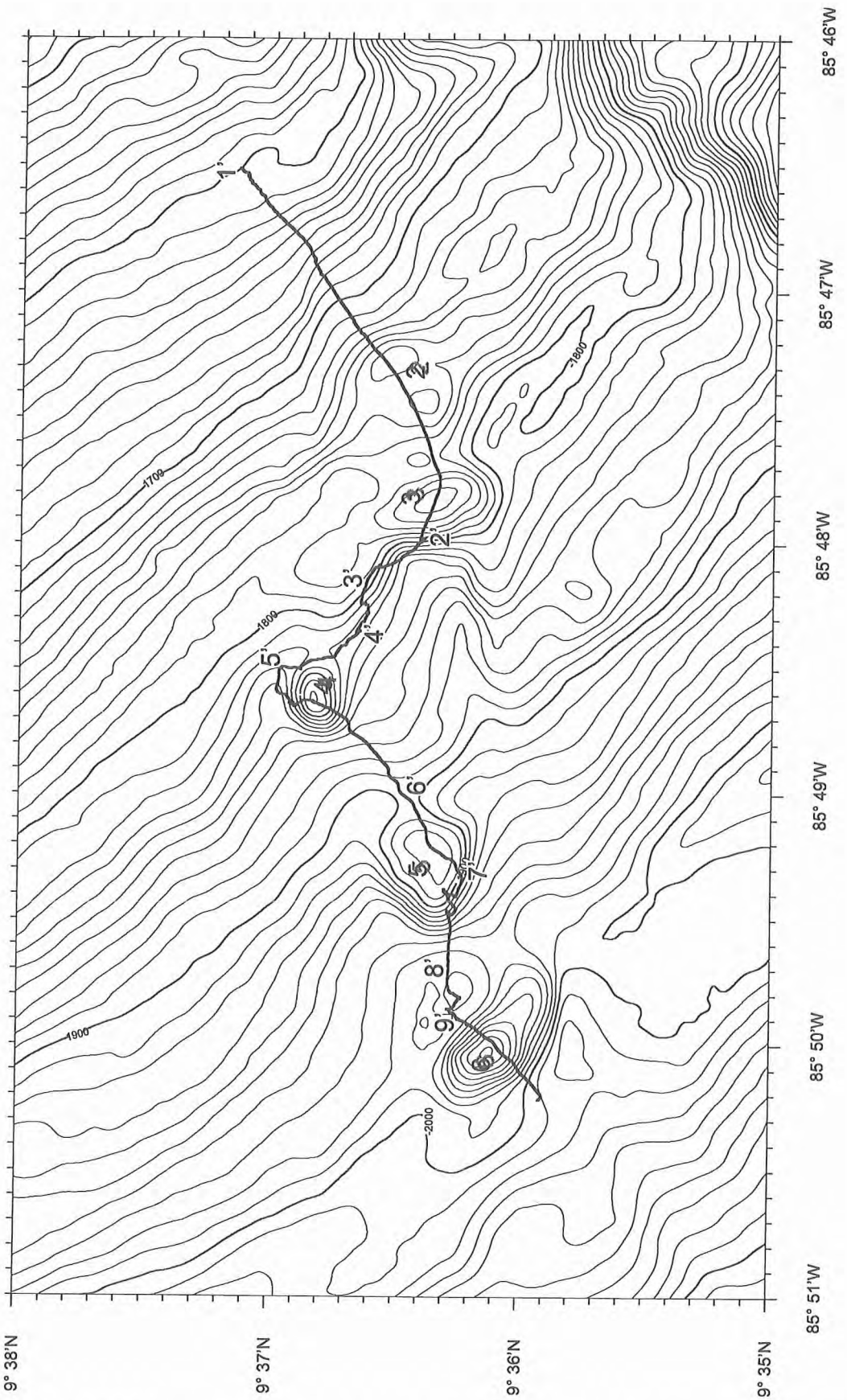


*Figure 6.4.1.6: OFOS 3 at Mound # 2-6. The survey revealed that: (1) the spotted high backscatter at the beginning ('1) corresponds to highly consolidated or lithified sediments, (2) slabs probably indicate the existence of a fault east of Mound # 2, (3) the sloping flanks of the mounds cause the pronounced high and low backscatter values, (4) layered carbonates crop out at the south flanks of Mound # 3 and 4, (5) low backscatter east of Mound # 6 (8'-9') caused by a difference in sediment texture or thickness (possibily recent sediment deposition in the lee of the mound).*

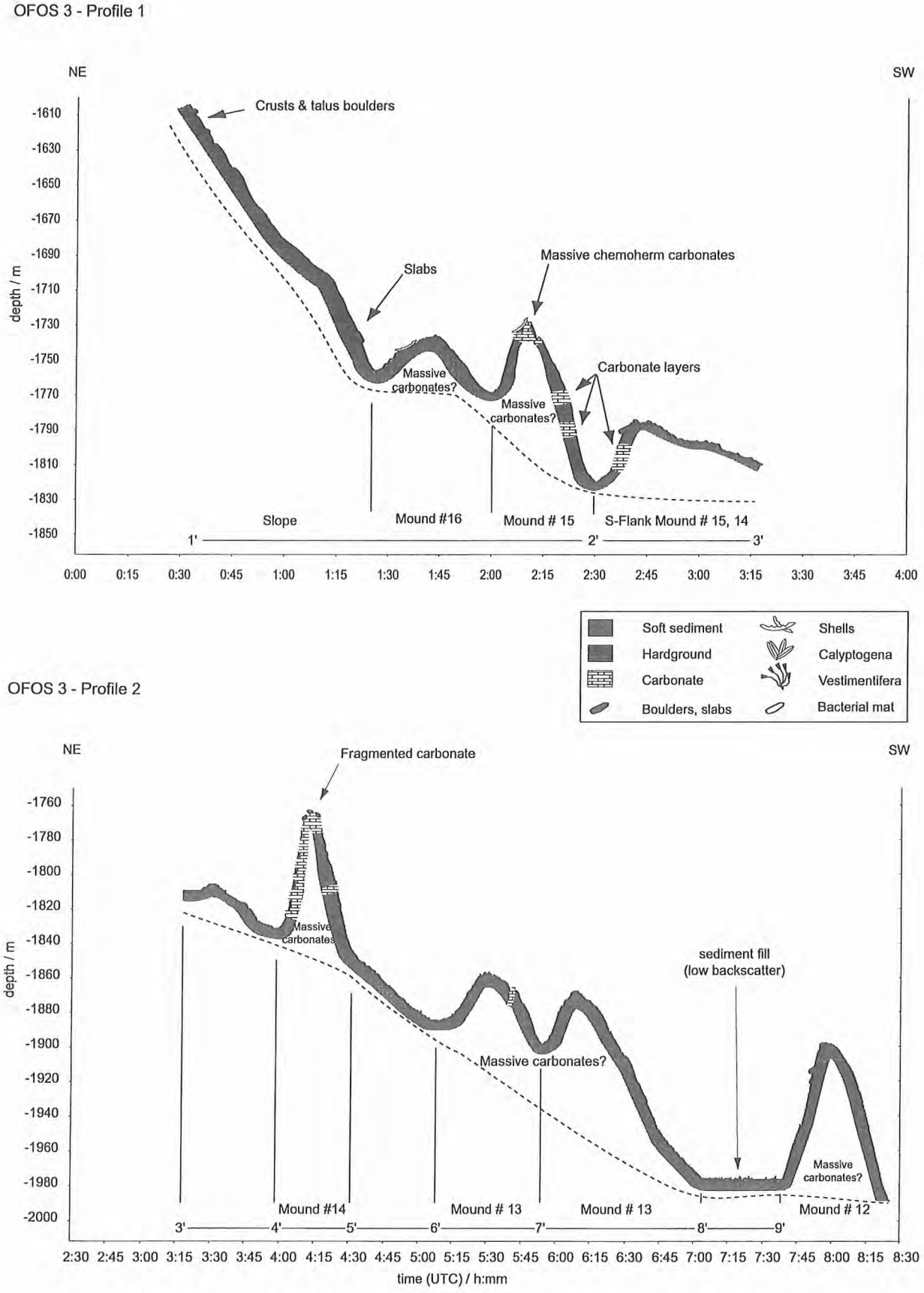


*Figure 6.4.1.7: OFOS 3 depth profiles at Mound # 2-6. The profile shows the shape of the mounds, the dotted line indicates the profile of the adjacent "mound-free" slope.*

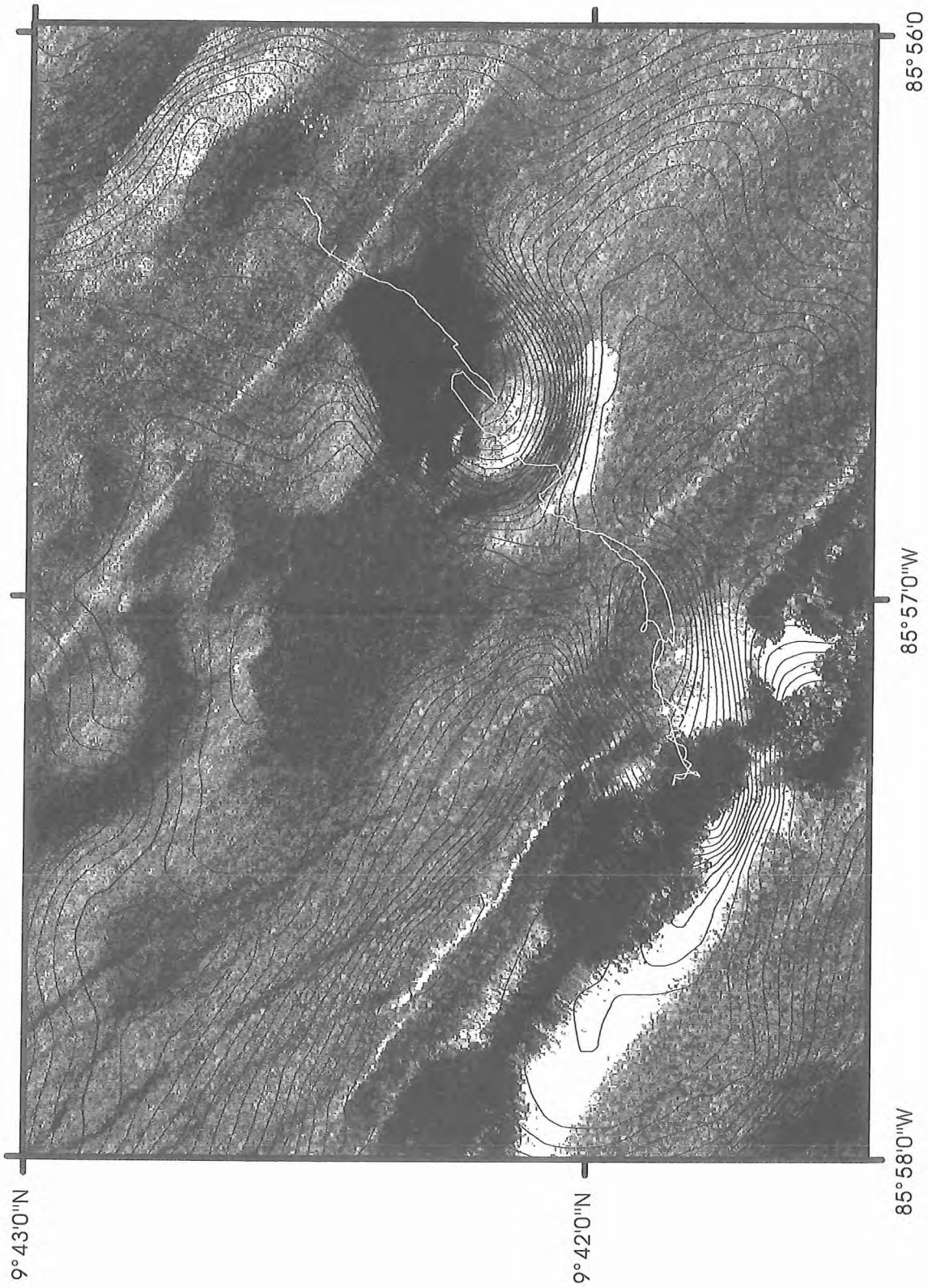


*Figure 6.4.1.8: TOBI image showing the same area as Figure 6.4.1.9. Linear, high and low backscatter features are faults. Mound 8 was poorly imaged as it lies directly beneath the TOBI track, but nevertheless still shows high backscatter.*

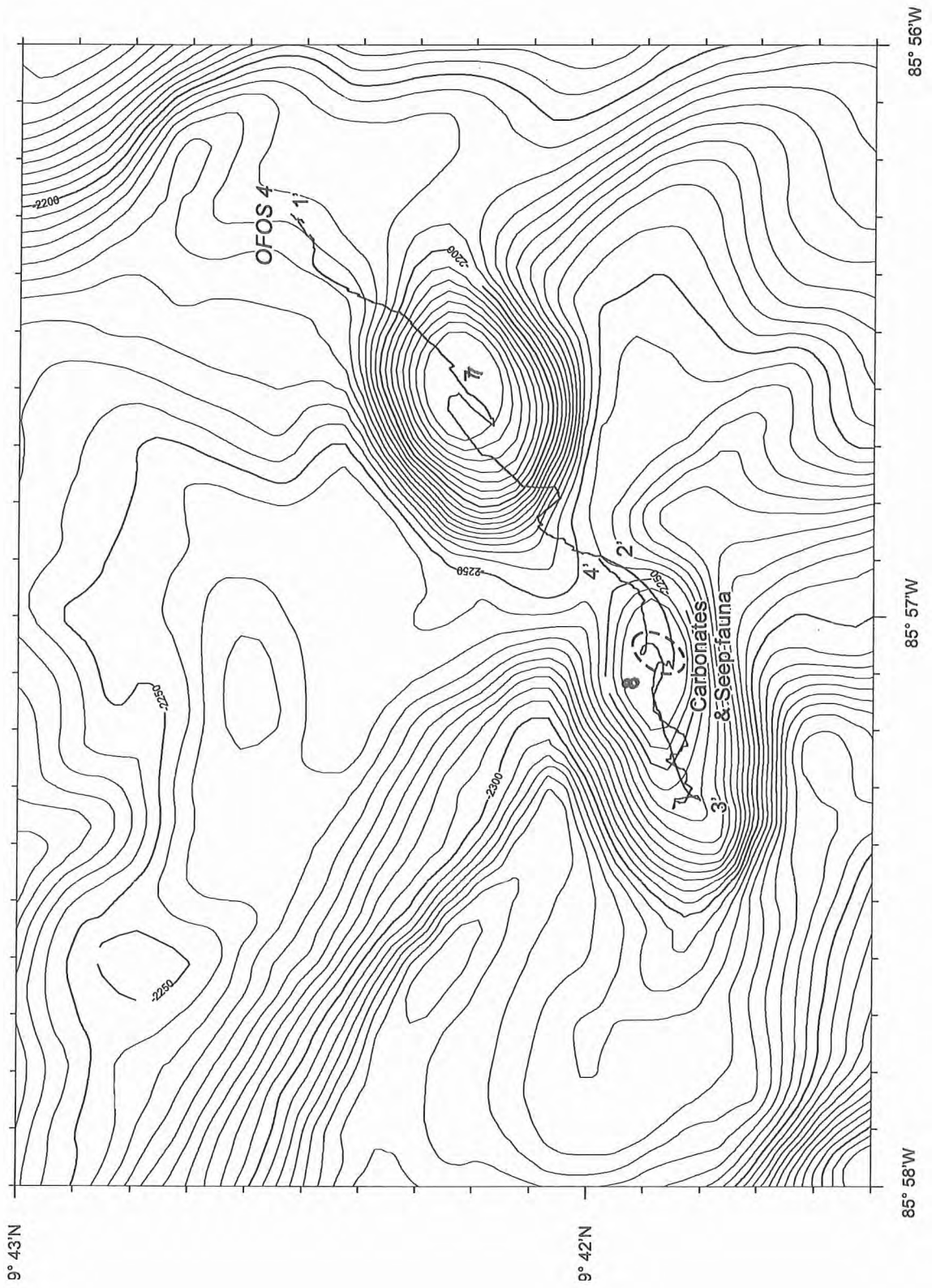


*Figure 6.4.1.9: OFOS 4 surveys at Mound # 7 and 8. Chemoherm-like carbonates, vestimentiferan tubeworms and clams were seen on top of Mound # 8.*

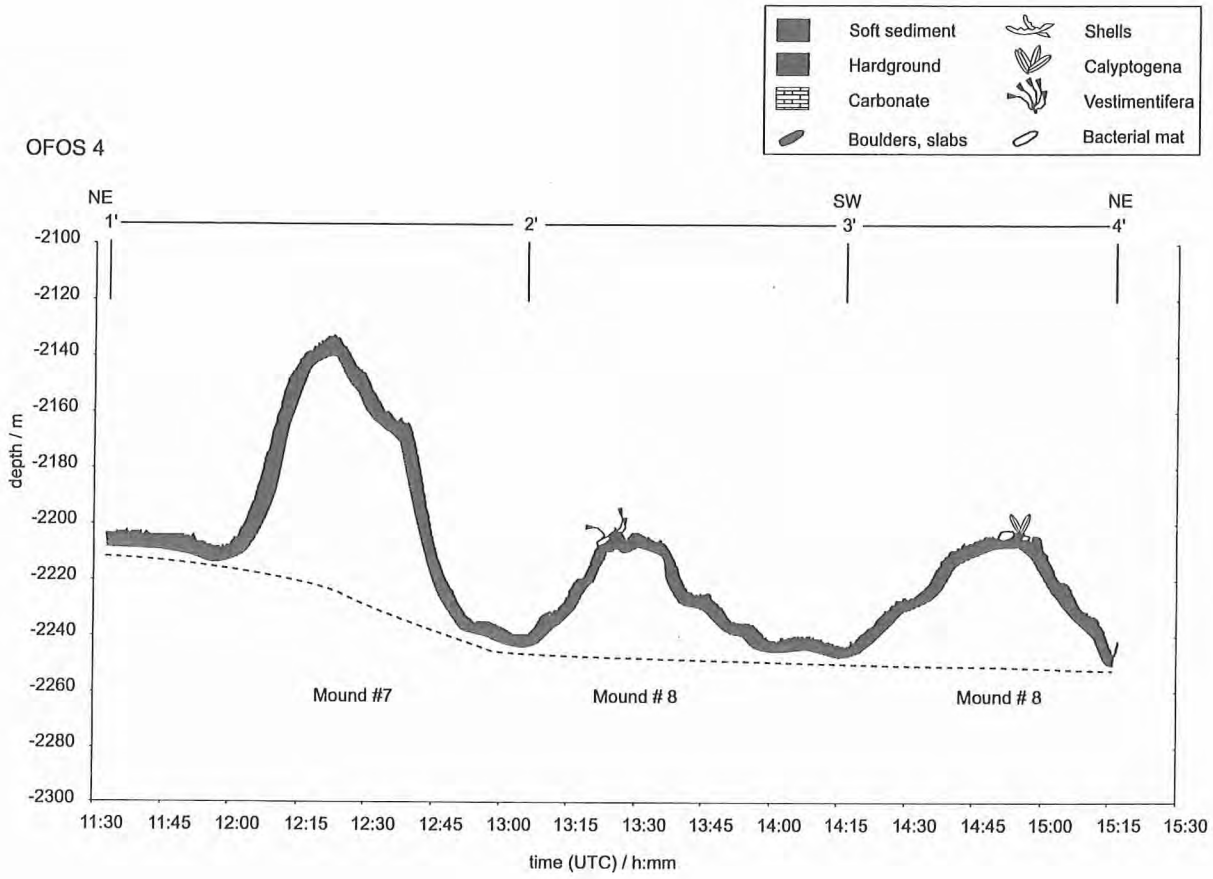


*Figure 6.4.1.10: OFOS 4 depth profile.*

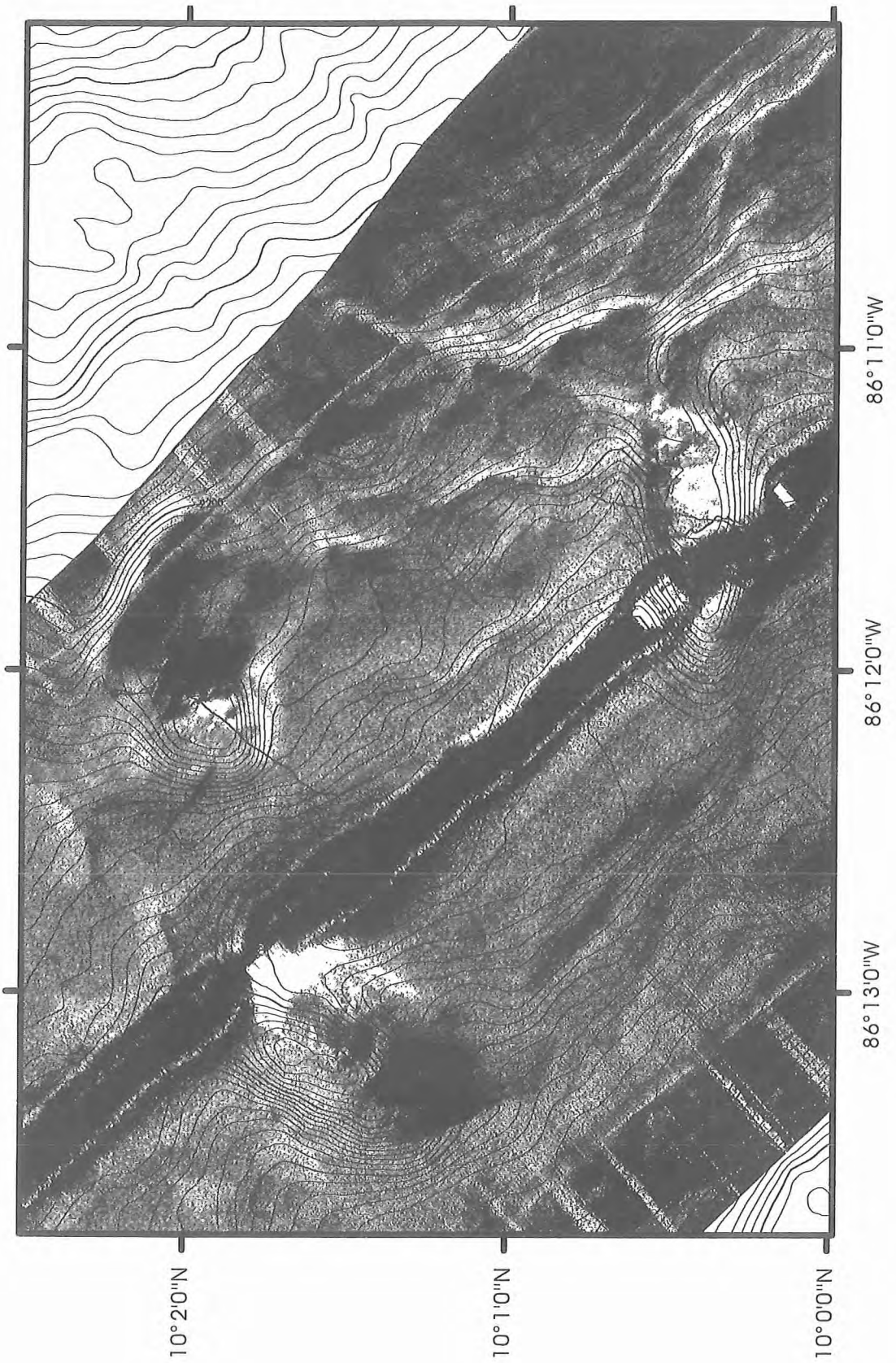


*Figure 6.4.1.11: TOBI image showing the same area as Figure 6.4.1.12. A complex fault pattern is shown by the pattern of linear features (mainly high backscatter) crossing the image, especially to the northeast of mound 10.*

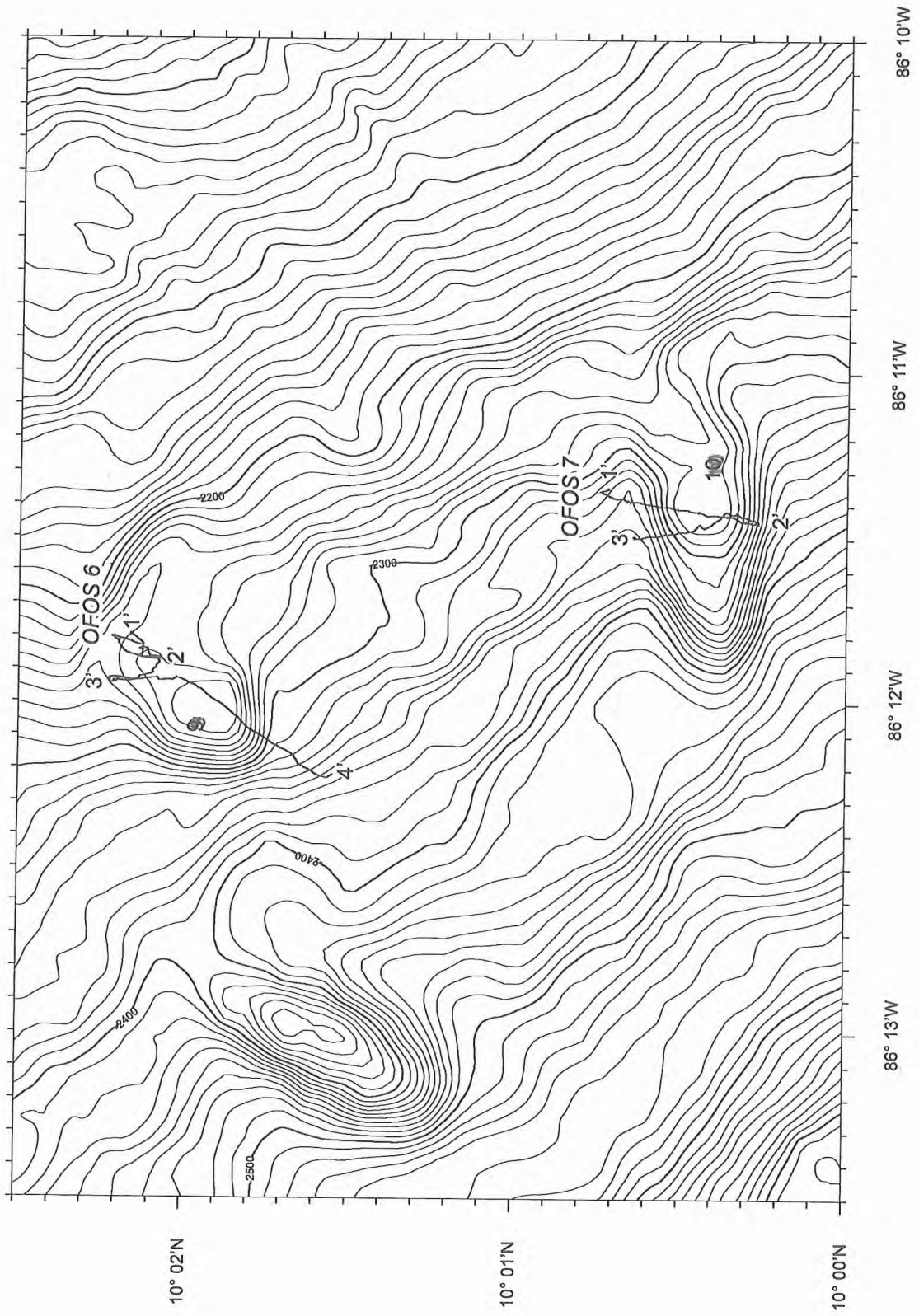


*Figure 6.4.1.12: OFOS profiles at mound # 9 and 10. High backscatter characterises the mounds (Figure 6.4.1.11). OFOS 6 surveyed Mound # 9 but did not reveal any signs of venting, i.e. carbonates or chemoautotrophic fauna. Mound # 10 is associated with faults (OFOS 7). At the northern flank and the top of this mound vigorous venting was indicated by an extensive clamfield and chemoherm carbonates.*

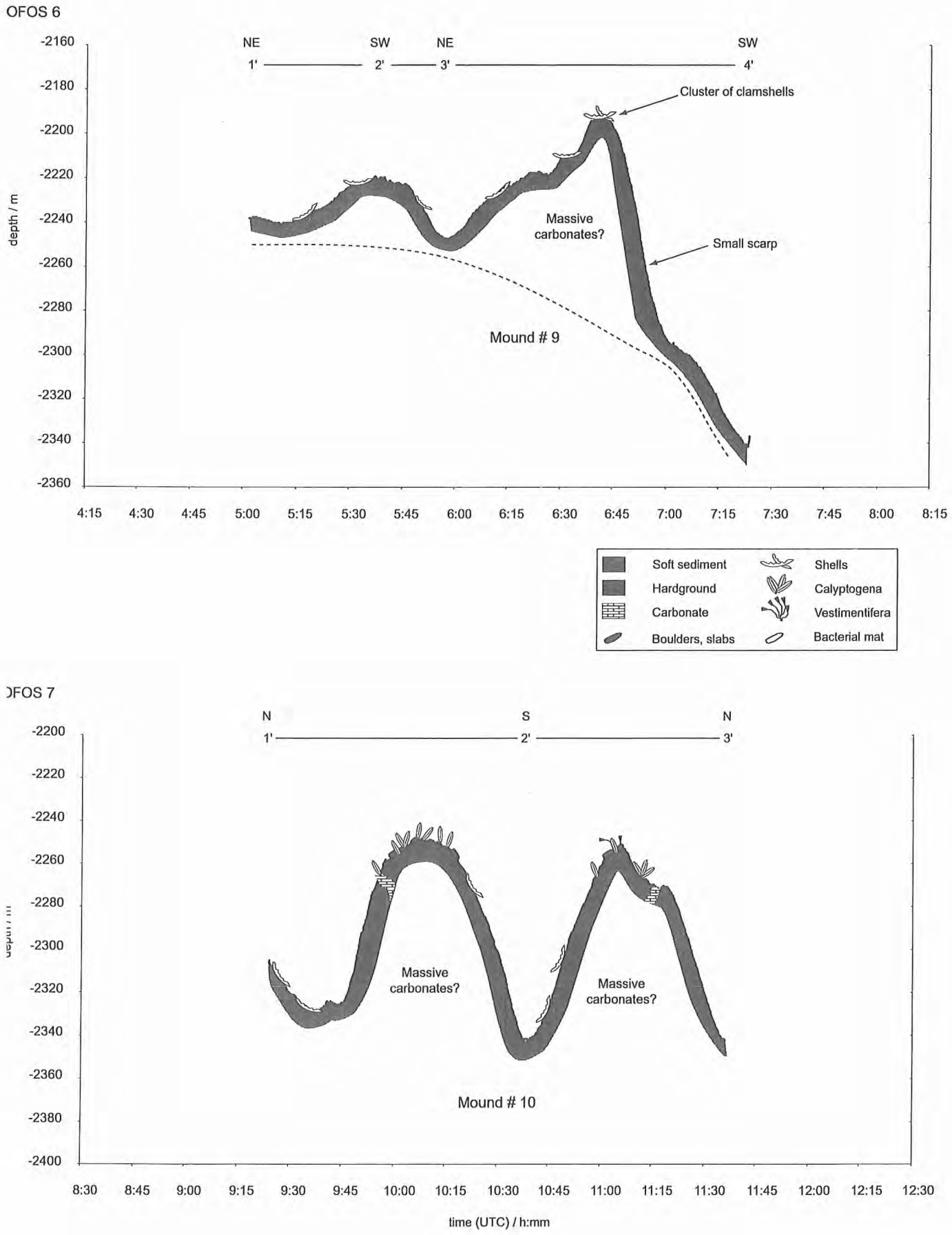


*Figure 6.4.1.13: Depth profiles of OFOS 6 at mound # 9 and OFOS 7 at Mound # 10.*

*Figure 6.4.1.14: Location of OFOS 19 and 21 at Mound # 11 and 12.*

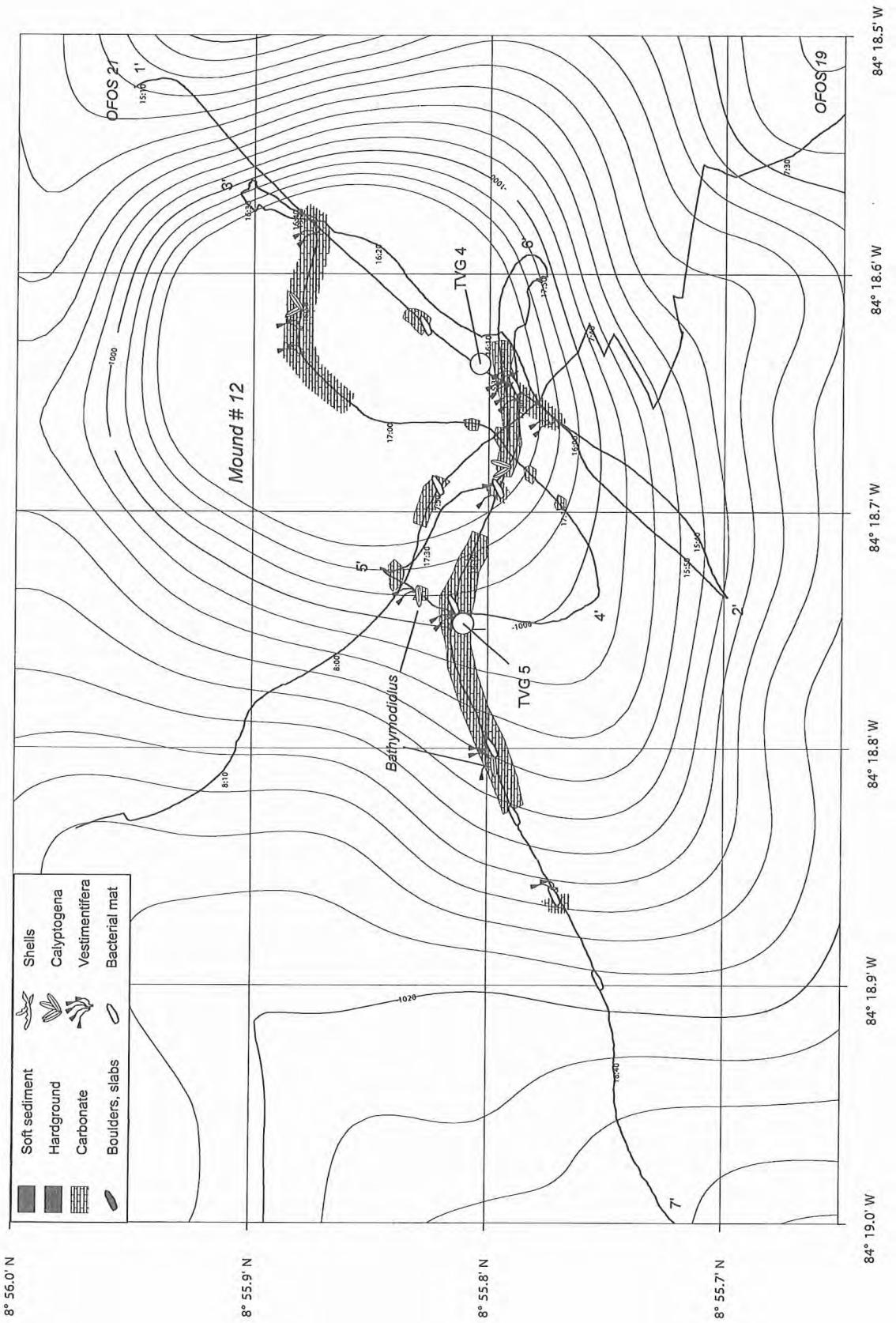


*Figure 6.4.1.15: Preliminary illustration of OFOS observations at Mound # 12. Please note that the bathymetry does not adequately image the small-scale morphology (Figure 6.4.1.15). The largest and most diverse seep area was found around the location of TVG 5.*

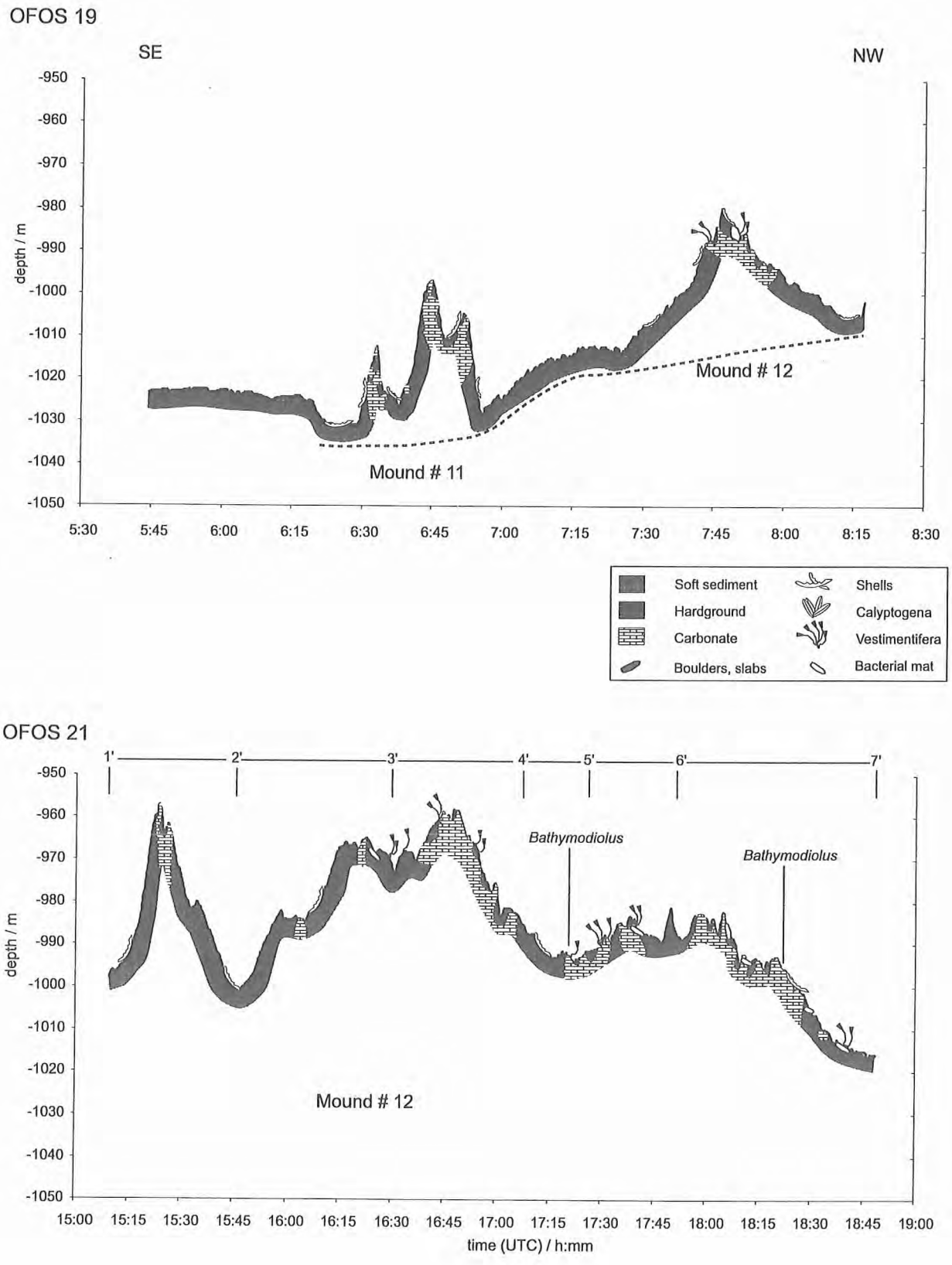


*Figure 6.4.1.16: Depth profiles of OFOS 19 and 21 at Mound # 11 and 12.*

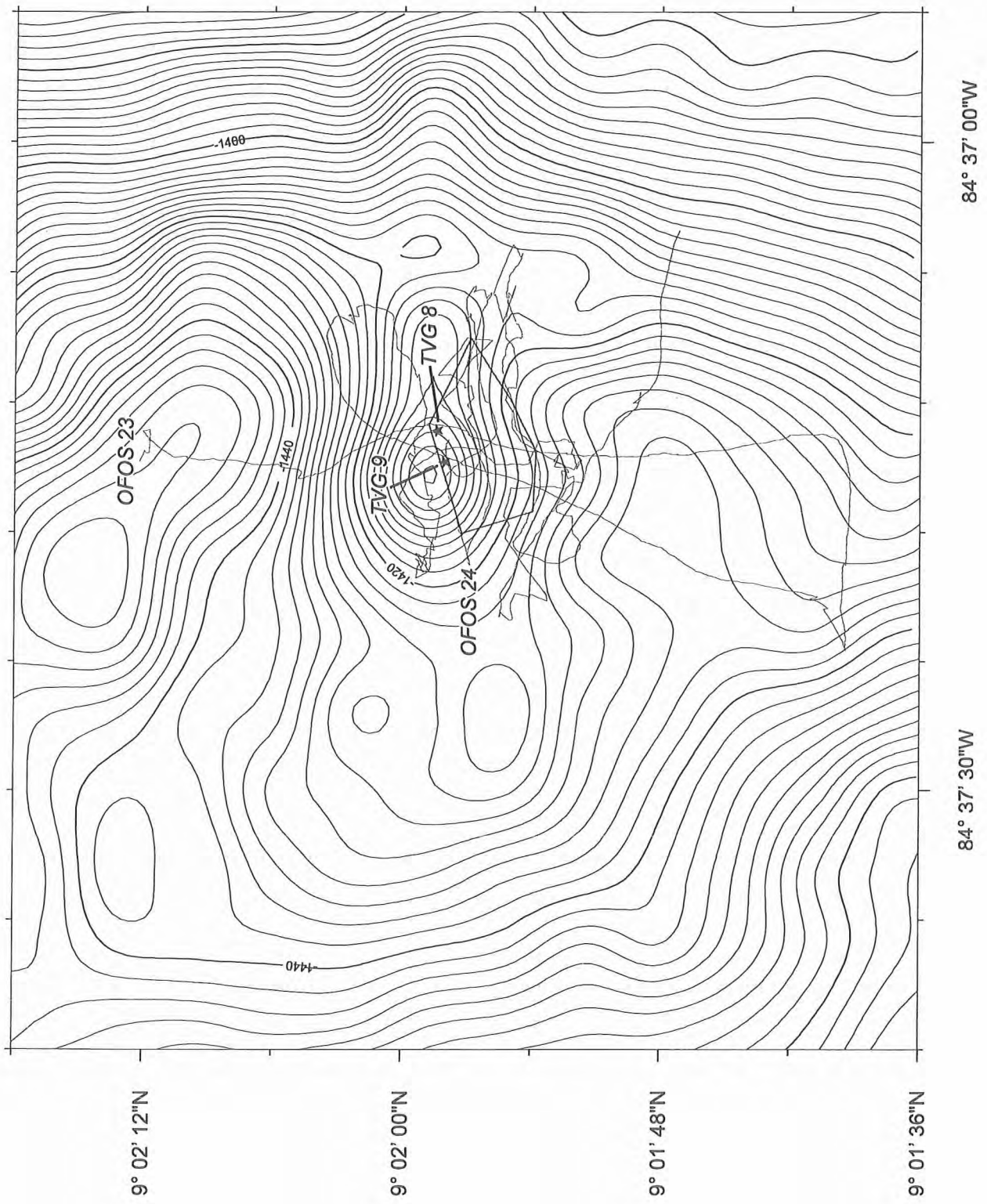


*Figure 6.4.1.17: Location of OFOS 23, 24 and TVG 8, 9 at "Ranero Mound". The polygon roughly indicates the extent of the vent field, i.e. the occurrence of carbonate, pogonophorans, mytilid and vesicomyid bivalves.*

In general, venting activity at Mound # 12 appears to be high, sustaining a luxuriant seep community. Further investigations should concentrate on this mound, which is among the most active ones surveyed during this cruise. Only at Mound # 13 the seep organisms occur in even larger areas.

Mound # 13 (Quepos Mound) OFOS 23, 24, TVG 8, 9
Mound # 13 were discovered a sampled during the last days of the cruise. The area influenced by methane seepage at this mound is by far the most extensive we have observed during this cruise.

### 6.4.2 High heatflux area

During the TicoFlux I expedition with R/V Maurice Ewing A. Fisher and the Shipboard Party conducted heatflux measurements as well as investigations on the porewater of sediments obtained by gravity- or pistoncorer. They report heatflux values (> 600 mW $m^{-2}$) and porewater compositions (high Ca concentrations) which strongly indicate hydrothermal venting. Based on these findings we surveyed this area located on the ocean plate with OFOS 8 and 9 (Fig. 6.4.2.1). The plan was to survey the two sites, at which the highest heatflux values were found, in a North-South transact by OFOS 8 and, then, to turn East in order to survey the flank of the seafloor elevation, which is the surface expression of a basement high (Fig. 6.4.2.2). Due to wind and currents we did not actually reached the (most Northward) point with the highest heatflux values. Furthermore, we had to heave OFOS for a while in order to allow the ship to adjust position. However, the track did not reveal any indications for fluid venting. A second OFOS profile (OFOS 9) were conducted at a second site with high heatflux values (> 300 mW $m^{-2}$) further to the North. Again, no indications for fluid venting were found.

### 6.4.3 Seamount subduction

The subduction of seamounts and ridges on the lower (oceanic) plate cause deformation of the upper plate. High resolution bathymetry and TOBI images show clearly the uplift and faulting processes of the overriding upper plate (dome), in addition to mass wasting processes in the wake of the subducted seamount or ridge (scarp). We have surveyed with OFOS several of these structures in order to, first, find indications for fluid venting and, second, reveal the surface expressions of tectonic processes.

Scarp of Fracture Zone Trace OFOS 5
A narrow ridge mark the boundary between the lithosphere formed at the East Pacific Rise and the Cocos-Nasca spreading center on the oceanic plate named Fracture Zone Trace (Barckhausen et al., 2001). The subduction of this fracture zone and its associated morphological structures has caused uplift of the upper plate sediments and landsliding in the wake of it, a feature we call here the Scarp of the Fracture Zone Trace. The TOBI image revealed high backscatter in the area of the multiple headwalls as well as in the deposit area. OFOS 5 surveyed the scarp from the headwalls between 2210 m and 2700 m and the deposit areas down to a depth of 3100 m (Fig. 6.4.3.1). In contrast to the seamount scarps surveyed during SO 144 cruise, this scarp does not show abundant indications for venting. The OFOS depth profile over the time (Fig. 6.4.3.2) traces well the tilted blocks. We found only few segments of the headwalls which show bedding. The talus blocks areas are also limited. Few scattered empty shells were observed. No vent indications were recorded at the deposit area where high backscatter was found. Mass wasting seems to be minor at present. Most structures are sediment covered.

Uplifted area above Christmas Ridge (Rio Bongo Scarp) OFOS 10
The Rio Bongo Scarp clearly indicates the location of the subducted Christmas Ridge. Due to the subduction of the Christmas Ridge the upper plate sediments are uplifted, forming a dome. The TOBI image, which covers only the area south of 9°19.5' N, indicated high reflectivity at the top of the dome. A survey (OFOS 8) during SO 144 revealed the existence of carbonates and clams at some sites on the NW Flank of the uplifted areas. With OFOS 10 we surveyed the top area of the dome and the eastern flank (Fig. 6.4.3.3). The

survey revealed that the whole top area at water depth above 550 m consists of hardground, that is probably carbonate. Although the origin of this carbonate is largely unknown, we speculate that tectonic processes in the course of ridge subduction have caused the carbonate exposure. Along the track we observed a few sites at which the hardground was cutted. There, NE-SW striking bedding was seen. We found no clear evidence for fluid venting. At some sites the outcropping rocks were very bright or had coating of whitish material, that may or may not be bacterial mats. Only at one location, around 20:17 h (UTC), whitish material on rocks as well as in depressions appeared to be bacterial mats. Here, rocks with sharp edges were seen, that could probably be chemoherm carbonates. Additionally, at 20:27:24 something was observed that could possibly have been rising gas bubbles. In general, we are not convinced that these structures are related to venting. The OFOS line was interrupted for a while because the captain was afraid that we caught a fishing line, thus, OFOS was heaved to the surface and lowered to the seafloor again. The following track surveyed faults that were largely sediment covered and did not show any indication for venting activity. In general, this structure is probably not a high priority target for future investigations.

Jaco Scarp OFOS 11, 12, TVG 3

A detailed image of Jaco Scarp was obtained by TOBI during SO 144. At that cruise OFOS tracks 1&2 surveyed the uplifted areas and the scarp. We used a variety of OFOS surveys to further understand tectonic processes and fluid venting patterns at this feature, which was also imaged by DTS # 3. That DTS covered along WE profiles the uplifted areas. The regular survey was followed by a high resolution (410 kHz) line, which was planed to cover the circular structures seen in the TOBI, but the DTS passed these structures to the south. The last line then followed the scarp downslope.

OFOS 11 was deployed in order to survey the circular structures with high backscatter. We crossed these with an east to west profile. Due to wind and currents the ships speed was very low. In the area of high backscatter the seafloor appears to be continuously paved by carbonates below a very thin sediment cover in which very scattered bivalves occur. At some areas, donut-shaped carbonates occur which are surrounded by clamshells. We deployed TVG 3 in order to sample these carbonates. Again, this grab felt to the we were able to sample this carbonates, 89 living specimens of the solemyid bivalve *Acharax johnsoni*, shells of vesicomyid and thyasirid clams and sediments with a week sulfidic odour. The high abundance of *Acharax*, that were approximately the same size (46.2 ± 8.7 mm), indicate that there is a considerable but low supply of sulfide. This sulfide is possibly produced by anaerobic methane oxidation and, thus, we conclude that methane venting does occur at present.

Additional OFOS surveys were conducted towards the end of the cruise (OFOS 25, 26). These did not reveal any further indications for fluid venting. With TVG # 7 we were able to sample carbonate rocks.

Parrita Scarp OFOS 13, 22

Two OFOS surveys during the SO 144 cruise and this leg revealed that only few indications for venting exist in the uplifted area of Parita Scarp. Additionally, during both cruises the area West of Parrita Scarp was surveyed. There, the TOBI image showed high backscatter reflectivities. Both OFOS runs showed only infrequent clamshells. Later during the cruise the area was surveyed by DTS and revealed the existence of very small mounds, which were hardly seen on the TOBI image and do not show up in the bathymetry. This small mounds were not surveyed by OFOS.

"Frontal collision" OFOS 15

With OFOS 15 we surveyed the collision zone between the accretionary wedge and a seamount. The area at the frontal wedge is characterised by very steep morphology. Beside few scattered clamshells we found no indication for methane seepage.

"Small Seamount Scarp" OFOS 16

With OFOS 16 we surveyed the uplifted area of a seamount, that is probably smaller than the seamounds subducted at Jaco or Parrita Scarp. We did not find any indications for methane seepage.

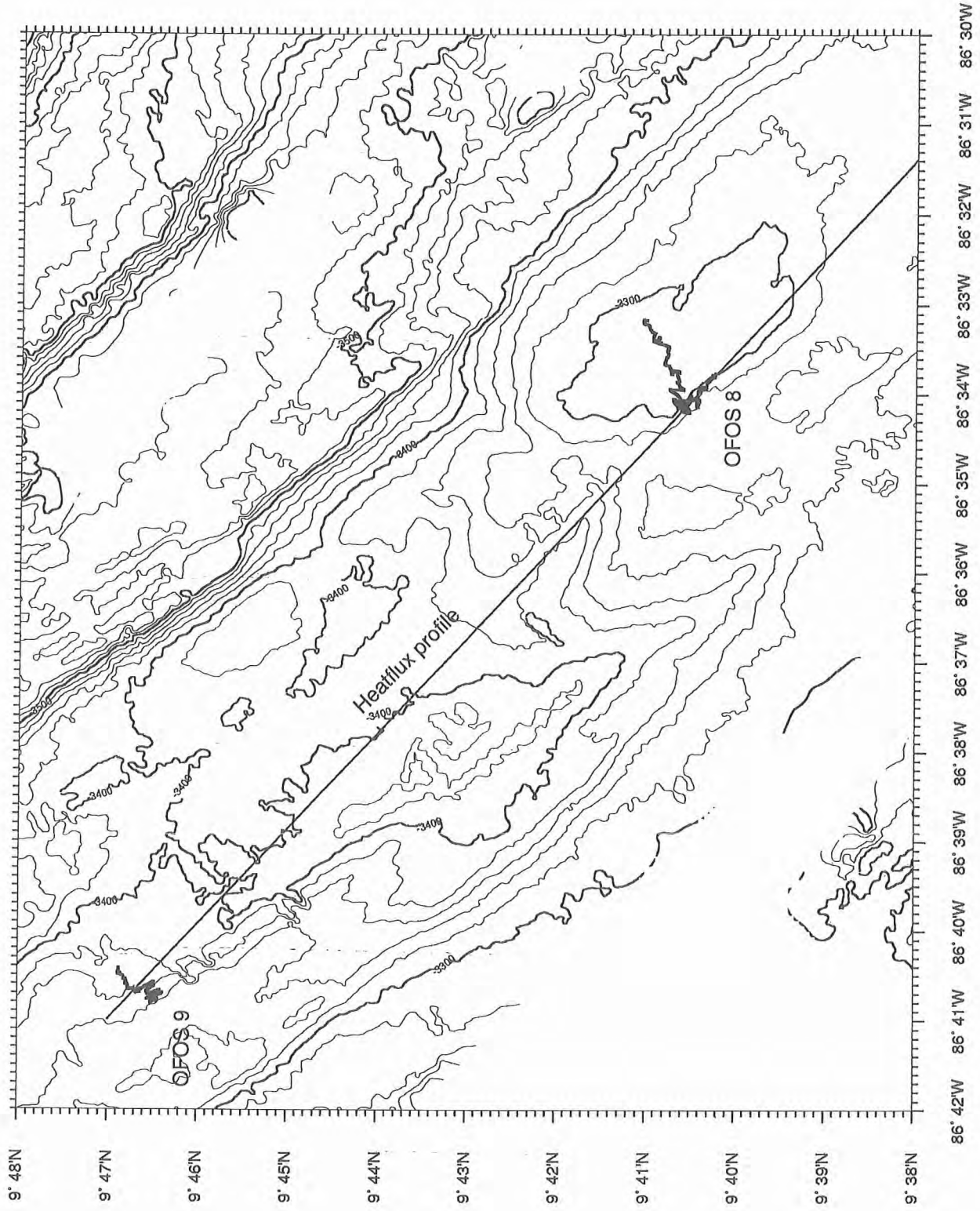


*Figure 6.4.2.1: Location of OFOS 8 and 9 profiles at the high heatflux sites on the ocean plate.*

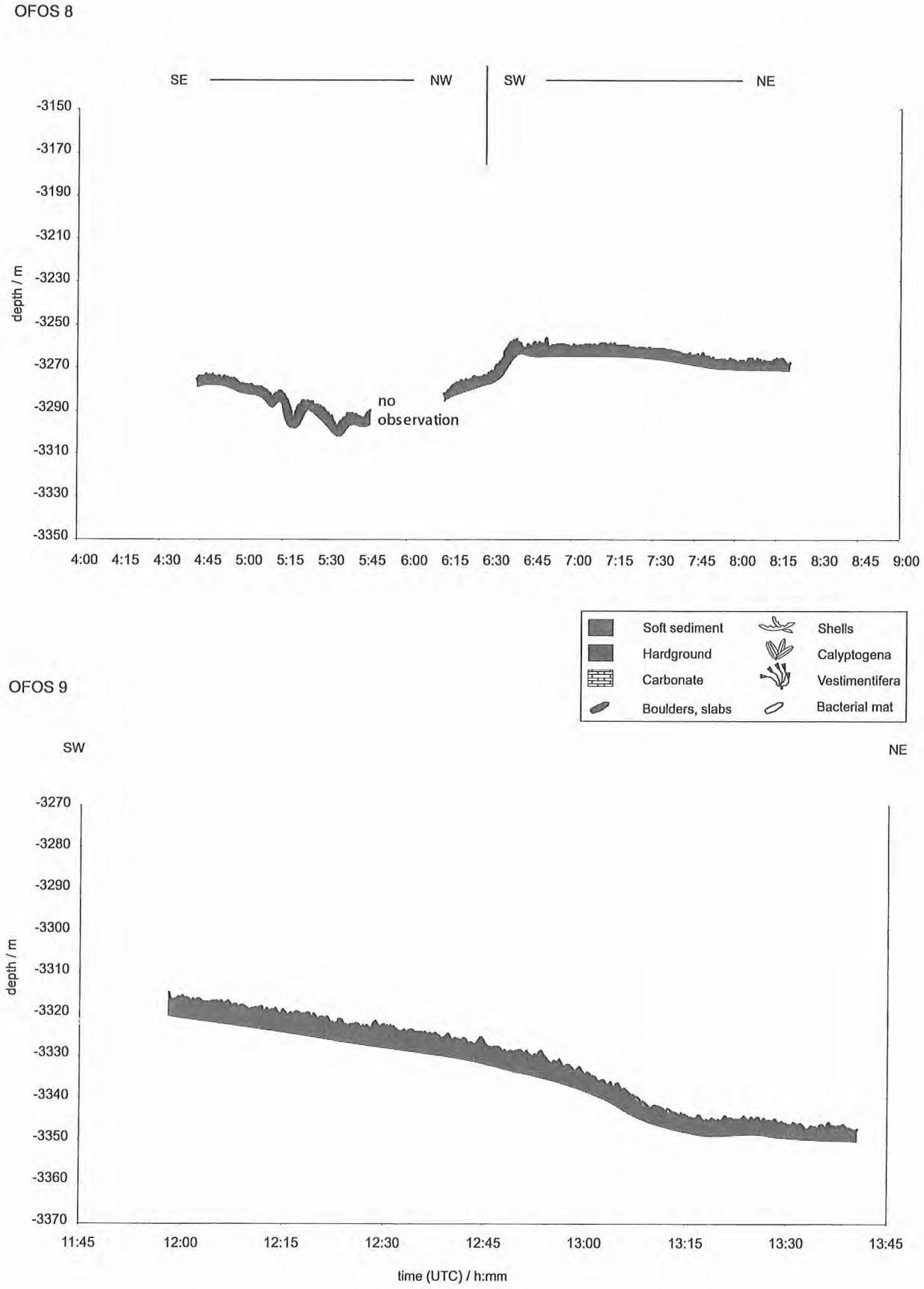


*Figure 6.4.2.2: Depth profiles of OFOS 8 and 9 at the high heatflux site on the ocean plate. We found no evidence for hydrothermal venting.*

### 6.4.4 Landslides

Quepos Landslide OFOS 18, 20, TVG 6
An OFOS survey conducted during SO 144 at the Quepos landslide (OFOS 4) revealed that enormous bacterial mats cover the sediments at and below the headwall of this landslide. Additionally, bacterial mats and clams were observed in the area of the slide tail. The occurrence of bacteria in the headwall area can be explained either by anaerobic methane oxidation or by anaerobic organic matter oxidation. We surveyed the area with two OFOS profiles (18 & 20), that run parallel to the SO 144 OFOS. OFOS 18 confirmed the existence of the bacterial mats covering the sediments below the headwall. Below, at the slide mass, we observed with OFOS 18 and 20 very few bacterial mats and no living clams or clamshells that are typical for methane venting. With TVG 6 we sampled sediments covered by bacterial mats just below the headwall. Just before the grab touched the ground we saw in the cameras, that thin Beggiatoa-like bacterial filaments were looking through the sediment surface. When the grab came close to the sea surface we saw bubbles rising from the grab. On deck, gas was released from the sediment. The grab was completely full of sediment that was still increasing in volume due to degassing. The entire sediment was mousse-au-chocolate-like, highly porous, although at the same time considerable "dry". It had a considerable sulfidic odour. Several 2-3 cm thick layers of cemented sediments were found throughout the sediment. The sediment surface did not remain intact and, thus, we did not find any bacterial mats. In conclusion, we believe that methane venting rather than anaerobic organic matter oxidation cause sulfidic conditions. Porewater studies are needed to confirm which geochemical pathway causes the sulfidic conditions. The area covered by this bacteria are large enough to be sample by conventional equipment, i.e. multicorer or gravitycorer.

### 6.4.5 Accretionary wedge

Accretionary wedge at graben at crest of Cocos Ridge (off Osa Peninsula)
The wedge where the graben (formed at the crest of the Cocos Ridge) collides with the upper plate is characterised by a largely undisturbed accretionary sequence. At the very frontal slope of these sequence linear patterns of alternating high and low backscatter imaged by TOBI exists. Based on geophysical data, that show the greatest porosity reduction at the frontal prism, this area should be influenced by fluid escape. With OFOS 14 we surveyed the front down to the oceanic plate, but could not detect any indication for fluid venting. The seafloor was covered by very soft sediment, thus, no geological features associated with deformation processes could be observed.

Accretionary wedge along seismic line SO 81 # 05
The accretionary wedge along the seismic line SO 81 # 05 (see (Huene et al., 2000) for location) was surveyed by OFOS 17 in order to search for evidence of fluid venting. This area is, as shown by the seismic line, highly influenced by deep-seated faults. The seafloor expressions of these faults are probably small displacements seen on the OFOS depth profile. We did not discover living chemoautotrophic species or carbonate precipitations during this deployment. The seafloor was uniformly covered by soft sediment. However, we found shells that probably originate from vesicomyid clams that are indicative for methane venting processes.

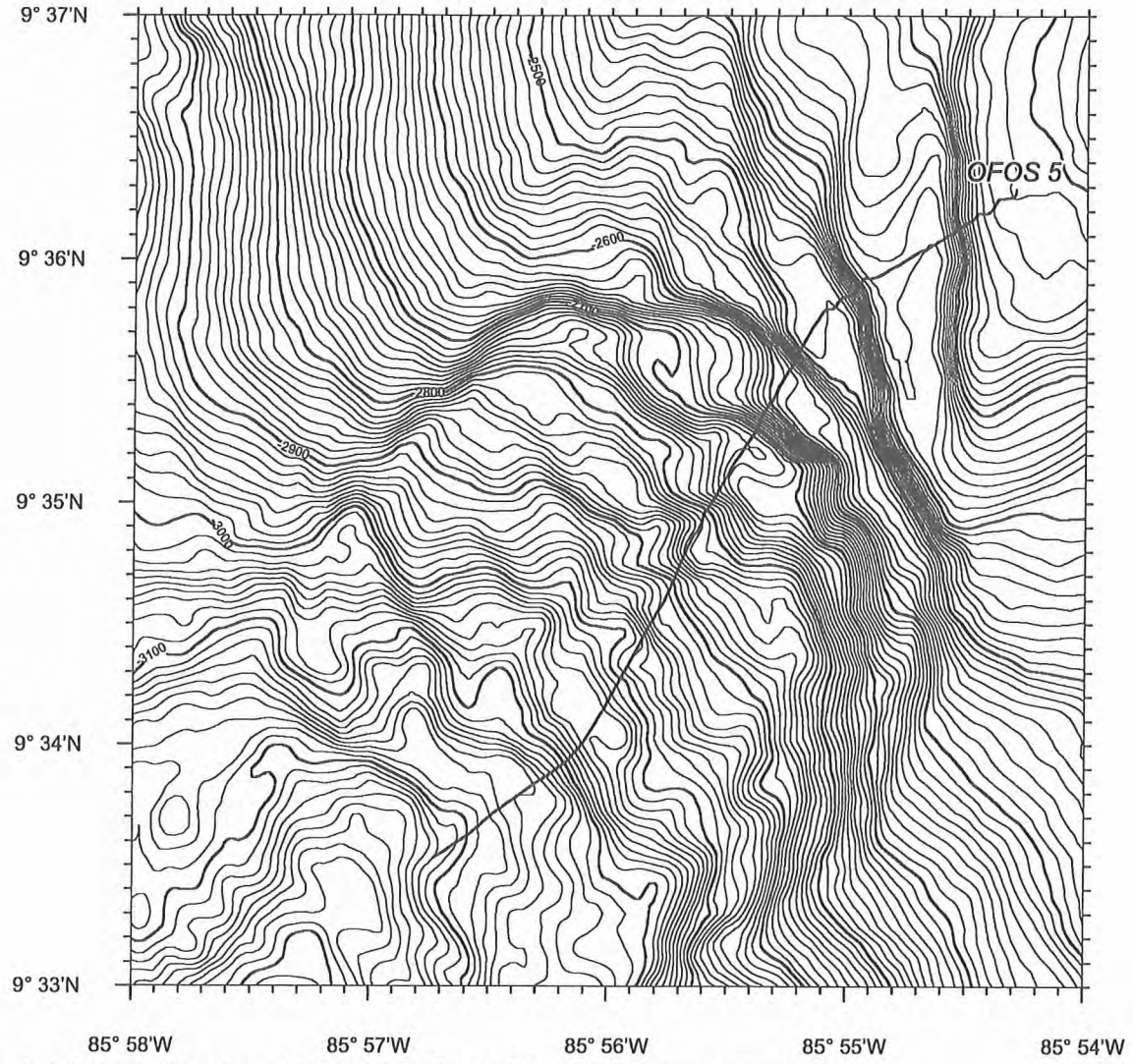


*Figure 6.4.3.1: Location of OFOS 5 profile at Scarp of Fracture Zone Trace.*

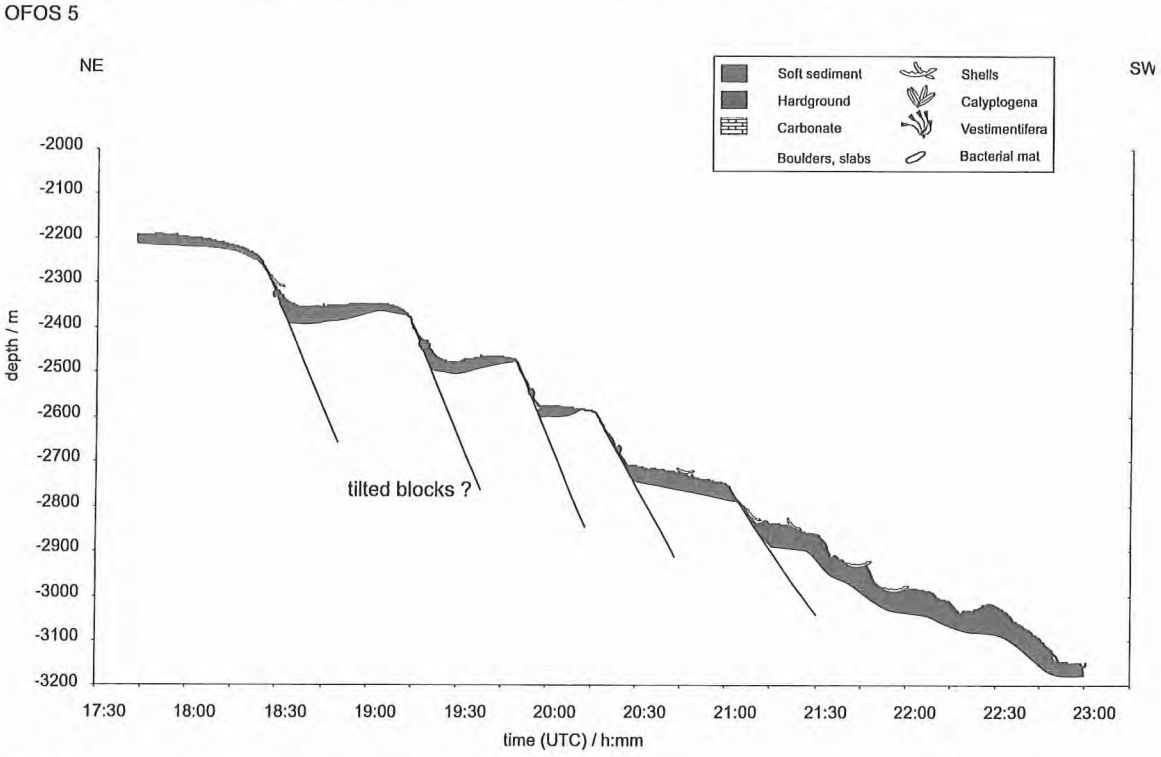


*Figure 6.4.3.2: OFOS 5 depth profile at Scarp of Fracture Zone Trace. Beside very few scattered clamshells we found no evidence for fluid venting.*

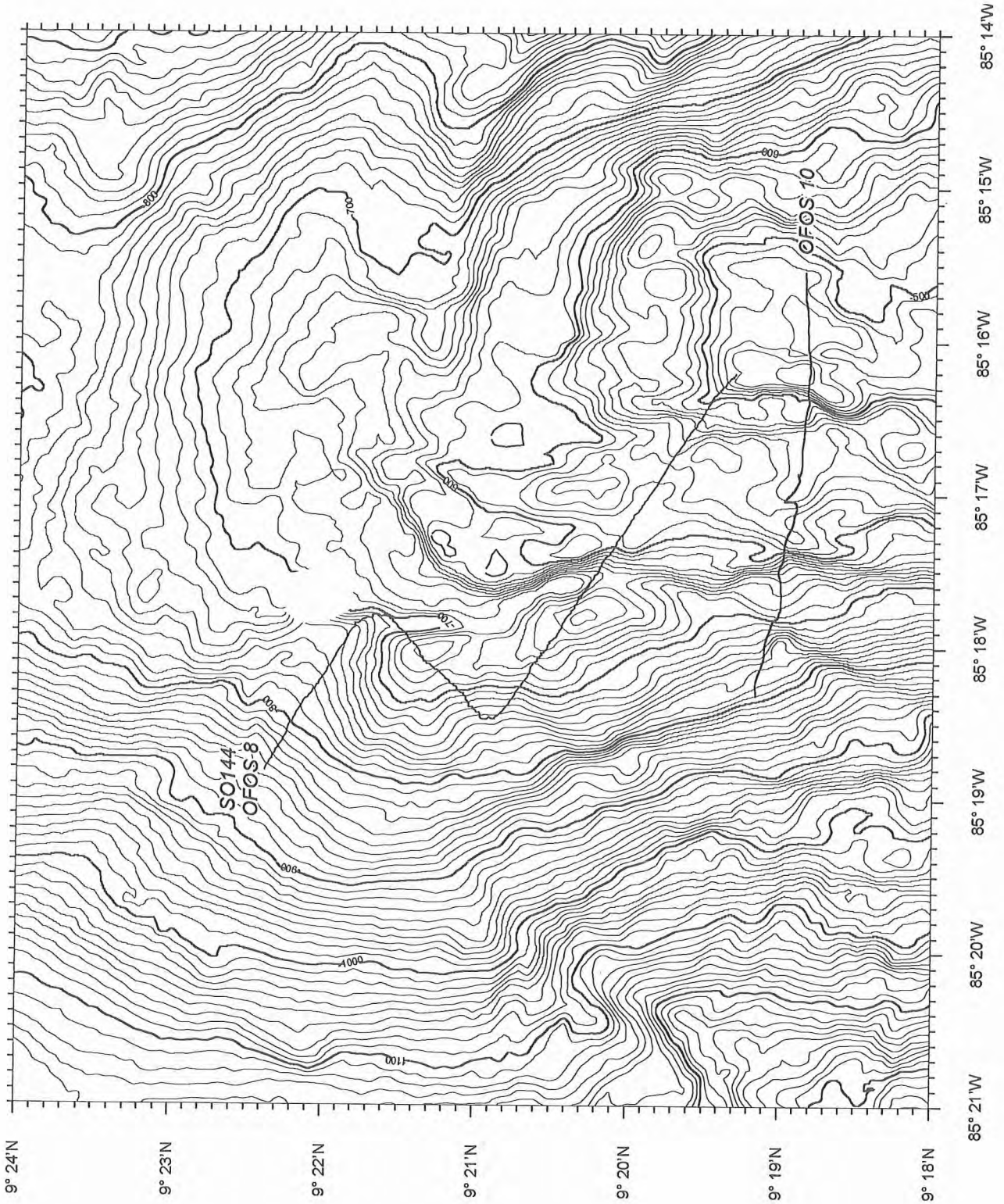


*Figure 6.4.3.3: Location of OFOS profiles at uplifted area of Rio Bongo Scarp.*

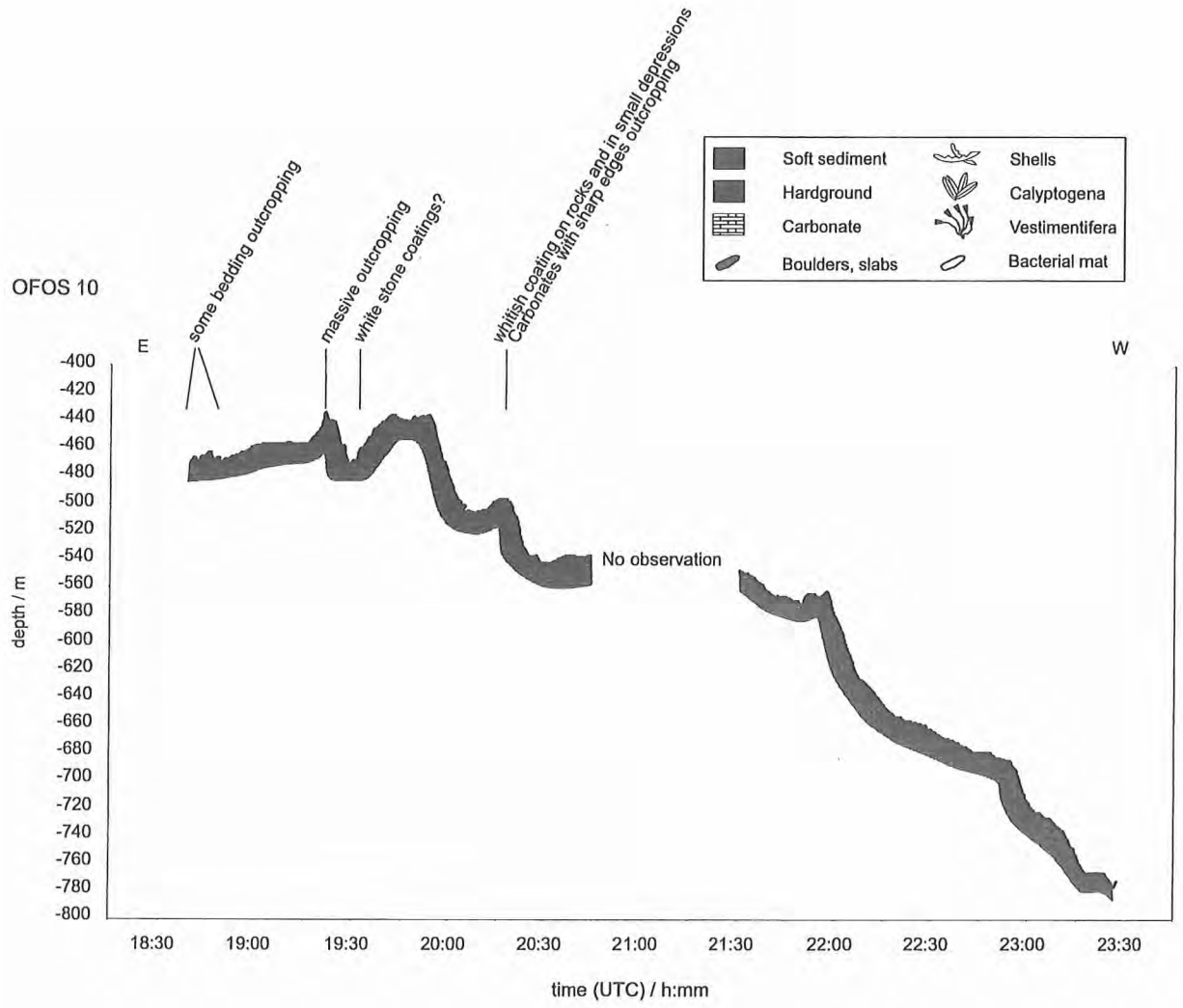


*Figure 6.4.3.4: OFOS 10 depth profile at uplifted area on Rio Bongo Scarp. The entire top area above 550-m water depth consists of hardground. This is probably outcropping massive carbonate forming a uniform flat plateau. The hardground is cutted at places, exposing bedding that is NE-SW striking. We found no indication for fluid venting beside whitish coatings on rocks and in depressions that can possibly be bacterial mats and chemoherm-like carbonates.*

*Figure 6.4.3.5: TOBI image of Jaco Scarp.*

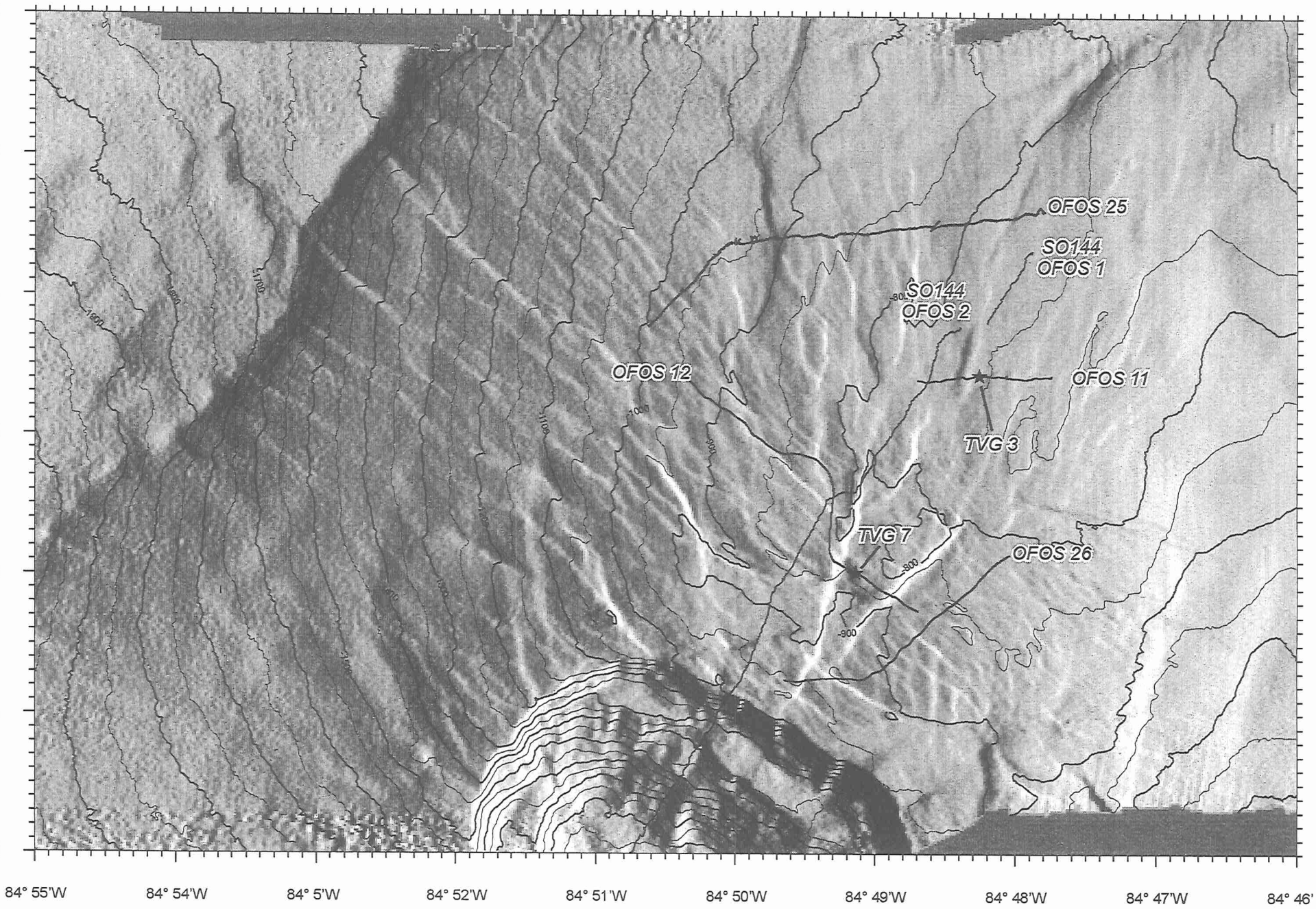


*Figure 6.4.3.6: Locations of OFOS tracks and TVG sampling stations at Jaco Scarp. The high-resolution bathymetry was obtained by the Simrad system during this cruise.*

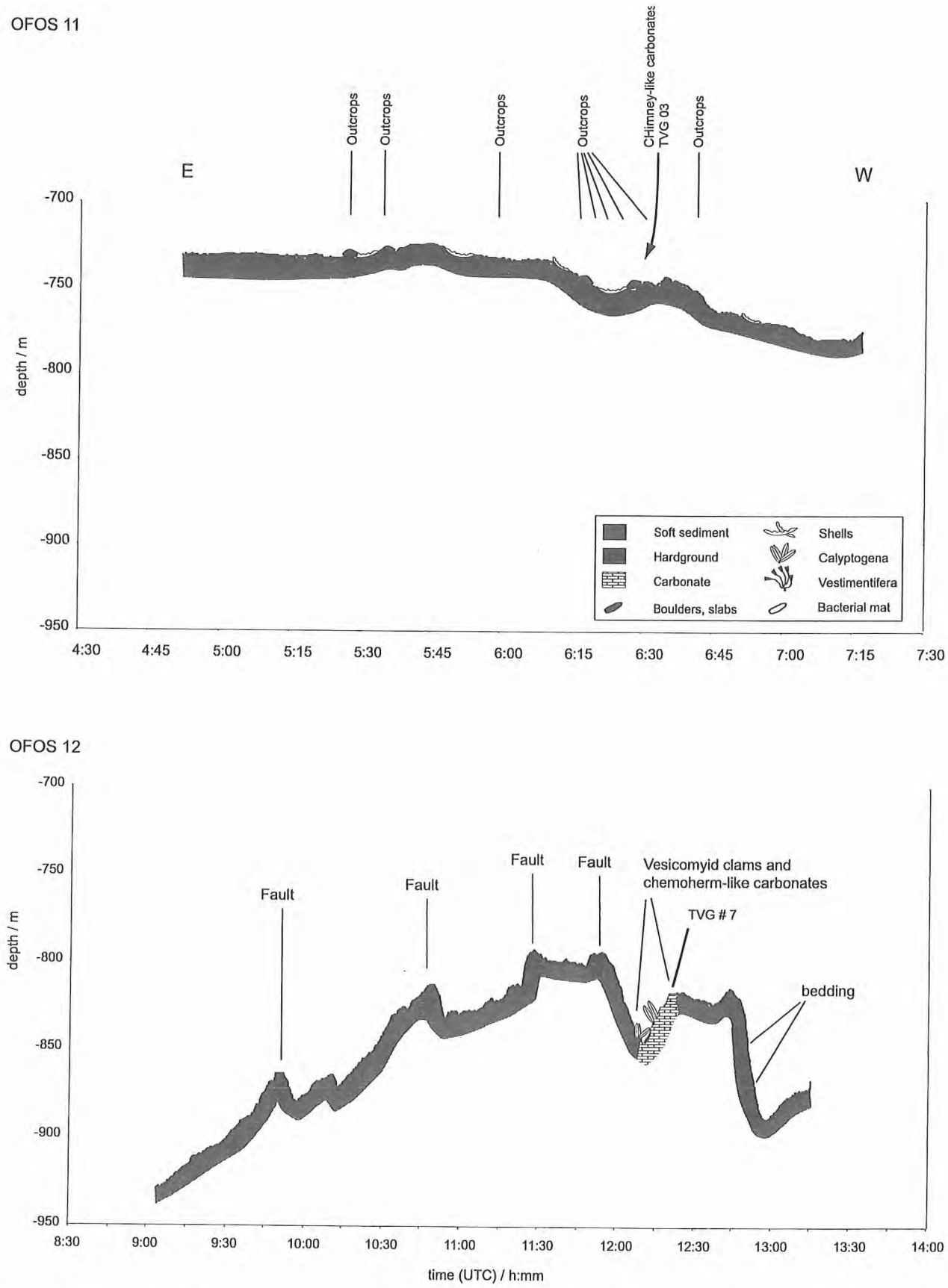


*Figure 6.4.3.7: OFOS 11 and 12 depth profiles at dome of Jaco Scarp. Circular high backscattter features were surveyed by OFOS 11. The locations of these features correspond to areas with outcrops. In addition, hard ground exists in a large area, in which scattered clamshells are abundant. Chimney or donut-like carbonates were observed around 6:25 (UTC) and sampled by TVG 03. These carbonates as well as abundant living solemyid bivalves indicate methane venting at this site. OFOS 12 surveyed the radial fault patterns. We crossed several faults at which outcrops were seen. We found indications for methane*

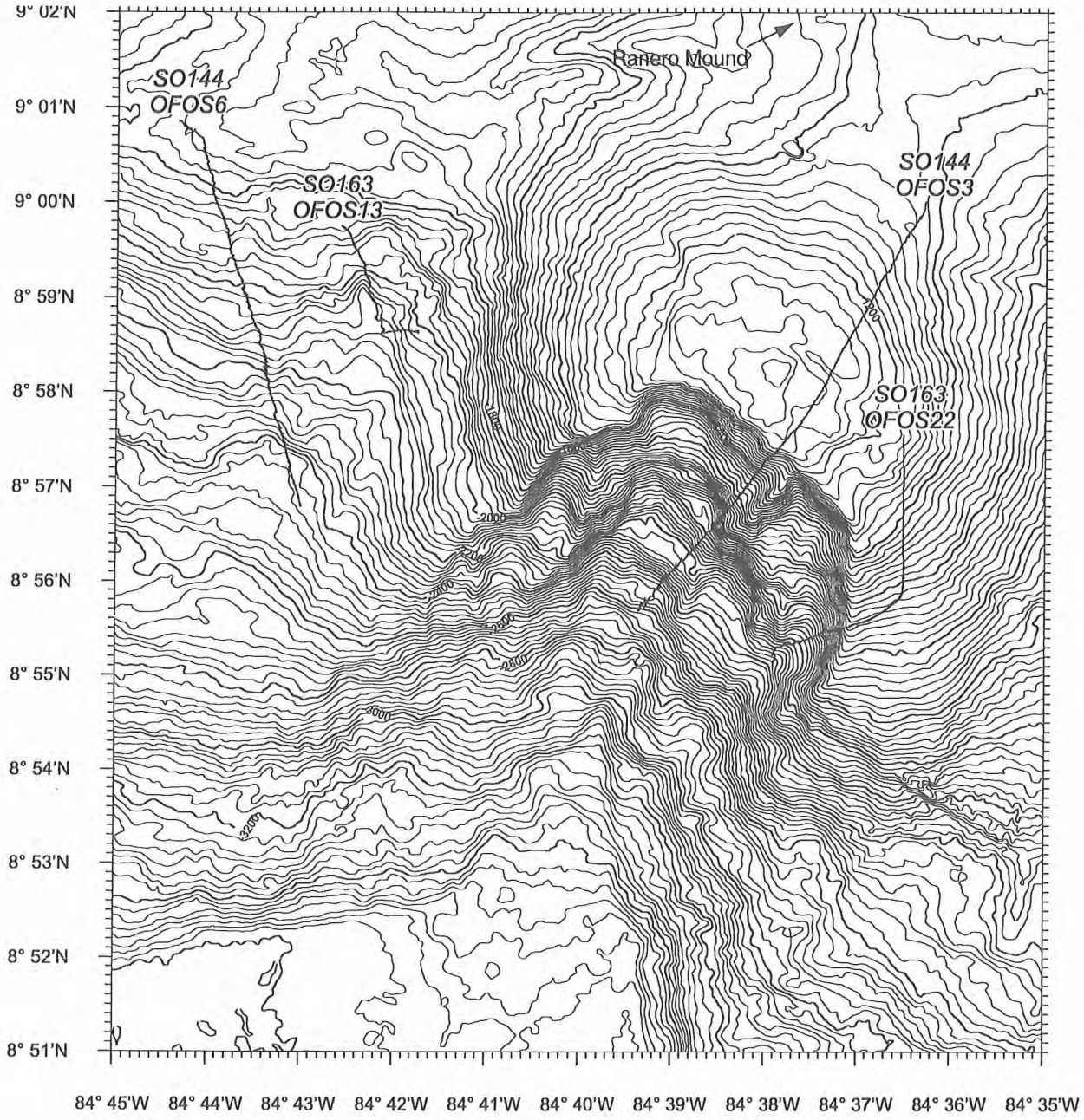


*Figure 6.4.3.8: Location of OFOS tracks at and near Parrita Scarp. SO 144 OFOS 3 and SO 163 OFOS 22 surveyed the uplifted area of Parrita Scarp. SO 144 OFOS 6 and SO 163 OFOS 13 were deployed in order to survey the seafloor at sites which revealed high backscatter in the TOBI image. Note that we discovered with DTS after the OFOS deployments the existence of very small features that are probably mounds. We did not survey these mounds with OFOS.*

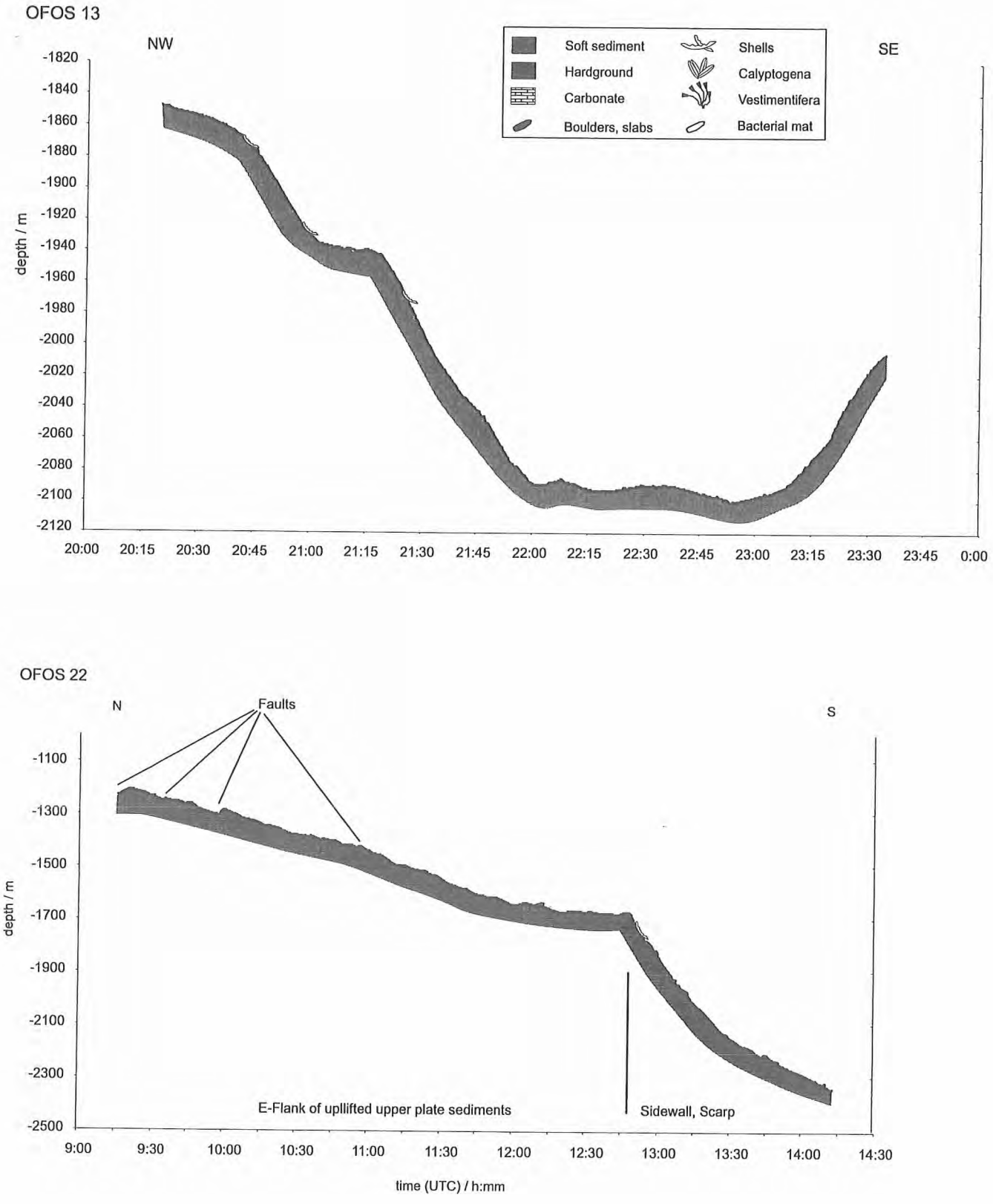


*Figure 6.4.3.9: OFOS 13 and 22 depth profile. OFOS 13 was designed to survey an area of high reflectivity E of Parrita Scarp. During the DTS profile it turned out that in this area small mounds are present, that we have just missed. OFOS 22 surveyed the E side of the uplifted area at Parrita Scarp but did not reveal any signs of venting.*

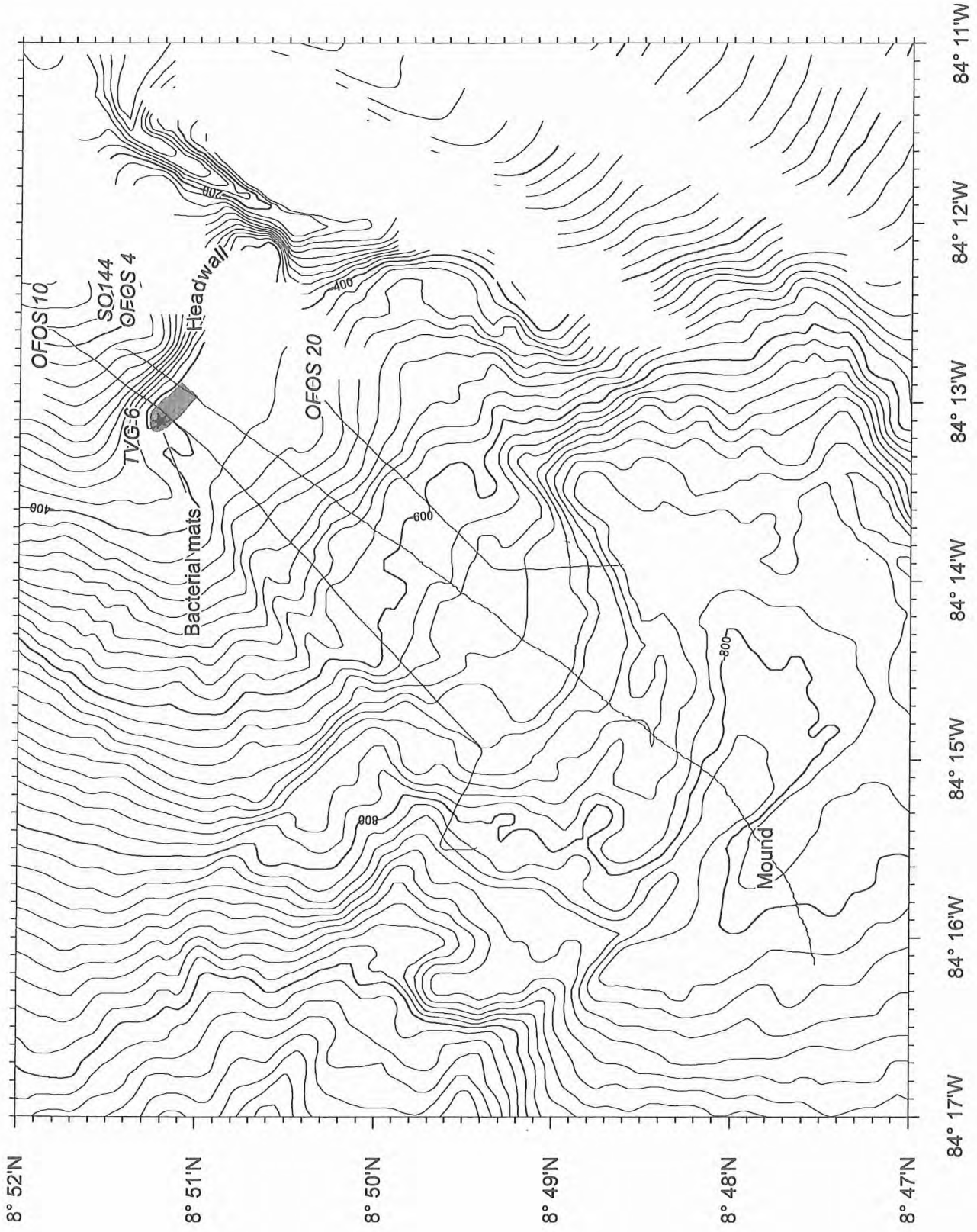


*Figure 6.4.4.1: The locations of OFOS profiles, TVG deployment and major bacterial mat occurrence at Quepos landslide. Notice that with SO 144 OFOS 4 by chance carbonates at a mound were surveyed.*

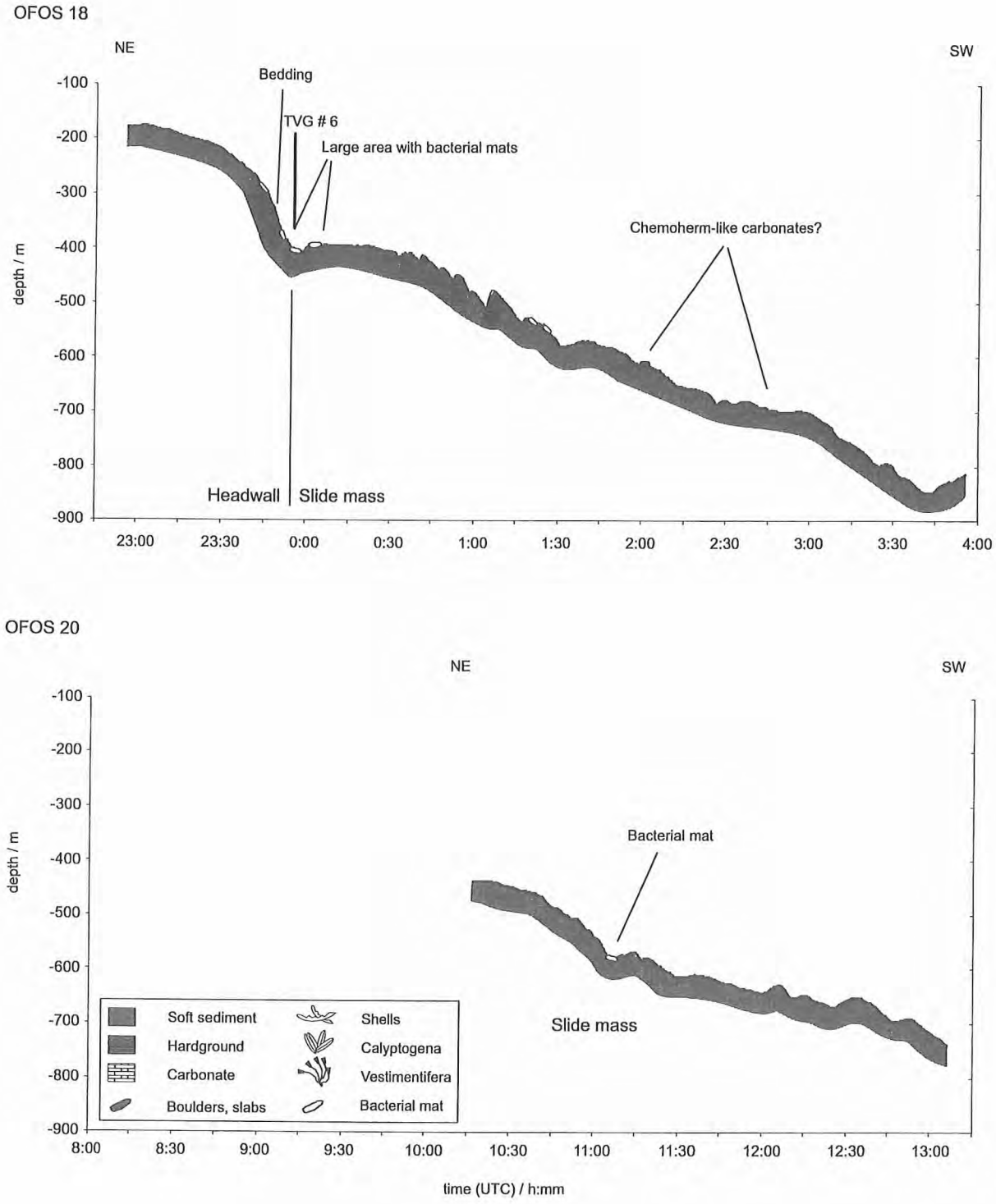


*Figure 6.4.4.2: OFOS 18 and 20 depth profiles. Below the headwall, the most extensive bacterial mats are present. In contrast to SO 144 OFOS 4 only few bacterial mats and no seep-typical living clams or clamshells were observed in the slide mass. The most extensive bacterial mats were observed between the points: 8°51.21'N, 84°13.10'W and 8°51.1'N, 84°13.10'W.*

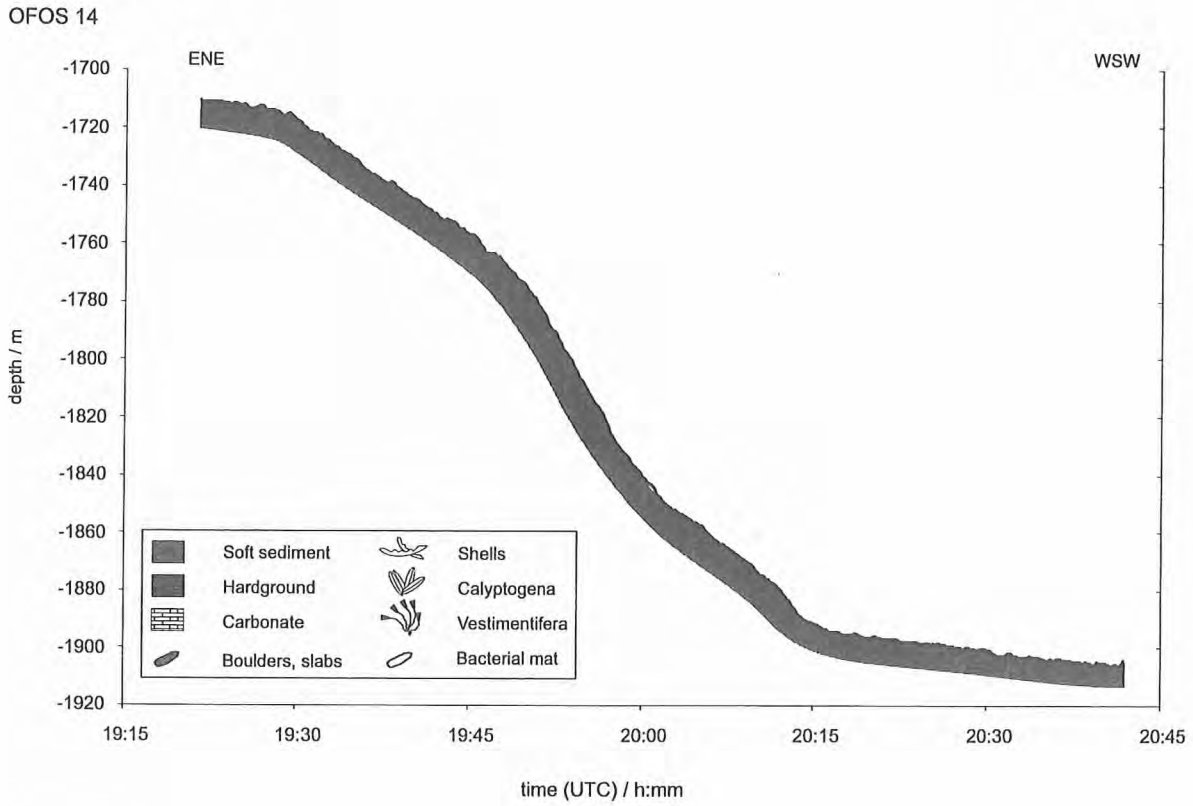


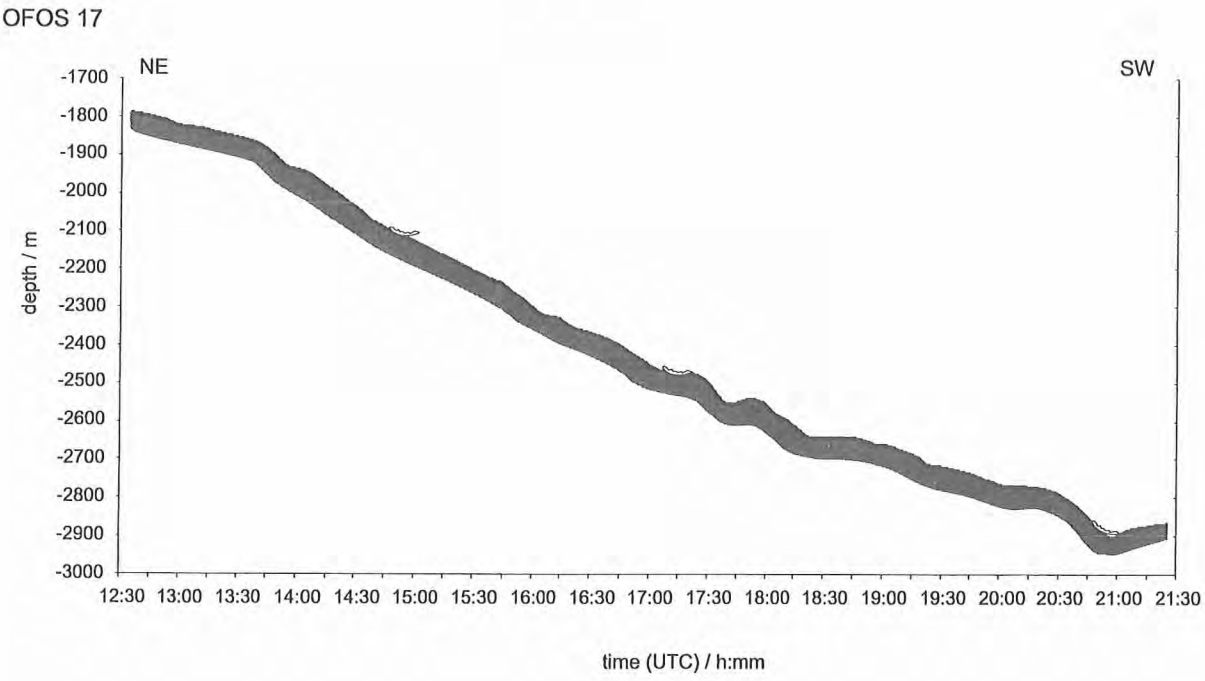


*Figure 6.4.5.1: OFOS 14 and 17 depth profiles at the accretionary wedge. For locations see Figure 6.4.2. Soft sediment prevails throughout the profiles.*

## 6.5 Magnetic Data

(P.O. Thierer)

During the cruise SO163-1 of R/V SONNE, in total 16 magnetic profiles were collected. The magnetometer was deployed during SIMRAD $^{EM}$ 120 bathymetry profiling and on transit between different working areas. Du to the technical parameters of the GeoMetrics G801/3 Marine Proton Magnetometer system, its maximum working depth is limited to 70 meters below seasurface. The measurement of the natural magnetic field requires that the influence of other, artificial magnetic fields is minimised. In consequence a distance of at least three times ship length between the vessel and the sensor is required; in case of R/V SONNE 300 meters. To keep the depth of the sensor above 70 meters below sealevel, the velocity of the ship is forced to be at least 4 nms per hour. Therefore magnetic profiling could not be done while TOBI or DTS-1 Side Scan Sonar profiles were done.

Interpretations of the magnetic data has been done on the total field magnetic raw data. No corrections as e.g. daily variations or latitude correction was done. Therefore, interpretations are of preliminary character.

The magnetic profiles obtained are shown in Figure 6.5.1 to 6.5.12. All profiles are situated on the Costa Rica continental margin.

Profile 1 is striking about 120 degrees and crosses the lower part of the slope. The magnetic data show variations in the magnetic field strength of about 400 nT, they amount to a relative maximum toward the continent. Furthermore, we can observe variations which correlate to the observed topography on the margin.

Profile 2 was carried out during SIMRAD $^{EM}$ 120 bathymetric profiling on the slope. We can observe variations in the total magnetic field strength and a local maximum in the outermost north of this survey area. Variations along the track might correlate to topographic features.

The magnetic profiles 3, 4 and 5 are only of short length and trends (except profile 5) parallel to the slope. They all show a constant magnetic field strength. Probably the wavelength of the magnetic variations is too long in relation to our profiles.

Near by the Nicoya Slide, the magnetic profile 6,7,8 and 9 were obtained. At this place, a seamount is subducting. The magnetic profiles show a relative homogeneous northern part and a distinct magnetic anomaly to the south in the near offset area of slide. This magnetic anomaly fits to the subducting seamount at this place and clearly evidences its influence to the change of the total magnetic field at this place.

Profile 10 is situated in the lower part of the slope and reaches near by point "A" the oceanic plate. We can observe a little change in the magnetic field strength which might be part of the magnetic anomaly pattern of the oceanic plate. Toward the slope, magnetic variations are only very little. They might be linked to the normally very homogeneous magnetic behaviour of continental slopes and the fact that the seafloor topography in this area is very smooth.

Profile 11 instead is located in higher position on the slope and furthermore to the north than profile 10. However, magnetic variations are not very distinct too; they might be explained as it is done for profile number 10.

Magnetic line 12 is situated on the lower slope, its geographical position is between profile 10 and 11. In contrast to these lines, magnetic line 12 shows distinct magnetic anomalies. The influence of the normal oceanic plate magnetic anomaly pattern to the total magnetic field strength could be observed. Furthermore, we can observe variations of the seafloor topography as shown on the bathymetric map. Probably, a portion of the observed magnetic anomalies might be caused by some of those small and

already subducted topographic features which might influence the magnetic anomaly pattern as shown in line 6 to 9.

During SO163-2 only four magnetic profiles were collected, two during transit and two while shooting on the oceanic plate offshore Nicoya peninsula.
The profiles are shown in Figures 6.5.13 to 6.5.16.

Profile 13 is located off Nicoya Peninsula and crosses the Pacific Costa Rica Margin, striking NE - SW. The total field strength is very constant along the profile. Variations are very weak, both, on the margin and in the deep sea basin. Furthermore, no significant correlation between topography and total magnetic field strength can be observed.

Profile 14 and 15 are located off the northern part of Nicoya Peninsula. Profile 14 is coincident with the northern part of profile 15. Along the profile, the bathymetry is very flat and not influenced by e.g. seamounts or other topographic features. The total magnetic field strength ranges about 35500 nT in the northern part; in the southern part of magnetic line 15, a weak and negative magnetic variation can be observed.

Magnetic line 16 was recorded during transit towards Panama. The line starts near to Jaco Scar and stops at the Costa Rica - Panama frontier, off Burica Peninsula. The line, runs on the ocean plate and crosses several topographic elements like Cocos Ridge and several seamounts. The total magnetic field strength shows many variations along the profile. In the outermost east at 83.1° W, a smooth shaped magnetic anomaly was found which has no correspondence in the bathymetric profile and can be interpreted as a part of the magnetic anomaly pattern of the oceanic plate. The eastern part of the profile can be divided into two parts, west and east of latitude 84.0° W respectively.
In the western part, the bathymetric and magnetic profiles are trending nearly parallel; bathymetric highs are corresponding to regions of high magnetic field strength. The eastern portion of the profile shows the opposite tendence. Bathymetric highs are related to relative minimum zones of the magnetic field strength.

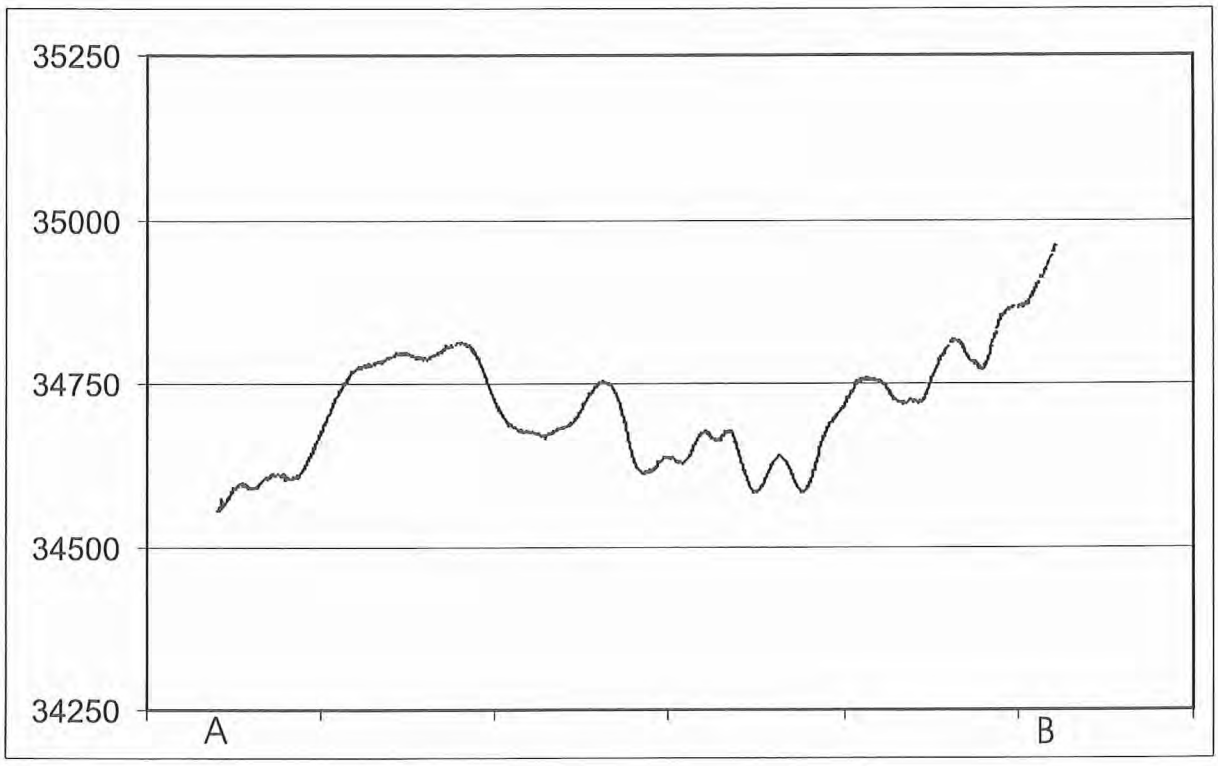


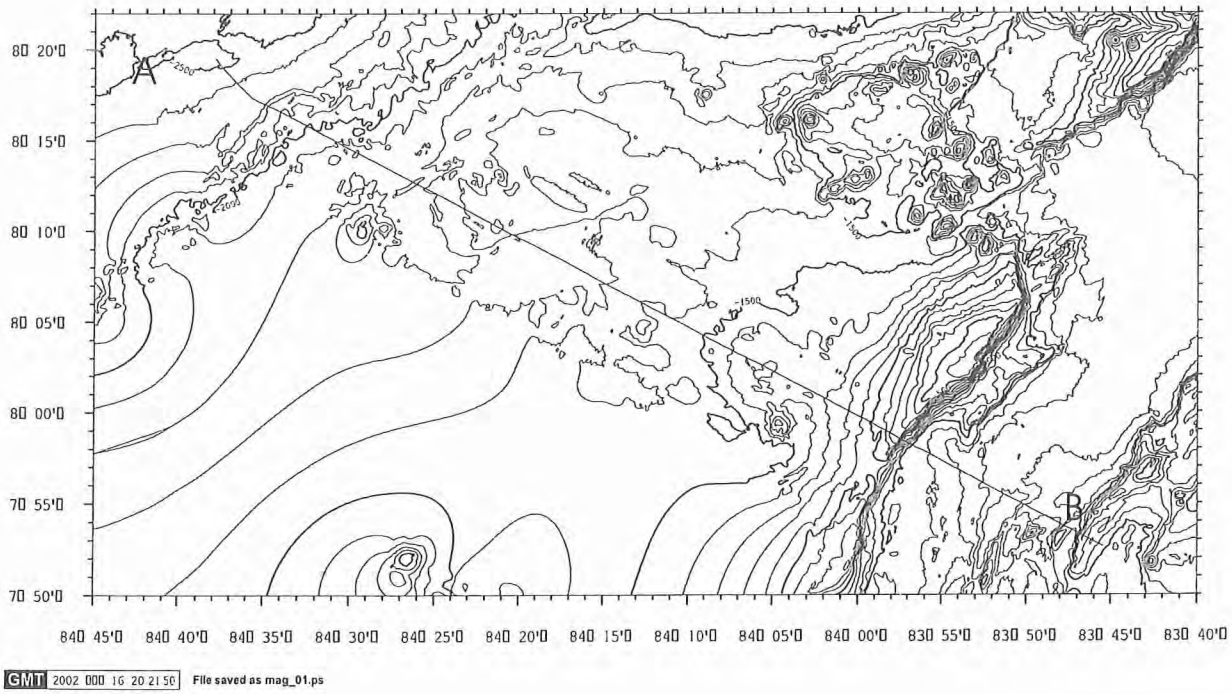


**Figure 6.5.1:**
Magnetic field strength [nT] and track line of magnetic profile 01, SO 163-1

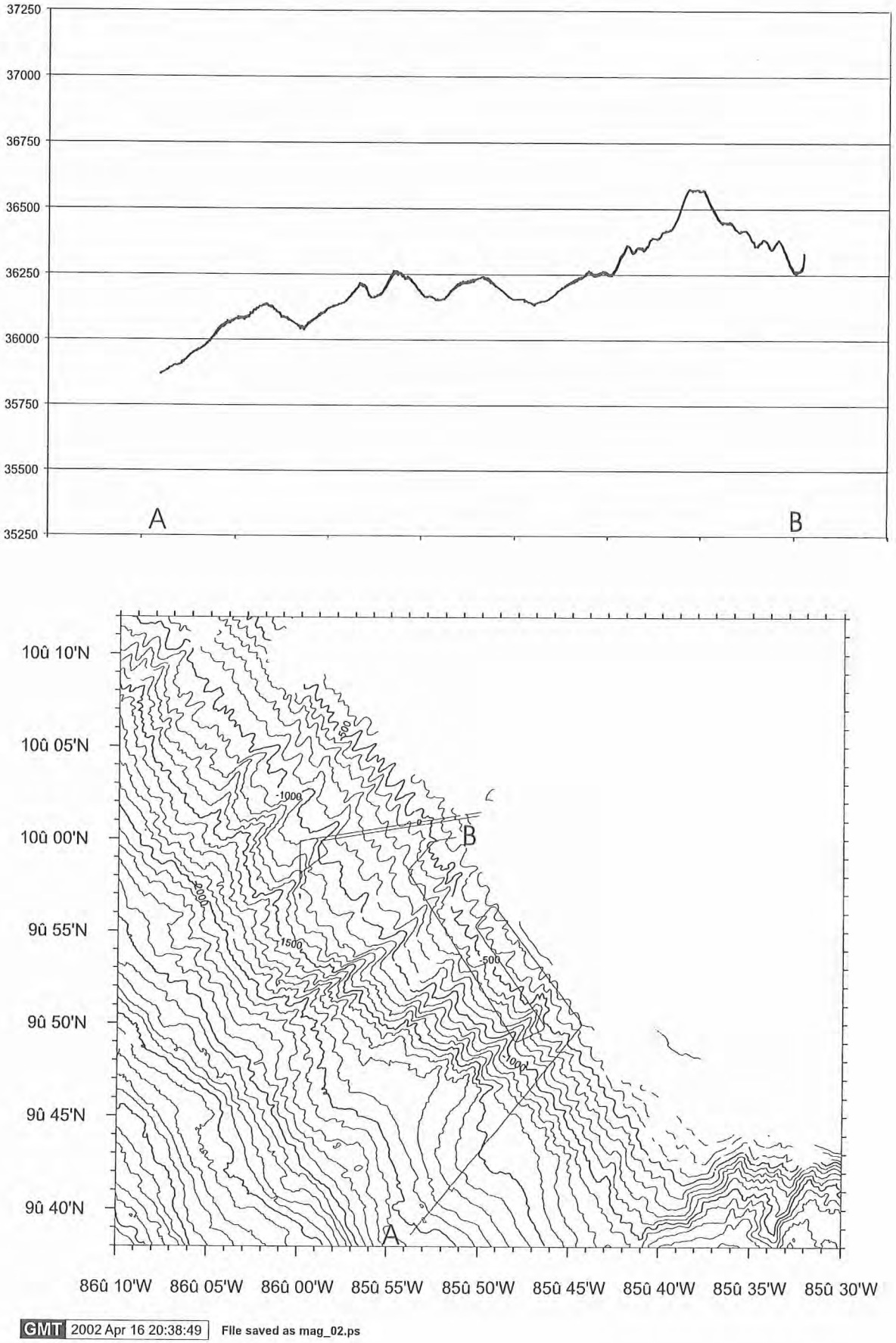


**Figure 6.5.2:**
Magnetic field strength [nT] and track line of magnetic profile 02, SO 163-1

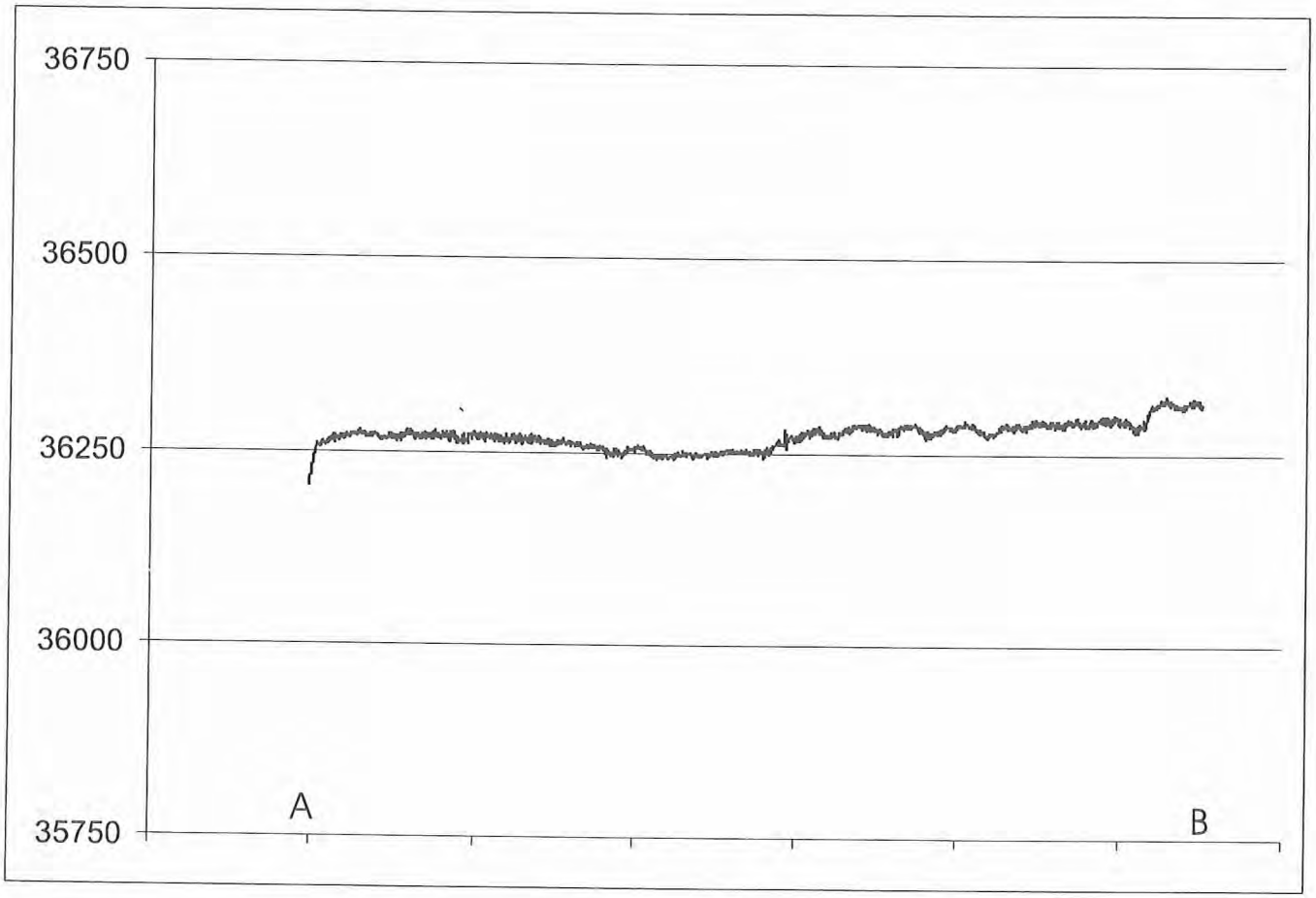


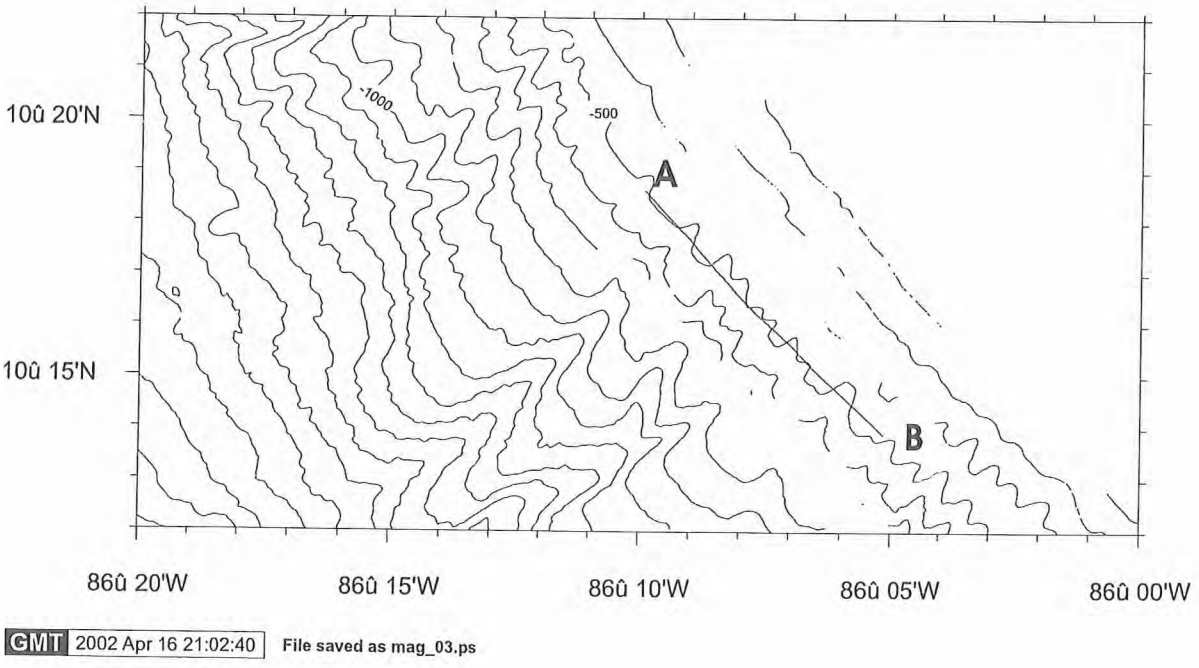


**Figure 6.5.3:**
Magnetic field strength [nT] and track line of magnetic profile 03, SO 163-1

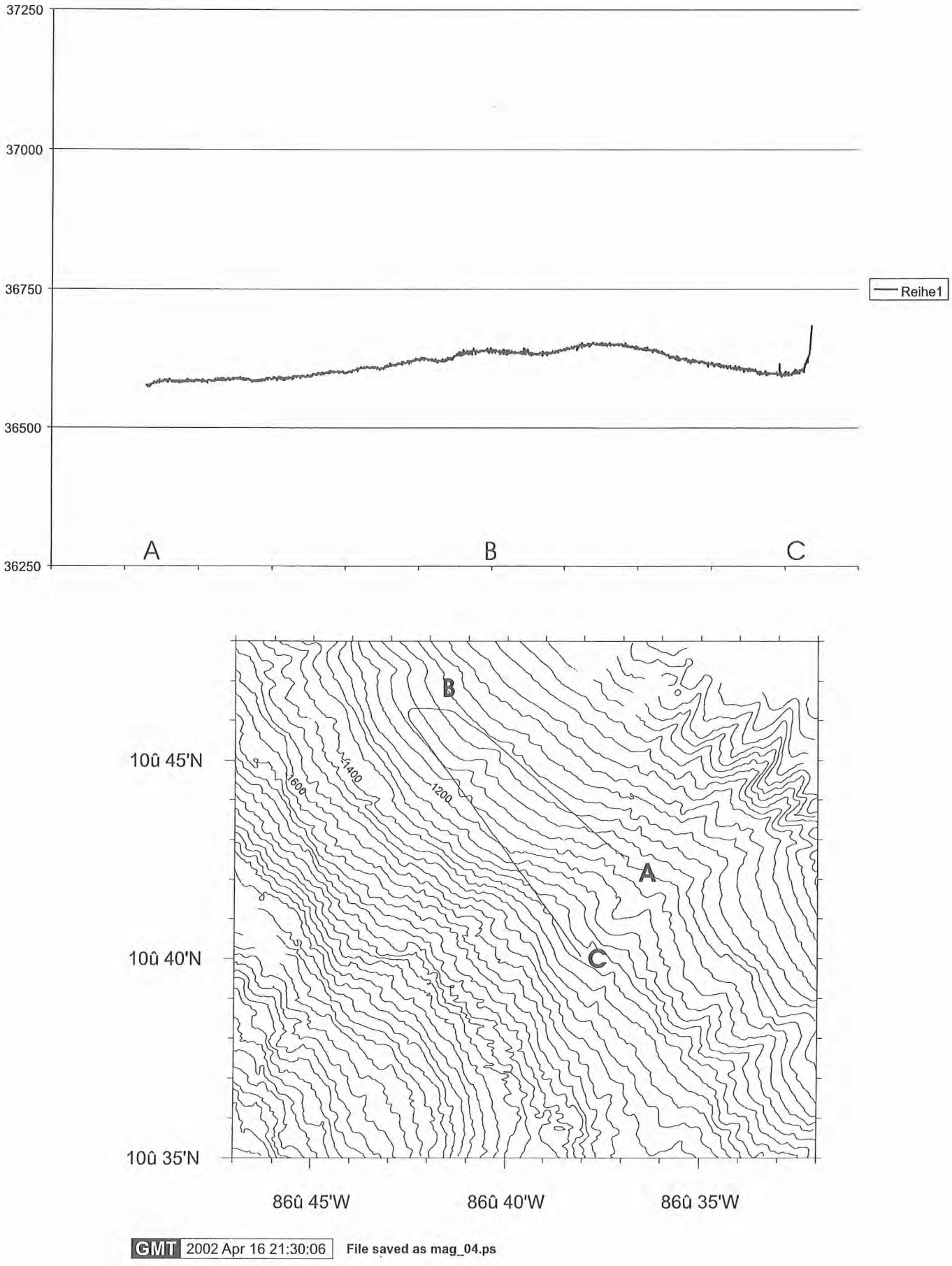


**Figure 6.5.4:**
Magnetic field strength [nT] and track line of magnetic profile 04, SO 163-1

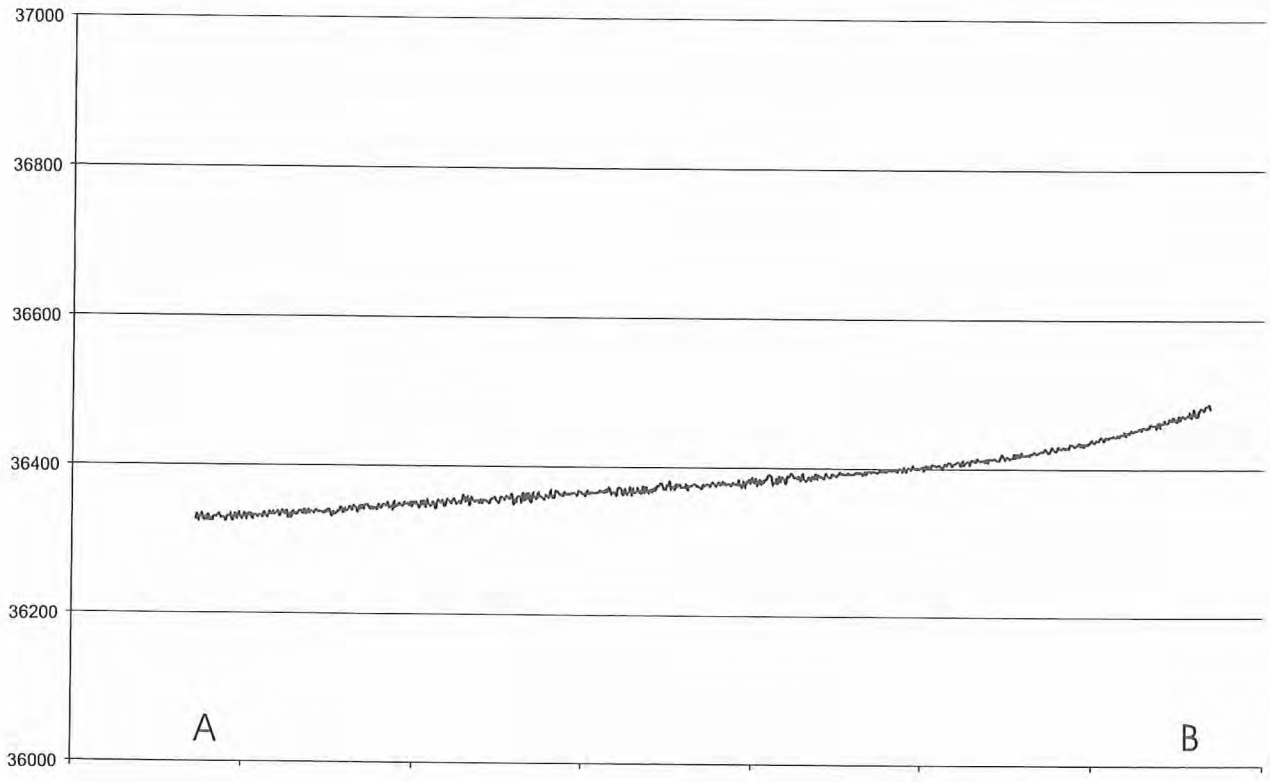


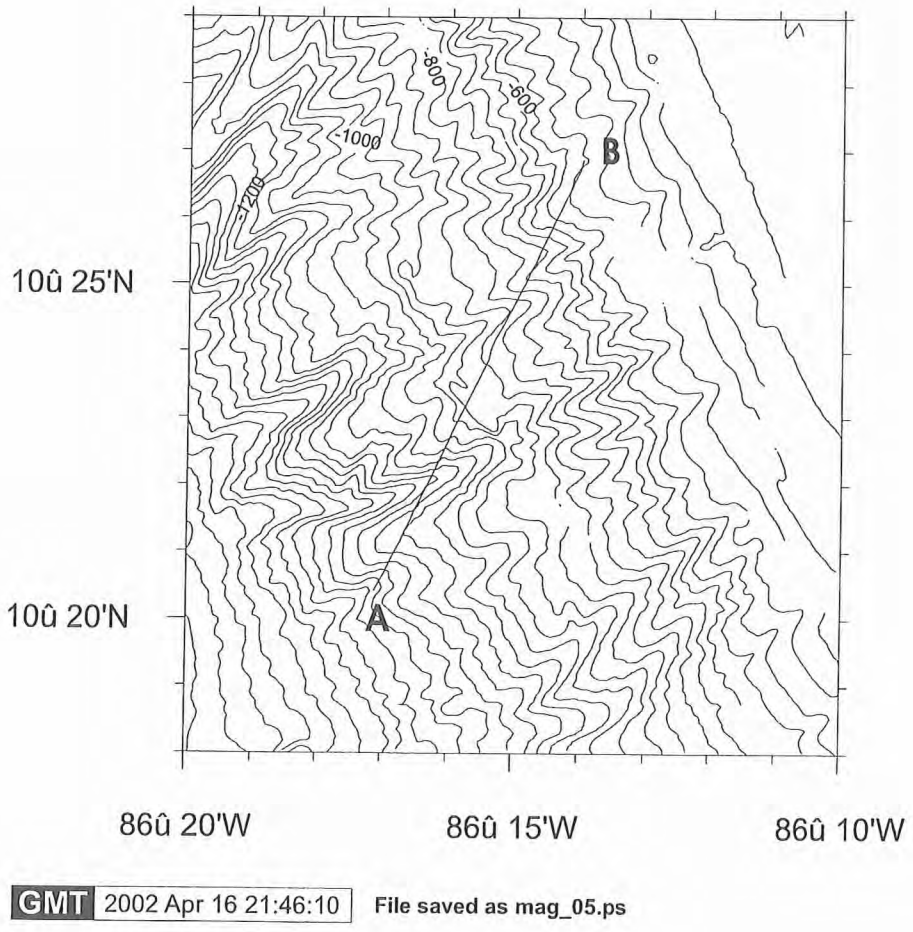


**Figure 6.5.5:**
Magnetic field strength [nT] and track line of magnetic profile 05, SO 163-1

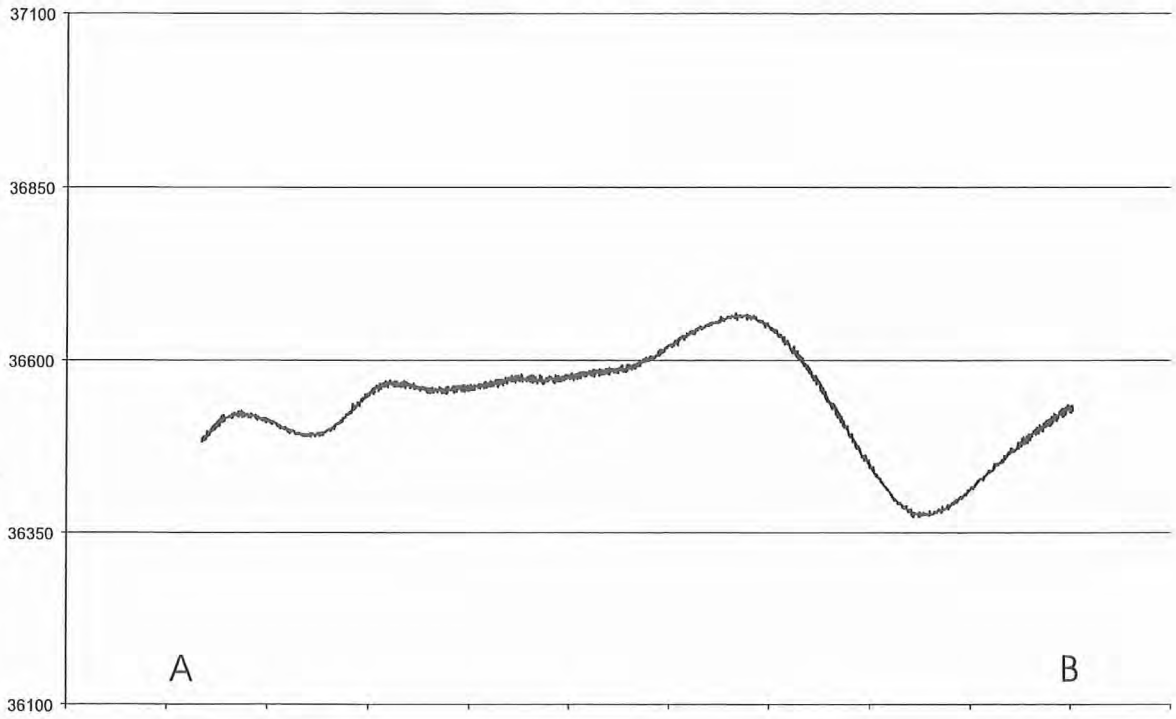


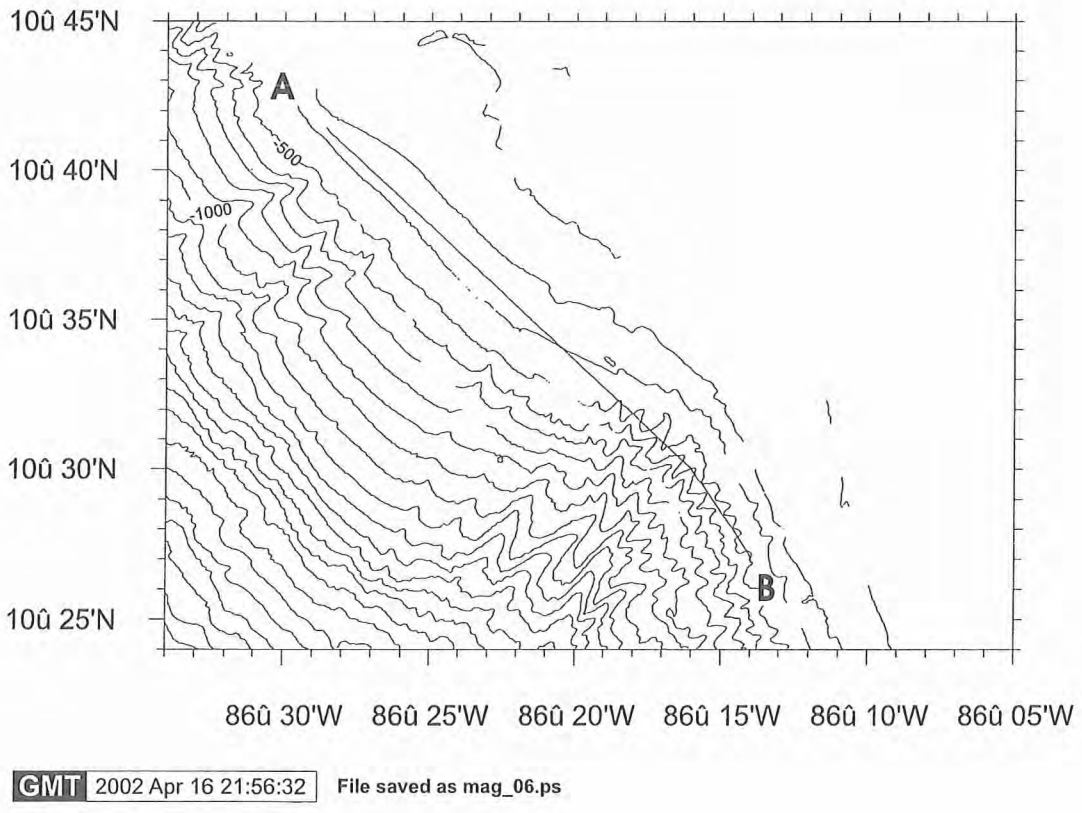


**Figure 6.5.6:**
Magnetic field strength [nT] and track line of magnetic profile 06, SO 163-1

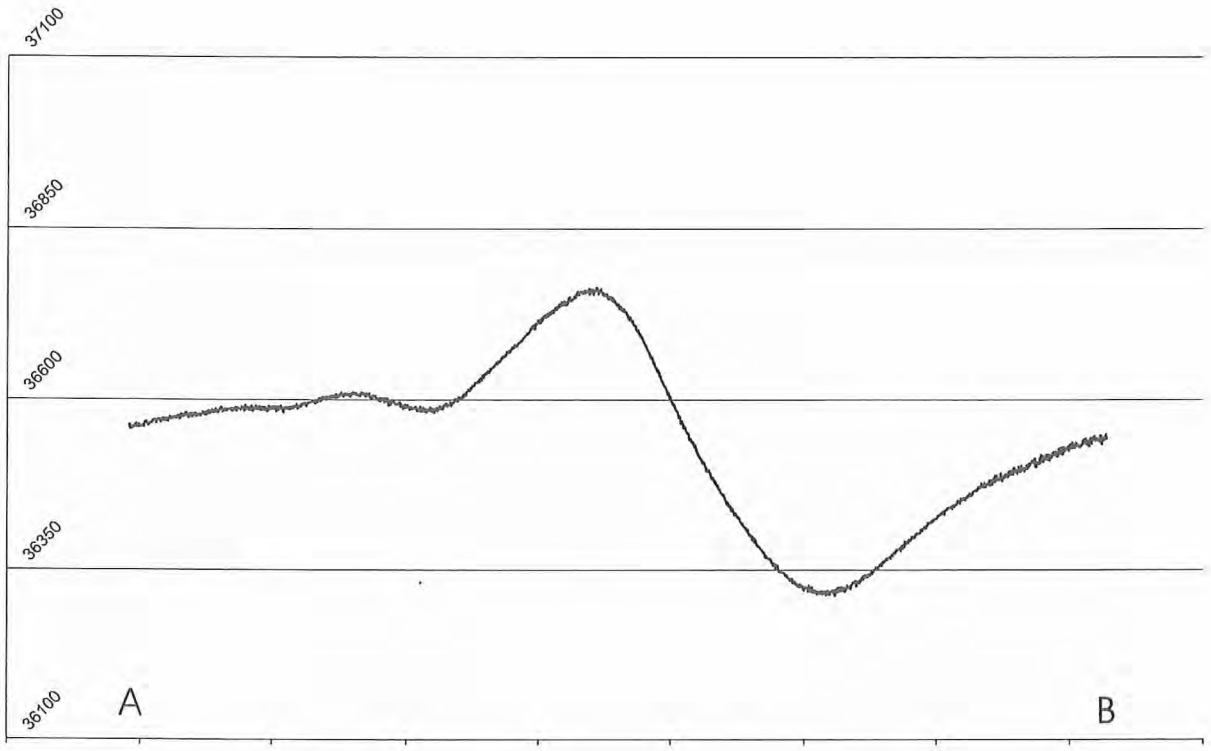


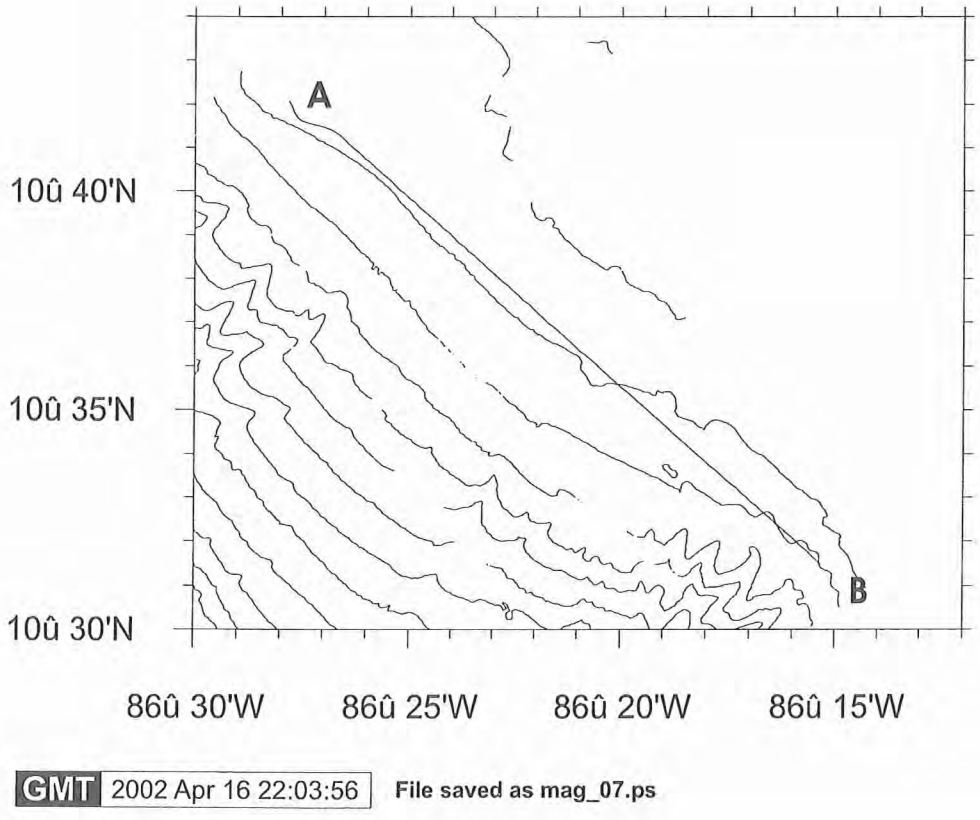


**Figure 6.5.7:**
Magnetic field strength [nT] and track line of magnetic profile 07, SO 163-1

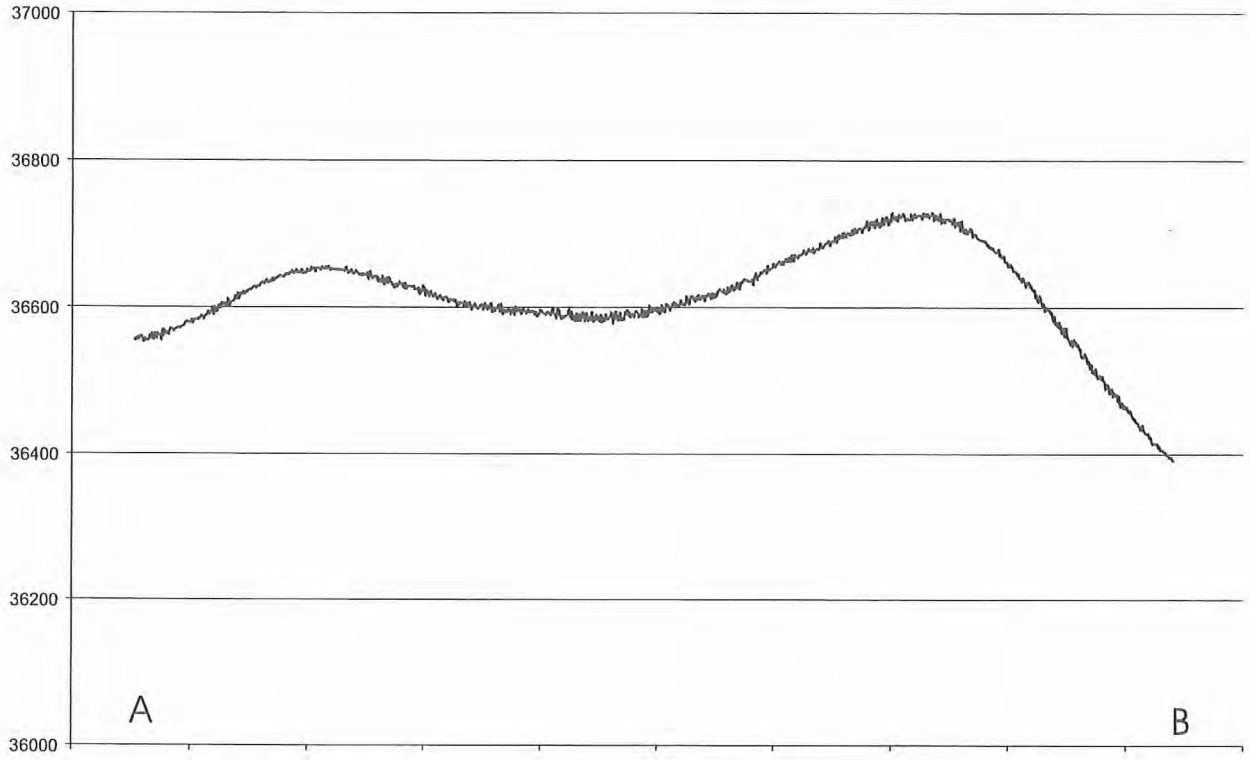


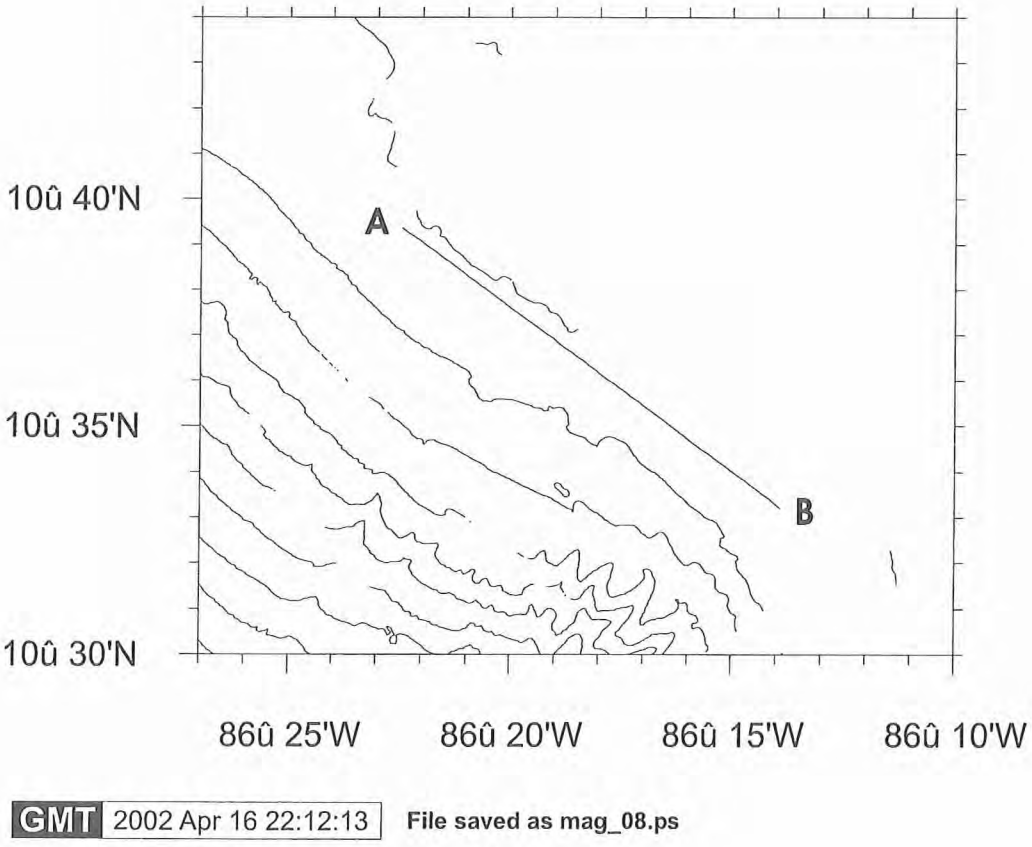


**Figure 6.5.8:**
Magnetic field strength [nT] and track line of magnetic profile 08, SO 163-1

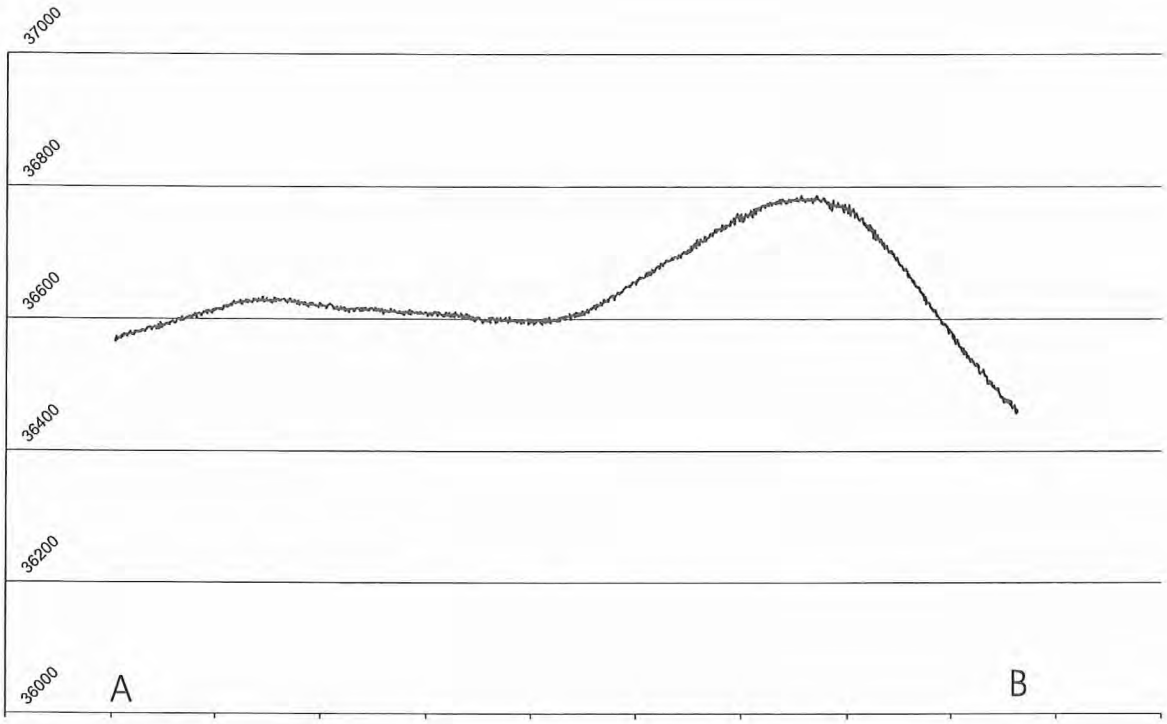


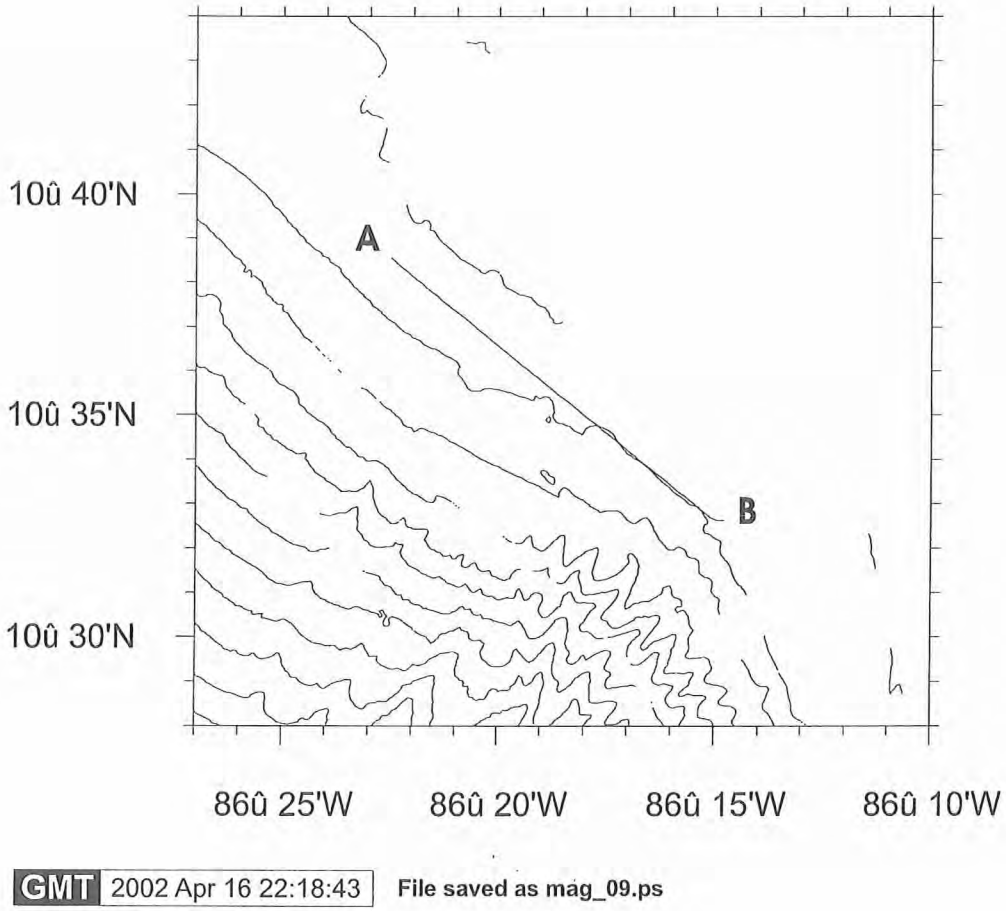


**Figure 6.5.9:**
Magnetic field strength [nT] and track line of magnetic profile 09, SO 163-1

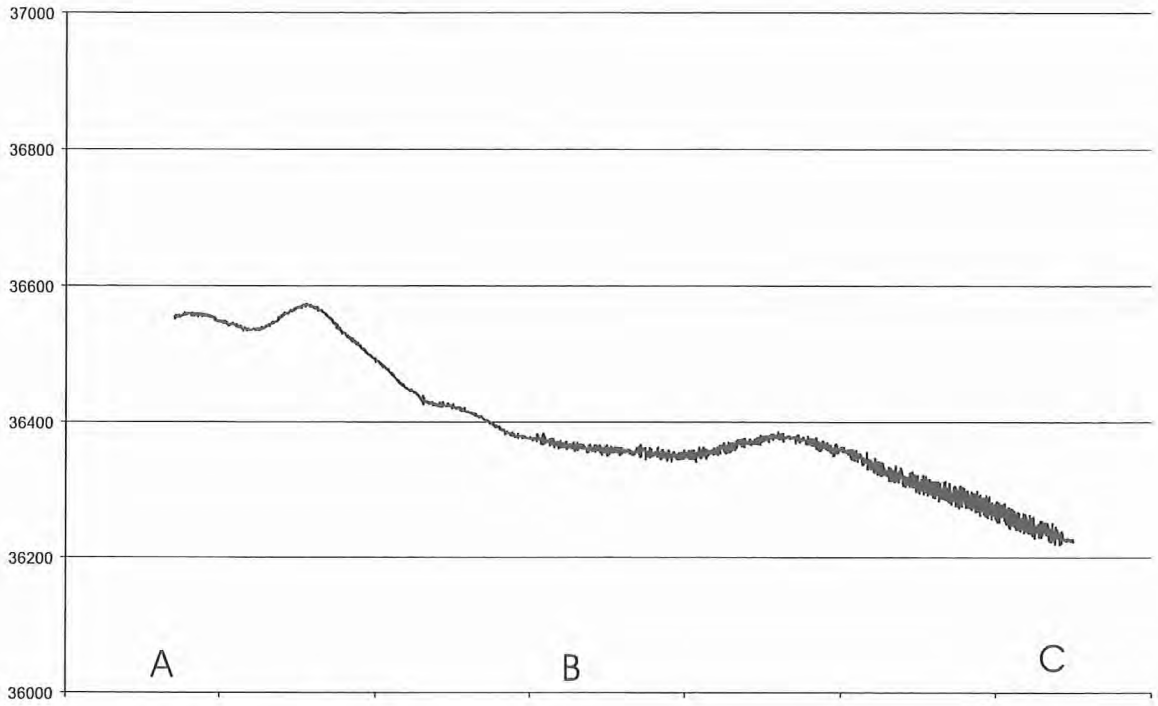


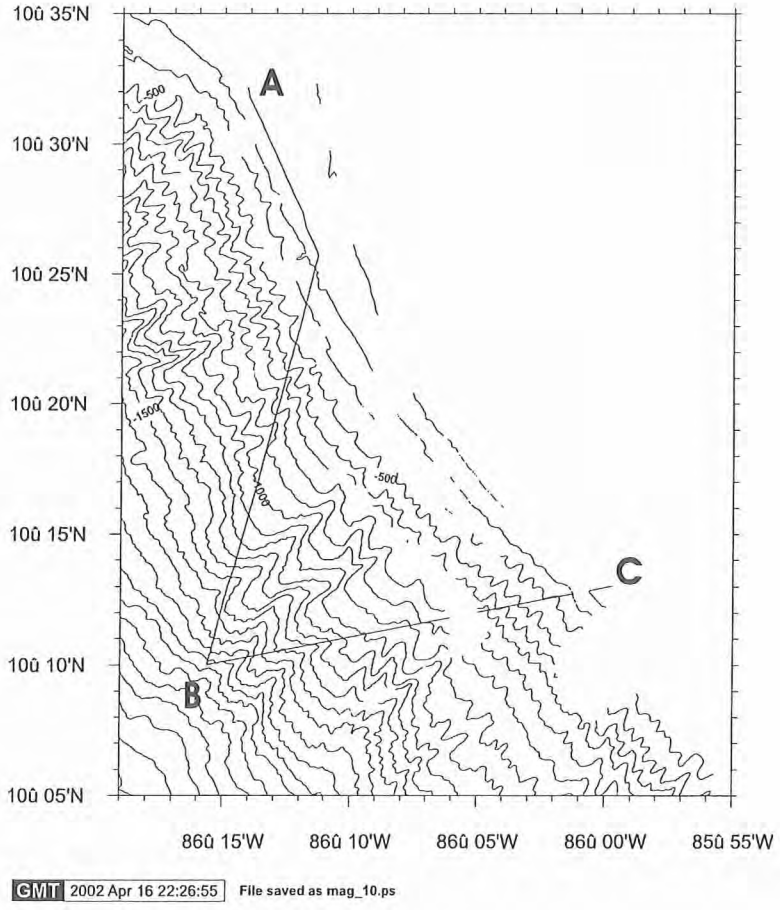


**Figure 6.5.10:**
Magnetic field strength [nT] and track line of magnetic profile 10, SO 163-1

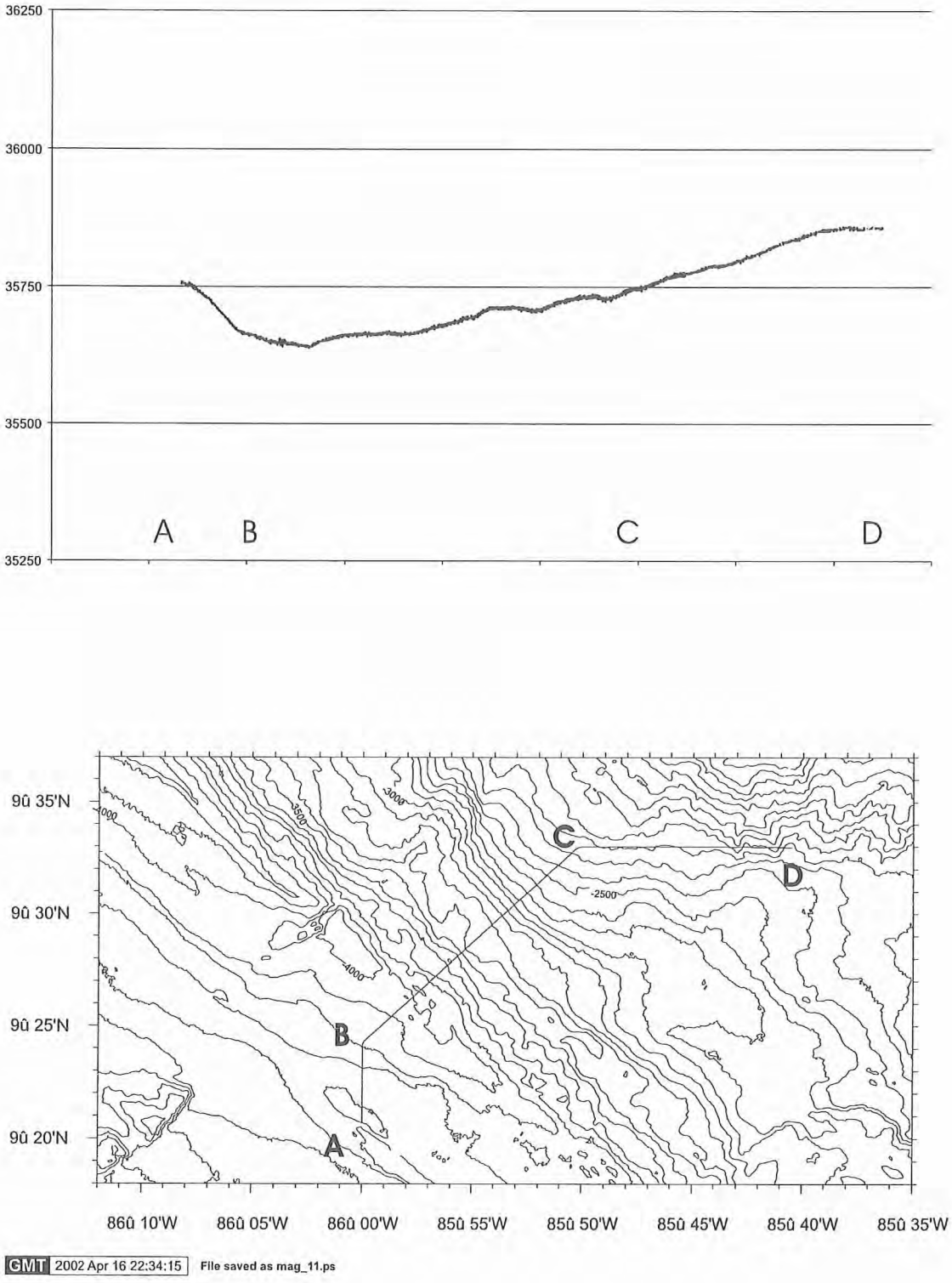


**Figure 6.5.11:**
Magnetic field strength [nT] and track line of magnetic profile 11, SO 163-1

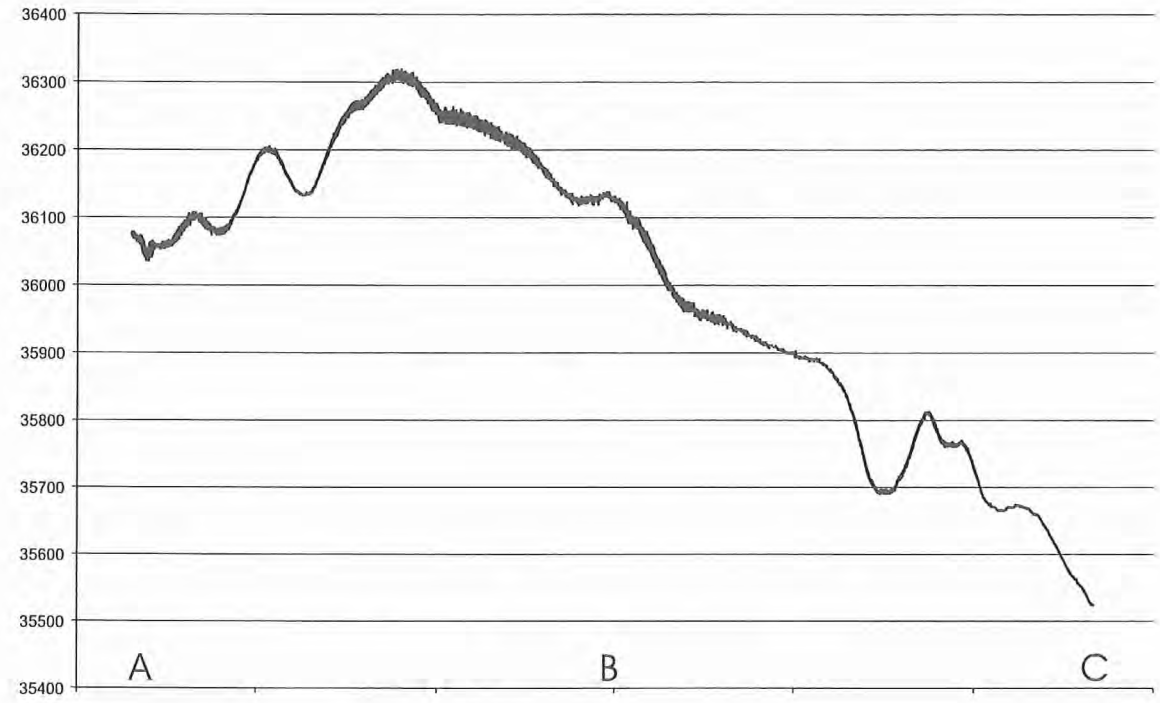


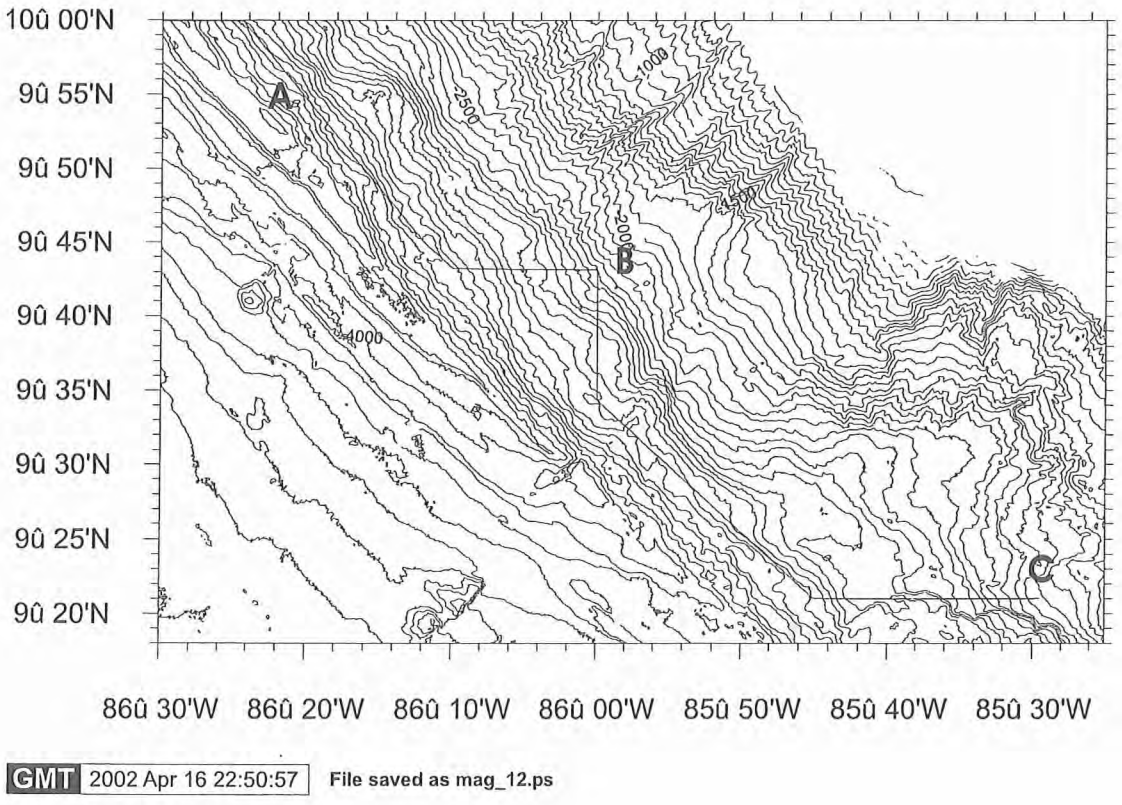


**Figure 6.5.12:**
Magnetic field strength [nT] and track line of magnetic profile 12, SO 163-1

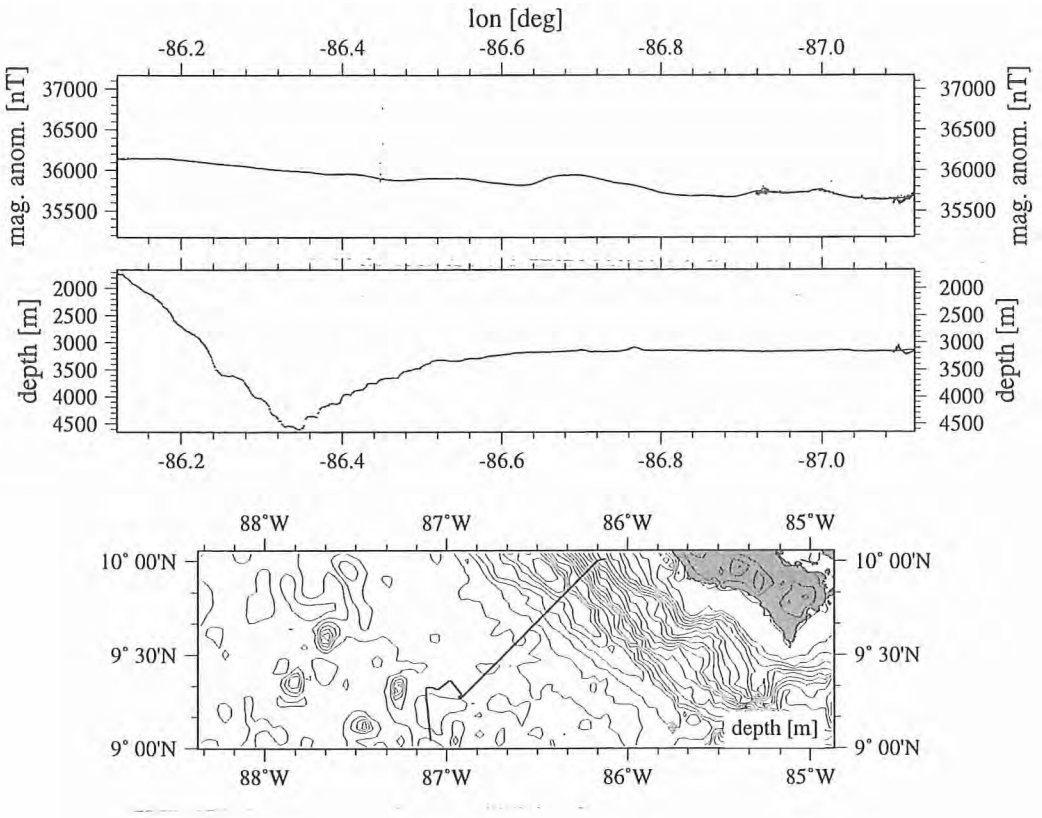


Figure 6.5.13: Magnetic field strength, bathymetry and track plot of magnetik profile SO 163, line 13

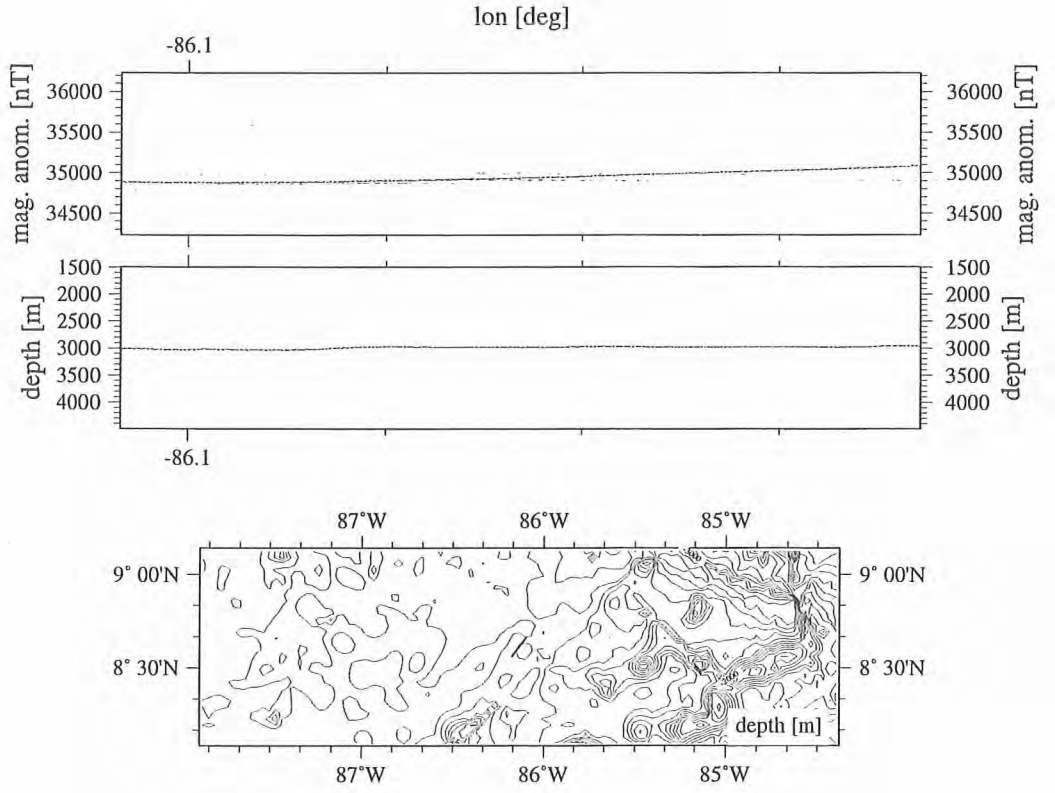


Figure 6.5.14: Magnetic field strength, bathymetry and track plot of magnetik profile SO 163, line 14

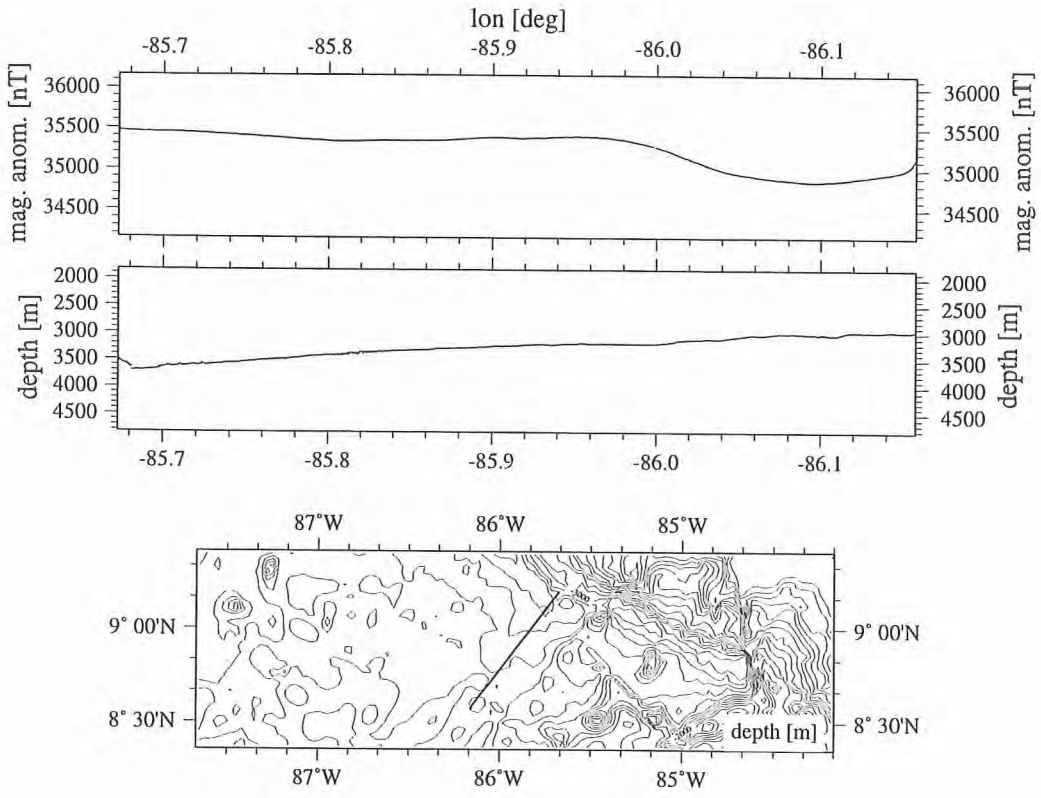


Figure 6.5.15: Magnetic field strength, bathymetry and track plot of magnetik profile SO 163, line 15

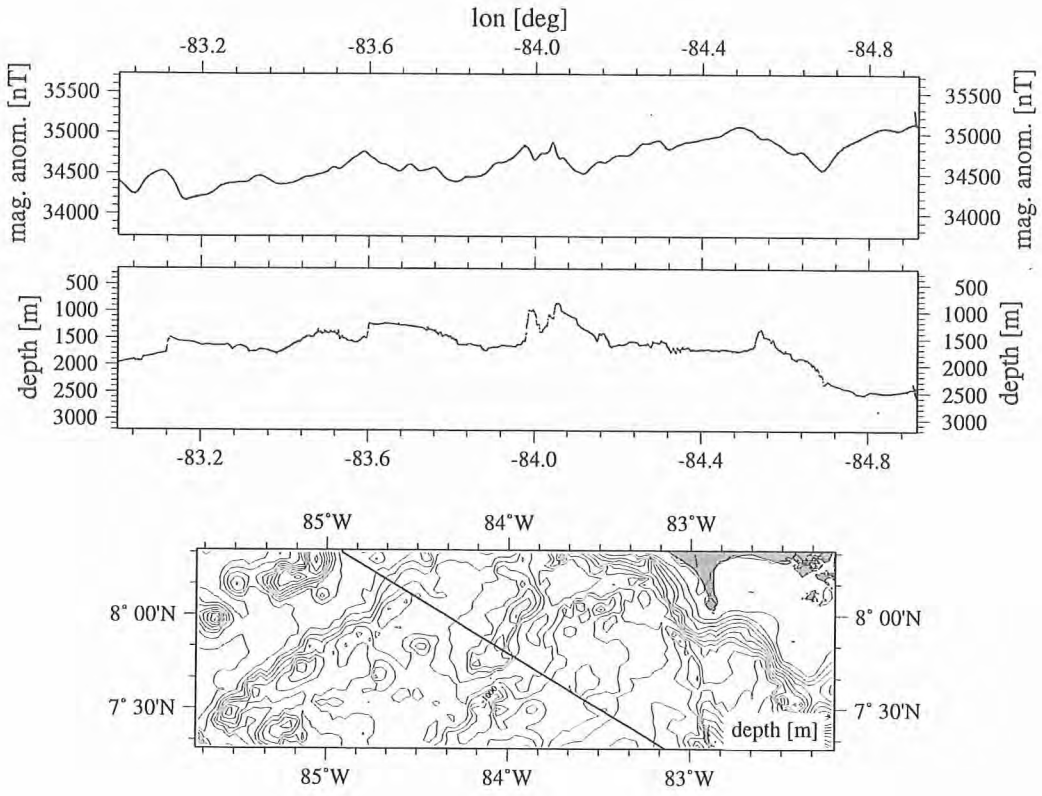


Figure 6.5.16: Magnetic field strength, bathymetry and track plot of magnetik profile SO 163, line 16

## 6.6 Seismic and seismological investigations
### Introduction

During cruise SO163-2 numerous seismic profiles were collected, using ocean bottom recorders and a four channel streamer. Several different airguns were used. All instruments are described in chapter 5.3, details of the profiles can be found in Appendices 9.5 and 9.6. In addition, seismological investigations were made, including a local network above an active venting site, where 10 instruments were deployed during cruise SO163-1 and recorded for about one month (Chapter 6.6.1). A larger network was deployed centered on Jaco Scar, here a total of 28 instruments were deployed and shall be recovered during METEOR Leg M54/3B in early October 2002. For this network seven instruments were recovered and redeployed during the cruise (chapter 6.6.5).
The active seismic work focussed on three main topics. Several data set were collected to study the feasability of modifying the receiver function method, that is well established in global seismology, for studies of shear wave velocities of gashydrates (chapter 6.6.2). The so called Megalense, a reflection identified on earlier MCS images, was a second target. Here, two dip and two strike lines were recorded by ocean bottom recorders and the streamer (chapter 6.6.3). The third target area was the decollement reflection, that in some places along the Costa Rican margin is especially strong and can be followed to the very tip of the upper plate. We choose the occurence of the strongest reflection known from existing data and collected additional wide angle data that should provide the base for further lithological investigation using AVO and other attribute information (Chapter 6.6.4). Since during this cruise two G-Gun arrays were available (generously provided on loan from *Sodera Inc.*), several tests of the guns using different towing depths were made throughout the cruise, including the registration of the far field signal using hydrophones at large depth but away from the seafloor. The corresponding results are summarized in the chapters according to the area they were made.
Finally, a short profile was aquired across one of the carbonate mounds on the margin in order to detect the thickness of the carbonate layers (chapter 6.6.6). An overview map of all instruments and profiles is shown in Figure 4.2.2.
In the following, the data processing and archiving is described.

### Seismic Processing: OBH/OBS Wide Angle Data and MCS Reflection Data

(A. Berhorst, N. Fekete, H. Kopp, L. Planert, M. Schnabel, and the GEOMAR wide-angle Working Group)

**Data Conversion**
The OBH/OBS data are recorded in continuous mode by the MLS and MBS units. Processing of the seismic and seismological data requires a prior conversion into pseudo SEG-Y format, which is conducted based on existing REFTEK routines modified for the instrument requirements and the available hardware platforms. Figure 6.6.1 illustrates the processing scheme applied to the raw data, of which a detailed description of the main tools is presented below.

**send2pas**
Data recording is performed on PC cards which store the compressed data file in the MLS and MBS recorders. After recovery of the instruments, the skew of the internal clock is determined and the flash cards are then transfered to a DOS/Windows based PC. The program send2pas decompresses the data stored on the cards. The data are converted to a PASSCAL data format in a 16 or 32 bit storage and written to the hard disk as well as copied to a SUN workstation via ftp as all other programs are UNIX based.
Send2pas will also detect any possible time slip errors which may have occurred during the recording on MLS units. The time slips are caused by a mismatch of the actual sampling rate of the MLS recorder compared to the desired sampling rate. This mismatch arises because the clock rate of the crystal oscillator in the MLS recorder is temperature dependent (Klaus Schleisiek, SEND GmbH, pers. comm.). The temperature dependence is known and corrected for in the determination of the

system time, but for performance reasons the sampling pulses are directly generated from the oscillator signal without any time correction. The send2pas routine detects and reports in the log-file when the accumulated inaccuracies of the sample rate cause an effective timing error of one sample. For the wide-angle data, the timing errors are considered by adding them to the skew of the internal clock, which is corrected within the dat2segy program (see below, note that the sign of skew and time slips are opposite, i.e., a negative sum of time slips corresponds to a positive skew). As each trace is at most a few tens of seconds long (vs. 1 hour and more between non-cancelling time slips), the corrected time is expected to be highly accurate with uncertainties well below one sample length.

**ref2segy**
The ref2segy program converts the output of send2pas to a pseudo SEG-Y trace consisting of one header and a continuous data trace containing all samples, as used by the PASSCAL suite of seismic utility programs. For each channel (consisting of pressure, vertical velocity, and velocity along two mutually perpendicular horizontal directions for OBS; pressure for OBH) one file is created with the name derived from the start time, the serial number of the Methusalem system, and the channel number. The file size of the pseudo-SEGY file is directly related to the recording time. For instance, a recording time of one hour sampled at 200 Hz (16 Bit) will produce a file size of 1.44 MB per channel. A record with two channels and a recording time of two days will produce a total data volume of 70 MB. After conversion to the pseudo SEG-Y trace, the seismic and seismological processing schemes diverge. The seismology data flow is described in the next section below.

**pql**
pql (Passcal Quick Look) is a simple display program for continuous seismic data. Its interactive zooming capability allows a rapid inspection of data quality.

**segy2trig**
The trigger signal, provided by the airgun control system, is recorded on an additional MBS unit during the shooting period. The trigger data are treated similarly to regular seismic data and downloaded to the hard disk via the send2pas and ref2segy programs. Then, the segy2trig program detects the shot times in the data stream by identifying the trigger signal through a given slope steepness, duration and threshold of the trigger pulse. The output is an ASCII table consisting of the shot number and the shot time. Accuracy of the shot time is one of the most crucial matters in seismic wide-angle work, and must be reproduced with a precision of a few ms. Due to this demand the shot times have to be corrected with the shift of the internal recorder clock. Additionally, the trigger file contains the profile number, the start/end time of the profile and the trigger recording, which will be merged with the ukooa file that links the information with the coordinates of the source and the hydrophones.

**ukooa**
The ukooa program is used to establish the geometric database by calculating the positions of sources at any given shot time and offset from the ship. The source is placed on the ship track using simple degree/meter conversions and then written to a file in UKOOA-P84/1 format. Corrections for offsets between antenna and airguns as well as consistency checks are included. This file will be used when creating a SEG-Y section via the dat2segy program. The program requires the trigger file to contain the shot times, the ship's navigation (see Chapter 5.1.1), and a parameter file containing information for the UKOOA file header.

**dat2segy**
The dat2segy program produces standard SEG-Y records either in a 16 or 32 bit integer format by cutting the single pseudo SEG-Y trace (the ref2segy output) into traces with a defined time length based on the geometry and shooting time information in the ukooa file. In addition, the user may set several parameters for controlling the output. These parameters contain information about the profile and the receiver station, number of shots to be used, trace length, time offset of the trace and reduction velocity (to determine the time of the first sample within a record). The clock drift of the recorder (skew) and possible time slip errors are also considered. The final SEG-Y format consists of the file header followed by the traces. Each trace is built up by a trace header followed by the data

samples. The output of the dat2segy program may be used as input for further processing with e.g. SEISMOS or Seismic Unix (SU).

**relobs**
Due to the drifting of the OBH and OBS instruments during deployment and possible errors in the ship's DGPS navigation system, the instrument positions may be mislocated by up to several 100 m. Since this error leads to asymmetry and incorrect travel time information in the record section, the instrument's position on the seafloor must be relocated, which is accomplished using the relobs program.
For input, the assumed OBH location, shot locations, and the picked travel times of the direct wave near to its apex are required. To simplify the picking procedure, a static correction with a hyperbolic equation is performed to flatten the direct wave. This yields a much more coherent direct arrival which would normally suffer from strong spatial aliasing in the uncorrected section making it difficult to track. By shifting the OBH position, relobs minimizes the deviation between computed and real travel times using a least mean square fitting algorithm (assuming a constant water velocity).
The distance from stern to the center of the airgun array was measured using a floating line. The source offset, i.e. the distance from the vessel's GPS antenna position was determined to be approximately 80 m, which is in good agreement with earlier calculations from previous cruises on RV SONNE.

**syntrigger**
In case of a corrupted trigger recording, it is necessary to generate a synthetic trigger signal to merge the shot times with the navigation coordinates in the ukooa file. This may be done using the syntrigger program which uses the shot interval as well as the time of the first and last shot of the profile to calculate a synthetic trigger slope. Due to the fact that the trigger has a small but linear drift, even non-integer trigger intervals (59.99983 s instead of 60 s) can be handled. The drift has to be calculated from neighbouring profiles.

**• OBH/OBS-data analysis and processing**

**Raw data:** As an example which was aquired with the Bolt air-gun, the raw OBH record section 28 for profile 09 is shown in Figure 6.6.2a. A broadband frequency filter is applied for display purpose. For the analysis, offset ranges between 0-13 km and 26-38 km west are presented in detail. For comparison, the seismic section of OBH 59 on profile 15, which was shot with the two G-guns, is presented in Figure 6.6.2b. The offset ranges from 0-9 km and 31-42 km east are used for the analysis. The parameter tests for the Prakla airgun-array, which was used for only 3 profiles, are not presented, but the applied processing sequence is displayed (see below).
**Frequency filter analysis:** To determine the frequencies of the seismic energy, filter panels with narrow frequency band passes for the near- and far offset ranges are shown in Figures 6.6.3 to 6.6.6. In the lower section of the figures the amplitude spectra of the corresponding filter panels are appended. The amplitude spectra of the applied Ormsby frequency filter operators are characterized by linear slopes. The filter applied, which is minimum delay, is described by four corner frequencies: Lower stop/pass band boundary and upper pass/stop band boundary. The frequencies on the filter panels correspond to the lower and upper pass frequencies. The main energy for the reflected phases in the near offset range is between 3-25 Hz for the Bolt-gun and 3-37 Hz for the G-guns while the direct waves show signals up to 110 Hz. The main energy of the far offset phases for both air-guns is between 3-16 Hz. As a broad frequency range is contained in the data, time and offset dependent filtering was applied (see below).
**Deconvolution analysis:** To improve the temporal resolution of the seismic data a deconvolution is applied to compress the basic seismic wavelet. The recorded wavelet has many components, including the source signature, recording filter, and hydrophone/geophone response. Ideally, deconvolution should compress the wavelet components and leave only the earth's reflectivity in the seismic trace. We applied Wiener deconvolution in successive trace segments, based on the following assumptions:

1. The earth's reflectivity is 'white'.
2. The wavelet shows the minimum-delay phase behavior.

As in this wide-angle data the amplitude spectra of the seismic traces vary with time and offset (e.g. reflected and refracted phases), the deconvolution must be able to follow these time and offset variations. Each trace is therefore divided into 3 s data gates with 1 s overlap, in which time invariant deconvolution operators are computed from the autocorrelation function of the data segment and applied to account for the non-stationarity of the seismic signals. The overall deconvolved trace results from a weighted merging of the independently deconvolved gates.
The raw data serves as input to the deconvolution process. As several recordings were influenced by a DC shift, a 0-3 Hz high-pass minimum delay Kaiser frequency filter with 60 dB attenuation between the pass and reject zone was applied prior to deconvolution in order to center the amplitudes around zero. The deconvolution test panels are shown in Figures 6.6.7 to 6.6.10 for the near and far offset ranges, respectively. In the lower section of the Figures the autocorrelation function is appended. Constant operator lengths of 200 and 300 ms (predictive length included) and a variation of the predictive length from 4 (spike) to 160 ms is displayed.
On the undeconvolved data of the Bolt-gun in Figures 6.6.7 and 6.6.8, strong energy is clearly visible in the autocorrelation function. The best resolution is obtained for a predictive length of 4 ms and an operator length of 300 ms, with a reduction of signal-to-noise ratio especially on the far offset traces. A predictive length of 100 ms and an operator length of 200 ms was chosen for this data set which is a compromise between temporal resolution and signal-to-noise ratio.
The autocorrelation function of the raw data from the G-guns in Figures 6.6.9 and 6.6.10 show much weaker energy behind zero leg than the Bolt-gun. Therefore the wavelet could be much better compressed. A predictive length of 60 ms and an operator length of 200 ms was finally selected.
After deconvolution an offset- and time-variant Ormsby filter with minimum delay characteristic was applied. As the seafloor depth changes along the seismic lines, each trace was statically corrected to a fixed seafloor travel time of 11 s based on the water depth before filtering. This information is available in the trace headers. After this filter was applied, the data were shifted back to their original travel times.

**Processed data:** Comparison of the data in Figure 6.6.11 to the unprocessed data in Figure 6.6.2a (Bolt-gun) and Figure 6.6.12 to Figure 6.6.2b for the G-guns respectively shows a clear reduction of the low and mono-frequency noise in the near and far offset traces and moderate (Bolt-gun) to good (G-gun) compression of the wavelet signal. For the picking of events and model building by raytracing both sections were used to keep all available seismic information.

- **Final processing sequence**
  - Input: SEGY-data, 4 ms or 5 ms sampling rate with complete geometry information.
  - Tapering the first 0.5 s to zero to reduce the response of the debias filter operator.
  - Kaiser highpass (debias).
  - Gated Wiener deconvolution: gate length 3 s, overlap 1 s, length of merge region 1 s,

| | | |
|---|---|---|
| Bolt-gun: | operator length 200 ms | prediction length 100 ms |
| G-gun: | operator length 200 ms | prediction length 60 ms |
| Prakla-array: | operator length 300 ms | prediction lenght 40 ms |

  - Static correction to a fixed seafloor traveltime of 11 s.
  - Time and offset-dependent Ormsby frequency filter.

On time-shifted traces with a reduced time scale of 6 km/s the following filter parameters were used:

| lower stop/pass Bolt-gun G-gun Prakla-array | upper pass/stop [Hz] | offset[m] | beginful[s] | endful[s] |
|---|---|---|---|---|
| 3/5 | 40/60 | | | |
| 3/5 | 57/77 | | | |
| 3/5 | 50/70 | 0 | 0 | 12.8 |
| | | 8000 | 0 | 12.6 |
| | | 48000 | 0 | 0 |
| 3/5 | 30/40 | | | |
| 3/5 | 38/53 | | | |
| 3/5 | 30/50 | 0 | 13.7 | 14.3 |
| | | 8800 | 13.5 | 14.4 |
| | | 13200 | 13.0 | 13.9 |
| | | 52000 | 1.0 | 2.0 |
| | | 107000 | 0 | 0 |
| 3/5 | 20/30 | | | |
| 3/5 | 22/35 | | | |
| 3/5 | 20/30 | 0 | 15.3 | 16.8 |
| | | 11700 | 15.1 | 16.6 |
| | | 19200 | 14.8 | 16.3 |
| | | 61700 | 7.0 | 10.1 |
| | | 114000 | 2.0 | 3.0 |
| | | 152000 | 0 | 0 |
| 3/5 | 10/20 | | | |
| 3/5 | 14/23 | | | |
| 3/5 | 10/20 | 0 | 19.0 | trace length |
| | | 20000 | 18.4 | trace length |
| | | 130000 | 3.5 | trace length |

**• Data exchange**

For the exchange of the OBH/OBS data, the SEGY-format on disk with a Sun tar-format was chosen. The raw segy data is in Integer2 format with trailer bytes between the record structure of SEGY. The processed data is in IBM-floating point without trailer bytes between the records.
For UTM transformation into Cartesian coordinates use: WGS84 spheroid, central meridian 85 0. 0. W, northern hemisphere.
This is the definition of the segy trace header for the GEOMAR OBS wide-angle reflection data. The extension of the standard SEGY header from 181 to 240 byte is a layout in order to process the data on the SEISMOS/SU software system. Reading bytes directly into this header will allow access to all of the fields.

**• MCS processing**

The airgun shots were also registrated by a 4 channel mini-streamer. The group spacing is 50 m and the first offset was calculated from the direct wave to approximate 130 m. Due to the different shot intervals from 10 to 60 s (≅ 10 to 120 m) and the variable data quality, the processing sequence was adjusted for each profile after a check of the raw data. During the first 14 profiles all 4 channels could be used for processing, while only 2 channels recorded data of good quality for profile 15 to 28 after which we continued with only one channel. The bad traces are degradated by high amplitude noise and a low signal to noise ratio. Problems with streamer depth variations between first and last channel were nearly eliminated by attaching a buoy at the tail of the streamer.

A standard processing job (-) was created with some variable modules (*), depending on the profile parameters and the data quality.

- Input: SEGY-data, 2 ms or 4 ms sampling rate with complete geometry information.
- * Resampling from 2 ms to 4 ms.
- Kaiser highpass (debias).
- Static correction to a fixed seafloor travel time of 10 s.
- Time-variant gather-oriented predictive deconvolution: always 5 traces of a common receiver gather are used to calculate the operator for the centre trace, gate length 3 s,

overlap 1 s, length of merge region 1 s.

| | | |
|---|---|---|
| Bolt-gun: | operator length 200 ms | prediction interval 100 ms |
| G-guns: | operator length 200 ms | prediction interval 40 ms |
| Prakla-array: | operator length 200 ms | prediction interval 32 ms |

- Time dependent Ormsby frequency filter.

| | depth interval below seafloor [s] | lower stop/pass[Hz] | upper pass/stop [Hz] |
|---|---|---|---|
| Bolt-gun/ | 0 – 0.1 | 3/5 | 65/85 |
| G-guns: | 0.5 – 0.9 | 3/5 | 45/65 |
| | 1.3 – 1.9 | 3/5 | 30/45 |
| | 2.3 – 2.8 | 3/5 | 20/30 |
| | 3.6 – trace length | 3/5 | 15/23 |
| Prakla-array: | 0 – 0.1 | 5/8 | 70/90 |
| | 0.5 – 0.9 | 5/8 | 50/70 |
| | 1.3 – 1.9 | 5/8 | 35/50 |
| | 2.3 – 2.8 | 5/8 | 25/40 |
| | 3.6 – trace length | 5/8 | 15/23 |

* Whole trace normalization for varying amplitude levels in the different channels.
* Removing of high amplitude noise by comparing trace amplitudes with the average amplitude of the surrounding traces.

- Seafloor mute.
- Remove static correction.
- Binning of traces, depending on the desired output spacing.
- Dip dependent trace interpolation of empty bins.
- Finite difference time migration with 1500 m/s.
- Automatic gain control.
- Output: SEGY-data.

For profile 22 the raw plot of one channel is presented in Figure 6.6.13 with a broad bandpass filter (5 to 60 Hz) applied. In the processed section (two channels) in Figure 6.6.14 the reveberations of strong reflectors are removed and the resolution is remarkable improved. The same seismic line was also shot with the Bolt-gun (Figure 6.6.15) and the Prakla airgun-array (Figure 6.6.16). The bolt gun reveals two strong reveberations at around 200 ms and 400 ms, while the Prakla airgun-array shows a sequence of reveberations of up to more than 300 ms.
The MCS profiles are displayed in the individual chapters of the wide-angle profiles.

## Processing of earthquake data (EQNET and JACO NET)

(I. Arroyo, J. Gossler, P.O. Thierer)

The initial processing of the data is identical to the processing sequence for wide angle data described in the previous section, i.e., reading of the flashcards, conversion into a REFTEK file, and conversion into a pseudo SEGY file. Following this step, the processing sequence of the earthquake data diverges from the one for wide angle data.

The single traces are cut into records of 25 hours length with one hour overlap between adjacent records, such that each record begins at 0:00:01 (except on the first day of recording, of course). The reason for this cutting is (a) to make file sizes smaller and hence the data more manageable, and (b) to be able to apply the time corrections on a daily basis. Routine for cutting: split_segy.pl

The timing of each 25 hour section of the data is corrected. Two timing errors need to be taken account of:

a) the occurrence of time slips (extra or missing samples) due to a mismatch of the desired and actual sample rates (see previous section for a more detailed discussion of time slips). The approach for correcting time slips differs from the approach used for the wide angle data because seismological analysis needs to refer back to the continuous data stream throughout. The occurrence time of all time

slips is read out from the send2pas log file. The time slips before the beginning of the record are added up and applied as static shift to the start time of the record. For time slips during the record a sample is added (positive time slips) or removed (negative time slips) at the appropriate time. This procedure is only approximate (a correct treatment would require resampling of the whole record, fraught with its own difficulties), and in general the apparent time of a sample can be off by up to half a sample length due to this approximation. Relative times within the same record can be off by up to one sample length if the time span straddles a time slip. Routine for time slip correction: unslip

b) the slow drift of the internal clock relative to GPS time. The system time is compared with GPS time at the beginning and end of the deployment, and a drift rate is inferred from the observed difference (skew). The time of each 25 hour record is corrected by applying the shift appropriate for the time 12.5 hours after the beginning of the record. The underlying assumption is that the system clock does indeed drift linearly, and that the drift over a 24 hour period is negligible, i.e. much less than one sample length, which was the case in this experiment. For some stations that ran out of power prematurely, no skew could be determined and therefore no drift correction carried out. Timing uncertainties for these stations accumulate at a rate 1.5-2 ms per day, starting with the first day of deployment. Routine for linear clock drift correction: clock_cor.pl

The data for each day are quality controlled and a table of station status prepared for each station (see Tables 6.6.1.1 and 6.6.5.1).

A short-term-average versus long-term-average (STA/LTA) trigger algorithm is then applied to the data to find out seismic events. Trigger parameters like length of the short term (s) and long term (l) time windows, the mean removal window length (m), the trigger (t) and detrigger ratio (d), minimum number of stations (S) and at least the time window length (M) in which trigger signals contribute to the same event must be found individually for each data set. We take s = 0.5 sec, l = 60 sec, m = 500 sec, t = 3.5, d = 0.8, S = 3, M = 10 sec for the EQNET small scale network, where the data are very noisy and most event locations are very close to the network, so that the waveforms are coherent and have higher frequencies than the noise, so that is possible to use a relatively high trigger ratio. For the JACO network, were the noise is reduced drastically compared to EQNET we decreased the trigger ratio to 2.8, and increased M to 20 sec because of the larger spatial dimension of the network. Data has been checked by eye view also, and it seems that the selected trigger values delivered good results. The so found events are cut from the time-corrected data, and stored in sub-directories, one per event. The events have been quality checked again. Bad triggers have been sorted out. Events are also inspected for traces, which are unusable for a particular event, e.g. because they contain only noise. Routine for trigger and event cutting: trig_all.sh, which uses reftrig program from the PASSCAL tool kit and collate_ev.pl, respectively.

The pseudo-SEGY traces in the event directories are converted first into SAC, and then into SEISAN waveform format, which makes it possible to store all traces associated with an event in one file. After the conversion the data are registered into the SEISAN database (Havskov and Ottemöller, 2001). Routines for conversion: segy2sac_all.csh, sacsei.sh, seisei.sh

At last, P and where possible S phases are picked and events preliminarily located with the program HYP, which employ an iterative solution to the nonlinear localisation problem (Lienert, 1994). For the sake of simplicity of onboard processing, a one-dimensional velocity model is assumed based on offshore refraction profile line 3 of RV Sonne cruise SO76 west of Nicoya peninsula (Ye et al., 1996). The coda magnitude is also determined for each event.

**Table 6.6.1:** 1D-Velocity model for earthquake localisation

| Vp(km/s) | Depth(km) |
|---|---|
| 2.0 | 0.0 |
| 4.2 | 2.0 |
| 6.0 | 7.0 |
| 7.2 | 12.0 |
| 8.1 | 80.0 |

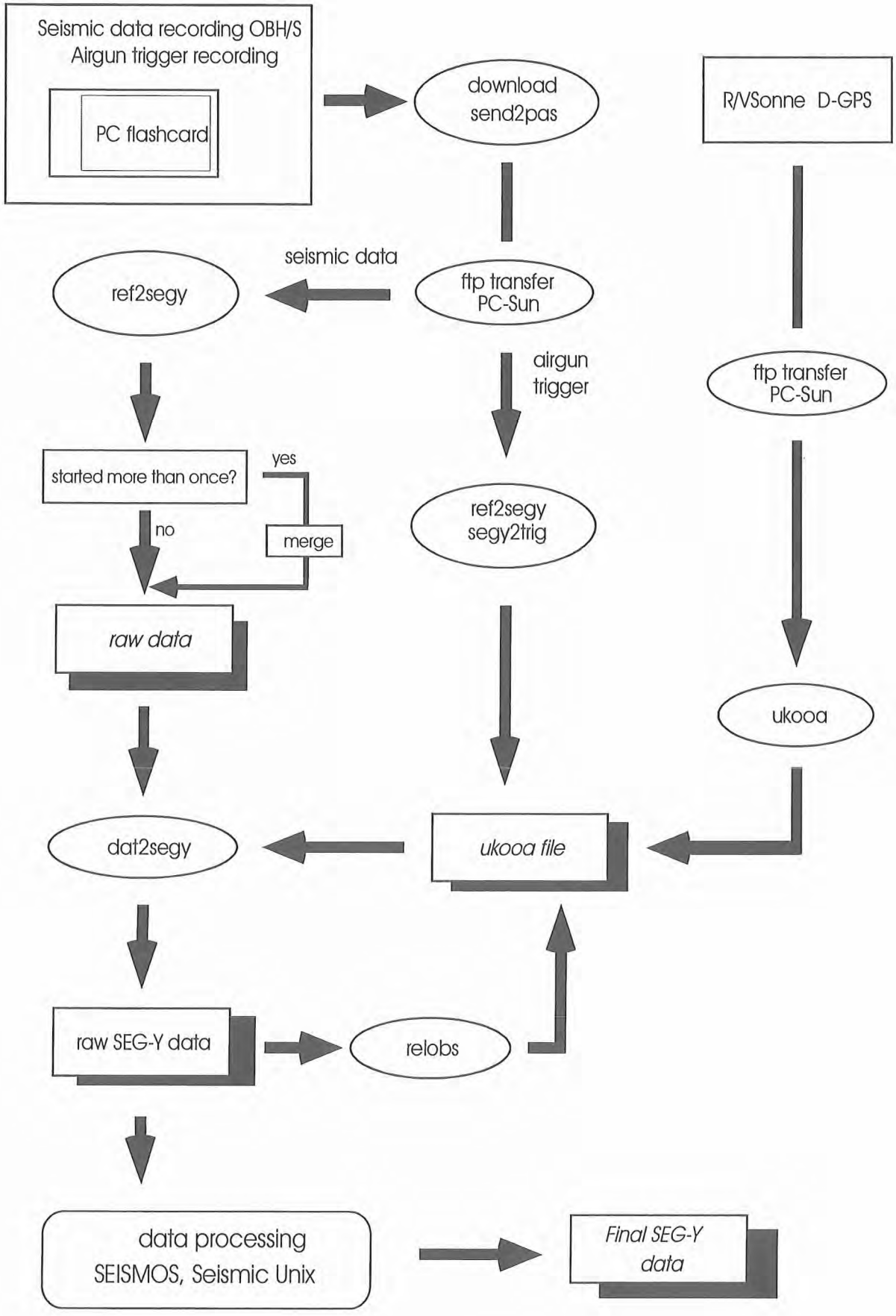


**Figure 6.6.1:** Processing flow of OBH/S data from raw data to SEG-Y records.

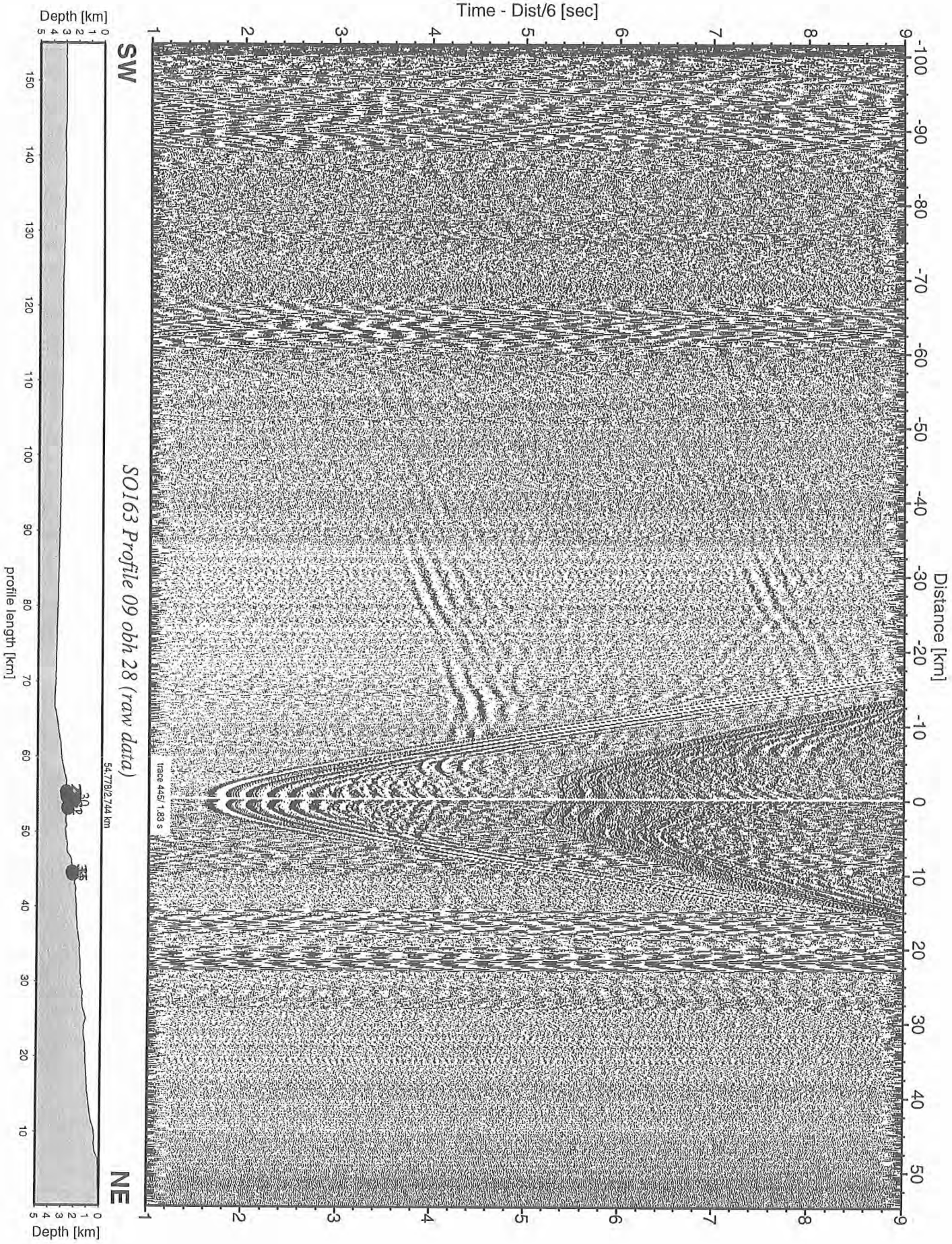


**Figure 6.6.2a:** Record section from obh 28 (raw data), Profile 09.

**Figure 6.6.2b:** Record section from obh 59 (raw data), Profile 15.

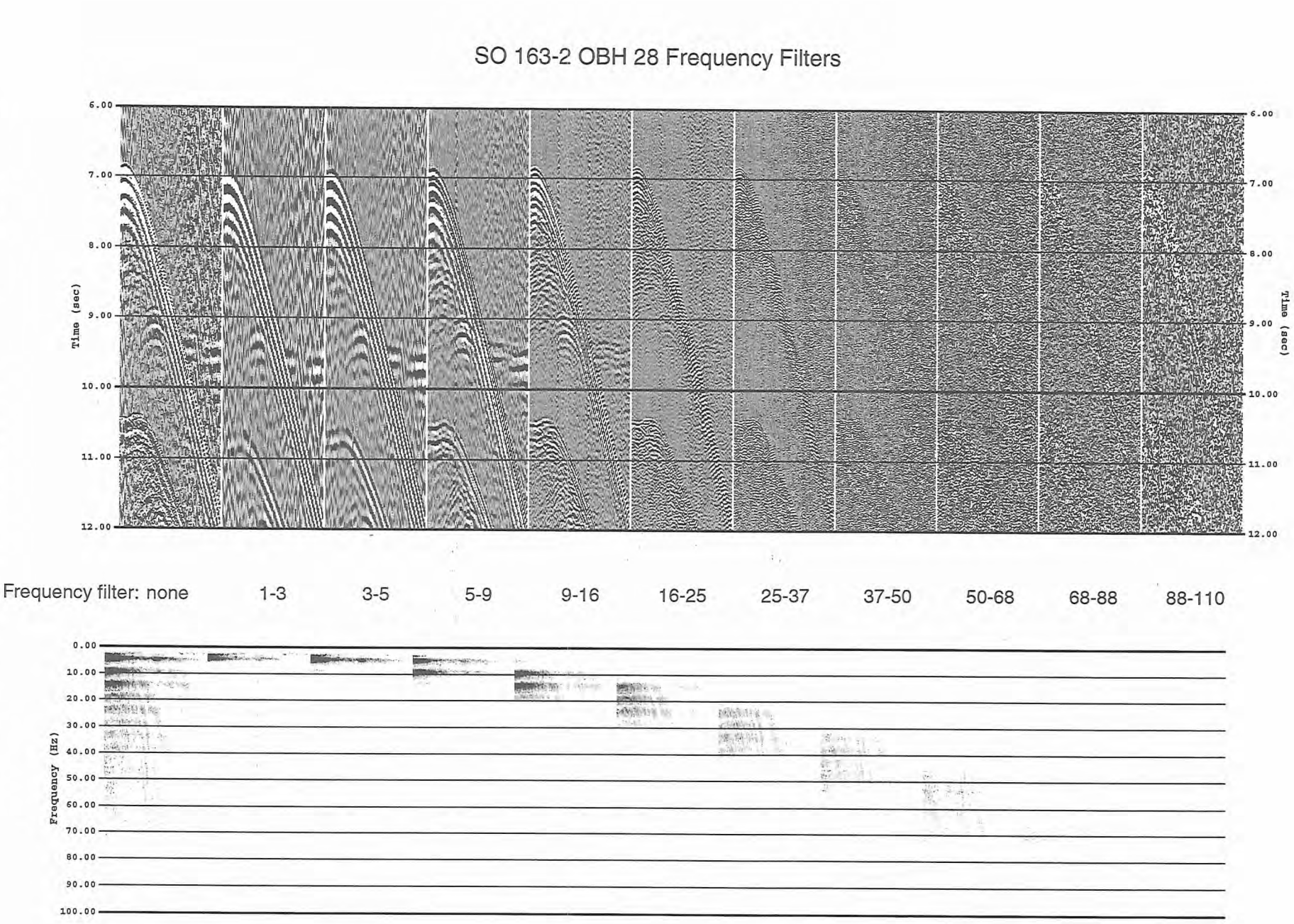


**Figure 6.6.3:** Frequency analysis of OBH28 (0-13 km offset, Bolt gun).

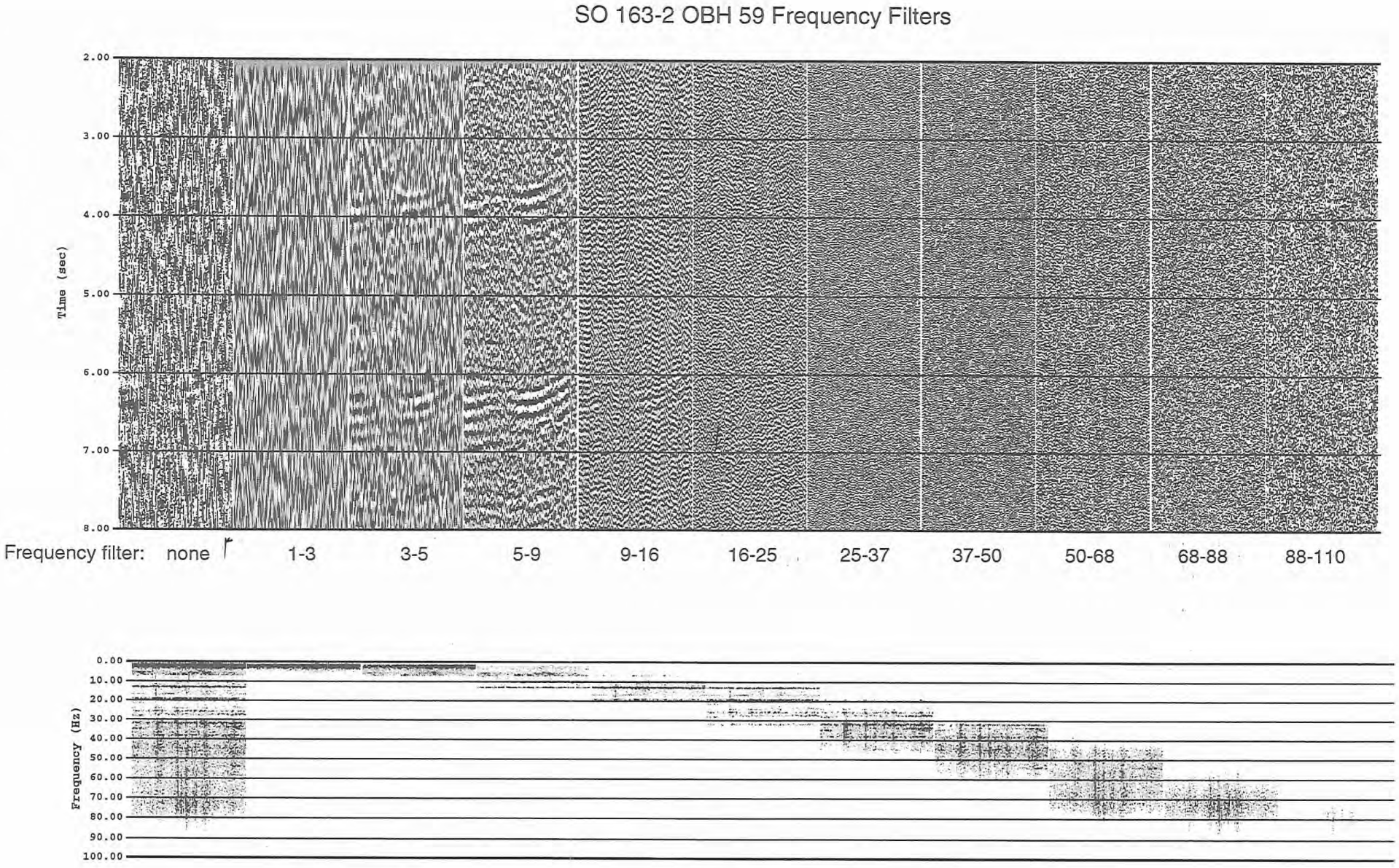


**Figure 6.6.6:** Frequency analysis of OBH59 (31-42 km offset, G-guns).

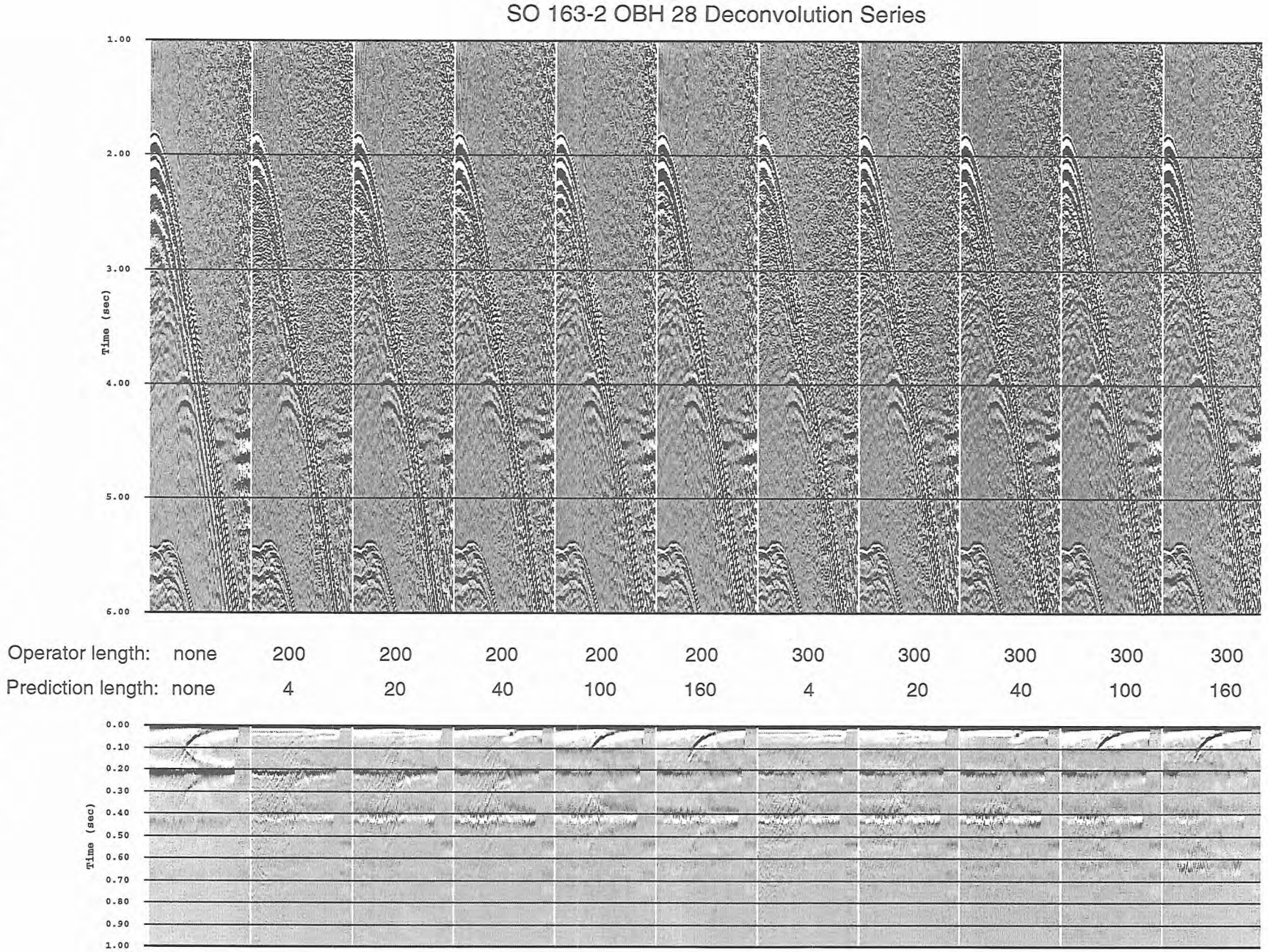


**Figure 6.6.7:** Deconvolution test of OBH 28 (0-13 km offset, Bolt gun).

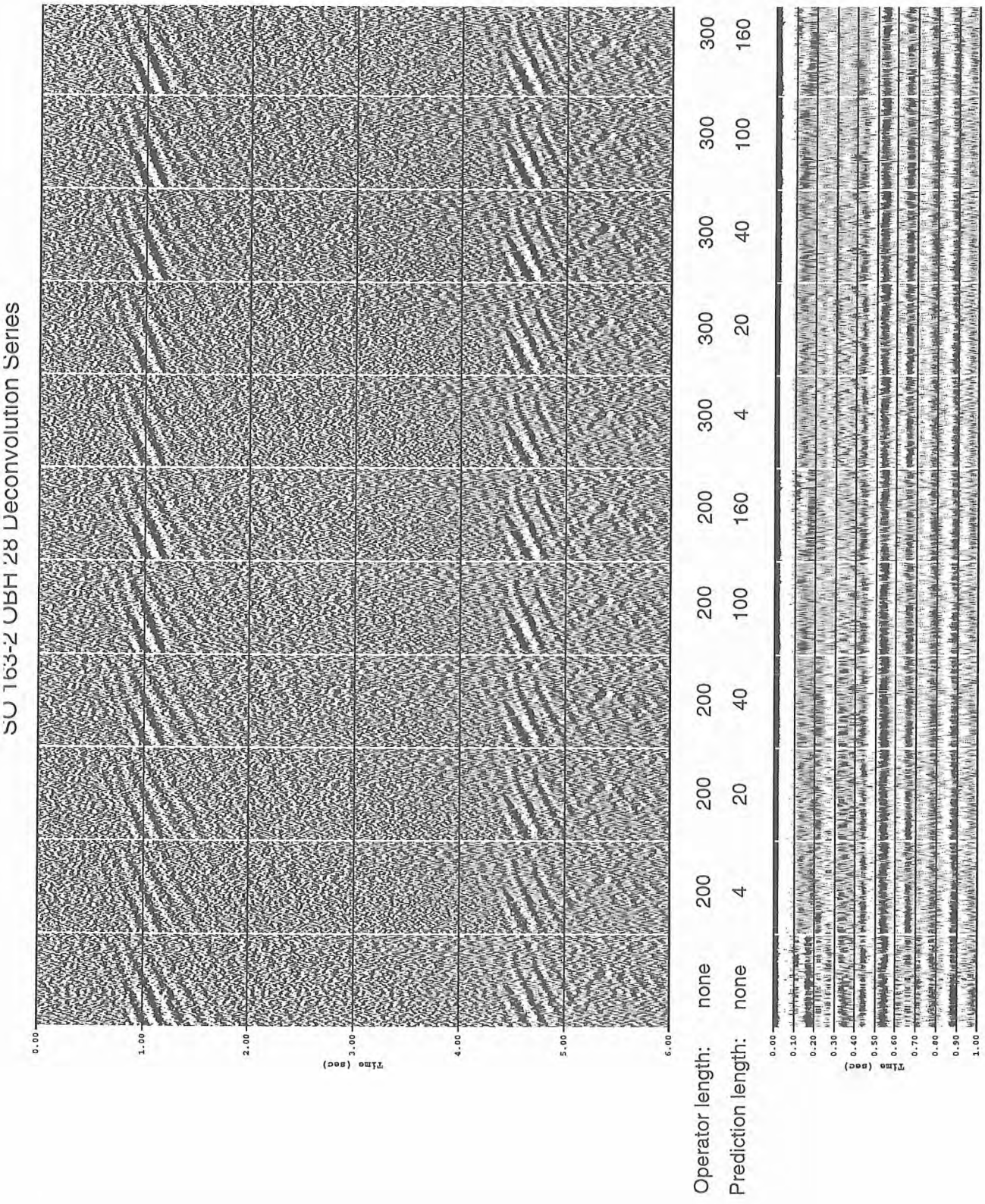


**Figure 6.6.8:** Deconvolution test of OBH 28 (26-38 km offset, Bolt gun).

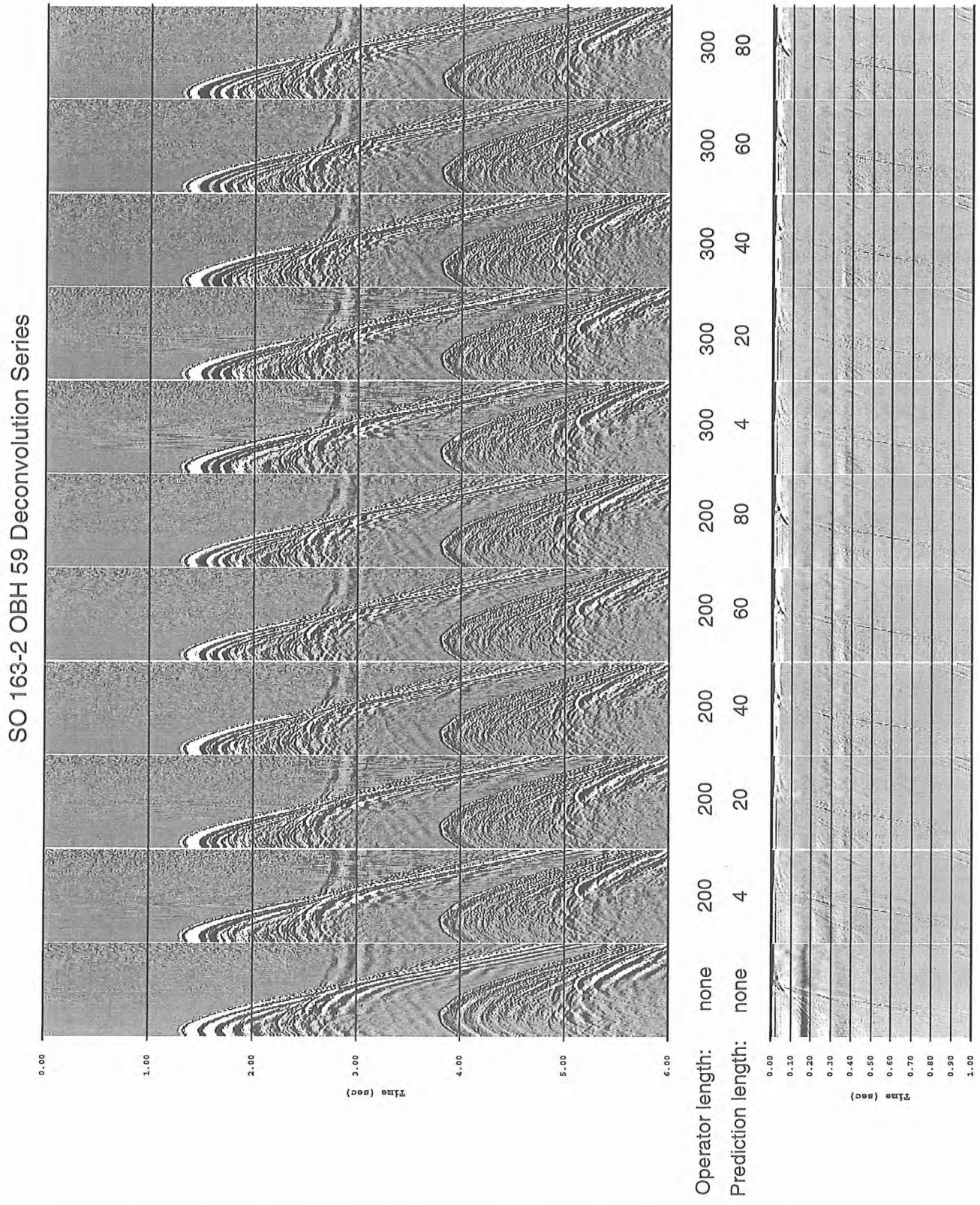


**Figure 6.6.9:** Deconvolution test of OBH 59 (0-9 km offset, G-guns).

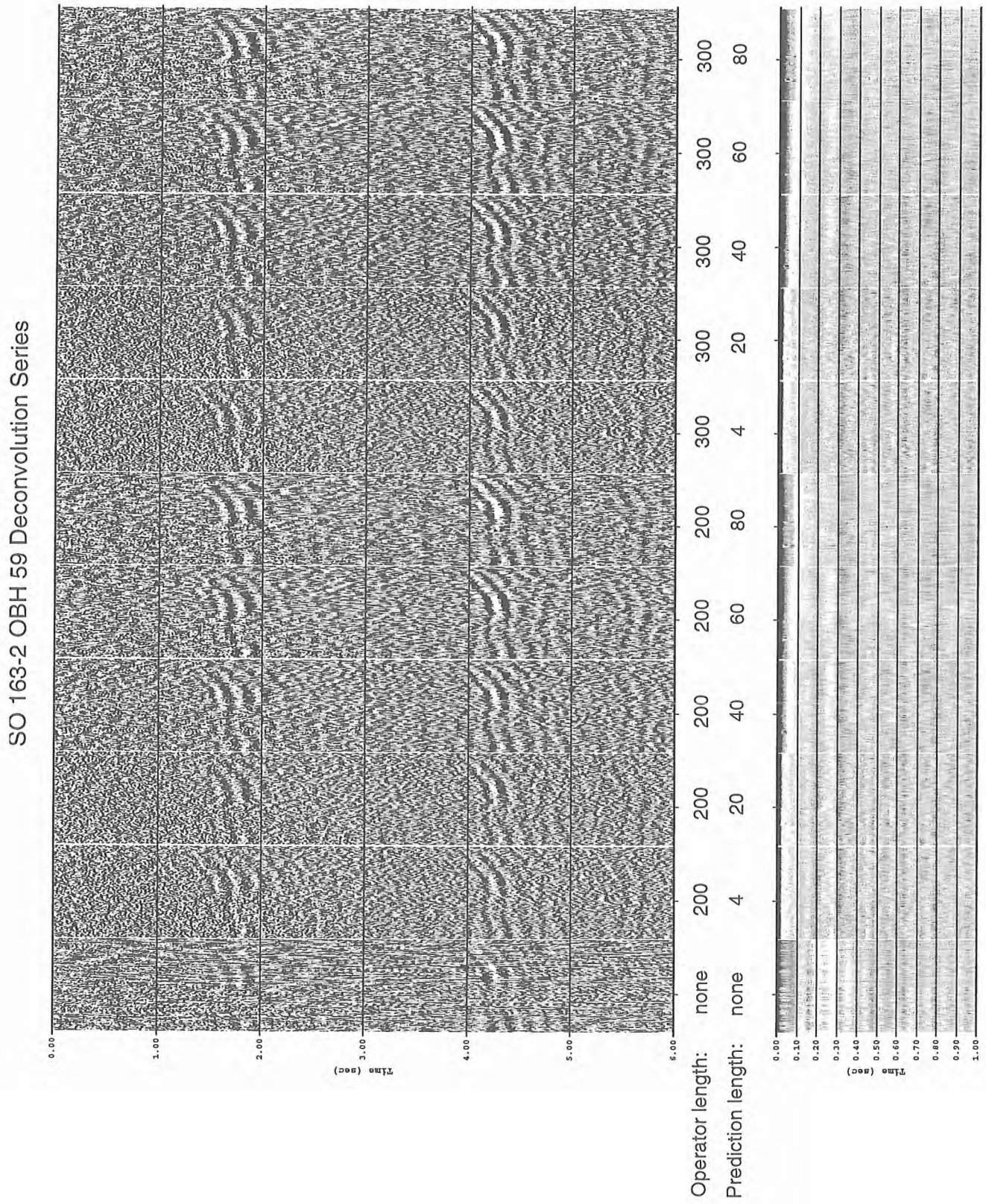


**Figure 6.6.10:** Deconvolution test of OBH 59 (31-42 km offset, G-guns).

**Figure 6.6.11:** Record section from obh 28 (processed data), Profile 09.

**Figure 6.6.12:** Record section from obh 59 (processed data), Profile 15.

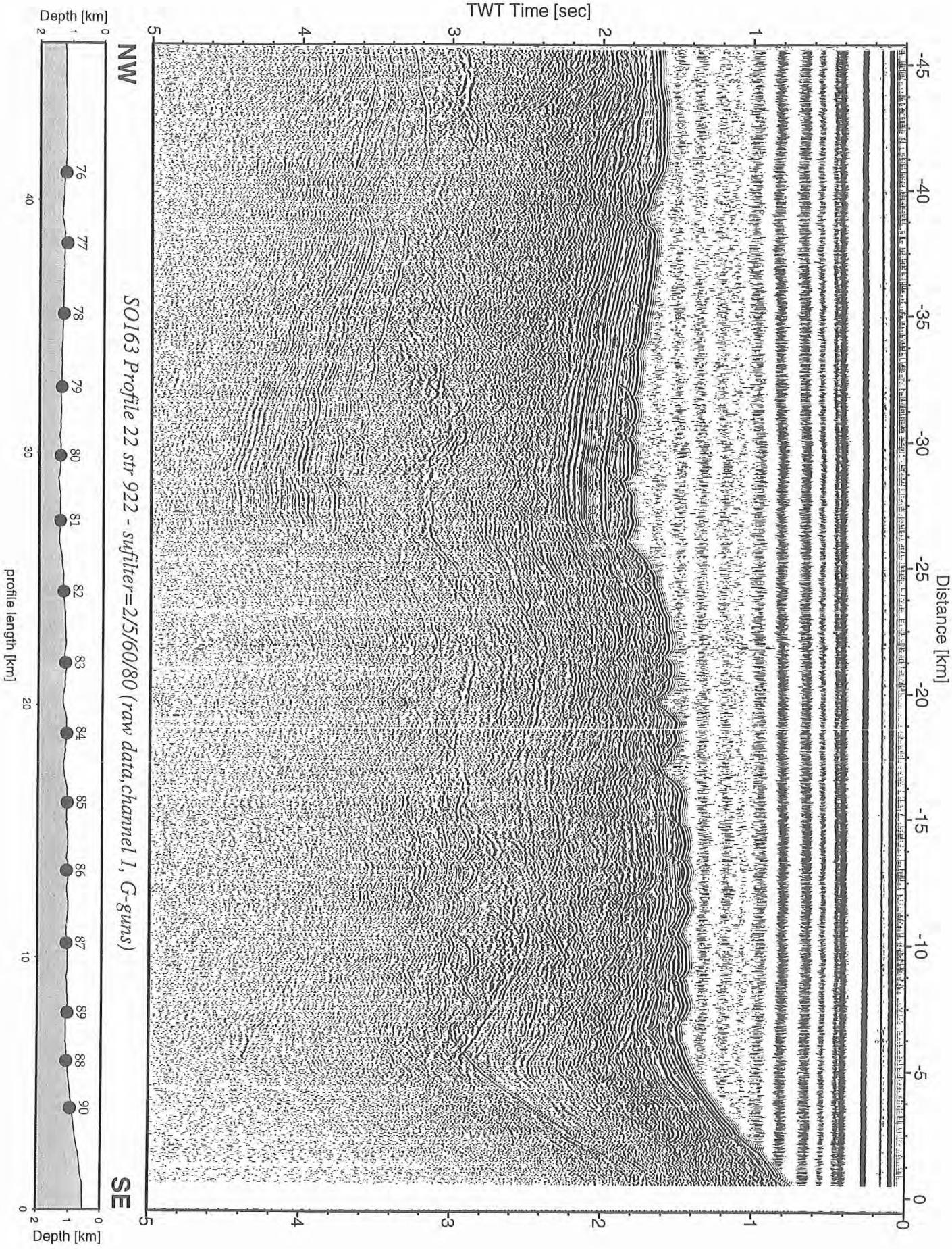


**Figure 6.6.13:** Record section from str 922 (raw data,channel1, G-guns), Profile 22.

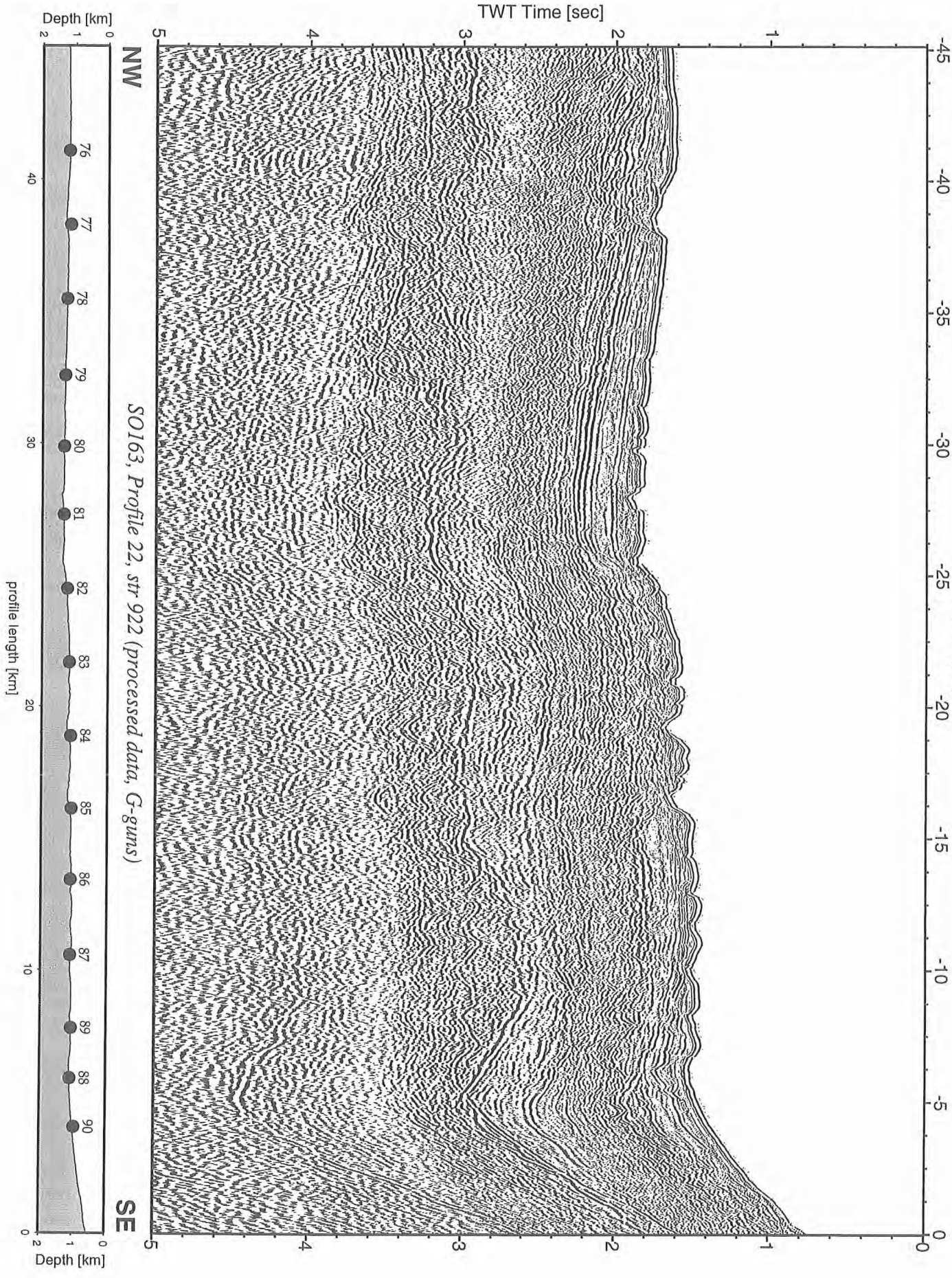


**Figure 6.6.14:** Record section from str 922 (processed data, G-guns), Profile 22.

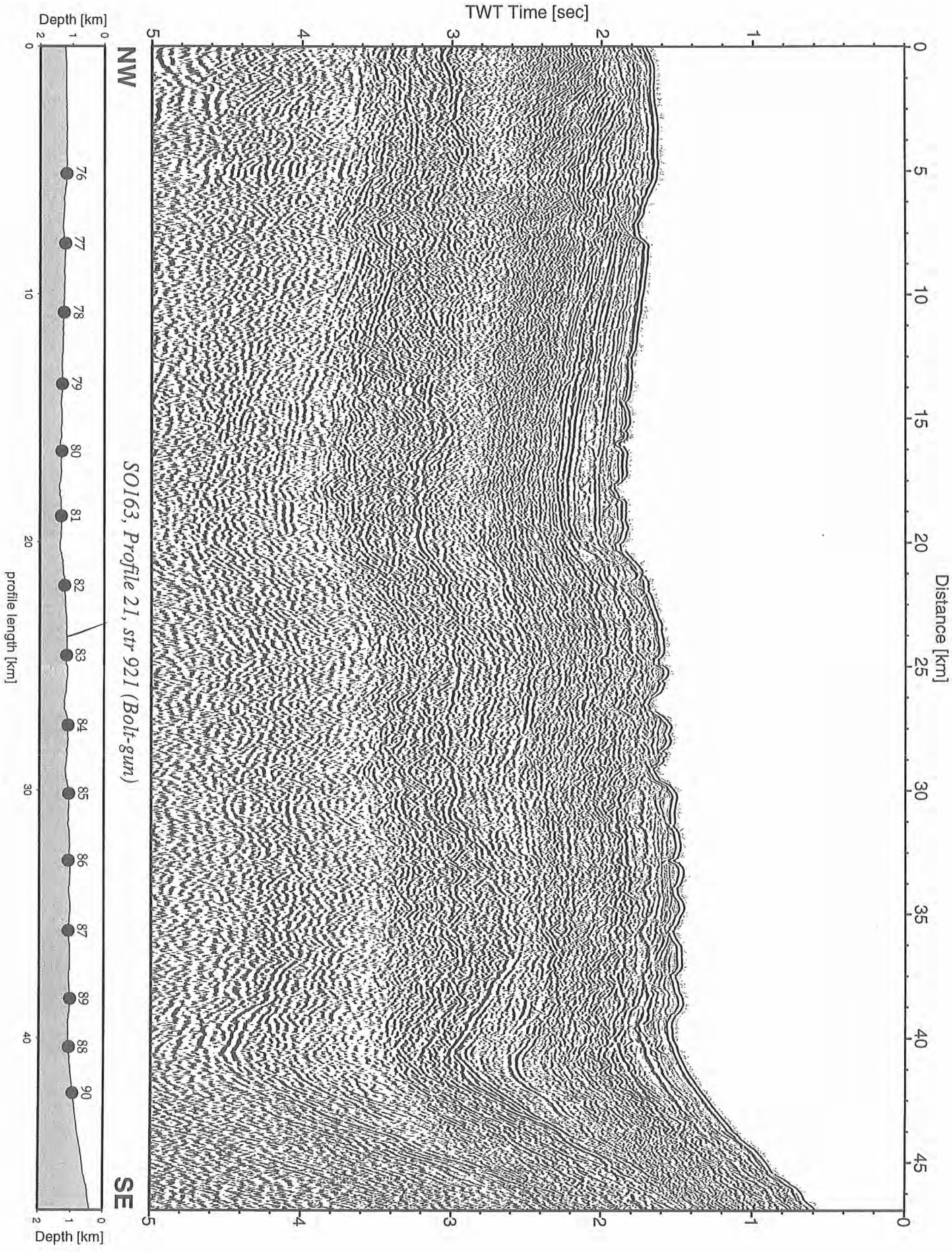


**Figure 6.6.15:** Record section from str 921 (Bolt-gun), Profile 21.

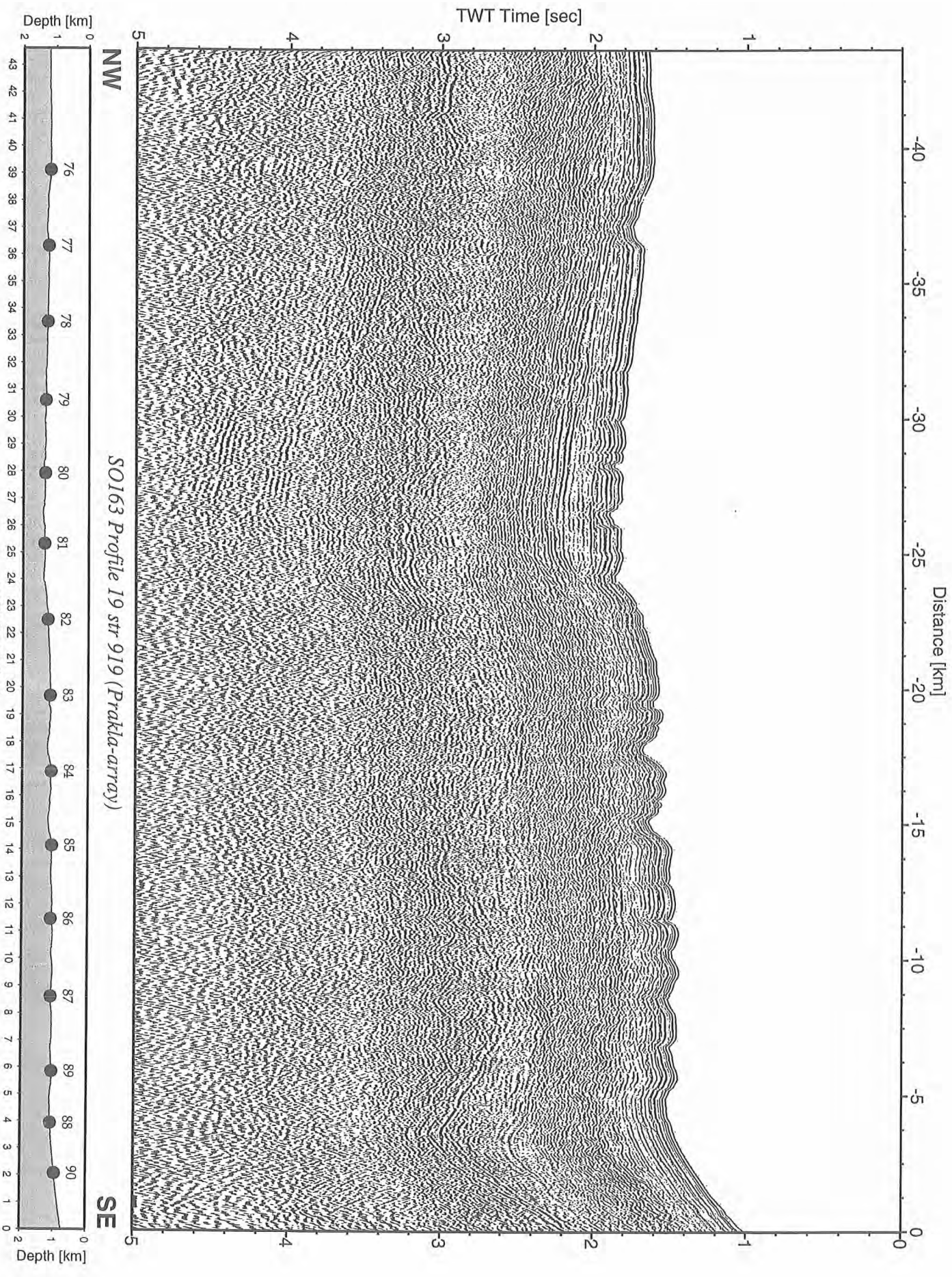


**Figure 6.6.16:** Record section from str 919 (Prakla-array), Profile 19.

## 6.6.1 The Local Earthquake Network and profiles P01-P06 (EQNET)

### Determination of the optimum source depth of the Bolt-gun (P01 – P06)

(A. Berhorst)

In order to determine optimum depth of the Bolt-gun, profiles P01 to P06 across EQNET (Figure 6.6.1.1) were shot along the same transect (Figure 6.6.1.11), revealing a doming structure of 1 km length, 100 m high and a central depression. The cable length between the airgun and its floatations has been varied between 3.5 m and 14 m. Medium and far-field source signal recorded by the streamer and an OBH placed 500 m above seafloor are presented in Figures 6.6.1.9 f. and 6.6.1.10 f., respectively. Peak amplitudes recorded by the streamer were clipped, but as all sections are recorded with the same gain, the signals are comparable in time domain. In the frequency domain, the clipping causes unpredictable frequency distortions, making this records less reliable for an analysis. The registrations of the OBH are not clipped. Due to the 500 m long anchor, the direct wave is not mixed with the first reflections of the seafloor, thus presenting the far-field source signal. In Figure 6.6.1.12 the images for a source depth of 7.5 m and 9.5 m are exchanged. The number of reverberations is increasing with the source depth, while the time interval between first peak and bubbles is decreasing with increasing source depth. The increasing time interval between first peak and first bubble is well imaged in the first maximum of the frequency spectrum and its overtones. This first frequency maximum is shifted from 4.5 Hz for a source depth of 3.5 m to 6 Hz for a source depth of 14 m. The peak amplitudes of the first arrivals indicate a maximum for a cable length of 7.5 m.

The frequency analysis of the refracted arrivals (Figure 6.6.1.13) is in good agreement with these observations, thus indicating that the analyzed wavelet is our far-field signature convoluted with the subsurface reflectivity. In order to operate the Bolt-gun with maximum amplitude of the first peak, we used a cable length of 7.5m after these test profiles.

### Velocity determination

(I.Arroyo)

The processed record of the OBH23 during the shooting of Profile 2 (Figure 6.6.1.3) was analyzed in order to obtain an 1-D velocity model of the upper sediment cover (~ 4 km). To achieve further studies in the far field, OBH23 was located 500 m above the sea floor. The pickings of the record are shown in Figure 6.6.1.14, together with the predicted arrivals modeled with the program R1D (Luetgert, 1992). The curvatures of the predicted arrivals nearly coincide with the observed phases. Four reflections were found, with P-velocities ranging from 1,5 to 2,0 km/s :

| Depth (m) | P velocity (km/s) |
|---|---|
| 0 – 1 430 (water) | 1,480 |
| 1 430 – 1 973 | 1,468 – 1,766 |
| 1 973 – 2 504 | 1,791 – 1,905 |
| 2 504 – 3 199 | 1,922 – 1,959 |
| 3 199 – 3 593 | 1,953 – 2,027 |

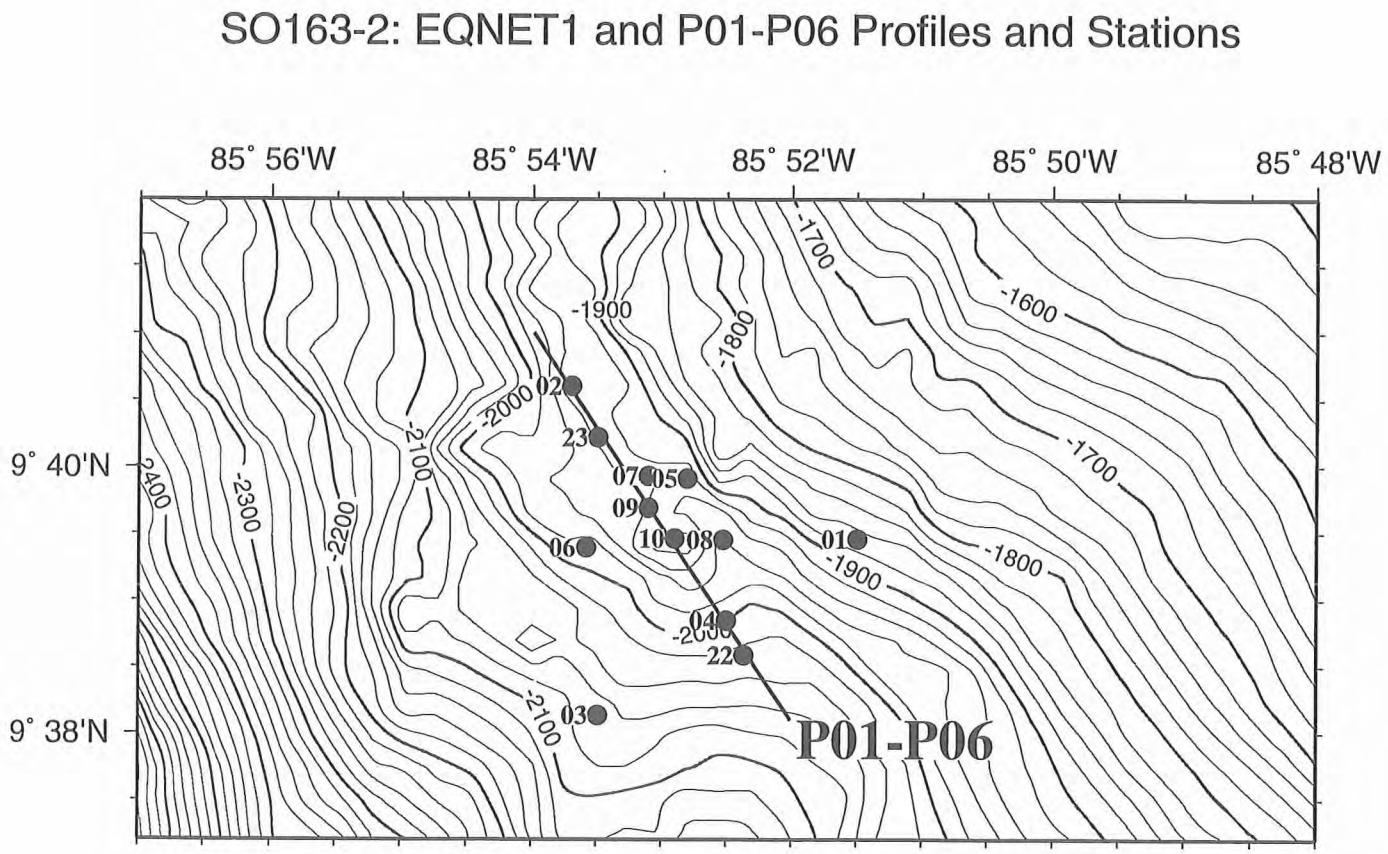


**Figure 6.6.1.1:** Location map of Eqnet1 and profiles 01-06 with 20 m isolines. Superimposed are the 10 OBH locations, covering the OFOS 10 mud volcano.

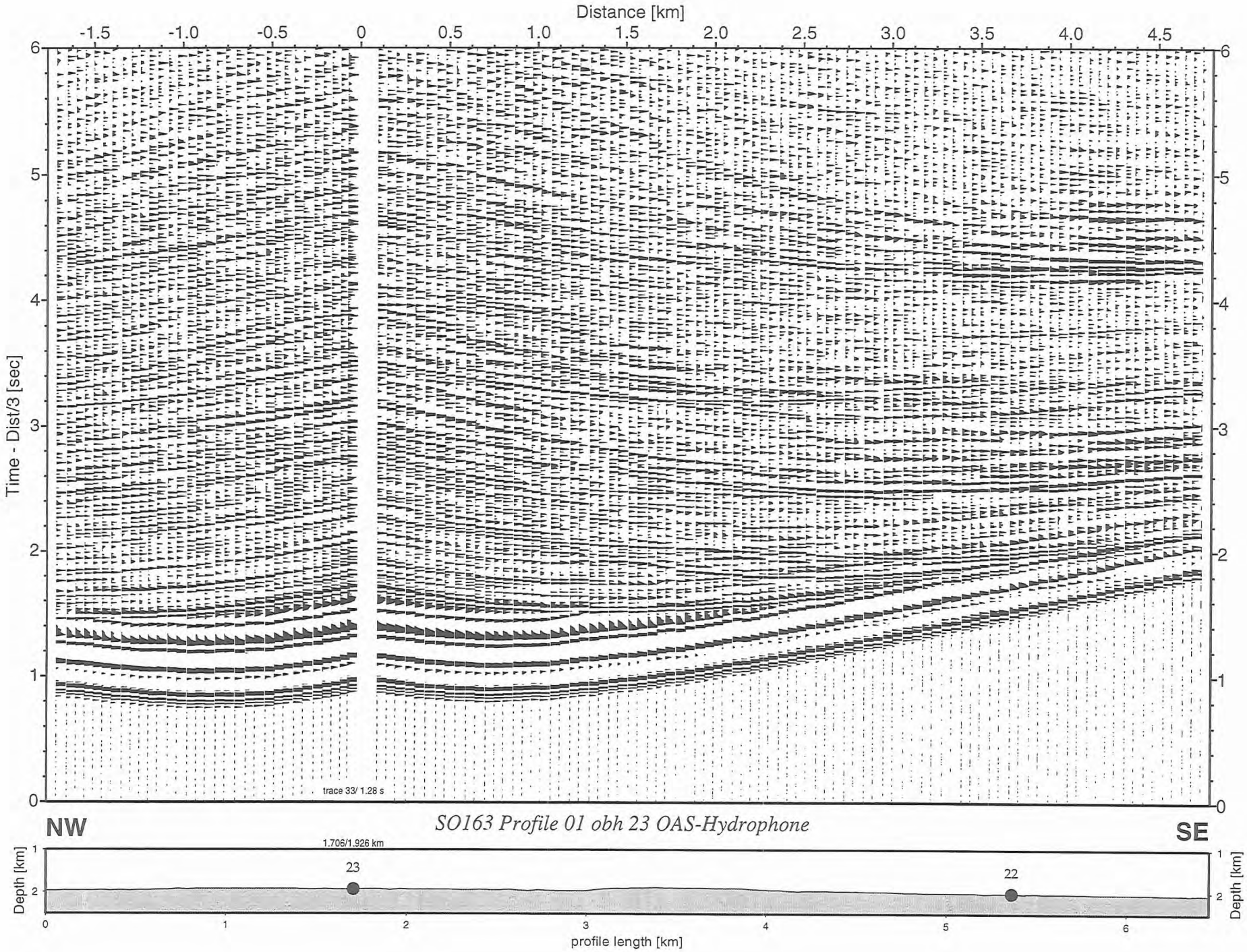


**Figure 6.6.1.2:** Record section from obh 23 OAS-Hydrophone, Profile 01.

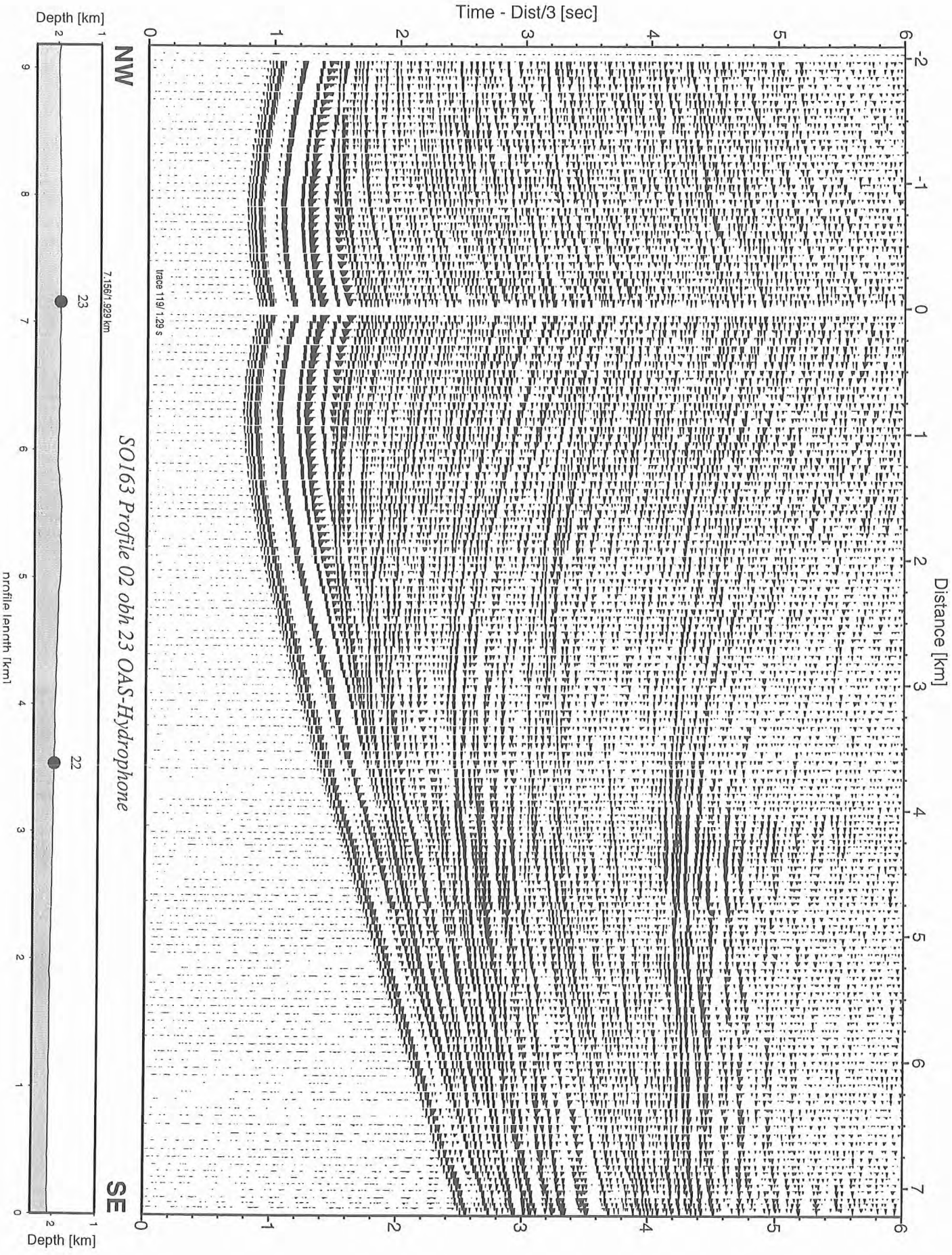


**Figure 6.6.1.3:** Record section from obh 23 OAS-Hydrophone, Profile 02.

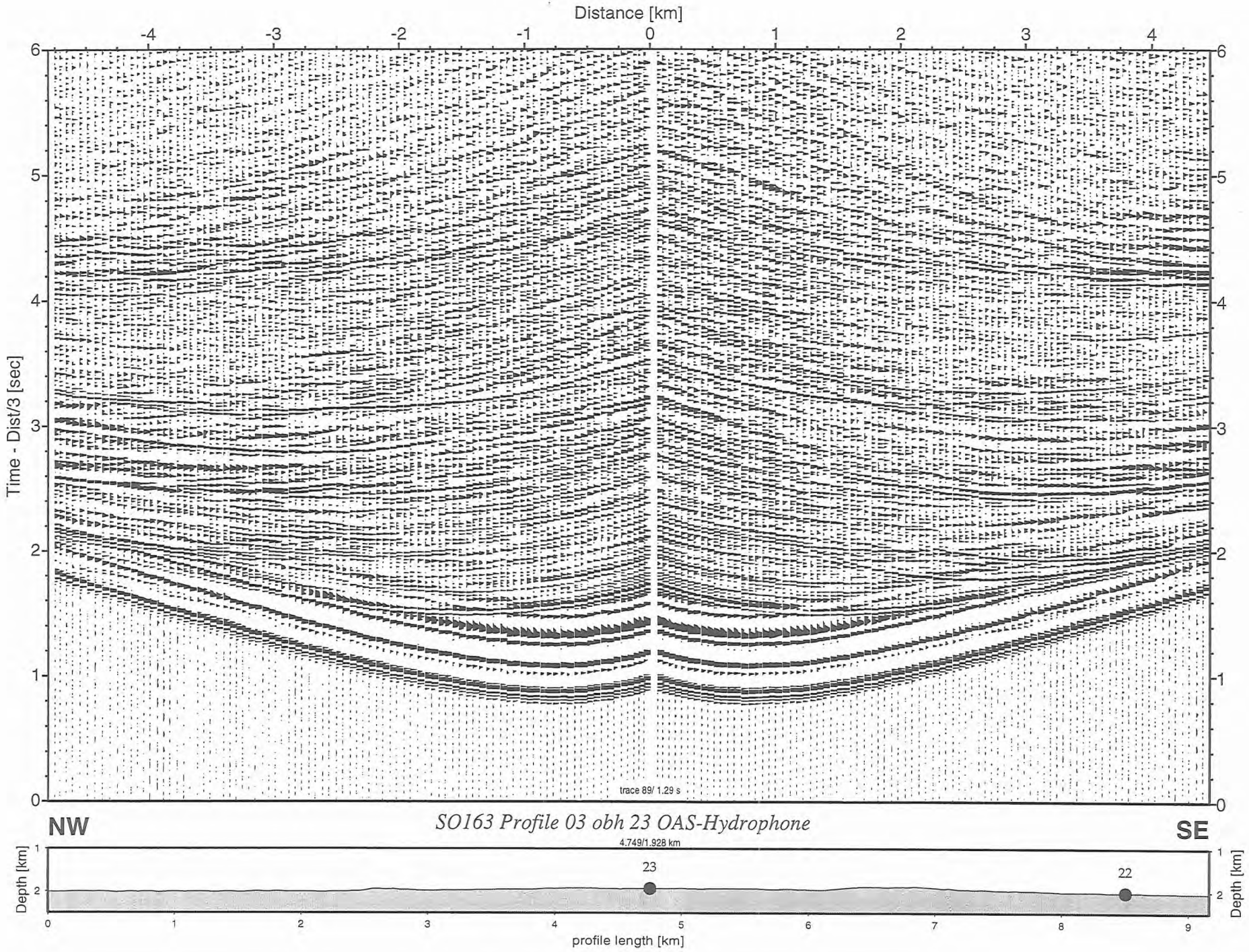


**Figure 6.6.1.4:** Record section from obh 23 OAS-Hydrophone, Profile 03.

**Figure 6.6.1.5:** Record section from obh 23 OAS-Hydrophone, Profile 04.

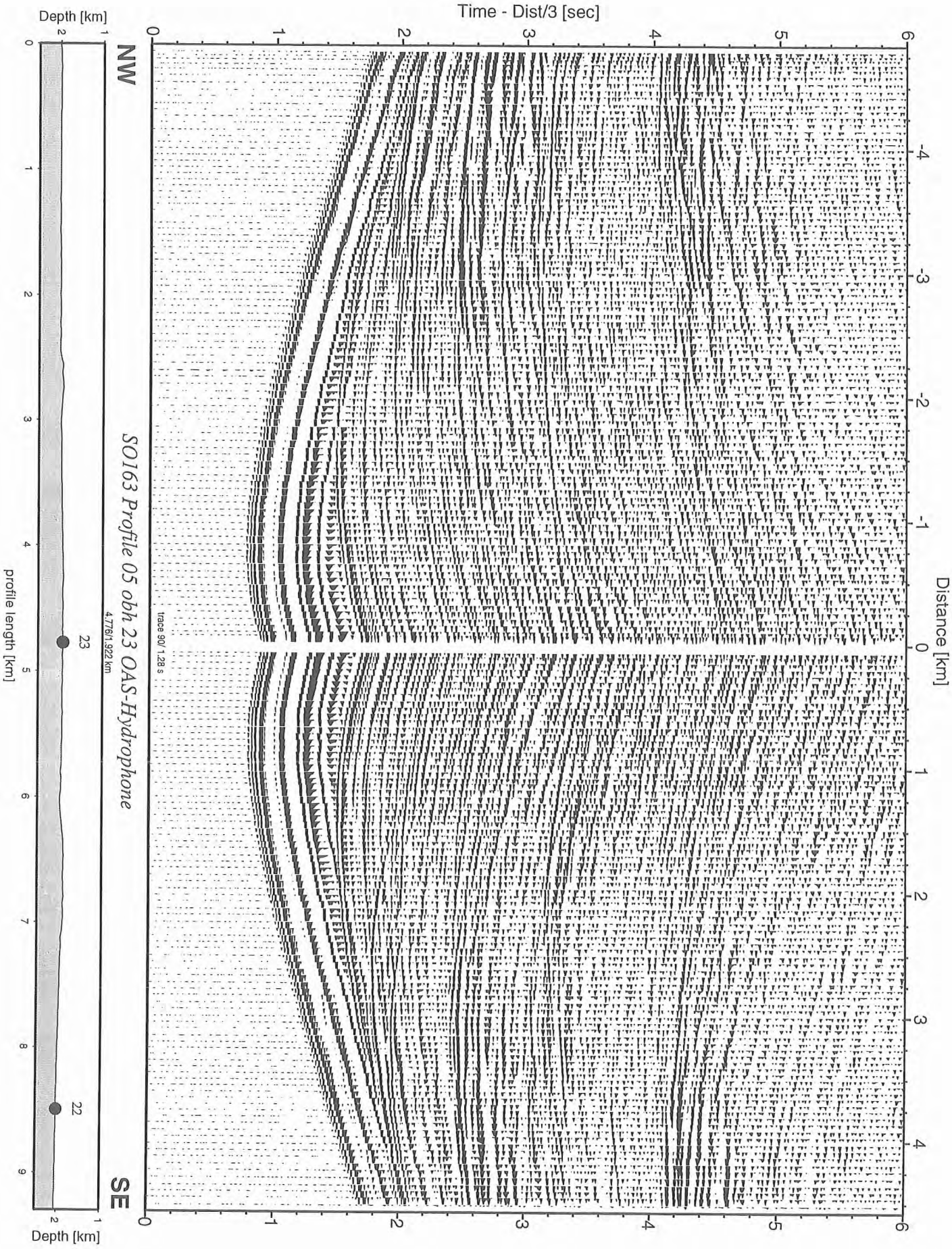


**Figure 6.6.1.6:** Record section from obh 23 OAS-Hydrophone, Profile 05.

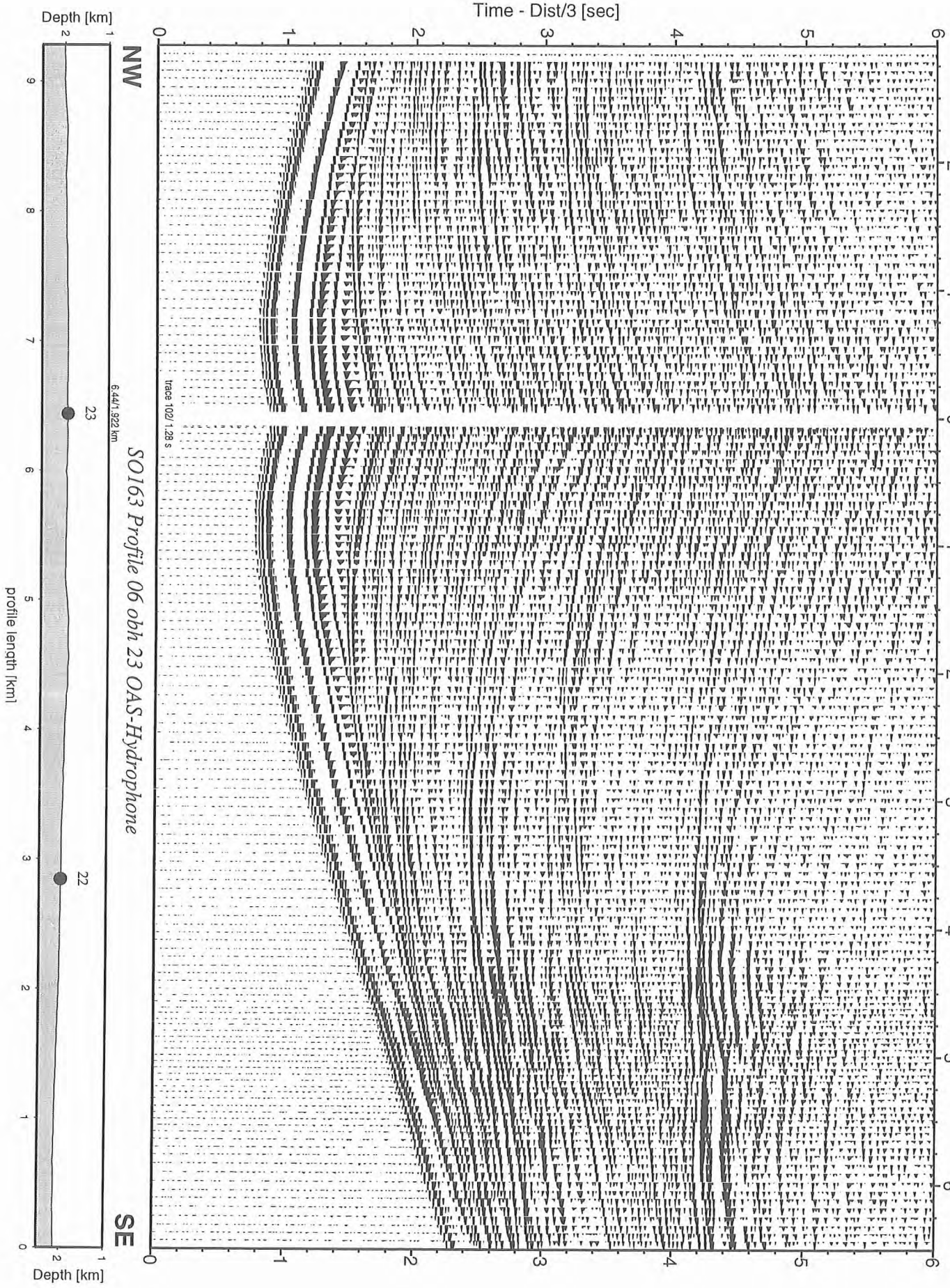


**Figure 6.6.1.7:** Record section from obh 23 OAS-Hydrophone, Profile 06.

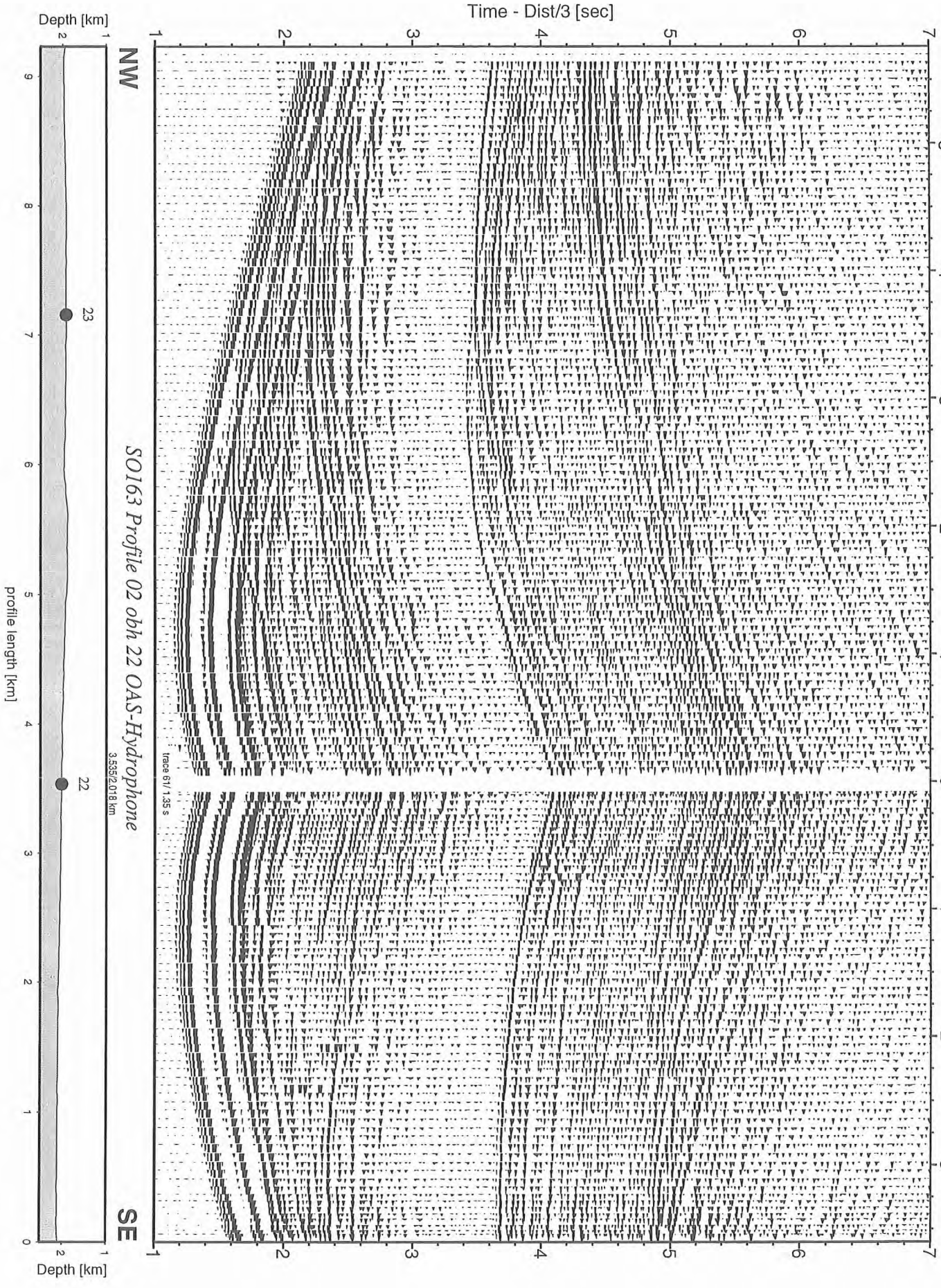


**Figure 6.6.1.8:** Record section from obh 22 OAS-Hydrophone, Profile 02.

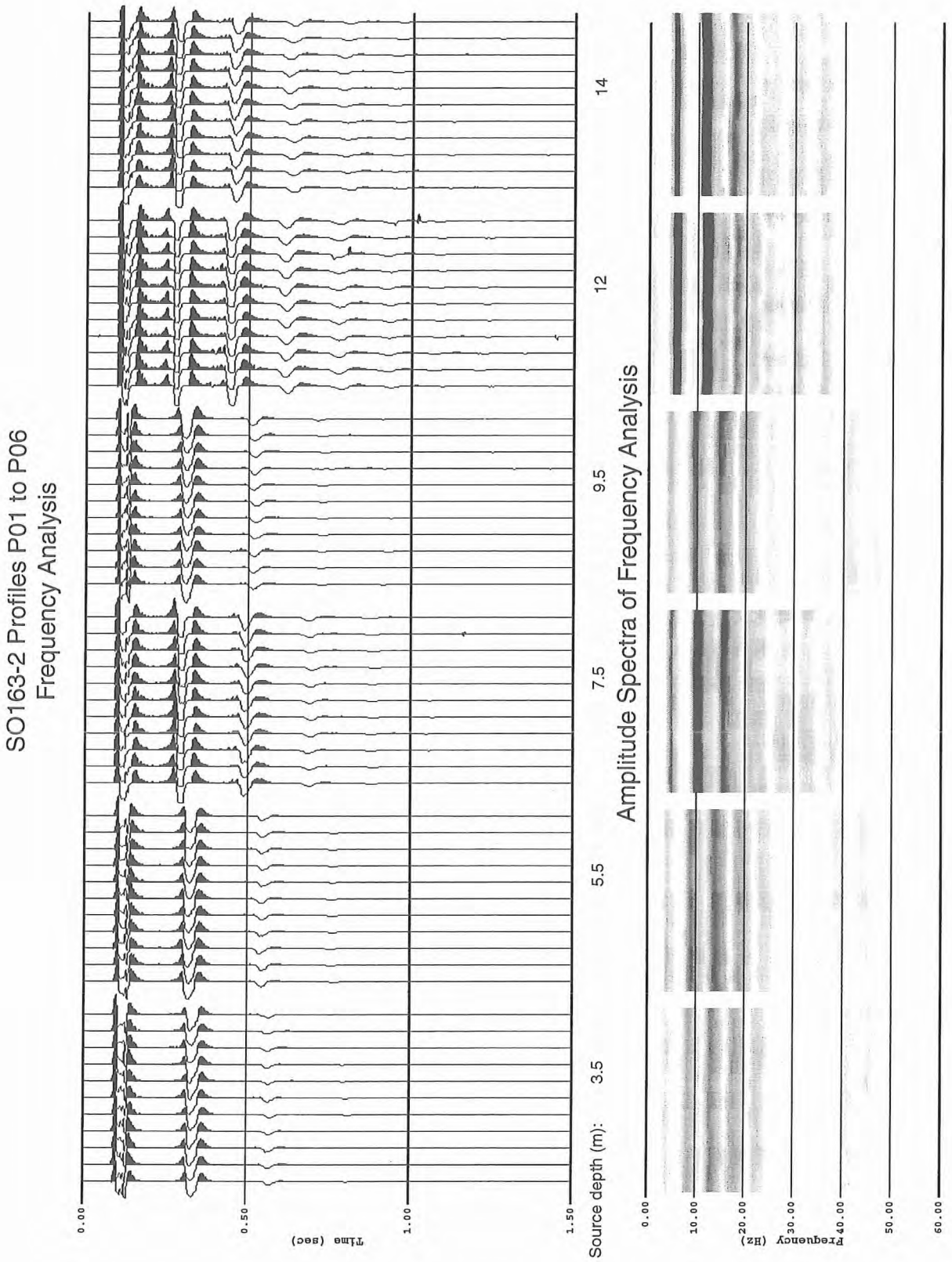


**Figure 6.6.1.9:** Frequency analysis of direct arrivals for different source depths (Bolt gun).

**Figure 6.6.1.10:** Frequency analysis of reflected waves for different source depths (Bolt gun).

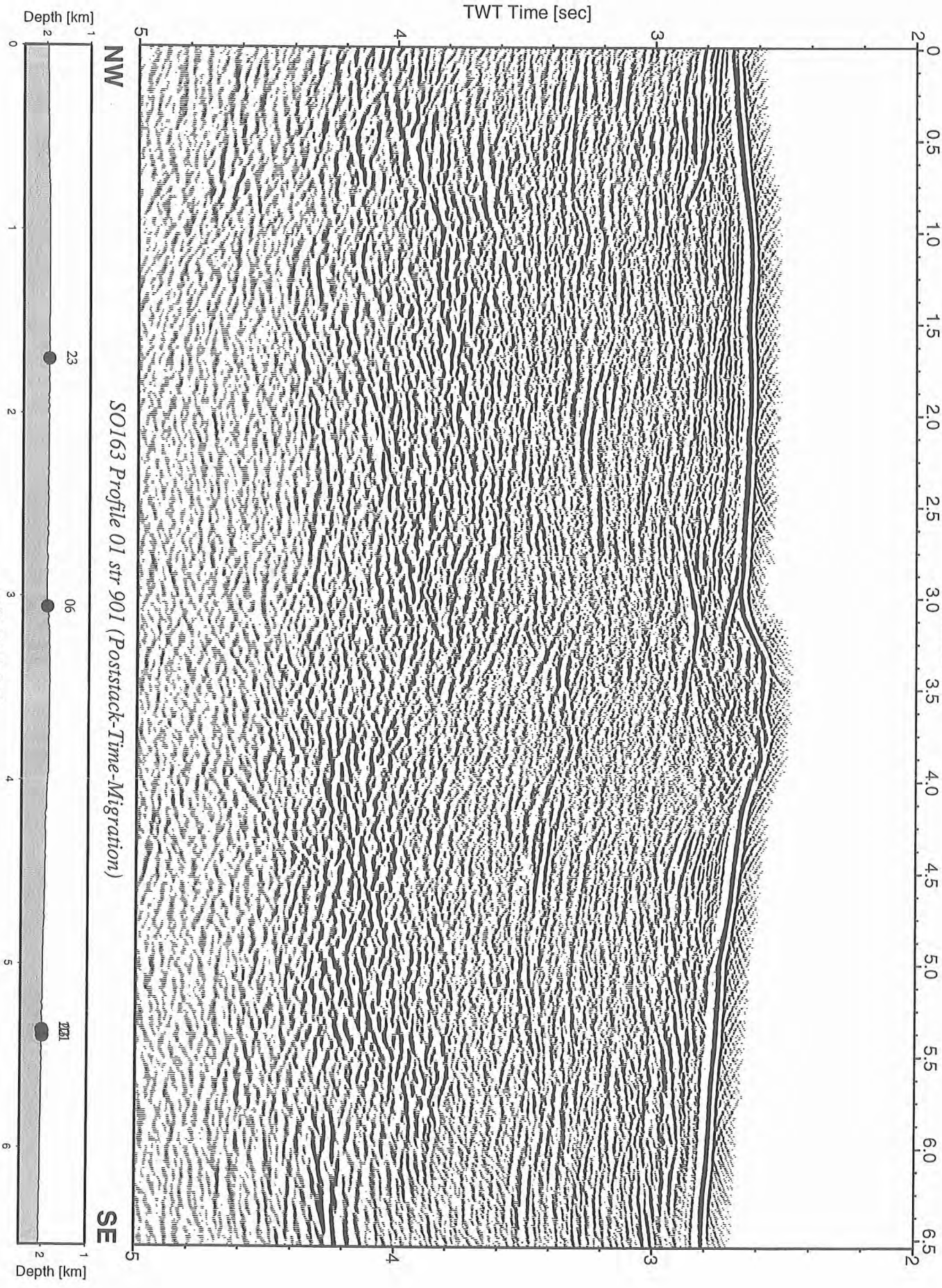


**Figure 6.6.1.11:** Record section from str 901 (Poststack-Time-Migration), Profile 01.

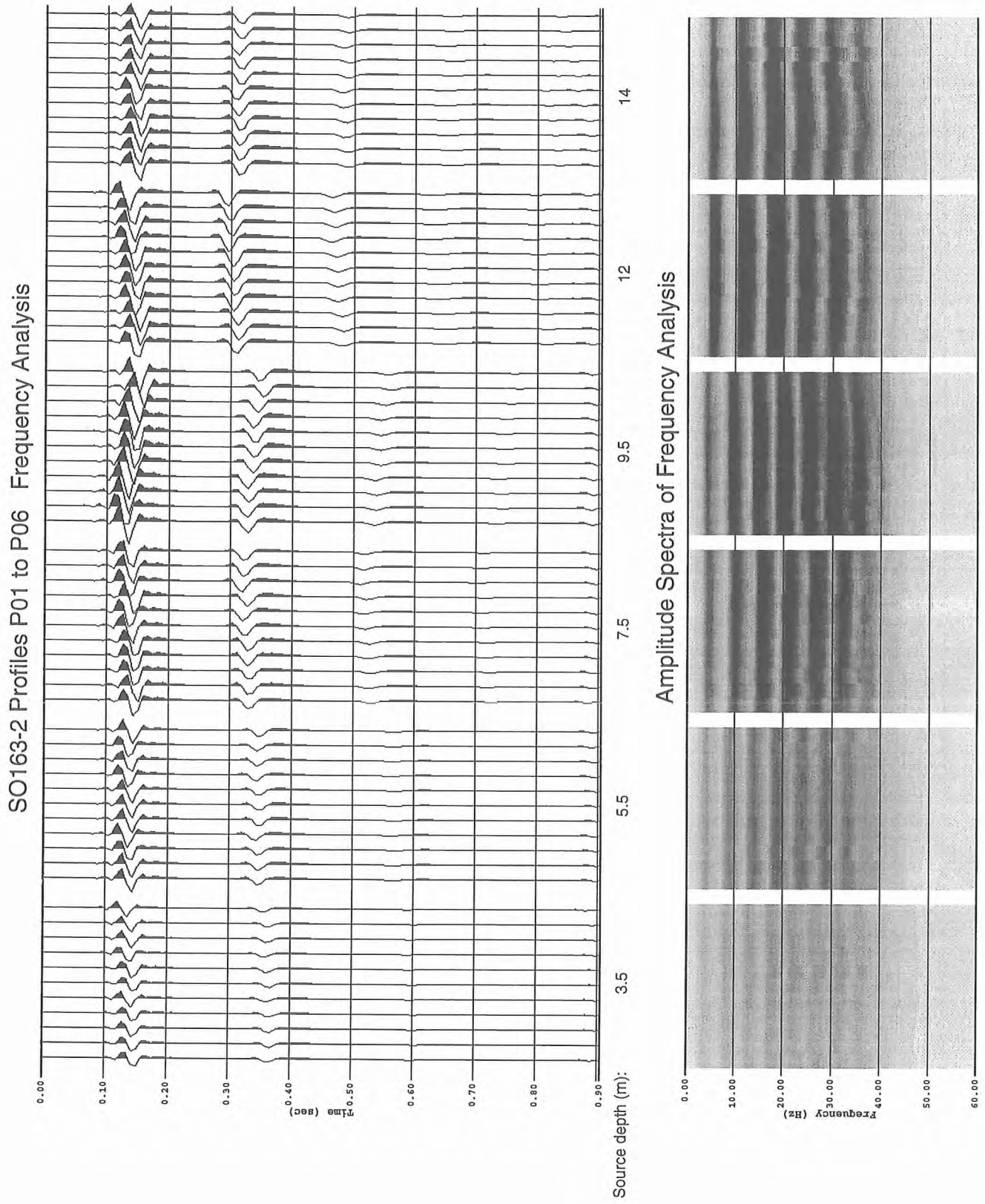


**Figure 6.6.1.12:** Frequency analysis of direct arrivals for different source depths (Bolt gun) recorded by station OBH 23 located 500 m above the seafloor.

**Figure 6.6.1.13:** Frequency analysis of refracted arrivals for different source depths (Bolt gun) recorded by station OBH 23 located 500 m above the seafloor.

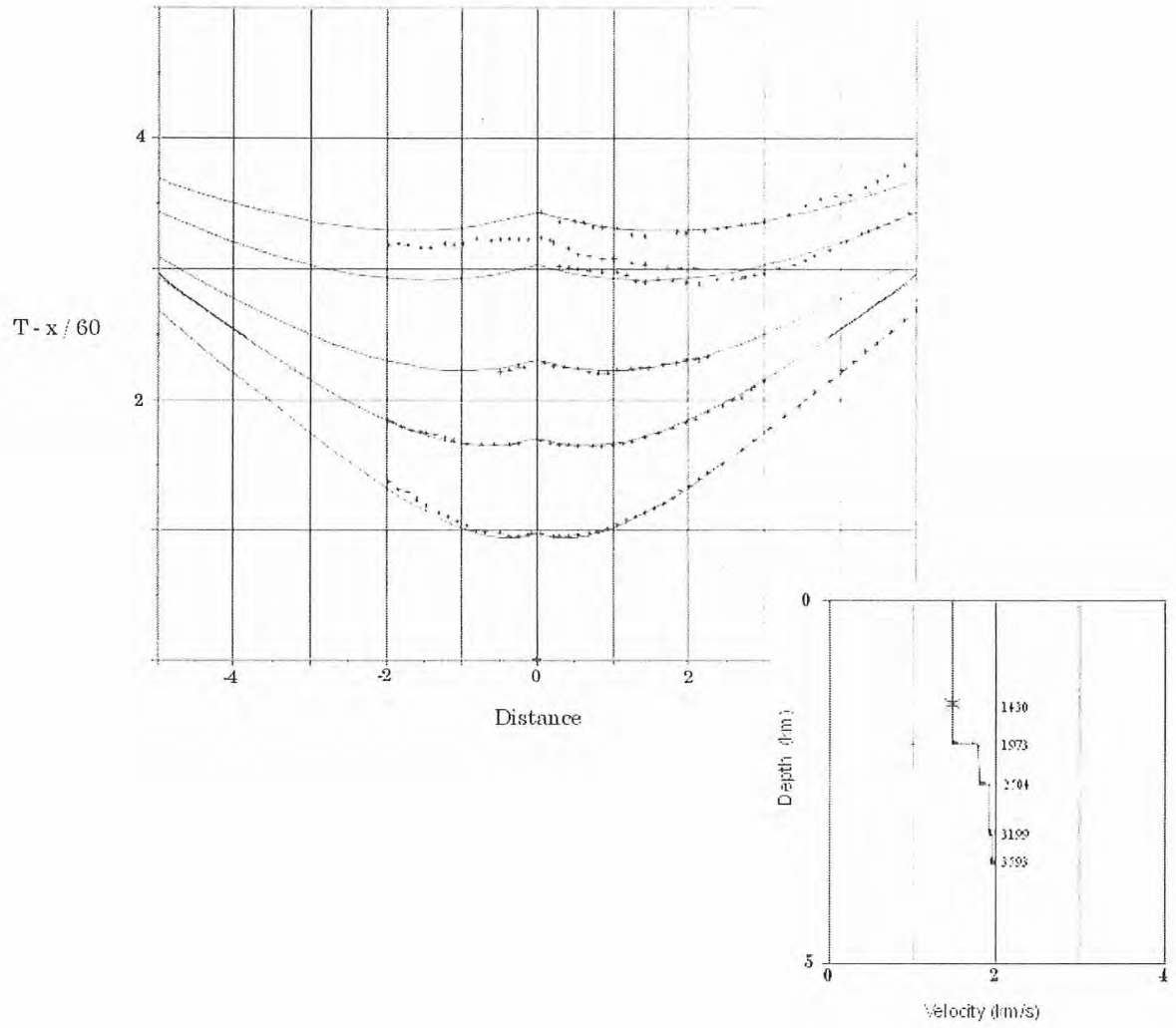


**Figure 6.6.1.14:** Pickings (crosses) from the record of the OBH23, Profile 2, and predicted arrivals according to the 1-D velocity model shown to the right.

The processed record of the OBH23 during the shooting of Profile 2 (Figure 6.6.1.3) was analyzed in order to obtain an 1-D velocity model of the upper sediment cover (~ 4 km). To achieve further studies in the far field, OBH23 was located 500 m above the sea floor. The pickings of the record are shown in Figure 6.6.1.14, together with the predicted arrivals modeled with the program R1D (Luetgert, 1992). The curvatures of the predicted arrivals nearly coincide with the observed phases. Four reflections were found, with P-velocities ranging from 1,5 to 2,0 km/s :

| Depth (m) | P velocity (km/s) |
|---|---|
| 0 – 1 430 (water) | 1,480 |
| 1 430 – 1 973 | 1,468 – 1,766 |
| 1 973 – 2 504 | 1,791 – 1,905 |
| 2 504 – 3 199 | 1,922 – 1,959 |
| 3 199 – 3 593 | 1,953 – 2,027 |

## The Local Earthquake Network (EQNET)

(I. Arroyo, J. Gossler, P. O. Thierer)

### Description of the network

On March, 16, 2002, a total of 10 Ocean Bottom Hydrophones were deployed in the Pacific Ocean off Costa Rica in order to record local earthquakes and microseismicity data of the OFOS 10 mudvolcano (9° 39.450 N and 85° 52.900 W). Furthermore, active GI-Gun shooting along the array, following the base lines of the array should provide a dense quasi 3-D dataset of the volcano. The duration of the passive part of the experiment is about 6 weeks. Nine stations were installed in three triangles, each triangle is rotated of 60 degrees against their neighboured one and one auxiliary station is placed in the center of the array (see Figure 6.6.1.15).

The main objective of this passive seismological experiment is to detect and register microseismicity events which are effected by the activity of the OFOS 10 mudvolcano. Furthermore, local and regional earthquakes which affects from the subducting Cocos Plate underneath the Caribbean Plate are supposed to be registrated. The experiment might moreover clear up possible relations between both kinds of seismological events, the large scale one in the context to plate dynamics and the local ones, produced by the active mudvolcano.
Active GI-Gun shooting along the the array should provide a dense quasi 3-D seismic dataset which allows to develope a precise velocity-depth model. Furthermore, when using the GI-Gun signals, a distinct relocation of the instruments could be done.

Two different types of hydrophones were installed; five short-period OAS hydrophones and five Differential Pressure Gauge hydrophones (DPG). Table 6.6.1.1 lists the station number, the hydrophone type used and the exact position of the ship when the station was deployed. These positions are not the final positions of the instruments at the seafloor, because while sinking to the seafloor, the instruments might drift with the current. The determination of the final position would be done by a full joint inversion of earthquake and station location and by using a minimum offset function of the GI-Gun shot points.

| Station Number | Sensor | Latitude | Longitude |
|---|---|---|---|
| **OBH 01** | OAS | 9° 39.456 N | 85° 51.494 W |
| **OBH 02** | OAS | 9° 40.605 N | 85° 53.698 W |
| **OBH 03** | OAS | 9° 38.135 N | 85° 53.489 W |
| **OBH 04** | DPG | 9° 38.849 N | 85° 52.508 W |
| **OBH 05** | DPG | 9° 39.911 N | 85° 52.805 W |
| **OBH 06** | DPG | 9° 39.394 N | 85° 53.584 W |
| **OBH 07** | OAS | 9° 39.930 N | 85° 53.109 W |
| **OBH 08** | DPG | 9° 39.450 N | 85° 52.528 W |
| **OBH 09** | OAS | 9° 39.691 N | 85° 53.108 W |
| **OBH 10** | DPG | 9° 39.461 N | 85° 52.905 W |

**Table 6.6.1.1:** Station number, type of sensor and ship position of deployment of the local earthquake network.

The ocean bottom array has been recovered on April 23 and 25, 2002 , at the beginning of RV SONNE cruise 163-2, the second Leg of the "SUBDUCTION" experiment.

### Data Quality and Noise

As mentioned above, all stations of the network were recovered successfully. Most of the stations operated as intended and recorded a large number of local earthquakes as well as the airgun source

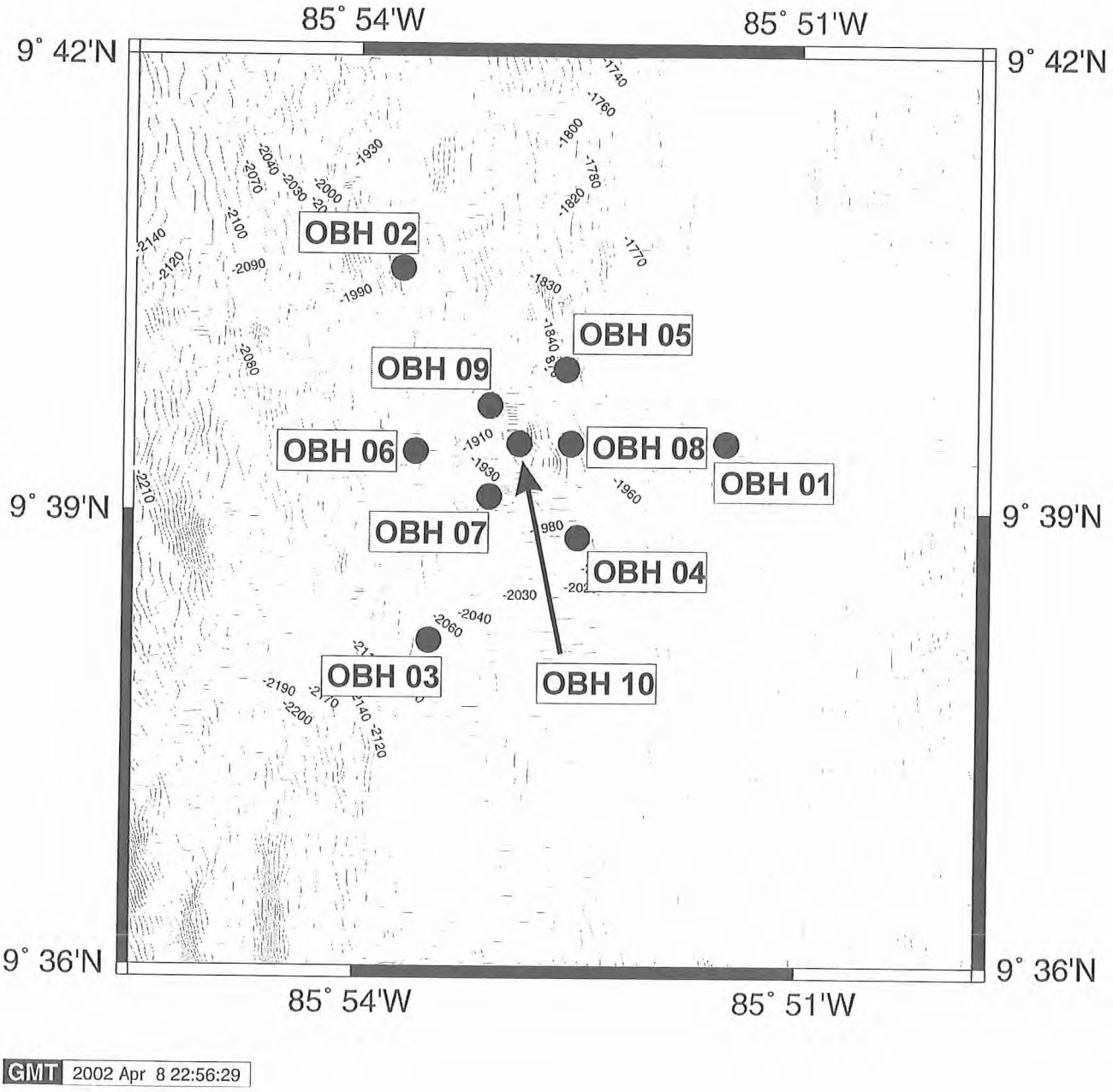


**Figure 6.6.1.15:** Location map of the 10 OBH, covering the OFOS 10 mud volcano

from MCS profiles 01 to 06 shot during leg 2 of SO163 (Figure 6.6.1.1). However, some problems occur with the instruments.

The DPG pressure sensor of station obh05 shows up with an almost complete loss of useful data, instead it produced only spikes and noise. This kind of sensor seems to be very delicate, because it is known for problems. The hydrophones of station obh01 and obh09 sometimes ran out of range. Because this problem occurs more often during the cruise with different instruments, it should be subject of a more detailed error analysis.

Apart from these faults the data from the EQNET network are very noisy, overall, which must be connected to environmental influences in this area. The network status is shown in table 6.6.1.2.

| Day of month | March | | | | | | | | | | | | | | | April | | | | | | | | | | | | | | | | | | | | | | | | | | Remarks |
|---|---|---|---|---|---|---|---|---|---|---|---|---|---|---|---|---|---|---|---|---|---|---|---|---|---|---|---|---|---|---|---|---|---|---|---|---|---|---|---|---|---|---|
| | 16 | 17 | 18 | 19 | 20 | 21 | 22 | 23 | 24 | 25 | 26 | 27 | 28 | 29 | 30 | 31 | 1 | 2 | 3 | 4 | 5 | 6 | 7 | 8 | 9 | 10 | 11 | 12 | 13 | 14 | 15 | 16 | 17 | 18 | 19 | 20 | 21 | 22 | 23 | 24 | 25 | |
| Julian day | 75 | | | | | 80 | | | | | 85 | | | | | 90 | | | | | 95 | | | | | 100 | | | | | 105 | | | | | 110 | | | | | 115 | |
| OBH01 | s | x | x | x | x | x | x | x | x | x | x | x | x | x | - | - | - | - | - | - | - | - | - | - | - | - | x | x | x | x | x | x | x | x | x | x | x | a | x | s | Hydrophone, noisy, 12 days out of range |
| OBH02 | s | x | x | x | x | x | x | x | x | x | x | x | x | x | x | x | x | x | x | x | x | x | x | x | x | x | x | x | x | x | x | x | x | x | x | x | x | a | x | s | Hydrophone, noisy |
| OBH03 | s | x | x | x | x | x | x | x | x | x | x | x | x | x | x | x | x | x | x | x | x | x | x | x | x | x | x | x | x | x | x | x | x | x | x | x | x | a | s | | Hydrophone |
| OBH04 | s | x | x | x | x | x | x | x | x | x | x | x | x | x | x | x | x | x | x | x | x | x | x | x | x | x | x | x | x | x | x | x | x | x | x | x | x | a | x | s | DPG pressure sensor, extremely noisy |
| OBH05 | s | - | - | - | - | - | - | - | - | - | - | - | - | - | - | - | - | - | - | - | - | - | - | - | - | - | - | - | - | - | - | - | - | - | - | - | - | - | - | s | DPG pressure sensor, only spikes and noise |
| OBH06 | s | x | x | x | x | x | x | x | x | x | x | x | x | x | x | x | x | x | x | x | x | x | x | x | x | x | x | x | x | x | x | x | x | x | x | x | x | s | | | DPG pressure sensor, noisy |
| OBH07 | s | x | x | x | x | x | x | x | x | x | x | x | x | x | x | x | x | x | x | x | x | x | x | x | x | x | x | x | x | x | x | x | x | x | x | x | x | a | x | s | Hydrophone, noisy and a lot of spikes |
| OBH08 | s | x | x | x | x | x | x | x | x | x | x | x | x | x | x | x | x | x | x | x | x | x | x | x | x | x | x | x | x | x | x | x | x | x | x | x | x | a | x | s | DPG pressure sensor, noisy and many spikes |
| OBH09 | s | x | x | x | x | x | x | x | x | - | x | - | - | - | - | - | - | - | x | x | x | x | x | x | x | x | x | x | x | x | x | x | x | x | x | x | - | - | - | s | Hydrophone, sometimes signal out of range |
| OBH10 | | s | x | x | x | x | x | x | x | x | x | x | x | x | x | x | x | x | x | x | x | x | x | x | x | x | x | x | x | x | x | x | x | x | x | x | x | x | x | s | DPG pressure sensor, many spikes |

| | |
|---|---|
| x | operating |
| s | deployment/recovery |
| a | active seismic airgun shots (data excluded) |
| - | inaccurate recording, so that data cannot be used |
| blank | not recording |

**Tabelle 6.6.1.2:** Station status of EQNET seismic network

**Seismic activity observed by EQNET**

During the operating period of EQNET of about 40 days we could identify 184 events (Table 6.6.1.2). For 33 events a preliminary determination of the hypocenter was made now (Figure 6.6.1.16).

We found a very strange looking kind of event, that we called "Hongo", which is Spanish and means mushroom, because of their shape (Figure 6.6.1.17-19). Those events, which have an almost dual-frequent spectrum (Figure 6.6.17), consist of a high freqent first part which lasts about 1 second with a frequency of about 36 Hz. The second part has smaller amplitudes, lasts about 2-3 seconds at a frequency of about 20 Hz.

We could identify 25 of those Hongo events and fairly locate most of them in the vincity of the OFOS 10 mud volcano (Figure 6.6.1.16). Another two Hongos are located on the edge of the depletion where a big subducted seamount entered the continental plate. The others are located on the continental margin.

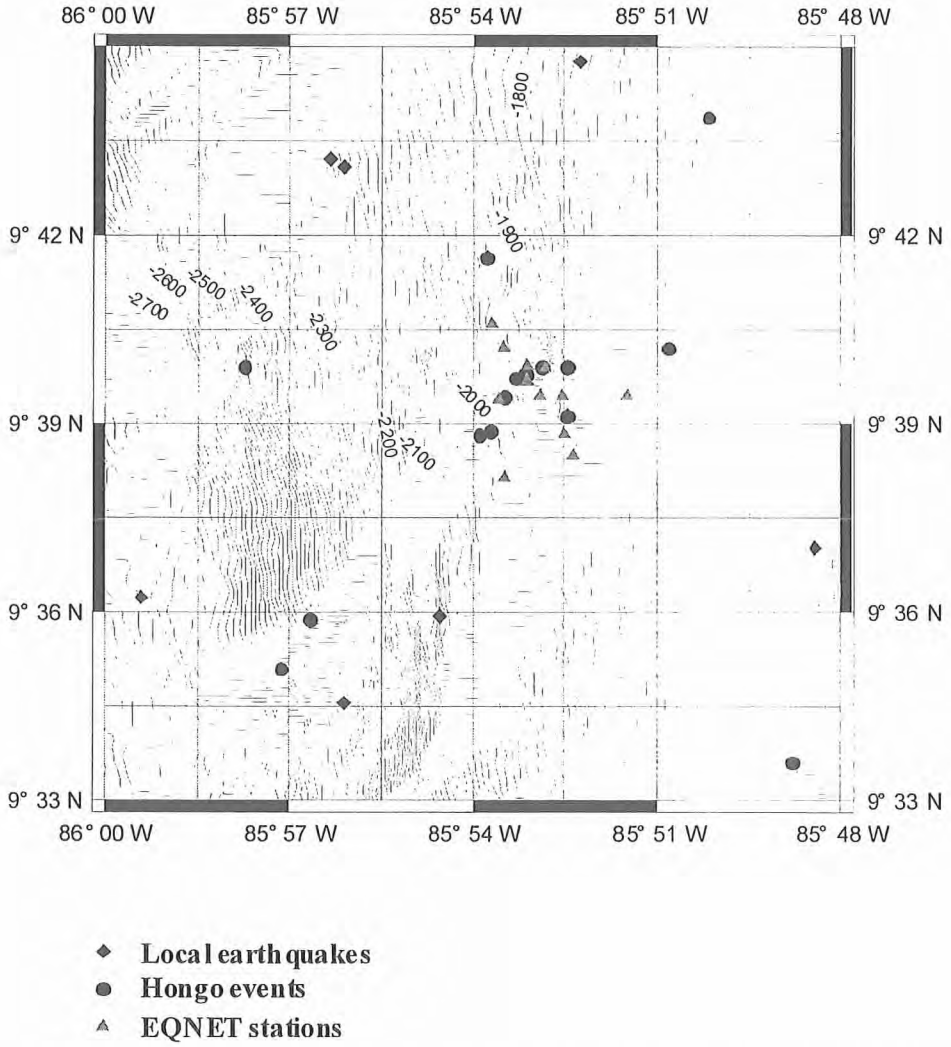


**Figure 6.6.1.16:** Epicenter locations of events located with the EQNET seafloor seismic network. The so-called Hongo events are located mainly very close to the OFOS 10 mud volcano in the center of the map. Some events occured in the vincity of the scarp of a big seamount. The EQNET array is marked due to better orientation.

| Date | | | Time | | | Type | Latitude | Longitude | Depth (km) | Magnitude |
|---|---|---|---|---|---|---|---|---|---|---|
| 2002 | 3 | 16 | 21 | 51 | 16.0 | D | | | | |
| 2002 | 3 | 17 | 2 | 52 | 37.0 | L | 9.744 | -85.759 | 43.0 | 3.2C |
| 2002 | 3 | 17 | 4 | 29 | 0.0 | L | | | | |
| 2002 | 3 | 17 | 8 | 44 | 9.8 | R | 11.177 | -87.412 | 20.0 | 4.7C |
| 2002 | 3 | 17 | 8 | 49 | 33.9 | L | 9.718 | -85.935 | 14.3 | 4.6C |
| 2002 | 3 | 17 | 9 | 1 | 4.5 | L | | | | |
| 2002 | 3 | 17 | 12 | 40 | 3.5 | L | 9.776 | -85.860 | 18.2 | |
| 2002 | 3 | 18 | 6 | 43 | 45.0 | L | | | | |
| 2002 | 3 | 18 | 9 | 42 | 11.0 | L | | | | |
| 2002 | 3 | 18 | 15 | 33 | 5.0 | L | | | | |
| 2002 | 3 | 19 | 1 | 55 | 6.0 | L | | | | |
| 2002 | 3 | 19 | 22 | 30 | 36.0 | L | | | | |
| 2002 | 3 | 20 | 2 | 30 | 39.5 | L | | | | |
| 2002 | 3 | 20 | 3 | 13 | 22.0 | L | | | | |
| 2002 | 3 | 20 | 5 | 28 | 11.0 | L | | | | |
| 2002 | 3 | 20 | 6 | 17 | 43.0 | L | | | | |
| 2002 | 3 | 20 | 6 | 58 | 45.0 | L | | | | |
| 2002 | 3 | 20 | 11 | 44 | 0.0 | L | | | | |
| 2002 | 3 | 20 | 20 | 25 | 48.0 | L | 9.599 | -85.909 | 13.9 | 2.8C |
| 2002 | 3 | 21 | 3 | 1 | 26.3 | L | | | | |
| 2002 | 3 | 21 | 12 | 18 | 5.0 | L | | | | |
| 2002 | 3 | 21 | 13 | 28 | 3.0 | L | | | | |
| 2002 | 3 | 21 | 16 | 17 | 9.7 | L | 9.576 | -85.935 | 13.9 | 2.7C |
| 2002 | 3 | 21 | 16 | 30 | 44.6 | L | 9.831 | -85.716 | 43.7 | 3.1C |
| 2002 | 3 | 21 | 17 | 29 | 42.6 | H | 9.585 | -85.952 | 2.0 | |
| 2002 | 3 | 21 | 17 | 42 | 51.1 | H | 9.560 | -85.813 | 2.0 | |
| 2002 | 3 | 21 | 17 | 57 | 13.8 | H | 9.598 | -85.944 | 1.5 | |
| 2002 | 3 | 21 | 18 | 13 | 4.0 | H | | | | |
| 2002 | 3 | 21 | 18 | 45 | 55.0 | L | | | | |
| 2002 | 3 | 21 | 18 | 53 | 1.0 | L | | | | |
| 2002 | 3 | 21 | 19 | 34 | 28.3 | H | 9.651 | -85.744 | 1.0 | |
| 2002 | 3 | 21 | 20 | 16 | 31.0 | H | | | | |
| 2002 | 3 | 22 | 3 | 27 | 22.2 | L | | | | 3.3C |
| 2002 | 3 | 22 | 3 | 48 | 26.0 | L | | | | |
| 2002 | 3 | 22 | 4 | 37 | 29.0 | L | | | | |
| 2002 | 3 | 22 | 10 | 29 | 20.7 | H | 9.752 | -86.044 | 1.0 | |
| 2002 | 3 | 22 | 19 | 19 | 59.0 | L | | | | |
| 2002 | 3 | 22 | 19 | 48 | 1.0 | H | | | | |
| 2002 | 3 | 22 | 20 | 20 | 46.2 | H | 9.731 | -85.836 | 0.7 | |
| 2002 | 3 | 22 | 20 | 28 | 38.4 | H | 9.665 | -85.874 | 0.5 | |
| 2002 | 3 | 22 | 20 | 35 | 2.7 | H | 9.663 | -85.886 | 1.7 | |
| 2002 | 3 | 22 | 20 | 43 | 26.9 | H | 9.662 | -85.888 | 0.7 | |
| 2002 | 3 | 22 | 20 | 56 | 52.0 | L | | | | |
| 2002 | 3 | 22 | 23 | 43 | 4.0 | L | | | | |
| 2002 | 3 | 23 | 13 | 24 | 12.0 | L | | | | |
| 2002 | 3 | 23 | 13 | 42 | 12.4 | L | 9.617 | -85.807 | 5.0 | |
| 2002 | 3 | 23 | 17 | 31 | 37.0 | H | | | | |
| 2002 | 3 | 23 | 17 | 40 | 46.0 | H | | | | |
| 2002 | 3 | 24 | 1 | 27 | 36.0 | L | | | | |
| 2002 | 3 | 24 | 3 | 29 | 16.0 | L | | | | |
| 2002 | 3 | 24 | 6 | 32 | 37.5 | L | 10.112 | -85.883 | 86.8 | 3.7C |
| 2002 | 3 | 24 | 12 | 15 | 29.0 | L | | | | |
| 2002 | 3 | 24 | 18 | 43 | 1.0 | L | | | | |
| 2002 | 3 | 25 | 0 | 30 | 57.0 | L | | | | |
| 2002 | 3 | 25 | 1 | 19 | 53.0 | L | | | | |
| 2002 | 3 | 25 | 4 | 36 | 43.4 | L | | | | |
| 2002 | 3 | 25 | 6 | 19 | 5.0 | L | | | | |
| 2002 | 3 | 25 | 8 | 11 | 32.7 | L | 9.885 | -86.117 | 69.9 | 4.4C |
| 2002 | 3 | 25 | 10 | 25 | 40.0 | L | | | | |
| 2002 | 3 | 25 | 11 | 16 | 15.9 | L | 9.746 | -85.871 | 18.7 | |
| 2002 | 3 | 25 | 12 | 0 | 20.0 | L | | | | |
| 2002 | 3 | 25 | 12 | 12 | 27.0 | L | | | | |

**Table 6.6.1.2:** Seismic events registered by EQNET station network (L = local, H = hongo event)

| Date | | | Time | | | Type | Latitude | Longitude | Depth (km) | Magnitude |
|---|---|---|---|---|---|---|---|---|---|---|
| 2002 | 3 | 26 | 2 | 59 | 10.0 | L | | | | |
| 2002 | 3 | 26 | 3 | 14 | 41.2 | L | | | | |
| 2002 | 3 | 26 | 4 | 47 | 31.0 | L | | | | |
| 2002 | 3 | 26 | 17 | 49 | 6.0 | L | | | | |
| 2002 | 3 | 26 | 18 | 36 | 10.0 | L | | | | |
| 2002 | 3 | 26 | 21 | 50 | 29.0 | L | | | | |
| 2002 | 3 | 27 | 2 | 11 | 15.3 | L | 9.852 | -85.941 | 43.8 | |
| 2002 | 3 | 27 | 5 | 54 | 30.0 | L | 9.720 | -85.939 | 21.2 | 1.8C |
| 2002 | 3 | 27 | 6 | 24 | 3.0 | L | | | | |
| 2002 | 3 | 28 | 5 | 0 | 11.0 | L | | | | |
| 2002 | 3 | 28 | 16 | 13 | 0.0 | L | | | | |
| 2002 | 3 | 28 | 16 | 38 | 45.0 | L | | | | |
| 2002 | 3 | 28 | 21 | 30 | 44.0 | L | | | | |
| 2002 | 3 | 31 | 7 | 9 | 18.0 | L | | | | |
| 2002 | 3 | 31 | 18 | 24 | 53.3 | L | 9.491 | -85.749 | 1.7 | |
| 2002 | 3 | 31 | 23 | 8 | 54.0 | L | | | | |
| 2002 | 3 | 31 | 23 | 16 | 50.0 | L | | | | |
| 2002 | 4 | 1 | 1 | 10 | 9.0 | L | | | | |
| 2002 | 4 | 1 | 20 | 4 | 15.0 | L | | | | |
| 2002 | 4 | 2 | 1 | 33 | 12.0 | L | | | | |
| 2002 | 4 | 2 | 8 | 24 | 36.0 | L | | | | |
| 2002 | 4 | 3 | 2 | 11 | 47.0 | L | | | | |
| 2002 | 4 | 3 | 8 | 37 | 36.0 | L | | | | |
| 2002 | 4 | 3 | 8 | 45 | 21.0 | L | | | | |
| 2002 | 4 | 3 | 10 | 35 | 26.0 | L | | | | |
| 2002 | 4 | 3 | 16 | 26 | 9.0 | L | | | | |
| 2002 | 4 | 3 | 21 | 53 | 25.0 | L | | | | |
| 2002 | 4 | 4 | 4 | 20 | 28.1 | L | 9.731 | -85.734 | 4.2 | 3.4C |
| 2002 | 4 | 4 | 6 | 5 | 17.0 | L | | | | |
| 2002 | 4 | 4 | 19 | 59 | 20.0 | L | | | | |
| 2002 | 4 | 5 | 4 | 25 | 46.0 | H | | | | |
| 2002 | 4 | 5 | 5 | 49 | 46.7 | H | 9.694 | -85.896 | 9.5 | |
| 2002 | 4 | 5 | 5 | 57 | 59.3 | H | 9.665 | -85.962 | 0.9 | |
| 2002 | 4 | 5 | 6 | 7 | 41.0 | H | 9.652 | -85.874 | 2.5 | |
| 2002 | 4 | 5 | 6 | 13 | 45.2 | H | 9.648 | -85.895 | 2.0 | |
| 2002 | 4 | 5 | 6 | 19 | 55.3 | H | 9.647 | -85.898 | 1.5 | |
| 2002 | 4 | 5 | 6 | 25 | 58.8 | H | 9.657 | -85.891 | 1.9 | |
| 2002 | 4 | 5 | 6 | 37 | 42.2 | H | 9.670 | -85.847 | 1.4 | |
| 2002 | 4 | 5 | 6 | 46 | 24.6 | H | 9.663 | -85.885 | 1.7 | |
| 2002 | 4 | 5 | 6 | 52 | 21.6 | H | 9.665 | -85.881 | 1.0 | |
| 2002 | 4 | 5 | 14 | 42 | 58.0 | L | | | | |
| 2002 | 4 | 5 | 15 | 31 | 2.0 | L | | | | |
| 2002 | 4 | 5 | 21 | 0 | 53.0 | L | | | | |
| 2002 | 4 | 6 | 3 | 26 | 42.0 | L | | | | |
| 2002 | 4 | 6 | 6 | 24 | 49.0 | L | | | | |
| 2002 | 4 | 6 | 9 | 23 | 38.0 | L | | | | |
| 2002 | 4 | 6 | 9 | 31 | 35.0 | L | | | | |
| 2002 | 4 | 6 | 16 | 38 | 40.7 | H | 9.604 | -85.990 | 2.0 | |
| 2002 | 4 | 6 | 20 | 41 | 27.0 | L | | | | |
| 2002 | 4 | 7 | 4 | 18 | 27.0 | L | | | | |
| 2002 | 4 | 7 | 11 | 33 | 46.0 | L | | | | |
| 2002 | 4 | 7 | 14 | 56 | 46.0 | L | | | | |
| 2002 | 4 | 7 | 18 | 44 | 42.0 | L | | | | |
| 2002 | 4 | 7 | 19 | 2 | 36.0 | L | | | | |
| 2002 | 4 | 7 | 20 | 47 | 21.0 | L | | | | |
| 2002 | 4 | 8 | 5 | 36 | 26.0 | L | | | | |
| 2002 | 4 | 8 | 11 | 51 | 7.0 | L | | | | |
| 2002 | 4 | 8 | 20 | 24 | 54.0 | L | | | | |
| 2002 | 4 | 9 | 4 | 58 | 13.0 | L | | | | 4.9C |
| 2002 | 4 | 9 | 7 | 38 | 9.0 | L | | | | |
| 2002 | 4 | 9 | 19 | 20 | 41.0 | L | | | | |
| 2002 | 4 | 9 | 22 | 52 | 5.0 | L | | | | |

**Table 6.6.1.2:** (continued)

| Date | | | Time | | | Type | Latitude | Longitude | Depth (km) | Magnitude |
|---|---|---|---|---|---|---|---|---|---|---|
| 2002 | 4 | 9 | 23 | 30 | 49.0 | L | | | | |
| 2002 | 4 | 10 | 0 | 32 | 52.0 | L | | | | |
| 2002 | 4 | 10 | 0 | 41 | 4.0 | L | | | | |
| 2002 | 4 | 10 | 1 | 11 | 40.0 | L | | | | |
| 2002 | 4 | 10 | 20 | 16 | 53.0 | L | | | | |
| 2002 | 4 | 11 | 0 | 0 | 43.0 | L | | | | |
| 2002 | 4 | 11 | 0 | 27 | 34.0 | L | | | | |
| 2002 | 4 | 11 | 9 | 50 | 30.0 | L | | | | |
| 2002 | 4 | 11 | 10 | 13 | 37.0 | L | | | | |
| 2002 | 4 | 11 | 13 | 23 | 42.0 | L | | | | |
| 2002 | 4 | 11 | 20 | 43 | 35.0 | L | | | | |
| 2002 | 4 | 11 | 21 | 39 | 15.0 | L | | | | |
| 2002 | 4 | 12 | 0 | 8 | 57.0 | L | | | | |
| 2002 | 4 | 12 | 15 | 6 | 20.0 | L | | | | |
| 2002 | 4 | 12 | 18 | 15 | 4.0 | L | | | | |
| 2002 | 4 | 13 | 19 | 28 | 34.0 | L | | | | |
| 2002 | 4 | 14 | 5 | 37 | 26.0 | L | | | | |
| 2002 | 4 | 15 | 9 | 17 | 44.0 | L | | | | |
| 2002 | 4 | 15 | 9 | 24 | 31.0 | L | | | | |
| 2002 | 4 | 15 | 10 | 7 | 54.0 | L | | | | |
| 2002 | 4 | 15 | 10 | 11 | 33.0 | L | | | | |
| 2002 | 4 | 15 | 10 | 28 | 31.0 | L | | | | |
| 2002 | 4 | 15 | 10 | 32 | 7.0 | L | | | | |
| 2002 | 4 | 15 | 10 | 53 | 36.0 | L | | | | |
| 2002 | 4 | 15 | 19 | 4 | 48.0 | L | | | | |
| 2002 | 4 | 16 | 16 | 20 | 21.0 | L | | | | |
| 2002 | 4 | 16 | 21 | 31 | 32.0 | L | | | | |
| 2002 | 4 | 17 | 4 | 53 | 23.0 | L | | | | |
| 2002 | 4 | 17 | 5 | 43 | 3.0 | L | | | | |
| 2002 | 4 | 17 | 12 | 35 | 40.0 | L | | | | |
| 2002 | 4 | 17 | 16 | 1 | 53.0 | L | | | | |
| 2002 | 4 | 17 | 18 | 51 | 47.0 | L | | | | |
| 2002 | 4 | 17 | 21 | 30 | 54.0 | L | | | | |
| 2002 | 4 | 17 | 21 | 34 | 22.0 | L | | | | |
| 2002 | 4 | 17 | 22 | 0 | 34.0 | L | | | | |
| 2002 | 4 | 18 | 5 | 3 | 45.0 | L | | | | |
| 2002 | 4 | 18 | 7 | 41 | 53.0 | L | | | | |
| 2002 | 4 | 18 | 8 | 46 | 21.0 | L | | | | |
| 2002 | 4 | 18 | 12 | 15 | 28.0 | L | | | | |
| 2002 | 4 | 18 | 12 | 18 | 43.0 | L | | | | |
| 2002 | 4 | 18 | 14 | 12 | 35.0 | L | | | | |
| 2002 | 4 | 18 | 16 | 13 | 7.0 | L | | | | |
| 2002 | 4 | 18 | 17 | 58 | 40.0 | L | | | | |
| 2002 | 4 | 18 | 18 | 15 | 21.0 | L | | | | |
| 2002 | 4 | 18 | 18 | 18 | 40.0 | L | | | | |
| 2002 | 4 | 19 | 1 | 42 | 59.0 | L | | | | |
| 2002 | 4 | 19 | 2 | 14 | 39.0 | L | | | | |
| 2002 | 4 | 19 | 2 | 45 | 56.0 | L | | | | |
| 2002 | 4 | 19 | 3 | 16 | 21.0 | L | | | | |
| 2002 | 4 | 19 | 11 | 26 | 39.0 | L | | | | |
| 2002 | 4 | 20 | 9 | 21 | 29.0 | L | | | | |
| 2002 | 4 | 21 | 12 | 19 | 25.0 | L | | | | |
| 2002 | 4 | 21 | 19 | 9 | 41.0 | L | | | | |
| 2002 | 4 | 21 | 19 | 57 | 11.0 | L | | | | |
| 2002 | 4 | 21 | 20 | 21 | 24.0 | L | | | | |
| 2002 | 4 | 22 | 3 | 13 | 42.0 | L | | | | |
| 2002 | 4 | 22 | 11 | 27 | 10.0 | L | | | | |
| 2002 | 4 | 22 | 14 | 2 | 34.0 | L | | | | |
| 2002 | 4 | 23 | 5 | 16 | 6.0 | L | | | | |
| 2002 | 4 | 23 | 7 | 48 | 31.0 | L | | | | |

**Table 6.6.1.2:** (continued)

We can imagine, that these Hongo events are caused by fluid currents which are pressed through a tube-like system, or something similar which lasts for about one second, e.g. the first part of the event, followed by a depression where those fluids may expand or flow back what can be observed as the second part of the event which lower frequency and amplitudes.

Further investigations should be done due to these strange events.

Further on we observed 53 emergent events which have not been located yet, due to the impossibility of identifying phase onsets (Figure 6.6.1.20). The origin of those events is not clear yet, although we know them from volcanoes. There, emergent events are tectonic events that run through a highly scattering media (U. Wegler, pers. com.).

Two tectonic events have been located in the vincity where the subducted seamount entered the continental lithosphere (Figure 6.6.1.16). Other earthquakes are spread over the continental margin.

Only one regional earthquake from Nicaragua has been registered during the operating period (Figure 6.6.1.21)

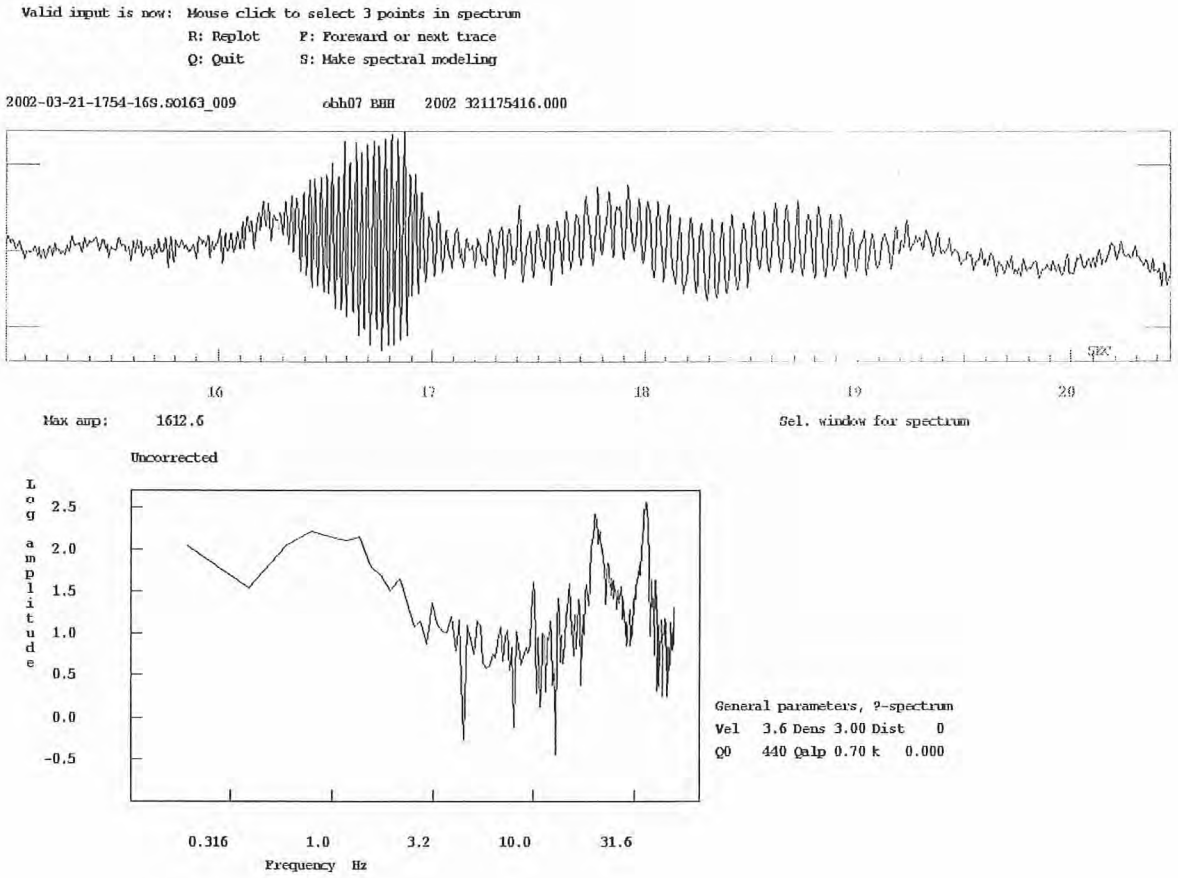


**Figure 6.6.1.17:** Hongo event from March 21, 2002 17:57 UTC registered at OBH07. The event is divided into two parts: the first one takes one second with a frequency of about 36 Hz (second peak in the spectrum below), while the second part has smaller amplitudes and stretches over 2.5 seconds. Ist frequency is at about 20 Hz (first prominent peak in the spectrum). The event may be connected to fluid processes of the OFOS 10 object.

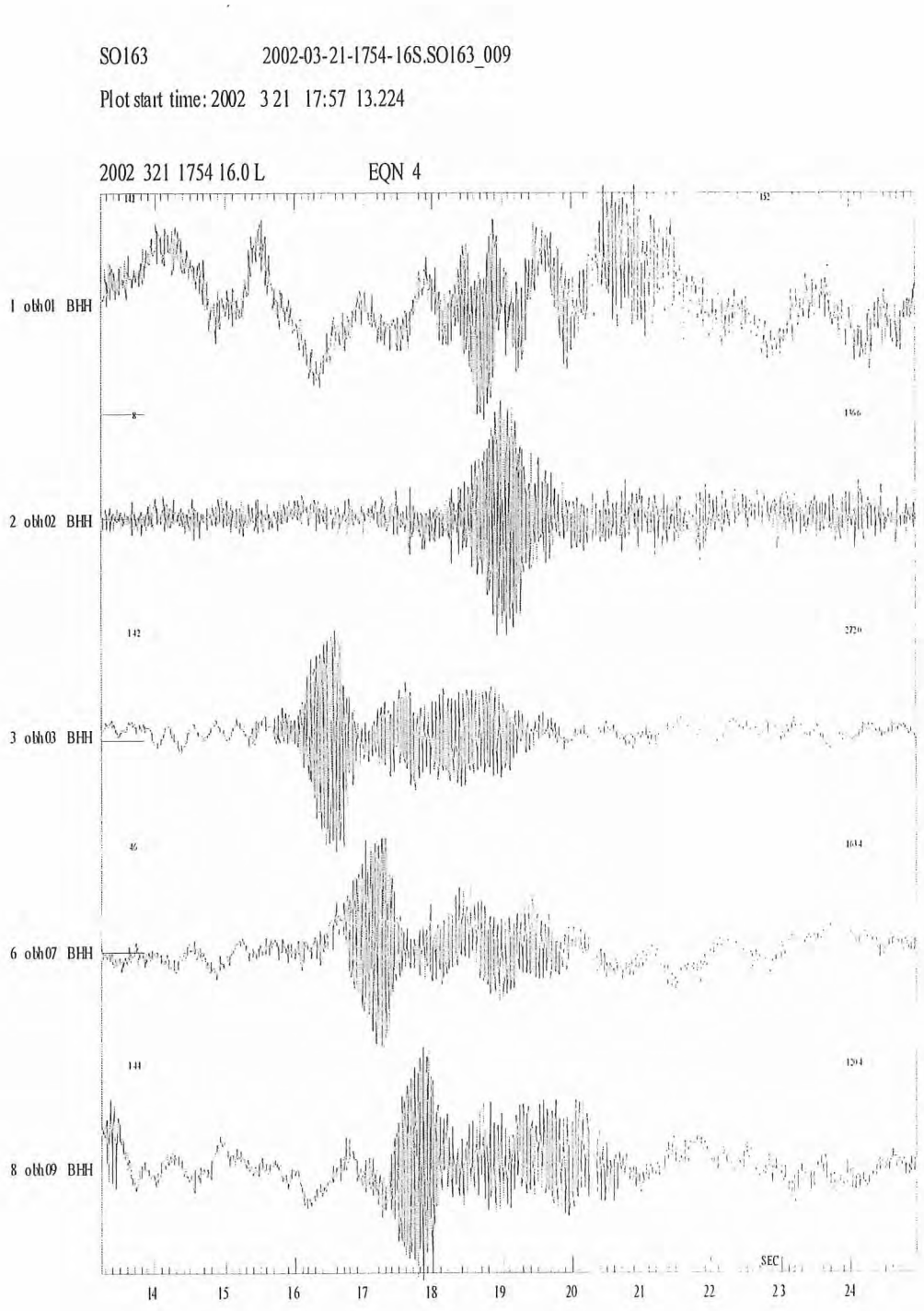


**Figure 6.6.1.18:** Seismograms of the Hongo event from previous figure, but for all stations of EQNET seafloor network.

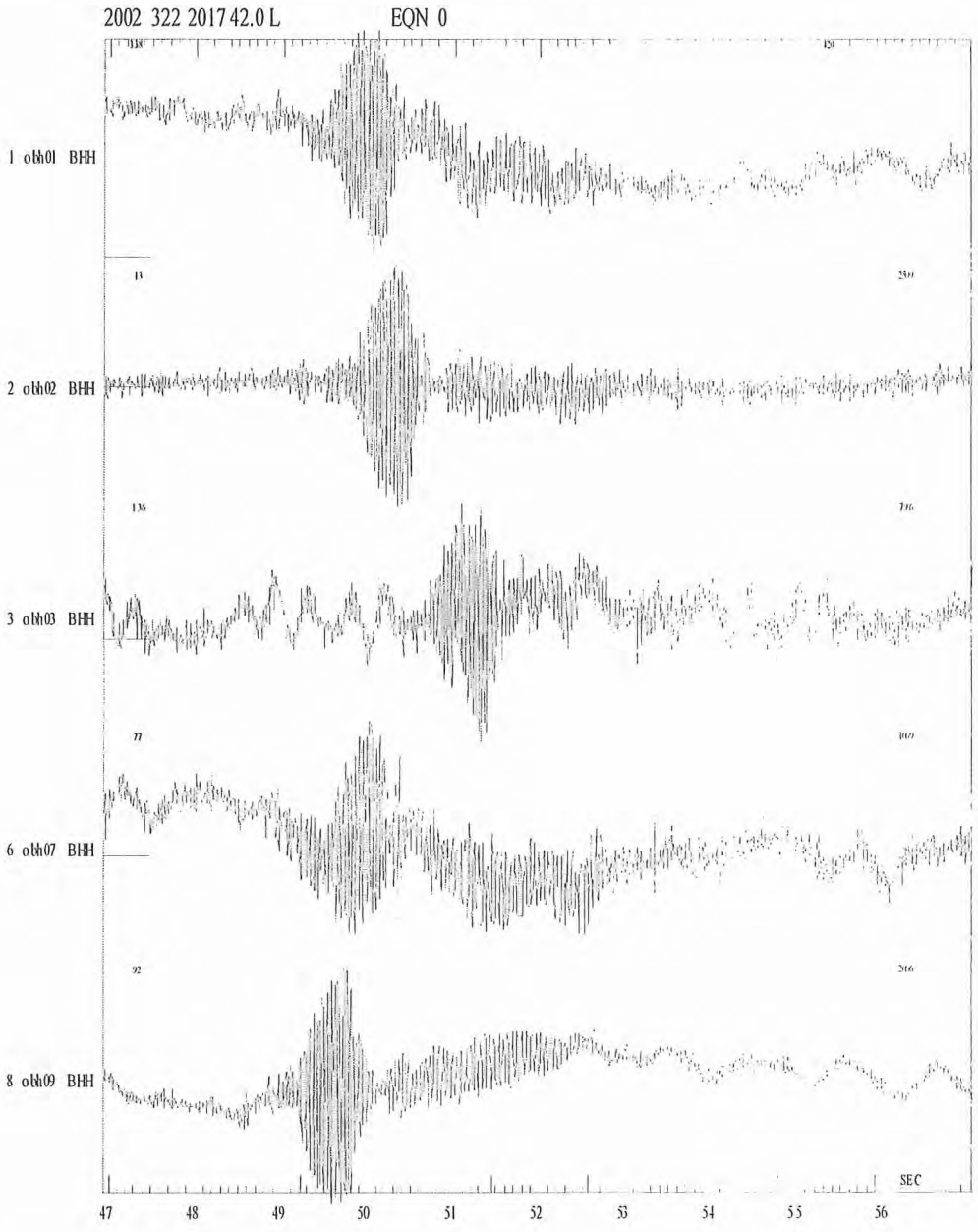


**Figure 6.6.1.19:** Another Hongo event from March 22, 2002 20:20 UTC observed at EQNET.

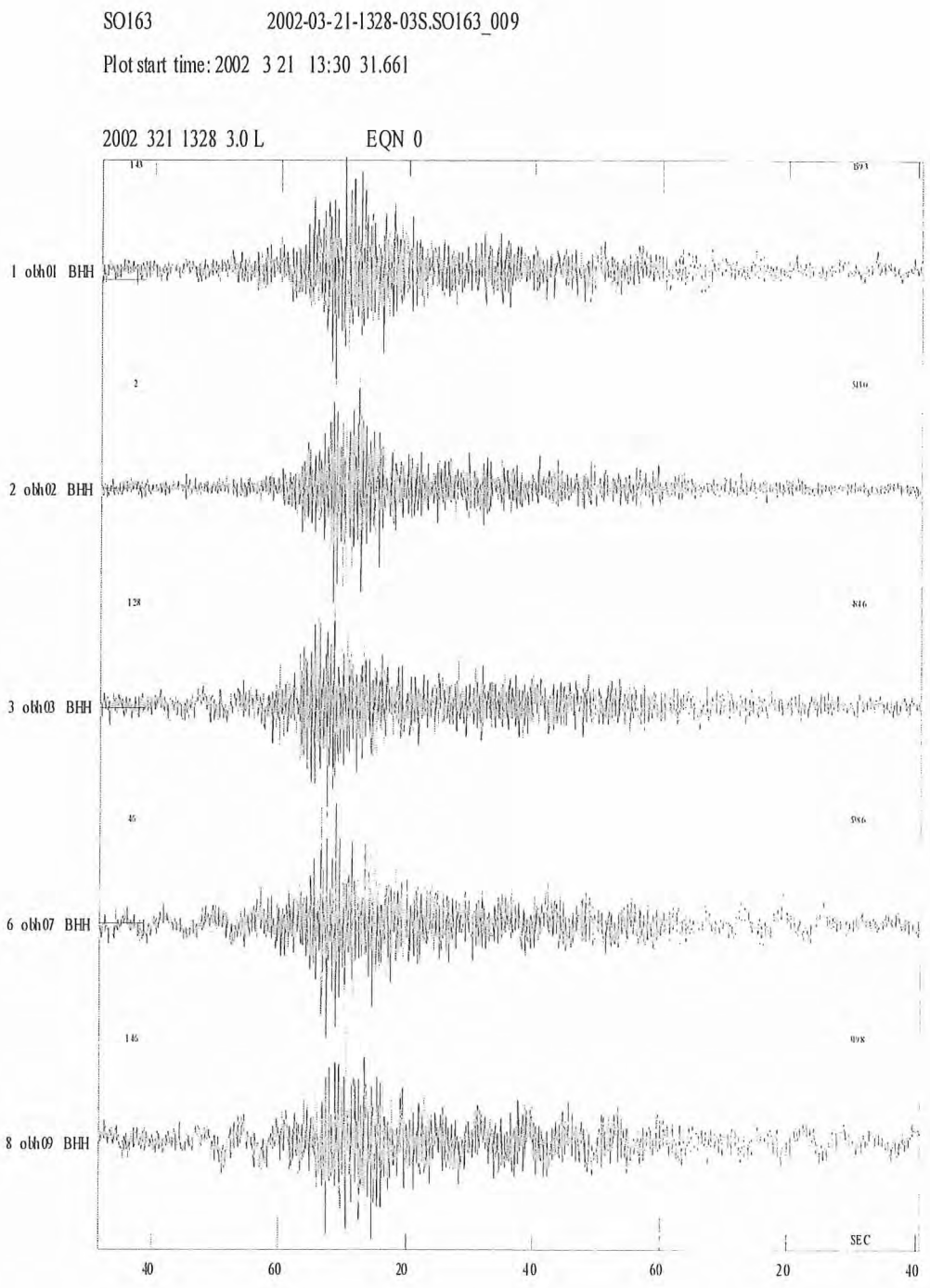


**Figure 6.6.1.20:** Emergent event observed on March 21, 2002 13:30 UTC at EQNET. The event cannot be easily located due to missing phase onsets. Those events are specific to volcanoes.

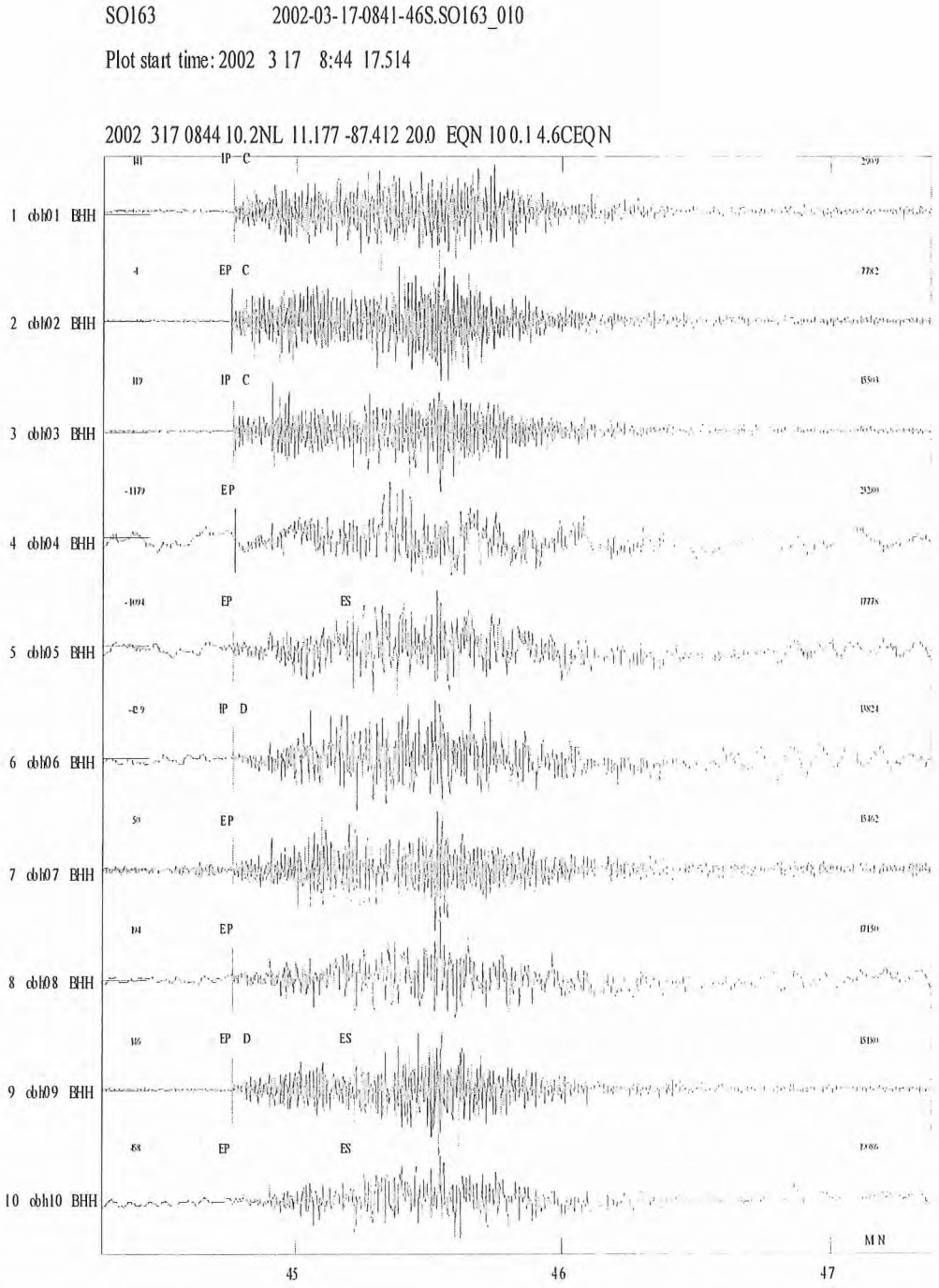


**Figure 6.6.1.21:** A magnitude 4.6 (Coda-magnitude) regional earthquake from Nicaragua on March 17, 2002 08:44 UTC. Localization was made with EQNET station array using mostly P onset. For distant events the earthquake waves are steep, so that their S waves oscillate parallel to the seafloor and do not produce pressure signals that can be registered from the OBH.

### 6.6.2 Gas-hydrates on Nicoya Slide

(D. De Nil, J. Goßler, A. Berhorst)

One objective of project B1 of the Sonderforschungsbereich 574 is to develop and to apply a new technique for determining shear wave velocity of marine gas-hydrates in order to discriminate different ways, in which gas-hydrate may be incorporated in sediment, as well as to estimate its amount. Gas-hydrates may be part of the pore fluid, part of the sediment matrix, or act as a cement for sediment grains in different ways. Especially, if the hydrate acts as a cement as described for cores from site 1041 of the Ocean Drilling Program (Kimura et al., 1997), shear wave velocity is increased significantly, even for small amounts of hydrate, because of the significantly risen shear strength. Discrimination of the different lithologies is especially important for understanding the role of gas-hydrates in slope stabilization and slope failures. Large slope failures may cause tsunamis and result in emitting large amounts of climate-relevant methane gas. Free gas that has been trapped beneath gas-hydrates may escape through faults and gas-hydrate in the sediment may dissociate due to reduced overburden load. Near ocean-bottom hydrate may also ascent directly due to its buoyancy.

An indicator for the presence of gas-hydrates are bottom-simulating reflectors (BSR), which are more or less distinct reflectors with a usually negative polarity due to an inverse velocity contrast caused by the bottom of hydrate-bearing sediment and possibly free gas beneath. They approximately follow the ocean-bottom reflection in a distance according to the pressure and temperature of the stability zone of gas-hydrates. The effect of the presence of the hydrate can be estimated by determining shear wave velocity of gas-hydrate saturated sediment above the BSR and the sediment without gas-hydrates below the BSR. The absence of a BSR does not indicate the absence of gas-hydrates. At the above mentioned drilling site off-shore Nicoya, gas-hydrates have been found included into sediment layers in different ways, but a BSR was not observed. However, for SONNE cruise SO-163-2 locations with relative strong BSRs have been chosen, because of the high dilatational wave velocity contrast there, which implies a possibly high shear wave velocity contrast. Furthermore, dilatational wave velocity and subsurface structure are already well determined at the chosen locations, so that shear wave velocity need not be determined absolutely, but can be determined by relative travel times as well.

According to the results of Pecher et al. (1998), BSRs observed offshore Costa Rica are best explained by a thin layer containing free gas beneath hydrate-bearing sediments. Poststack time-migrated streamer sections acquired and processed during SONNE cruise SO-163-2 show, that regions with strong BSRs coincide with low amplitudes of later phases (compare e.g. Figure 6.6.2.10), which can be attributed to attenuation by free gas beneath the gas-hydrate stability zone. This observation matches well with the result of Pecher et al. (1998). Since free gas can escape along fractures, bottom simulating reflectors are mostly absent in areas affected by slumping. A prominent example where a BSR has been observed in a structure interpreted as slump mass, is Nicoya slide. One possible explanation is, that the sediment slumped as a block and stratification was not disrupted at this location so that the gas cannot escape. Another possible explanation is, that the BSR re-formed after slumping. Different origins might result in a different fine structure causing different seismic velocities.

Profiles P09 and P10 (Figure 6.6.2.1a) follow the seismic reflection line SO-81-21 and refraction line SO-81-300 (Hinz et al. (1992), Pecher et al. (1998) and Ye et al. (1996)) across Nicoya Slide. The data has been recorded by the four-channel-streamer and ocean bottom seismometers and hydrophones. The new data complements SO-81-21 and SO-81-300 especially by three-component registration of reflected and refracted waves. While profile P09 was shot by the 32l-Bolt-gun (with 7.5 m cable to floatations, about 34 m behind and about 3 m portsides the vessel), profile P10 was shot by the four-G-gun-cluster (with 4 m cable to floatations, portside guns about 32 m and starboard side guns about 22.5 m behind the vessel). A group of four OBSs and five OBHs, including one OBH placed 500 m above seafloor for recording the far-field source signal, was deployed onto Nicoya Slide, a smaller group consisting of one OBS and two OBHs was deployed north-east of the headwall landward of this slide (Figure 6.6.2.1b, respectively Appendix 9.5). The smaller group has been recovered after

shooting of line P10 was completed, while the larger group was complemented by two test-instruments (OBH36 and OBH37). Sampling rate was 200 or 250 Hz, depending on the capabilities of the instruments. The following profiles P11, P12, P13 and P14 have been shot mainly for testing different source configurations (varied cable lengths of the G-gun-clusters of 4m and 6m, varied distances behind the vessel and lateral symmetries) for later measurements and for enabling a three-dimensional localization of the larger group of OBSs and OBHs by cross-lines. These profiles also provide additional information about lateral variations near to the ocean bottom. After profile 14 was finished, all instruments were recovered successfully. Except for OBS 24 and one approximately horizontal channel of OBS 25, all ocean bottom instruments recorded useful data. Standard processing as described in Section 6.6.1 has been applied. Selected sections are presented in Figures 6.6.2.2 ff.

The individual locations where the instruments were deployed onto the slump mass were mainly chosen because of the seismically almost transparent region below the BSR on the slide observed in migrated MSC sections provided by C.R. Ranero (personal communication). The stations landward of the headwall serve as similar but non-slided reference. Additionally, waves which entered the sediment through the headwall can be observed at this location, but all in all, subsurface structures appeared relatively simple, compared to other potential locations. According to preliminary two-dimensional re-localization of the ocean-bottom-instruments, their drift was in the order of the smallest planned station distances, but rather similar for all instruments. Deploying the instruments in groups, enables estimating very local effects, e.g. caused by small scaled structures and different coupling due to local variations of the ocean bottom material. Furthermore, the redundant information enables stacking of corresponding components in order to enlarge signal-to-noise ratio. The not completely known effective transfer functions of the rather different kinds of receivers makes comparisons difficult, however, it appears reasonable to assume that receivers of one kind have similar transfer functions. The difference in amplitudes between OBS 26 and OBS 31 might be caused by softer near-surface material at OBS 26. The transfer functions of the receivers shall be examined in more detail in future work, so that receiver effects may be eliminated from the data and differences due to local variations in subsurface and coupling at the surface may be estimated more precisely from different kinds of instruments, too. Unfortunately, during these measurements there where only the five deployed OBSs available. However, at intermediate and large angles of incidence, shear waves have a vertical displacement component and can be recorded by hydrophones as well.

The area around Nicoya Slide will probably be studied during Meteor cruise 54-1 in July and August 2002 by high frequency 3D reflection seismic and further ocean bottom seismic measurements, again. The data acquired during SONNE cruise SO-163-2 serve as a basis for later studies on gas-hydrates at locations with weak and perhaps lacking BSR and more complex subsurface structures. In addition to studies performed on Nicoya Slide during SONNE cruise SO-163-2, we also recorded two profiles offshore north-west Nicoya corresponding the MSC line BRG-99-39 and three profiles at a location on line SO-81-09 which has been studied in details by Pecher et al. (1998) and McGee (2000). This way, we are getting a rough idea of the variety of shear wave characteristics at locations with distinct BSRs offshore Nicoya. The subsurface structure at these locations is relatively simple, too. We chose two-dimensional layouts (Figures 6.6.2.1a, 6.6.2.1c and 6.6.2.1d and station-list in Appendix 9.5), so that we may identify phases arriving from outside the profile plane caused by lateral heterogeneities by array or network techniques. The OBSs were complemented by a larger number of OBHs in order to cover a larger region. Offshore north-west Nicoya, we deployed the stations at 2 km distances covering almost the whole slope, while we had chosen distances of 200 m at the location on SO-81-09 in order to study very local effects.

The source wavelet of the G-gun array is effectively shorter, but especially at large offsets the higher signal amplitudes of the Bolt-gun is advantageous, although the Bolt-gun has a rather powerful bubble interfering with phases to be evaluated. On recordings of some instruments of profiles P09 and P10, diving wave phases from the mantle may be observed even at very large distances up to 100 km, however, mostly the reasonably interpretable data probably ends at about 50 to 75 km due to a small signal-to-noise ratio and/or an insufficient dynamic and pre-amplification, respectively. At very large offsets, distortions from the direct water wave, its multiples and other late phases of the preceeding shot are significant at a shot-interval of 60 s, which was chosen as a compromise with respect to spatial resolution. For the sake of higher source energy, profile P32 (corresponding to multi-channel

seismic line BGR-99-39) was shot by the Bolt-gun (with 7.5m cable to floatations, about 34 m behind and 3 m portsides the vessel) and portside and starboard side GI-guns (with 4m cables to floatations, about 35 m behind the vessel) combined, while the cross-profile P32 (with 30 s shot interval) and profiles P35 to P37 offshore Nicoya were shot with 60 s shot-interval by the GI-gun cluster, only.

All ocean-bottom instruments deployed for profiles P32 (OBH142-OBH161) and P33 (OBH148-OBH165) and P35 to P37 (OBH173-OBH192) were recovered successfully. OBH146 and the seismometer channels of OBS159 did not record any useful data. The quality of the data of the other stations especially of line P32 and P33 is rather inhomogeneous and some of the stations recorded useful data only temporarily. Especially the data of OBH148, OBH173 and seismometer channels of OBS174 were severely contaminated by electronic noise and several stations e.g. OBH149 and the seismometer-channels of OBS184 recorded rather weak amplitudes. At other hydrophones the direct wave was already clipped. OBH147, OBH163 and OBH173 additionally served as hydrophone tester. Probably, only some of the recordings can be evaluated reasonably, depending on the processing technique. Comparability of different shots of line P33 might be affected by problems with the floatations of the starboard side G-guns resulting in a different source depth. Examples of processed OBH- and OBS-sections are presented in Figures 6.6.2.22 ff. Lines P35-P37 were shot only a few days before the end of the cruise have not been processed, yet. Data examples are presented in Figures 6.6.2.38 ff.

Further processing and analysis of the acquired data to be performed at Kiel University after the expedition includes evaluation of the three-component data by receiver functions (e.g. Yuan et al., 1997) focussing on determining shear wave velocity in the vicinity of the BSR. Receiver functions result of a deconvolution of a dilatational wave signal from a corresponding converted shear wave signal and describe the conversion operator. They are comparable to deconvolution of the source signal from an acoustic signal yielding reflectivity or transmissivity and the corresponding impulse response, respectively. Since dilatational and shear arrivals cannot be separated by component rotation completely in general, and since exact deconvolution of sampled and noisy data is instable (Oldenburg, 1981), the procedure is not completely straight forward. However, several sophisticated approaches to stabilise receiver functions have been developed and successfully applied in seismology, where receiver functions are a well established technique. Refer to Endrun (2001) for an overview and comparison of different approaches to receiver functions with seismological examples. Since active seismic data is not extremely different from earthquake recordings beside a difference in typical main frequencies of the signals and the different scale of the structures we are interested in, it is reasonable to assume that the principle ideas of receiver functions are transferable to active seismics. Possibly, receiver functions are a valuable complementary technique for determining shear wave velocity directly by picking shear arrivals and amplitude versus offset analysis.

Relative high amplitude horizontal motion of reflected and refracted waves has been recorded by several stations. Especially in the recordings of stations on SONNE lines SO-81-21 and SO-21-09, arrivals that are probably P to S-converted shear waves from the BSR can be identified even in unprocessed data (see Figure 6.6.2.47), although e.g. the waveform inversion performed by Pecher (1995) at the location on profile SO-81-09 works well without assuming a shear wave velocity contrast at the BSR which is necessary for the conversion of waves. However, waveform inversion of streamer data is not very sensitive to shear wave velocity and especially according to the models of Carcione and Tinivella (2000) and the results of Tinivella and Accaino (2000), we expect at least a small change in shear wave velocity causing at least a weak shear wave signal that might not necessarily be visible in unprocessed data. For a reliable, detailed interpretation, further processing is necessary, but could not be conducted on board due to a lack of time.

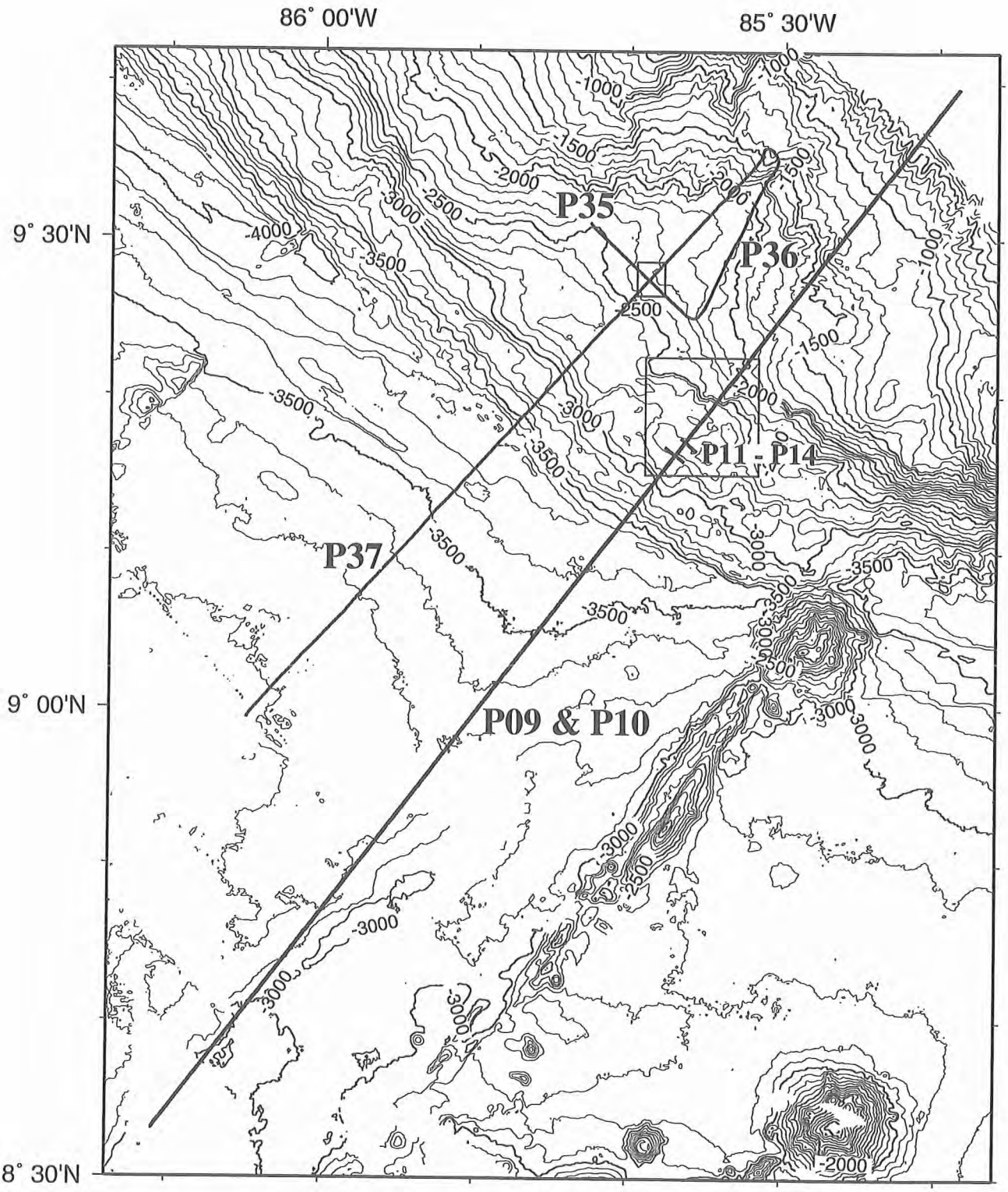


**Figure 6.6.2.1a:** Location map of profiles P09-P14 and P35-P37 (overview) with 100m isolines, compare figures 6.6.2.1b and 6.6.2.1c.

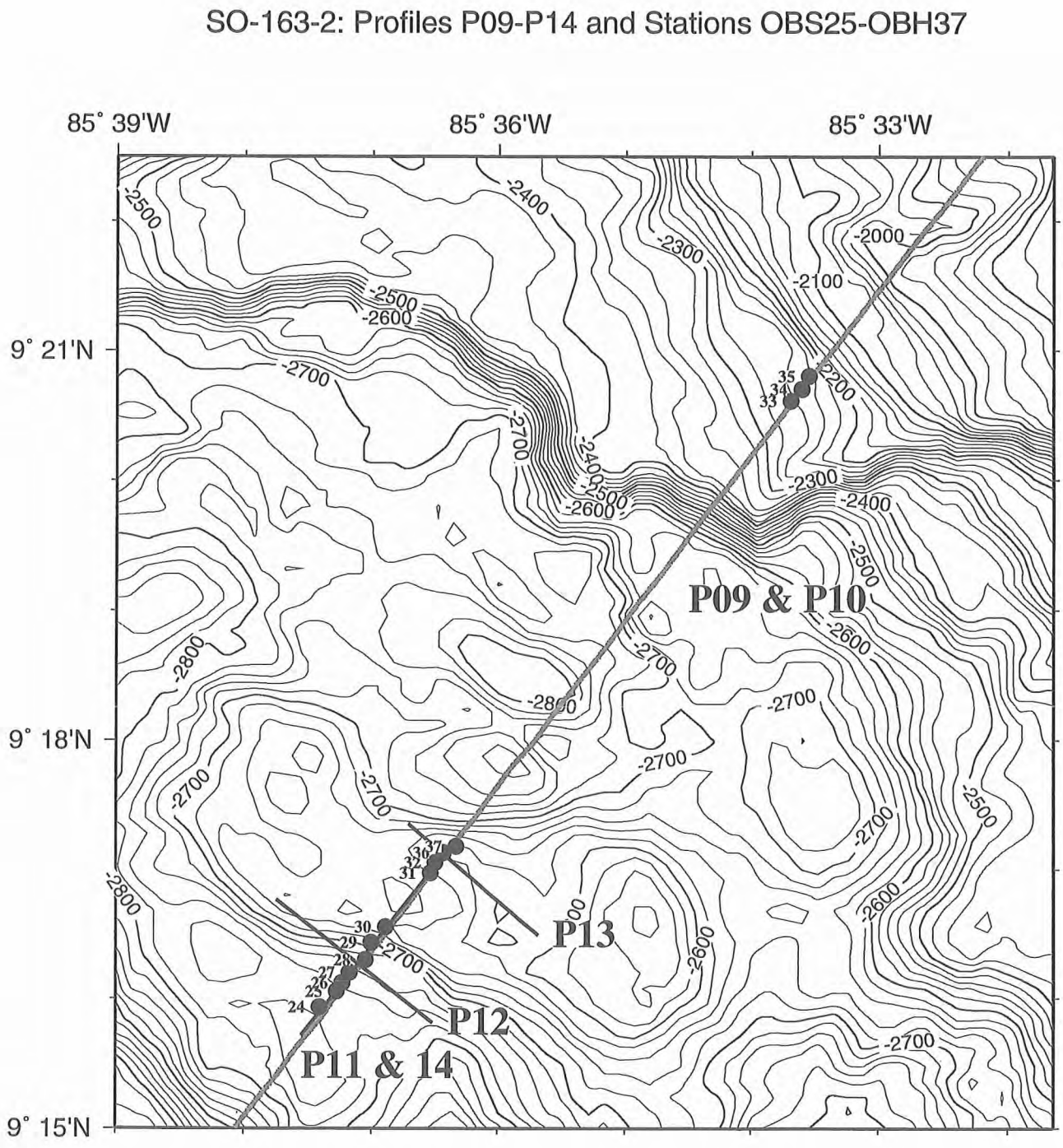


**Figure 6.6.2.1b:** Location map of profiles P09-P14 and stations OBS25-OBH37 (relocated) with 20m isolines, compare figure 6.6.2.1a.

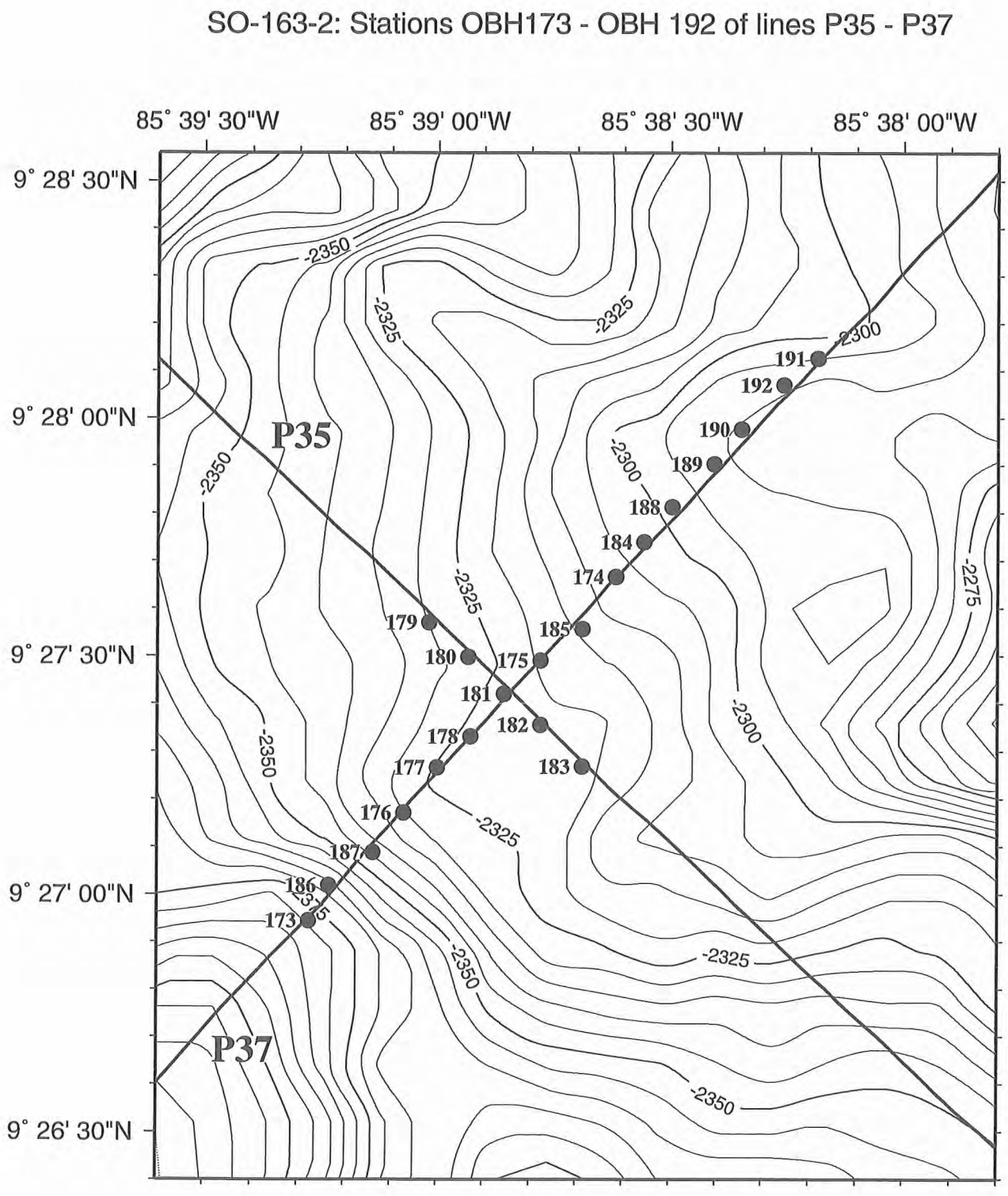


**Figure 6.6.2.1c:** Location map of OBH173-OBH192 (deployment co-ordinates) on profiles P35 and P37 with 5m isolines, compare figure 6.6.2.1a.

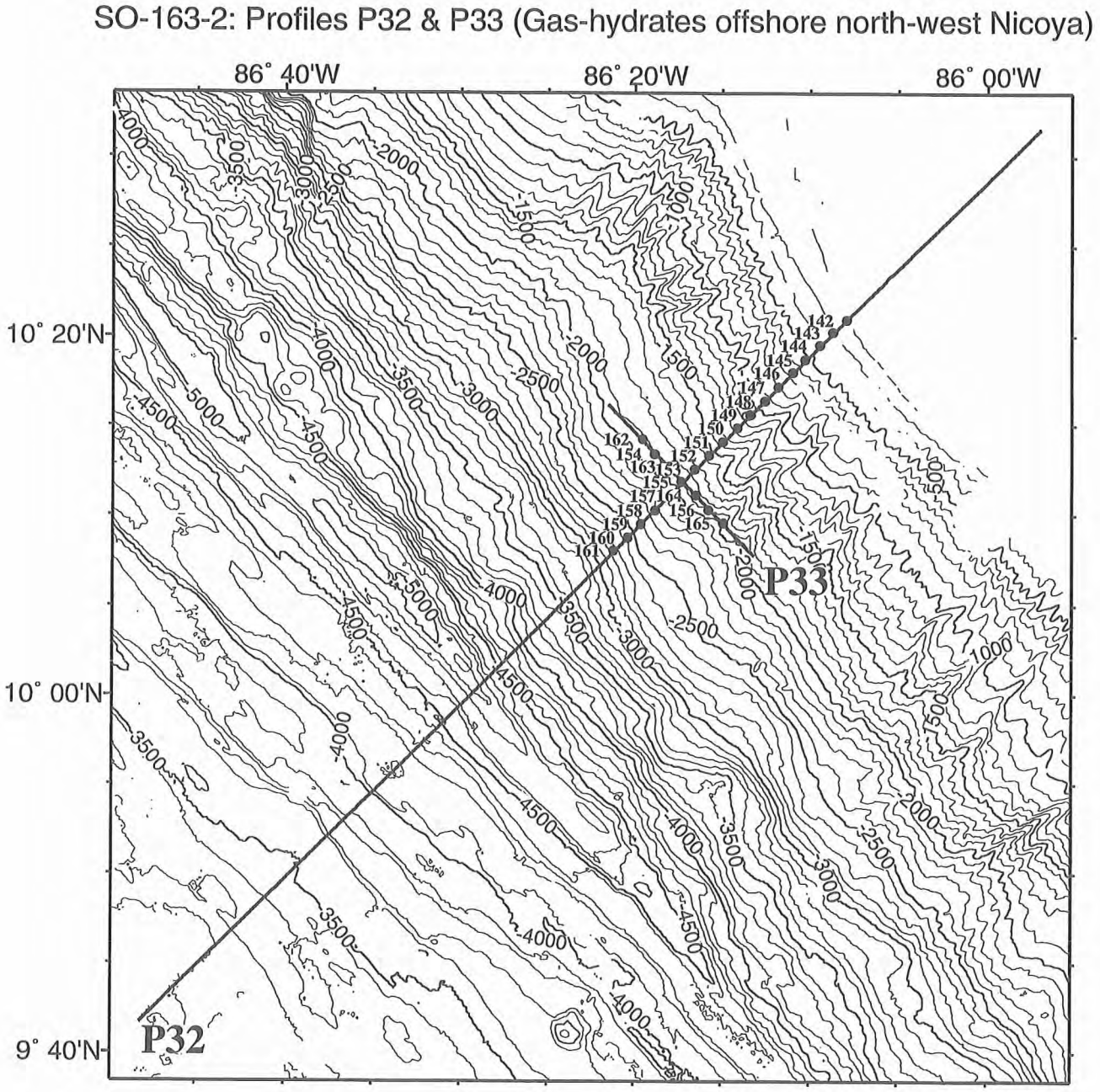


**Figure 6.6.2.1d:** Location map of profiles P32 and P33 with 100m isolines. Stations OBH142-OBH165 are superimposed.

**Figure 6.6.2.2:** Record section from obs 25 (HTI-Hydrophone), Profile 09.

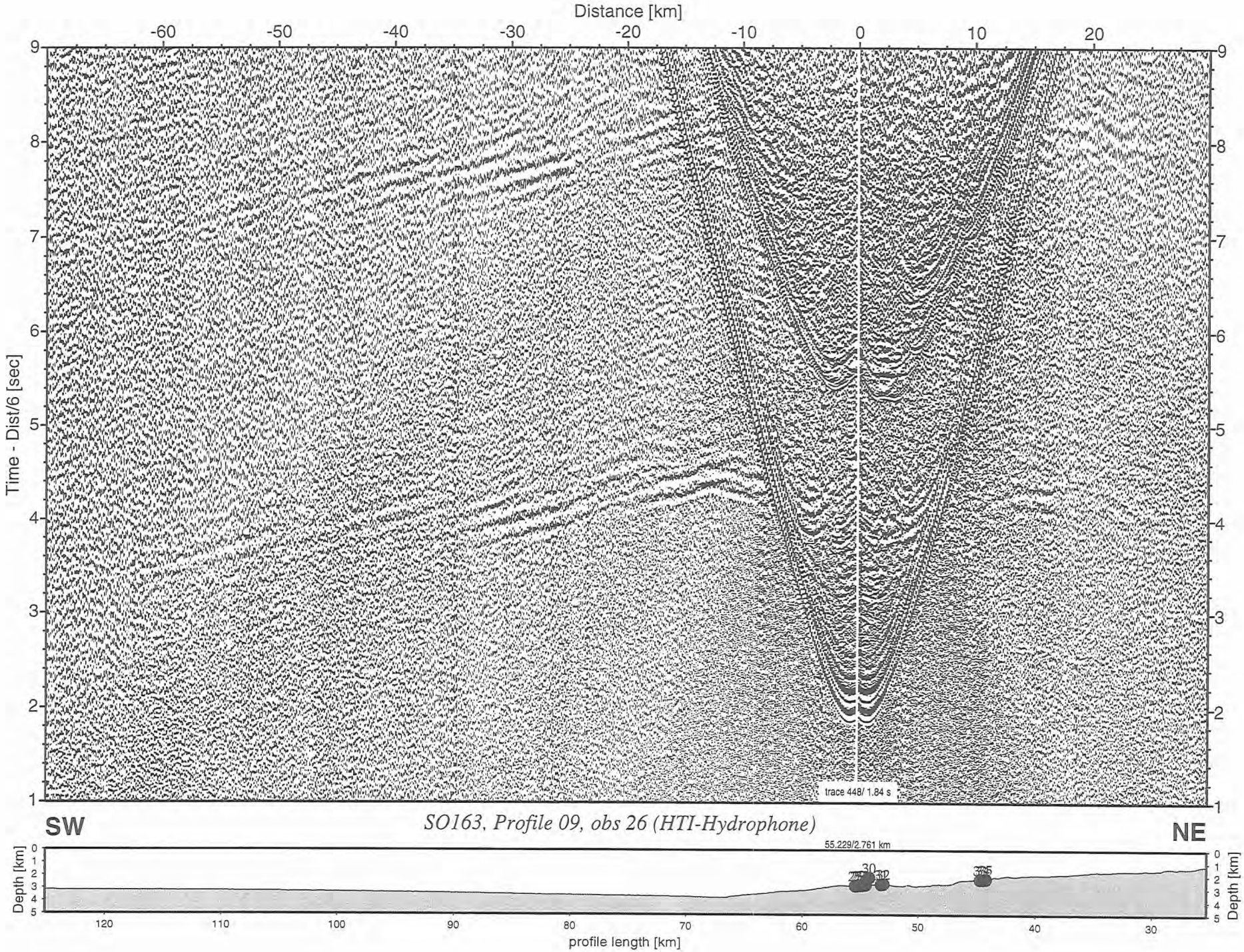


**Figure 6.6.2.3:** Record section from obs 26 (HTI-Hydrophone), Profile 09.

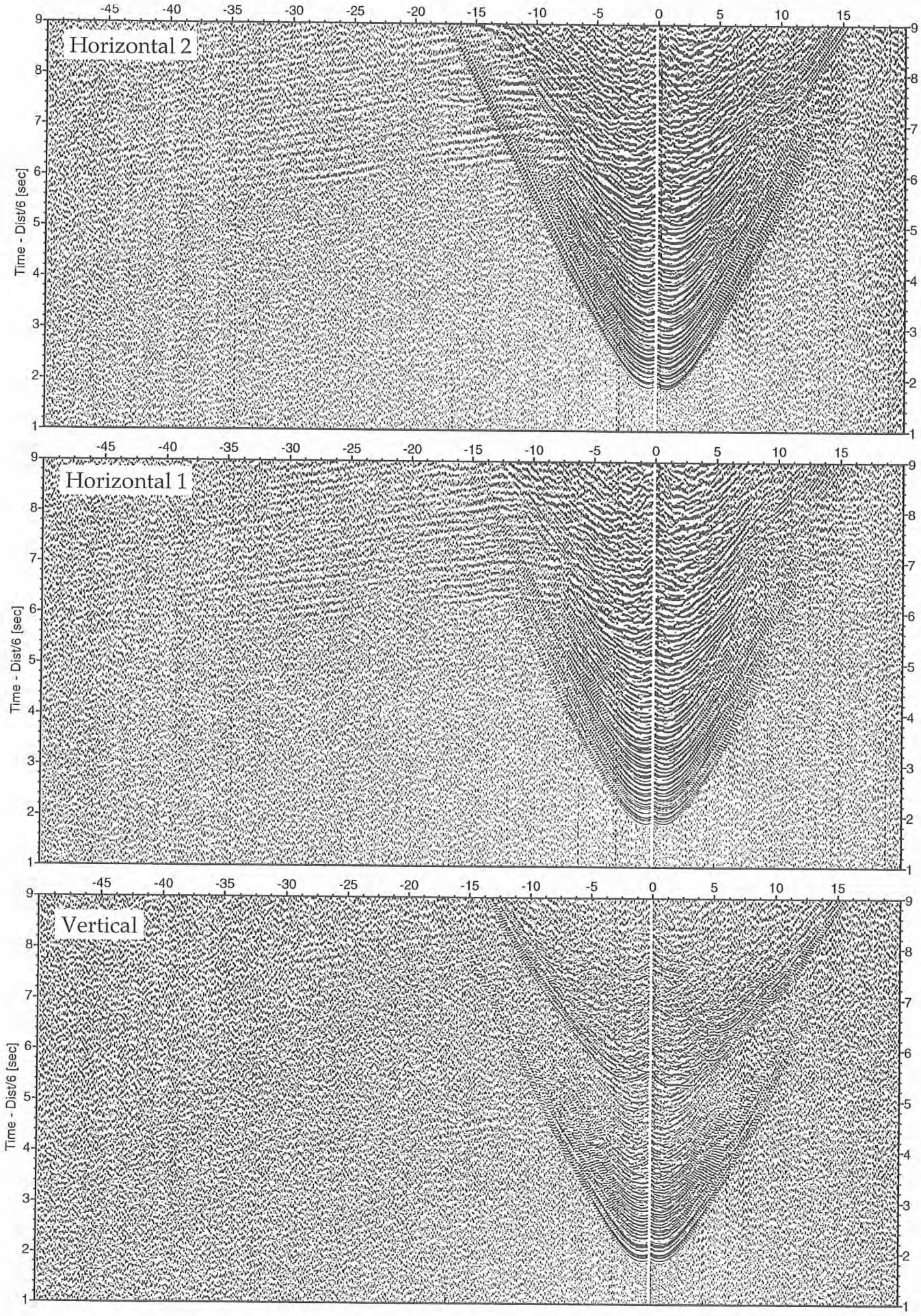


**Figure 6.6.2.4:** Record sections from obs 26 (Owen-4.5Hz), SO163, Profile 09.

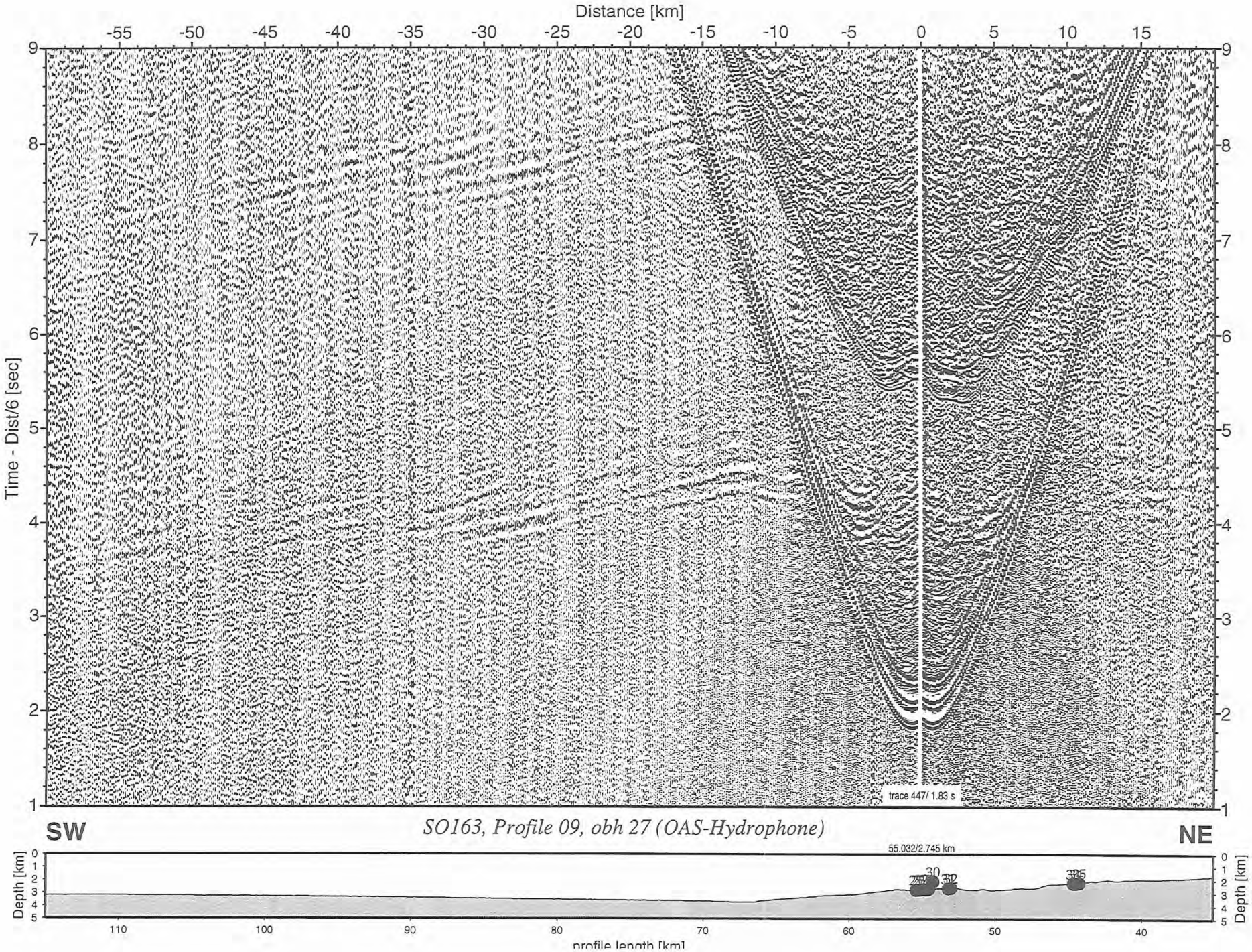


**Figure 6.6.2.5:** Record section from obh 27 (OAS-Hydrophone), Profile 09.

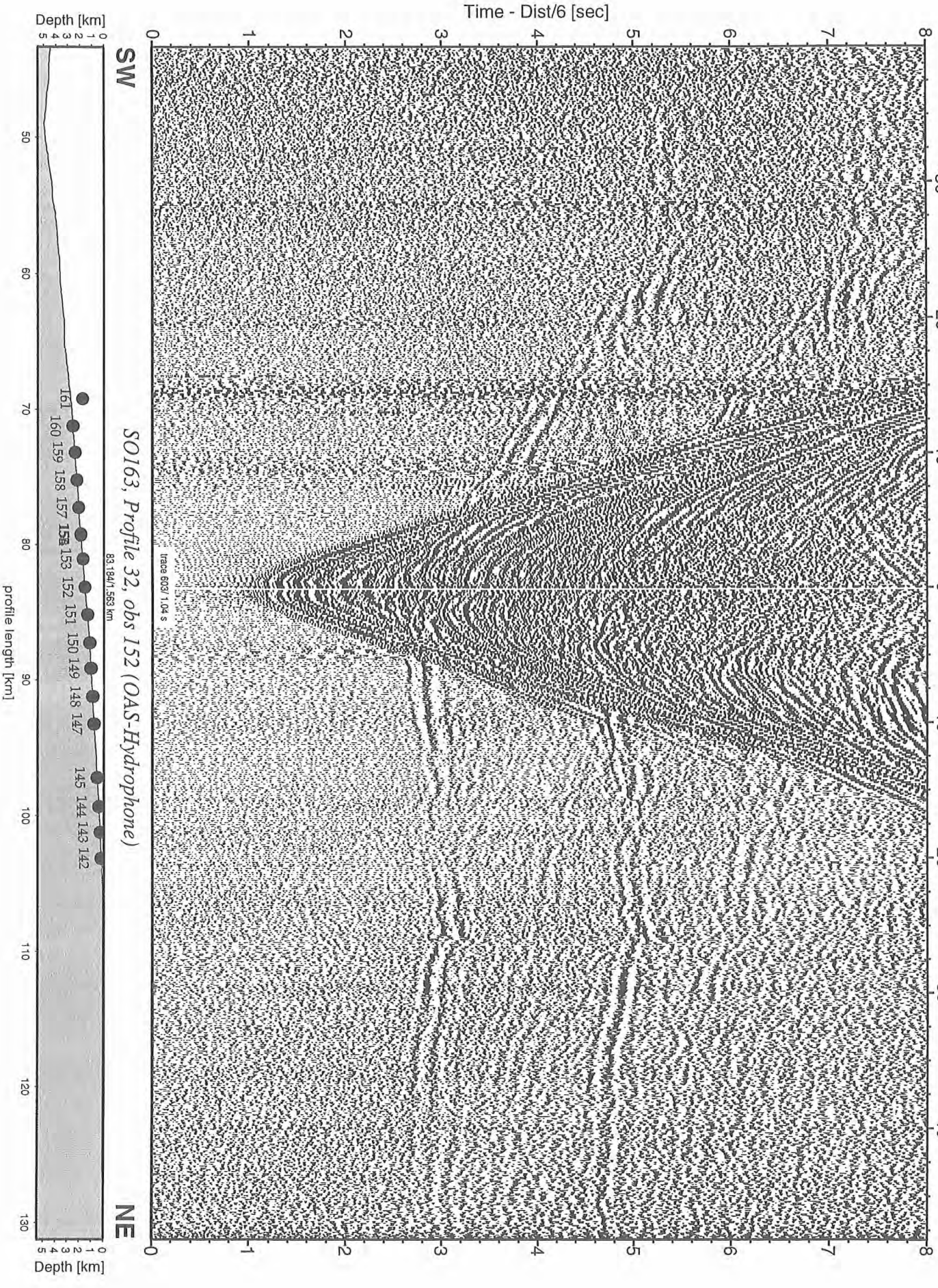


**Figure 6.6.2.28** Record section from obs 152 (OAS-Hydrophone), Profile 32.

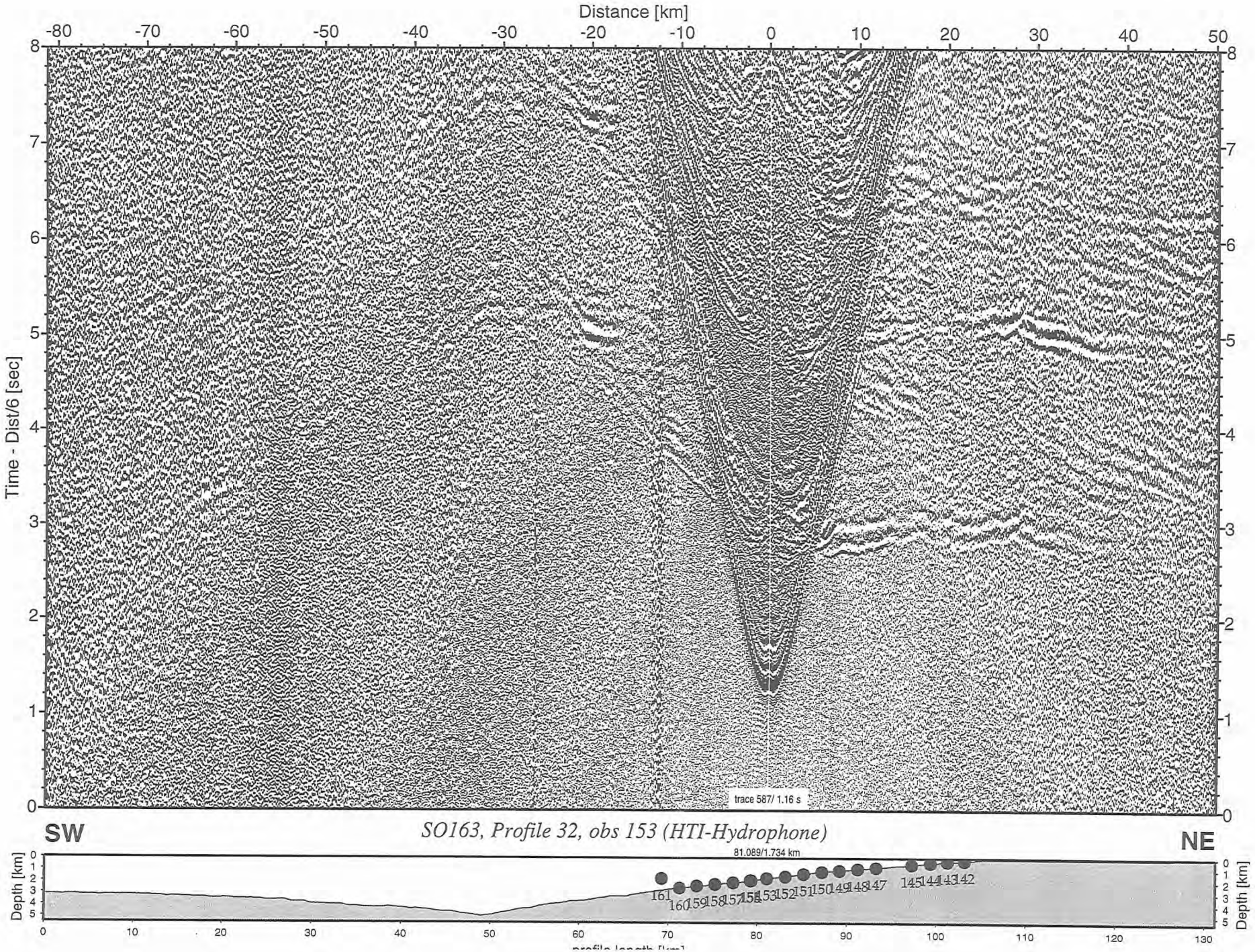


**Figure 6.6.2.29** Record section from obs 153 (HTI-Hydrophone), Profile 32.

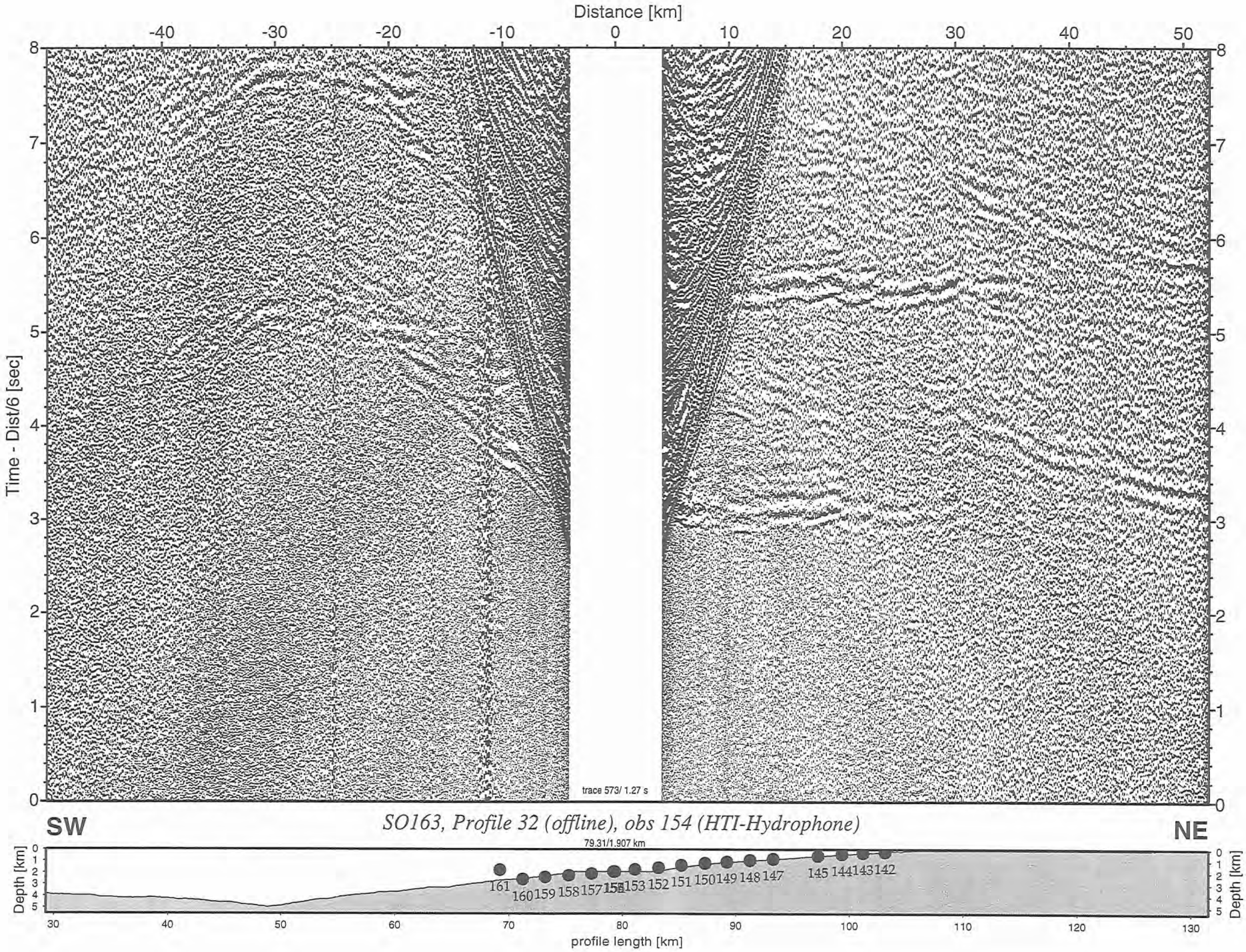


**Figure 6.6.2.30** Record section from obs 154 (HTI-Hydrophone), Profile 32.

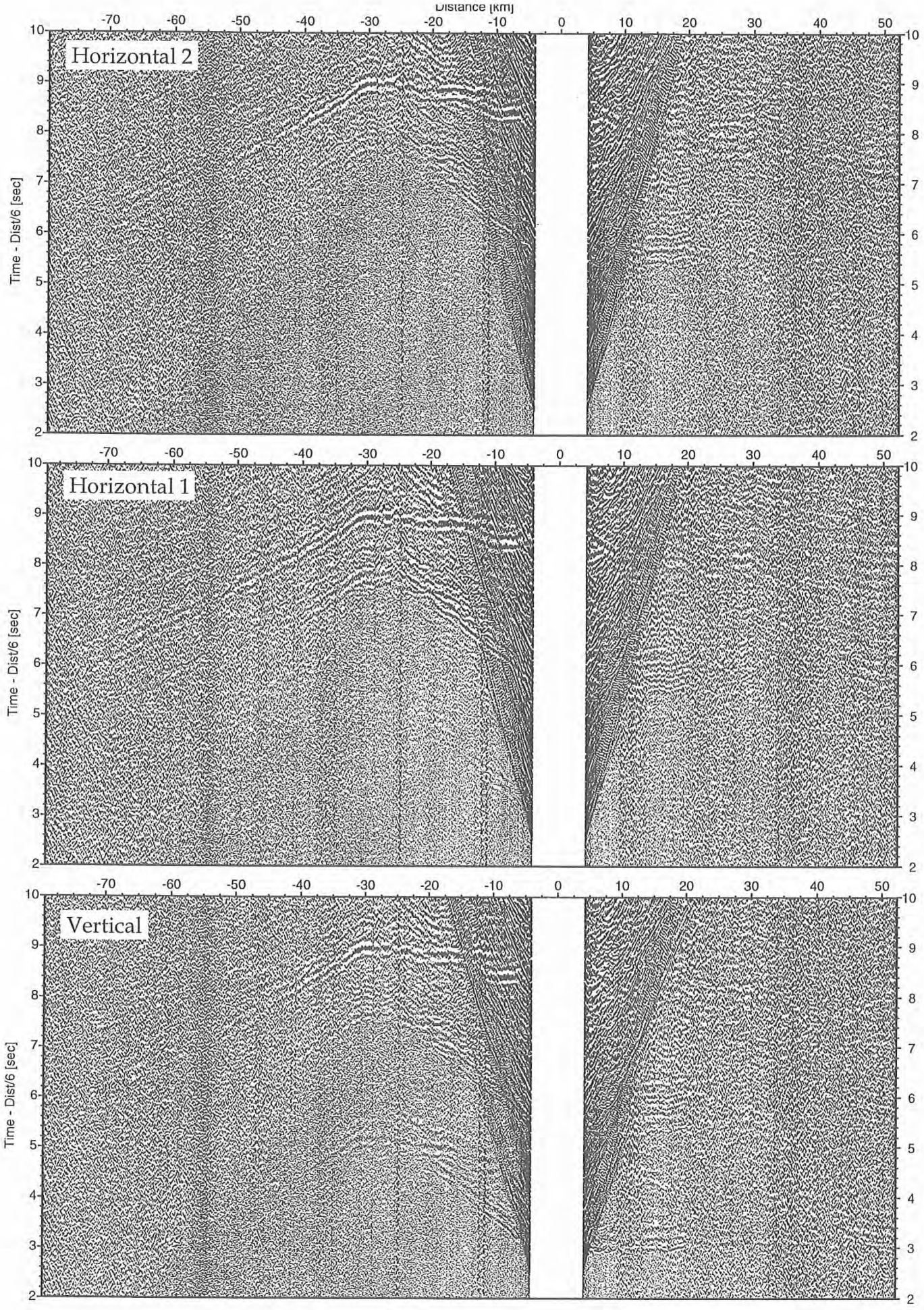


**Figure 6.6.2.31** Record sections from obs 154 (Owen-4.5Hz), SO163, Profile 32 (offline).

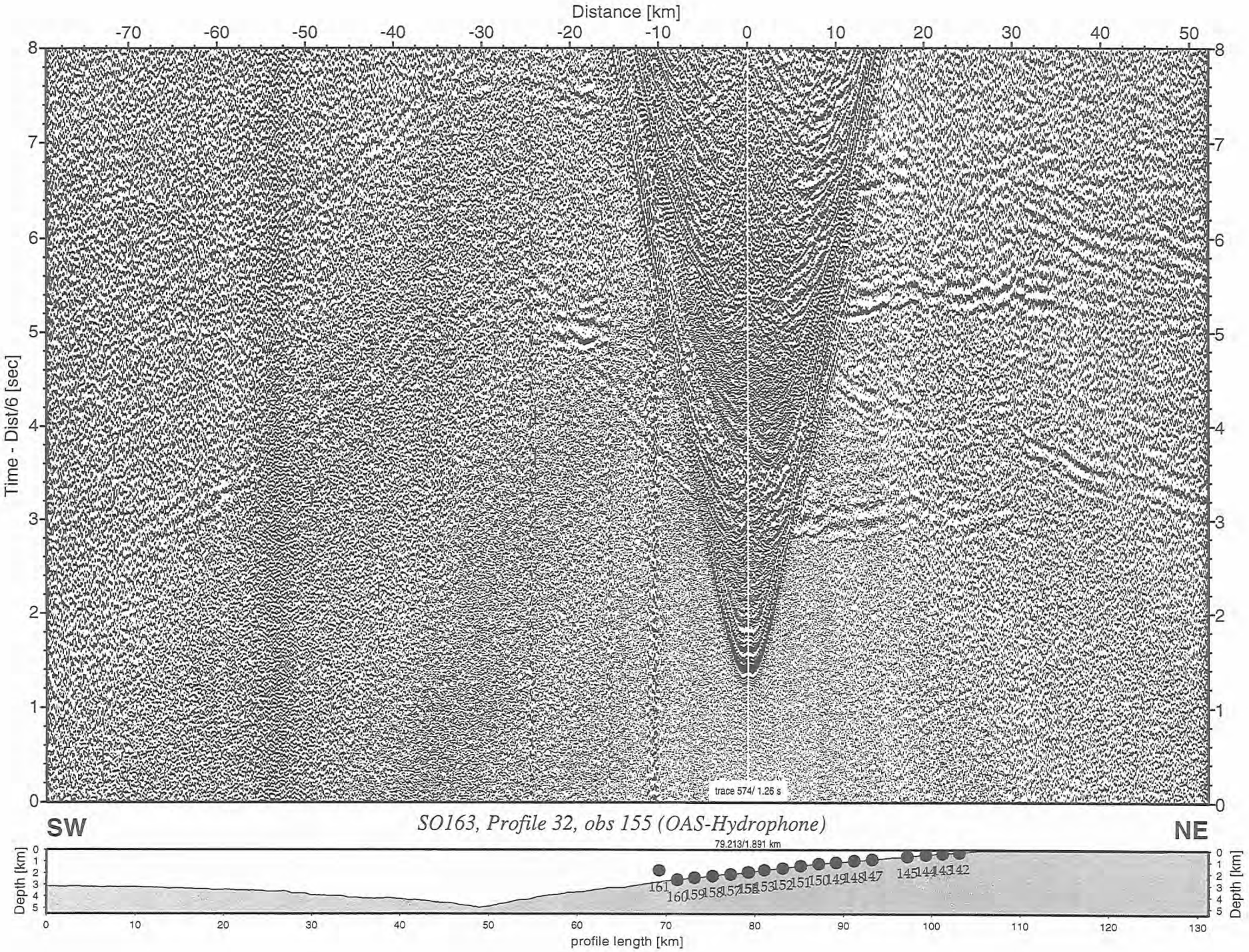


**Figure 6.6.2.32** Record section from obs 155 (OAS-Hydrophone), Profile 32.

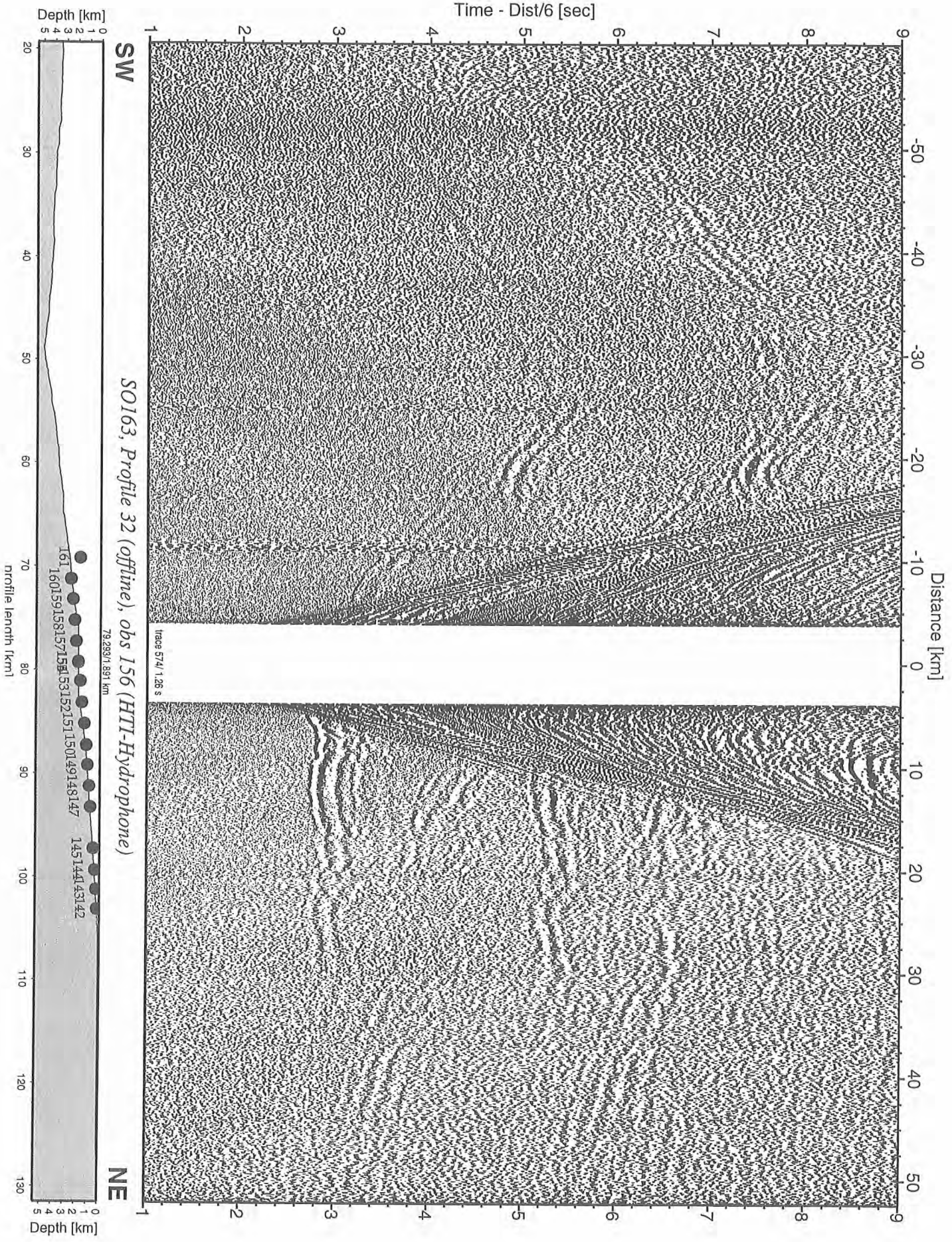


**Figure 6.6.2.33** Record section from obs 156 (HTI-Hydrophone), Profile 32.

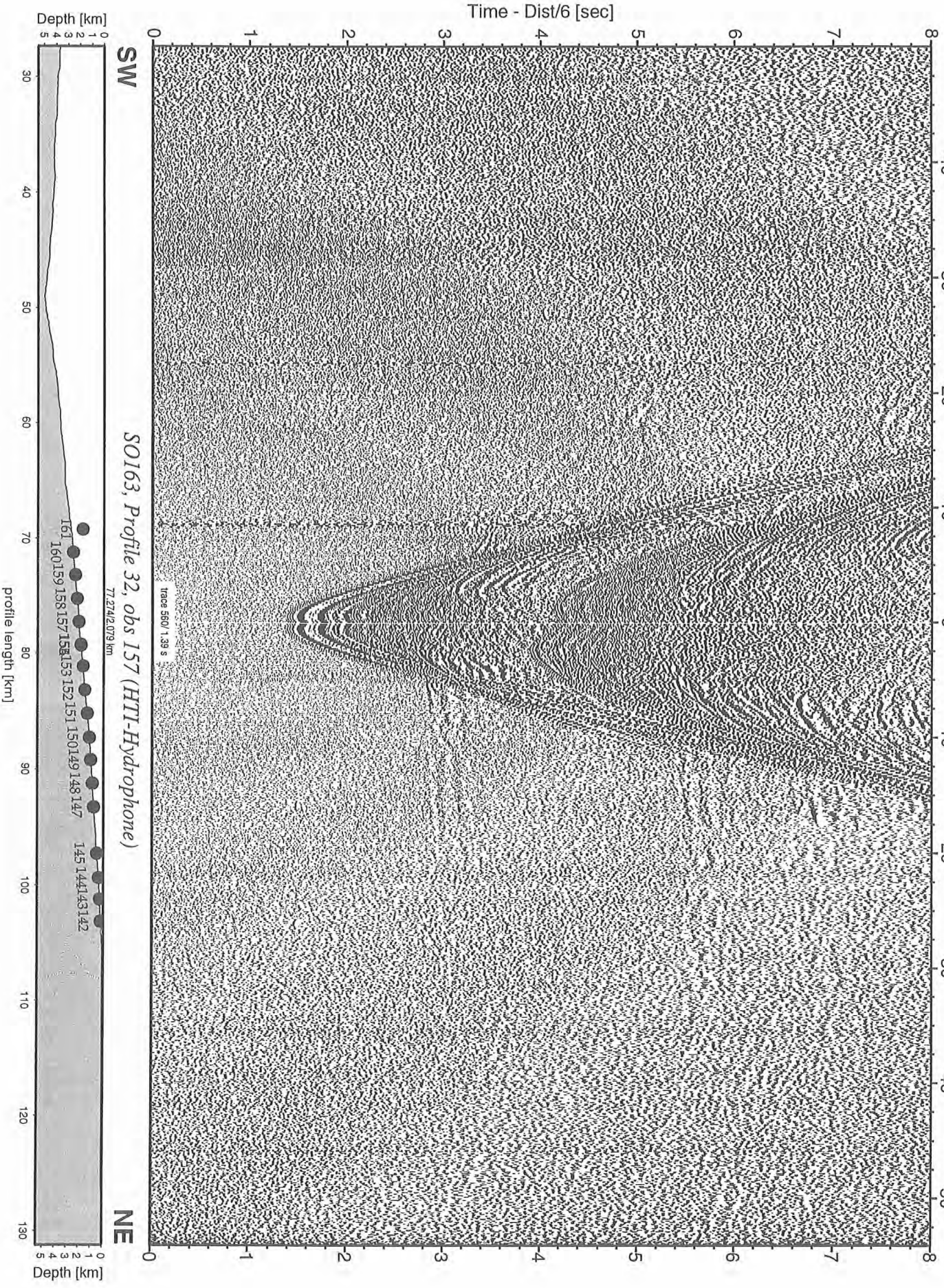


**Figure 6.6.2.34** Record section from obs 157 (HTI-Hydrophone), Profile 32.

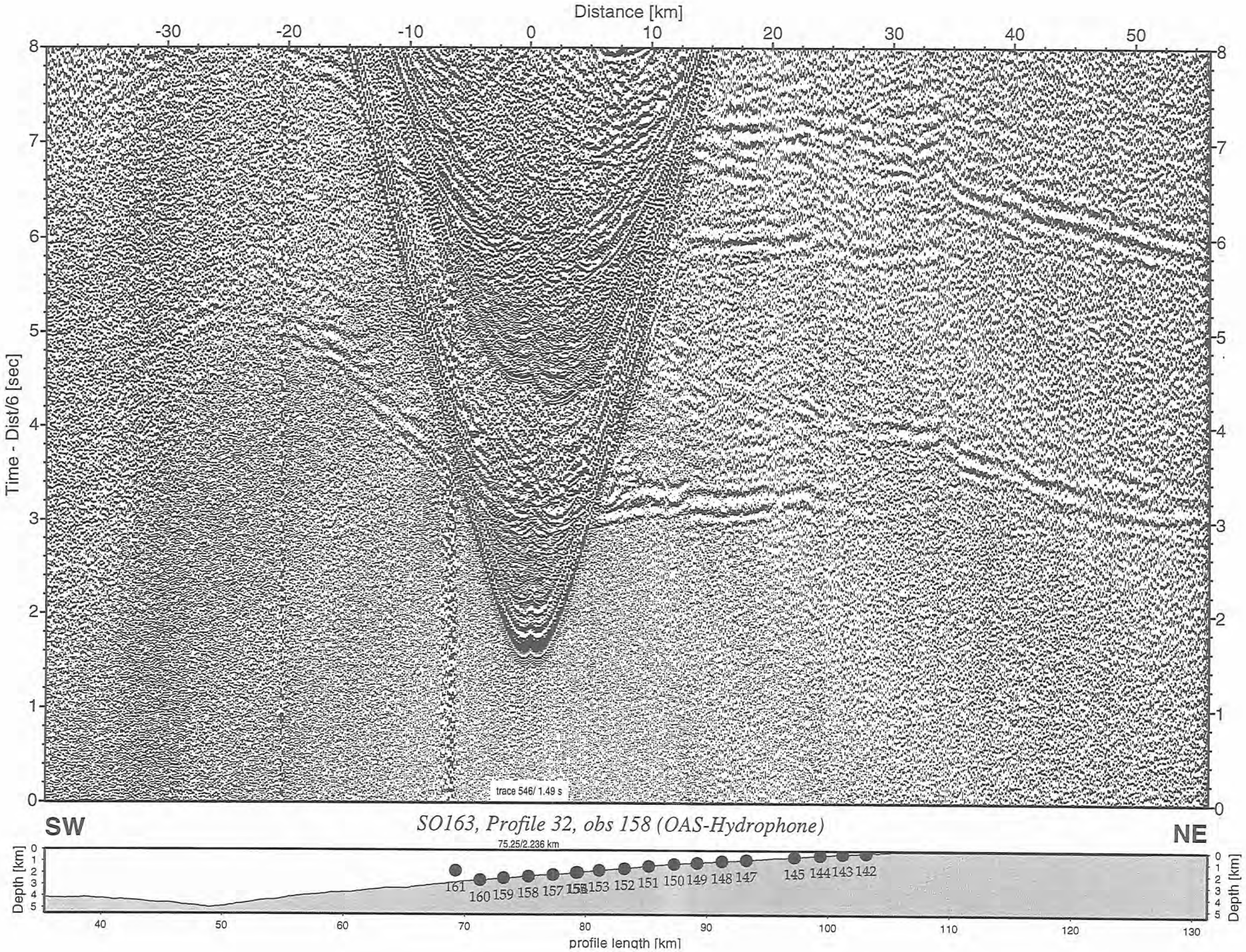


**Figure 6.6.2.35** Record section from obs 158 (OAS-Hydrophone), Profile 32.

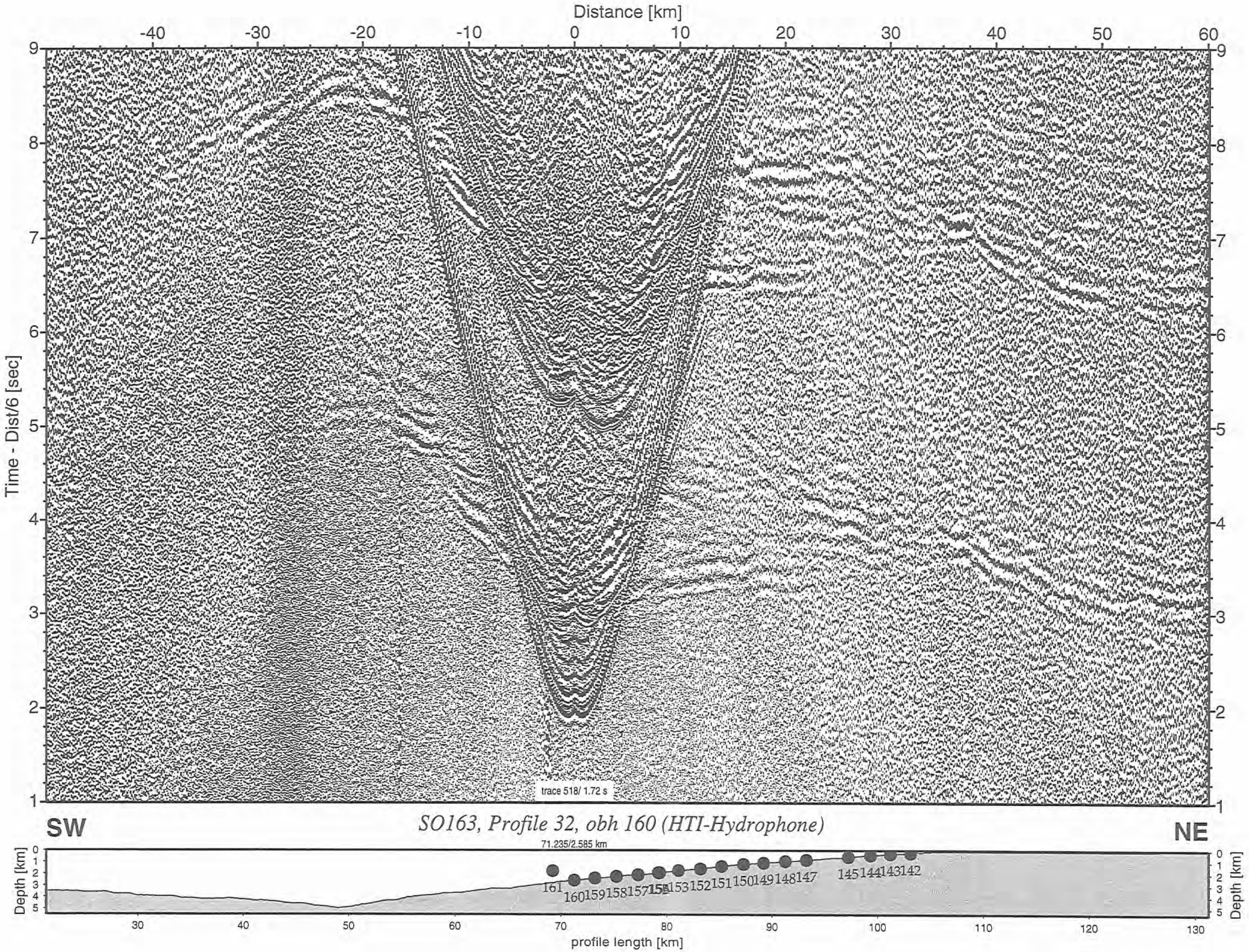


**Figure 6.6.2.36** Record section from obh 160 (HTI-Hydrophone), Profile 32.

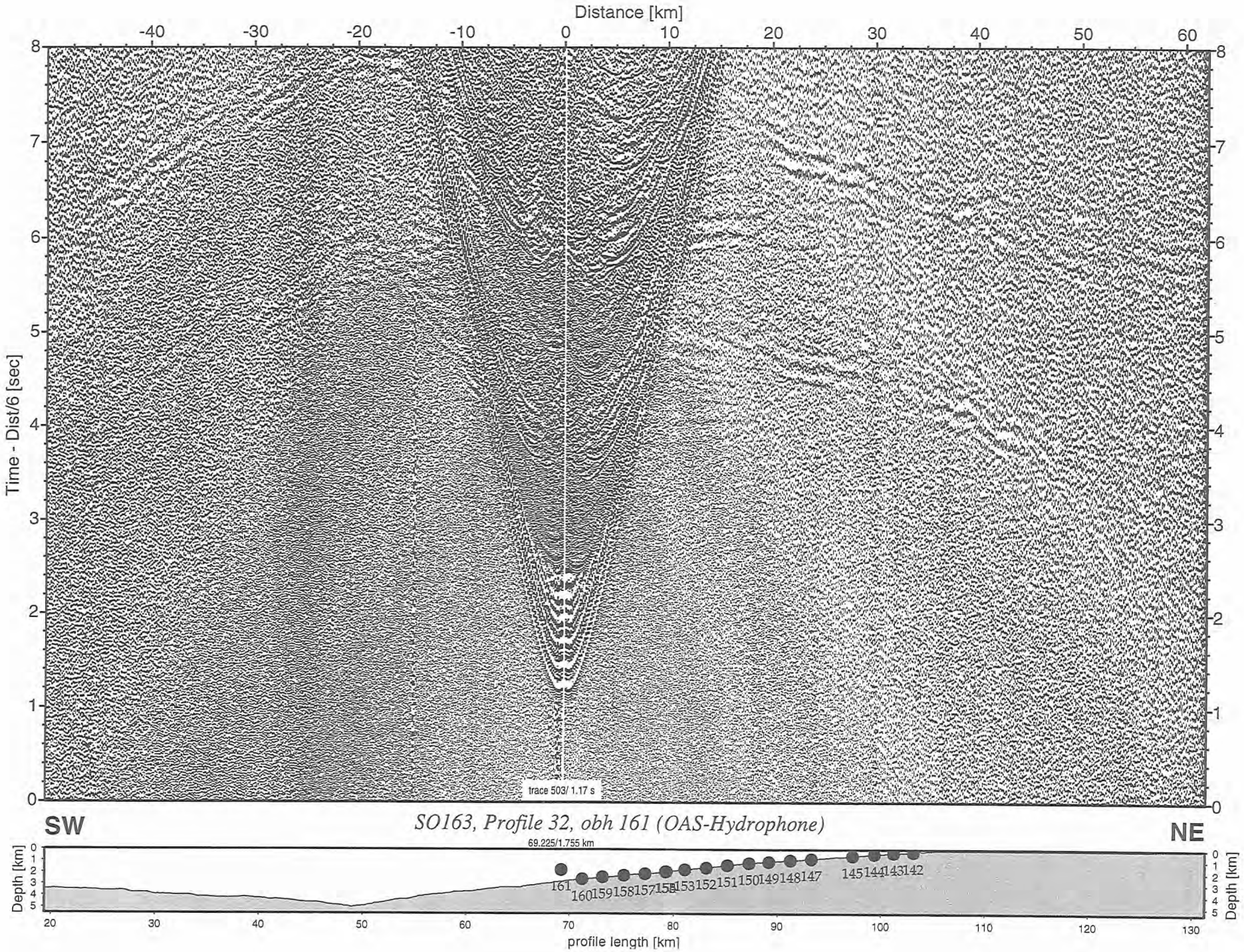


**Figure 6.6.2.37** Record section from obh 161 (OAS-Hydrophone), Profile 32.

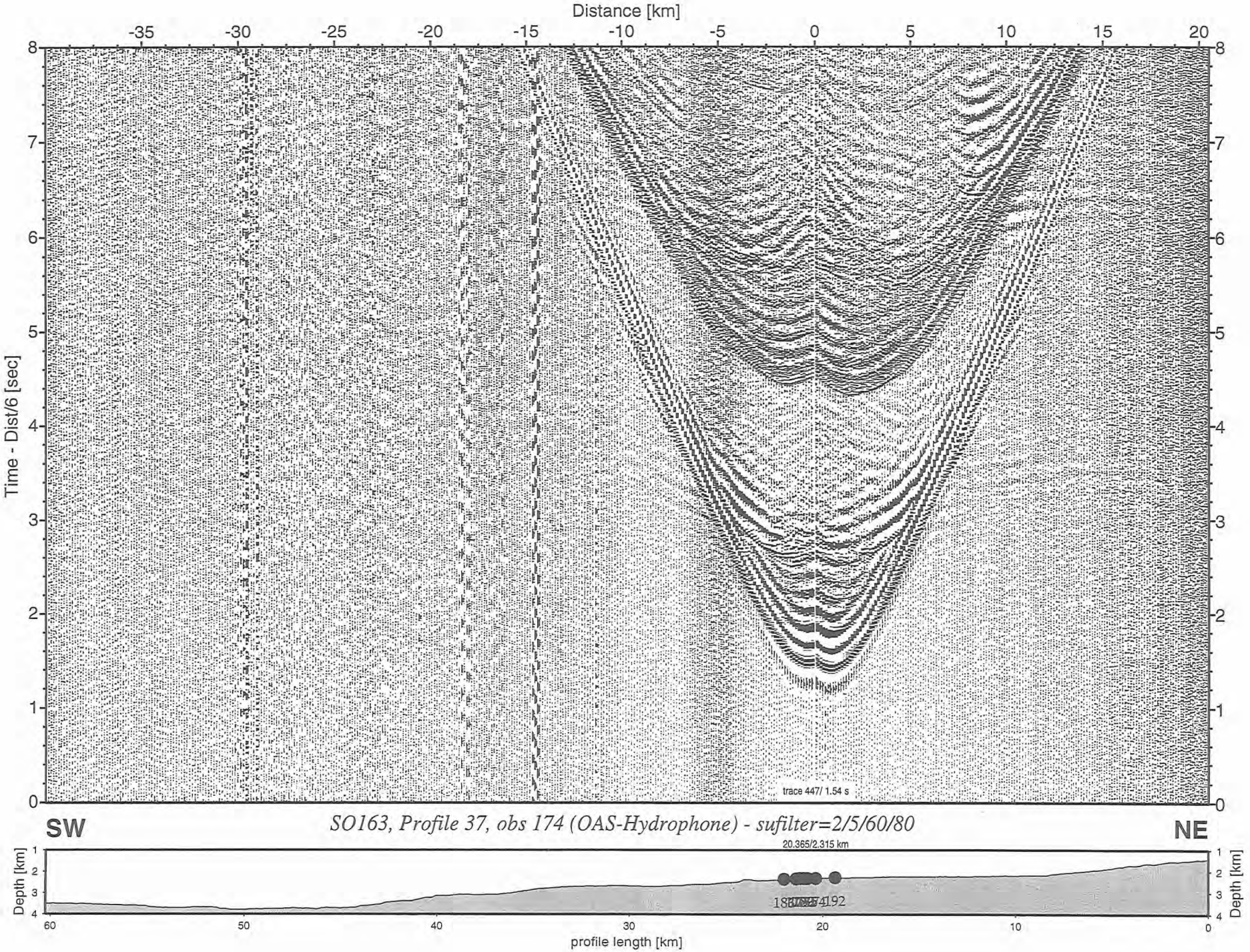


**Figure 6.6.2.38:** Record section from obs 174 (OAS-Hydrophone), Profile 37.

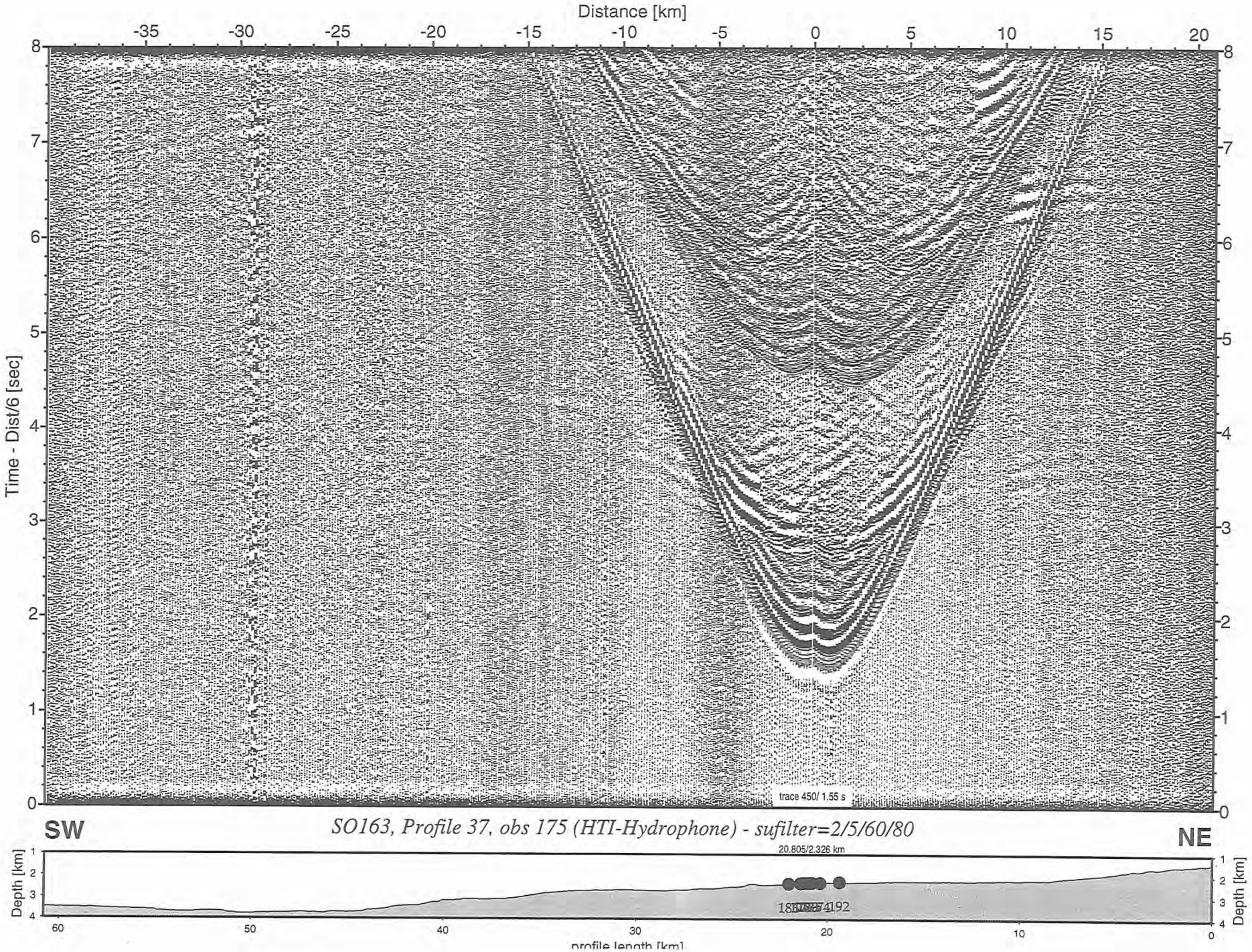


**Figure 6.6.2.39:** Record section from obs 175 (HTI-Hydrophone), Profile 37.

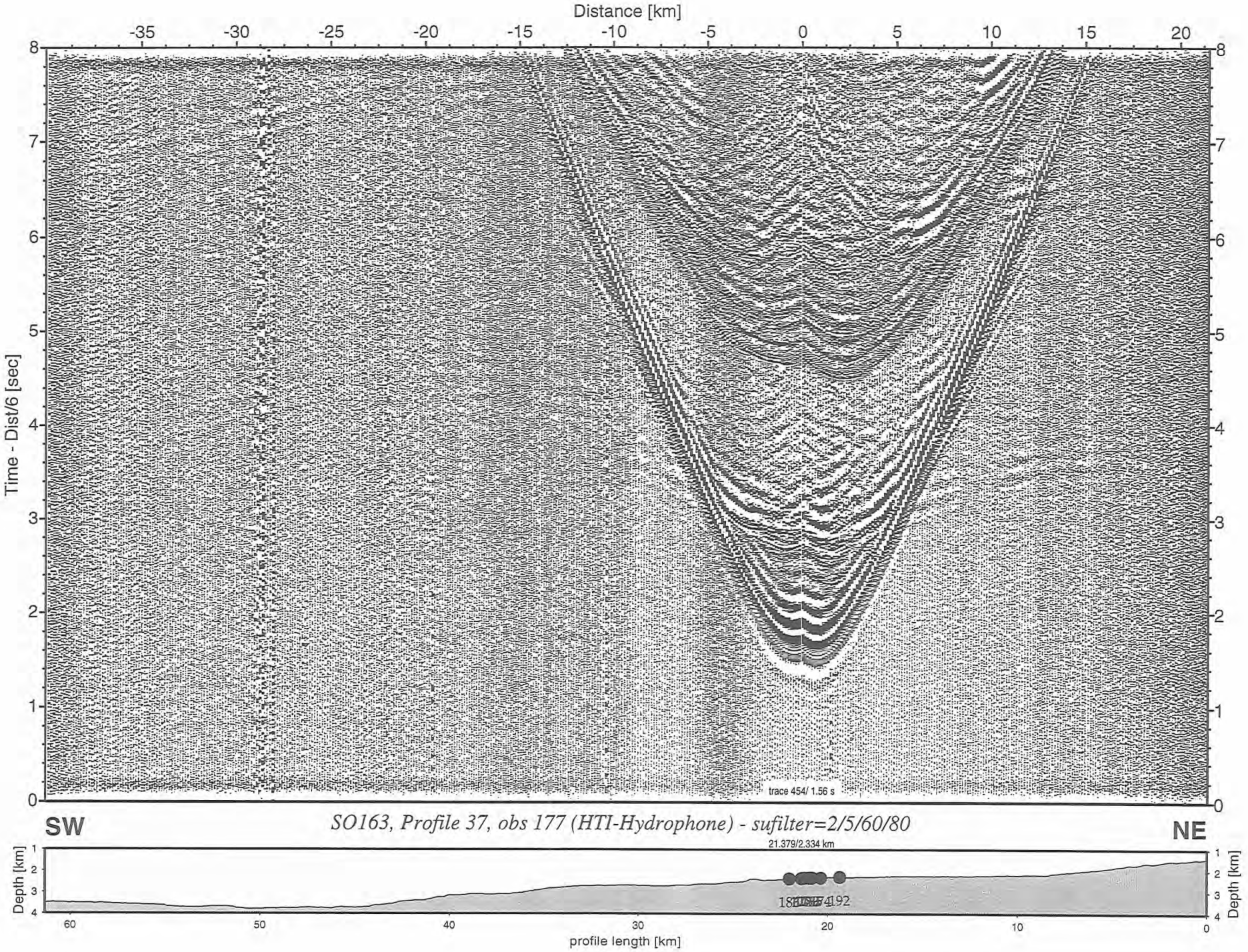


**Figure 6.6.2.40:** Record section from obs 177 (HTI-Hydrophone), Profile 37.

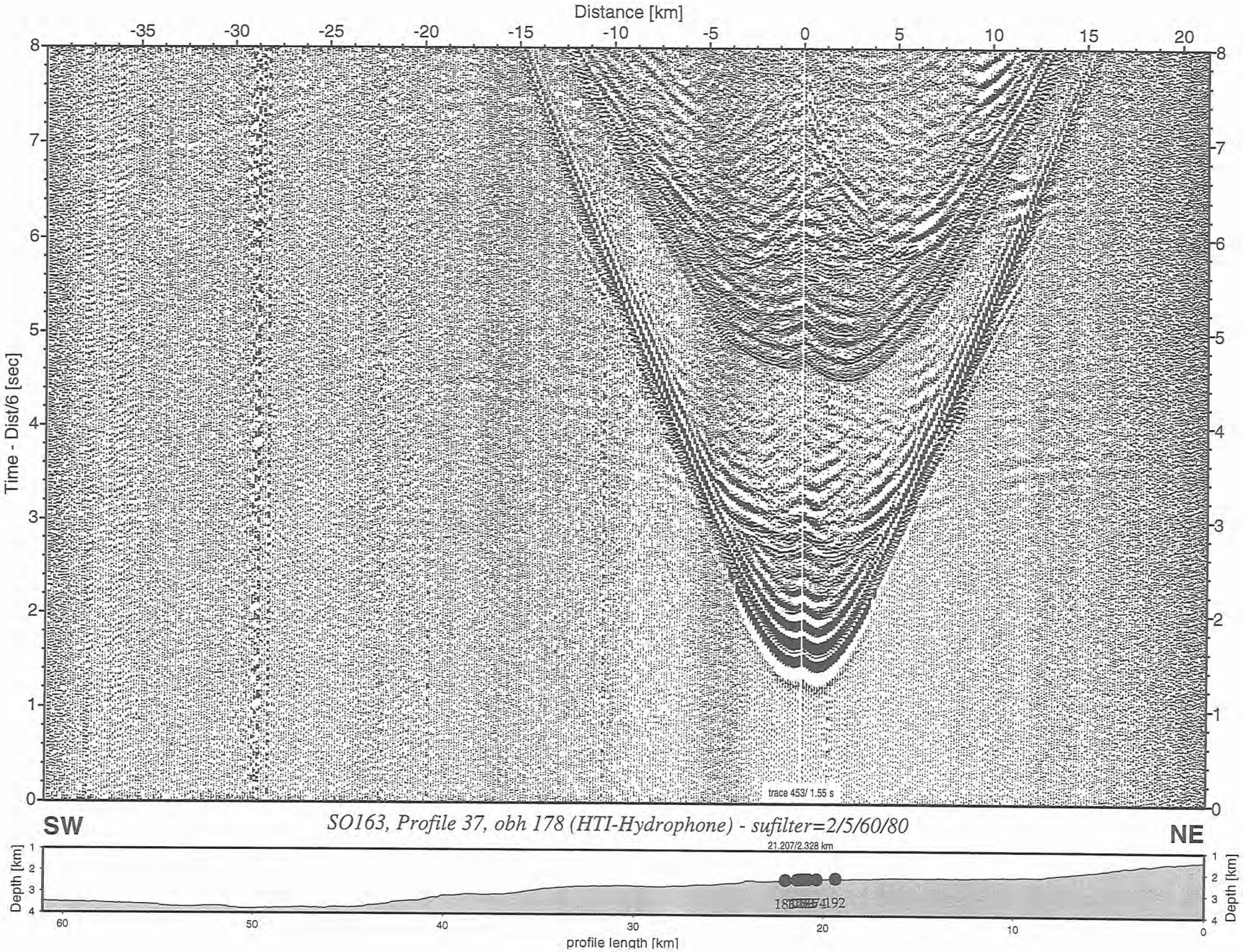


**Figure 6.6.2.41:** Record section from obh 178 (HTI-Hydrophone), Profile 37.

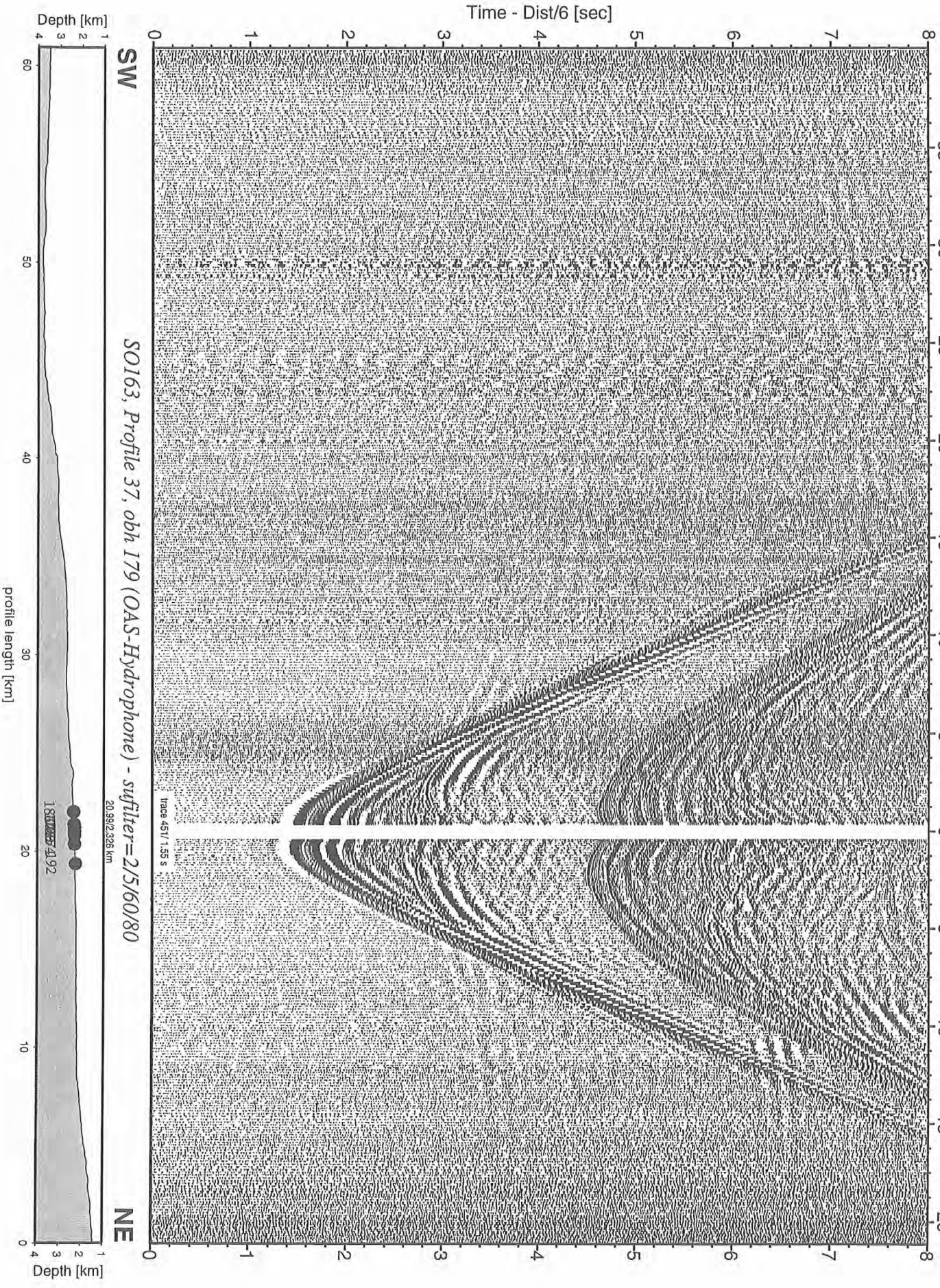


**Figure 6.6.2.42:** Record section from obh 179 (OAS-Hydrophone), Profile 37.

**Figure 6.6.2.43:** Record section from obs 180 (HTI-Hydrophone), Profile 37.

**Figure 6.6.2.44:** Record section from obs 183 (OAS-Hydrophone), Profile 37.

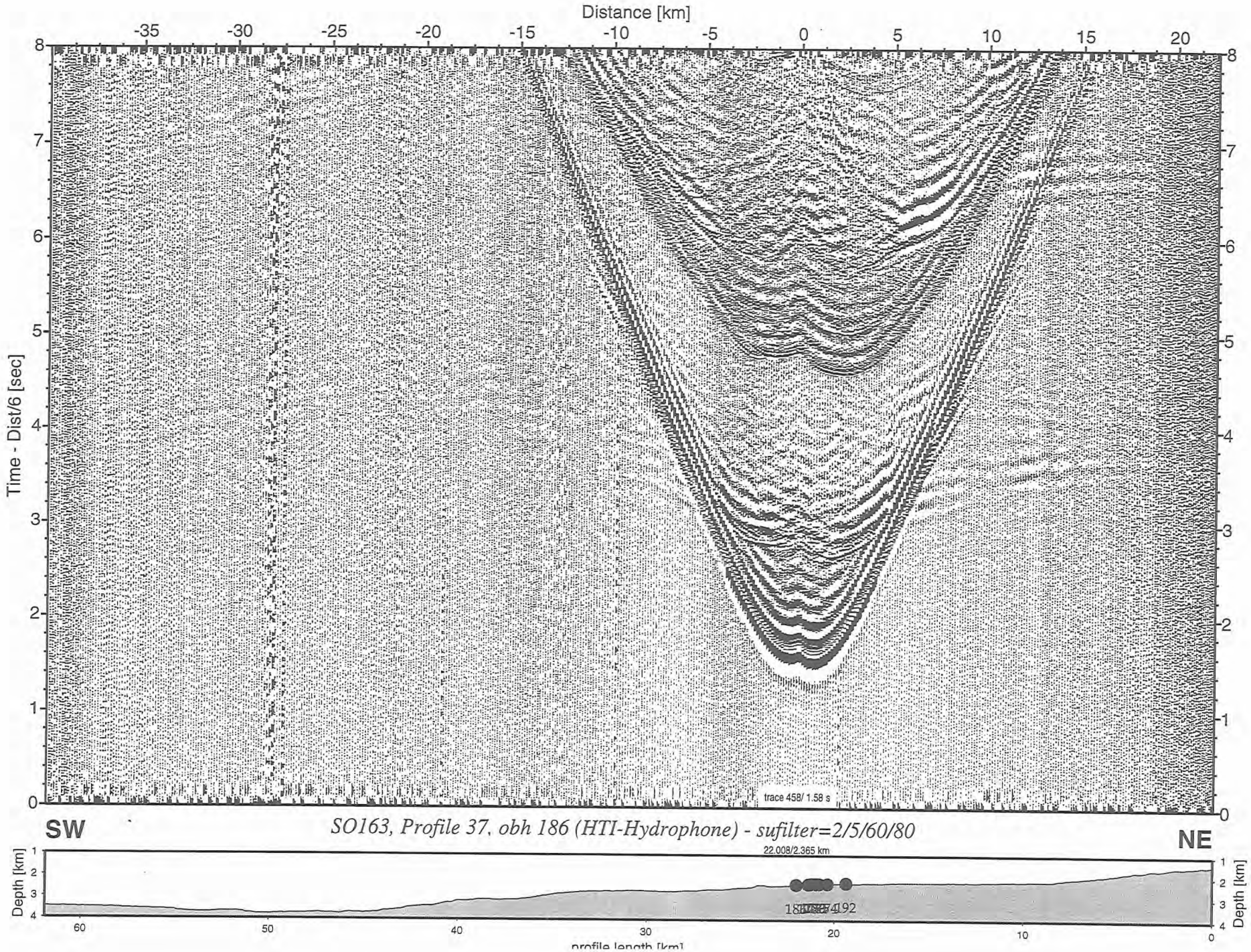


**Figure 6.6.2.45:** Record section from obh 186 (HTI-Hydrophone), Profile 37.

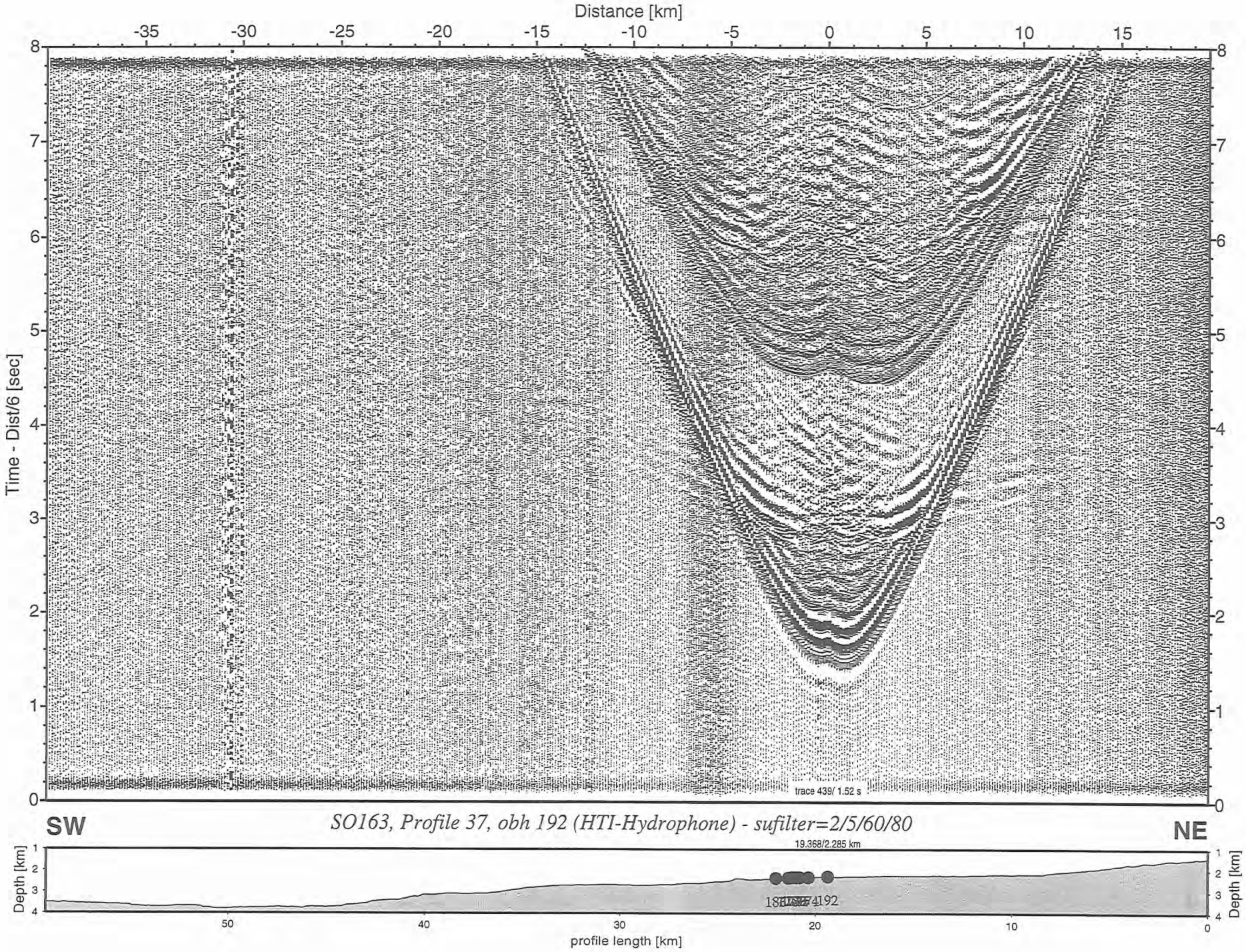


**Figure 6.6.2.46:** Record section from obh 192 (HTI-Hydrophone), Profile 37.

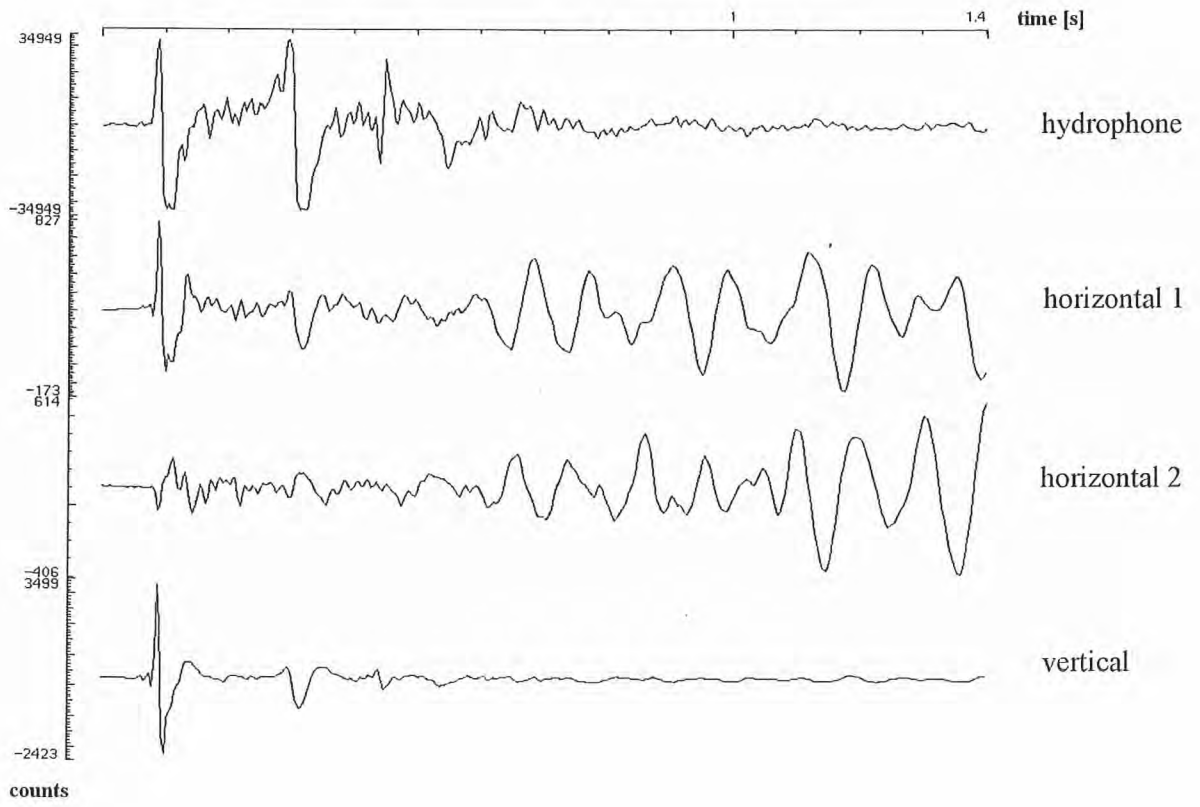


**Figure 6.6.2.47:** Example of unprocessed, trace-normalized components of a short offset recording of OBS31 on line P09. Hydrophone and approximately vertical trace are dominated by the direct wave consisting of three discrete oscillations and the reflected dilatational wave from the BSR with clear negative polarity on the hydrophone trace between second and third oscillation of the source signal. On the hydrophone trace peaks of the direct wave are clipped. On the approximately horizontal components, after the less powerful signature of the source signal, a phase with approximately horizontal polarization (probably a P to S converted phase from the BSR) follows. One might even identify a second shear phase in the coda (which might be a shear wave reflection from the BSR which has been converted into a shear wave already at the seafloor).

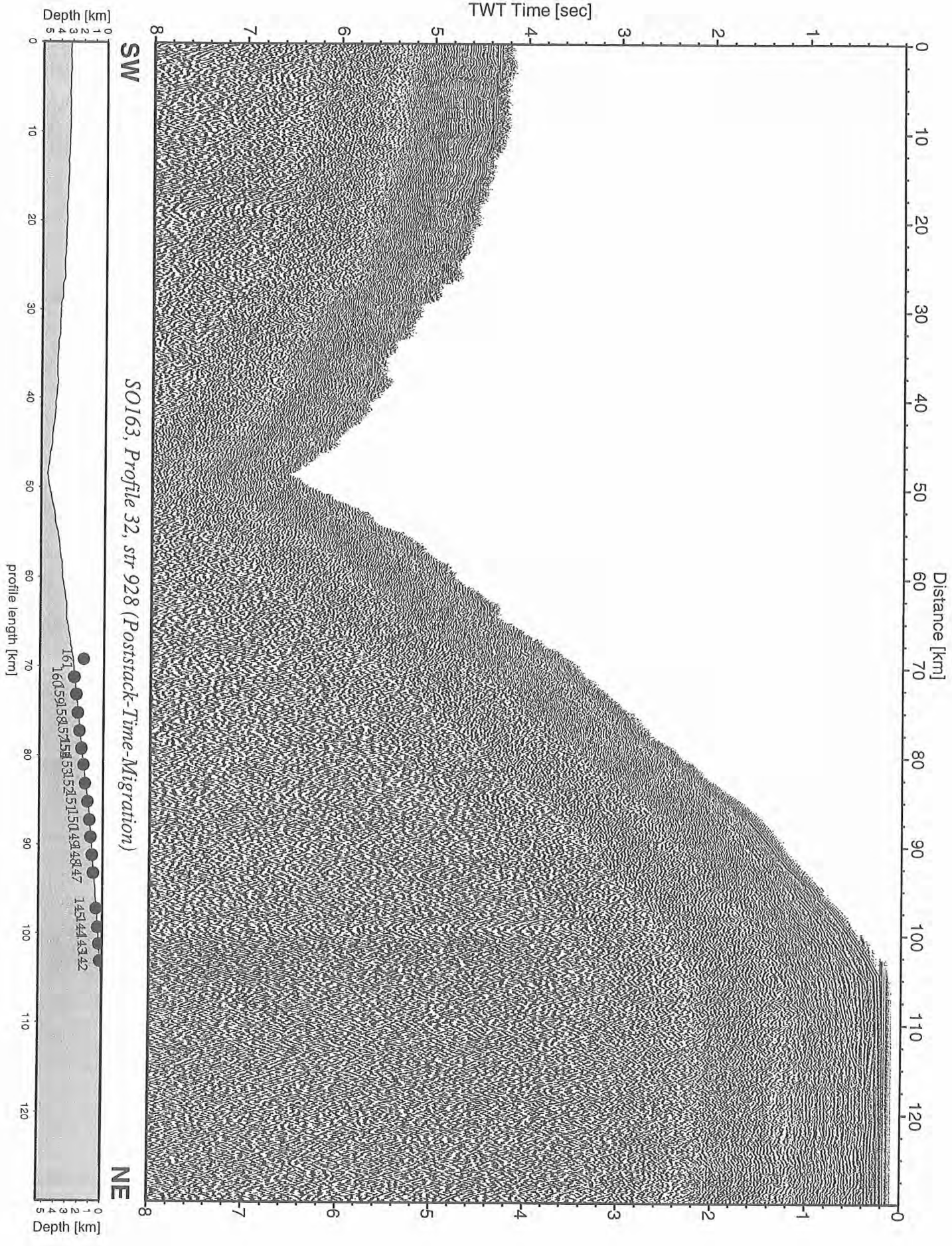


**Figure 6.6.2.48:** Record section from str 928 (Poststack-Time-Migration), Profile 32.

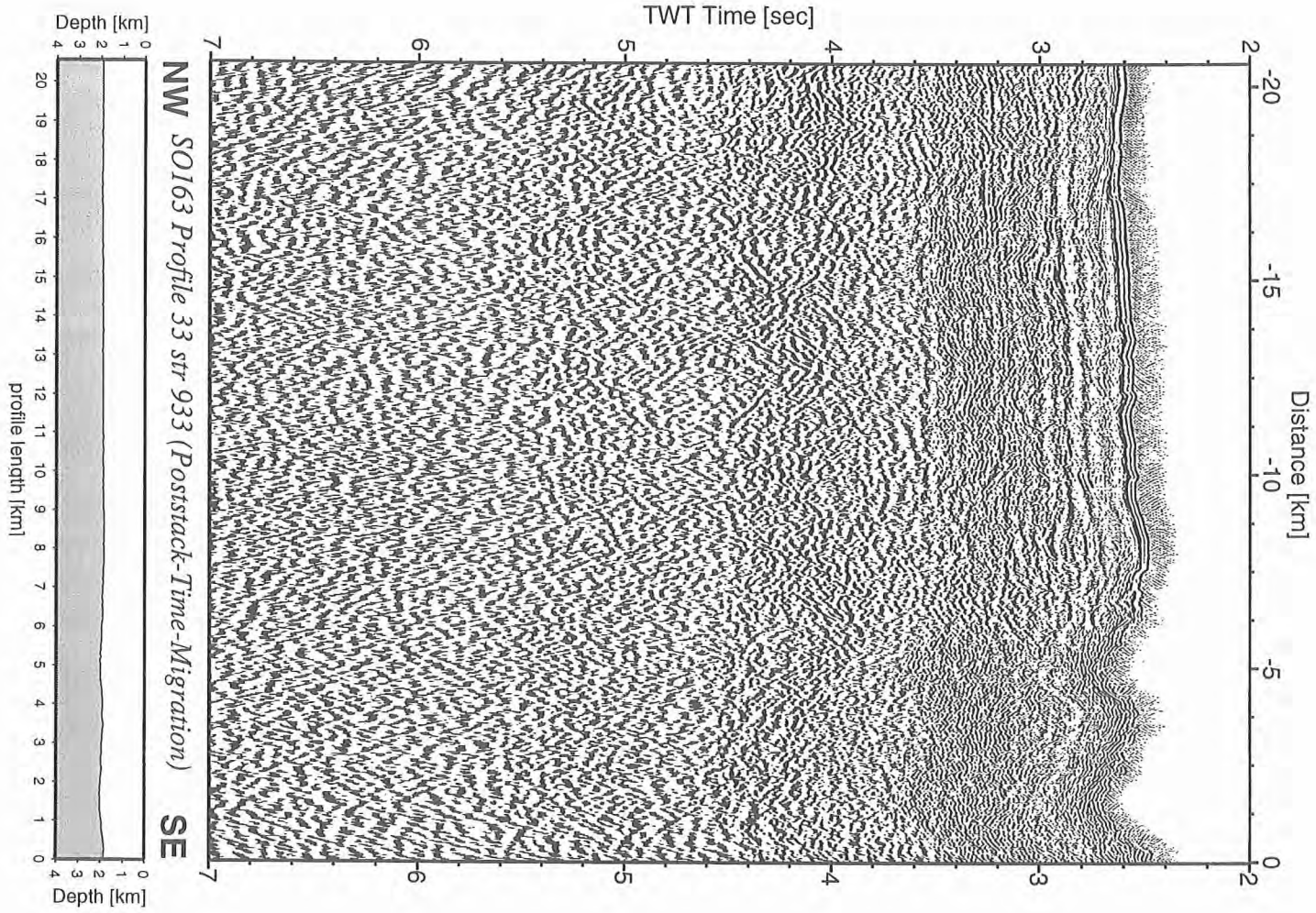


**Figure 6.6.2.49:** Record section from str 933 (Poststack-Time-Migration), Profile 33.

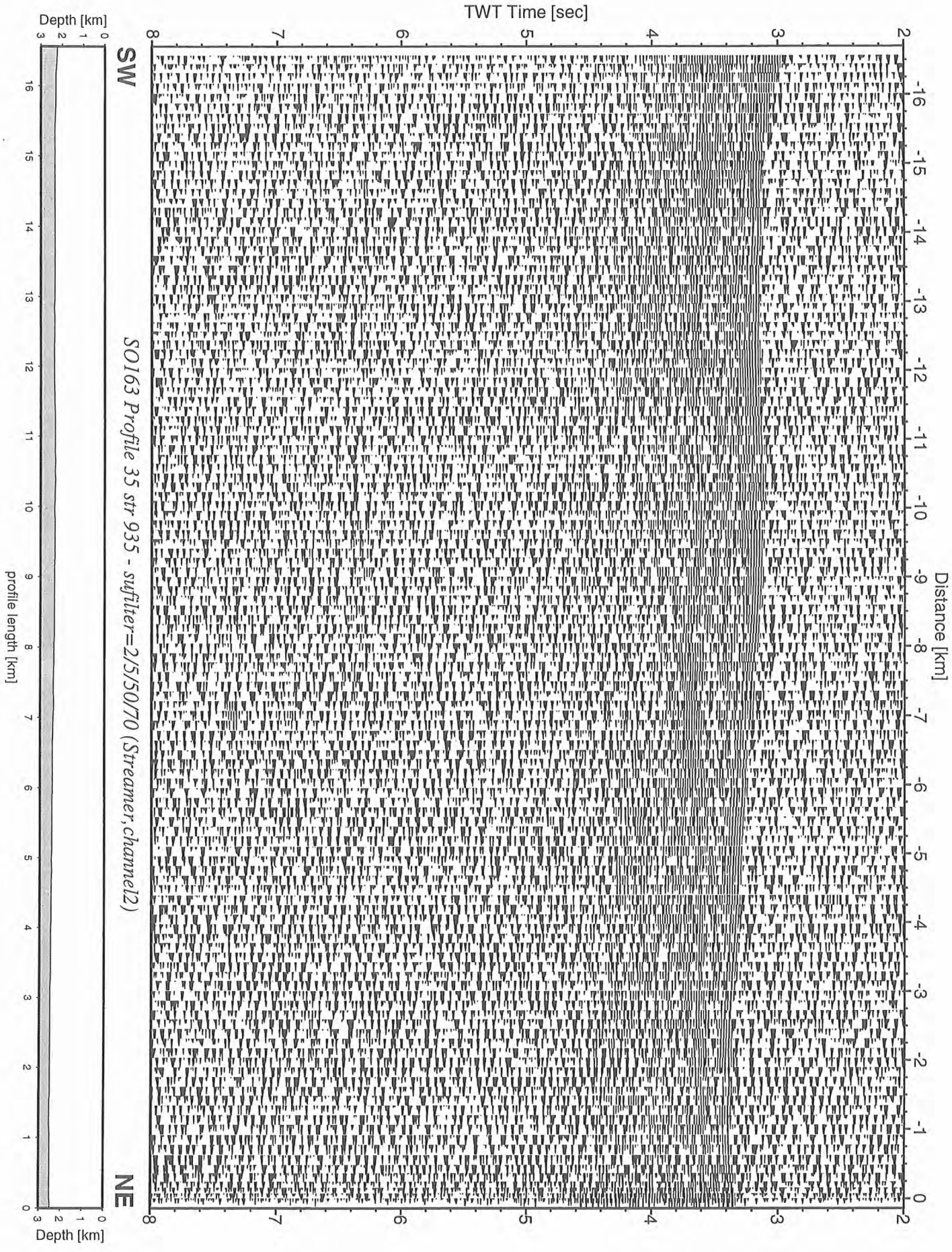


**Figure 6.6.2.50:** Record section from str 935 (Streamer,channel2), Profile 35.

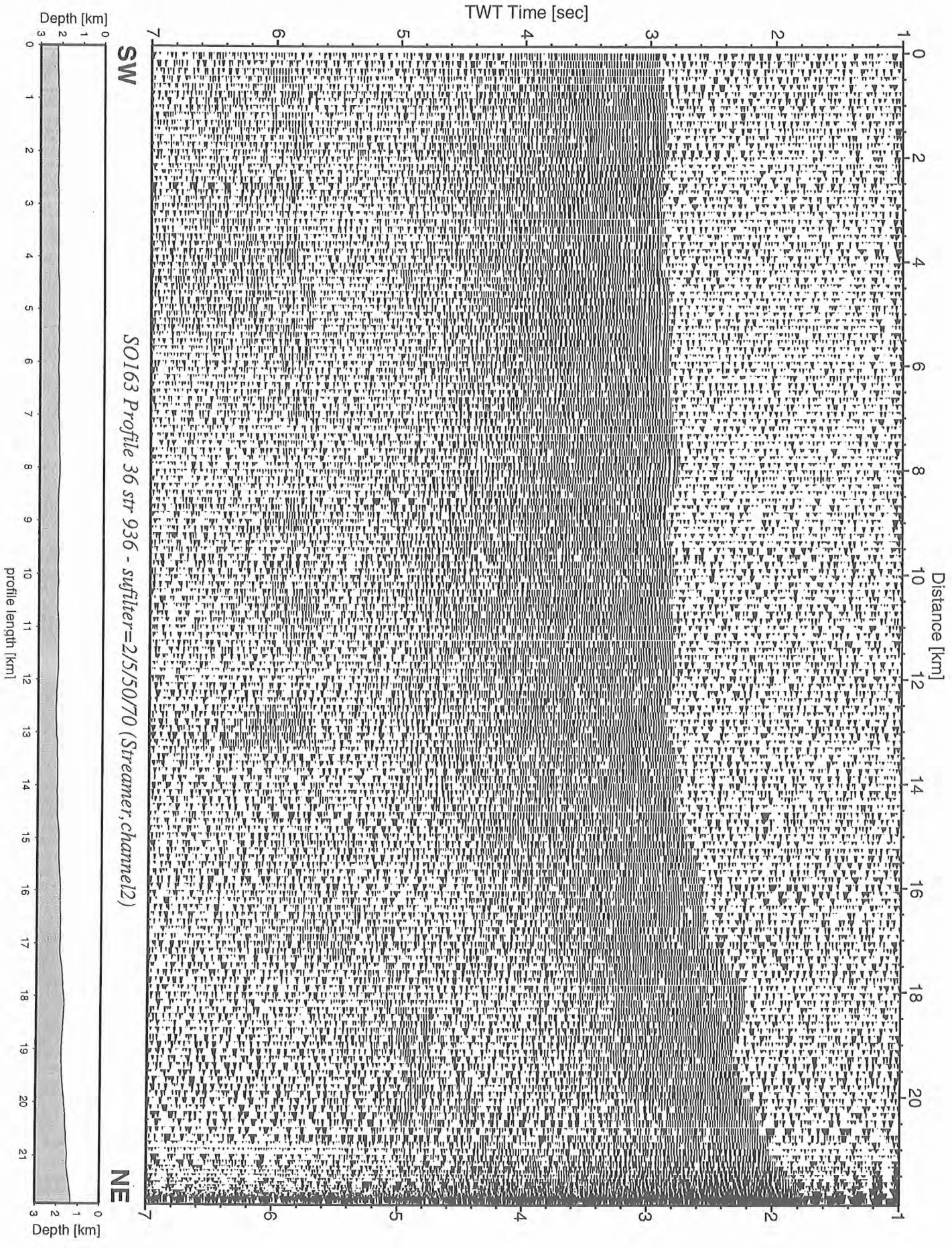


**Figure 6.6.2.51:** Record section from str 936 (Streamer,channel2), Profile 36.

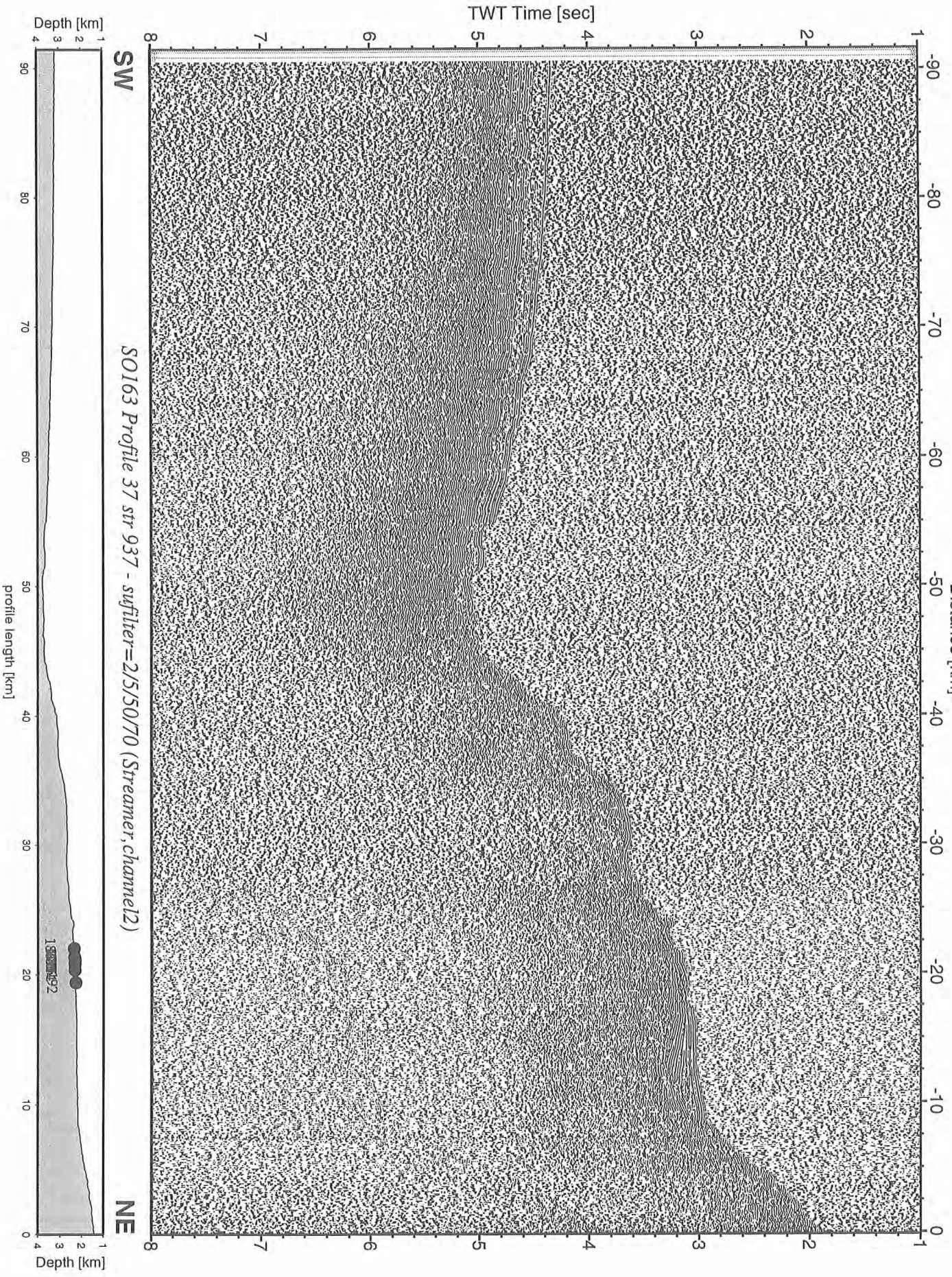


**Figure 6.6.2.52:** Record section from str 937 (Streamer,channel2), Profile 37.

### 6.6.3 The megalens

(M. Schnabel, P.-O. Thierer)

For the first period of the SFB 574, the largely erosive subduction zone off Central America was chosen as the target area for investigation. Concerning the erosion, Ranero & v. Huene (2000) identified two mechanisms: erosion by tunneling and basal removal of rock lenses from the overriding plate. Those megalenses are 10-15 km long and 1.5-2 km high, and they are surrounded by plate-boundary reflections. Seismics and bathymetry show a relative stable slope above these lenses, which is not consistent with a subducting seamount. The megalenses occur at depths at which temperatures indicate that the smectite-illite transition has occured, and the plate interface is entering the zone of stick-slip behaviour. Thus, the lenses could be associated with active erosion in an environment of increasing friction. One such seismic reflection image is shown in Figure 6.6.3.1.

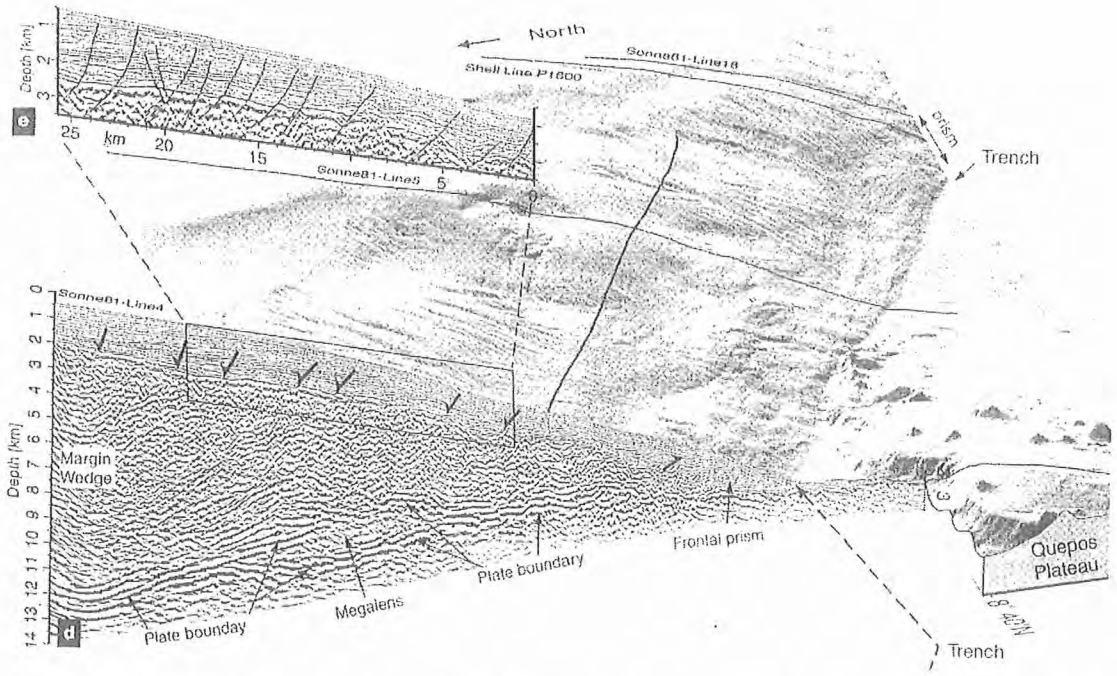


**Figure 6.6.3.1:** Prestack depth migration of SO81 line 4 projected on bathymetry perspectives. Plate-boundary reflections bifurcate at ~ 6km depth and surround a rock megalens (Ranero & v. Huene, 2000).

One of the aims of the subproject A2 within SFB 574 is to map the lateral extend of this megalense and its continouity. The lithological properties causing the surrounding reflections should be investigated. With the new data collected on SO163-2, we will be able to perform AVO-analysis to describe these reflections in greater detail.
Based on the results of Ranero & v. Huene (2000), we decided to collect seismic wide-angle data in the surrounding of profile 5 of Sonne-Cruise SO81. Four profiles were layed out, with a minimum of at least 9 OBH and 5 OBS. Along each line, several airgun configurations were used (see App. 9.5.4 to 9.5.6 and 9.6 for details on instrumentation and shots). In Figure 6.6.3.2 the location of the profiles and instruments are given. Selected record sections are shown in Figures 6.6.3.3 to 6.6.3.82.
The data quality along all profiles was quiet good. Only a few stations situated on the uppermost slope near the shore showed only short offsets. All other stations recorded shots over large distances (up to 50 km). Onboard forward modelling with the ray tracing application „MacRay“ (Luetgert 1992) resulted in the velocity-depth models shown in Figure 6.6.3.84 and Figure 6.6.3.87.

The principal geometry as deduced from the ray tracing show good agreement. The topmost layers are interpreted as sediments. The upper one shows P-wave velocities ranging from 1.6 to 2.0 km/s and has a thickness up to about 1000m. The velocity in the second layer is significant higher (2.5 to 4.0 km/s), and could therefore be interpreted as compacted and cemented sediments.
Refractions from the margin wedge are seen in all of the records. The velocity in the outer wedge is about 3.5km/s, increasing up to 4.2 near the coast. The velocity at the lower end of the wedge ranges from 4.0 km/s near the trench up to 4.8km/s.
For a few stations, reflections from the Mohorovičič-discontinuity could be identified (Figure 6.6.3.83a). The velocity of the oceanic layer 3 ranges from 6.0 to 6.9 km/s and the Moho is situated at a depth of 12.5 km at 30 km landward behind the trench.

## Profile P22, SO 163-2

(I. Arroyo, H. Kopp, E. Flueh)

Profiles 19 and 21-23 were carried out as part of the detailed research focusing around the megalense and the Quepos mound. The location map with bathymetric lines every 100 m is shown in Figure 6.6.3.2. These profiles consisted of 15 OBHs (from 76 to 90), with an average offset between stations of 1,5 nm (2,7 km) for a total length of almost 40 km with an orientation NW-SE, parallel to the trench axis. Details and coordinates of the stations could be found in Appendix 9.5.4.

The shooting of the profiles were performed by using different airguns arrays: Prakla array with a trigger interval of 10 s (profile 19), 32 l airgun (profiles 21 and 23) and G-Gun (profile 22) with trigger interval of 30 s. The records were stored and processed as described in Section 6.6. The clearest records were obtained with profile 22 (Figure 6.6.3.49 to 6.6.3.63), which is the one analyzed on board.

The profiles were located over the upper continental slope, with OBHs at depths ranging from 960 to 1350 m. This sector is part of the broad embayment in the upper and middle slope that opposite the subduction of the Quepos Plateau. Here, the margin slope is characterized also by deep canyons that end at the upper part of the frontal prism of the margin (von Huene et al., 2000).

Profil 22 shows high quality data. Due to the relative similarity of the records and the limited time on board, only the phase arrivals of three stations (OBH 76, 80 and 86) were picked in order to achieve 1-D velocity models. OBH 80 shows one of the most interesting and rich records (see Figure 6.6.3.51). The pickings of the record are shown in Figure 6.6.3.86, together with the predicted arrivals modeled with the program R1D (Luetgert, 1992). A very good correlation between the observed and the predicted arrivals was achieved (Figure 6.6.3.86). From this 1-D modeling, the following layers were detected (Figure 6.6.3.86):

| **Depth (m)** | **P velocity (km/s)** |
|---|---|
| 0 – 1 350 (water) | 1,500 |
| 1 350 – 1 664 | 1,550 |
| 1664 – 2 401 | 1,633 – 1,867 |
| 2 401 – 3 156 | 3,467 – 4,067 |
| 3 156 – 6415 | 4,300 – 5,400 |
| 6 415 – 6 621 | 4,833 |
| 6 621 – 10 669 | 5,467 – 5,533 |
| 10 669 – 12 487 | 6,333 – 6,533 |

There is a top cover of about 300 m of slope sediments (1,6 km/s), underlayed by another sedimentary section of about 700 m with velocities increasing from 1,6 to 1,9 km/s. Below this sedimentary layers, velocities raise up to 3,5 km/s at a depth of 3 km and increase to 5,5 km/s at 10 km. These velocities may correspond to the presence of igneous rocks of the Nicoya Complex. There is a 200-m thick low-velocity layer at a depth of around 6,5 km, included to explain a strong reflection at about 3 s reduced travel time. In this sector of the continental margin, the plate boundary is at 11-12 km depth, according to the seismic line 4 (Figure 6.6.3.1) of the leg Sonne 81 (Ranero & von Huene, 2000). The model presented here shows another pronounced discontinuity at this depth.

The streamer record of this profile is also in concordance with the described model. Figure 6.6.3.81 shows an upper well-layered sedimentary cover, with some disturbances to the SE, approaching the erosional scarp that represents the edge of the embayment. This layer fits the described velocities from 1,6 to 1,9 km/s. A strong reflection comes from a depth of about 3 s that coincides with the strong change in velocities.

These results are in agreement with the continental margin configuration proposed by von Huene & Flueh (1994) and Hinz et al. (1996) for Costa Rica, where the subduction erosion is the dominant process.

## Profile 18, SO 163-2

(Fekete, N.)

Profile P18, with a total length of 53.058 km, was acquired using the bolt gun in a NW-SE direction, parallel to the trench axis as well as to profiles P21-23 and crossing the profile P24 approximately at its middle. The data of 13 instruments (OBH62 – 69 and OBH 71 – 75) were of good quality, showing offsets of up to 50 km. The distance between the instruments was approximately 3.5 km.

Onboard forward modelling with the ray tracing application „MacRay" (Luetgert 1992) resulted in the velocity-depth model shown in Figure 6.6.3.85. The uppermost two layers are identified as sedimentary, and have velocities of 1.6 – 2.1 km/s and 3.1-4.3 km/s and thicknesses of about 1 and 1.5 km, respectively. The sediments show a topographic stepdown in the middle of the profile, accompanied by an increase in velocity. The next layer is interpreted as the wedge, with seismic velocities ranging from 4.4 – 4.9 km/s and a thickness of 3 km. Beneath that, a 4-km thick oceanic upper crust is found, characterised by a velocity between 5.0 – 5.2 km/s. The topography of these latter two layers do not reflect that of the sediments. At a depth of about 9.5 km, a layer of 5.5 - 6.2 km/s can be found. This is interpreted as the oceanic basement, and reaches a thickness of as much as 7 km, down to the seismic boundary at a depth of 15.5 km that is thought to be the Mohorovičič discontinuity.

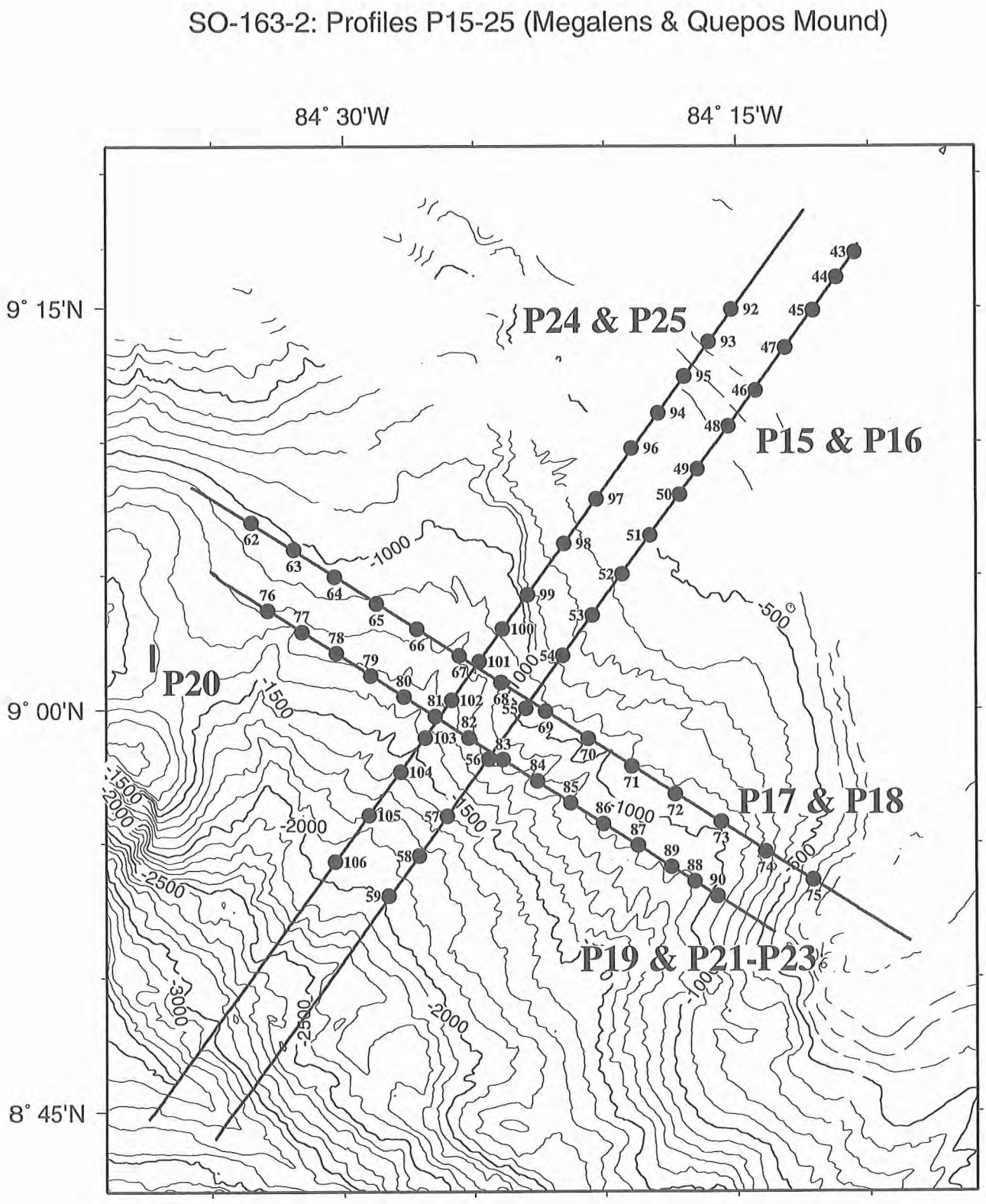


**Figure 6.6.3.2:** Location map of profiles P15-P25 with 100 m isolines. Stations OBH43-OBH57 (profiles P15 and P16), OBH62-OBH75 (profiles P17 and P18), OBH76-OBH90 (profiles P19-P23) and OBH92-OBH106 (profiles P24 and P25) are superimposed.

**Figure 6.6.3.3:** Record section from obh 43 (OAS-Hydrophone), Profile 15.

**Figure 6.6.3.4:** Record section from obh 44 (OAS-Hydrophone), Profile 15.

**Figure 6.6.3.5:** Record section from obh 45 (OAS-Hydrophone), Profile 15.

**Figure 6.6.3.6:** Record section from obs 46 (HTI-Hydrophone), Profile 15.

**Figure 6.6.3.7:** Record section from obs 47 (HTI-Hydrophone), Profile 15.

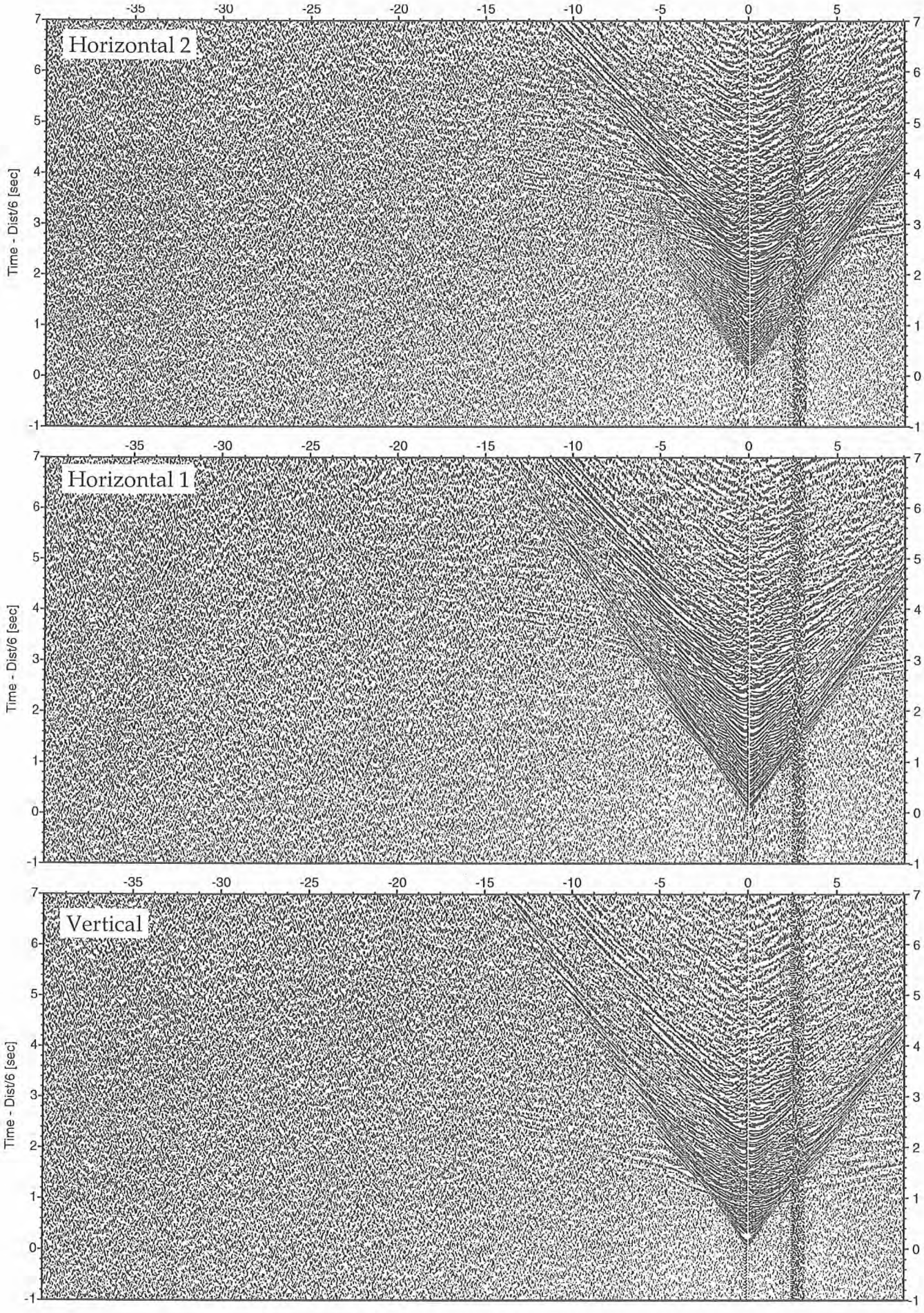


**Figure 6.6.3.8:** Record sections from obs 47 (Owen-30Hz), SO163, Profile 15.

**Figure 6.6.3.9:** Record section from obs 48 (HTI-Hydrophone), Profile 15.

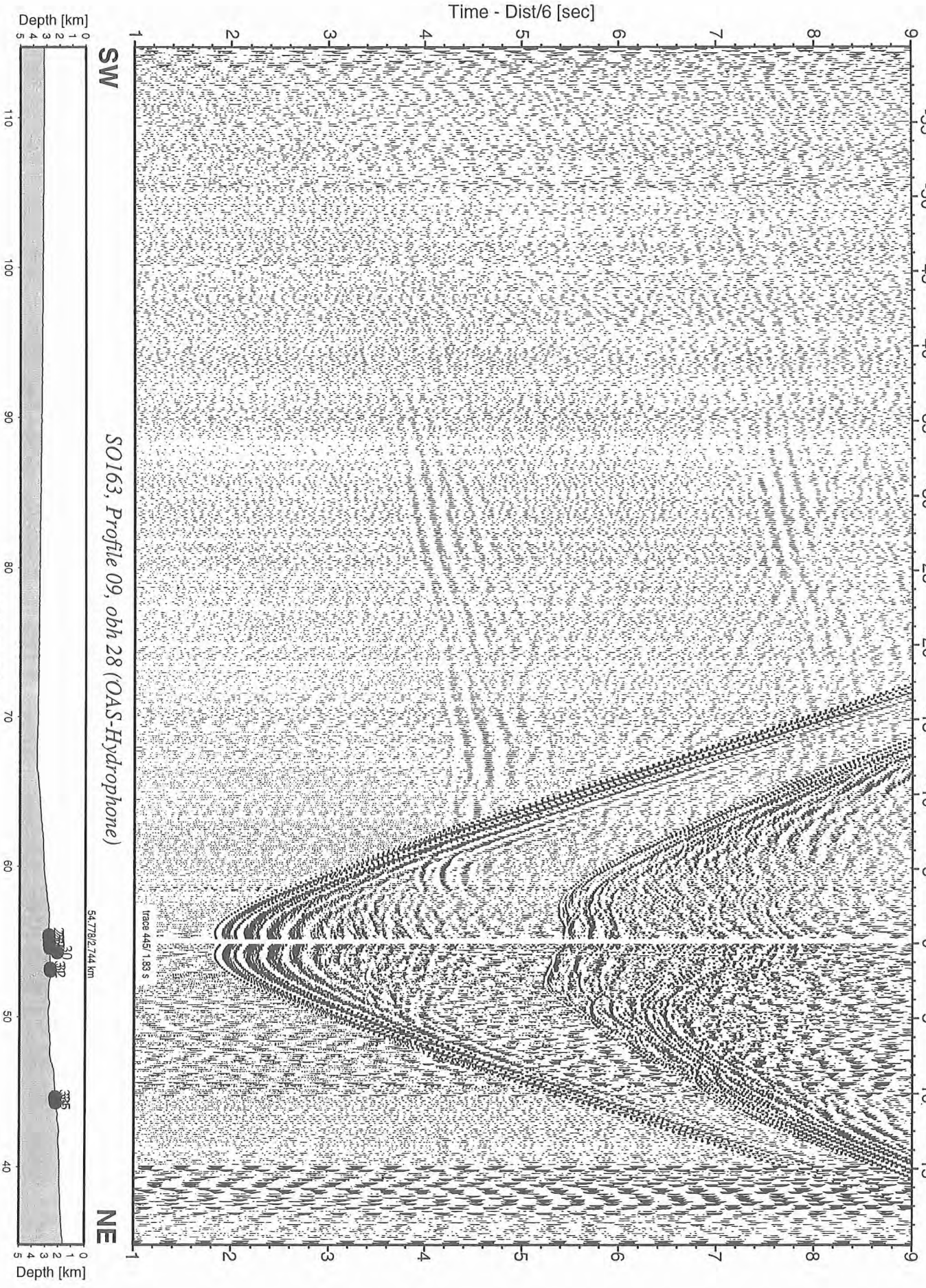


**Figure 6.6.2.6:** Record section from obh 28 (OAS-Hydrophone), Profile 09.

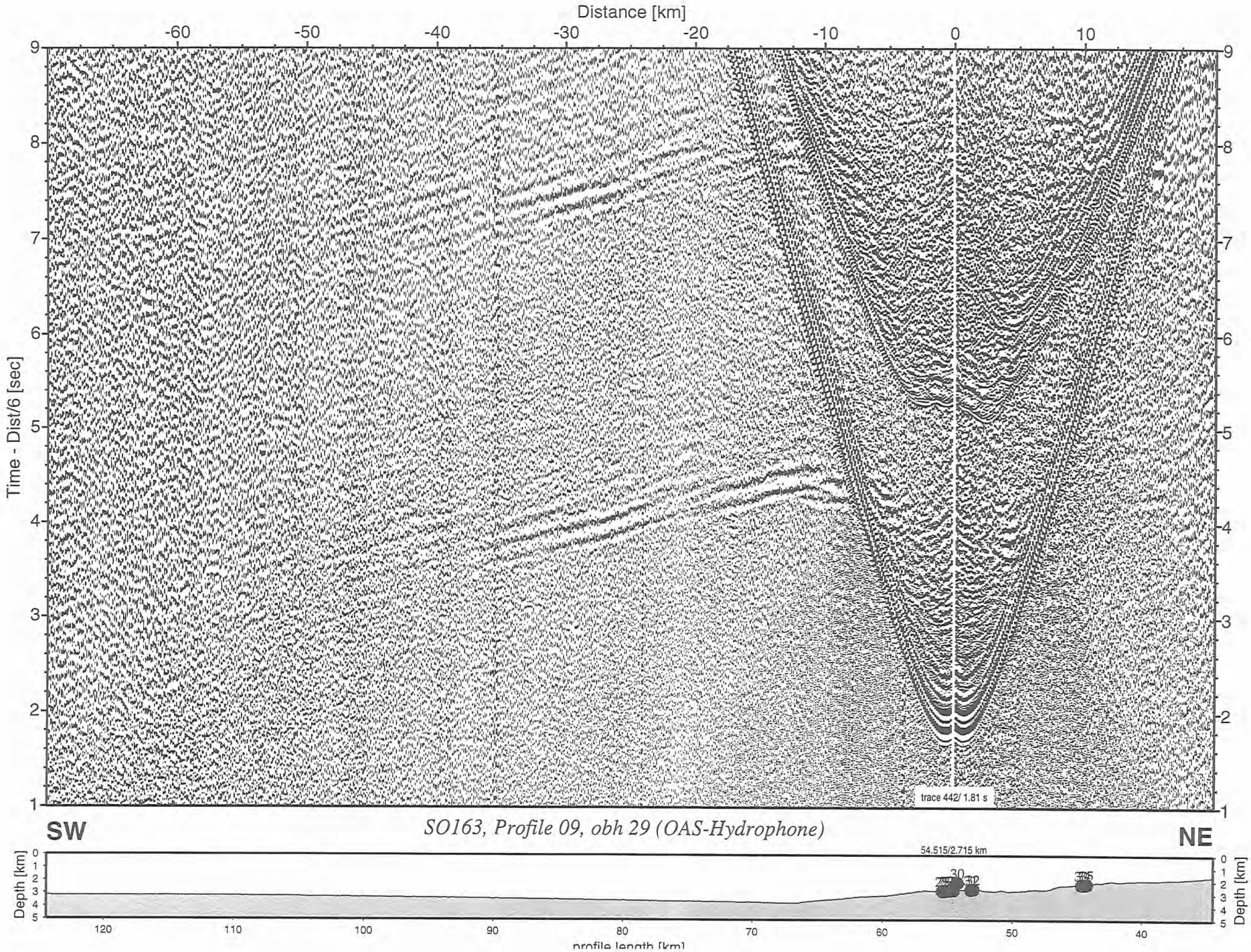


**Figure 6.6.2.7:** Record section from obh 29 (OAS-Hydrophone), Profile 09.

**Figure 6.6.2.8:** Record section from obh 30 (OAS-Hydrophone), Profile 09.

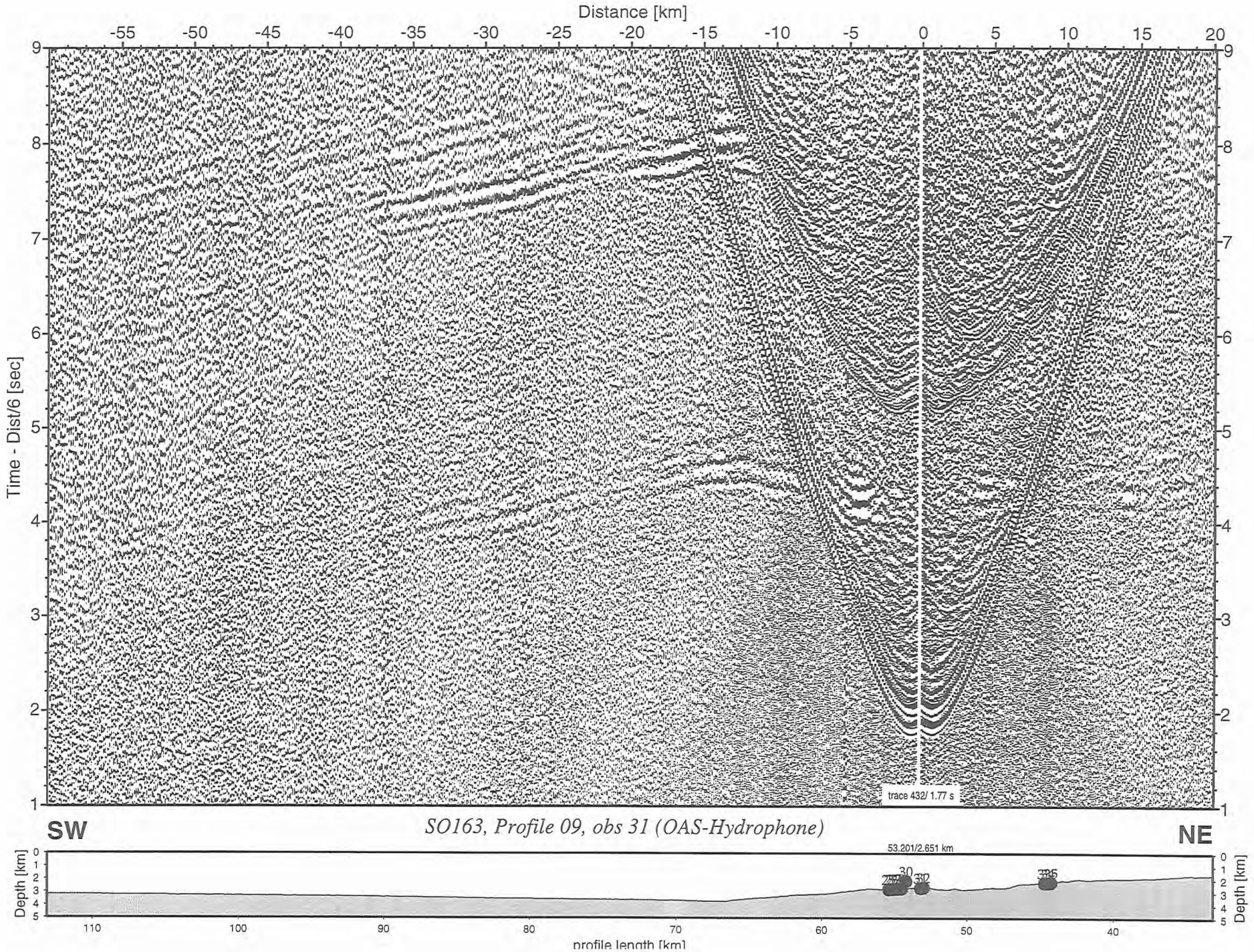


**Figure 6.6.2.9:** Record section from obs 31 (OAS-Hydrophone), Profile 09.

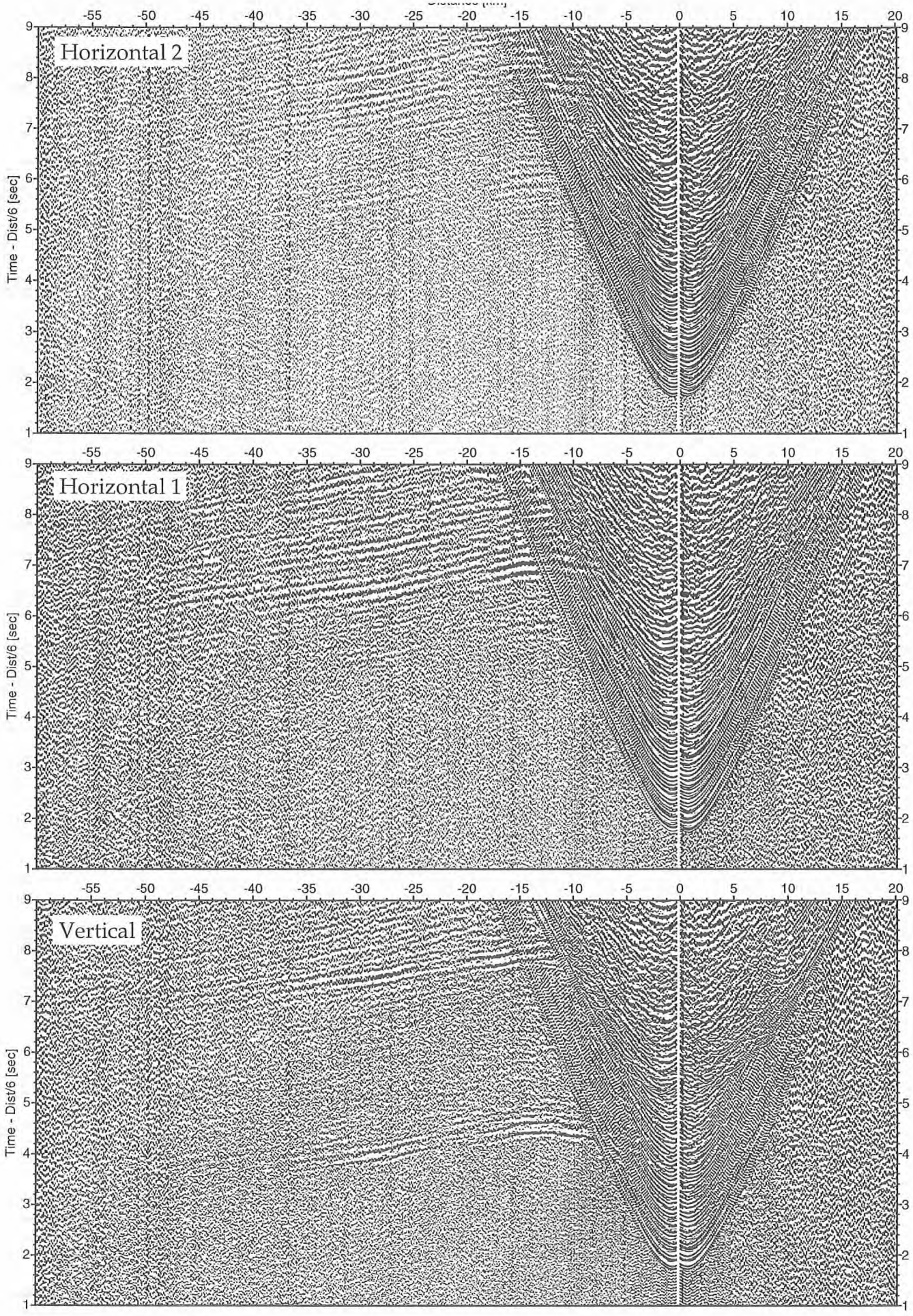


**Figure 6.6.2.10:** Record sections from obs 31 (Owen-4.5Hz), SO163, Profile 09.

**Figure 6.6.2.11:** Record section from obh 32 (OAS-Hydrophone), Profile 09.

**Figure 6.6.2.12:** Record section from obh 33 (OAS-Hydrophone), Profile 09.

**Figure 6.6.2.13:** Record section from obs 34 (HTI-Hydrophone), Profile 09.

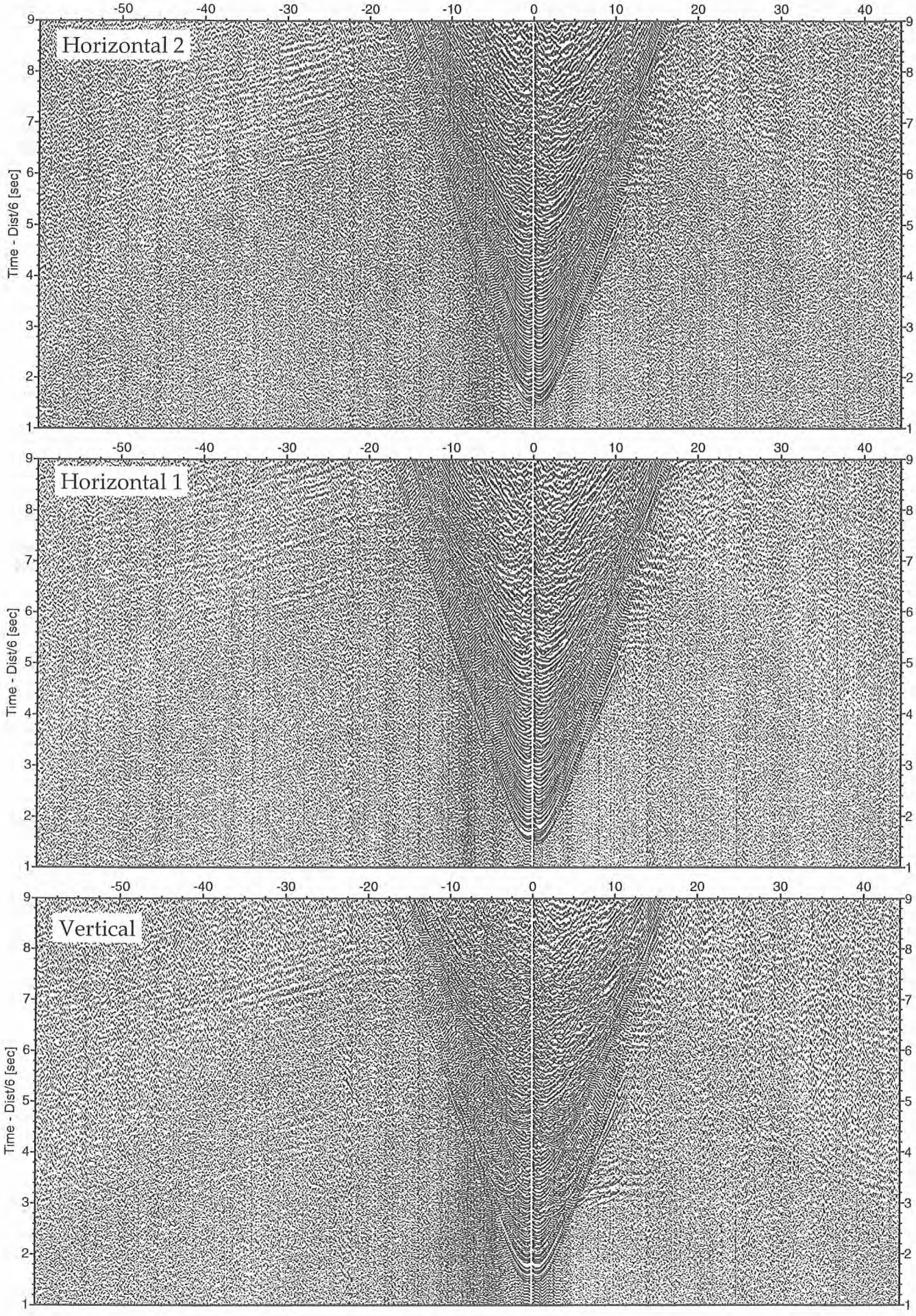


**Figure 6.6.2.14:** Record sections from obs 34 (Owen-4.5Hz), SO163, Profile 09.

**Figure 6.6.2.15:** Record section from obh 35 (HTI-Hydrophone), Profile 09.

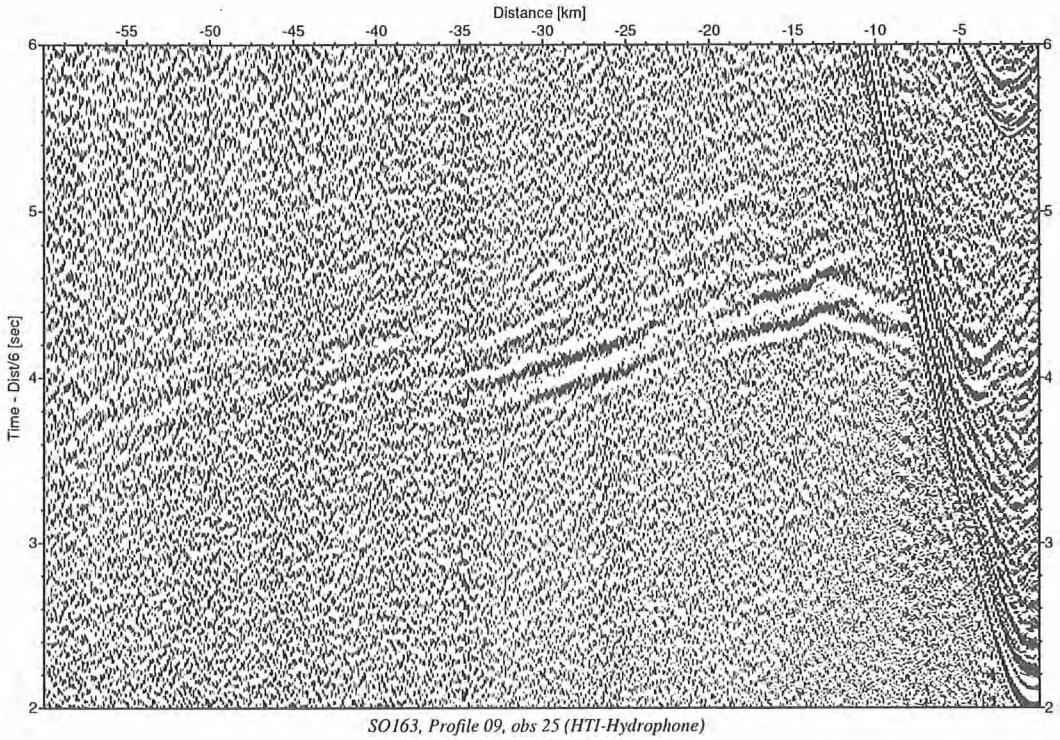


*SO163, Profile 09, obs 25 (HTI-Hydrophone)*

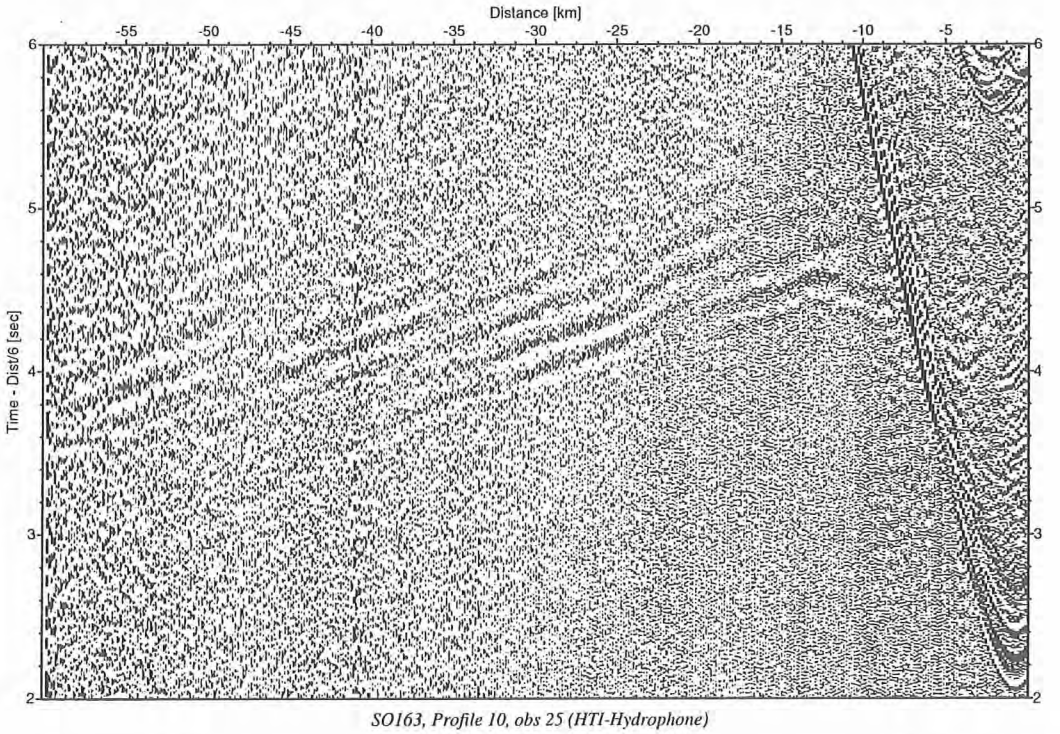


*SO163, Profile 10, obs 25 (HTI-Hydrophone)*

**Figure 6.6.2.16.:** Comparison between profiles P09 (Bolt gun) and P10 (G-gun) for station OBS 25.

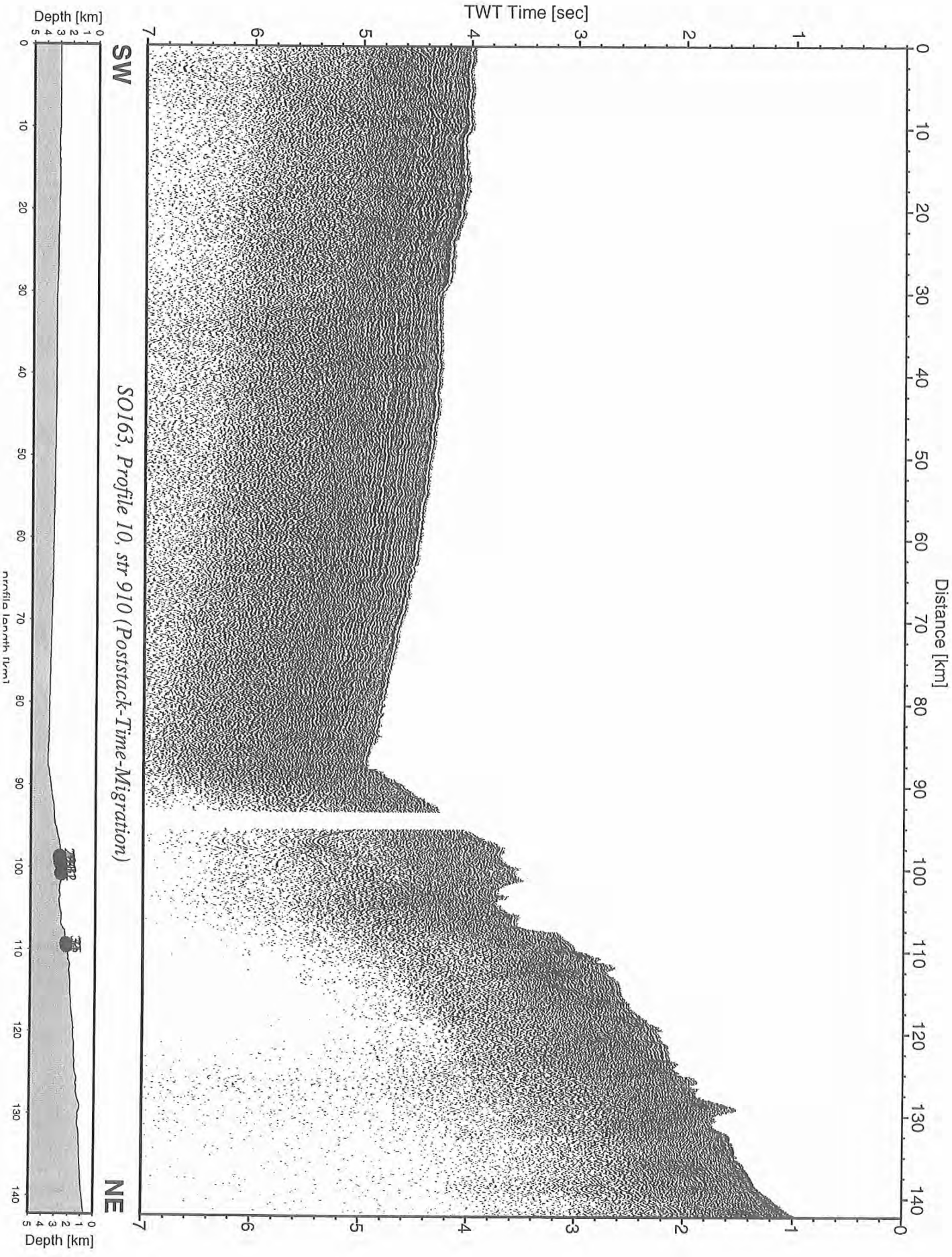


**Figure 6.6.2.17:** Record section from str 910 (Poststack-Time-Migration), Profile 10.

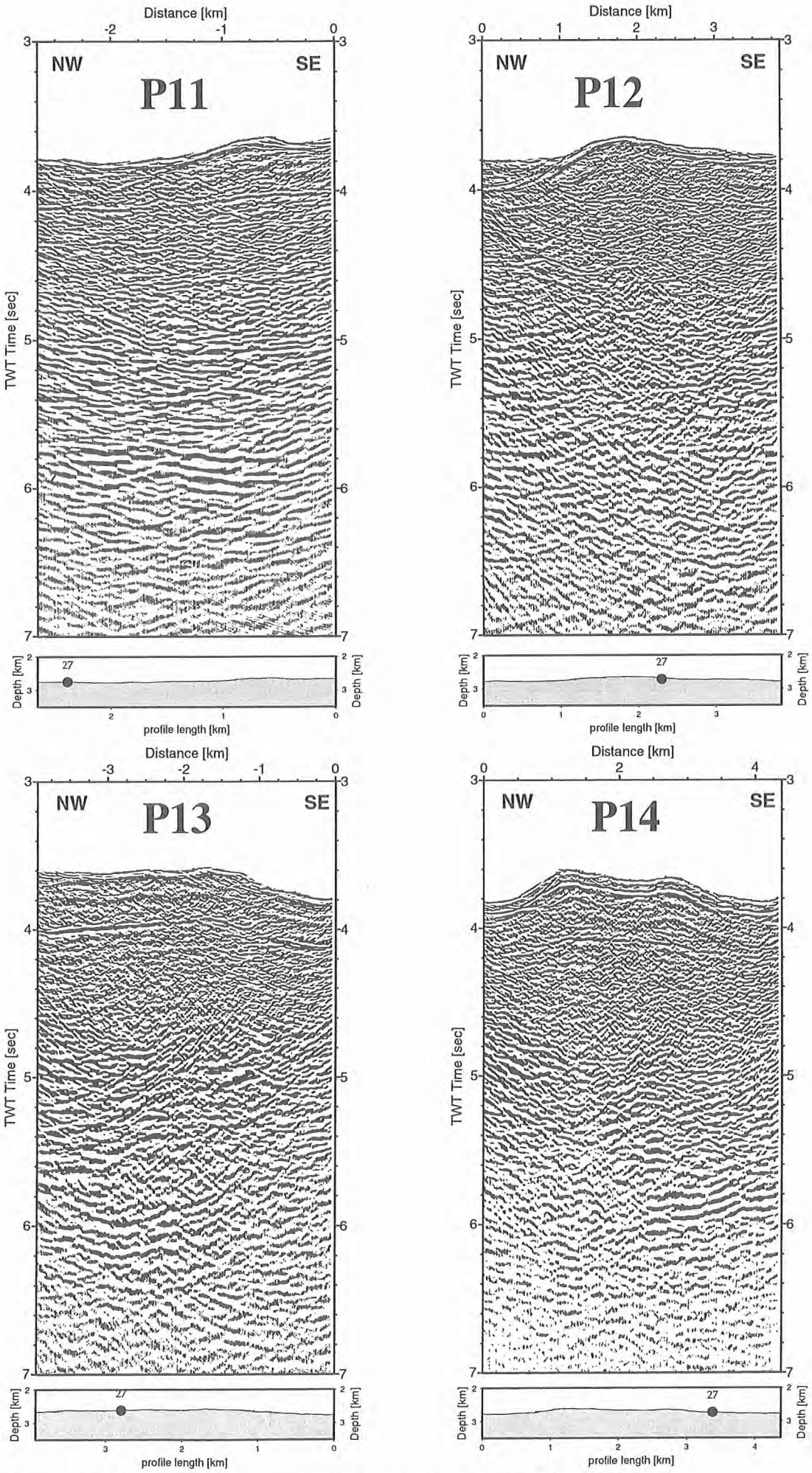


**Figure 6.6.2.18:** Post-stack time migrated sections for profiles P11-P14.

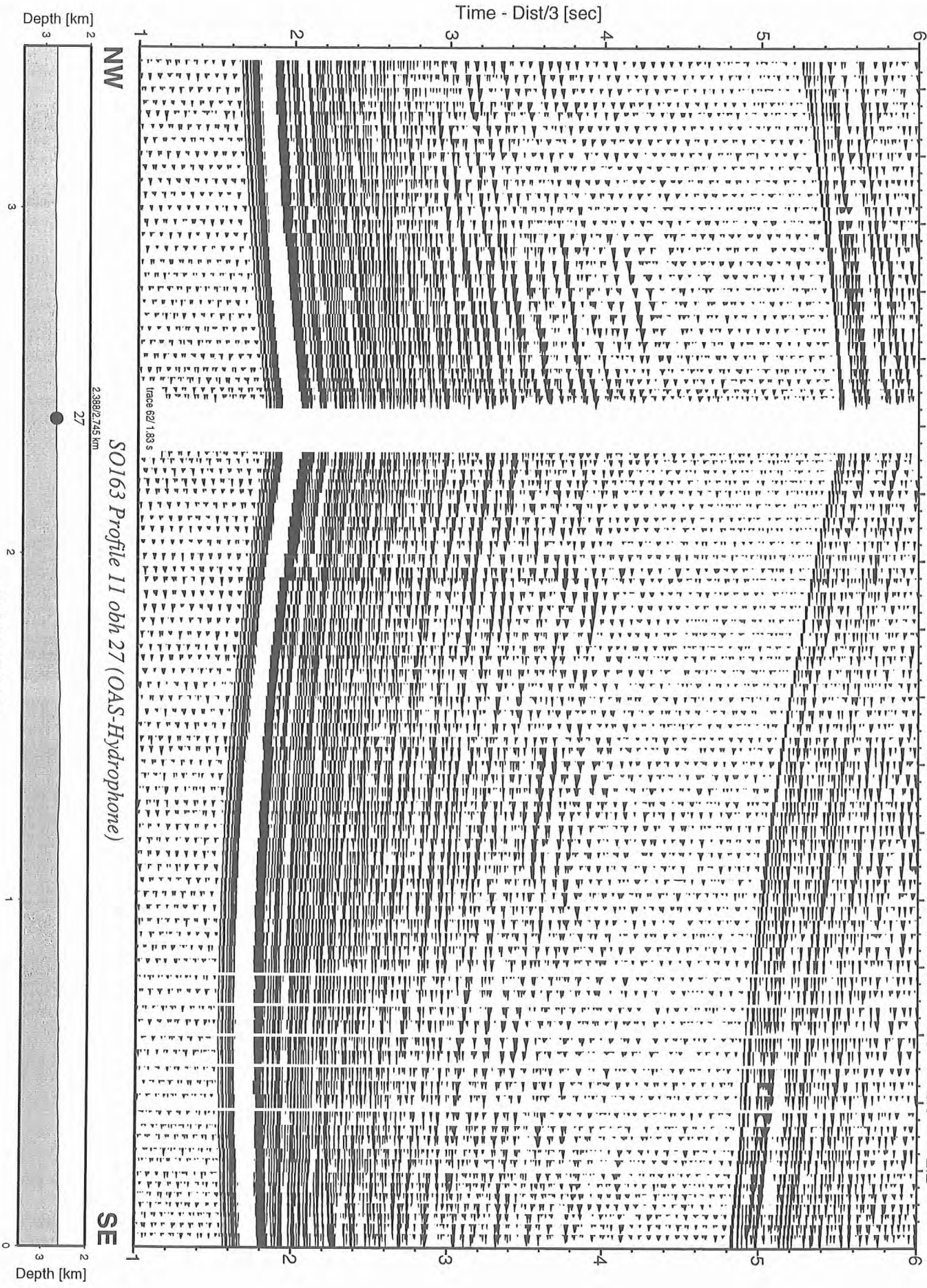


**Figure 6.6.2.19:** Record section from obh 27 (OAS-Hydrophone), Profile 11.

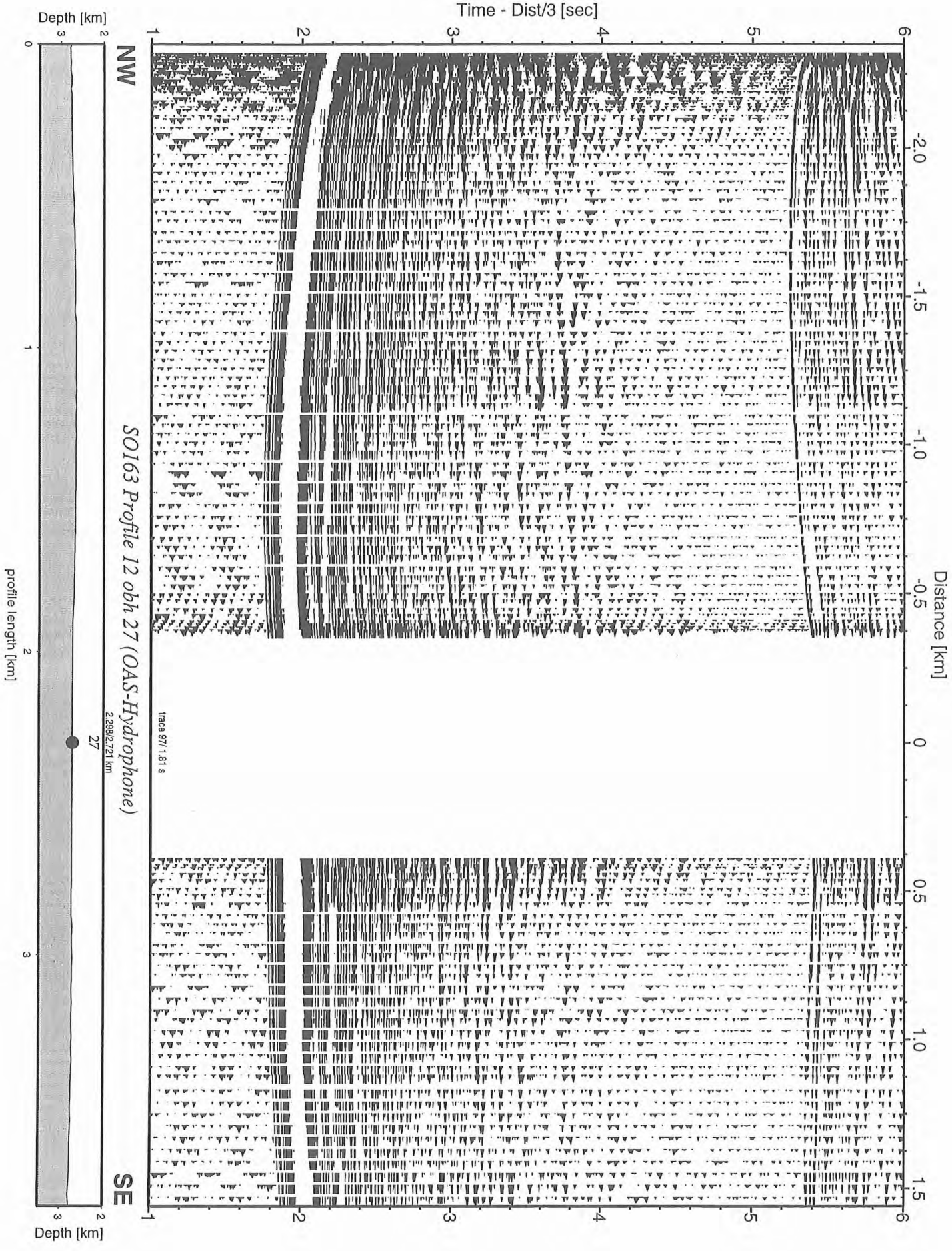


**Figure 6.6.2.20:** Record section from obh 27 (OAS-Hydrophone), Profile 12.

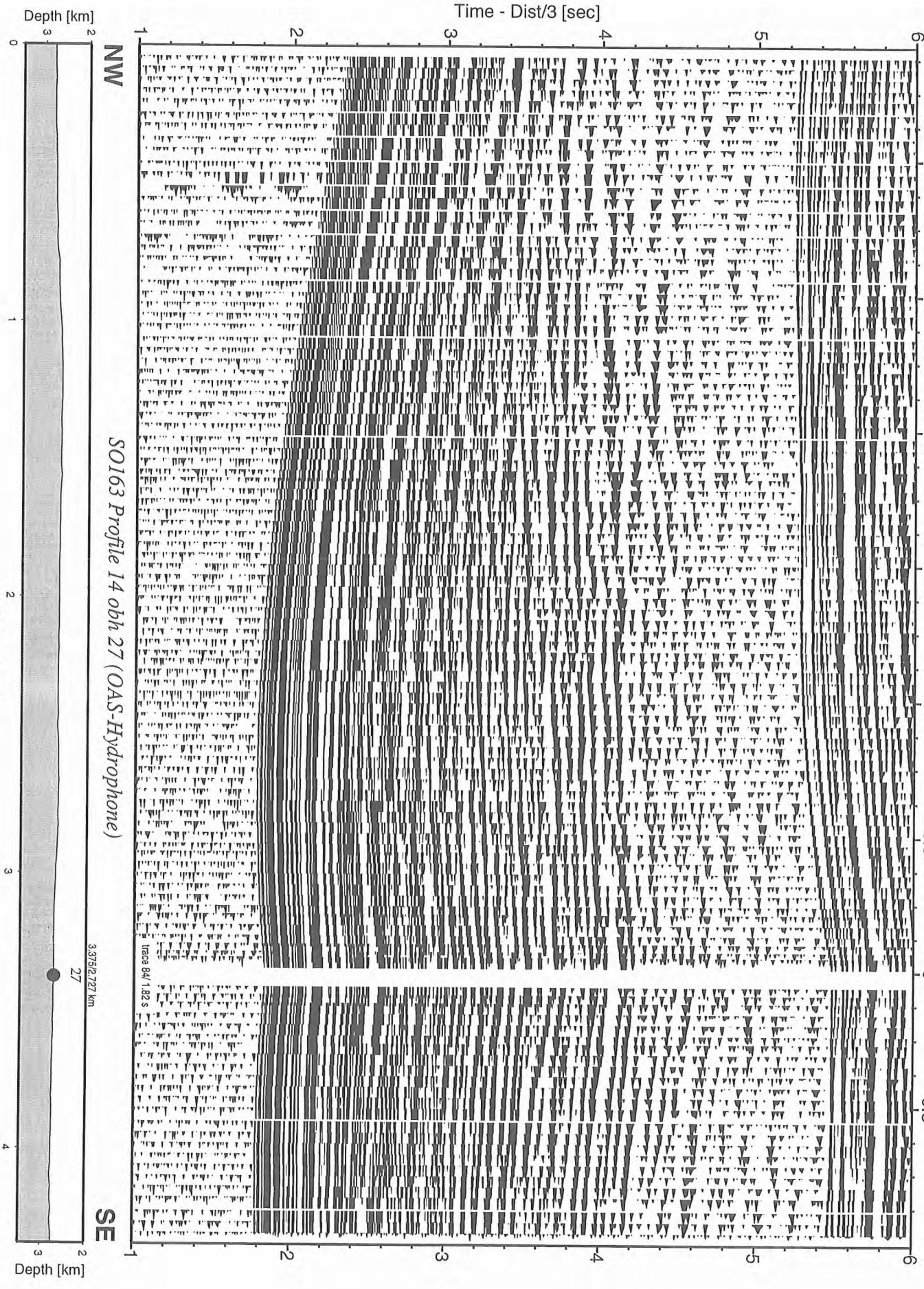


**Figure 6.6.2.21:** Record section from obh 27 (OAS-Hydrophone), Profile 14.

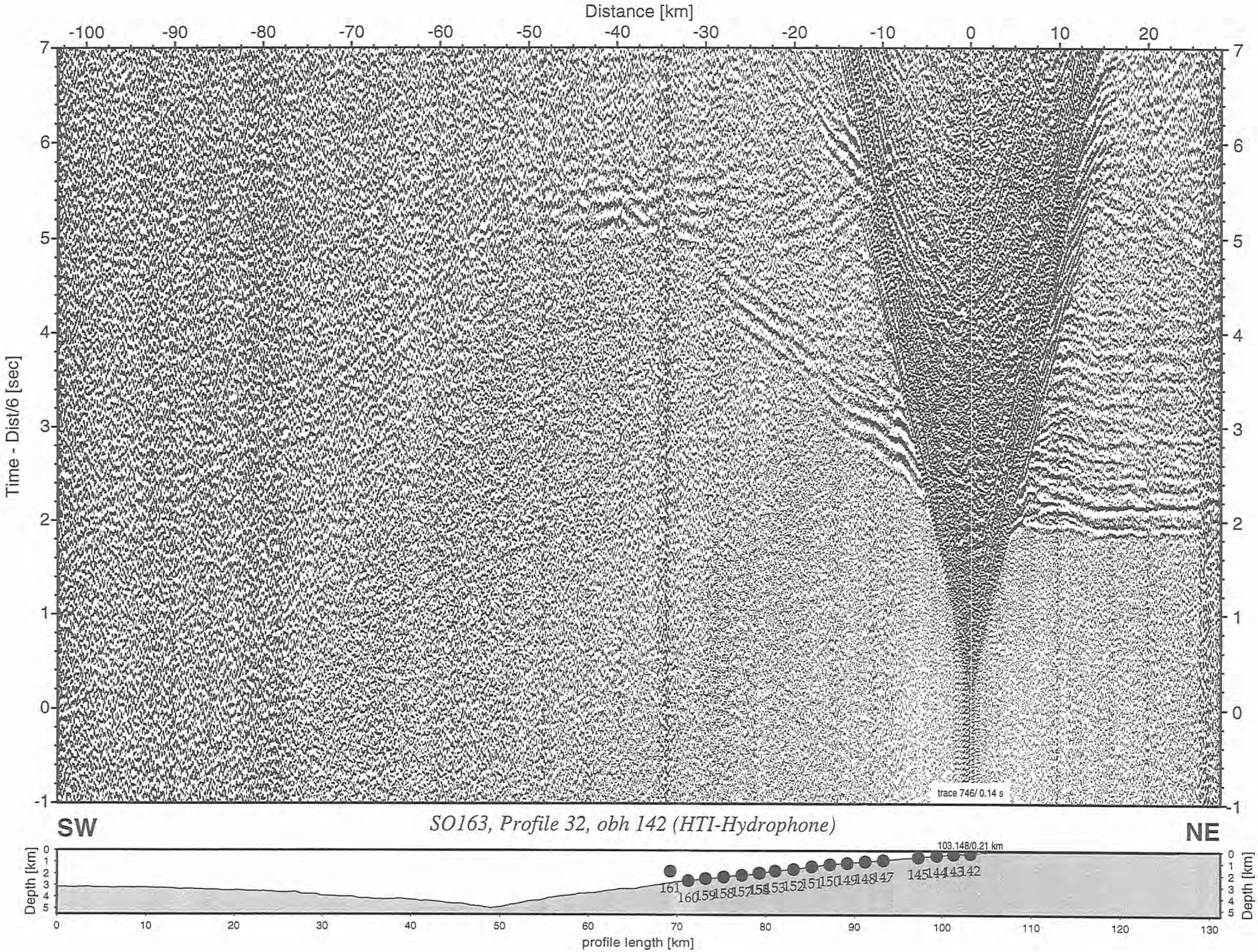


**Figure 6.6.2.22** Record section from obh 142 (HTI-Hydrophone), Profile 32.

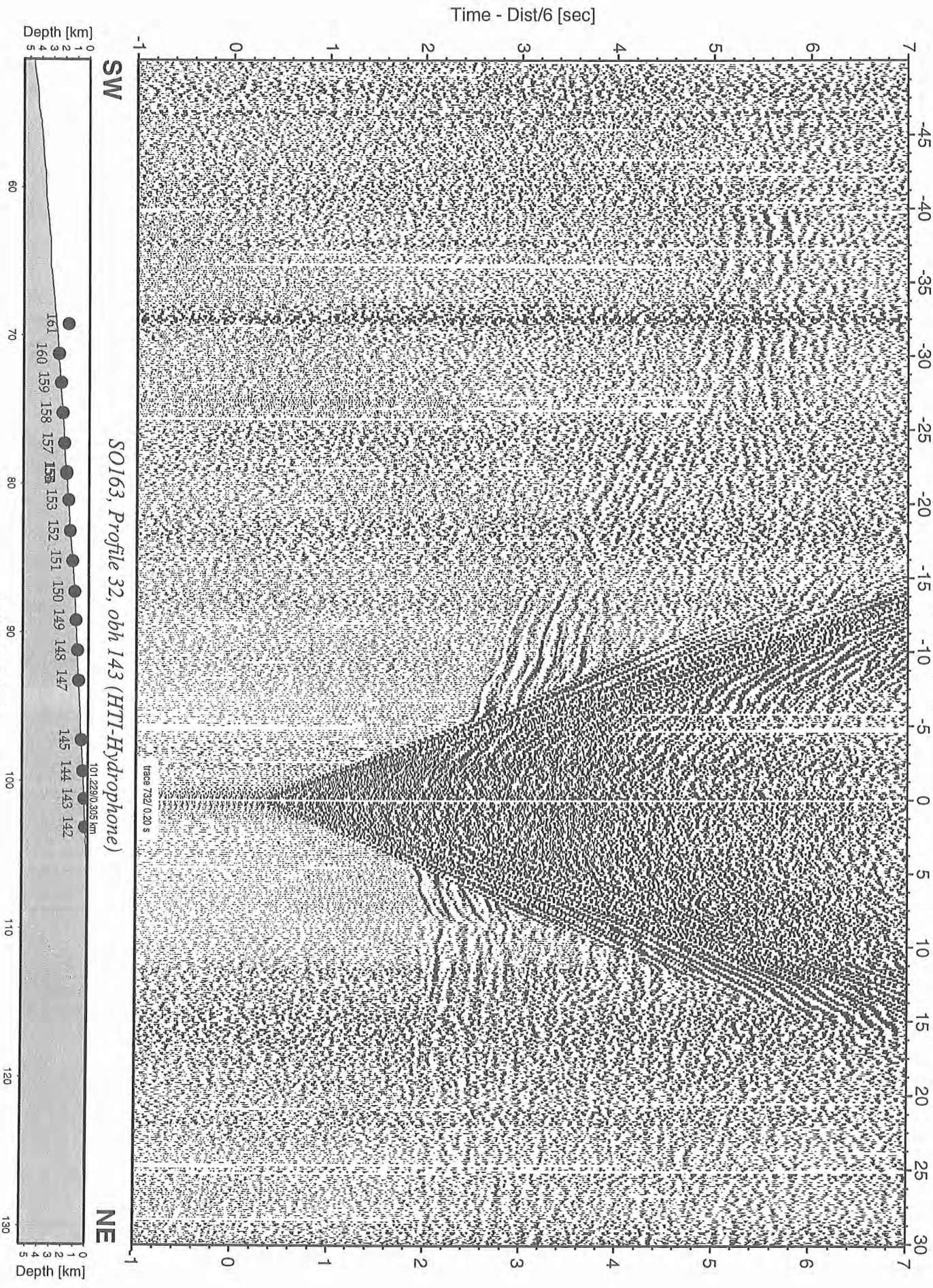


**Figure 6.6.2.23** Record section from obh 143 (HTI-Hydrophone), Profile 32.

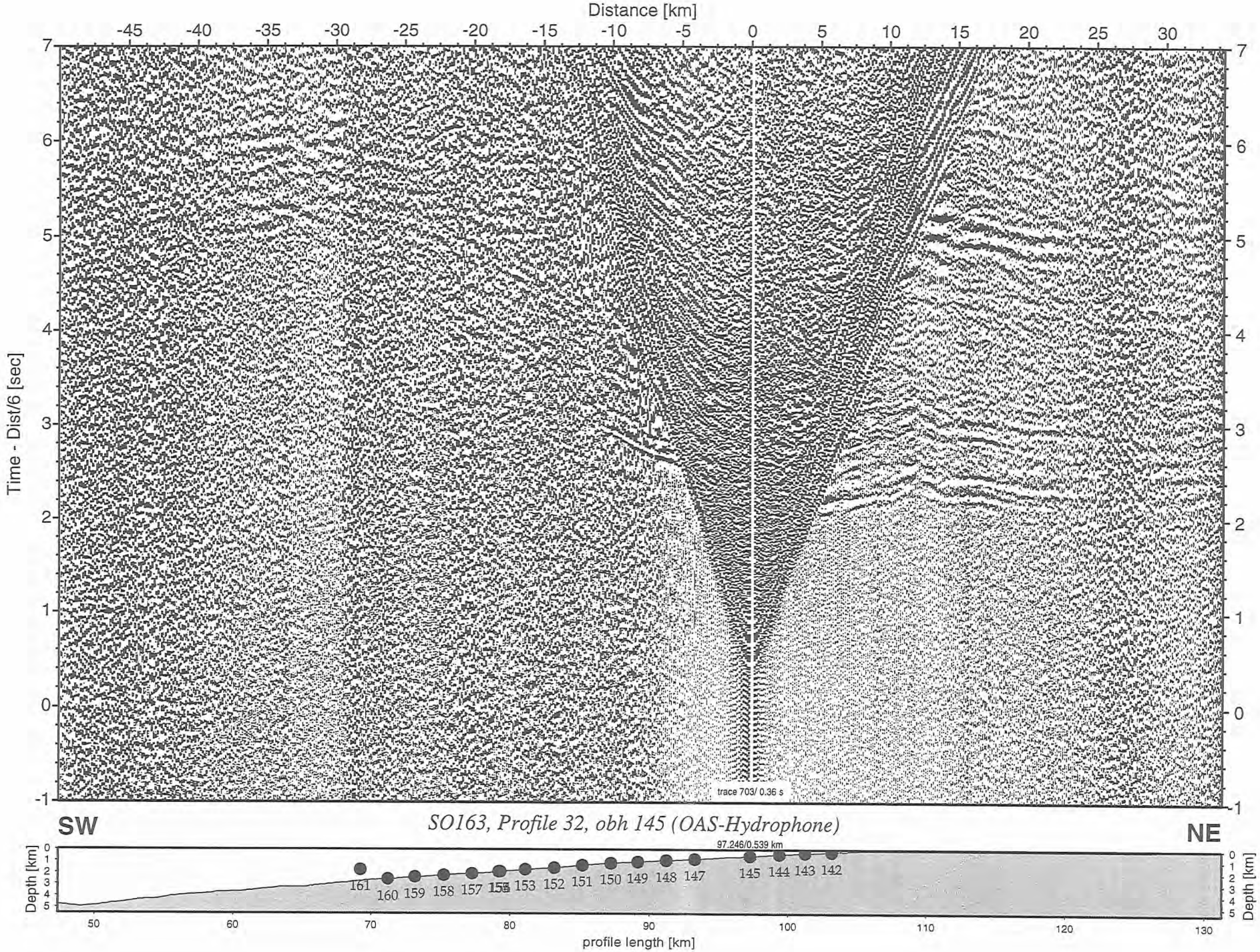


**Figure 6.6.2.24** Record section from obh 145 (OAS-Hydrophone), Profile 32.

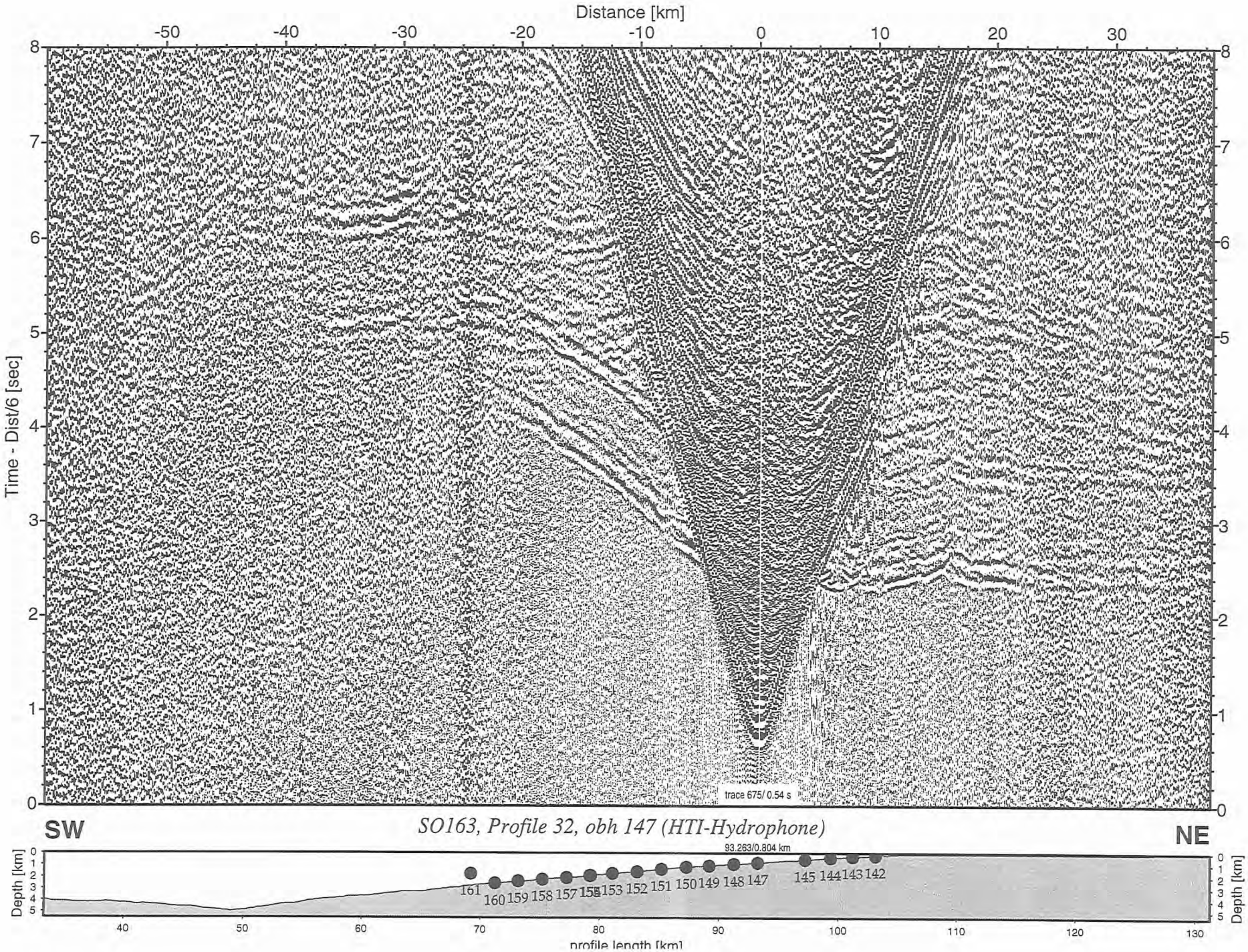


**Figure 6.6.2.25** Record section from obh 147 (HTI-Hydrophone), Profile 32.

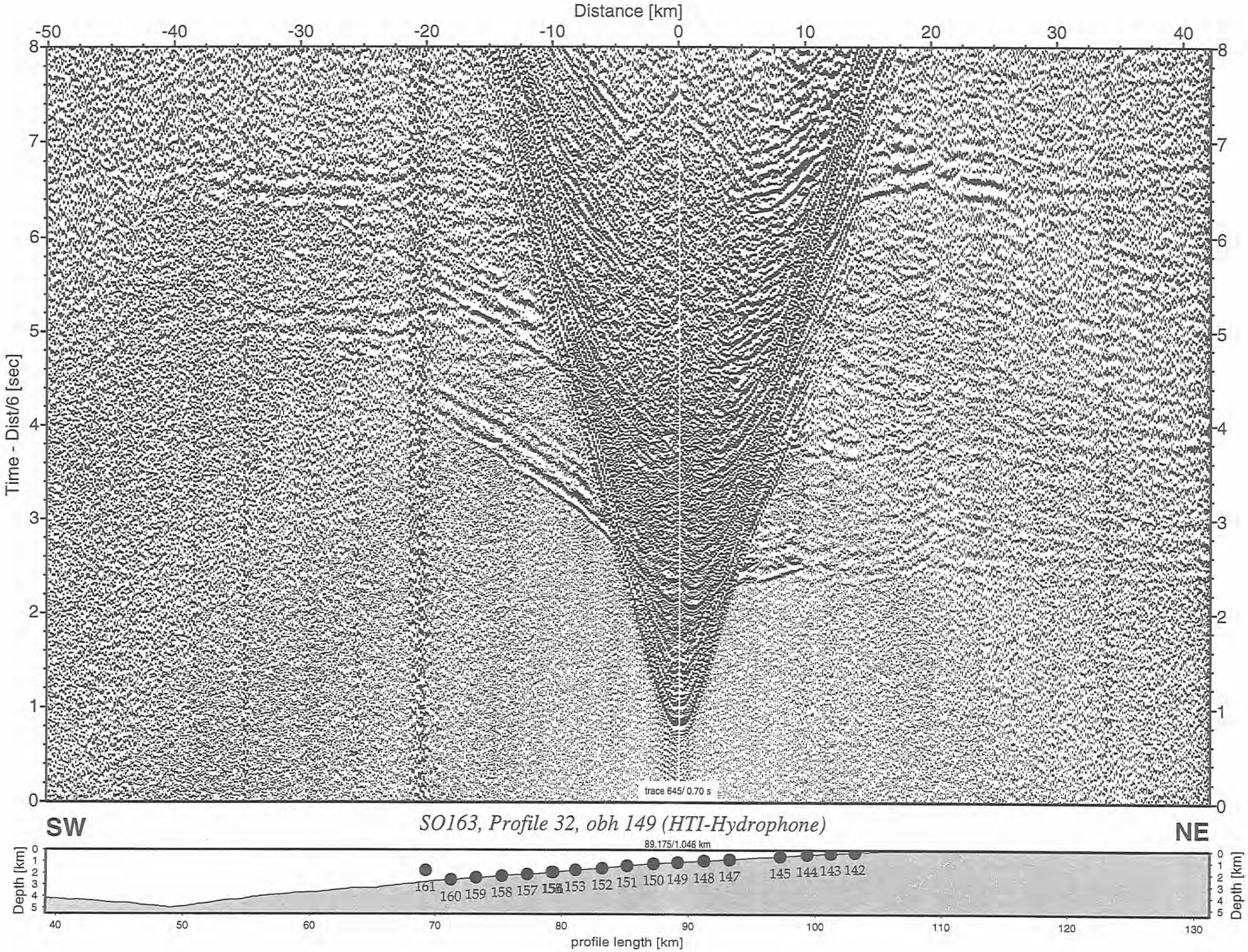


**Figure 6.6.2.26** Record section from obh 149 (HTI-Hydrophone), Profile 32.

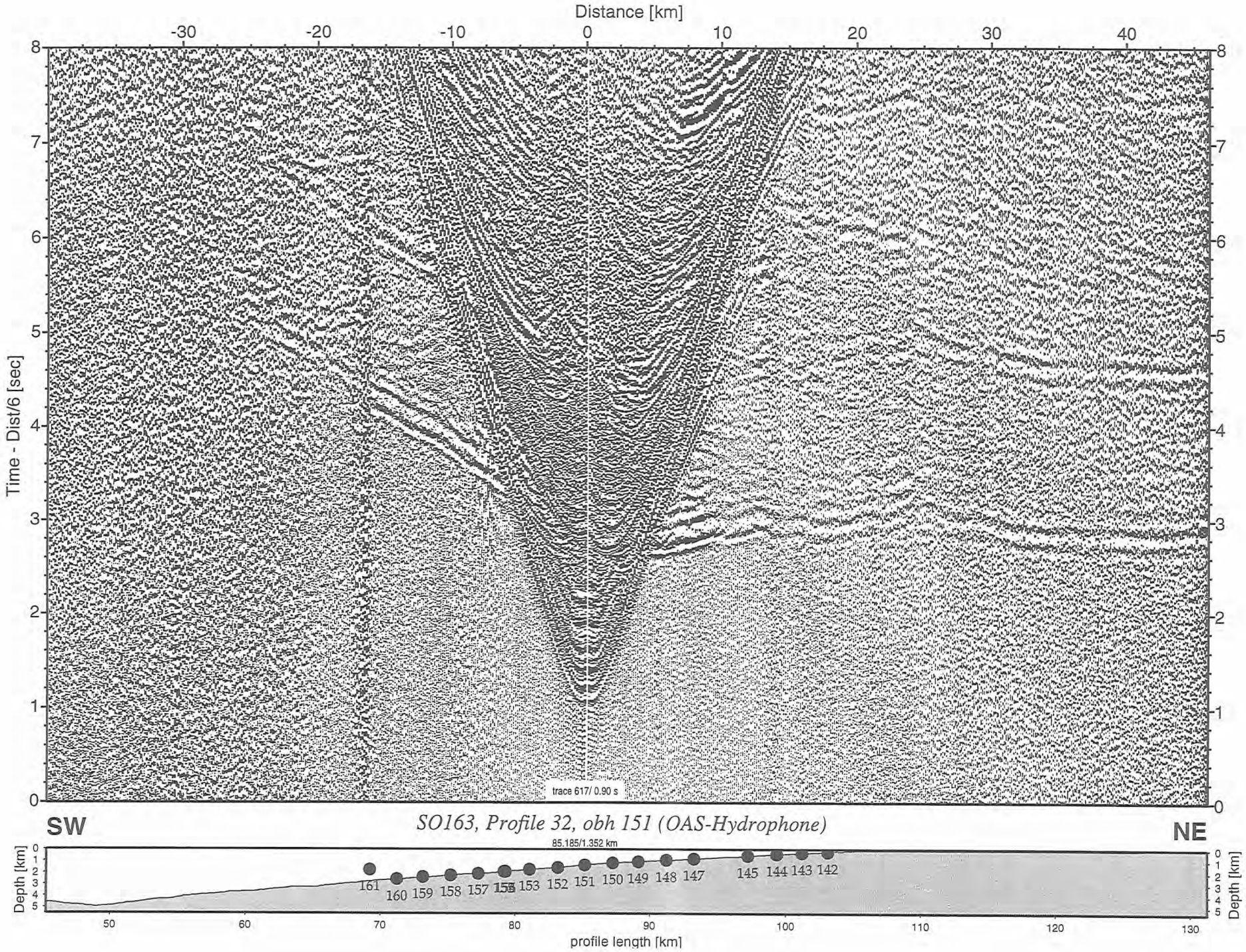


**Figure 6.6.2.27** Record section from obh 151 (OAS-Hydrophone), Profile 32.

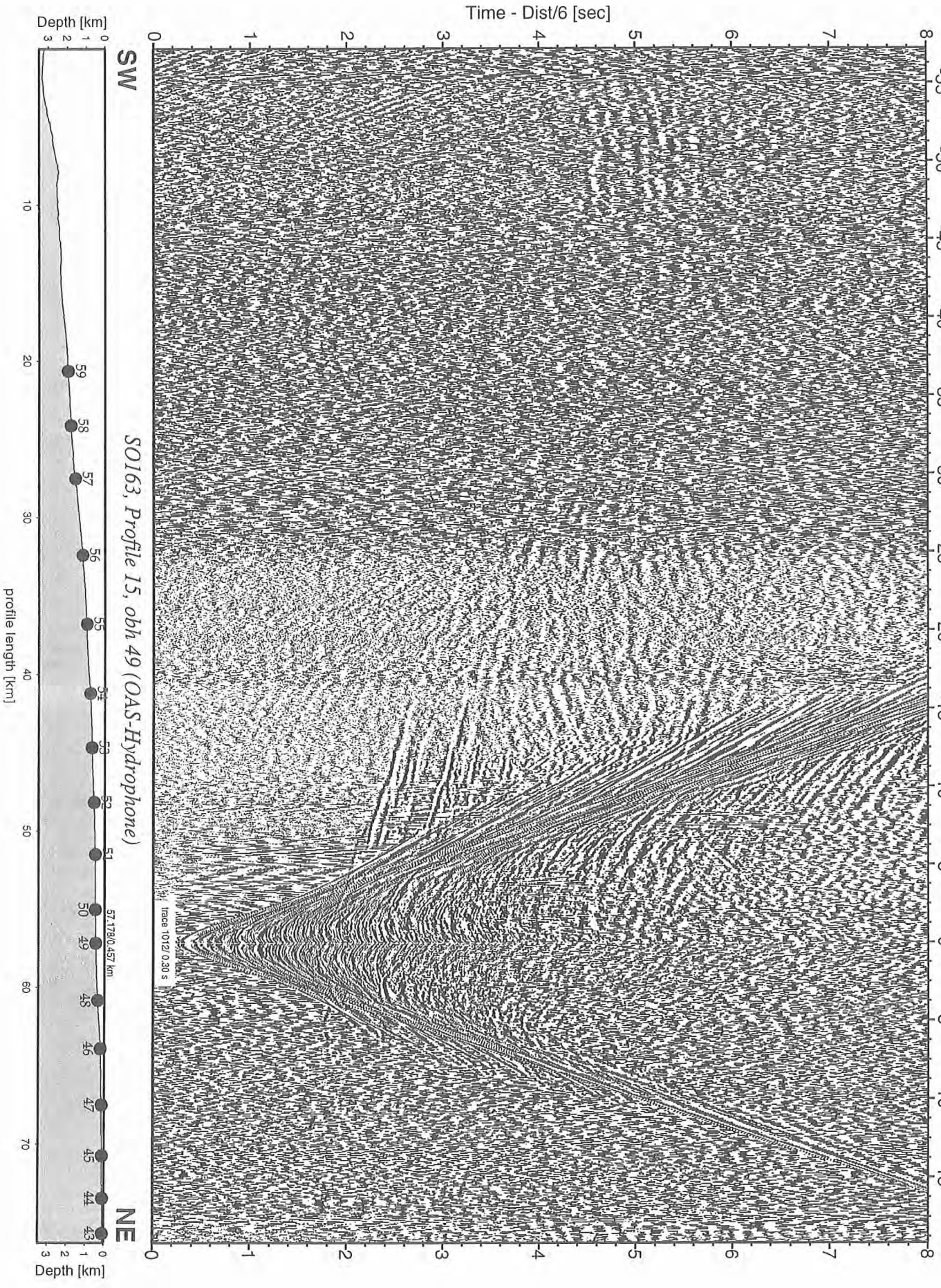


**Figure 6.6.3.10:** Record section from obh 49 (OAS-Hydrophone), Profile 15.

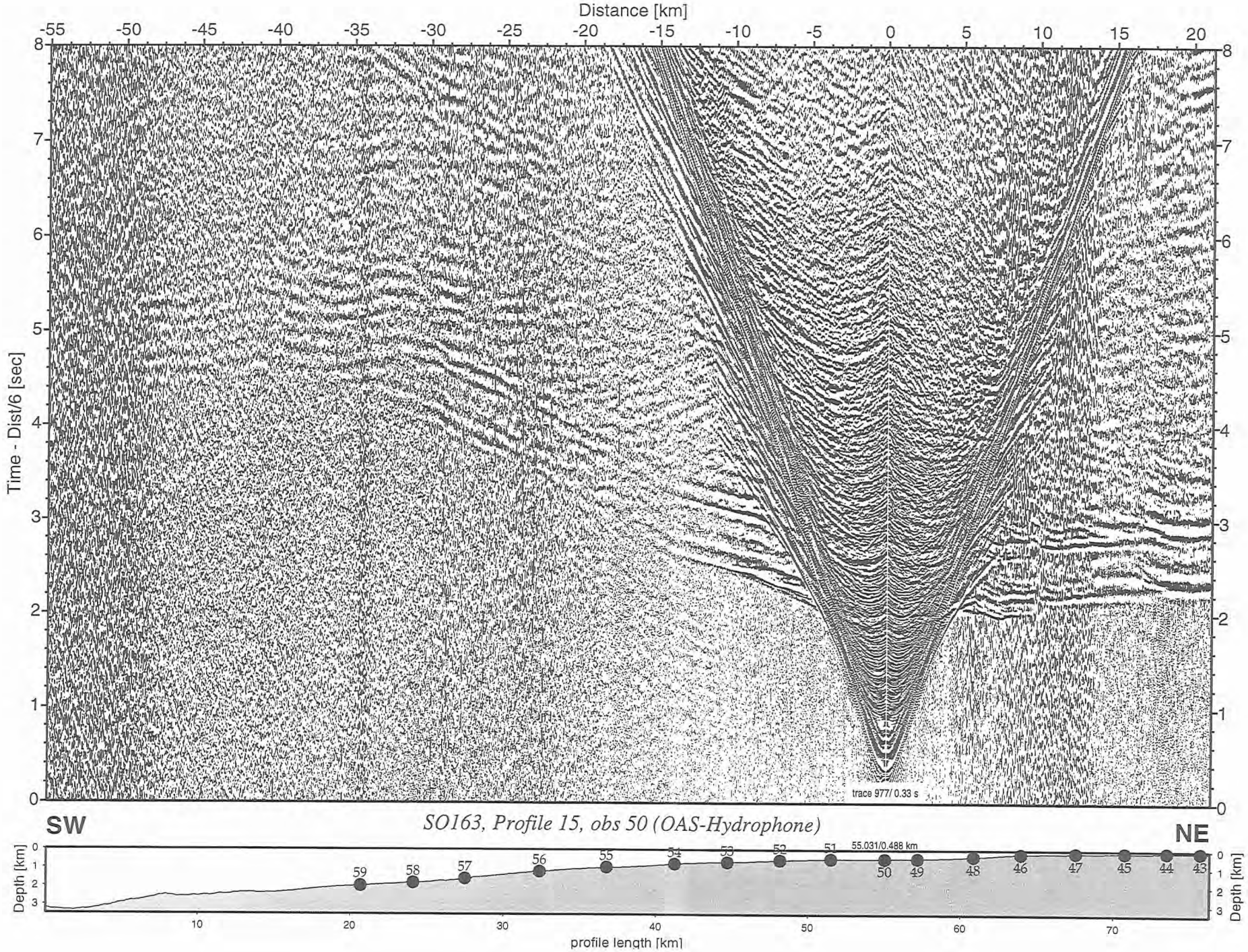


**Figure 6.6.3.11:** Record section from obs 50 (OAS-Hydrophone), Profile 15.

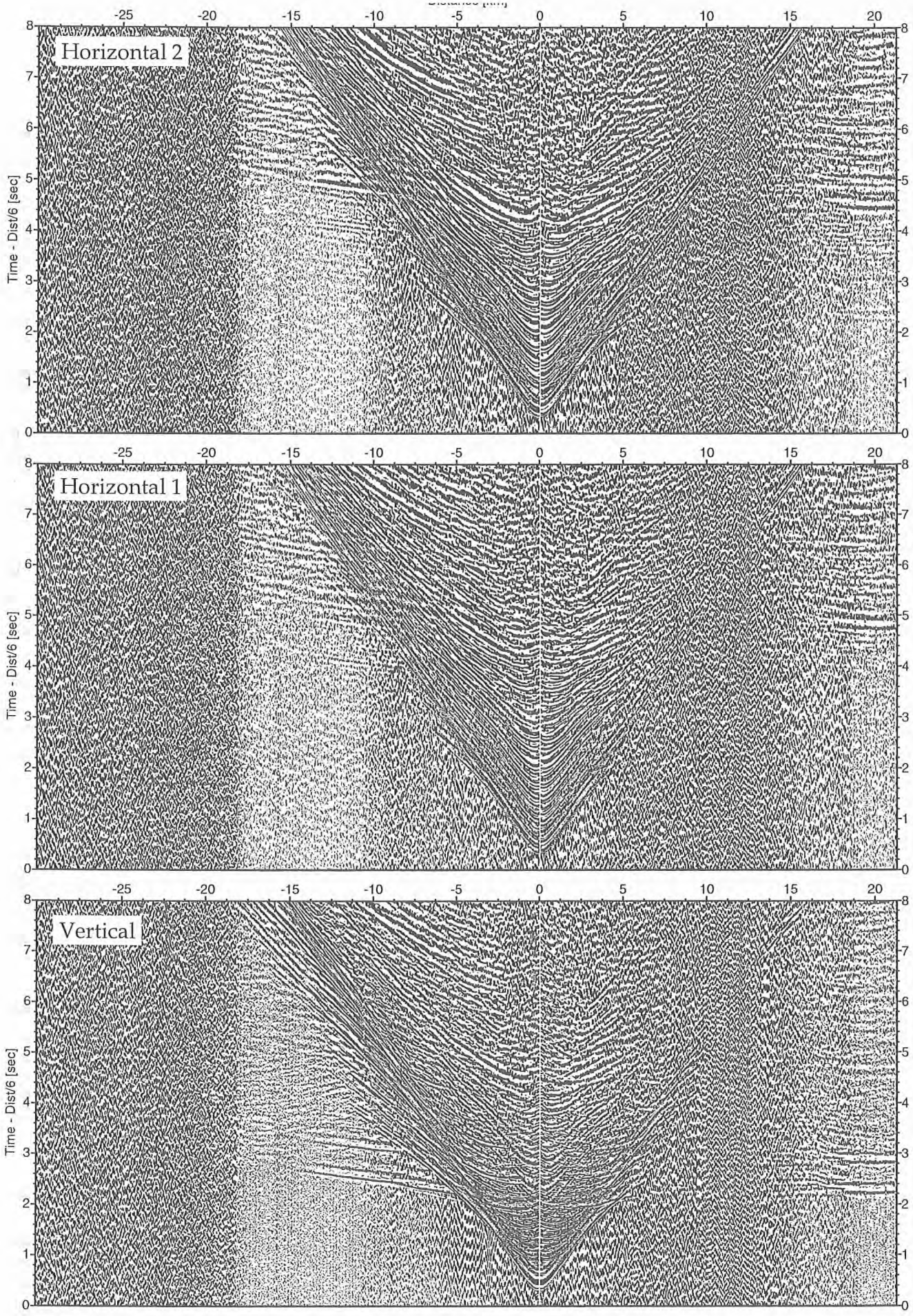


**Figure 6.6.3.12:** Record sections from obs 50 (Owen-4.5Hz), SO163, Profile 15.

**Figure 6.6.3.13:** Record section from obh 51 (OAS-Hydrophone), Profile 15.

**Figure 6.6.3.14:** Record section from obs 52 (HTI-Hydrophone), Profile 15.

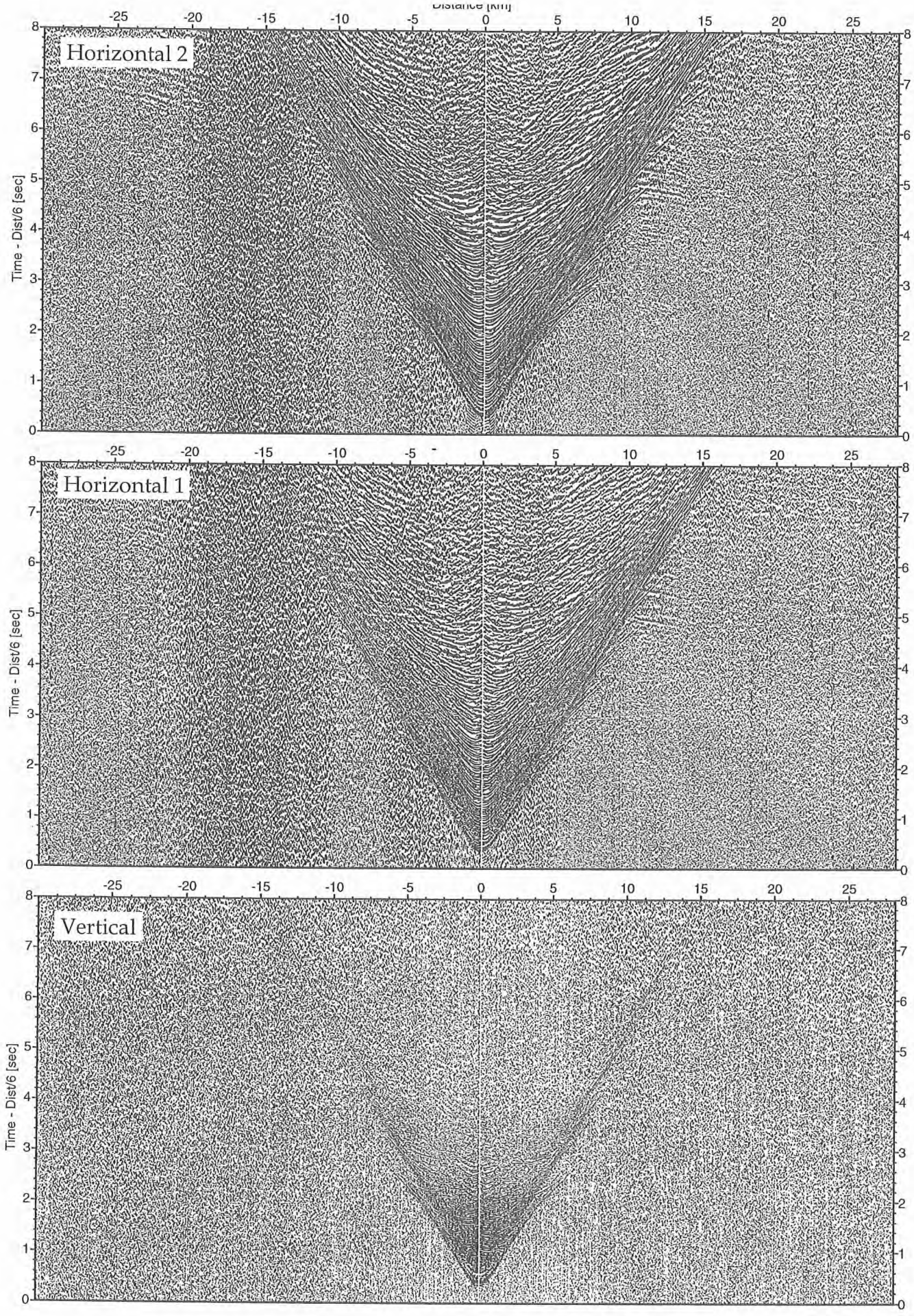


**Figure 6.6.3.15:** Record sections from obs 52 (Owen-30Hz), SO163, Profile 15.

**Figure 6.6.3.16:** Record section from obh 53 (OAS-Hydrophone), Profile 15.

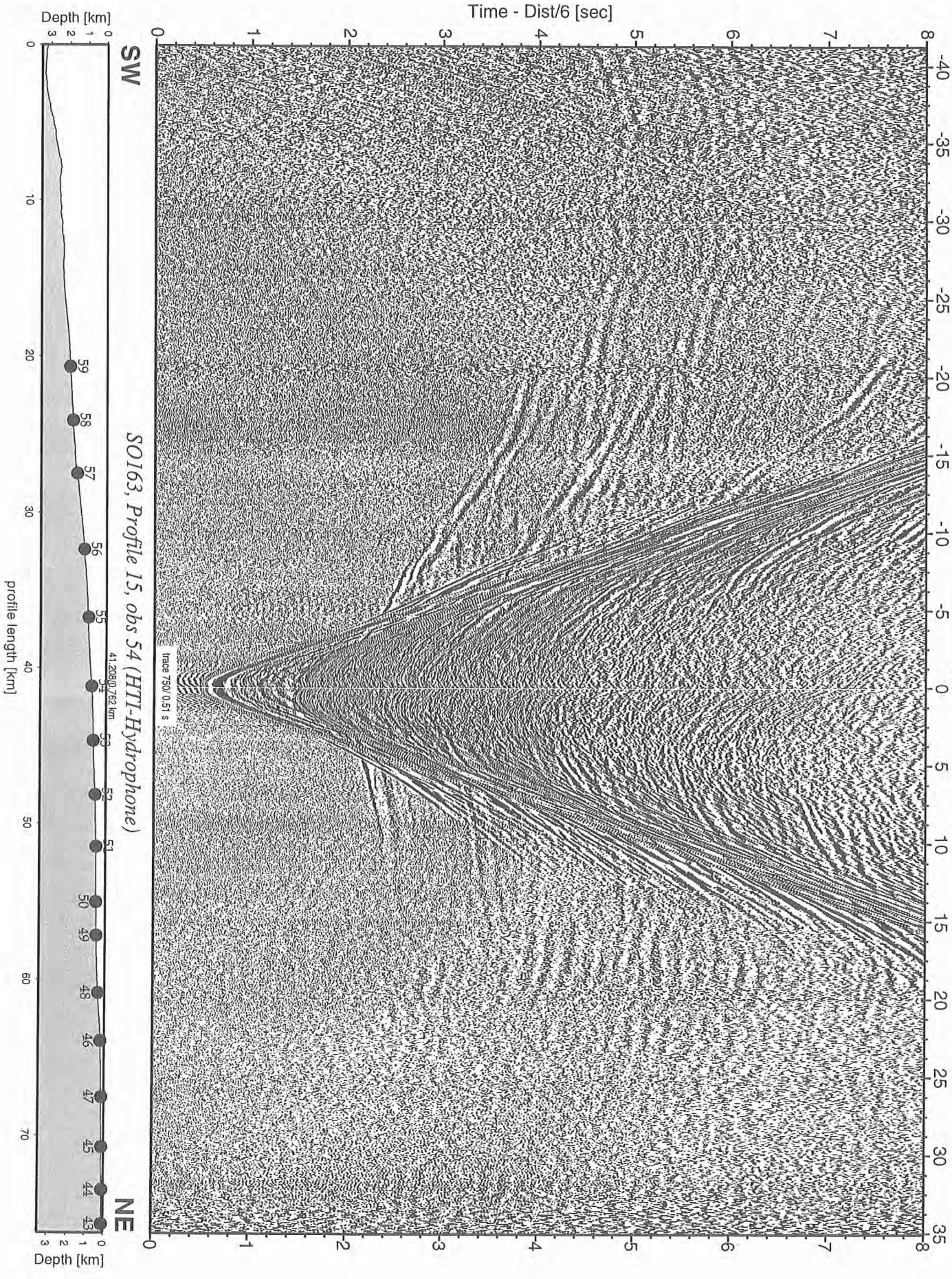


**Figure 6.6.3.17:** Record section from obs 54 (HTI-Hydrophone), Profile 15.

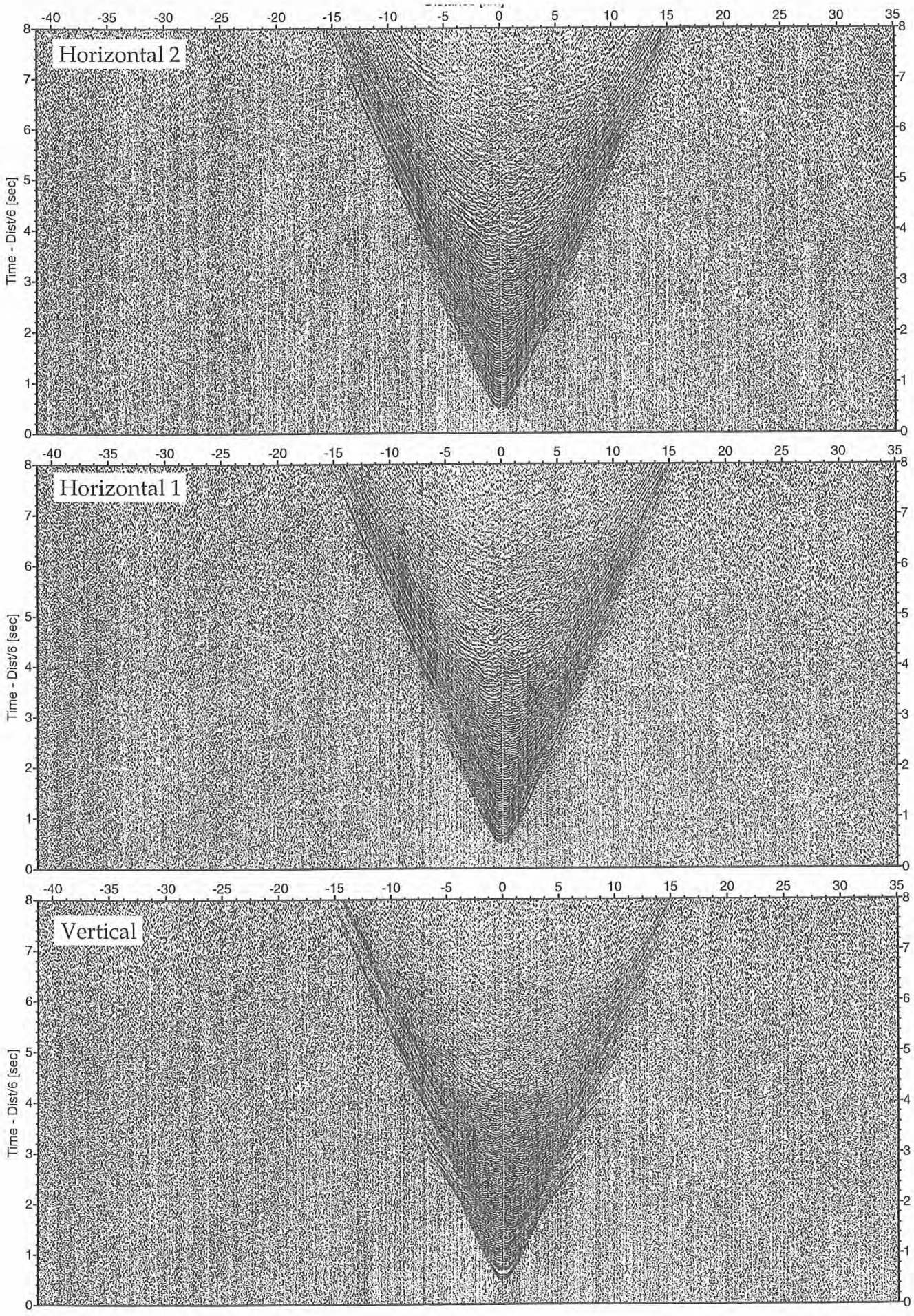


**Figure 6.6.3.18:** Record sections from obs 54 (Owen-30Hz), SO163, Profile 15.

**Figure 6.6.3.19:** Record section from obh 55 (HTI-Hydrophone), Profile 15.

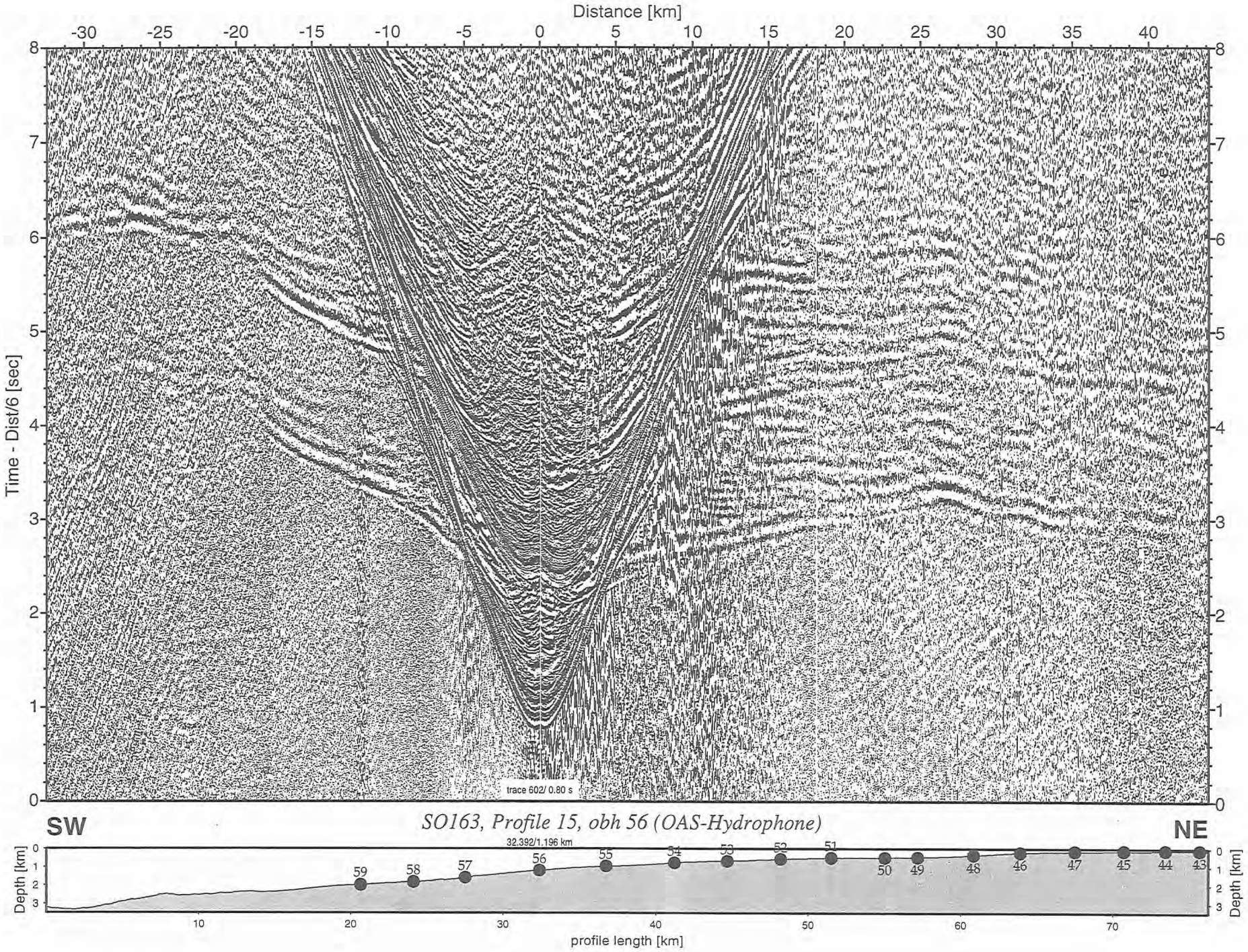


**Figure 6.6.3.20:** Record section from obh 56 (OAS-Hydrophone), Profile 15.

**Figure 6.6.3.21:** Record section from obs 57 (OAS-Hydrophone), Profile 15.

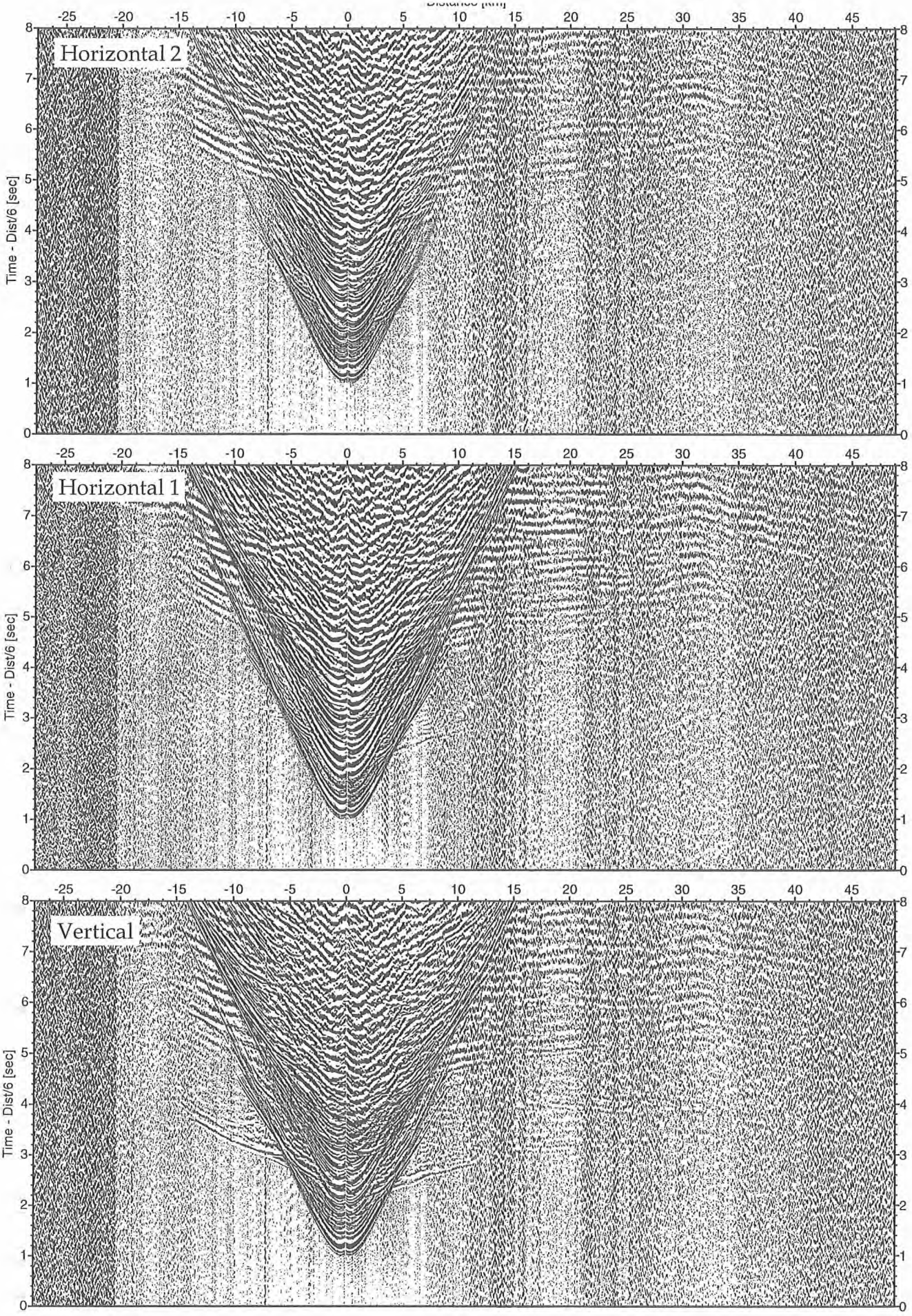


**Figure 6.6.3.22:** Record sections from obs 57 (LG-4.5HZ), SO163, Profile 15.

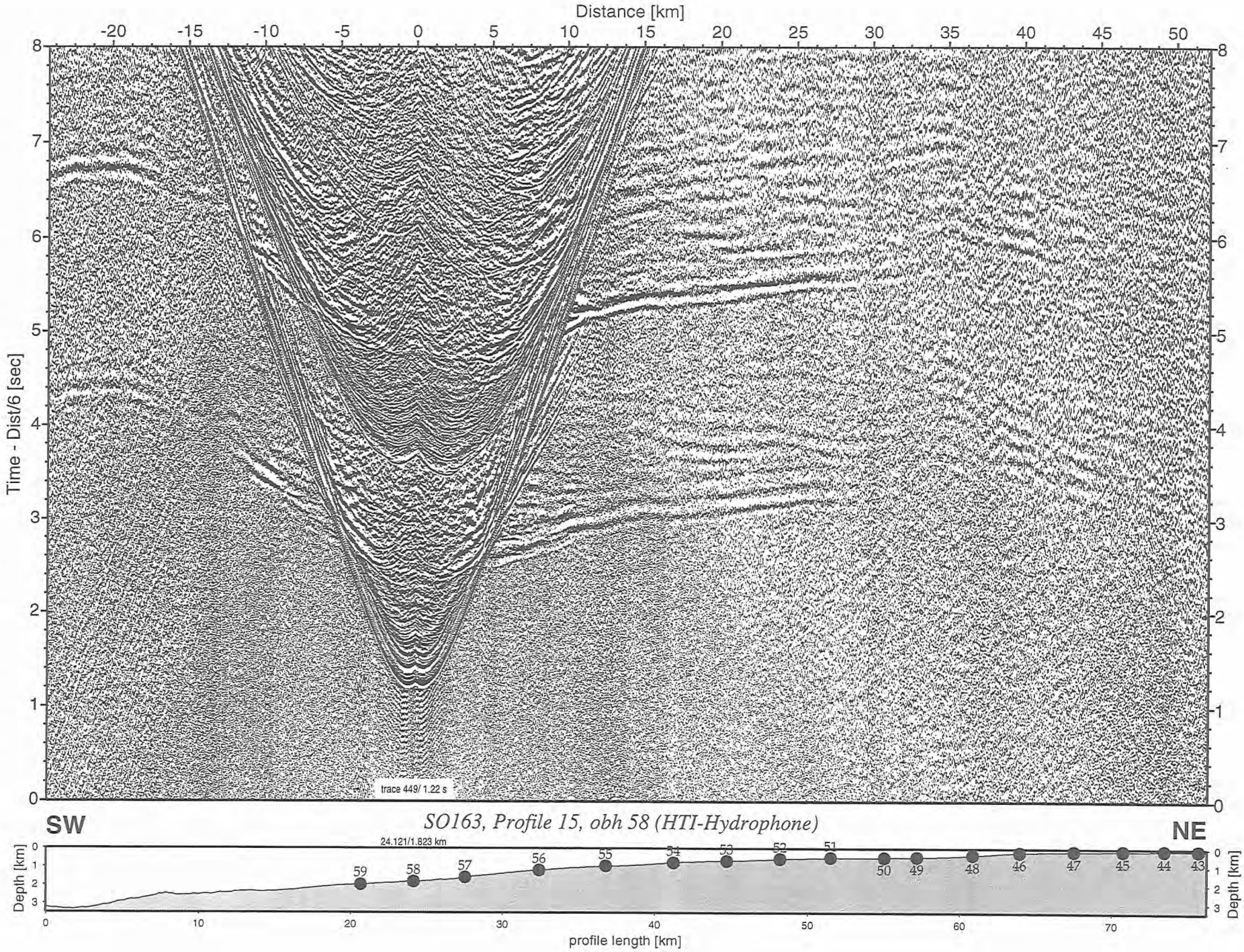


**Figure 6.6.3.23:** Record section from obh 58 (HTI-Hydrophone), Profile 15.

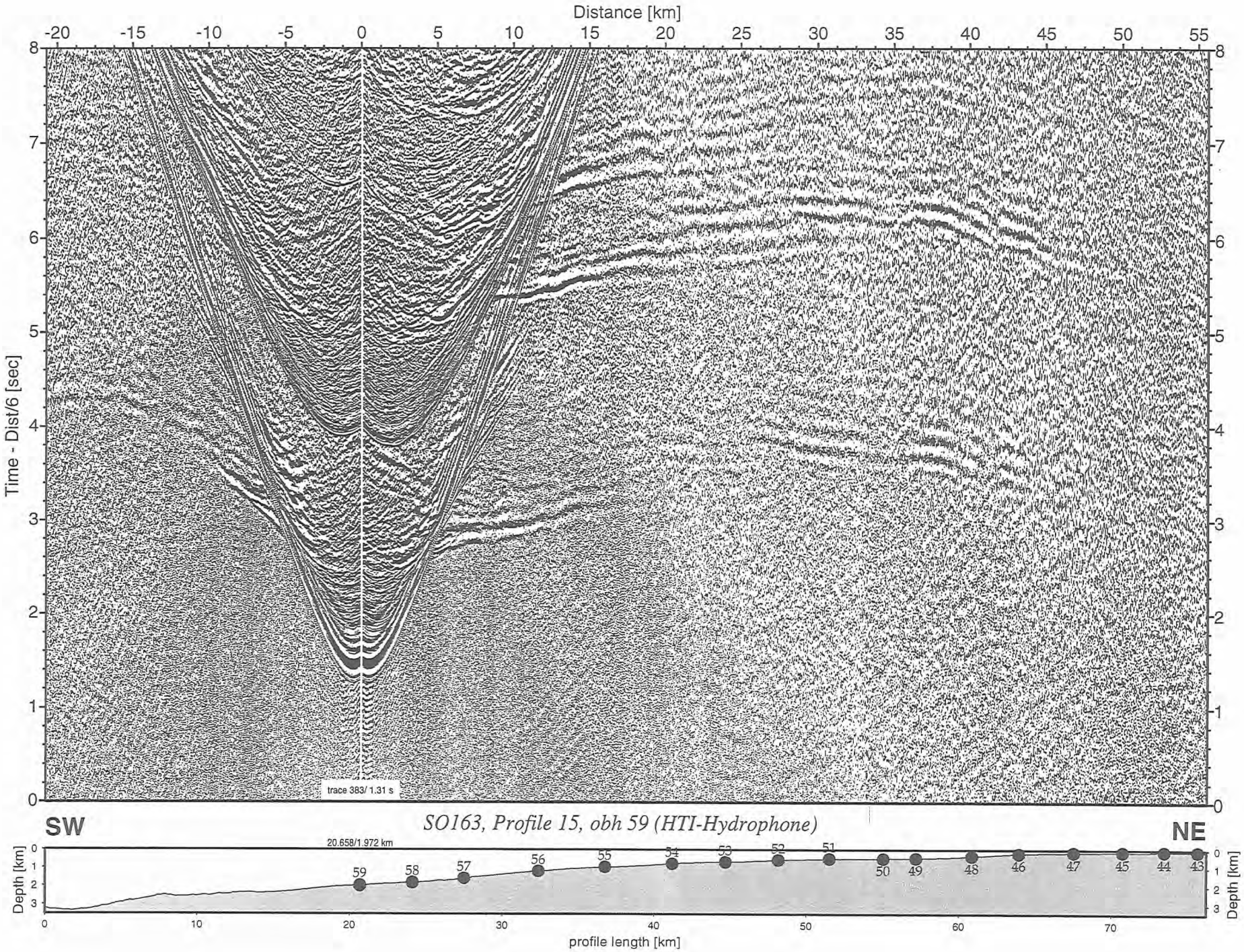


**Figure 6.6.3.24:** Record section from obh 59 (HTI-Hydrophone), Profile 15.

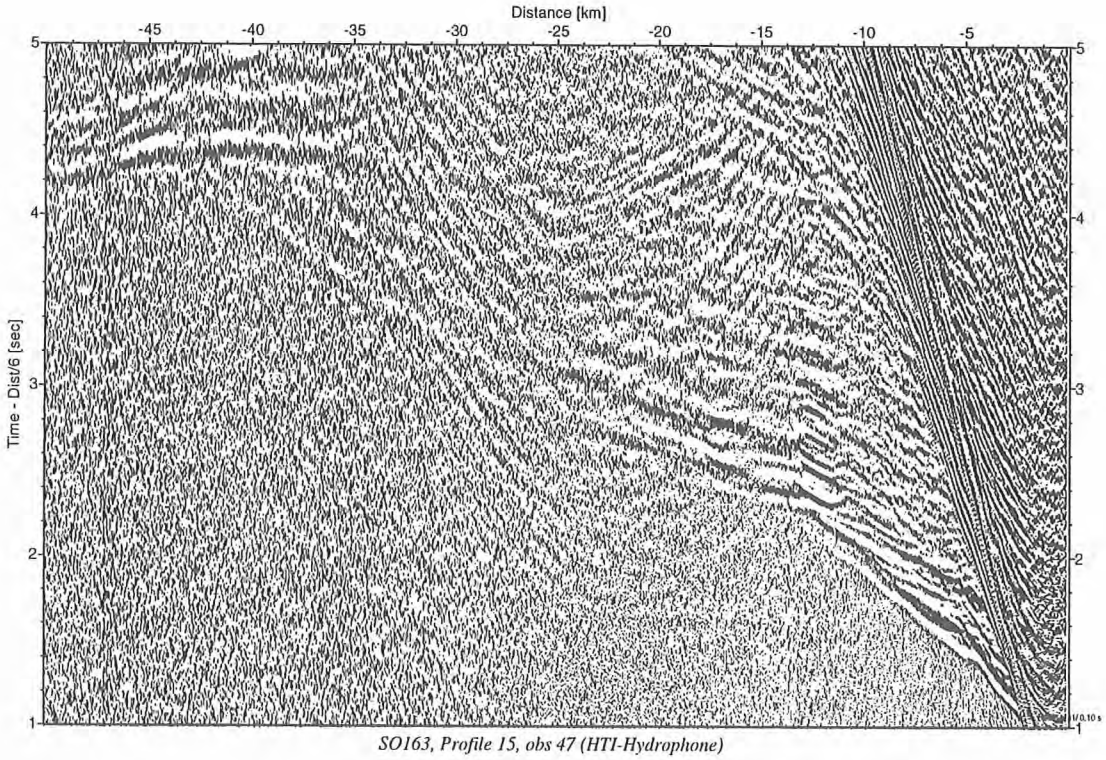


*SO163, Profile 15, obs 47 (HTI-Hydrophone)*

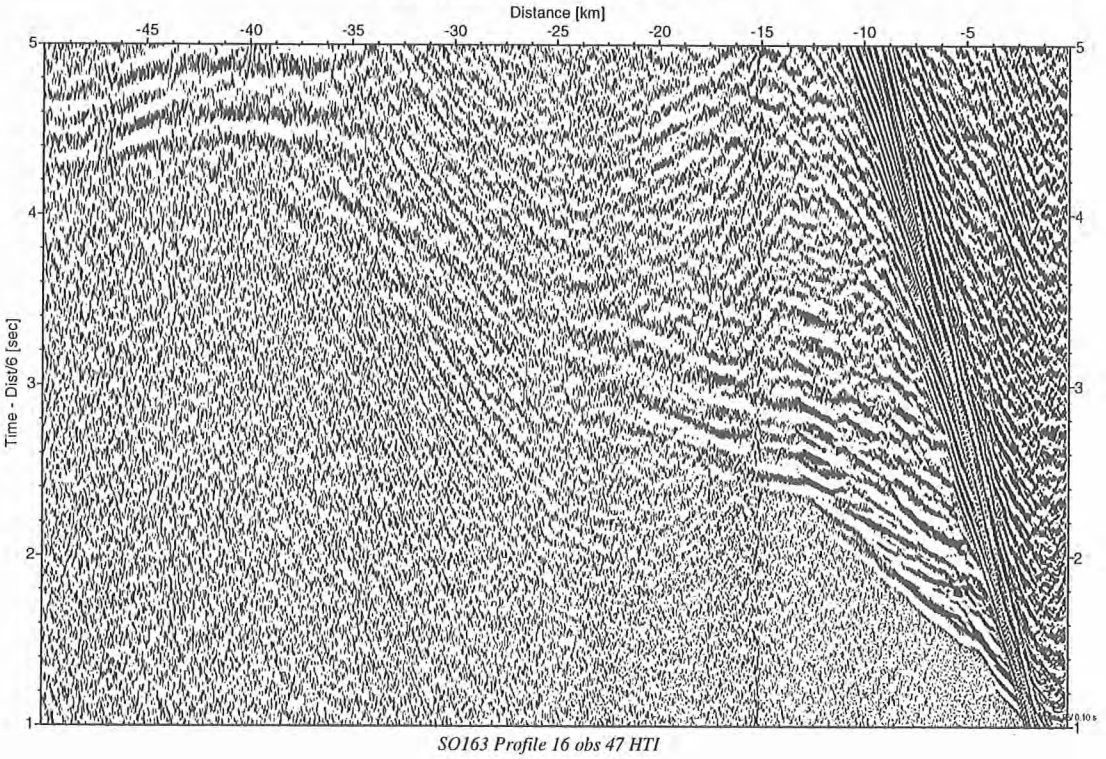


*SO163 Profile 16 obs 47 HTI*

**Figure 6.6.3.25.:** Comparison between profiles P15 (G-gun) and P16 (Bolt gun) for station OBS 47.

**Figure 6.6.3.26:** Record section from obh 62 (OAS-Hydrophone), Profile 18.

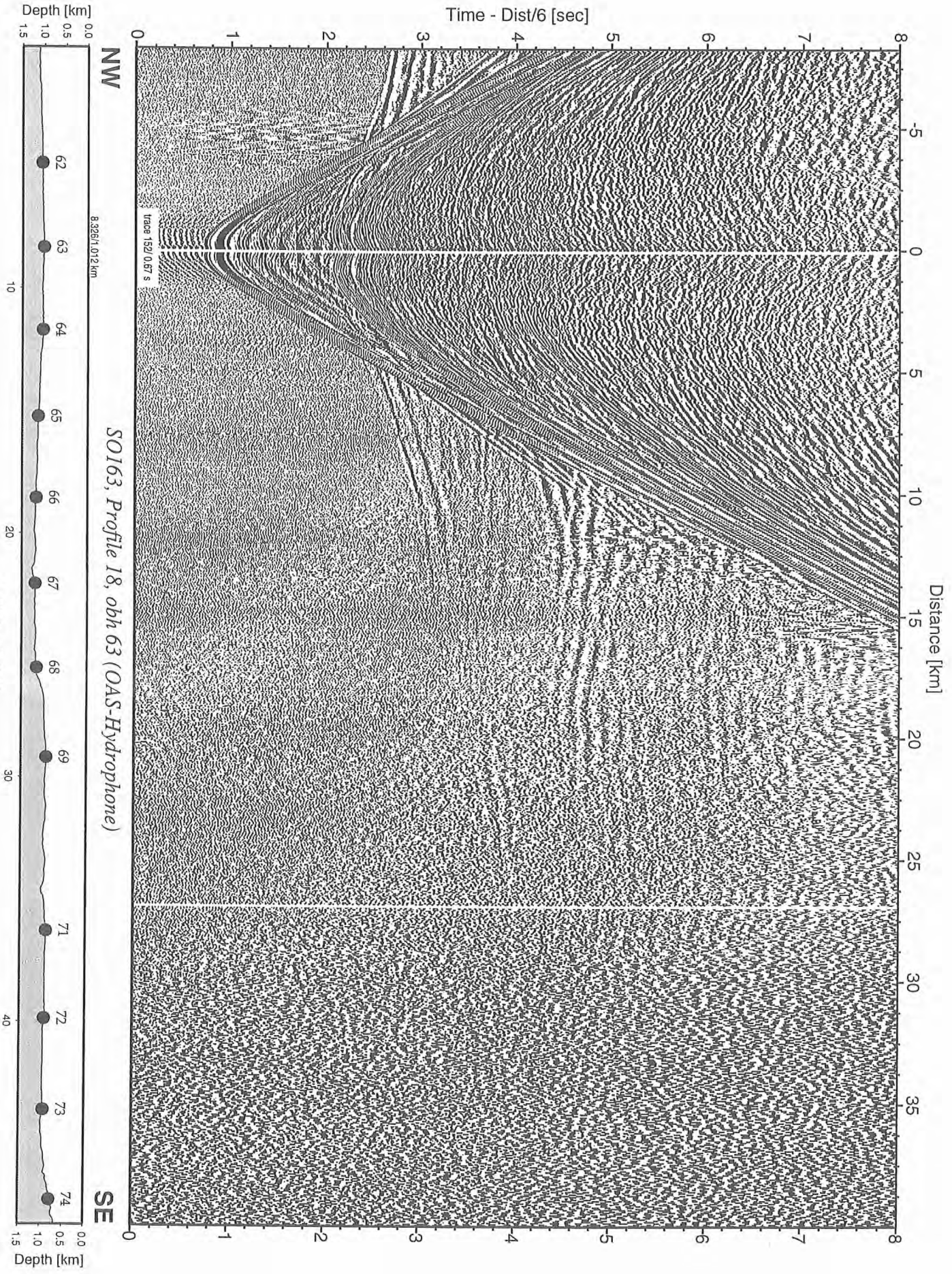


**Figure 6.6.3.27:** Record section from obh 63 (OAS-Hydrophone), Profile 18.

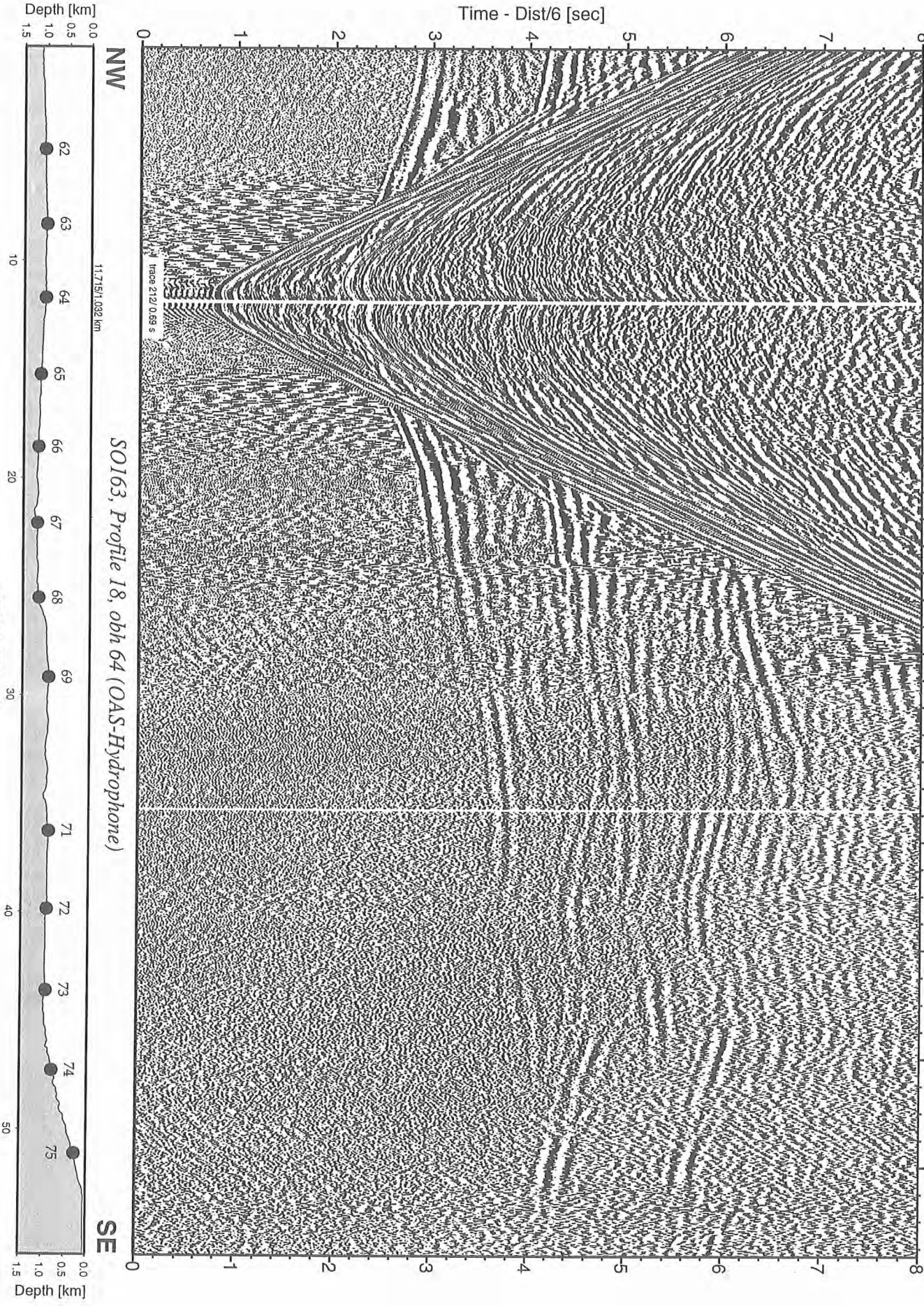


**Figure 6.6.3.28:** Record section from obh 64 (OAS-Hydrophone), Profile 18.

**Figure 6.6.3.29:** Record section from obs 65 (HTI-Hydrophone), Profile 18.

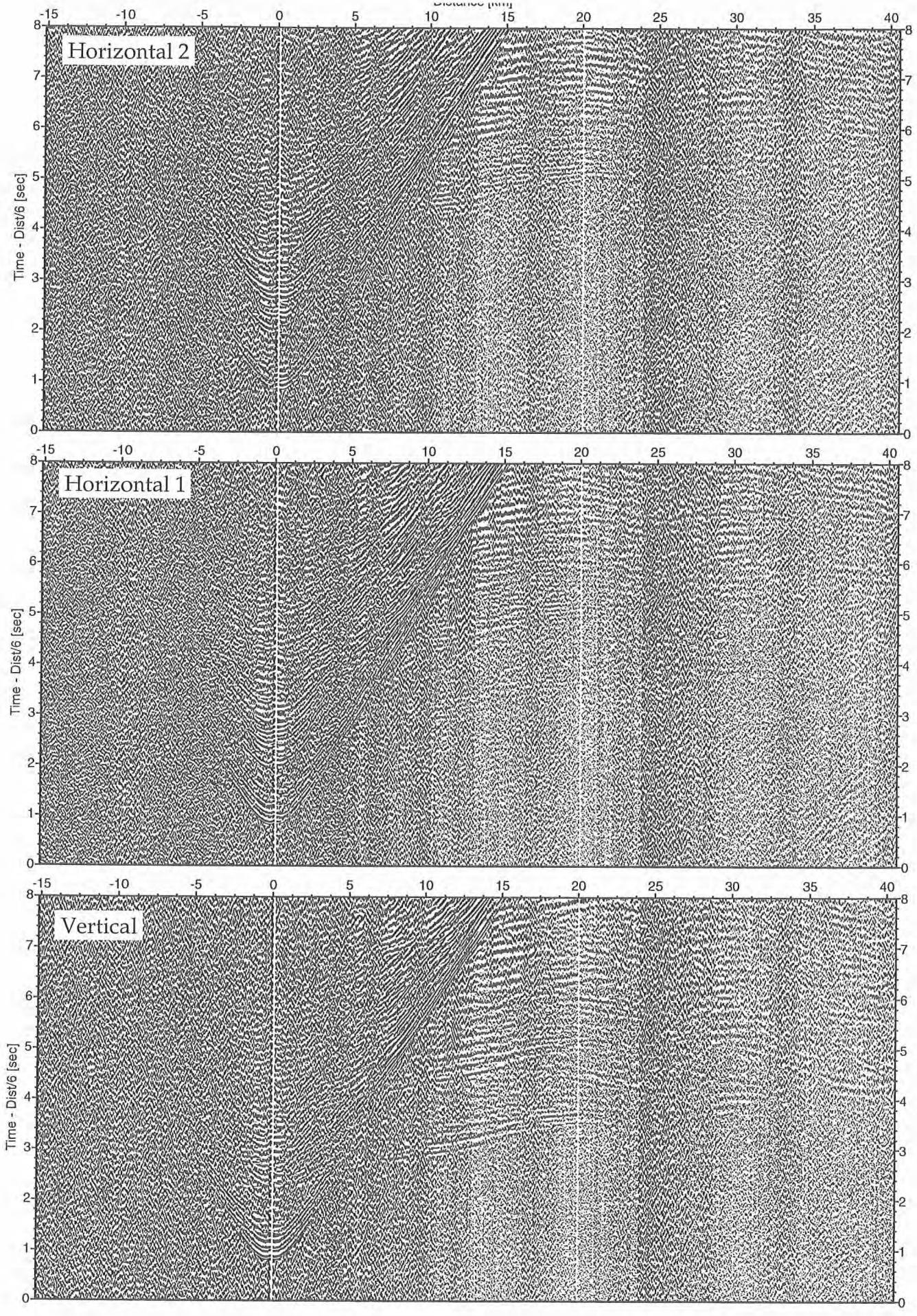


**Figure 6.6.3.30:** Record sections from obs 65 (Owen-4.5Hz), SO163, Profile 18.

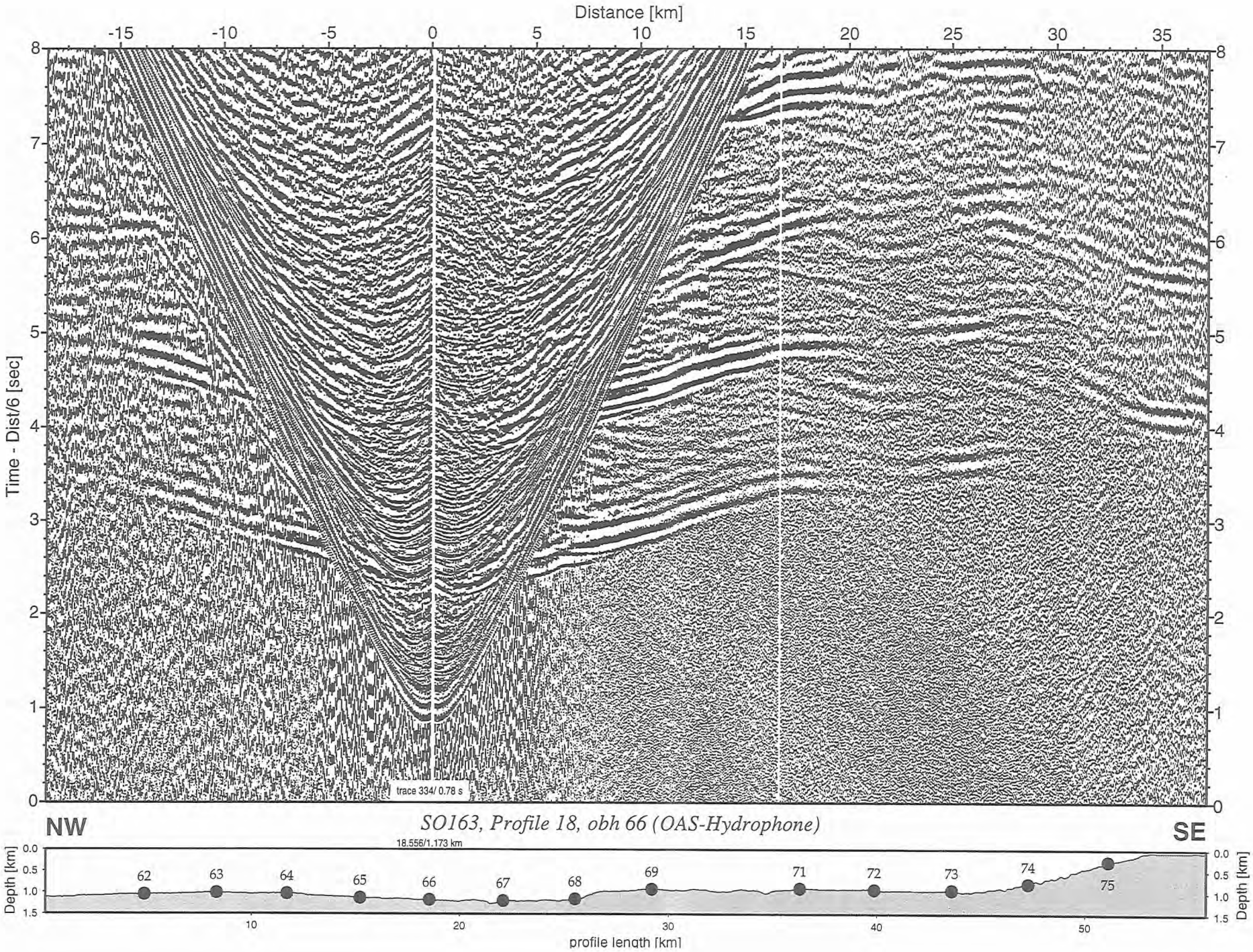


**Figure 6.6.3.31:** Record section from obh 66 (OAS-Hydrophone), Profile 18.

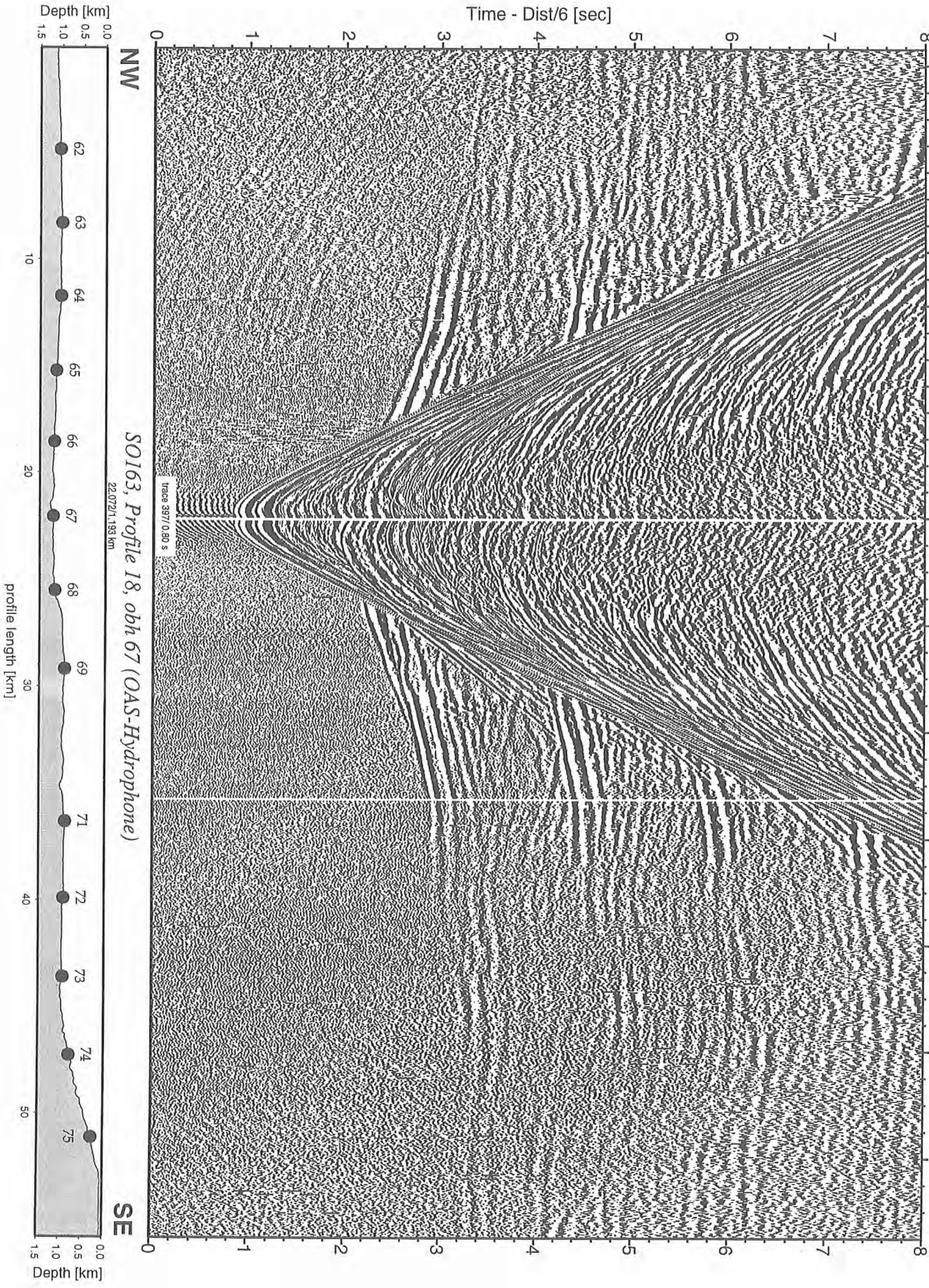


**Figure 6.6.3.32:** Record section from obh 67 (OAS-Hydrophone), Profile 18.

**Figure 6.6.3.33:** Record section from obs 68 (HTI-Hydrophone), Profile 18.

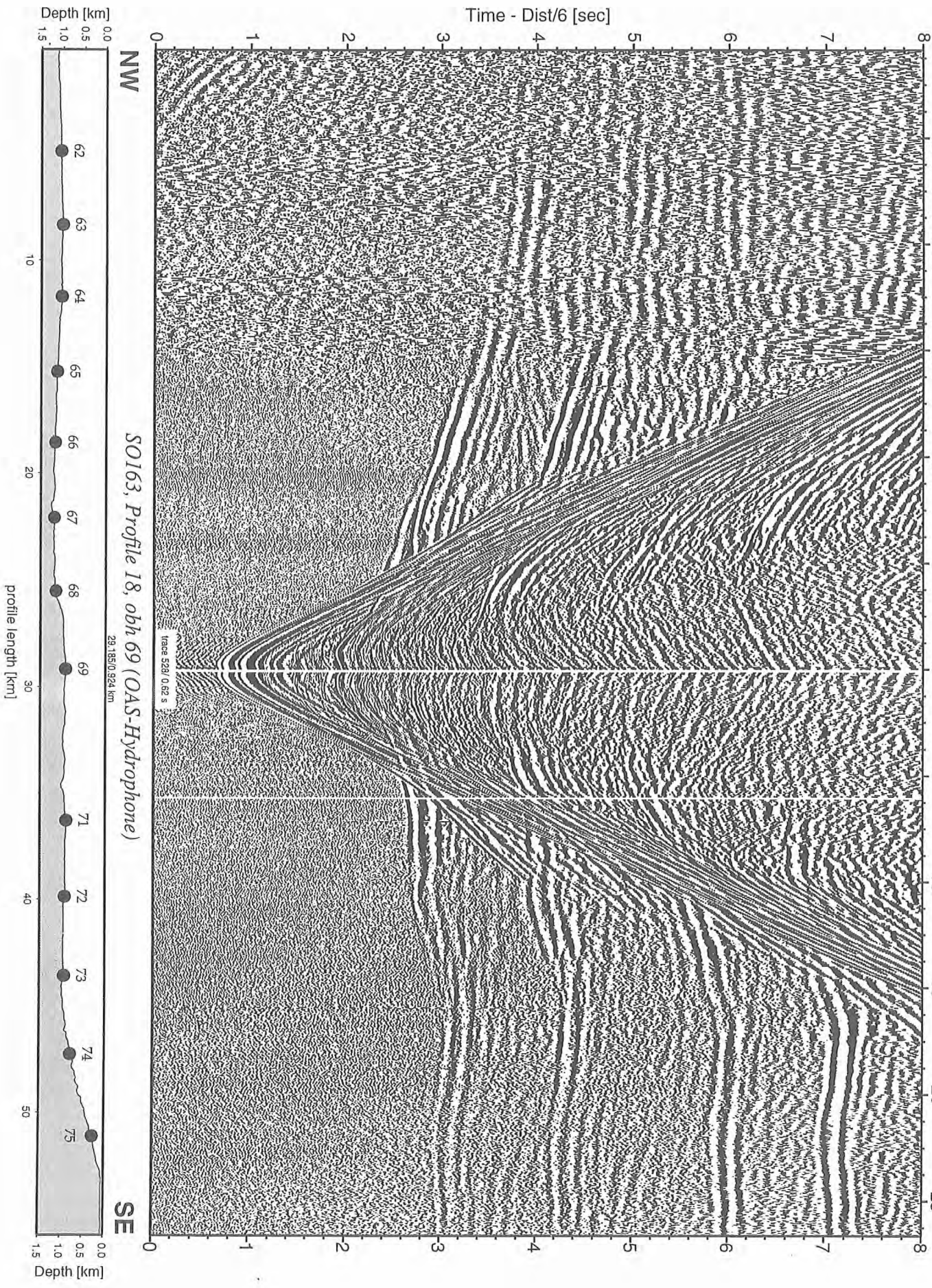


**Figure 6.6.3.34:** Record section from obh 69 (OAS-Hydrophone), Profile 18.

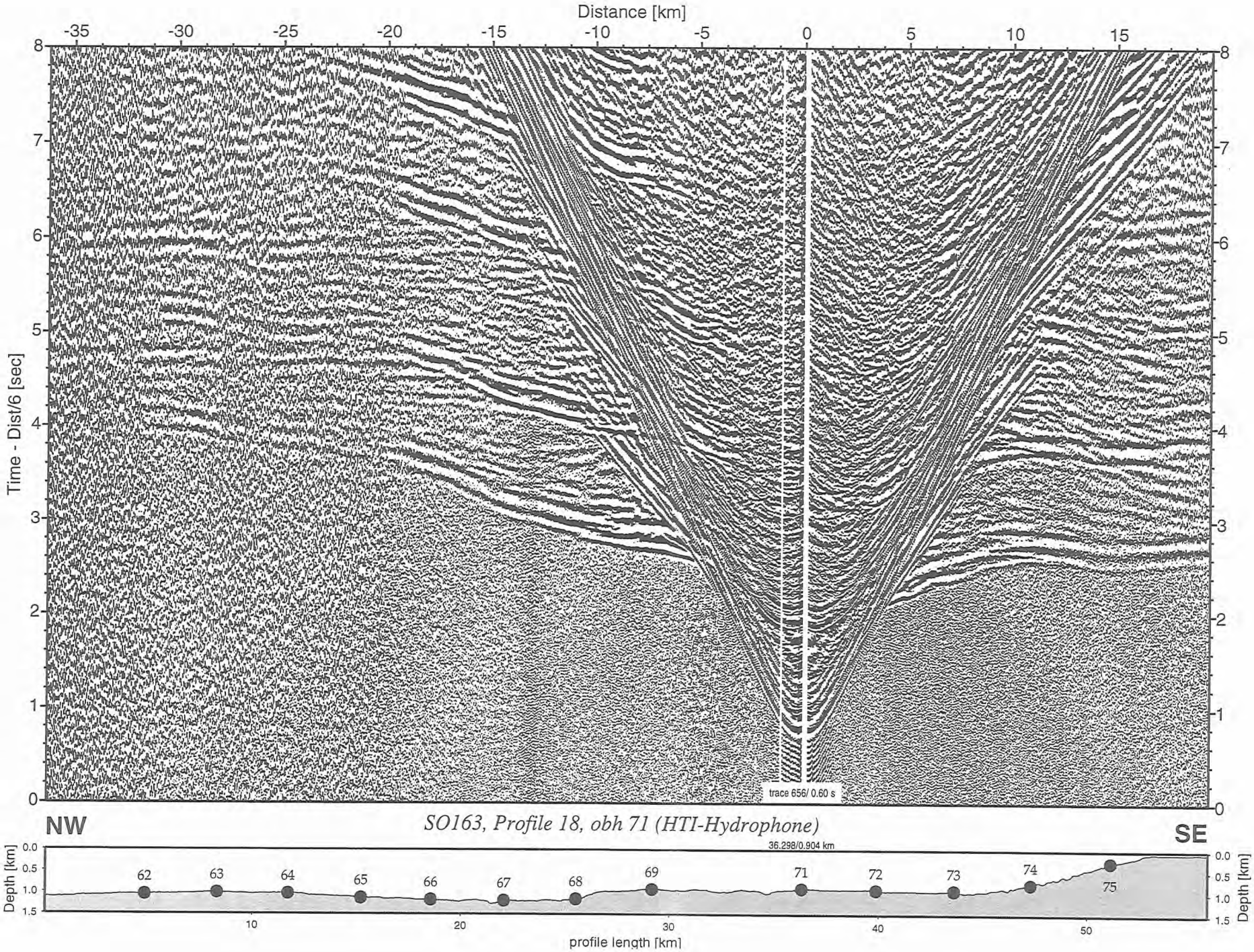


**Figure 6.6.3.35:** Record section from obh 71 (HTI-Hydrophone), Profile 18.

**Figure 6.6.3.36:** Record section from obs 72 (HTI-Hydrophone), Profile 18.

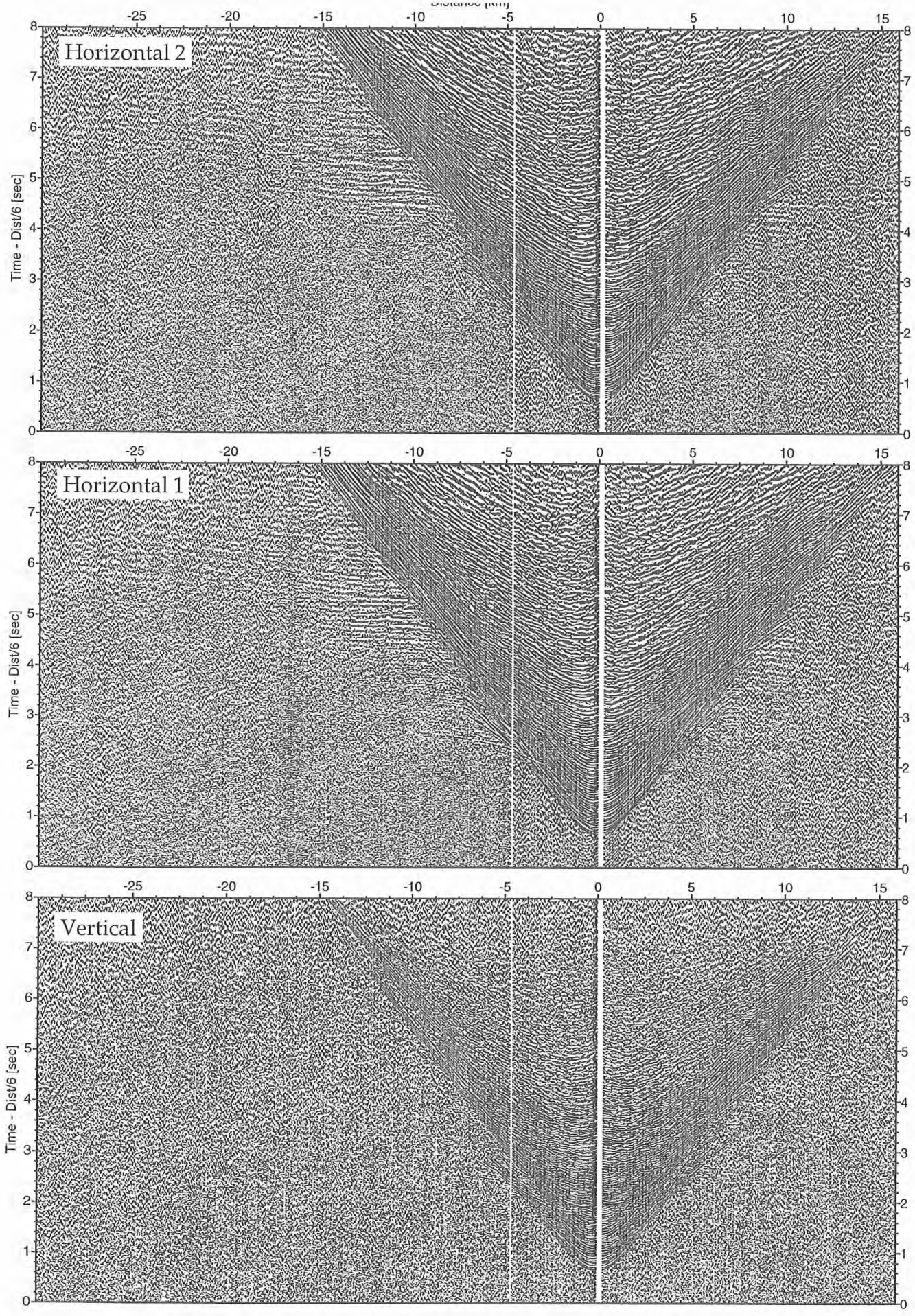


**Figure 6.6.3.37:** Record sections from obs 72 (Owen-30Hz), SO163, Profile 18.

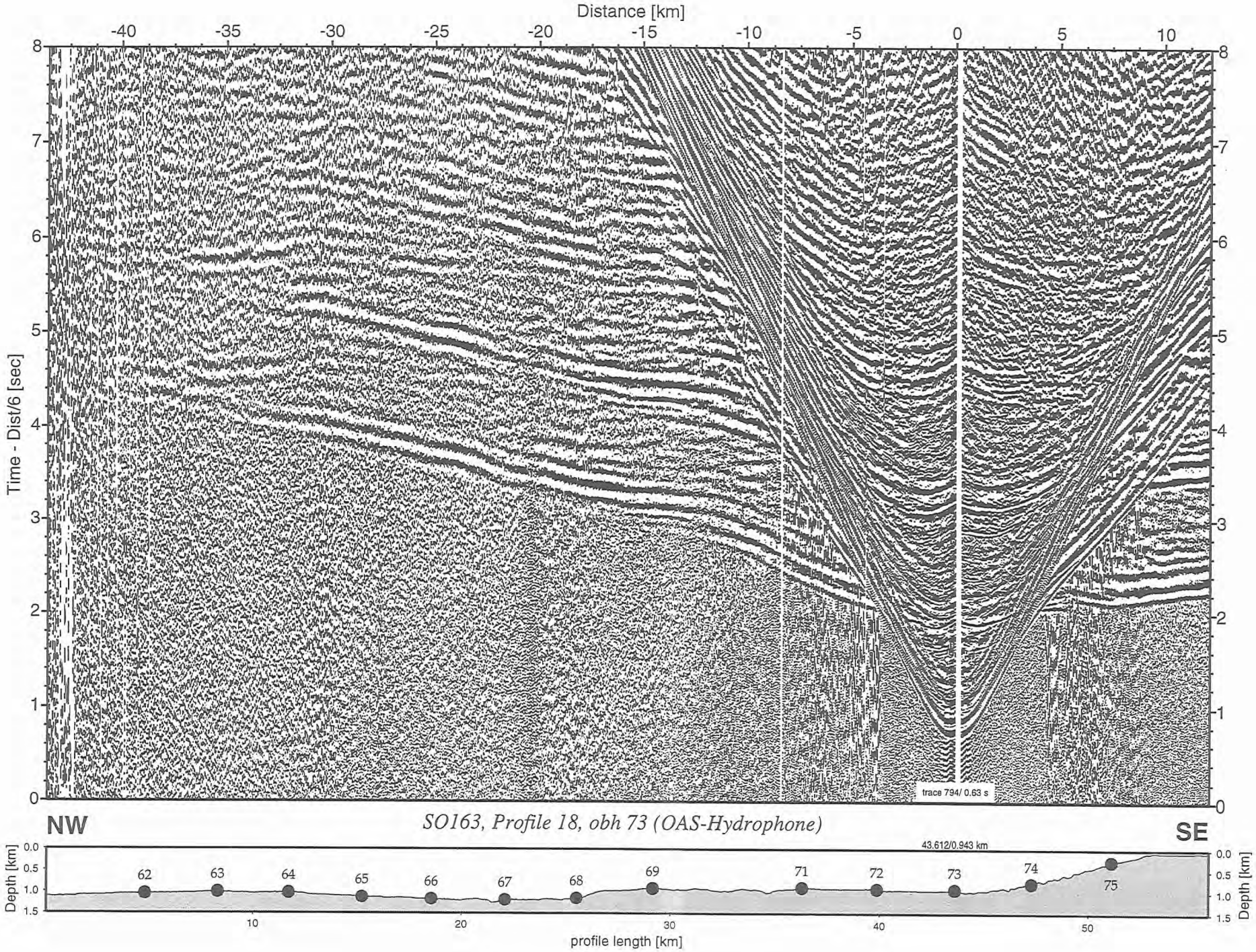


**Figure 6.6.3.38:** Record section from obh 73 (OAS-Hydrophone), Profile 18.

**Figure 6.6.3.39:** Record section from obs 74 (OAS-Hydrophone), Profile 18.

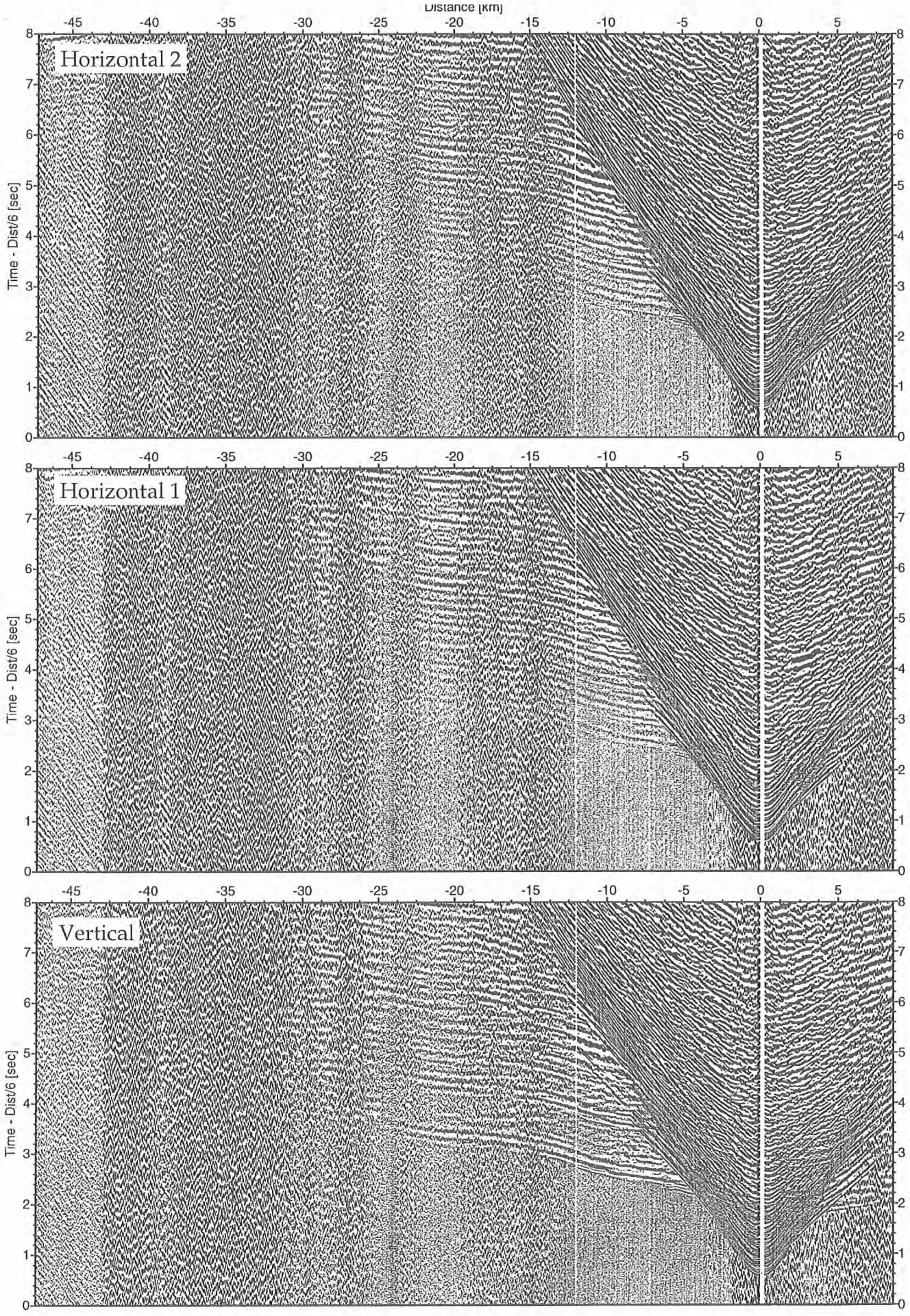


**Figure 6.6.3.40:** Record sections from obs 74 (LG-4.5Hz), SO163, Profile 18.

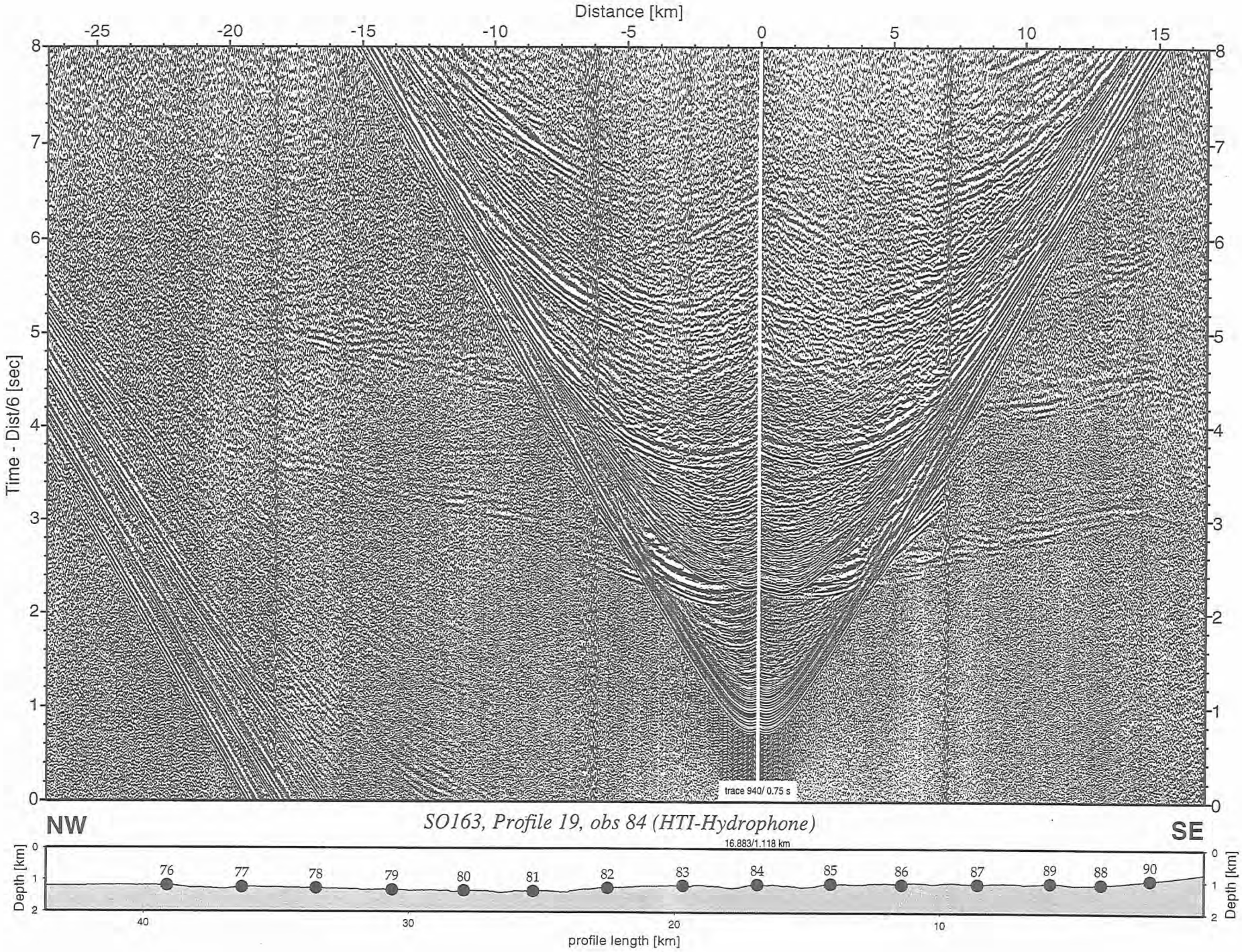


**Figure 6.6.3.43:** Record section from obs 84 (HTI-Hydrophone), Profile 19.

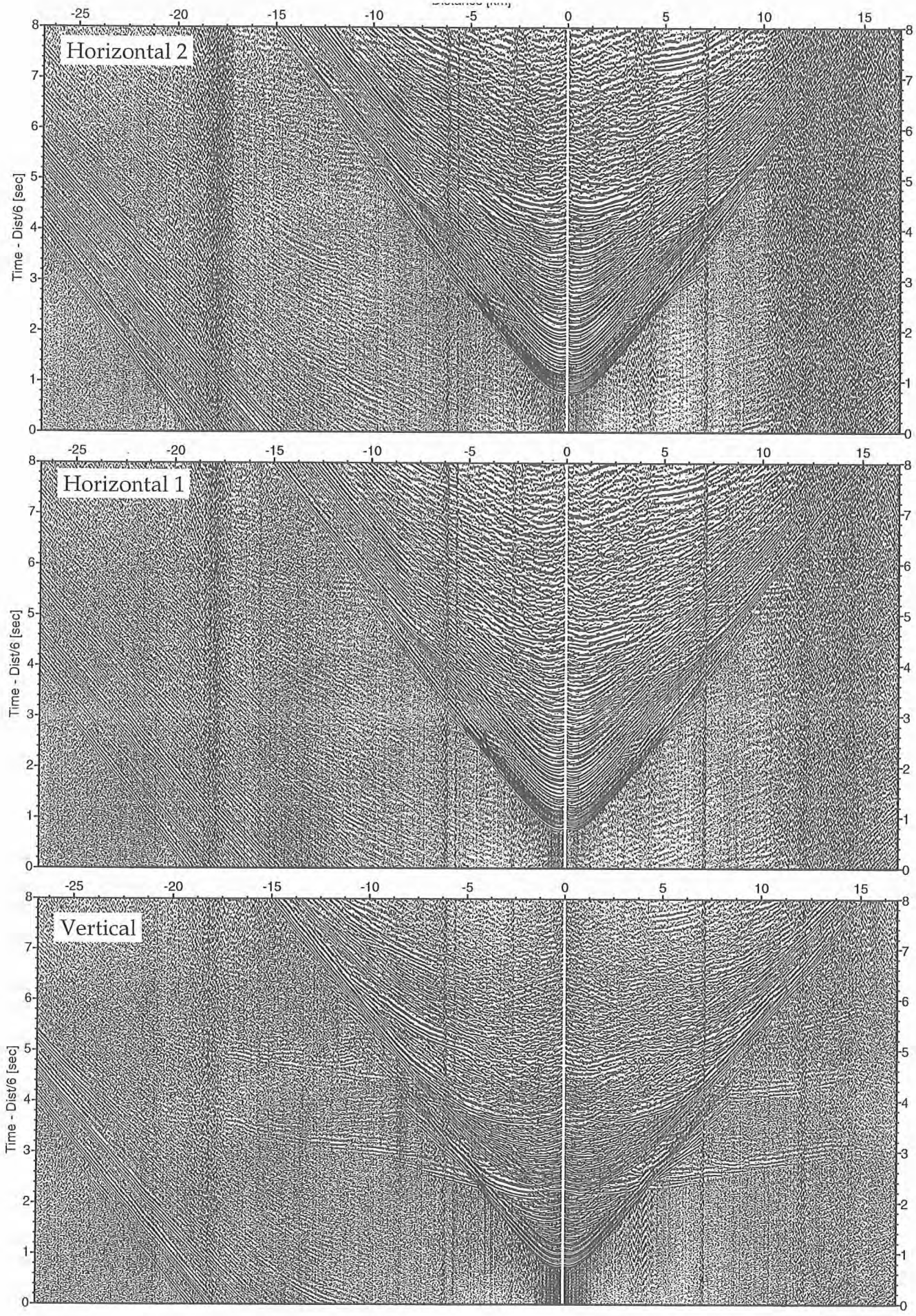


**Figure 6.6.3.44:** Record sections from obs 84 (Owen-4.5Hz), SO163, Profile 19.

**Figure 6.6.3.47:** Record section from obh 76 (OAS-Hydrophone), Profile 22.

**Figure 6.6.3.48:** Record section from obh 77 (OAS-Hydrophone), Profile 21.

**Figure 6.6.3.49:** Record section from obh 78 (OAS-Hydrophone), Profile 22.

**Figure 6.6.3.50:** Record section from obh 79 (OAS-Hydrophone), Profile 22.

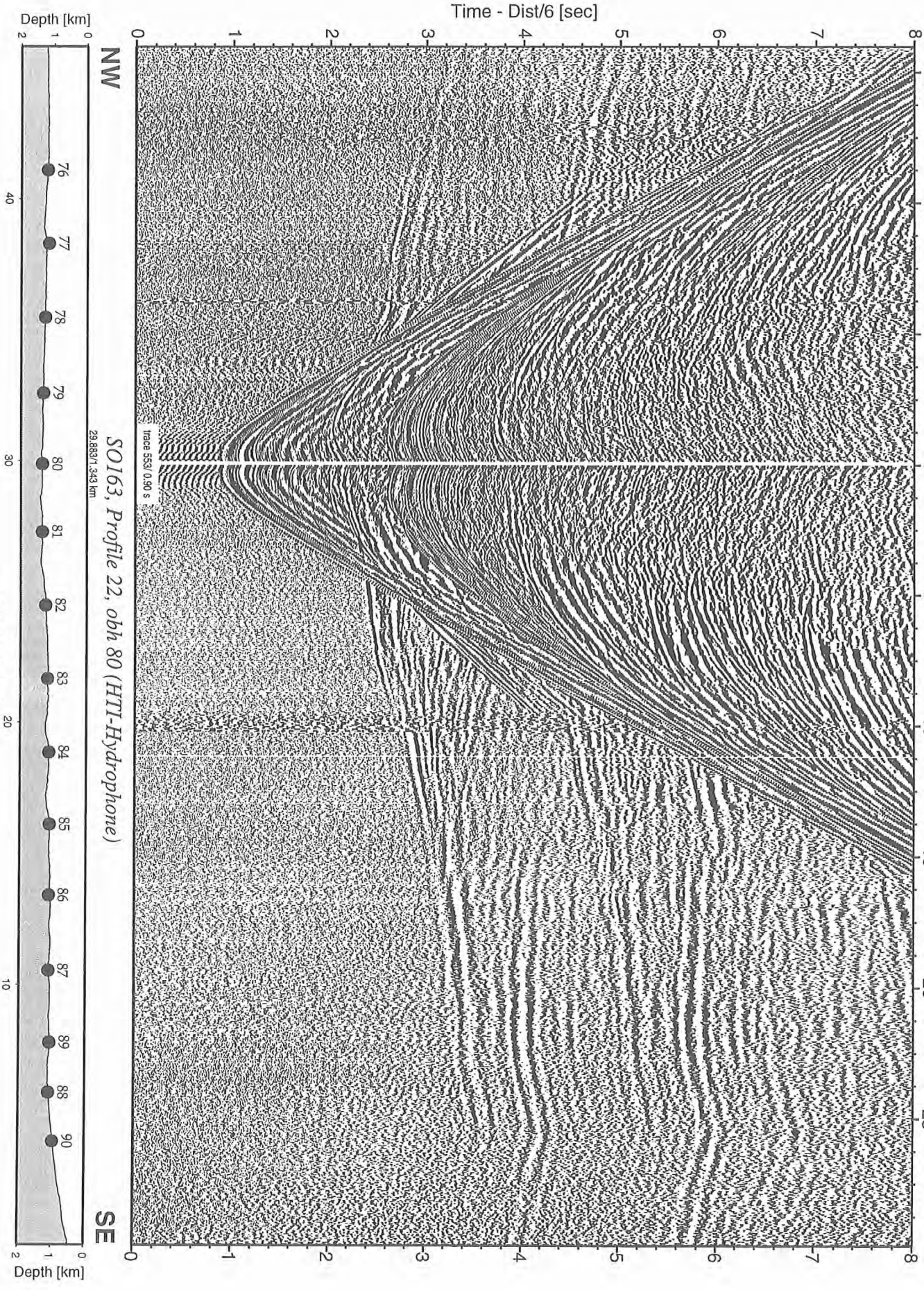


**Figure 6.6.3.51:** Record section from obh 80 (HTI-Hydrophone), Profile 22.

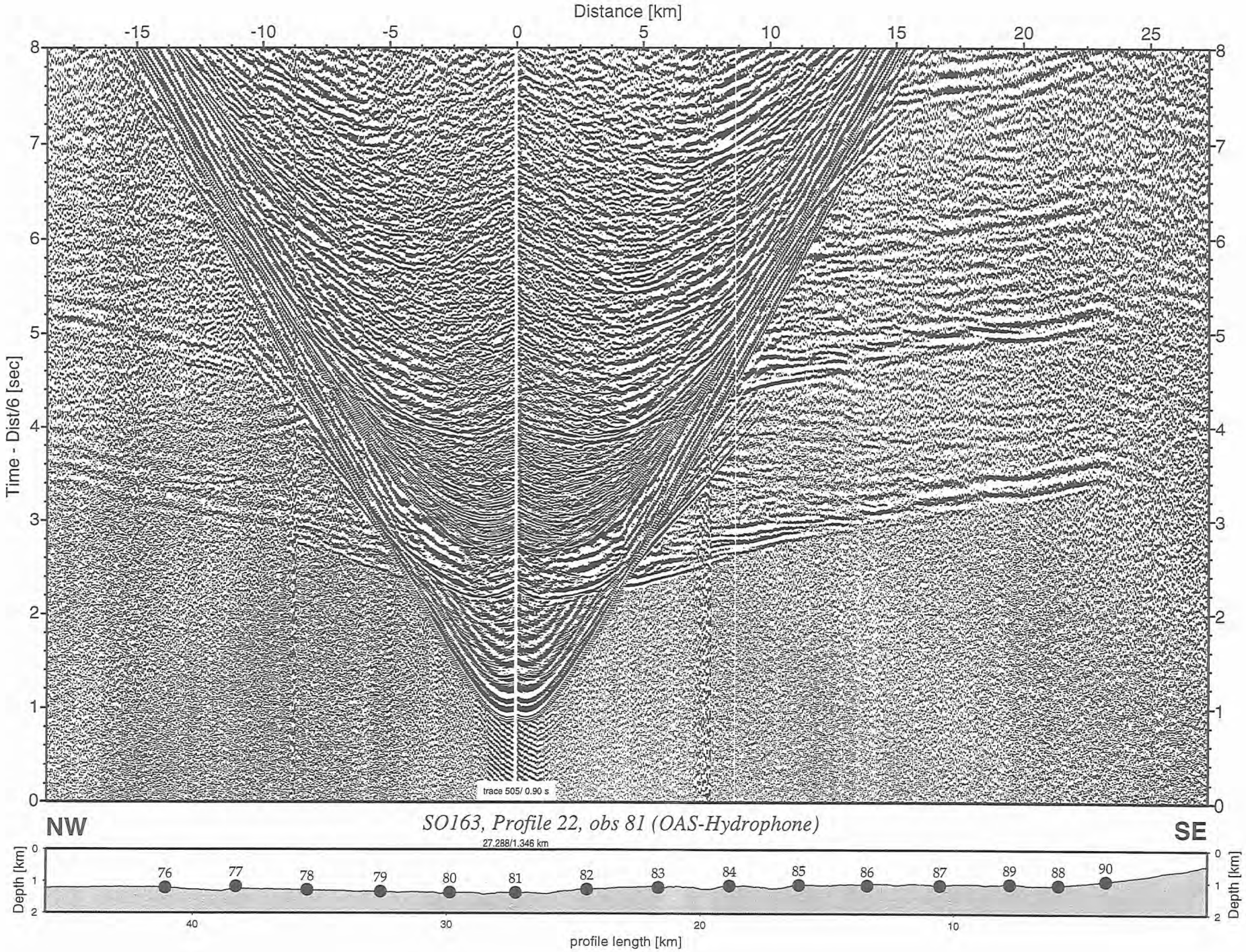


**Figure 6.6.3.52:** Record section from obs 81 (OAS-Hydrophone), Profile 22.

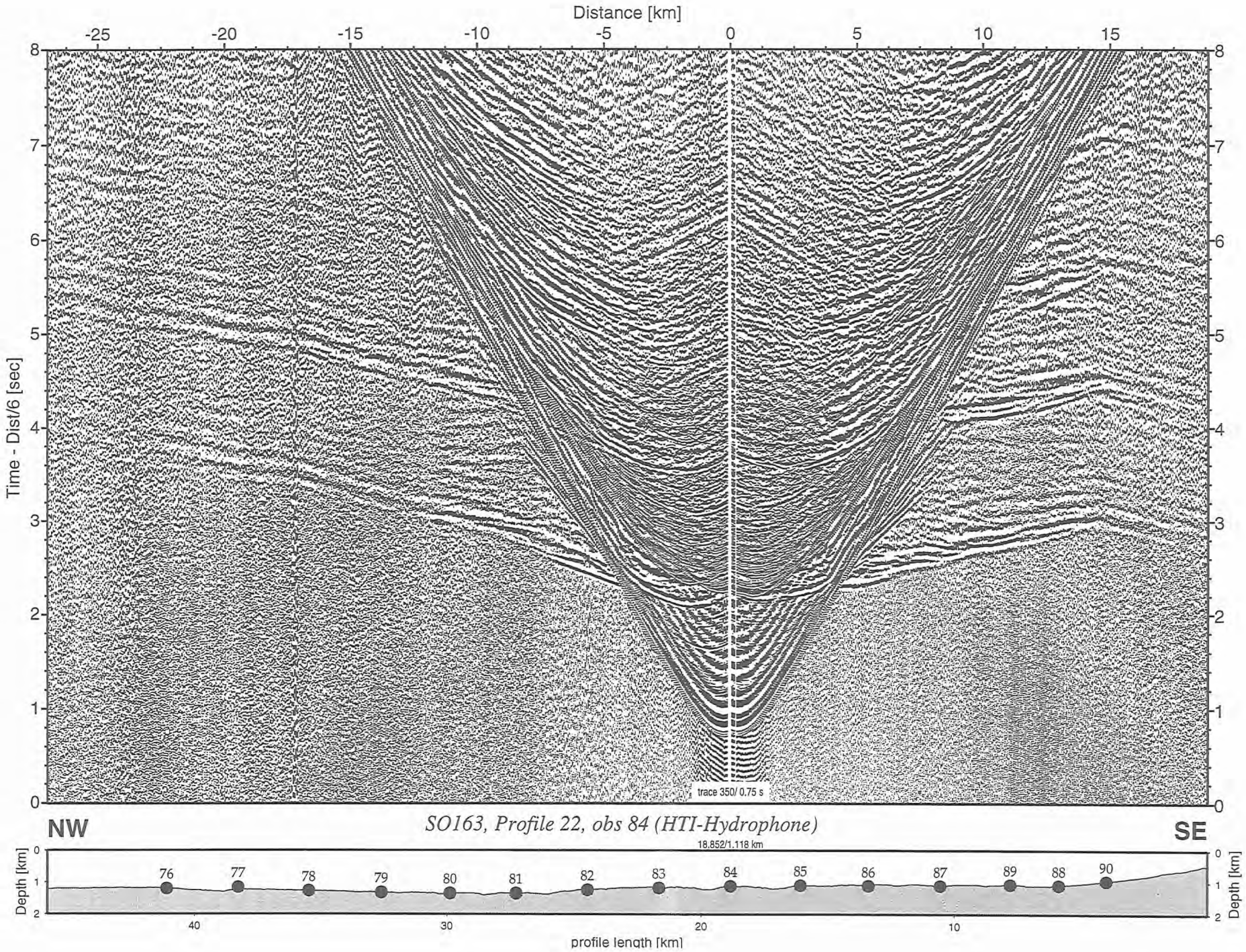


**Figure 6.6.3.55:** Record section from obs 84 (HTI-Hydrophone), Profile 22.

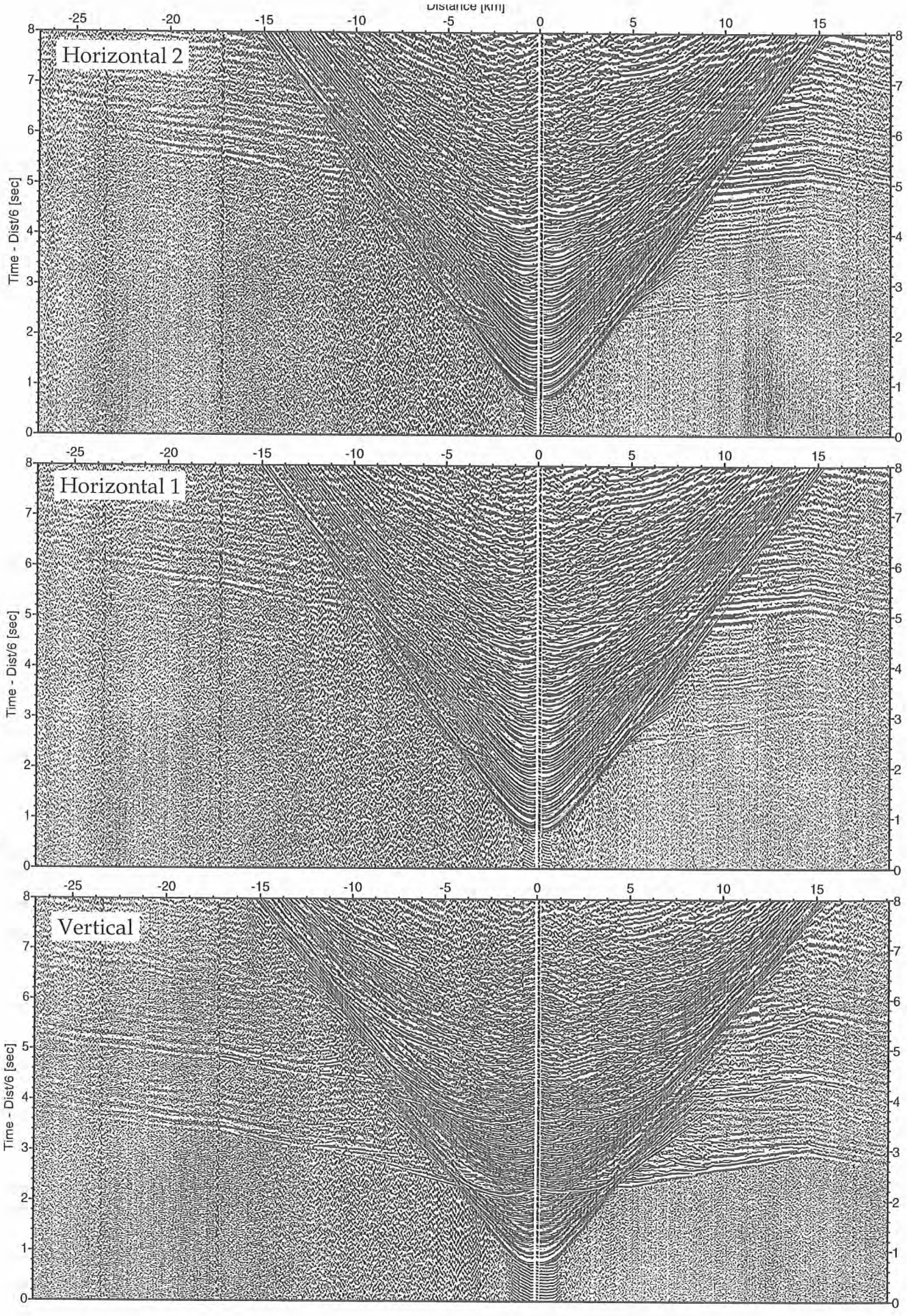


**Figure 6.6.3.56:** Record sections from obs 84 (Owen-4.5Hz), SO163, Profile 22.

**Figure 6.6.3.57:** Record section from obs 85 (OAS-Hydrophone), Profile 22.

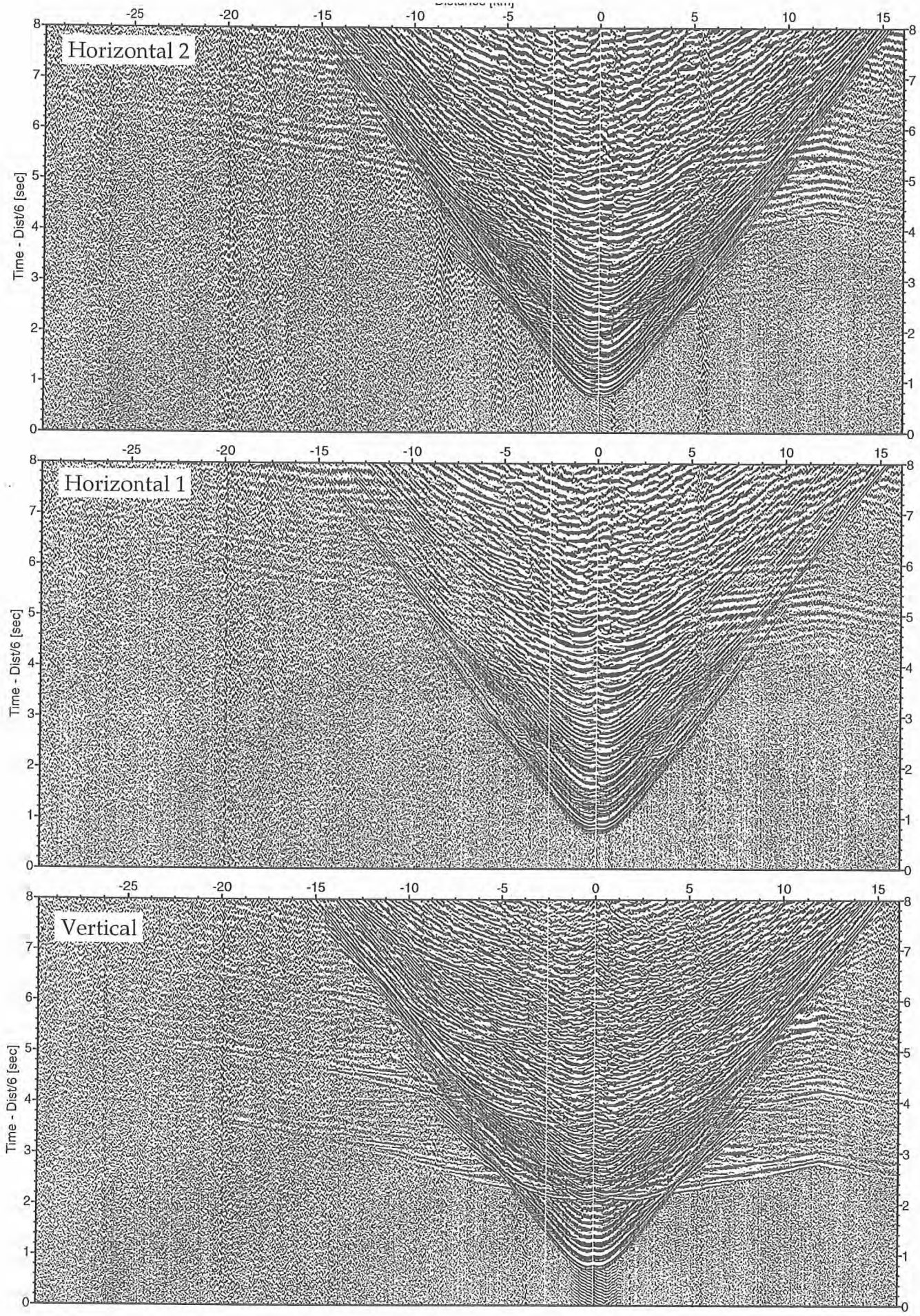


**Figure 6.6.3.58:** Record sections from obs 85 (LG-4.5Hz), SO163, Profile 22.

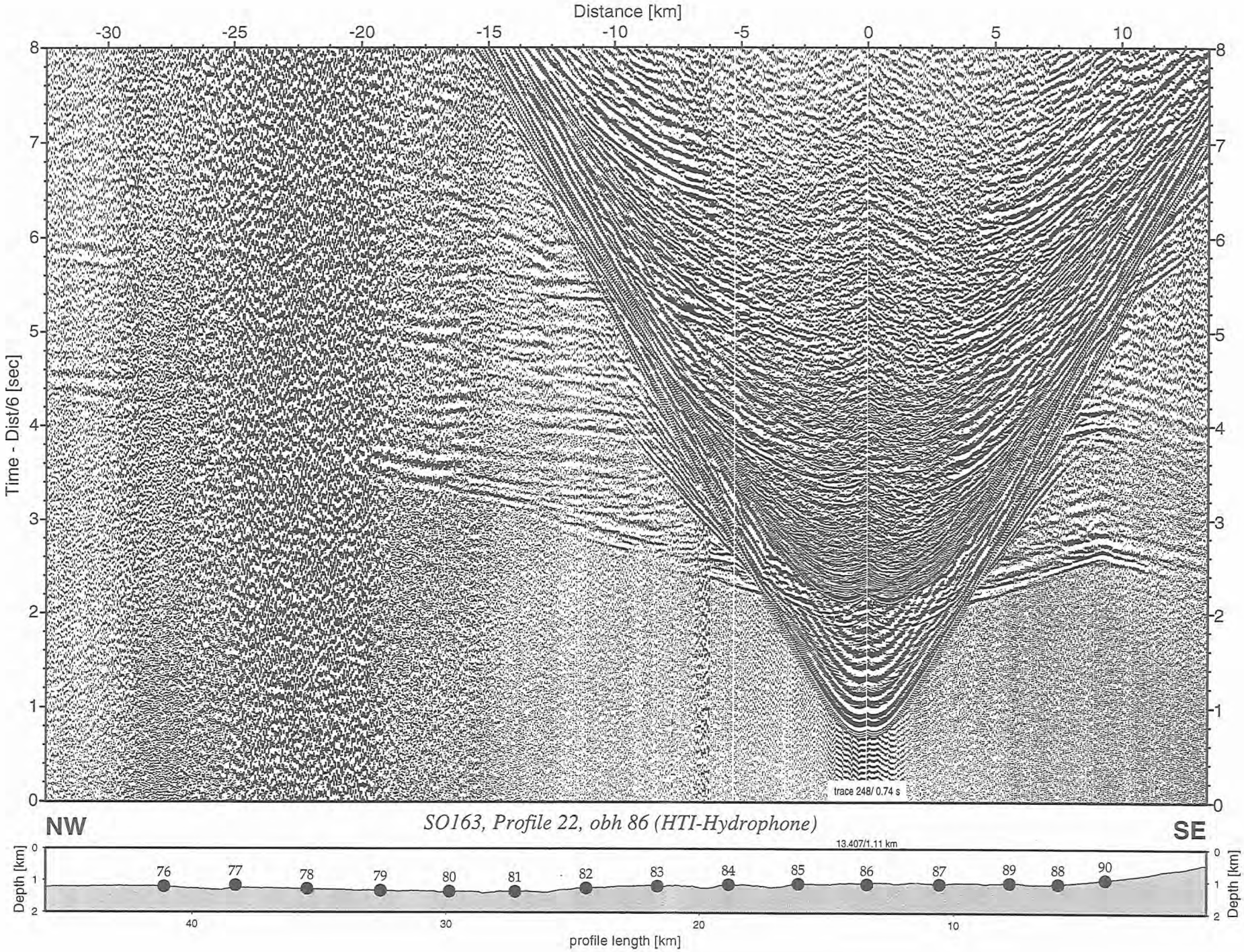


**Figure 6.6.3.59:** Record section from obh 86 (HTI-Hydrophone), Profile 22.

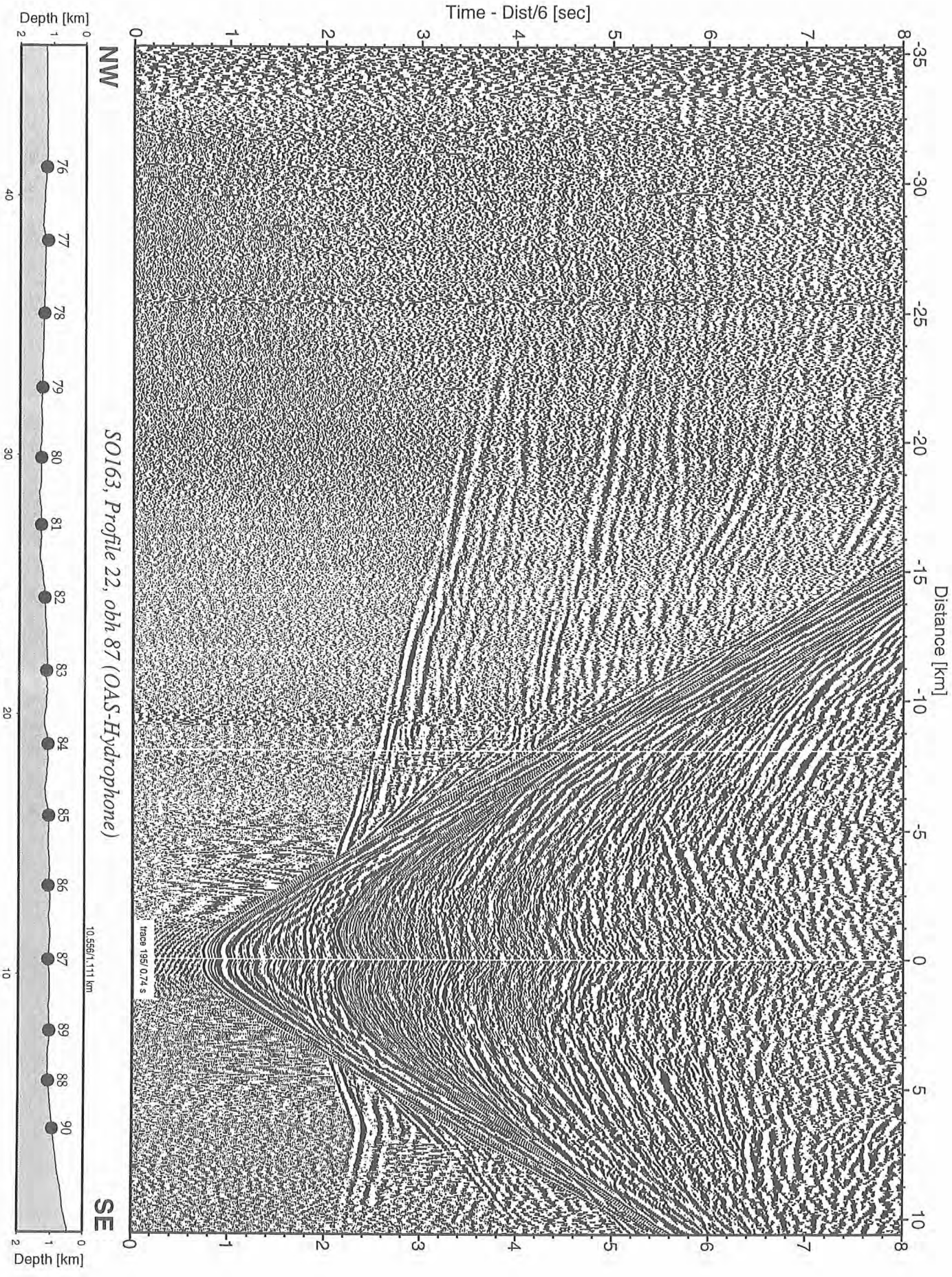


**Figure 6.6.3.60:** Record section from obh 87 (OAS-Hydrophone), Profile 22.

**Figure 6.6.3.61:** Record section from obh 88 (OAS-Hydrophone), Profile 22.

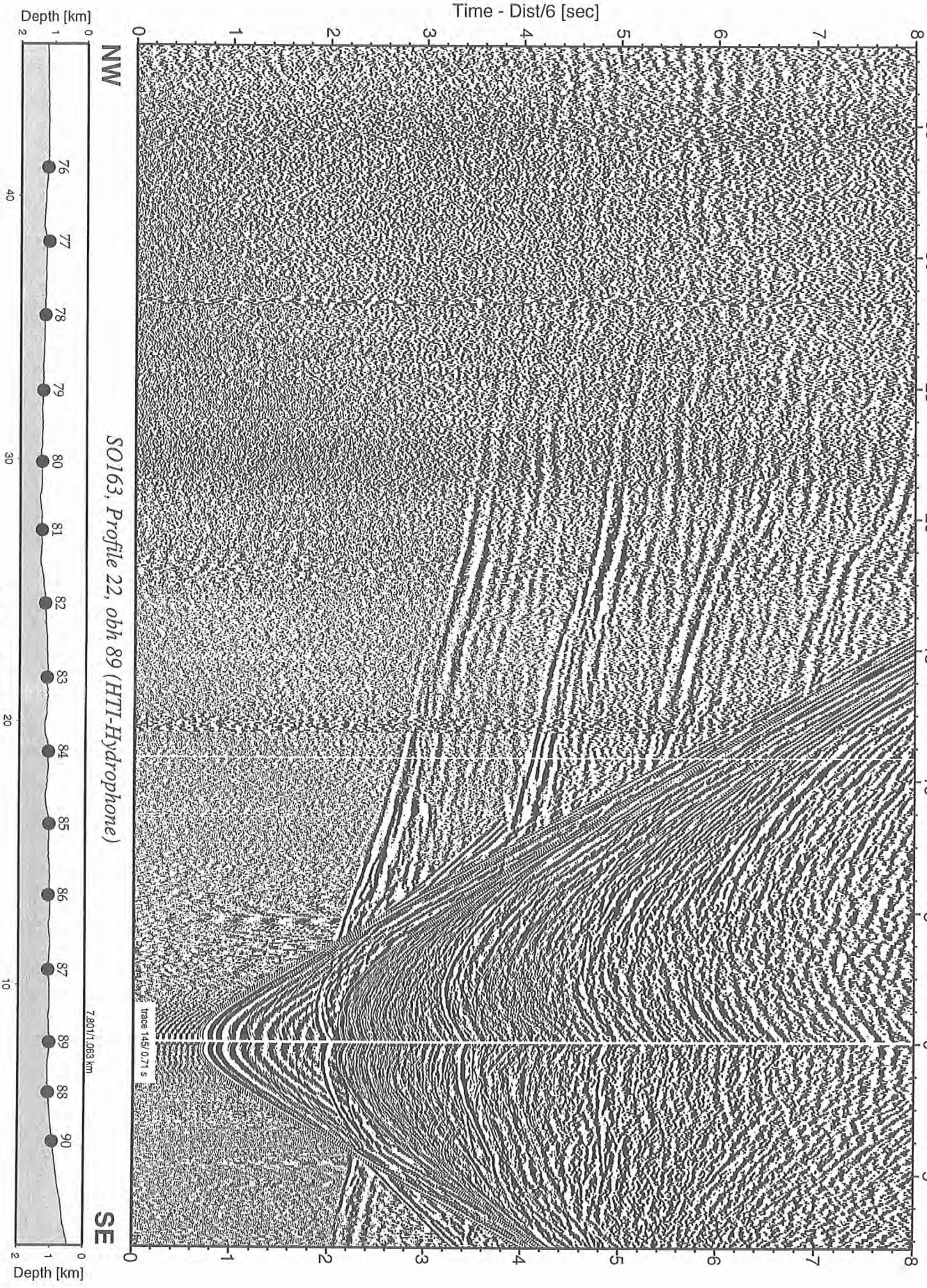


**Figure 6.6.3.62:** Record section from obh 89 (HTI-Hydrophone), Profile 22.

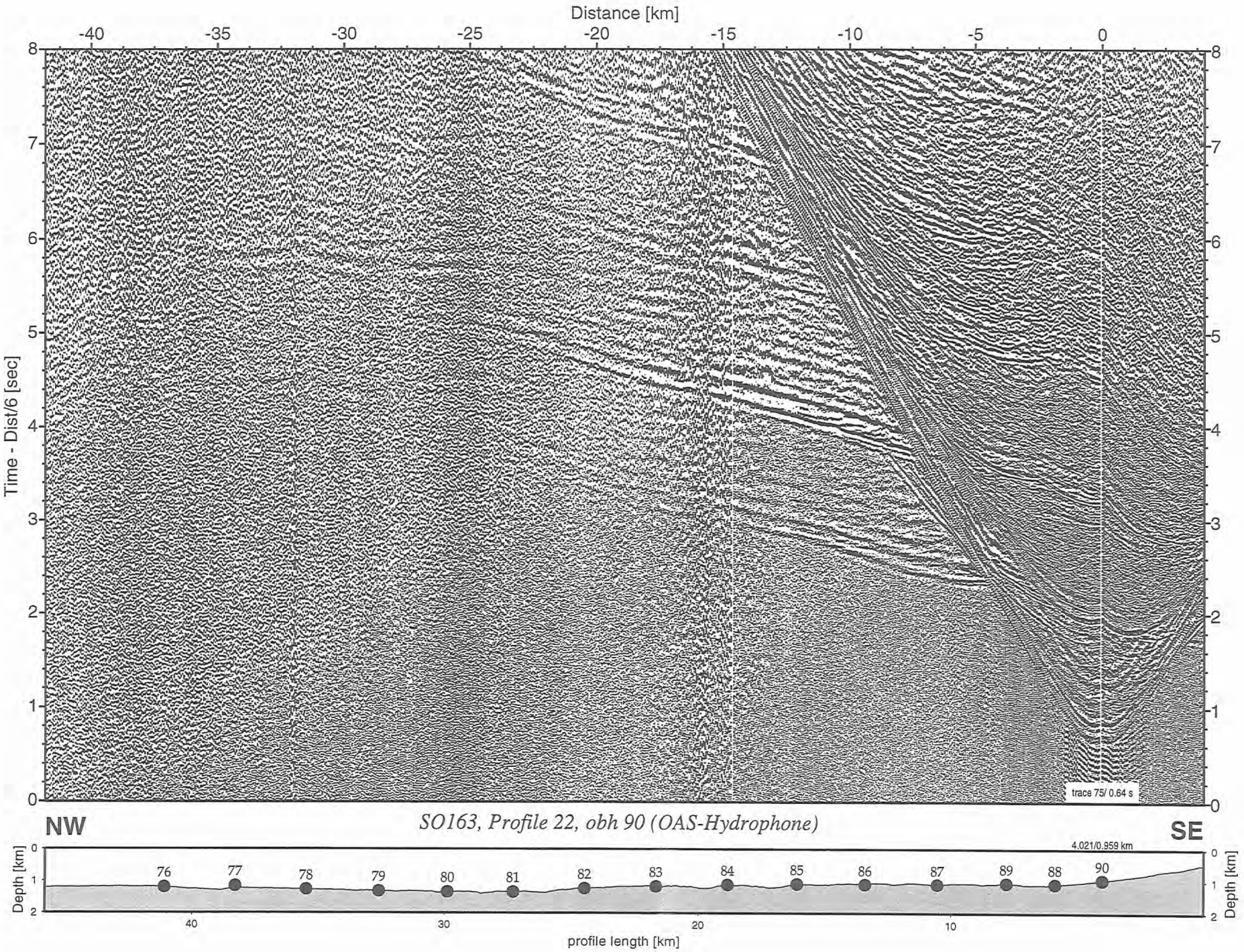


**Figure 6.6.3.63:** Record section from obh 90 (OAS-Hydrophone), Profile 22.

**Figure 6.6.3.64:** Record section from obh 92 (OAS-Hydrophone), Profile 24.

**Figure 6.6.3.69:** Record section from obs 97 (HTI-Hydrophone), Profile 24.

**Figure 6.6.3.70:** Record section from obs 98 (HTI-Hydrophone), Profile 24.

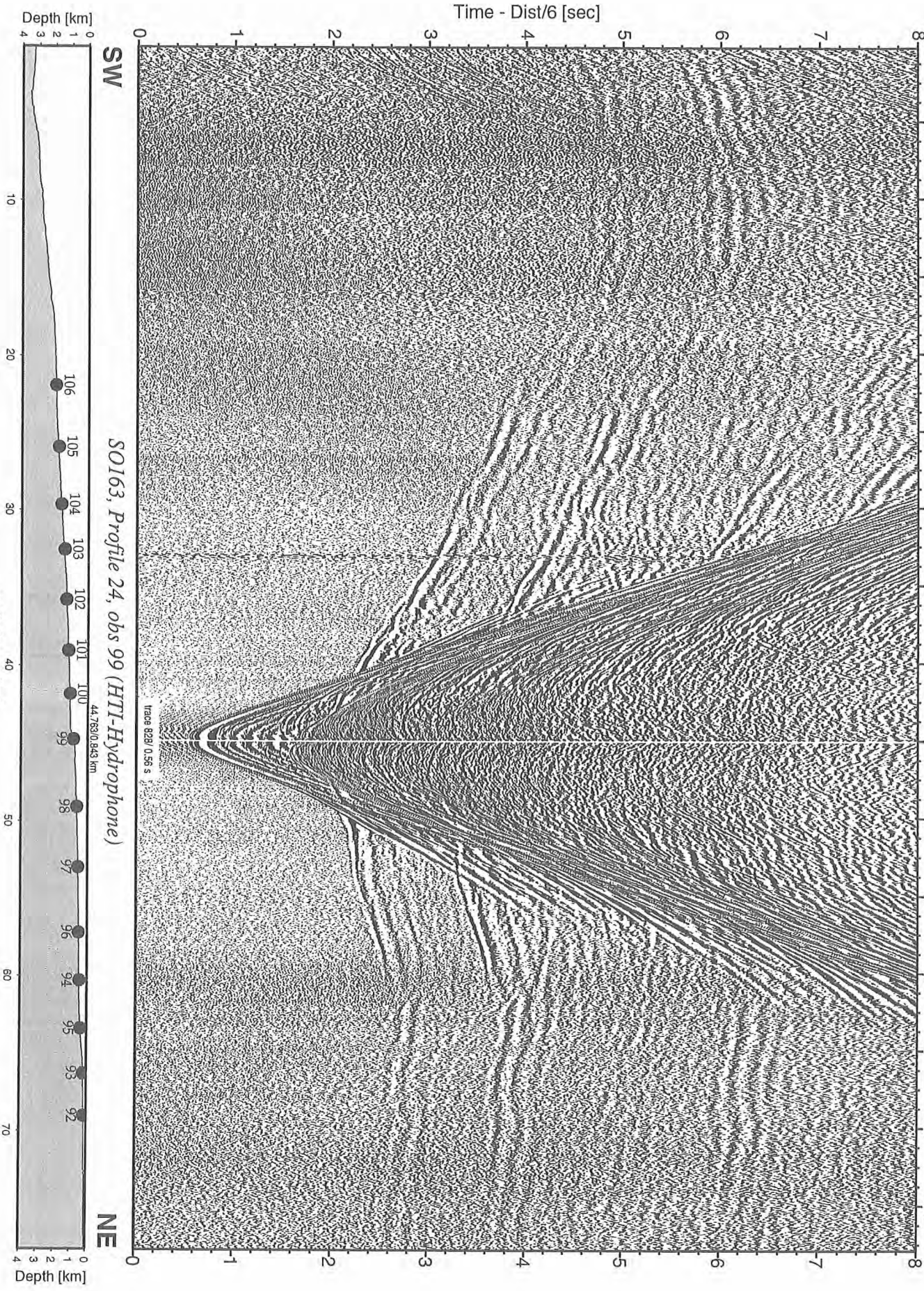


**Figure 6.6.3.71:** Record section from obs 99 (HTI-Hydrophone), Profile 24.

**Figure 6.6.3.72:** Record section from obs 100 (OAS-Hydrophone), Profile 24.

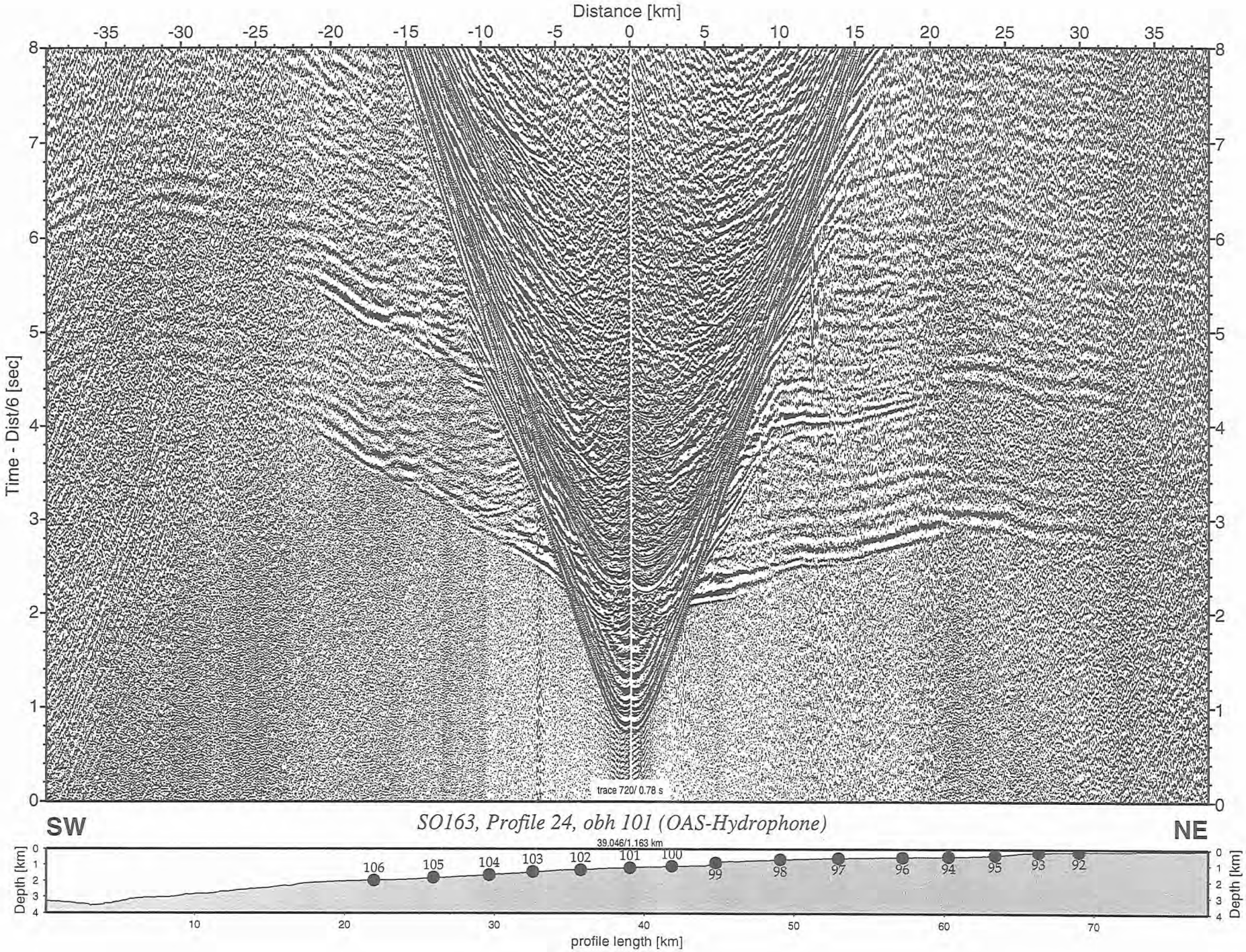


**Figure 6.6.3.73:** Record section from obh 101 (OAS-Hydrophone), Profile 24.

**Figure 6.6.3.74:** Record section from obh 102 (HTI-Hydrophone), Profile 24.

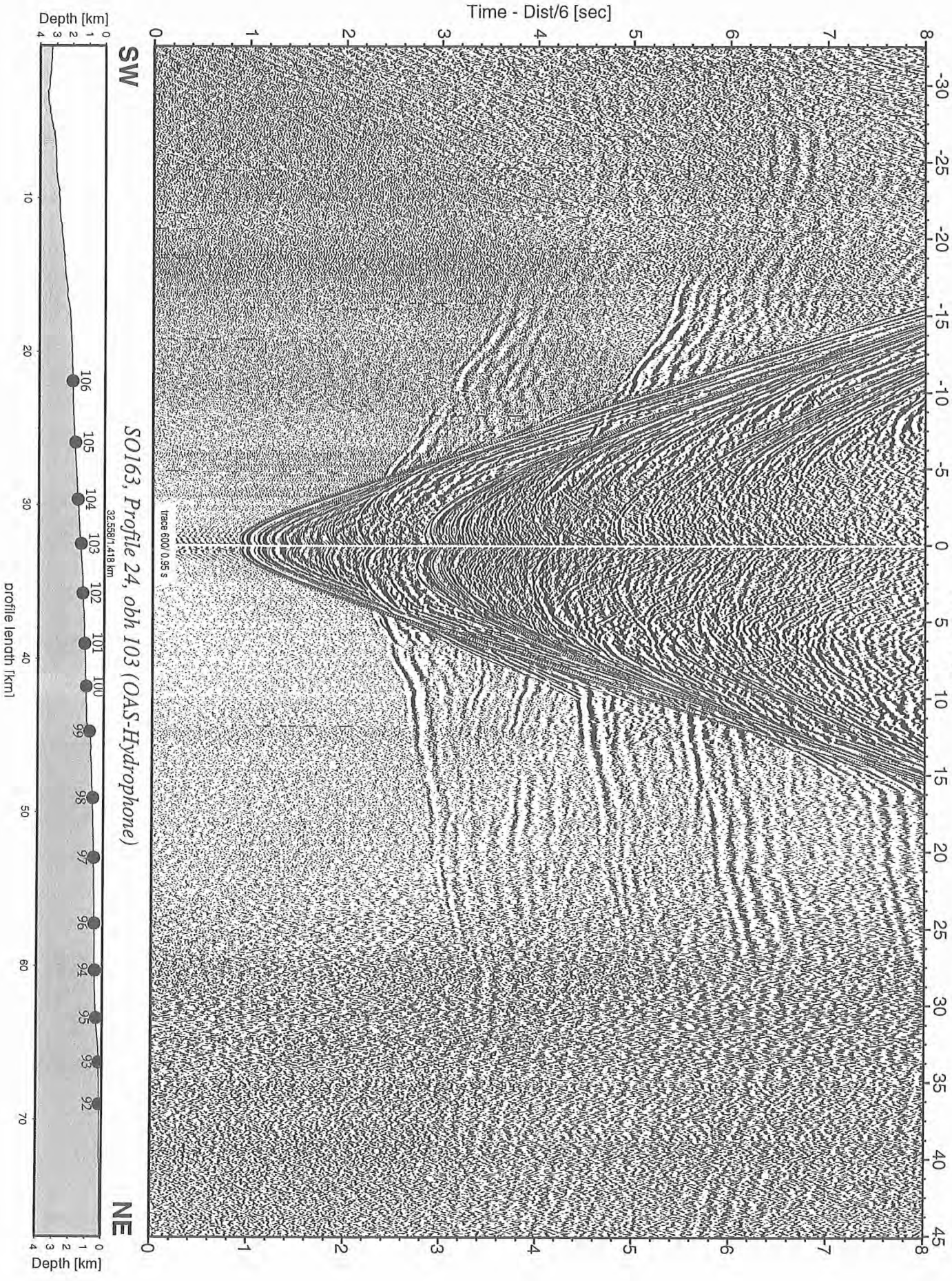


**Figure 6.6.3.75:** Record section from obh 103 (OAS-Hydrophone), Profile 24.

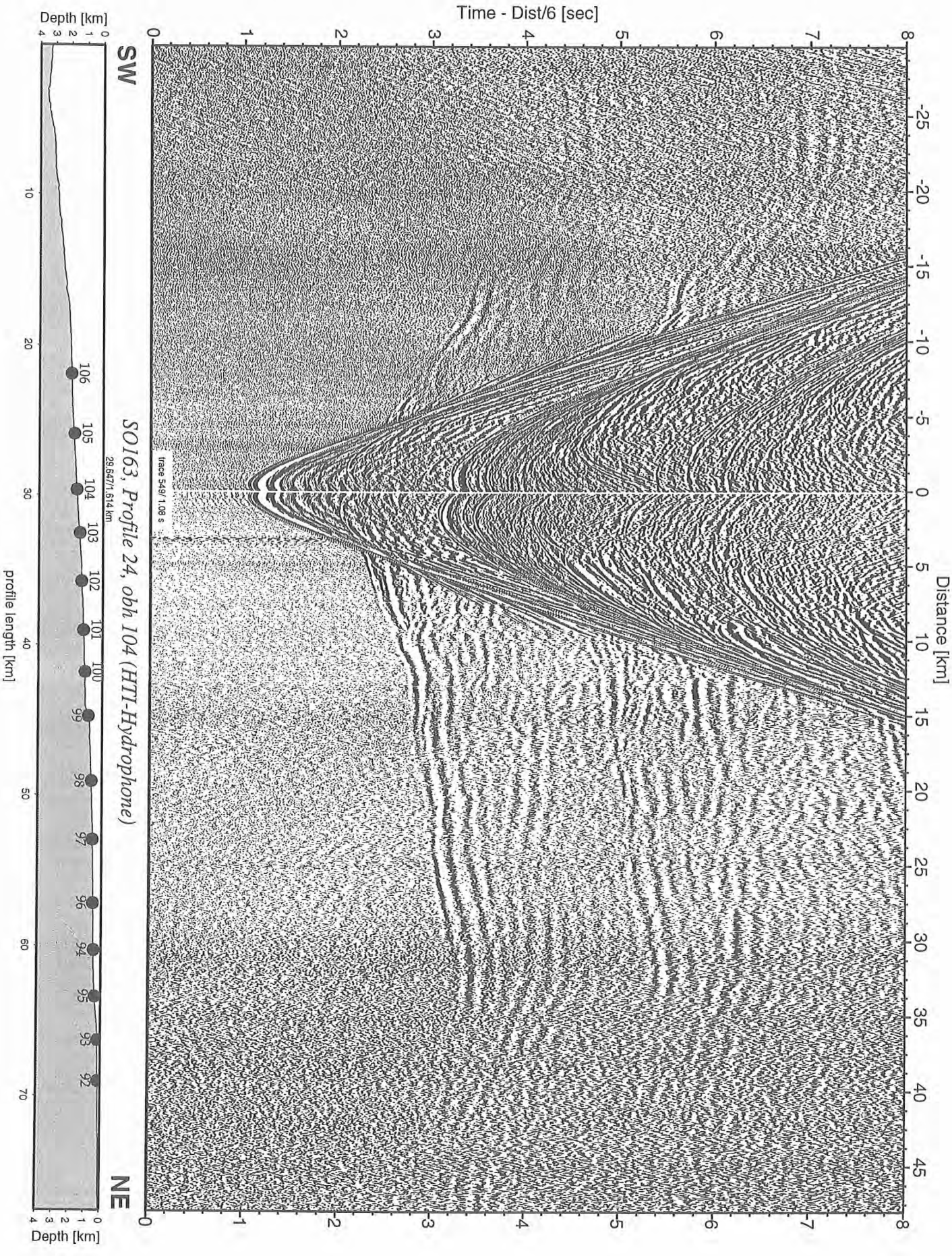


**Figure 6.6.3.76:** Record section from obh 104 (HTI-Hydrophone), Profile 24.

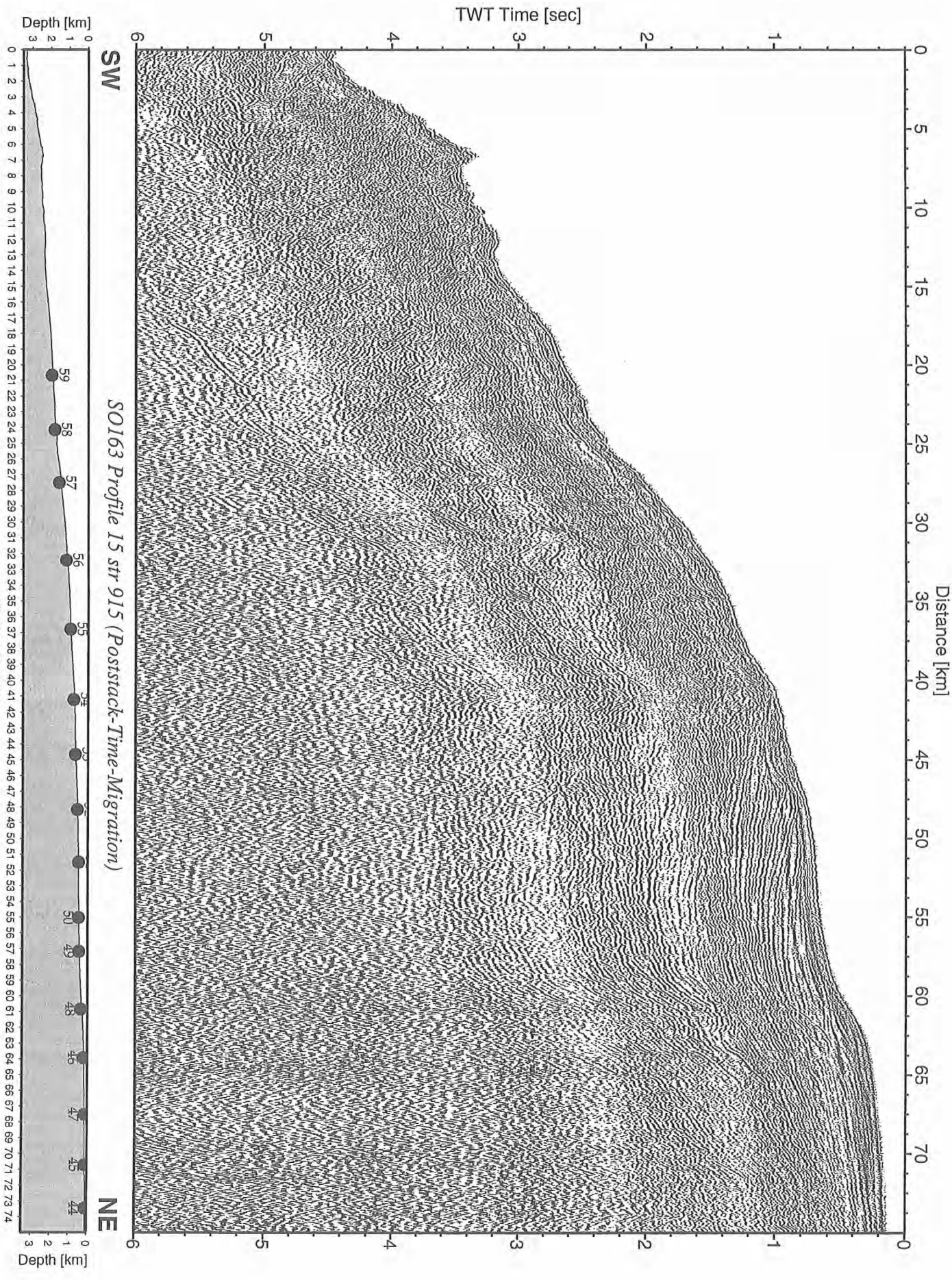


**Figure 6.6.3.79:** Record section from str 915 (Poststack-Time-Migration), Profile 15.

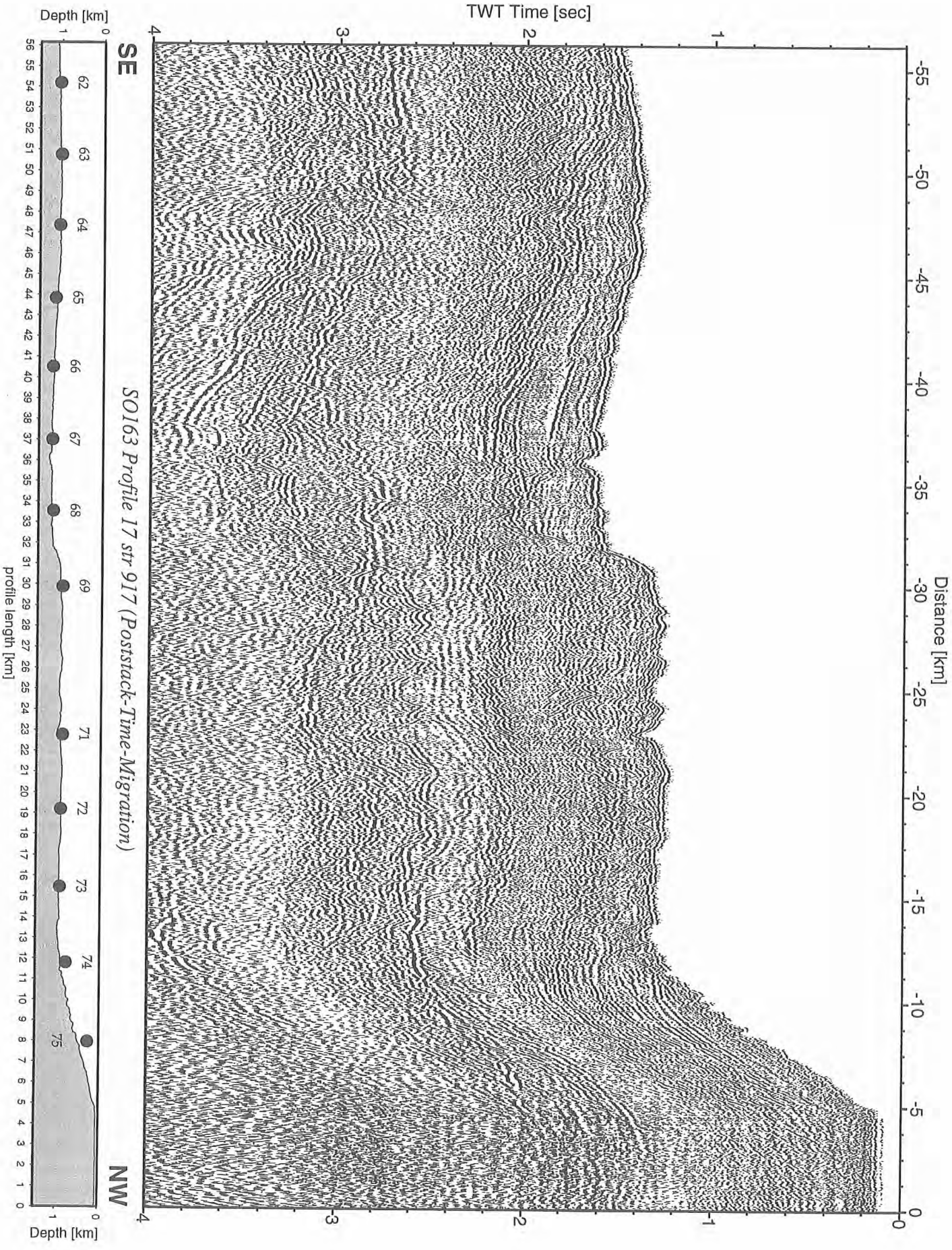


**Figure 6.6.3.80:** Record section from str 917 (Poststack-Time-Migration), Profile 17.

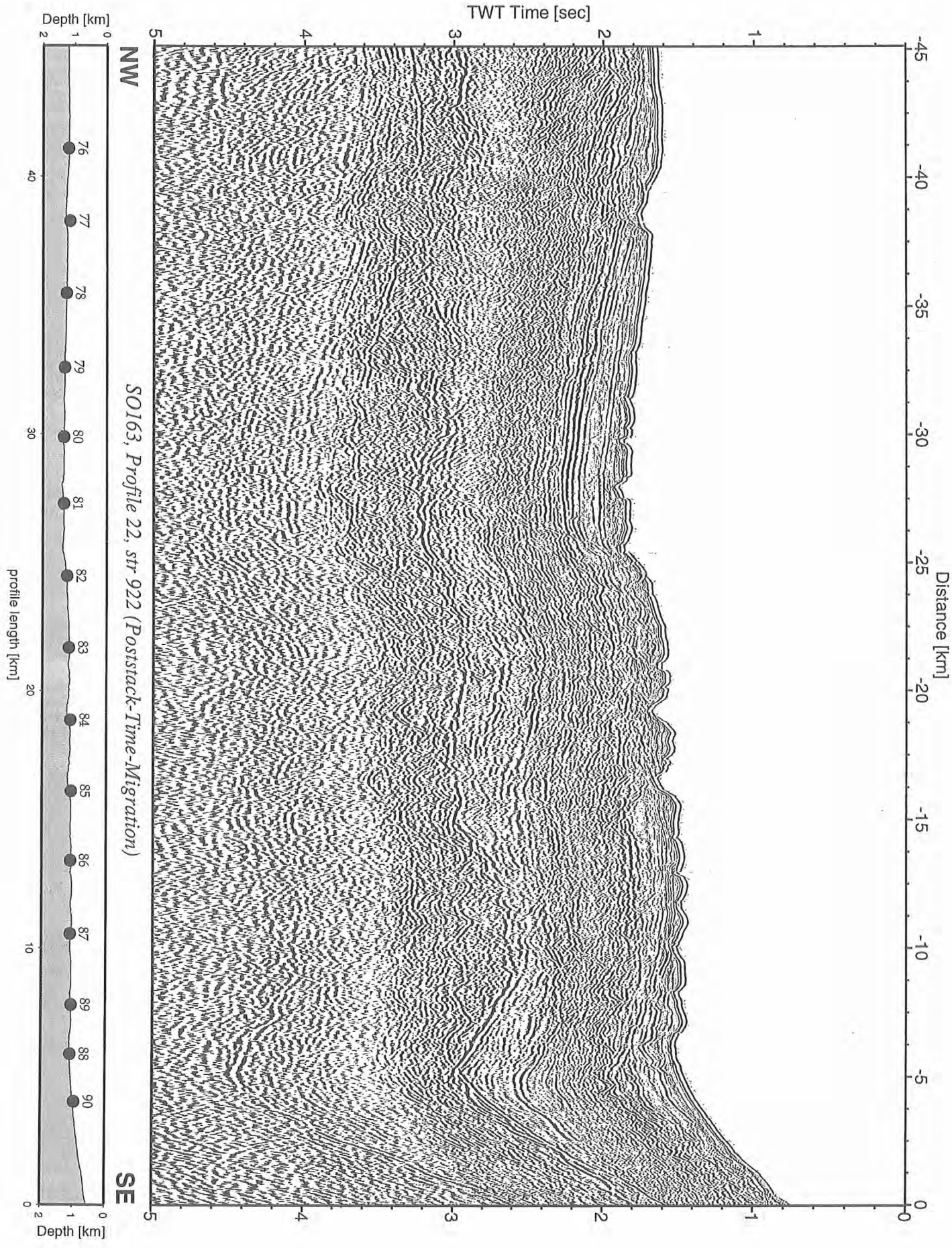


**Figure 6.6.3.81:** Record section from str 922 (Poststack-Time-Migration), Profile 22.

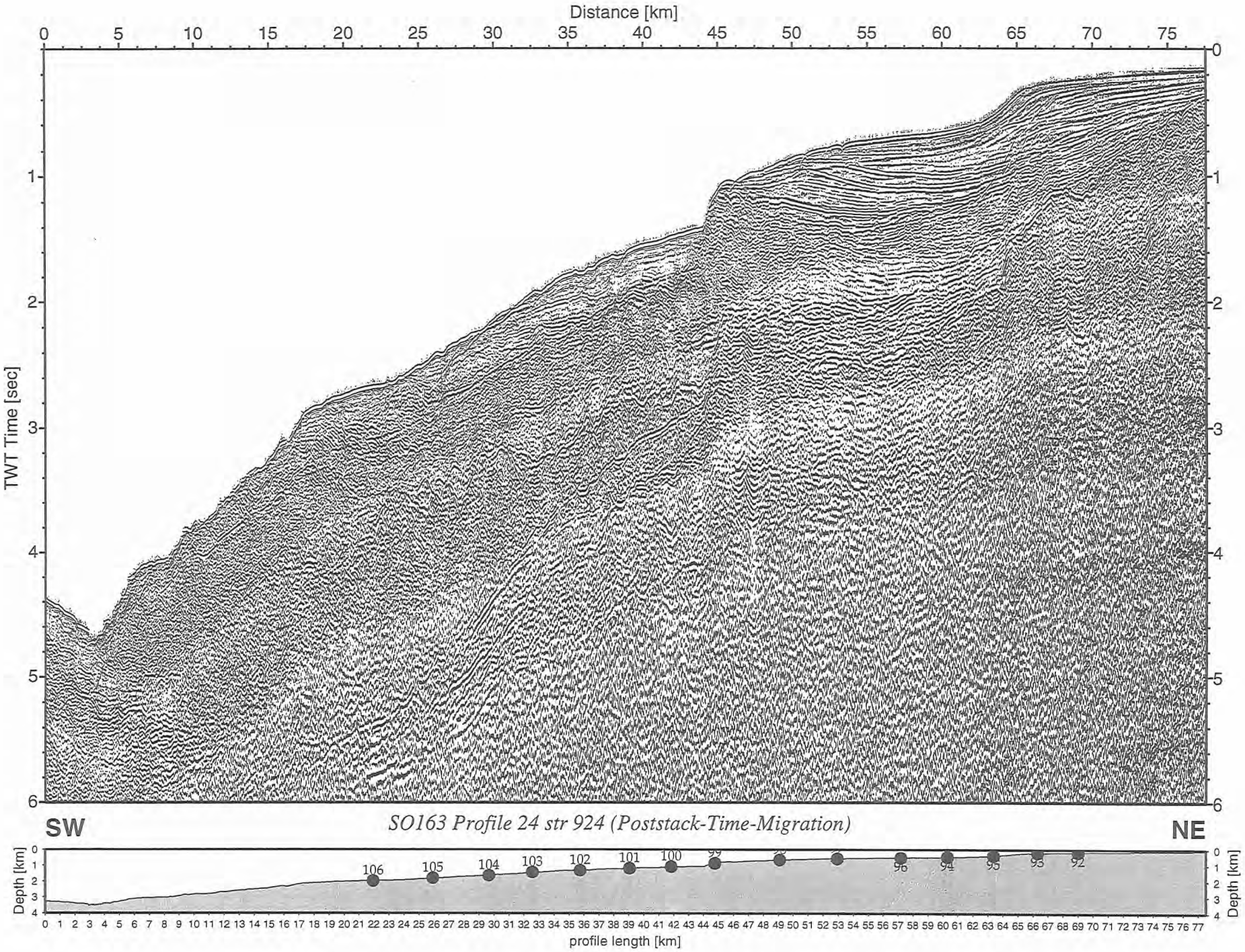


**Figure 6.6.3.82:** Record section from str 924 (Poststack-Time-Migration)S, Profile 24.

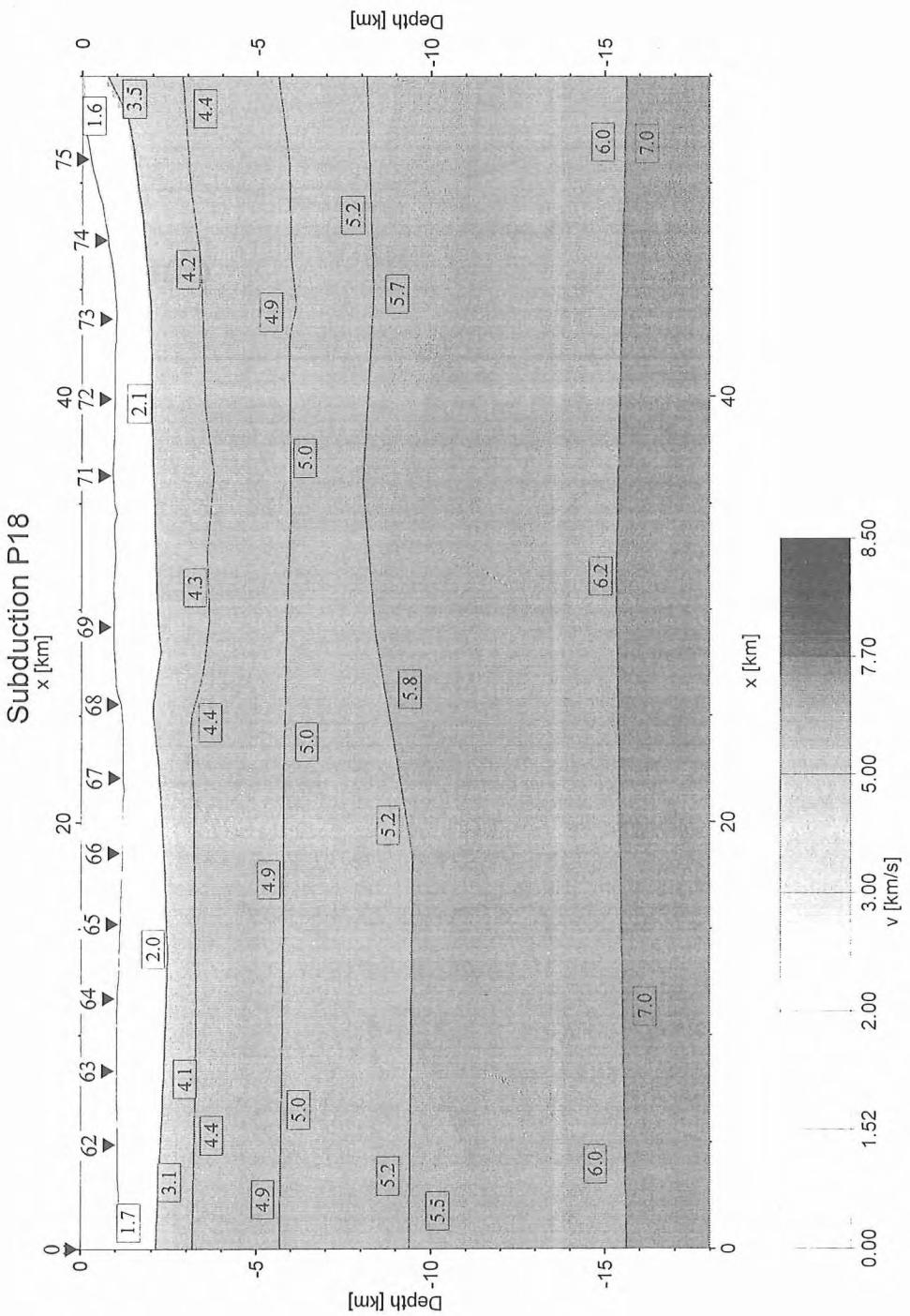


Figure 6.6.3.85: Velocity-depth model of profile P18, SO 163-2. Velocities are give in km/s.

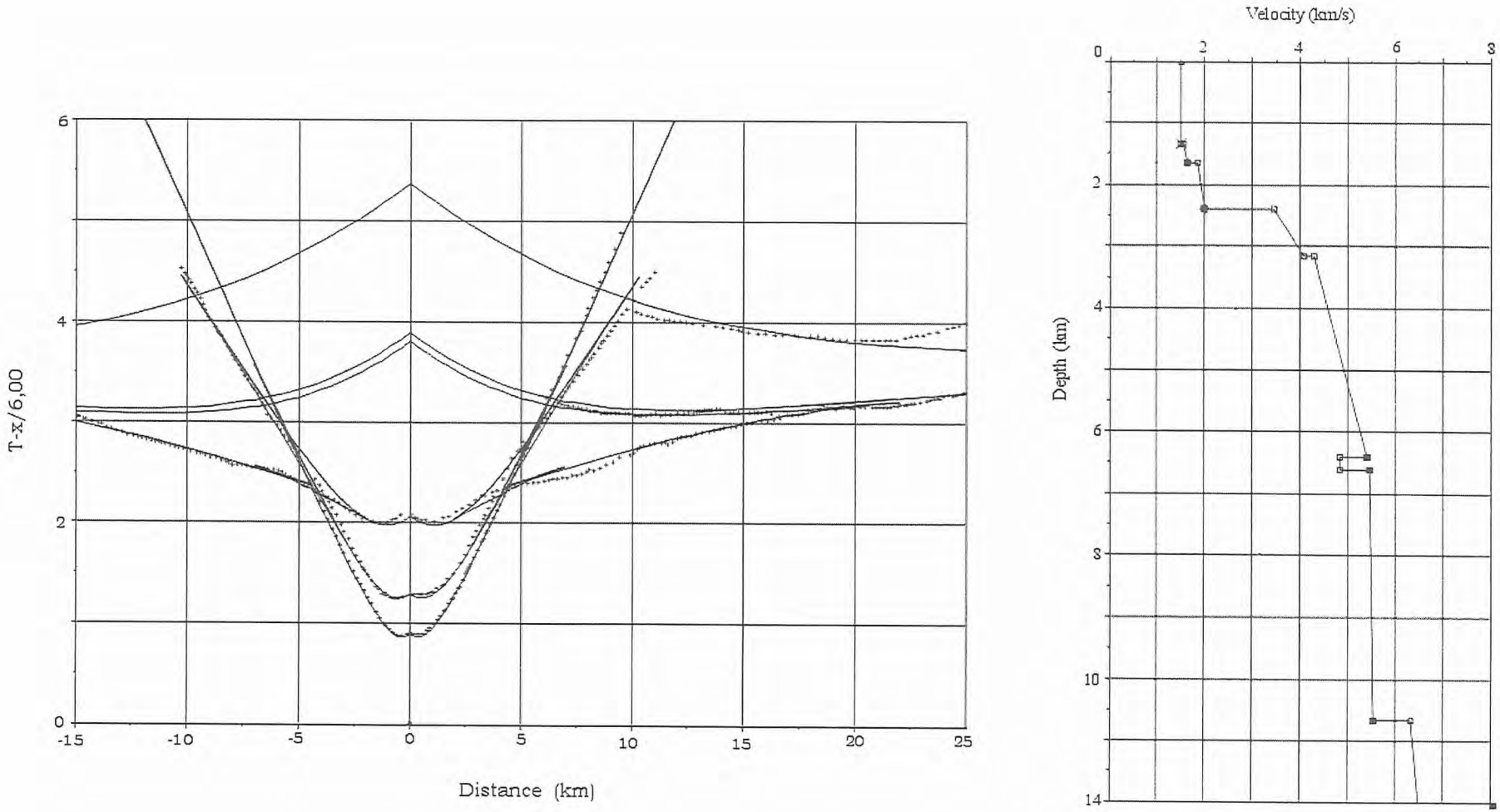


**Figure 6.6.3.86:** Pickings (crosses) from the record of the OBH80, Profil 22, and predicted arrivals according to the 1-D velocity model shown to the right.

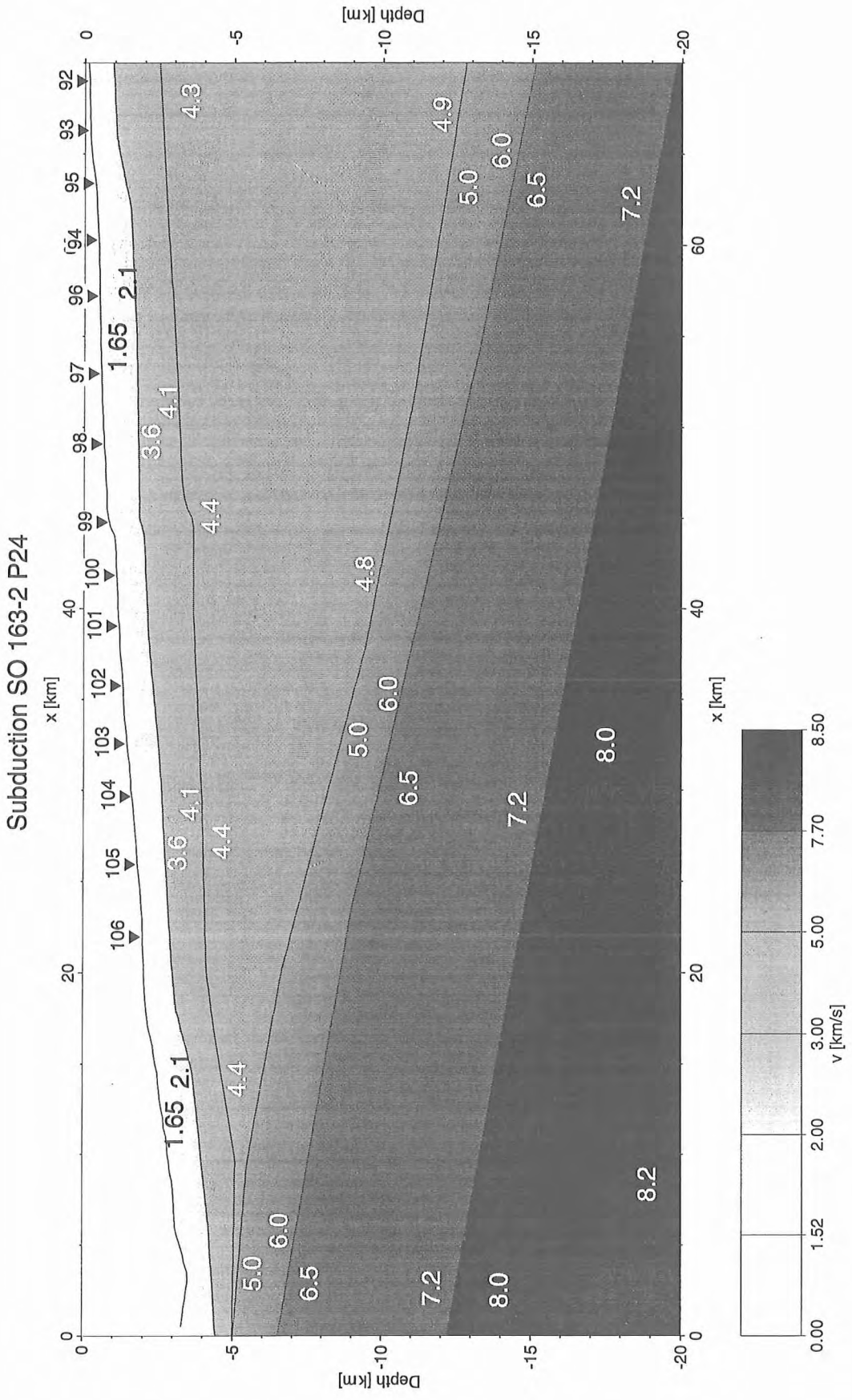


Figure 6.6.3.87: Preliminary Velocity-depth model of profile P24, SO 163-2. Velocities are given in km/s.

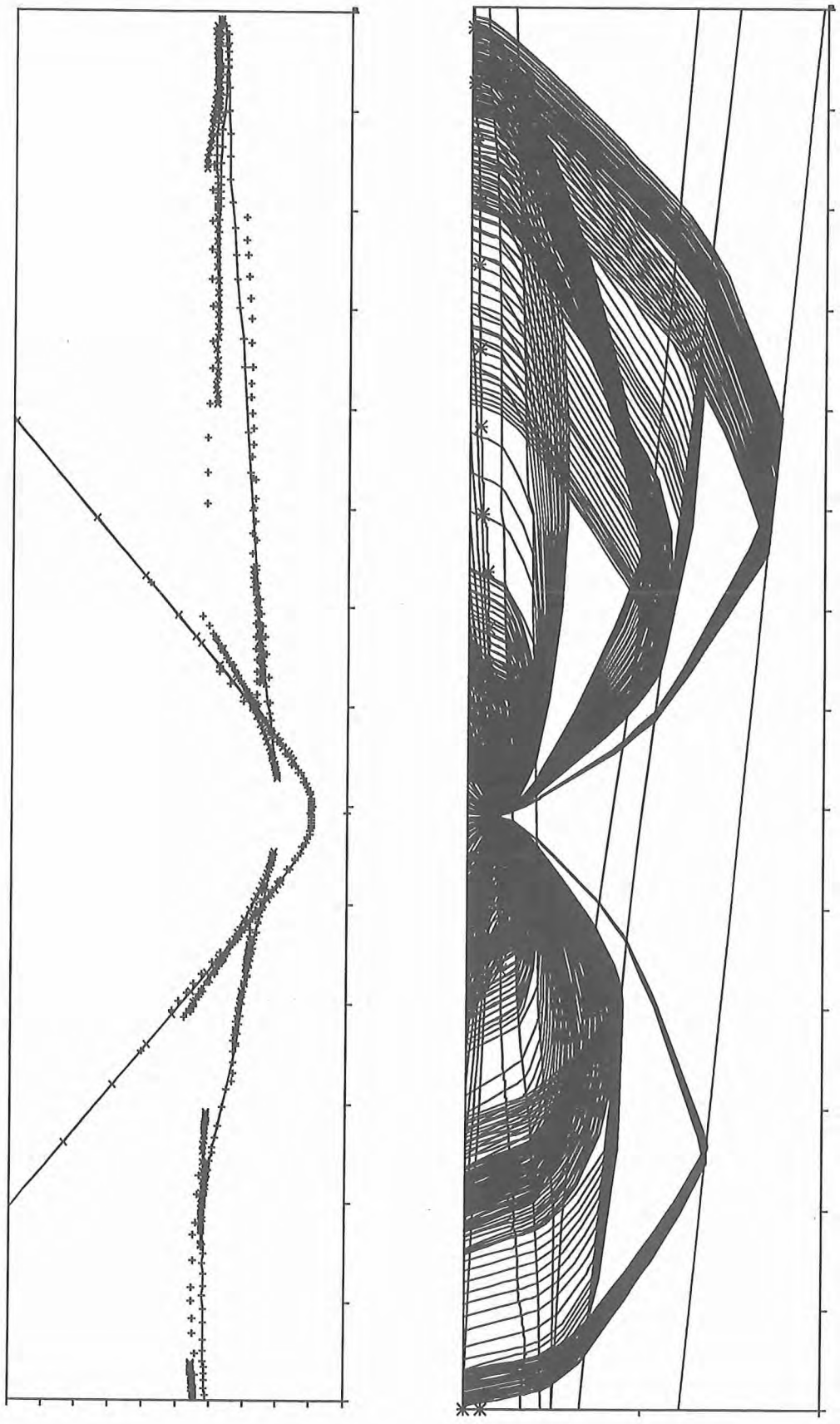

Figure 6.6.3.88: Travel times and ray penetration for OBH 106 of profile P24, SO163-2.

### 6.6.4 The décollement

(M. Schnabel)

The main objectives within the subproject A2 are to determine the key factors that lead to accretion or erosion at convergent margins. The coupling and mass-transfer between upper and lower plate should be studied and seismic images of the resulting tectonic units should be delivered. One target-area is the décollement, which separates the upper and lower plate.
The décollement zone plays an important role in the volatile budget of an subduction zone. It is the focus of mechanical compaction, which releases pore water. New volatile reservoirs are generated by the alteration of sediments. Off Costa Rica, the décollement has in places a high reflectivity, which implies a massive dewatering within about 4 km of the deformation front (Shipley & Moore, 1986). In this zone, porosity decreases from perhaps 50 to 25%. Based on ODP Leg 170, Kimura et al. (1997) showed that the décollement reflection is a result of a very sharp boundary in physical properties, with higher porosities below than above, indicating marked mechanical decoupling. The plate boundary décollement off Costa Rica is structurally divisible into an upper brittle-fracture-dominated domain overlying a lower, ductile domain (Tobin et al., 2001).
During SO163, we wanted to collect new seismic wide-angle data, which should enable us to describe the décollement reflections in greater detail. We are especially interested in the lithological properties, which may be used to analyse and quantify the amount of sediment incorporated in the subduction channel and indicate potential locations of porosity changes and fluid losses. Further on, we hope to deliver important informations for the subproject A3, which is concerned about diagenetic reactions and alterations of sediment.
Along profile line SO81-5, which showed one of the best reflections of the décollement in this region (Hinz et al., 1996), we deployed a profile with 10 OBH and 5 OBS across the lower slope (Figure 6.6.4.1). After a first look at the streamer recording of this profile, we decided to deploy two strike-profiles, the first 2 km, and the second 3.2 km behind the trench. Selected record sections are given in Figures 6.6.3.2 to 6.6.3.41.
The data quality on these profiles were very high on profile 26 up to 29. All hydrophones were recording and showed strong reflections. Only 2 seismometer delivered weak data.
On profile 30 and 31, there were problems with two stations. OBH 124 had not enough battery power, and OBH 130 recorded just electronic noise. But for the rest of the stations, the data quality was very satisfiing. No onboard velocity modelling was done with these stations.
Figures 6.6.4.39 up to 6.6.4.42 show streamer recordings. All three profiles were shot with the G-Gun array and a shot intervall of 20 seconds. The data is poststack time migrated.
On profile 28, the décollement is clearly imaged up to 5 km behind the trench. Below the detachment, a graben-like-structure can be seen.
On the strike-profiles, the décollement can be found at 4.4 seconds TWT. The oceanic crust shows again large fault planes. These fault planes might be pathways for fluids rising from the deeper crust, explaining the high reflectivity of the décollement above. A further analysis of the amplitudes might give answer to this question.

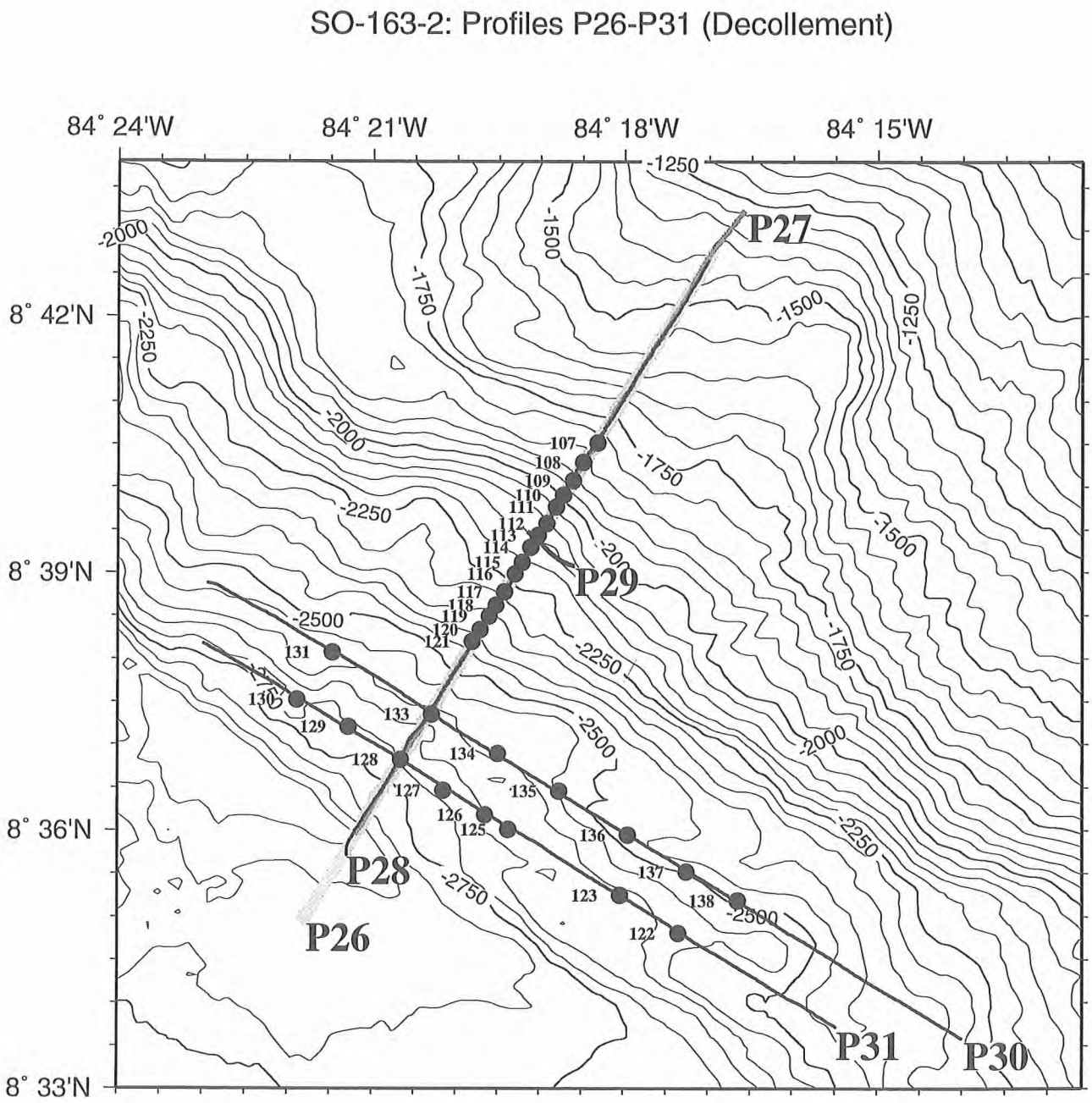


**Figure 6.6.4.1:** Location map of profiles P26-P31 with 50 m isolines. Stations OBH107-OBH121 (lines P26-P29, relocated) and OBH122-OBH138 (lines P30 and P31) are superimposed.

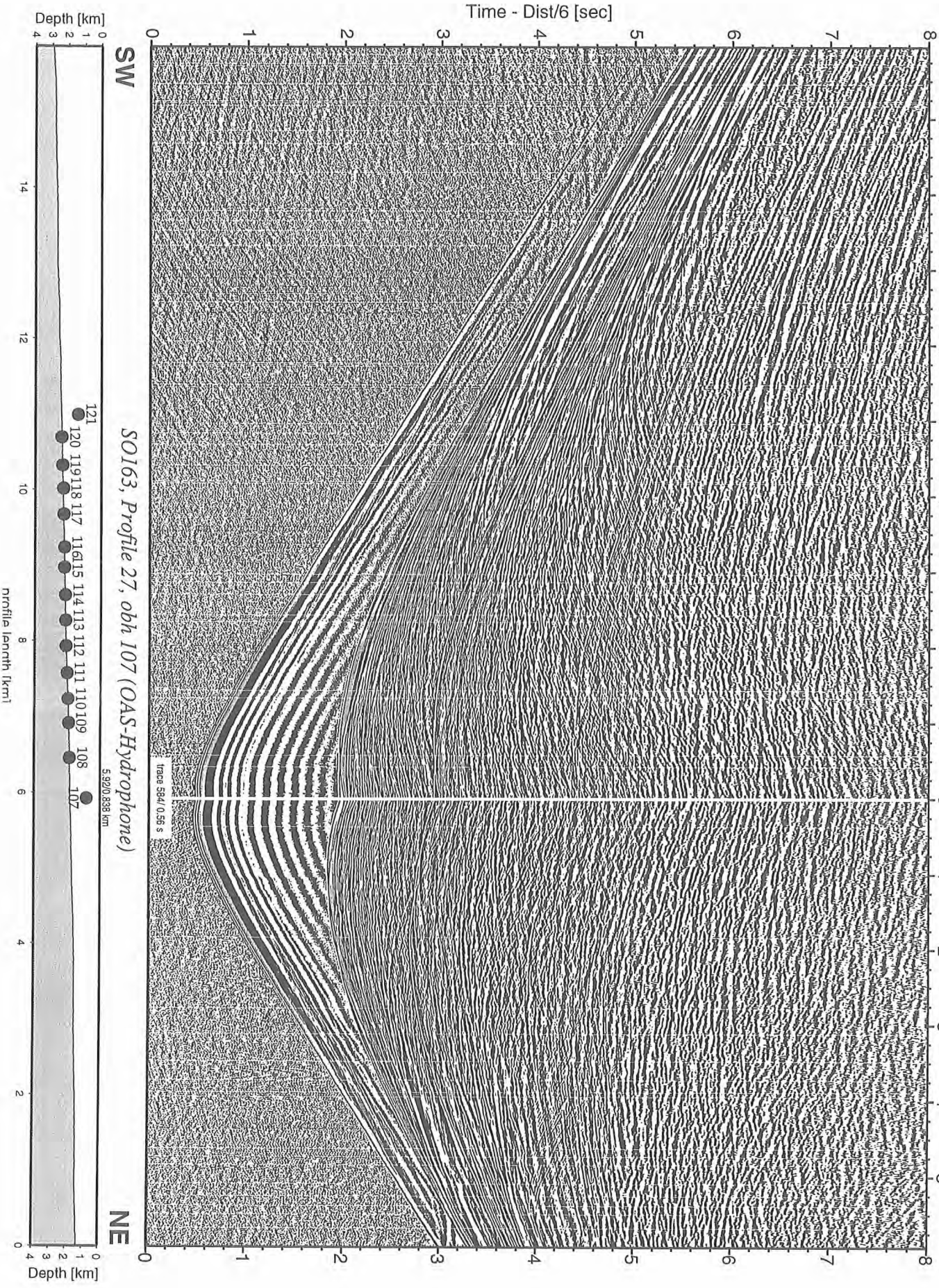


**Figure 6.6.4.2:** Record section from obh 107 (OAS-Hydrophone), Profile 27.

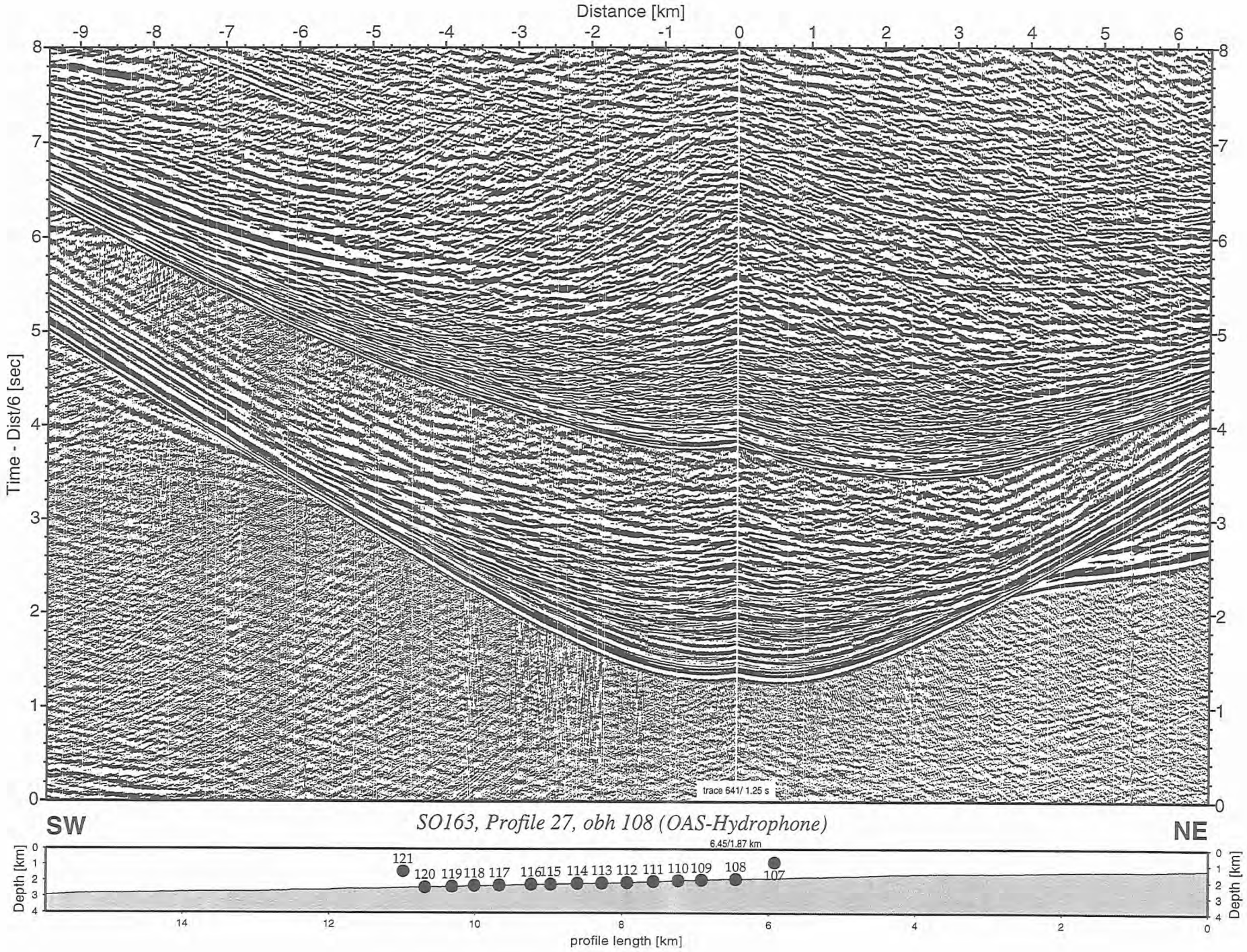


**Figure 6.6.4.3:** Record section from obh 108 (OAS-Hydrophone), Profile 27.

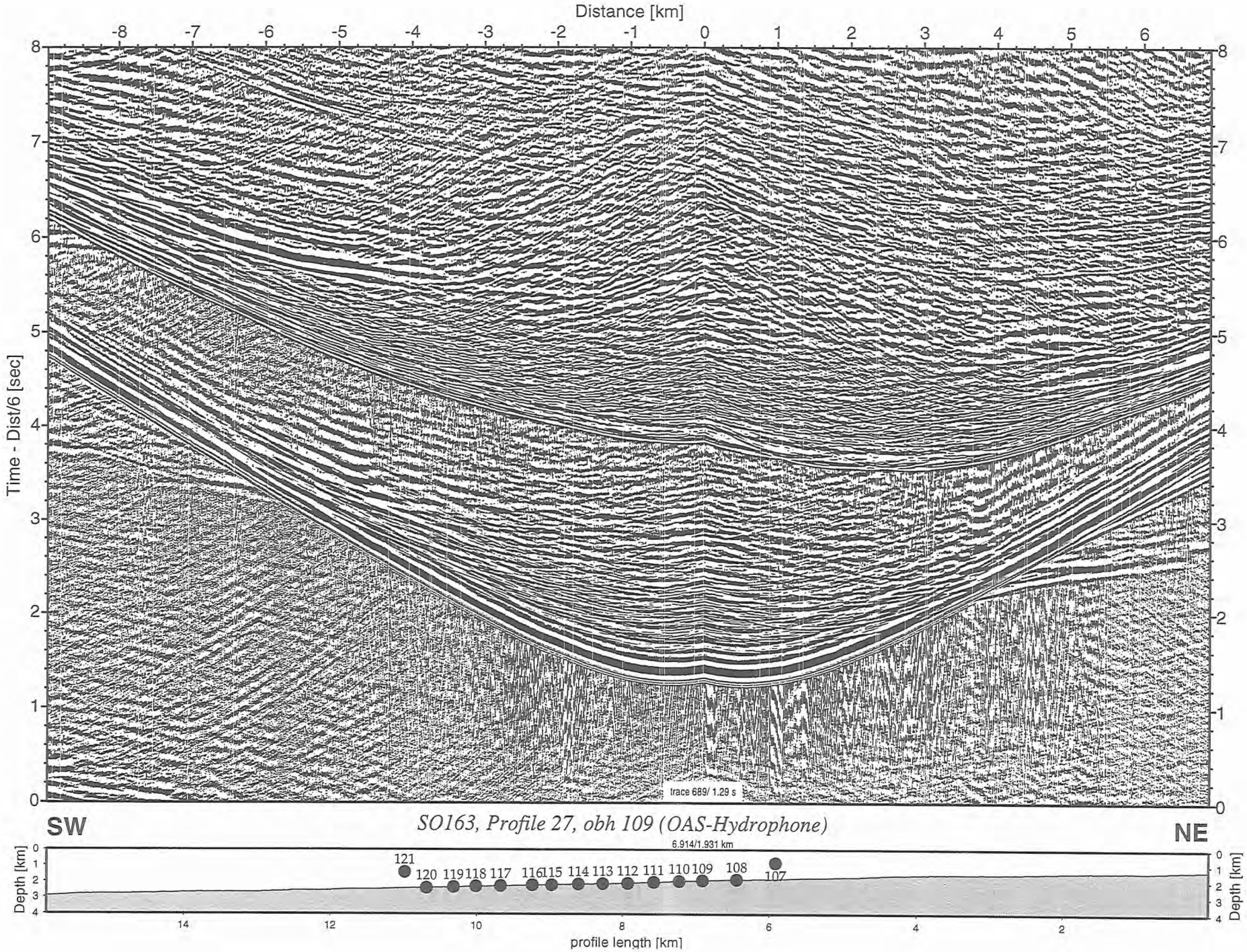


**Figure 6.6.4.4:** Record section from obh 109 (OAS-Hydrophone), Profile 27.

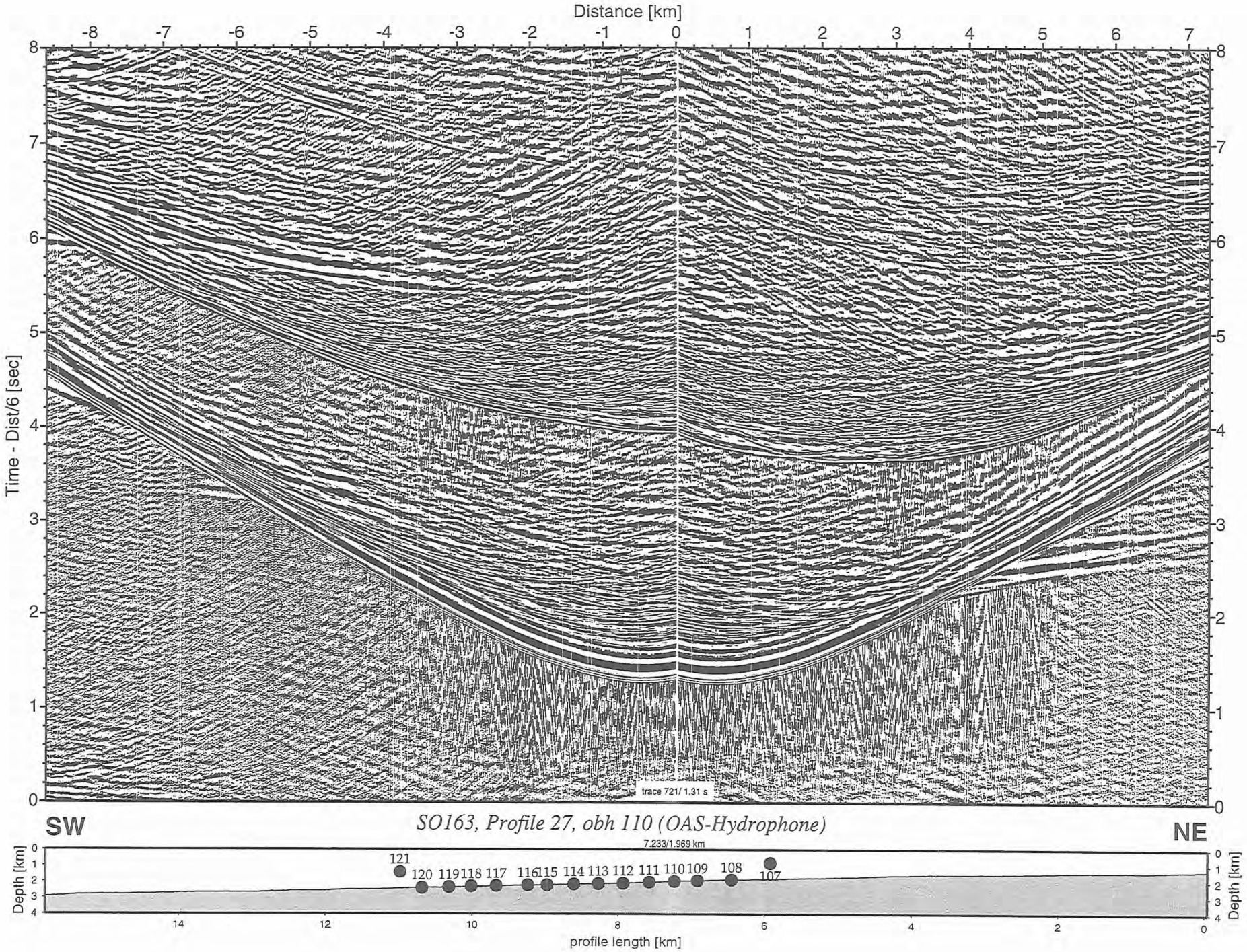


**Figure 6.6.4.5:** Record section from obh 110 (OAS-Hydrophone), Profile 27.

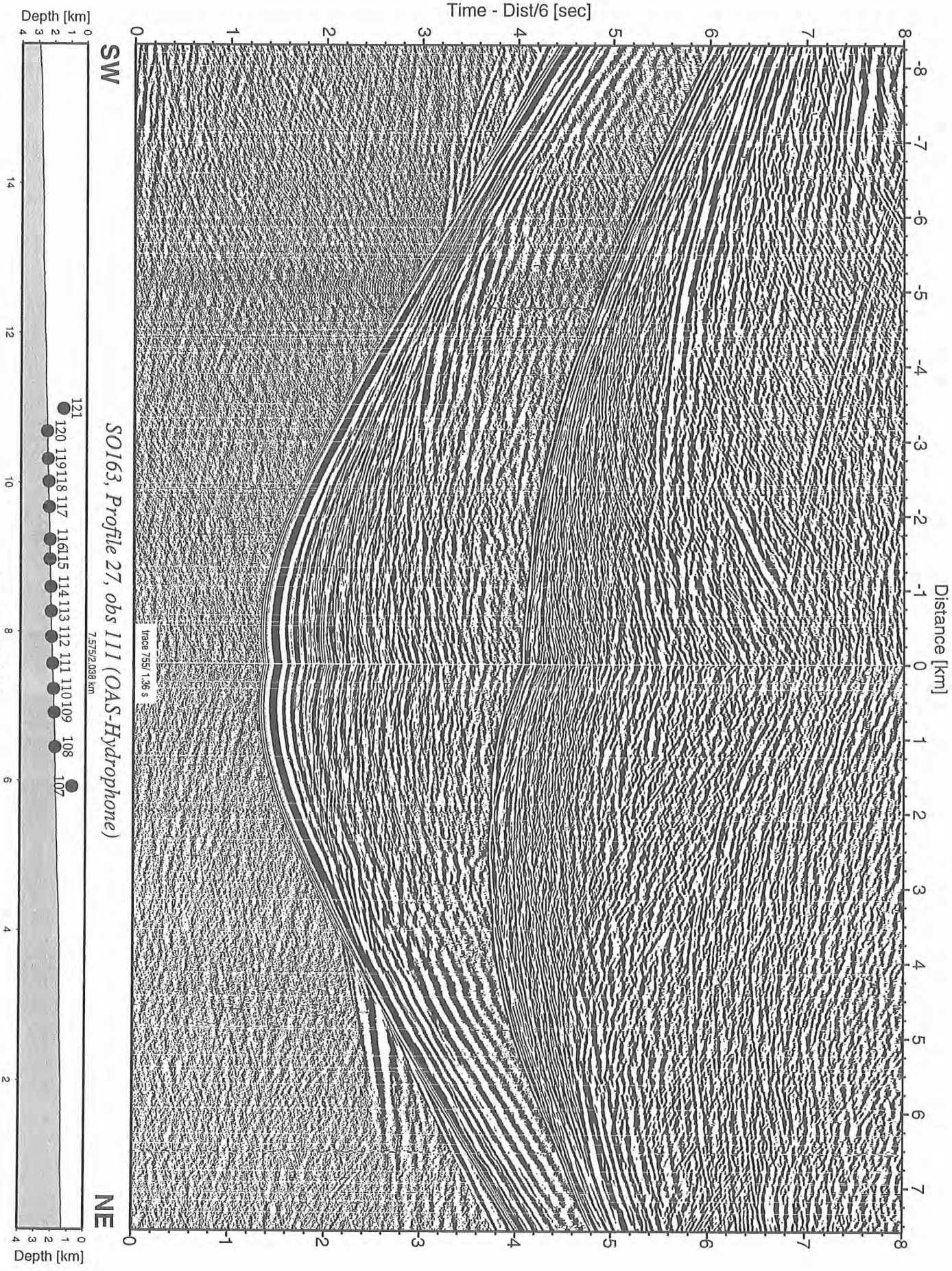


**Figure 6.6.4.6:** Record section from obs 111 (OAS-Hydrophone), Profile 27.

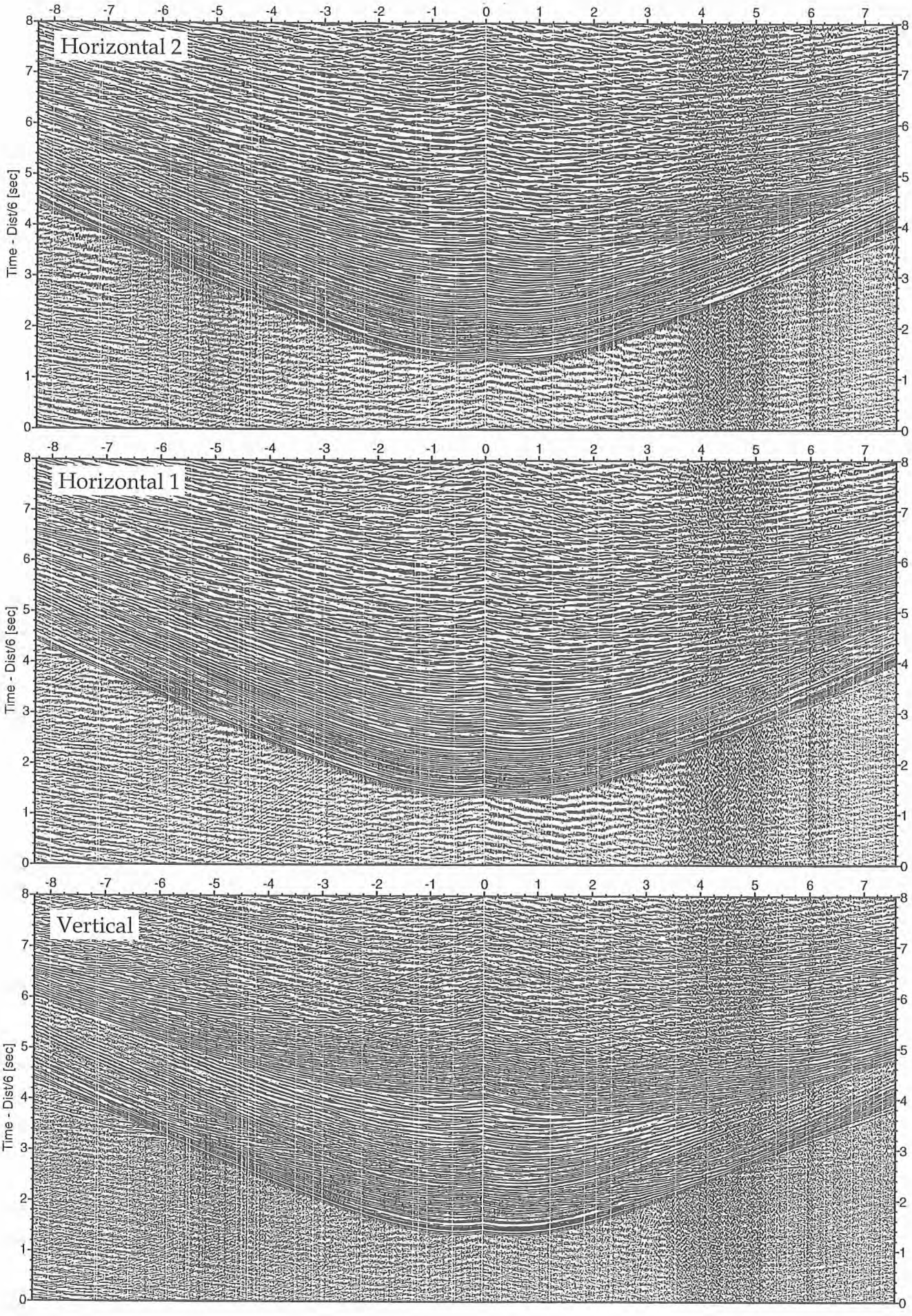


**Figure 6.6.4.7:** Record sections from obs 111 (Owen-30Hz), SO163, Profile 27.

**Figure 6.6.4.8:** Record section from obs 112 (HTI-Hydrophone), Profile 27.

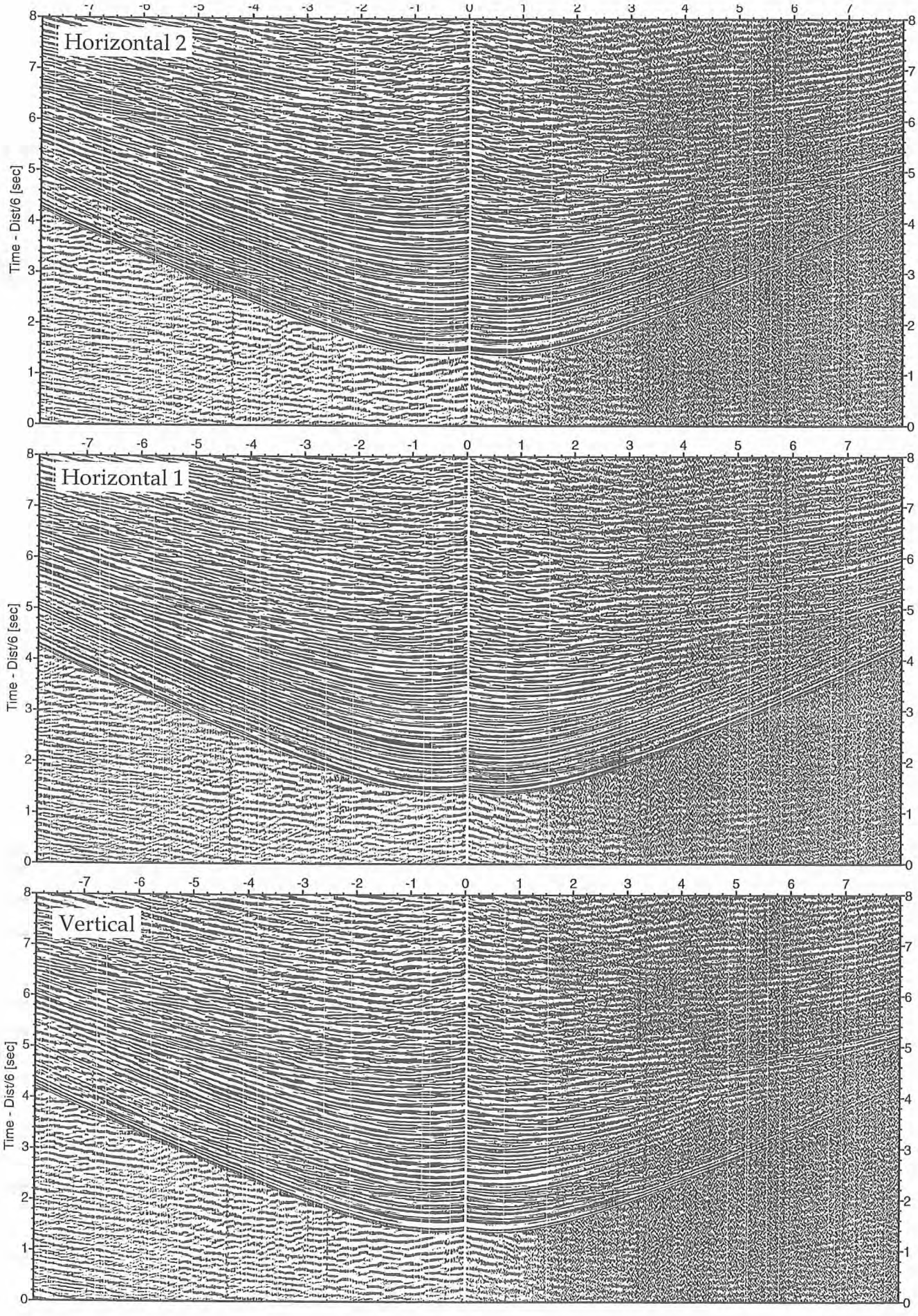


**Figure 6.6.4.9:** Record sections from obs 112 (Owen-4.5Hz), SO163, Profile 27.

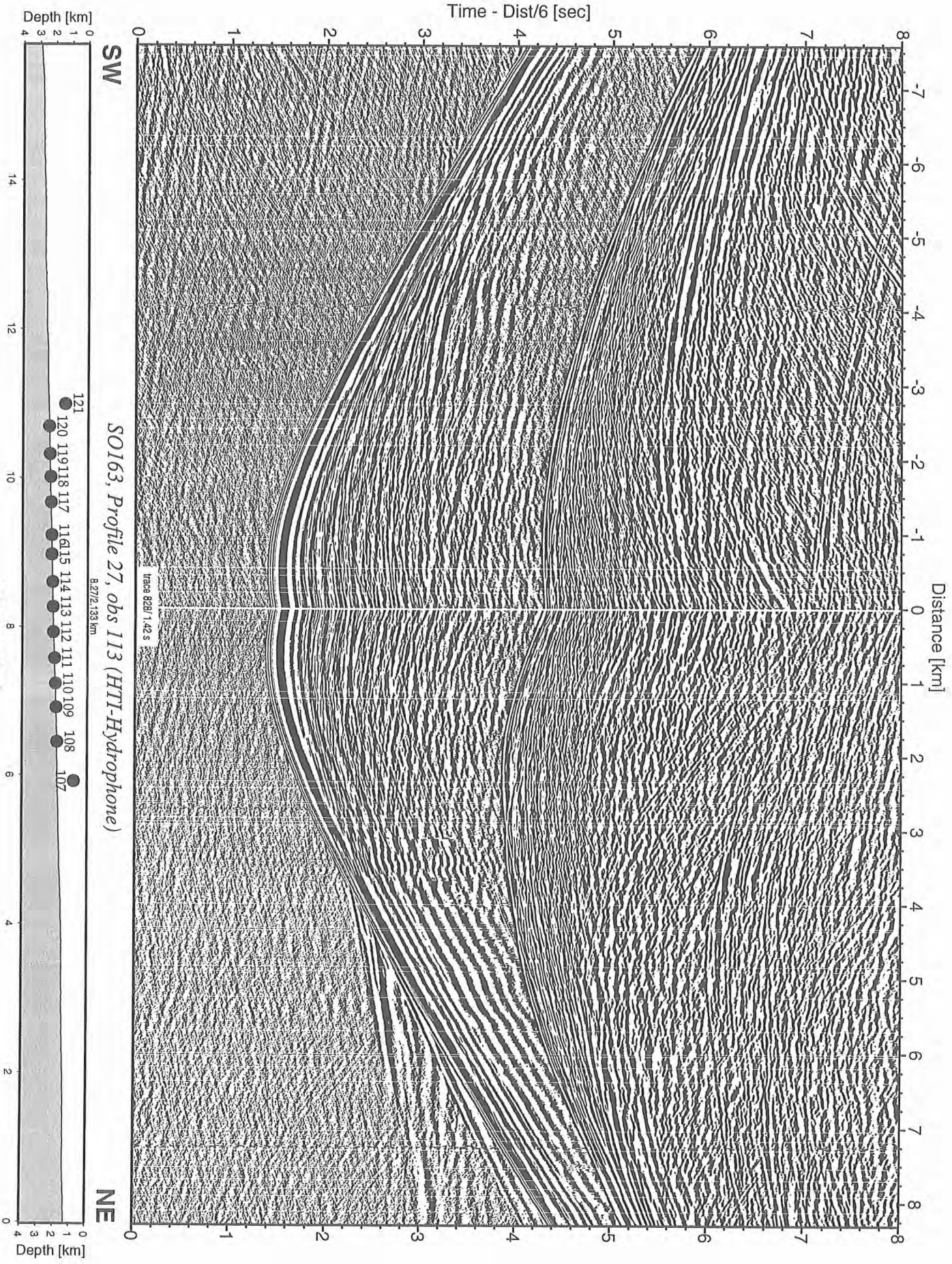


**Figure 6.6.4.10:** Record section from obs 113 (HTI-Hydrophone), Profile 27.

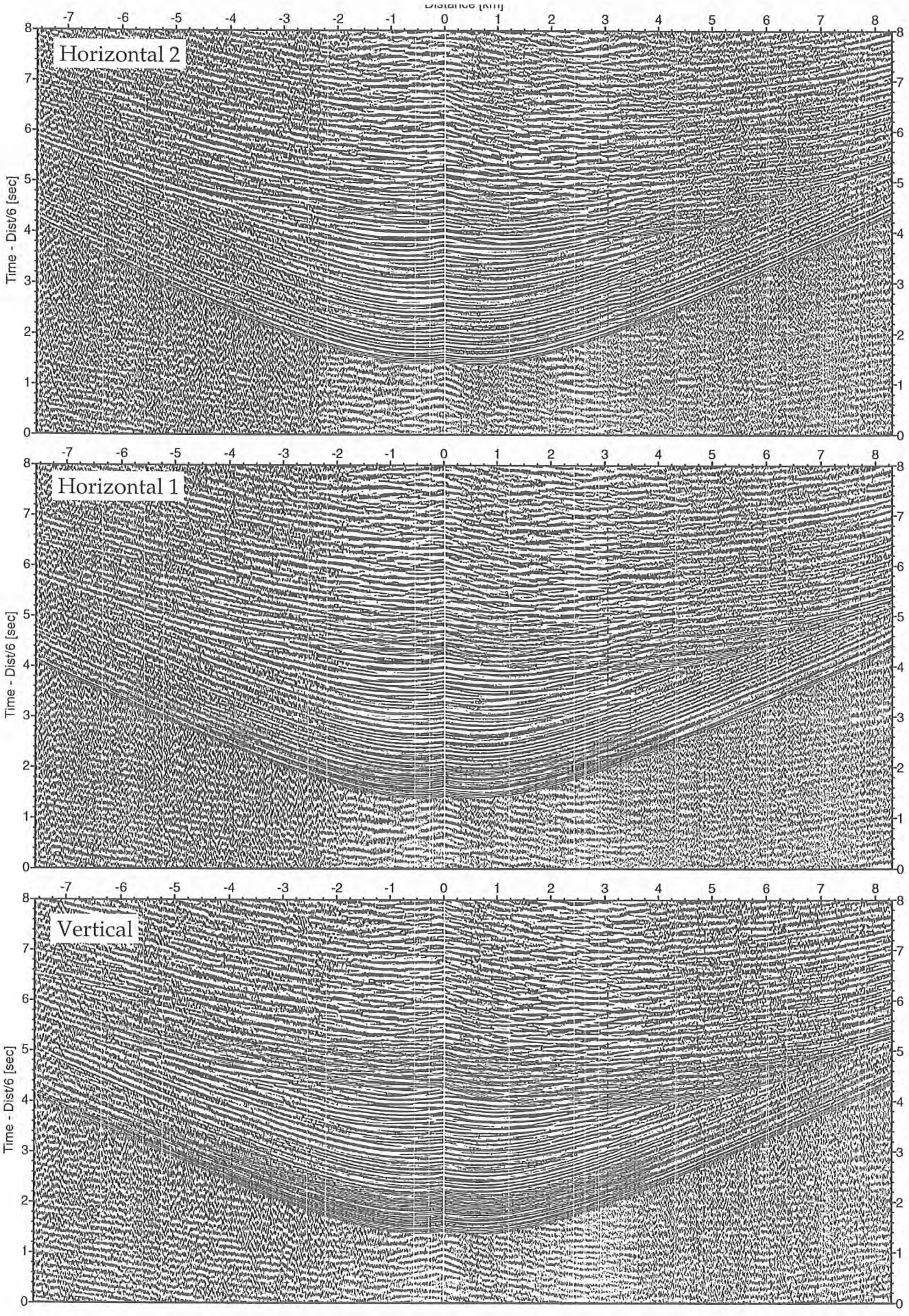


**Figure 6.6.4.11:** Record sections from obs 113 (Owen-4.5Hz), SO163, Profile 27.

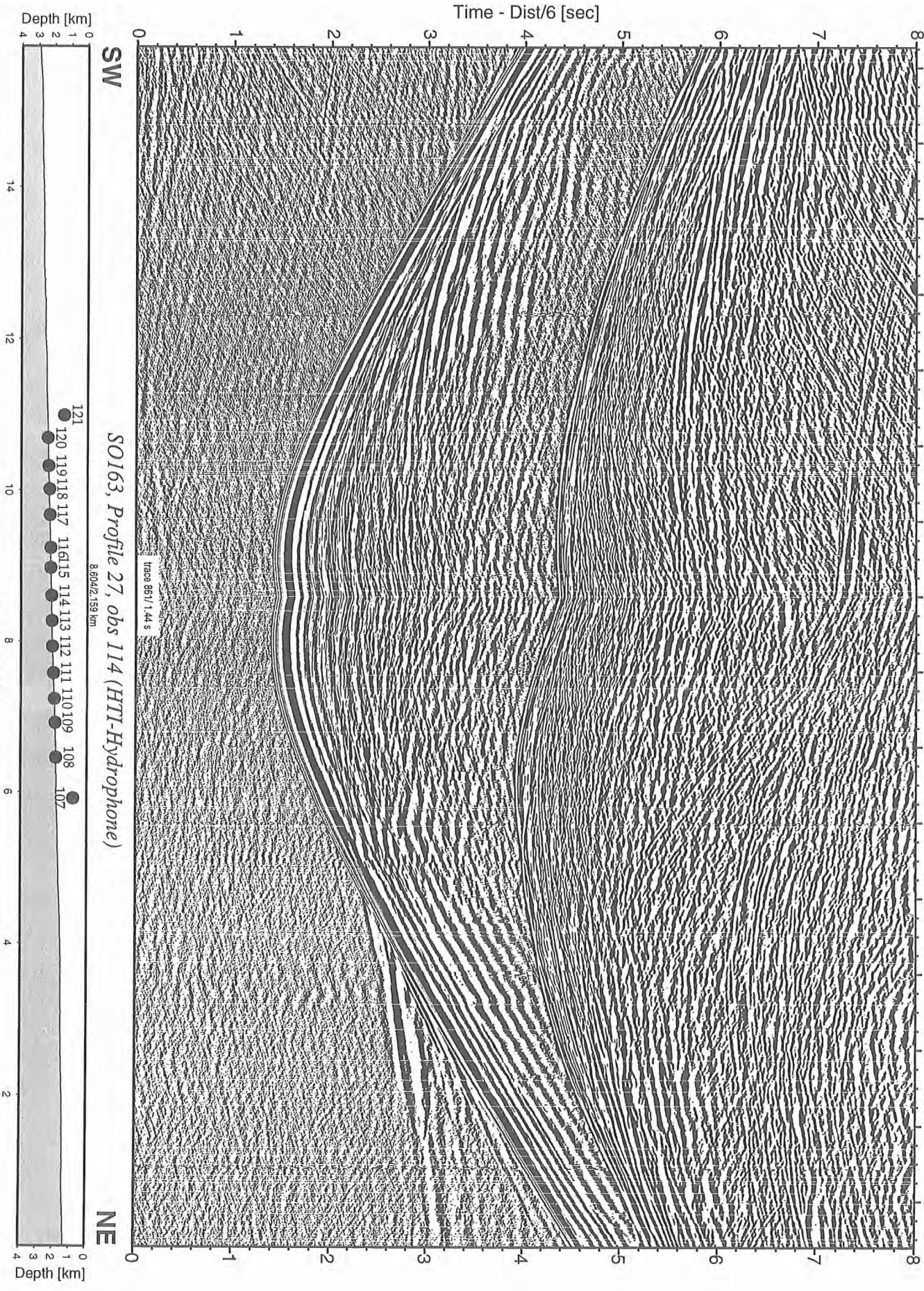


**Figure 6.6.4.12:** Record section from obs 114 (HTI-Hydrophone), Profile 27.

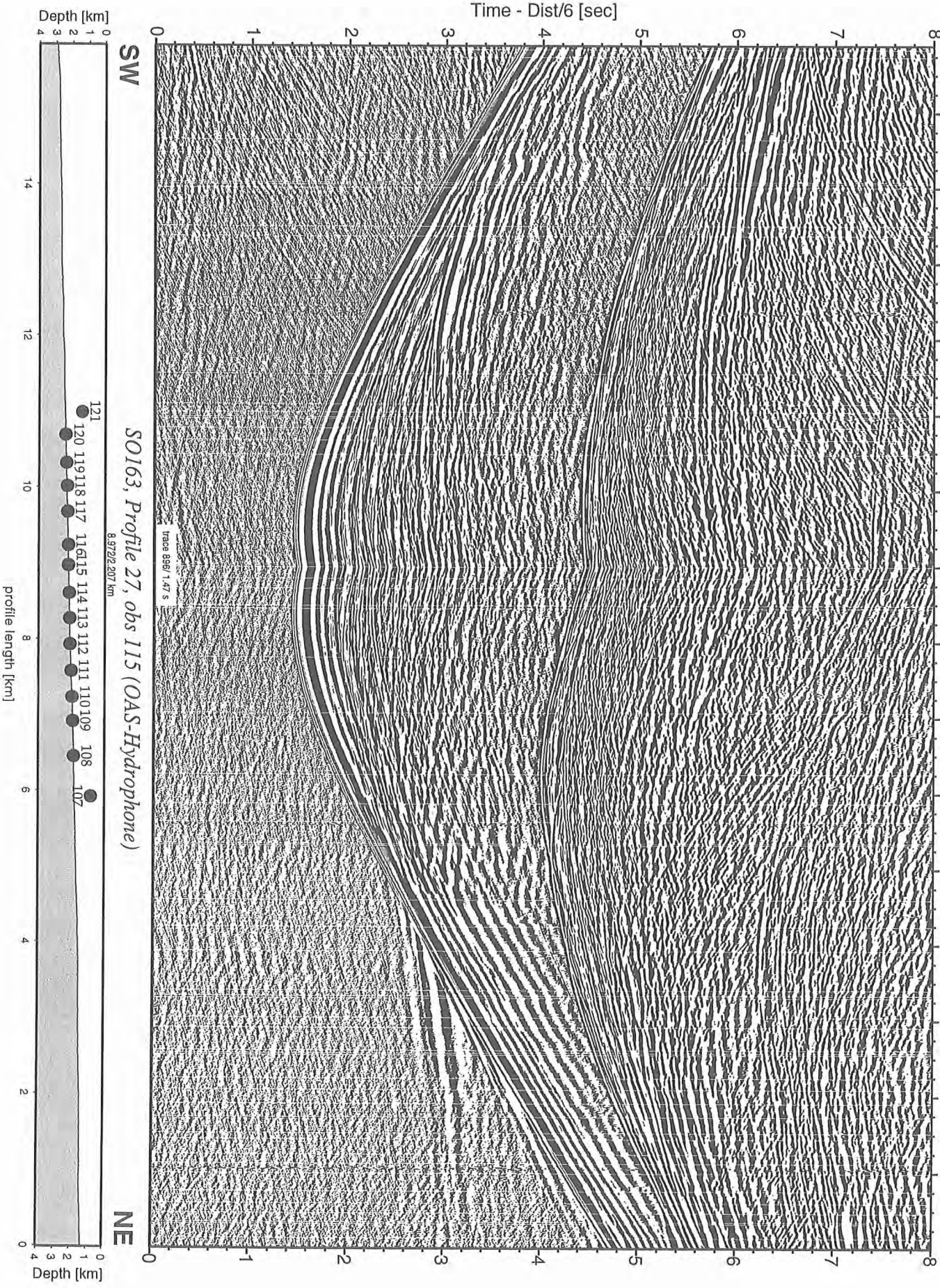


**Figure 6.6.4.13:** Record section from obs 115 (OAS-Hydrophone), Profile 27.

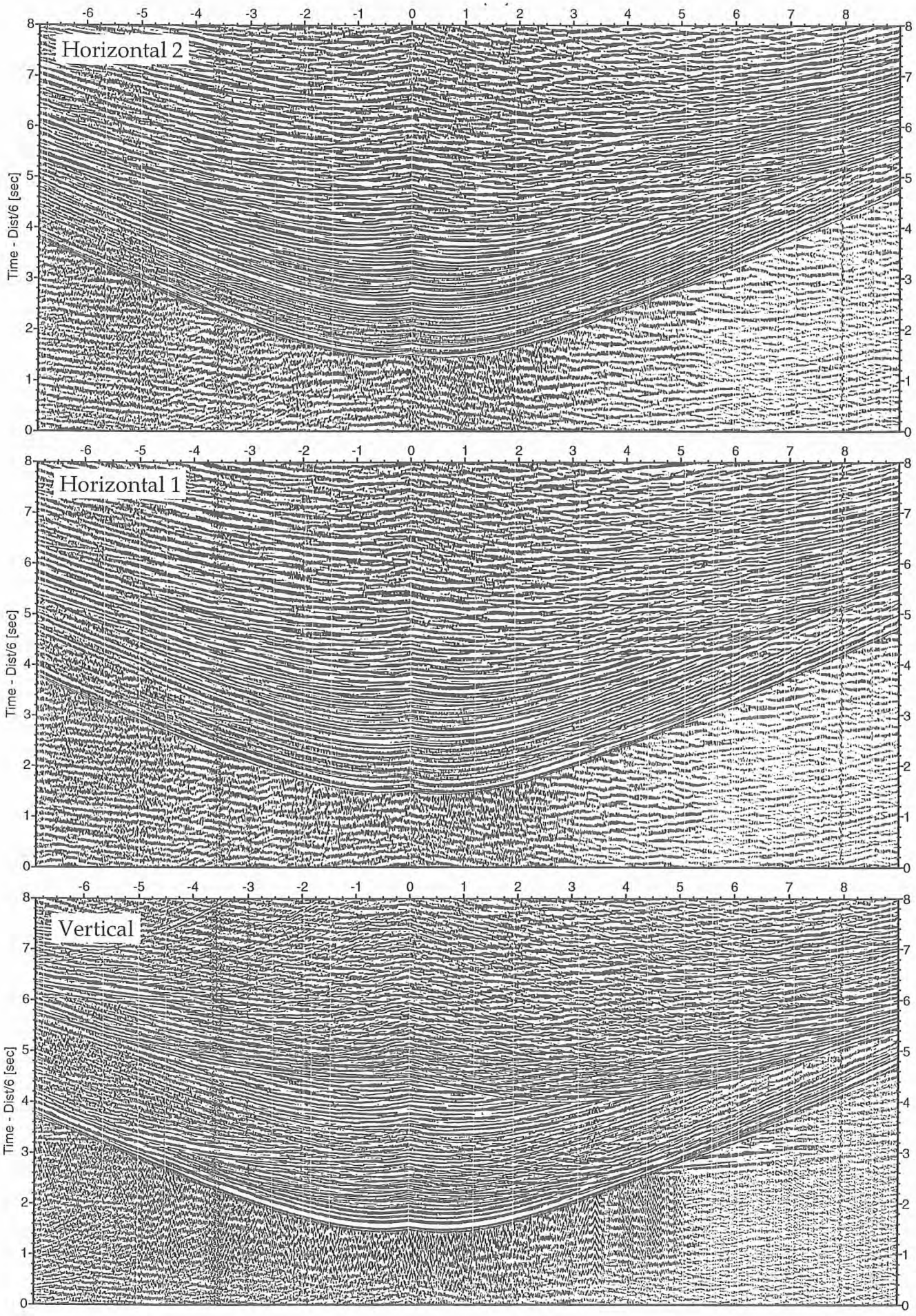


**Figure 6.6.4.14:** Record sections from obs 115 (Owen-30Hz), SO163, Profile 27.

**Figure 6.6.4.15:** Record section from obh 116 (OAS-Hydrophone), Profile 27.

**Figure 6.6.4.18:** Record section from obh 119 (HTI-Hydrophone), Profile 27.

**Figure 6.6.4.19:** Record section from obh 120 (OAS-Hydrophone), Profile 27.

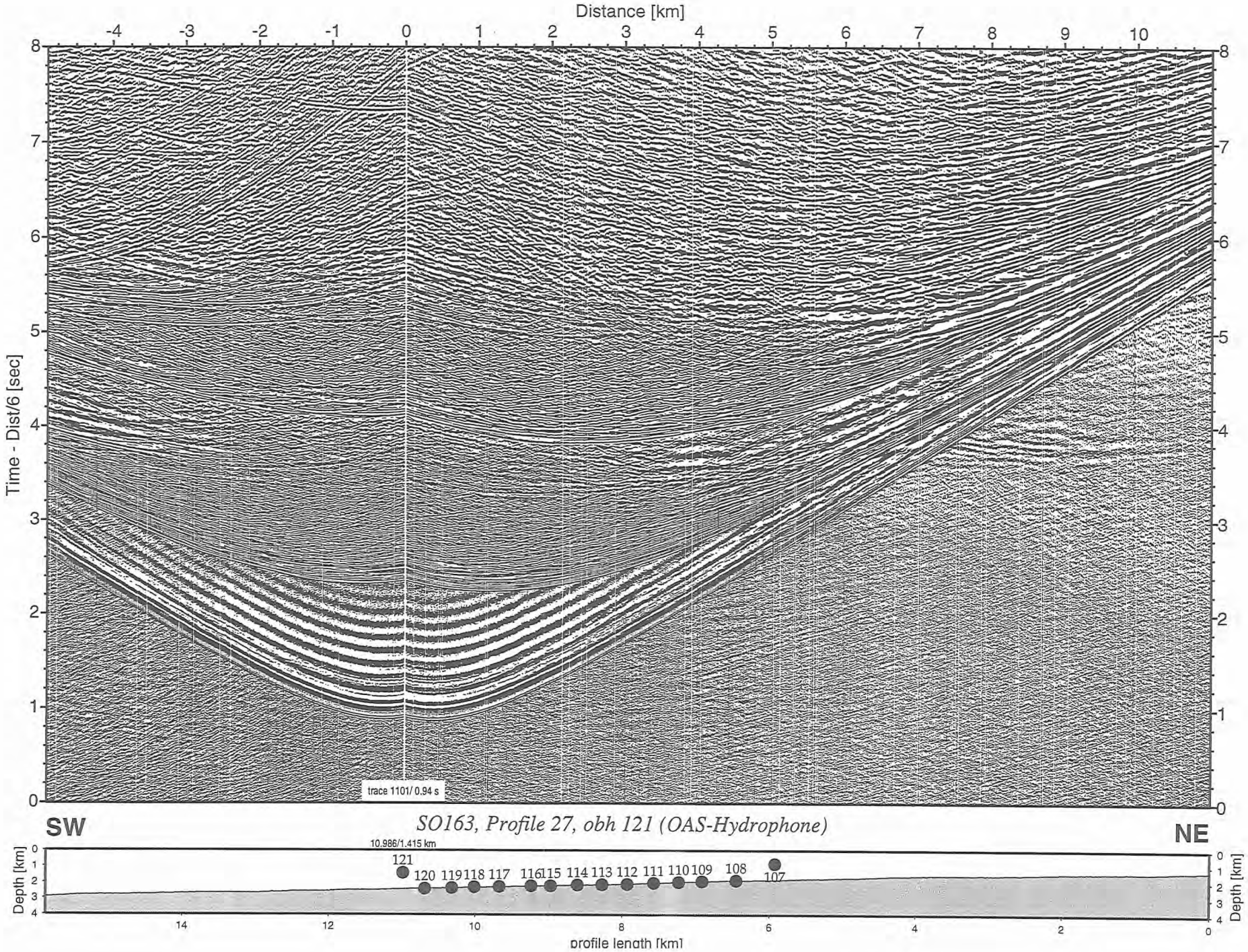


**Figure 6.6.4.20:** Record section from obh 121 (OAS-Hydrophone), Profile 27.

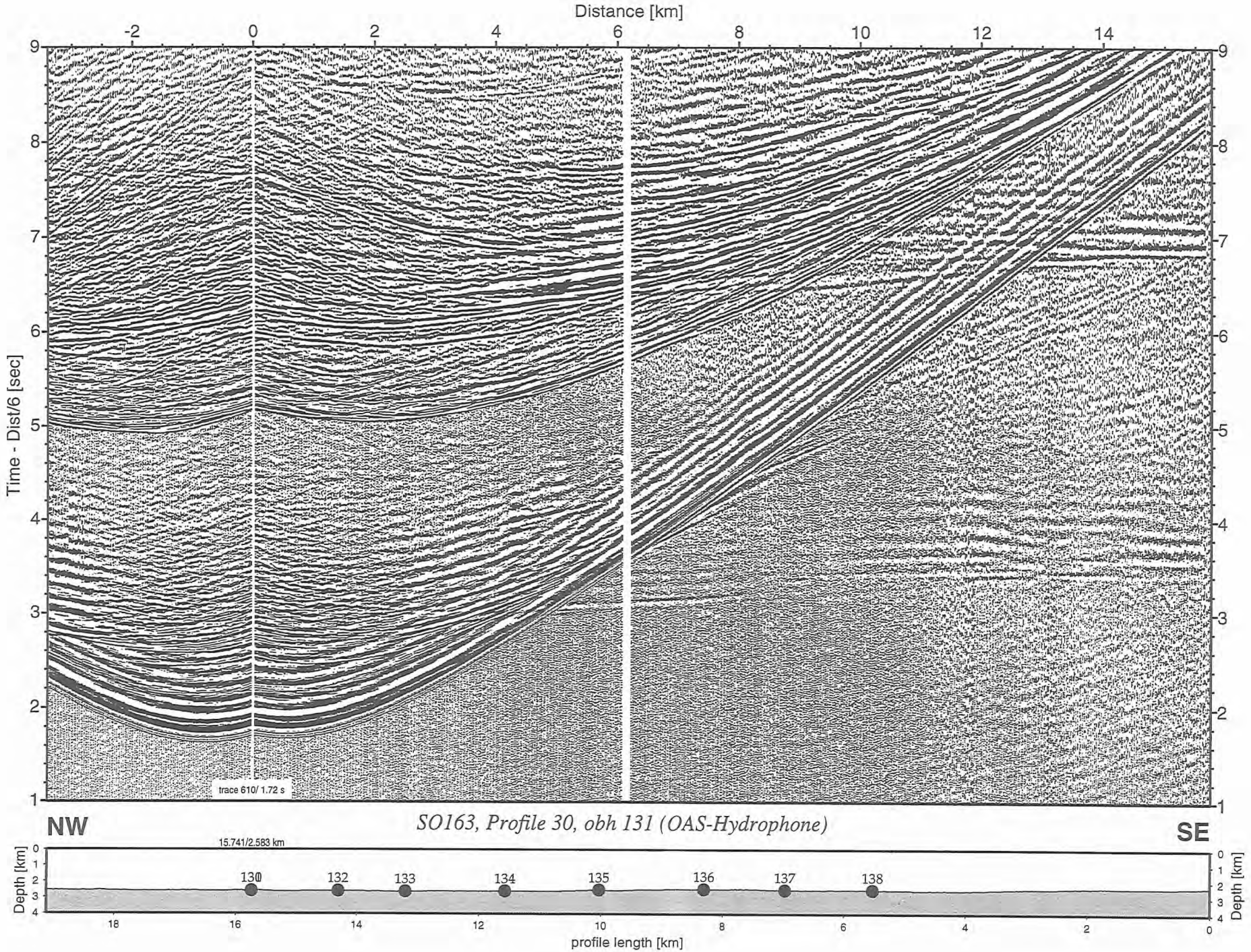


**Figure 6.6.4.21:** Record section from obh 131 (OAS-Hydrophone), Profile 30.

**Figure 6.6.4.22:** Record section from obs 132 (HTI-Hydrophone), Profile 30.

**Figure 6.6.4.23:** Record section from obh 133 (HTI-Hydrophone), Profile 30.

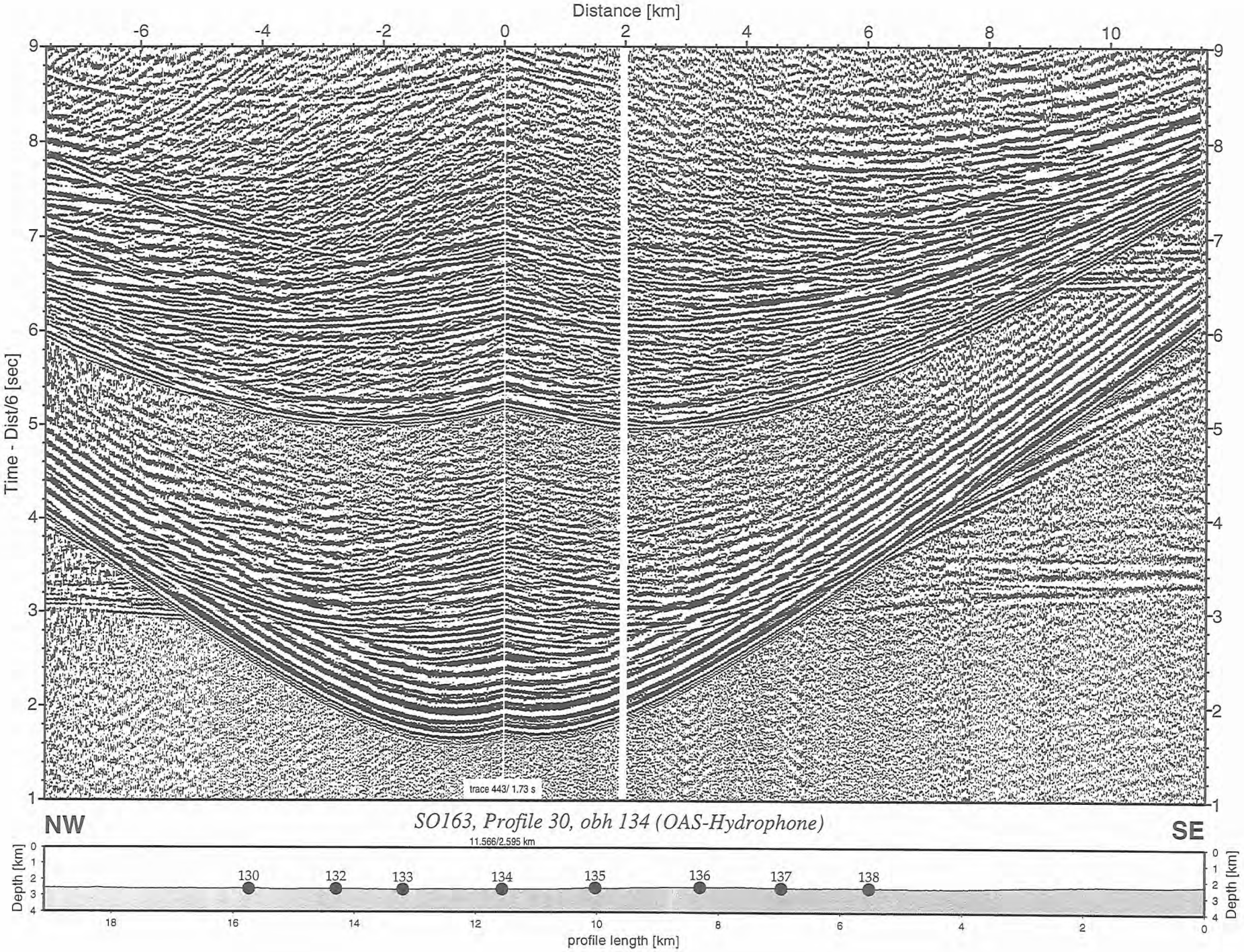


**Figure 6.6.4.24:** Record section from obh 134 (OAS-Hydrophone), Profile 30.

**Figure 6.6.4.25:** Record section from obh 135 (OAS-Hydrophone), Profile 30.

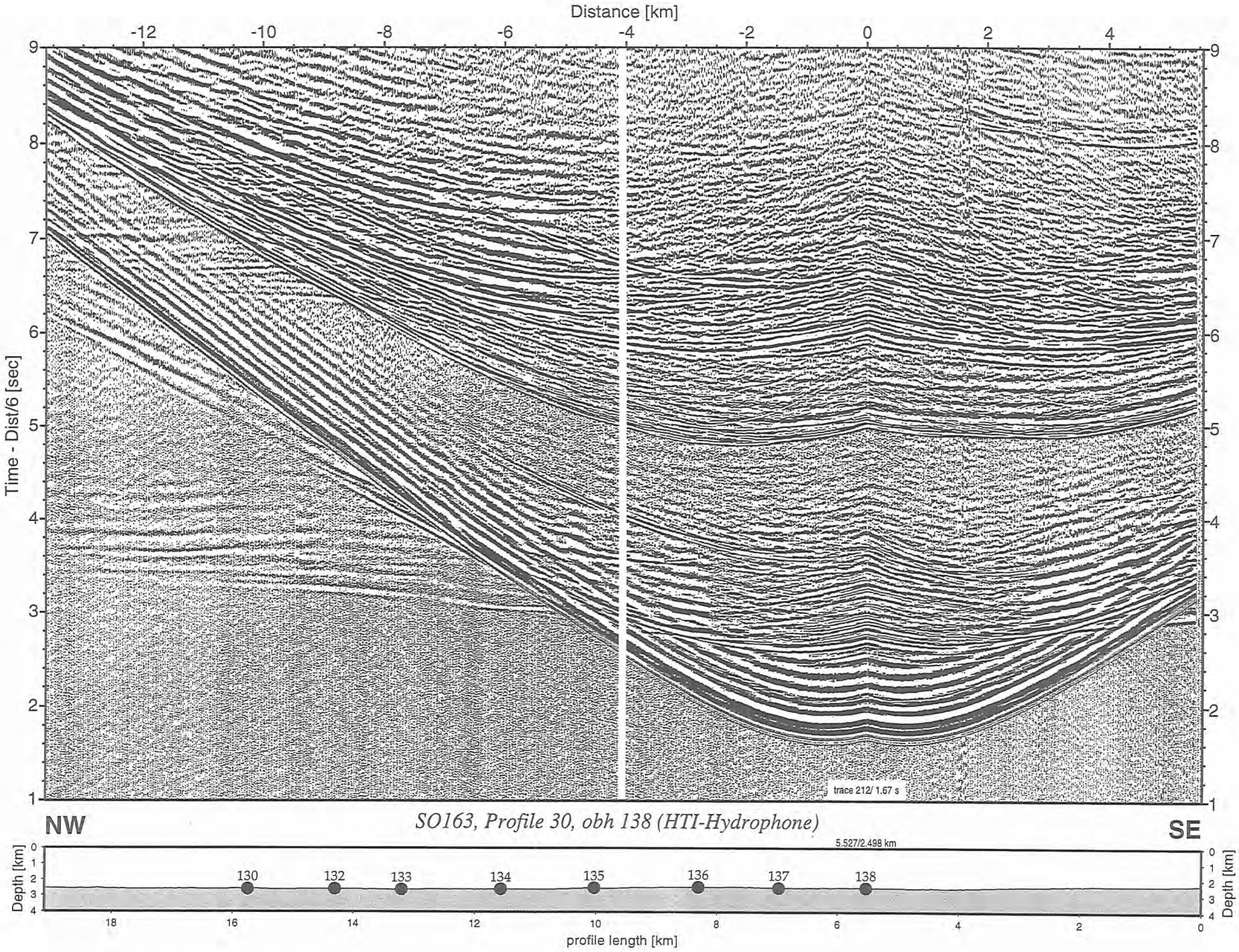


**Figure 6.6.4.28:** Record section from obh 138 (HTI-Hydrophone), Profile 30.

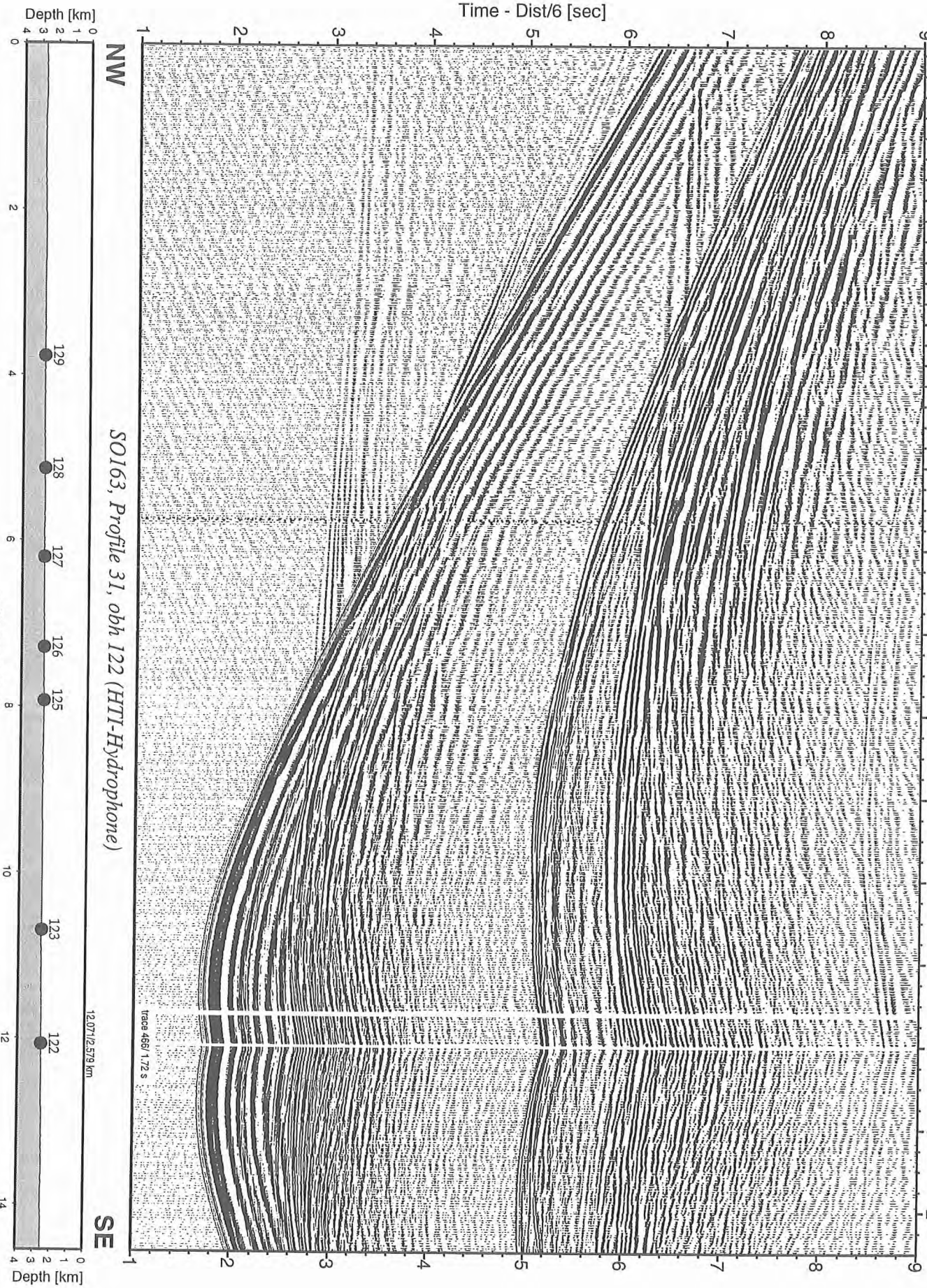


**Figure 6.6.4.29:** Record section from obh 122 (HTI-Hydrophone), Profile 31.

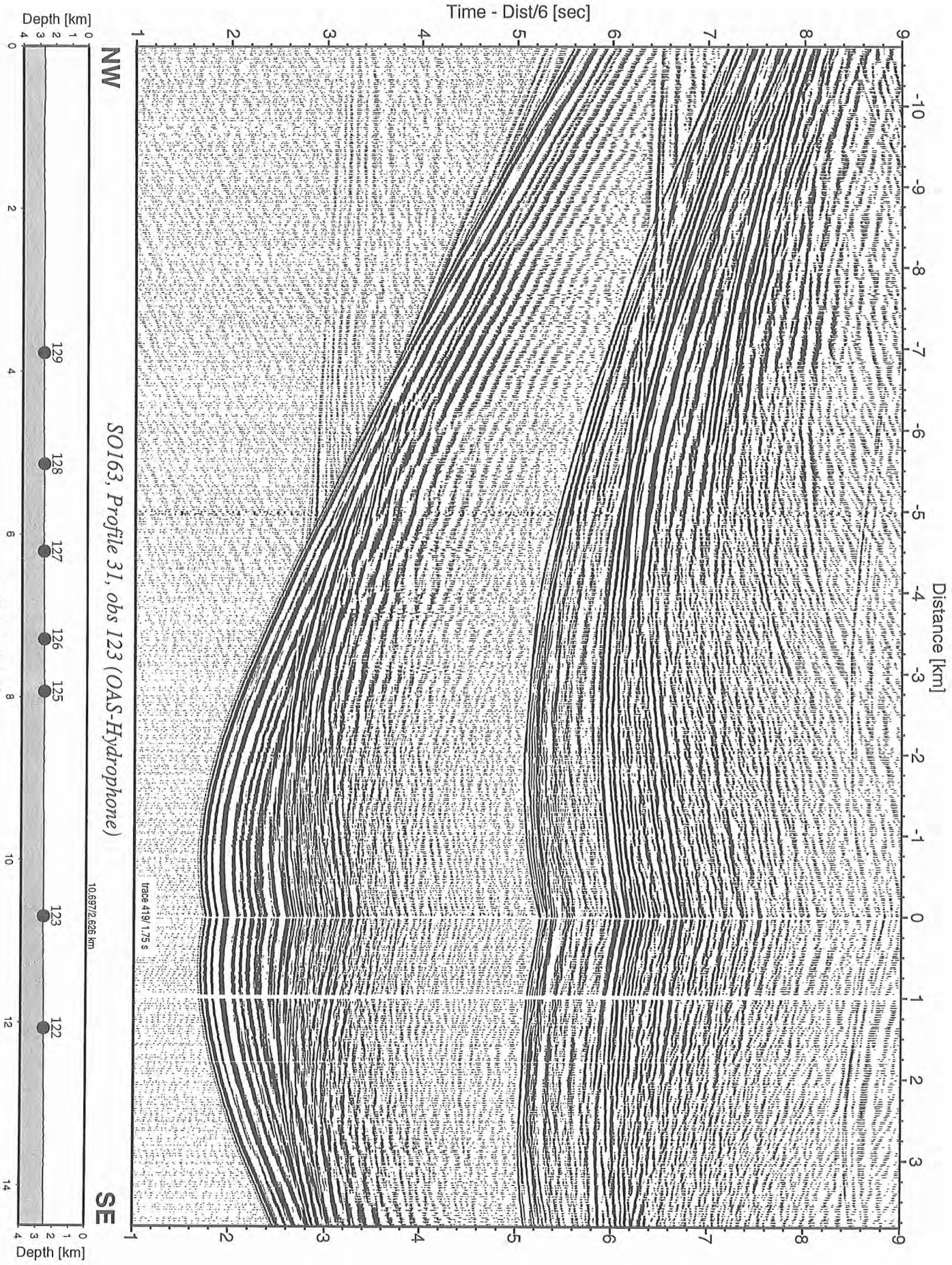


**Figure 6.6.4.30:** Record section from obs 123 (OAS-Hydrophone), Profile 31.

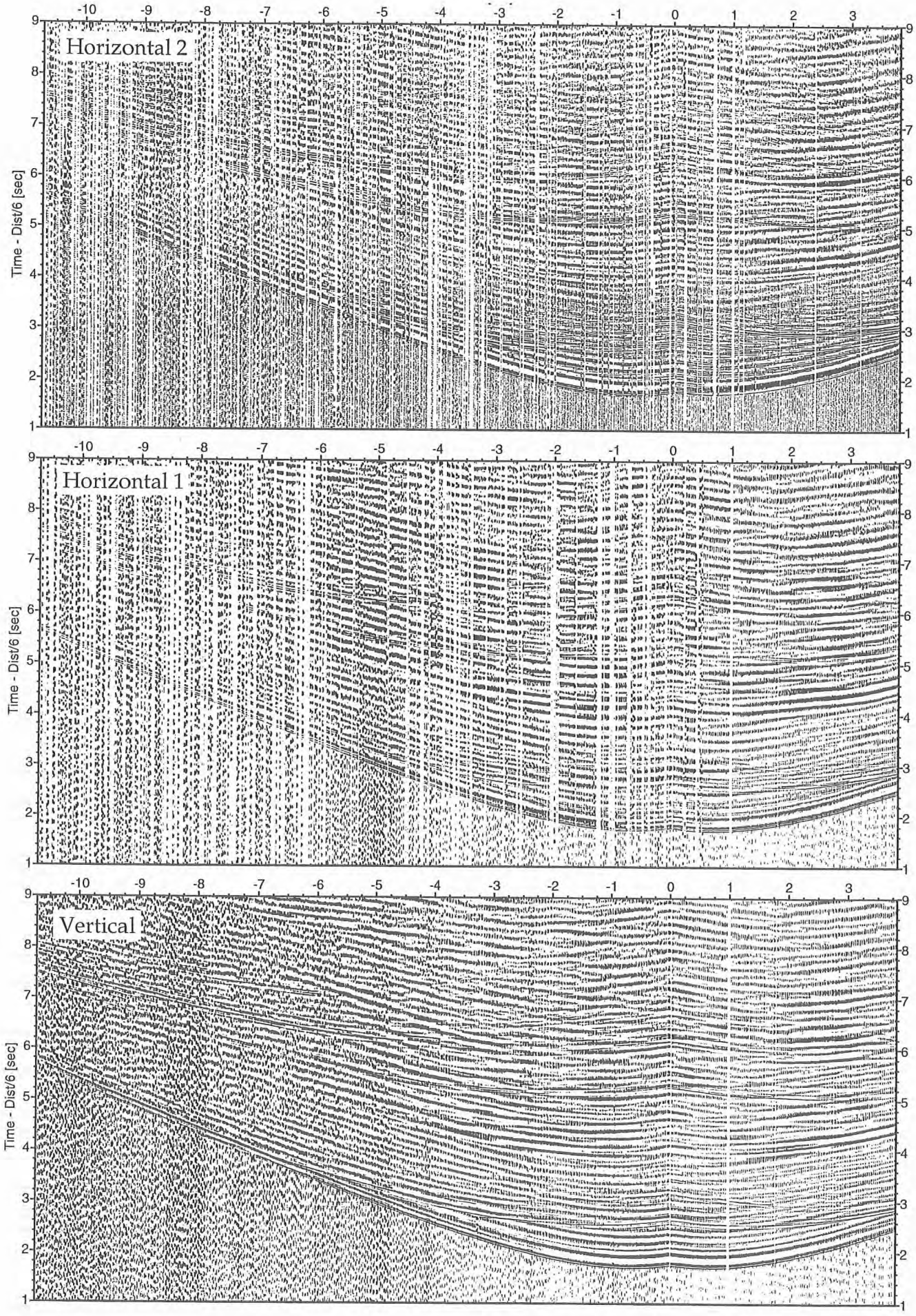


**Figure 6.6.4.31:** Record sections from obs 123 (PMD), SO163, Profile 31.

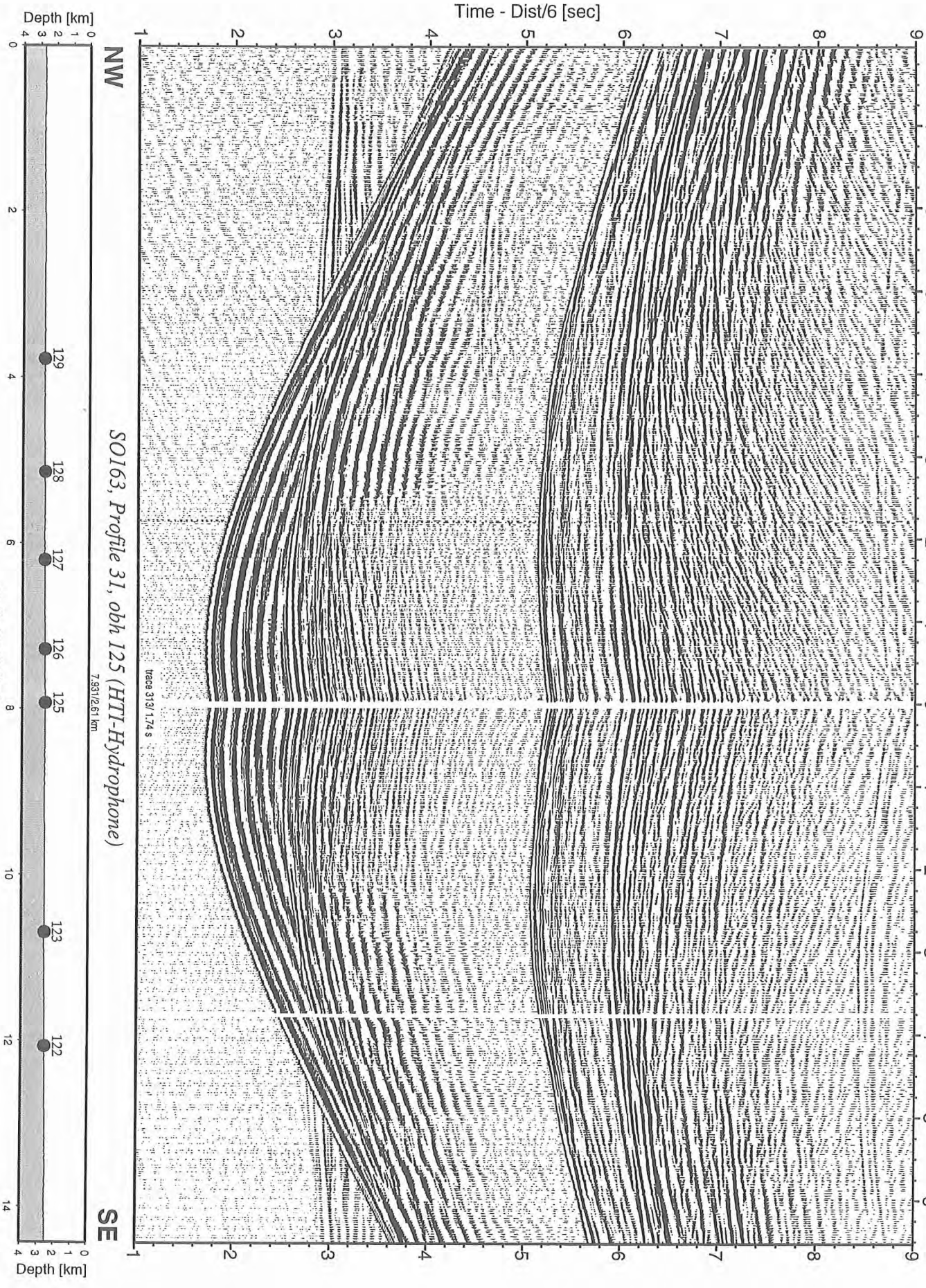


**Figure 6.6.4.32:** Record section from obh 125 (HTI-Hydrophone), Profile 31.

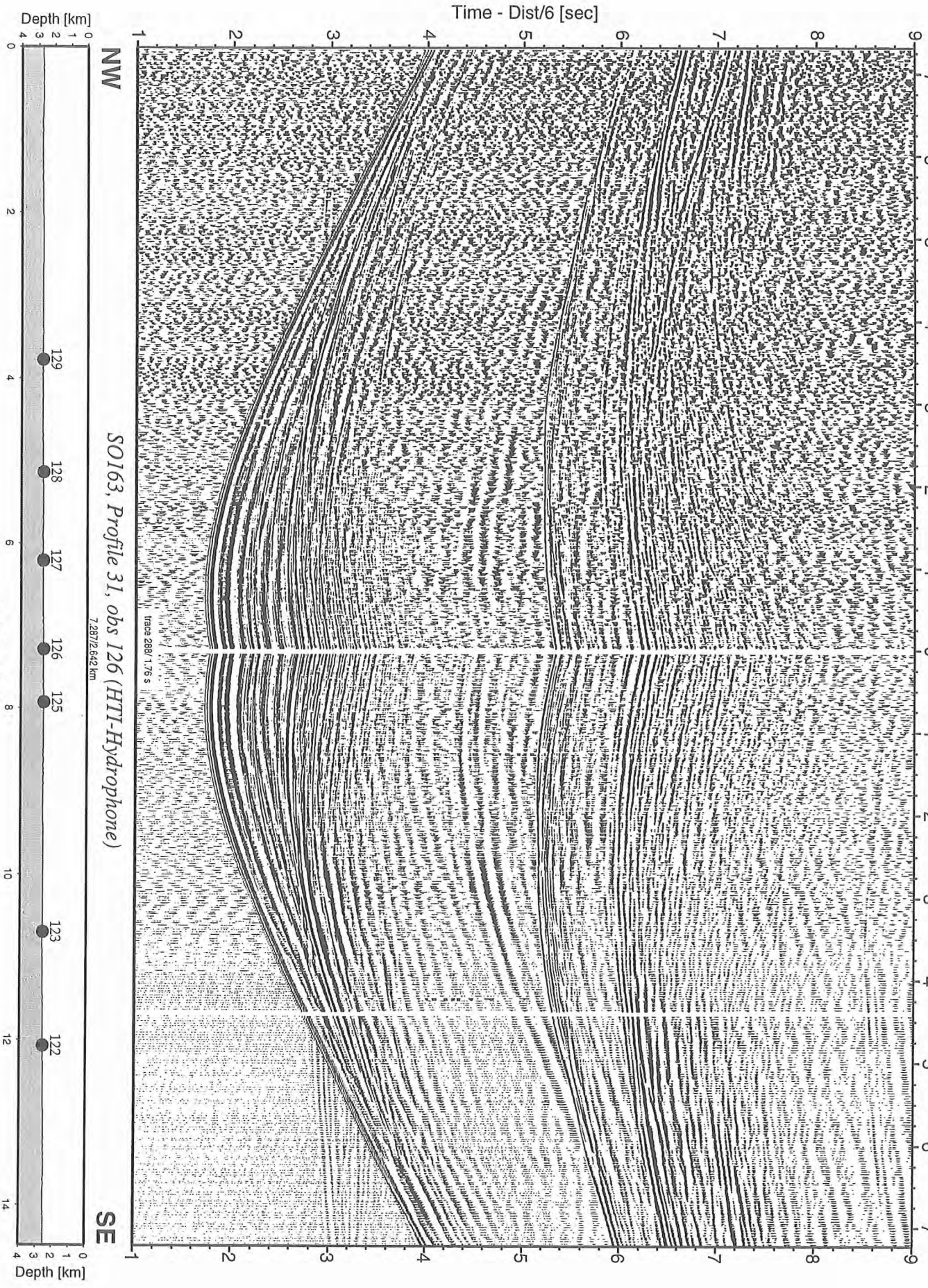


**Figure 6.6.4.33:** Record section from obs 126 (HTI-Hydrophone), Profile 31.

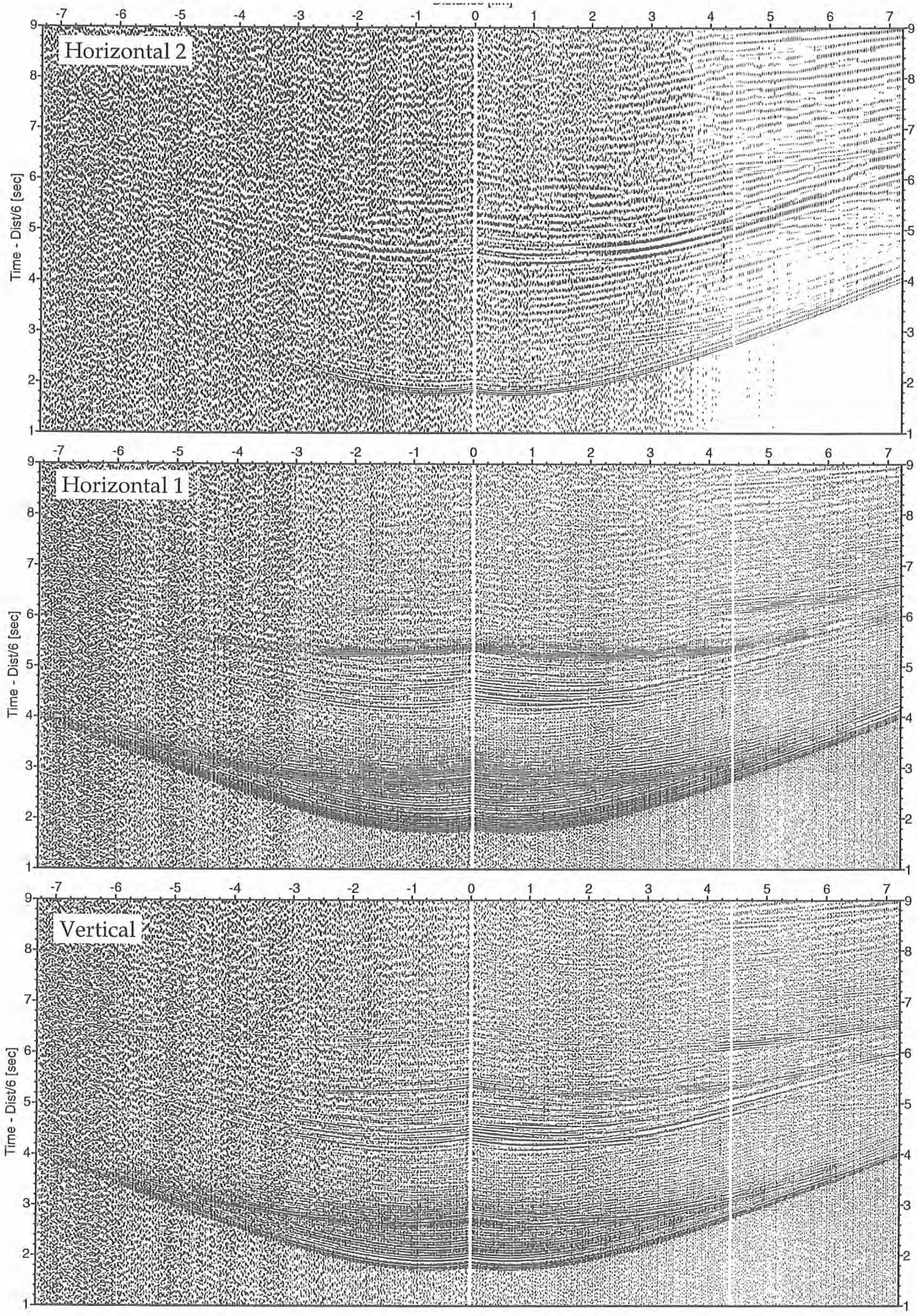


**Figure 6.6.4.34:** Record sections from obs 126 (Owen-4.5Hz), SO163, Profile 31.

**Figure 6.6.4.35:** Record section from obh 127 (DPG-Hydrophone), Profile 31.

**Figure 6.6.4.36:** Record section from obs 128 (OAS-Hydrophone), Profile 31.

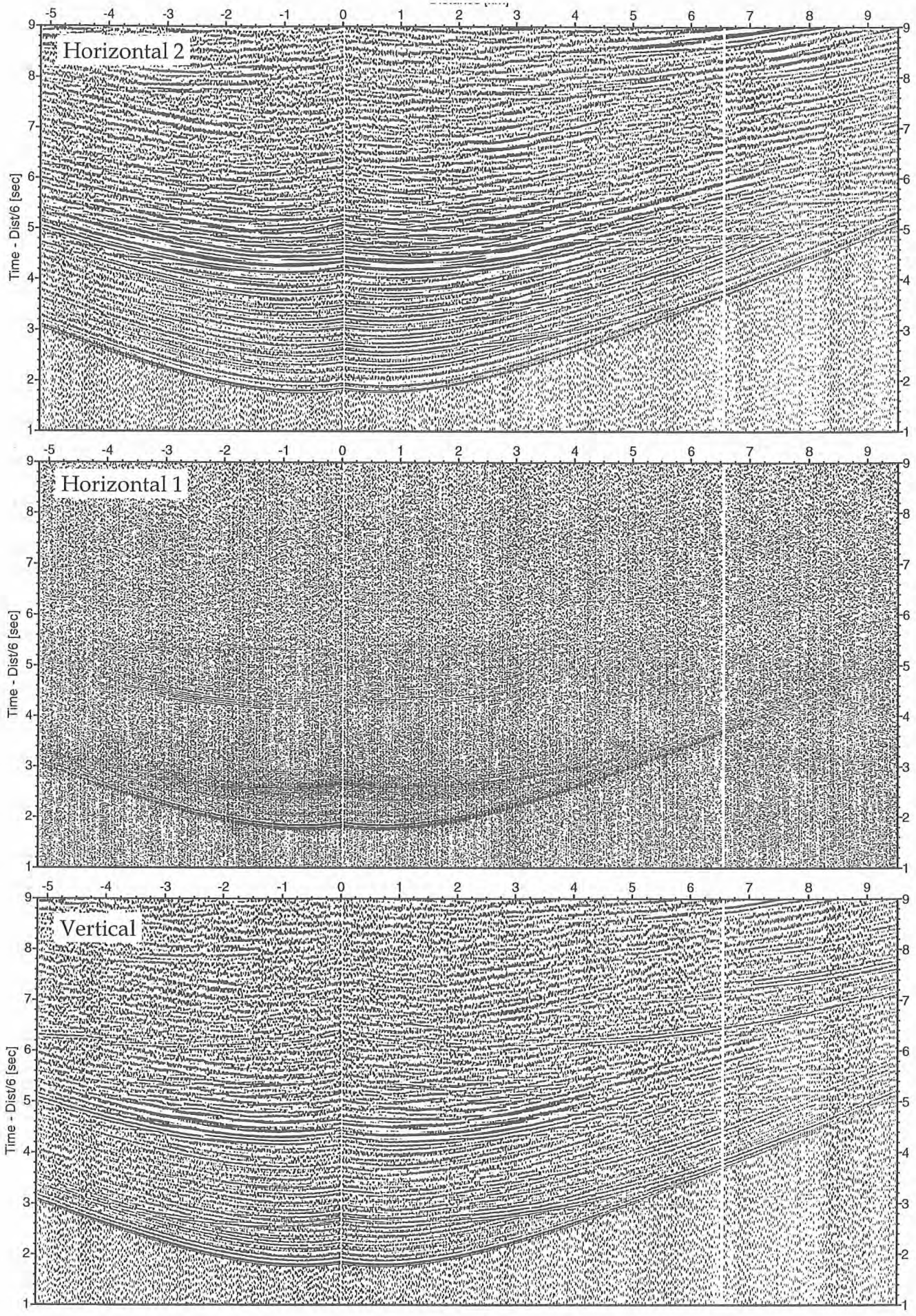


**Figure 6.6.4.37:** Record sections from obs 128 (Owen-4.5Hz), SO163, Profile 31.

**Figure 6.6.4.38:** Record section from obh 129 (OAS-Hydrophone), Profile 31.

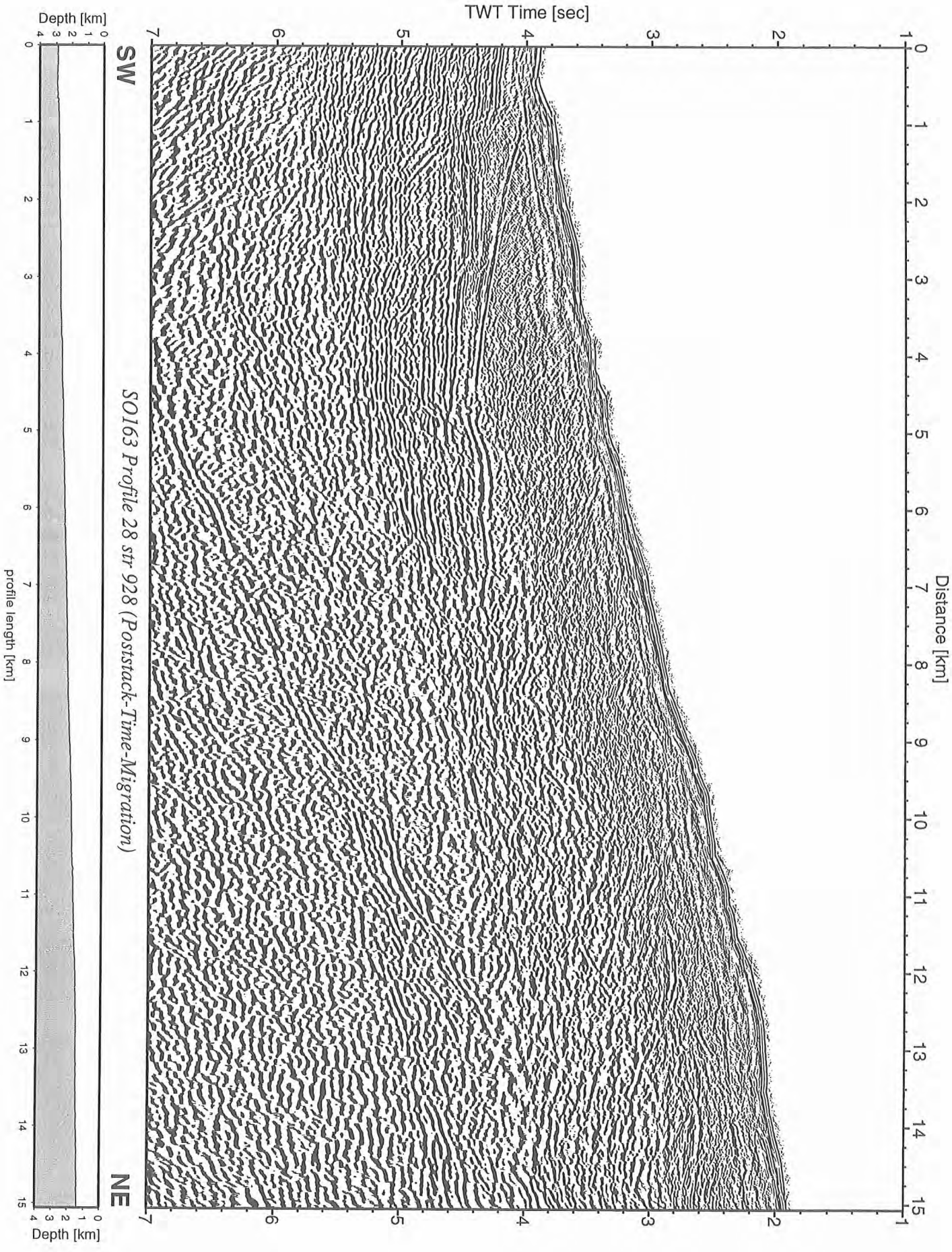


**Figure 6.6.4.39:** Record section from str 928 (Poststack-Time-Migration), Profile 28.

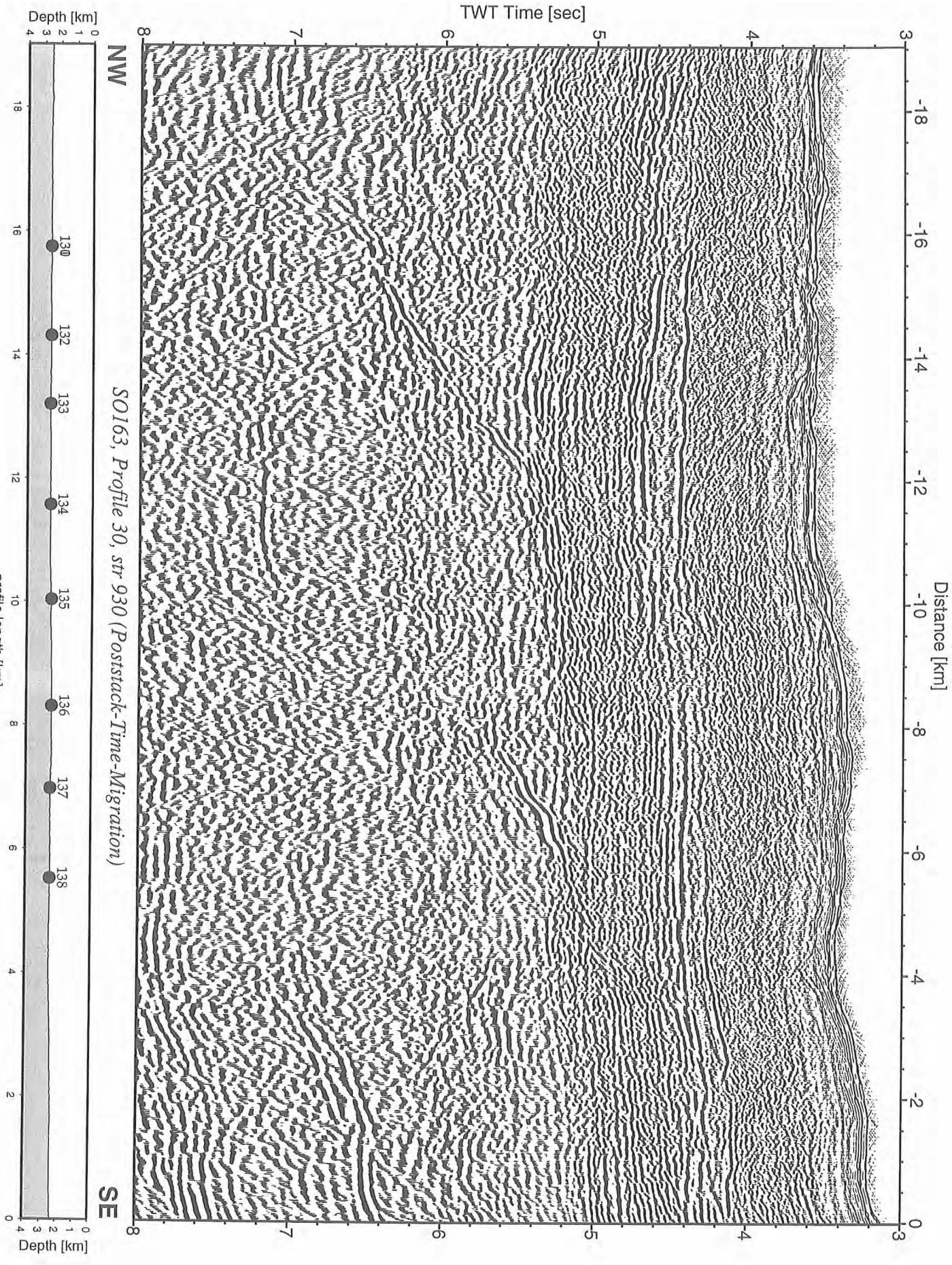


**Figure 6.6.4.40:** Record section from str 930 (Poststack-Time-Migration), Profile 30.

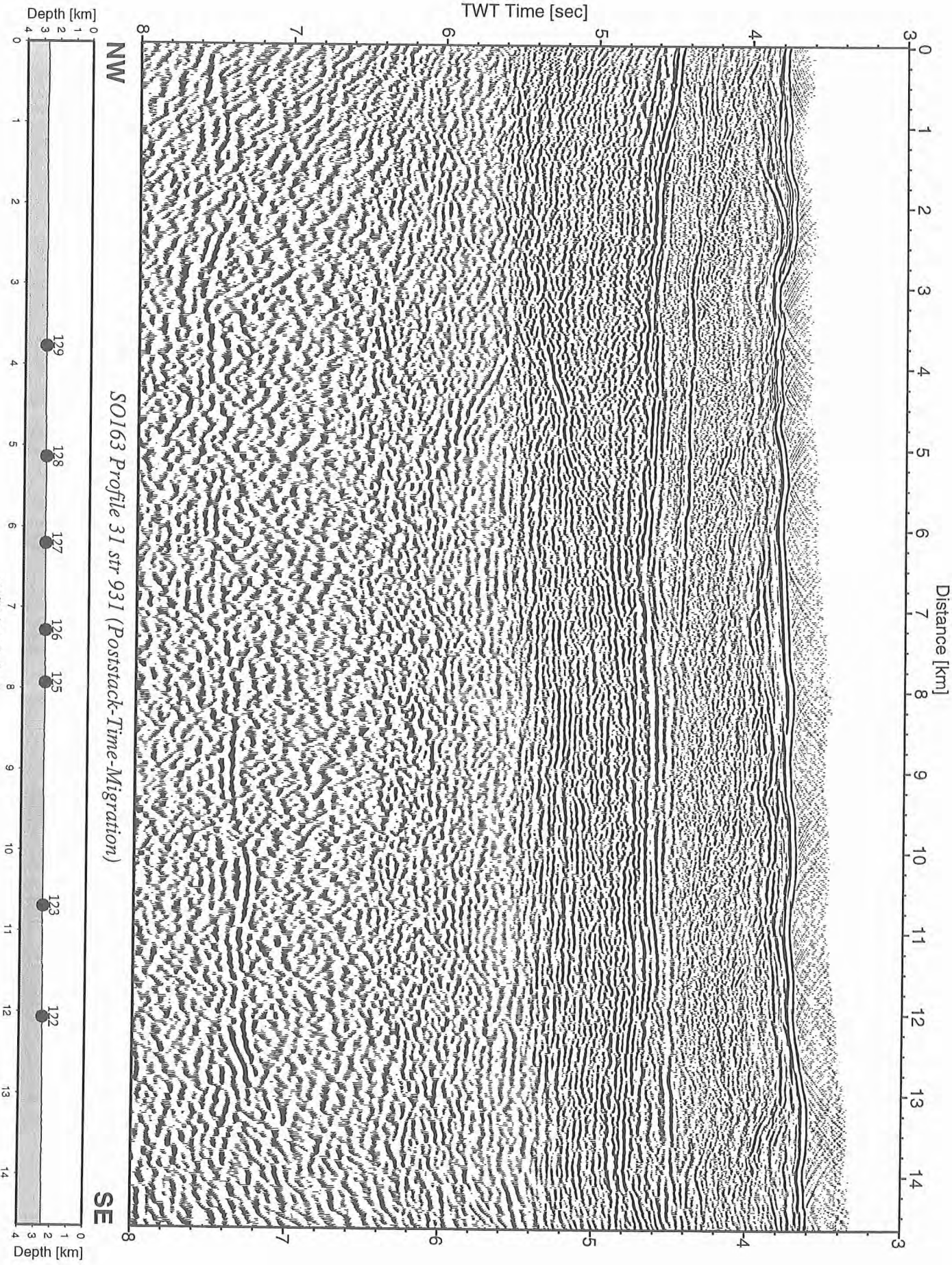


**Figure 6.6.4.41:** Record section from str 931 (Poststack-Time-Migration), Profile 31.

### 6.6.5 The Jaco Scar seismological Network

(I. Boschini, J. Gossler, P.O. Thierer)

**Description of the network**

A larger network than installed on OFOS 10 mudvolcanoe was deployed centered on Jaco Scar. Here a total of 23 instruments were deployed and shall be recovered during METEOR Leg M54/3B in early October 2002. Another five OBH have been deployed east of the network on Quepos Mound, which may be included into the Jaco Scar network. The Quepos Mound stations will be recovered in July. In a first portion, seven ocean bottom instruments were deployed. To the end of SO163-2, we recovered the instruments and redeployed them after checking the quality of the obtained data (Figure 6.6.5.1).

Contemporaneously with the ocean botton deployment of the ten OBH, the Instituto Costaricense de Electricidad (ICE) together with GEOMAR and the University of Kiel are running a land based local earthquake network. The additional data from the land stations will be used for further constrain earthquake locations and should provide more data for focal mechanism analysis of events located nearby the marine ocean bottom array (Figure 6.6.5.1).

Additionally to the passive seismological recordings, active seismic shootings were carried out following the baselines of the network. Shooting was done using two G-Gun arrays and an additional single Bolt gun of 32 liters volume.

The Jaco Scarp region is a structural place were a seamount is subducting underneath the Caribbean Plate. As seen in the multibeam bathymety, the subducting seamount produces an uplift of the upper part of the margin right beneath. Moreover, numerous recent fractures are cutting the Jaco uplift area at that place.

The main objectives of this passive seismological experiment is to detect and register the seismicity induced by the convergent dynamics between the subducting seamount and the Caribbean Plate. The spatial dimensions of the joined marine and land network are designed to register local tectonic events of the subducting plate.

| | April | | | | | | | May | | | | | | | | | |
|---|---|---|---|---|---|---|---|---|---|---|---|---|---|---|---|---|---|
| **Day of month** | 22 | 23 | 24 | 25 | 26 | 27 | 28 | 29 | 30 | 1 | 2 | 3 | 4 | 5 | 6 | 7 | 8 | 9 |
| **Julian day** | | | | 115 | | | | | 120 | | | | | 125 | | | | | Remarks |
| **OBS14** | s | o | o | o | o | o | o | o | o | o | | | | | | | | s | Hydrophone channel out of range, only vertical seismometer component was fairly working. Because of power problems recording stopped after 10 days |
| **OBH15** | s | - | - | - | - | - | - | - | - | - | - | - | - | - | - | - | - | s | DPG pressure sensor did not work |
| **OBH16** | s | x | x | x | x | x | x | x | x | x | x | x | x | x | x | x | x | s | Hydrophone |
| **OBH18** | | s | x | x | x | x | x | x | x | x | x | x | x | x | x | x | x | s | Hydrophone |
| **OBS19** | | s | o | o | o | o | o | o | o | o | o | o | o | o | | | | s | Hydrophone sometimes out of range, only one seismometer channel was fairly working. Because of power low recording stopped after 13 days |
| **OBH20** | | s | - | - | - | - | - | - | - | - | - | - | - | - | - | - | - | s | recorder problem |
| **OBH21** | | s | x | x | x | x | x | x | x | x | x | x | x | x | x | x | x | s | Hydrophone |

| | |
|---|---|
| x | operating |
| s | deployment/recovery |
| o | data with specific problems but at least one component usable (see comment column) |
| - | inaccurate recording, so that data cannot be used |
| blank | not recording |

**Table 6.6.5.1:** The station status of the first deployed JACO net stations, that have been already recovered during RV sonne cruise SO 163-2.

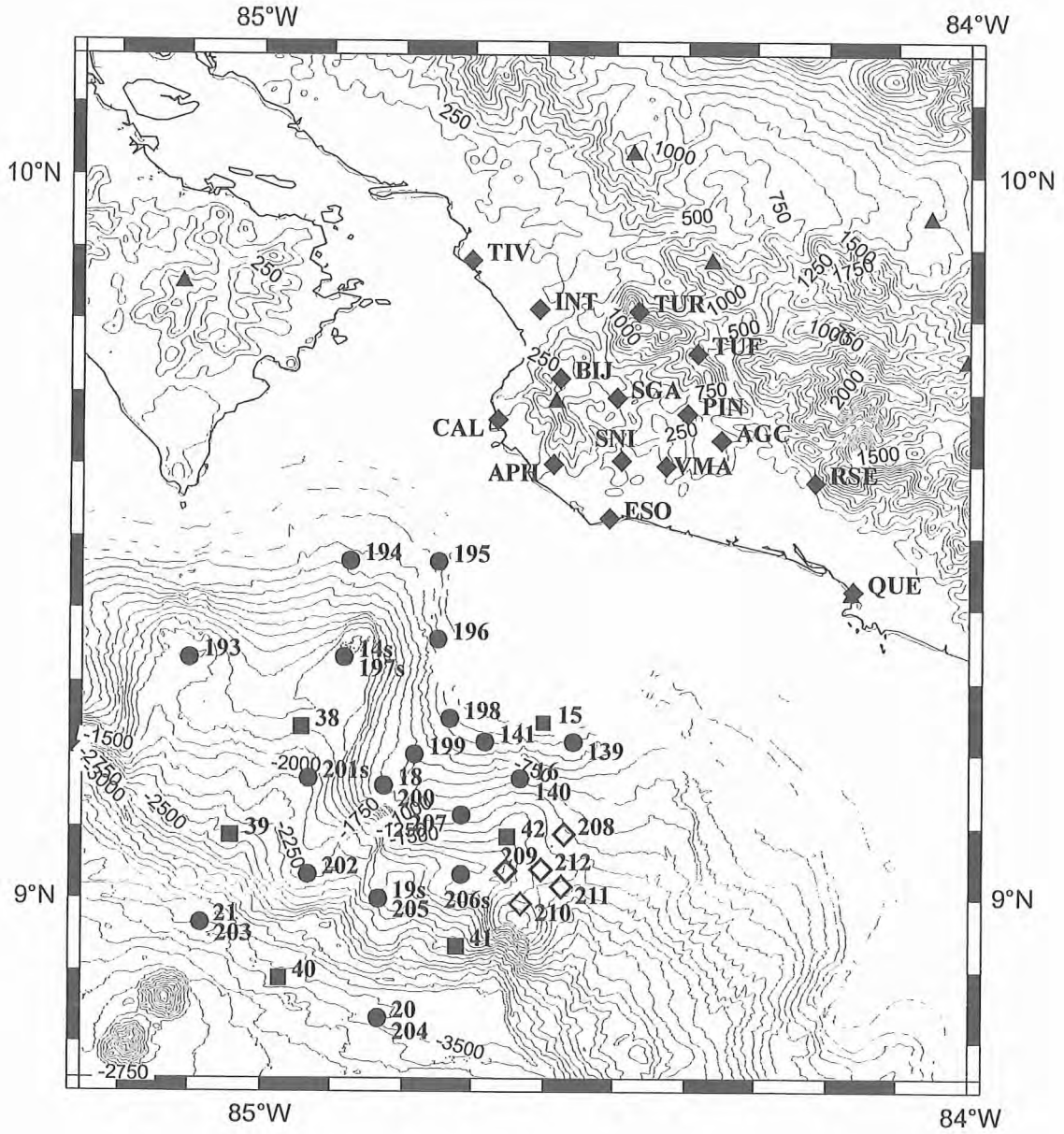


■ **JACO ocean net (first deployment)**

● **JACO ocean net (second deployment)**

◇ **QUEPOS MOUND subnet**

◆ **JACO land stations**

▲ **permanent land stations**

**Figure 6.6.5.1:** The combined land and seafloor seismic network of the JACO area. The land stations have been installed in April 2002. The ocean bottom instruments have been deployed during RV Sonne cruise SO 163-1 and SO 163-2. The traces of the subducting seamounts are clearly visible as large depressions in the contiental margin.

The interpretations on both datasets, the seismic and seismological data, must be done interactive. Active shooting allows to develope a precise velocity-depth model which is elementary for further seismological investigations. Furthermore, a distinct relocalisation of the instruments could be done. Hypocenter determination and calculations of fault plane solutions of the registered earthquake events is as well planed

**Data Quality and Noise characteristics**

As mentioned above, seven stations of the network were recovered successfully and have been deployed again. Half of the stations operated as intended and recorded high quality data of local and regional earthquakes that occur during their deployment period of 17 days, as well as the airgun source from MCS profiles shot during leg 2 of SO163 (Table 6.6.5.1). Data recovery was not complete because of a number of factors.

1. The PMD seismometers installed at obs14 and obs19 seemed to draw more power than specified such that those stations ran out of power prematurely. Furthermore these instruments jumped often between the minimum and maximum offset, so that only a small potion of their data could be used. Because this failure could not be fixed during the cruise, the PMD sensors have not been deployed again, but will be shipped to the manufacturer for repair.
2. The DPG pressure sensor at station obh15 also did not work correctly and produced a lot of noise and spikes, so that only stronger events could be registered successfully. This sensor also has not been deployed any more.
3. Obh20 failed due to recorder problems.
4. Some of the stations are affected by spikes, and more mysteriously, by bursts of almost monochromatic noise with a fundamental frequency close to 5 Hz, as already reported on RV Sonne cruise SO 161-3 often supplemented by overtones. The noisy periods can last up to several hours. Because of its relative monochromaticity this type of noise can be relatively easily removed by filtering.
5. No problem occur with the new 1 Gbyte flash disks, so that they could be read out completely. Hopefully that will be the same in October when the stations will be recovered and the amount of data is much larger than on the first deployment.

**Combination of MLS recorders with Owen-type 4.5 Hz OBS**

In Figure 6.6.5.2 we compare the signals of a hydrophone (upper seismogram) with the signals of a seismometer during a shooting session together with a coinciding earthquake. While the shot amplitudes on the hydrophone are larger than the biggest earthquake signals, it is opposite on the seismometer channels (lower seismograms). There, the shot peaks can only hardly be recognized besides the earthquake signal.

Because hydrophones are pressure sensitive, while naturally the seismometer records mainly ocean bottom displacement, the different behaviour is clear.

Though, the foreseen PMD broadband seismometer could not be used due to malfunction, we tested the 4.5 Hz Owen-type sensor in combination with a MLS recorder. Usually these sensors are only used together with MBS recorders, which cannot stay longer than a few weeks at the sea floor, without being recovered for changing the batteries. Although that kind of sensor is not as sensitive to lower frequencies as the broadband sensor, it is sufficient for the detection of local earthquakes.

Testing the direct connection of the sensor to the recorder seismometer connector failed due to unsufficient amplification of the sensor's signals. In a quick action a 10-times pre-amplifier has been constructed. In the labaratory testing was successful, so that we decided to use three 4.5 Hz

seismometers for the long-term survey, though we could not test it because deployment has to be do done immediately.

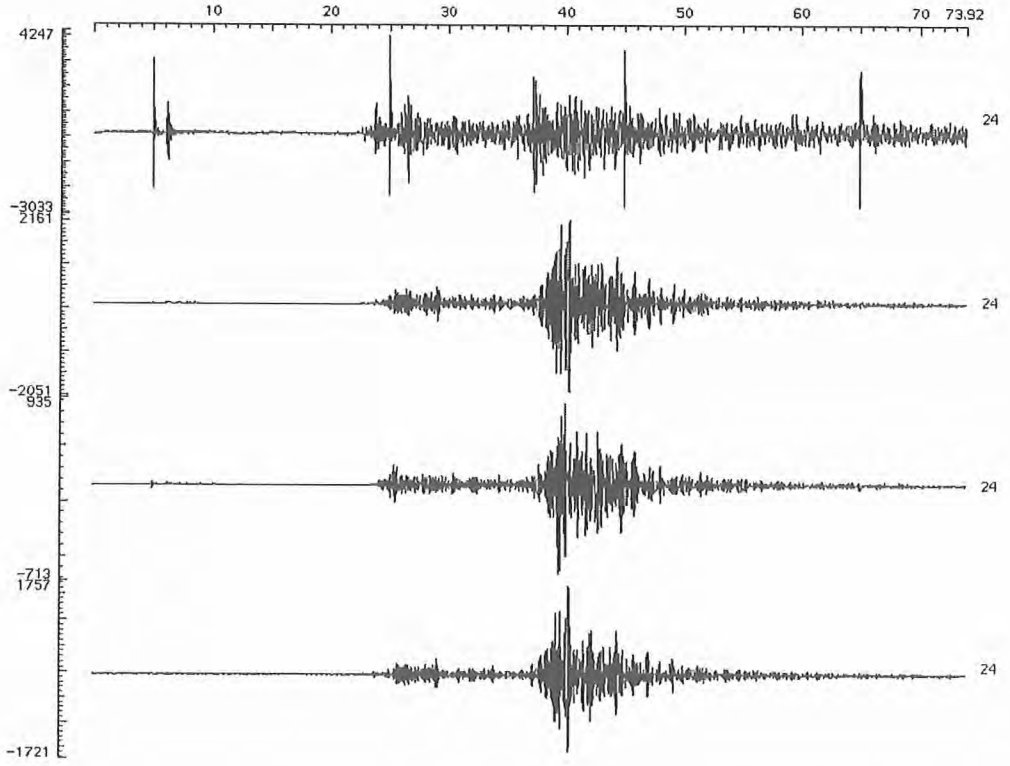


**Figure 6.6.5.2:** Comparison of hydrophone (upper trace) with seismometer signals during the coincidence of airgun shooting and a local earthquake (lower three traces) on May 8, 2002 19:58 UTC. The shot signals are equally spaced every 20 seconds, with the first shot at the 5$^{th}$ second of the registration window. The earthquake first arrival is 23 seconds after trace start.

**The JACO network ocean bottom instruments**

A total of 20 OBH and 3 combined OBH/OBS stations are deployed in the JACO seismological network. The instruments sites have been choosen to cover the area of three prominent subducted seamounts, promising a lot of seismicity due to tension when the seamounts pass through the continental lithospheric plate.

Furthermore, a small network of five OBH is closely placed east of the JACO net, to investigate the so called Quepos Mound, a fluid vent site on the subducting plate. These instruments will be recovered in July, earlier than the JACO net stations. Nevertheless, their signals can be combined with the JACO data set, too.

Table 6.6.5.2 specifies the instruments and their deployment date. The first 8 stations including a tiltmeter station are from the first deployment, and have already been recovered. Some of the stations of the second deployment occupy their sites. Data from the already recovered stations will be presented in the following section.

| SFB 574 Jaco Earthquake Net (ocean bottom instruments) | | | | | | | | | | | | | |
|---|---|---|---|---|---|---|---|---|---|---|---|---|---|
| STATION | LAT (N) | | LON (W) | | DEPTH | DEPLOYMENT | RECOVERY | RELEASER | ANTENNA | RECORDER | SENSORS | | |
| | D | M | D | M | (m) | (Date) | (Date) | CODE | CH. | S/N | HYDROPHONE | SEISMOMETER | TILTMETER |
| obs14 | 9 | 19.985 | 84 | 52.996 | 1741 | 22. Apr | 09. Mai | 0399+0355 | C | 706 | OAS 34 | PMD 540 | |
| obh15 | 9 | 14.661 | 84 | 36.046 | 114 | 22. Apr | 09. Mai | 0398+0355 | A | 711 | DPG 95 | | |
| obh16 | 9 | 9.975 | 84 | 38.015 | 944 | 22. Apr | 09. Mai | 0397+0355 | C | 10405 | HTI 302 | | |
| obt17 | 9 | 9.405 | 84 | 49.577 | 824 | 22. Apr | 28. Apr | 03BC+0355 | C | 20303 | | | 4948 |
| obh18 | 9 | 9.397 | 84 | 49.588 | 827 | 23. Apr | 09. Mai | 4A44 | C | 10402 | OAS 18 | | |
| obs19 | 8 | 59.996 | 84 | 50.055 | 2206 | 23. Apr | 09. Mai | 03B9+0355 | C | 10401 | OAS 31 | PMD 509 | |
| obh20 | 8 | 50.006 | 84 | 49.996 | 3473 | 23. Apr | 09. Mai | 03B7+0355 | D | 991238 | HTI 602 | | |
| obh21 | 8 | 58.032 | 85 | 5.046 | 3602 | 23. Apr | 09. Mai | 03BB+0355 | C | 991243 | HTI 102 | | |
| | JACO network (until October 2002) | | | | | | | | | | | | |
| obh38 | 9 | 14.271 | 84 | 56.637 | 1752 | 28. Apr | | 03BD+0355 | D | 713 | DPG 93 | | |
| obh39 | 9 | 5.280 | 85 | 2.560 | 2496 | 28. Apr | | 03B6+0355 | C | 991249 | DPG 75 | | |
| obh40 | 8 | 53.328 | 84 | 58.432 | 3420 | 28. Apr | | 03B5+0355 | C | 991237 | DPG 91 | | |
| obh41 | 8 | 56.043 | 84 | 43.428 | 2615 | 28. Apr | | 03B3+0355 | C | 991242 | DPG 87 | | |
| obh42 | 9 | 5.173 | 84 | 39.092 | 1481 | 28. Apr | | 03B8+0355 | C | 991250 | DPG 92 | | |
| obh139 | 9 | 13.023 | 84 | 33.508 | 379 | 12. Mai | | 03B7+0355 | C | 991247 | OAS 02 | | |
| obh140 | 9 | 10.017 | 84 | 37.993 | 939 | 12. Mai | | 03BB+0355 | A | 10405 | OAS 04 | | |
| obh141 | 9 | 13.016 | 84 | 41.022 | 351 | 12. Mai | | 03B9+0355 | A | 10402 | OAS 29 | | |
| obh193 | 9 | 19.989 | 85 | 6.063 | 1880 | 16. Mai | | 3659 | C | 991238 | HTI 502 | | |
| obh194 | 9 | 28.015 | 84 | 52.503 | 560 | 16. Mai | | 039A+0355 | D | 707 | OAS 18 | | |
| obh195 | 9 | 28.001 | 84 | 44.997 | 324 | 16. Mai | | 0387+0355 | B | 991256 | OAS 18 | | |
| obh196 | 9 | 21.531 | 84 | 45.034 | 413 | 16. Mai | | 3624 | C | 10401 | HTI 302 | | |
| obs197 | 9 | 20.022 | 84 | 53.006 | 1745 | 17. Mai | | 03BA+0355 | C | 10404 | HTI 702 | Owen 22 (4.5 Hz) | |
| obh198 | 9 | 14.975 | 84 | 44.001 | 291 | 16. Mai | | 3674 | C | 991243 | OAS 27 | | |
| obh199 | 9 | 12.016 | 84 | 46.990 | 734 | 16. Mai | | 03B1+0355 | D | 20303 | HTI 802 | | 4949 |
| obh200 | 9 | 9.419 | 84 | 49.601 | 824 | 16. Mai | | 03B2+0355 | C | 20302 | HTI 602 | | 4948 |
| obs201 | 9 | 10.013 | 84 | 56.020 | 2080 | 17. Mai | | 0397+0355 | D | 991252 | OAS 31 | LG 01 (4.5 Hz) | |
| obh202 | 9 | 1.992 | 84 | 56.010 | 2237 | 17. Mai | | 0386+0355 | D | 991236 | HTI 102 | | |
| obh203 | 8 | 57.974 | 85 | 5.004 | 3561 | 17. Mai | | 3614 | D | 706 | OAS 18 | | |
| obh204 | 8 | 50.000 | 84 | 49.995 | 3474 | 17. Mai | | 3629 | D | 991246 | OAS 38 | | |
| obh205 | 8 | 59.985 | 84 | 49.996 | 2207 | 17. Mai | | 3669 | B | 991241 | HTI 902 | | |
| obs206 | 9 | 1.996 | 84 | 43.006 | 1726 | 17. Mai | | 03BC+0355 | D | 10403 | OAS 46 | Owen 21 (4.5 Hz) | |
| obh207 | 9 | 7.000 | 84 | 43.003 | 1159 | 17. Mai | | 3609 | C | 711 | OAS 22 | | |
| | Quepos Mound Net (until July 2002) | | | | | | | | | | | | |
| obh208 | 9 | 5.376 | 84 | 34.248 | 1155 | 17. Mai | | 0399+0355 | D | 991248 | HTI 202 | | |
| obh209 | 9 | 2.296 | 84 | 39.205 | 1615 | 17. Mai | | 3664 | A | 991244 | OAS 75 | | |
| obh210 | 8 | 59.579 | 84 | 37.907 | 1202 | 17. Mai | | 03B4+0355 | D | 708 | HTI 101 | | |
| obh211 | 9 | 1.004 | 84 | 34.461 | 1411 | 17. Mai | | 6334 | C | 616 | OAS 09 | | |
| obh212 | 9 | 2.387 | 84 | 36.203 | 1326 | 17. Mai | | 4A44 | B | 971202 | OAS 28 | | |

**Table 6.6.5.2:** The seafloor stations of the JACO network and the Quepos Mound Net

**The JACO network earthquake dataset from the first deployment**

During the two and a half week period of the first deployment from April 23 to May 8, 2002 a total of 34 earthquakes has been detected by the JACO seismological network. Preliminary hypocenter locations have been determined for 20 events (Table 6.6.5.3).

| Date | | | Time | | | | Latitude | Longitude | Depth | Magnitude |
|---|---|---|---|---|---|---|---|---|---|---|
| 2002 | 4 | 23 | 13 | 44 | 7.0 | L | | | | |
| 2002 | 4 | 25 | 6 | 58 | 52.0 | L | | | | |
| 2002 | 4 | 26 | 16 | 24 | 49.7 | L | | | | |
| 2002 | 4 | 26 | 21 | 51 | 12.1 | L | 9.365 | -84.862 | 24.2 | 2.1C |
| 2002 | 4 | 26 | 22 | 2 | 17.3 | L | 9.332 | -84.869 | 1.6 | 2.3C |
| 2002 | 4 | 26 | 22 | 27 | 51.1 | L | 9.370 | -84.857 | 31.2 | 2.4C |
| 2002 | 4 | 26 | 23 | 14 | 42.4 | L | 9.334 | -84.867 | 1.3 | |
| 2002 | 4 | 27 | 0 | 10 | 8.1 | L | 9.329 | -84.888 | 1.6 | 1.9C |
| 2002 | 4 | 27 | 0 | 29 | 38.5 | L | 9.349 | -84.874 | 1.3 | 2.0C |
| 2002 | 4 | 27 | 1 | 30 | 55.7 | L | 9.352 | -84.867 | 1.3 | 2.2C |
| 2002 | 4 | 27 | 1 | 37 | 31.9 | L | 9.340 | -84.854 | 1.7 | 2.1C |
| 2002 | 4 | 27 | 2 | 29 | 42.5 | L | 9.340 | -84.877 | 1.2 | 2.0C |
| 2002 | 4 | 27 | 3 | 26 | 38.2 | L | 9.308 | -84.886 | 1.9 | 2.2C |
| 2002 | 4 | 27 | 10 | 52 | 23.3 | L | 9.368 | -84.856 | 34.7 | 2.3C |
| 2002 | 4 | 28 | 1 | 52 | 44.0 | L | | | | |
| 2002 | 4 | 28 | 13 | 55 | 47.2 | L | 9.247 | -84.455 | 53.9 | 2.3C |
| 2002 | 4 | 28 | 19 | 4 | 11.2 | R | | | | |
| 2002 | 4 | 29 | 2 | 44 | 30.2 | L | 9.087 | -84.669 | 11.0 | |
| 2002 | 4 | 29 | 5 | 15 | 21.1 | L | 10.104 | -84.580 | 134.1 | 2.9C |
| 2002 | 4 | 30 | 18 | 54 | 7.0 | L | | | | |
| 2002 | 5 | 1 | 5 | 21 | 18.2 | L | 9.752 | -84.458 | 121.7 | |
| 2002 | 5 | 2 | 14 | 35 | 52.0 | L | | | | |
| 2002 | 5 | 3 | 8 | 14 | 58.0 | L | | | | |
| 2002 | 5 | 4 | 4 | 33 | 37.0 | L | | | | |
| 2002 | 5 | 5 | 0 | 6 | 18.0 | L | | | | |
| 2002 | 5 | 5 | 2 | 36 | 38.0 | L | | | | |
| 2002 | 5 | 5 | 3 | 29 | 3.0 | L | | | | |
| 2002 | 5 | 5 | 3 | 34 | 3.0 | L | | | | |
| 2002 | 5 | 5 | 13 | 14 | 25.3 | L | 10.096 | -84.685 | 96.0 | 3.2C |
| 2002 | 5 | 5 | 13 | 21 | 4.2 | L | 8.662 | -85.335 | 7.3 | |
| 2002 | 5 | 6 | 1 | 29 | 43.6 | L | 9.062 | -84.738 | 7.1 | 2.6C |
| 2002 | 5 | 8 | 1 | 24 | 19.1 | L | 9.121 | -84.895 | 3.4 | 1.9C |
| 2002 | 5 | 8 | 14 | 12 | 28.7 | L | 9.053 | -84.740 | 7.1 | 3.0C |
| 2002 | 5 | 8 | 23 | 50 | 56.8 | L | | | | |

**Table 6.6.5.3:** Preliminary earthquake catalogue from the JACO seismic ocean bottom network. Origin times are only valid for localized events, all others are the start time of the time window, which starts three minutes before the triggered event. L means local, R regional event, latitude and longitude are in ° (deg), depth is in km, magnitude is the coda-magnitude due to missing receiver transfer functions.

Half of the earthquakes have been located exactly at the place where a big seamount has already entered into the continental lithosphere (Figure 6.6.5.3). Eleven of those events belongs to a swarm that occured between April 26, 21:51 and April 27, 03:26. The other subducted seamounts did not produce heavy seismicity in the observed time intervall. One event could be detected on the track subducted seamounts draw below the Caribbean plate. Three earthquakes have been observed beneath the continent at depth around 100 km, which are originating from the subducting oceanic plate (Benioff Zone).

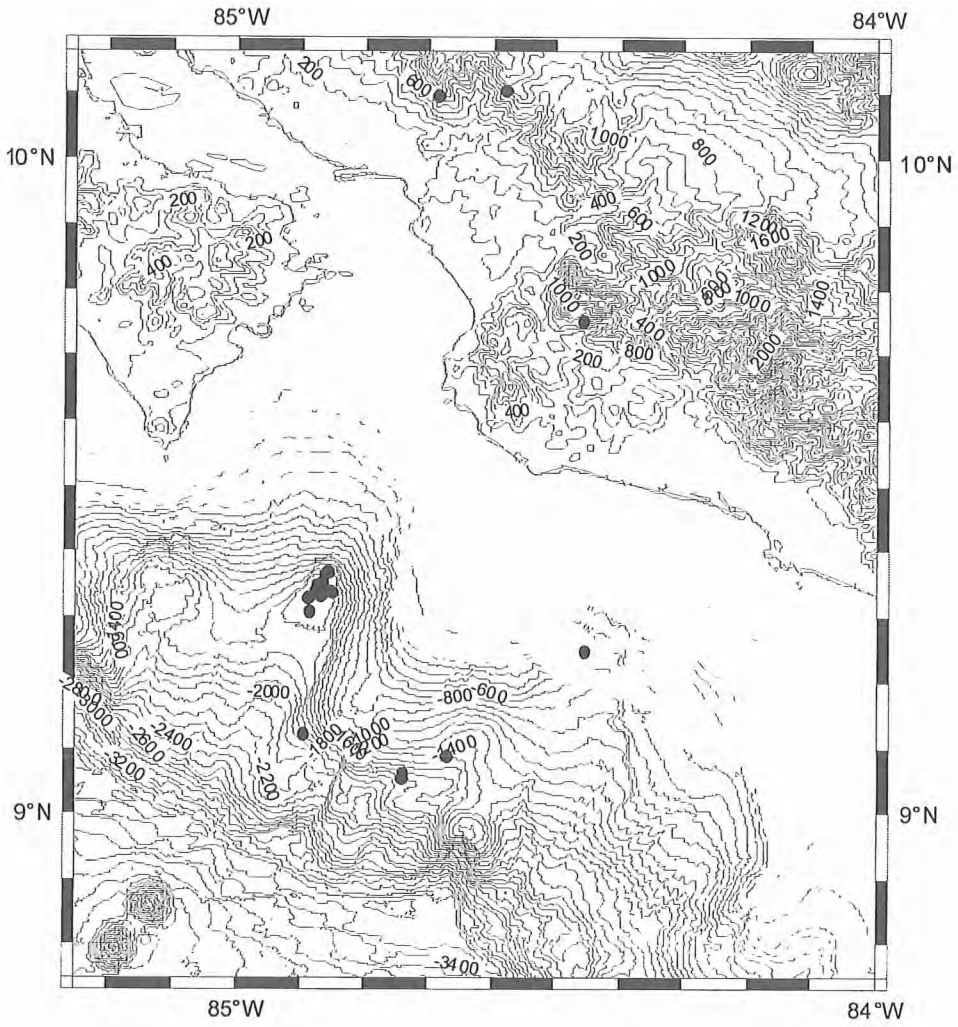


**Figure 6.6.5.3:** Earthquake epicenters that have been located with the JACO seismic network during April 23 and May 8, 2002 (first deployment)

The following pages show examples of earthquakes recorded at the JACO net array. They serve to illustrate the signal quality to be expected from the different instruments. In general, P phases can be clearly identified on all instruments in the unfiltered records, however, seismometer records are often dominated by long period microseismic noise. Fortunately, the dominant frequencies of this noise (<1 Hz) are sufficiently removed from the dominant band excited by local earthquakes (>3-4 Hz, see Figures 6.6.5.4-9) to be easily filtered out, or, for high precision onset and polarity picking (which can be affected adversely by filtering), to only appear as a trend or DC shift after zooming in on an arrival with a window size of only tenths of a second. For a first inspection, a 10-49 Hz bandpass filter was found to be the most suitable.

S-waves could occasionally be picked, too. As expected, these phases were quite clear on the seismometer data, particularly on the horizontal components, but much harder or impossible to see in the hydrophone records.

In the following plots, the event origin time and hypocentral co-ordinates as determined by phase picks on the ocean bottom stations are indicated by the heading above the seismograms. Component label BHH is used to indicate hydrophone channels, while BHZ, BH1, and BH2 are the vertical and two horizontal seismometer components. Amplitude and polarity of all data are 'raw', i.e., uncorrected for instrumental response, preamplifier gain, and polarity flips. All times are UTC. First, an event from the subducting plate is shown, then examples of oceanic events.

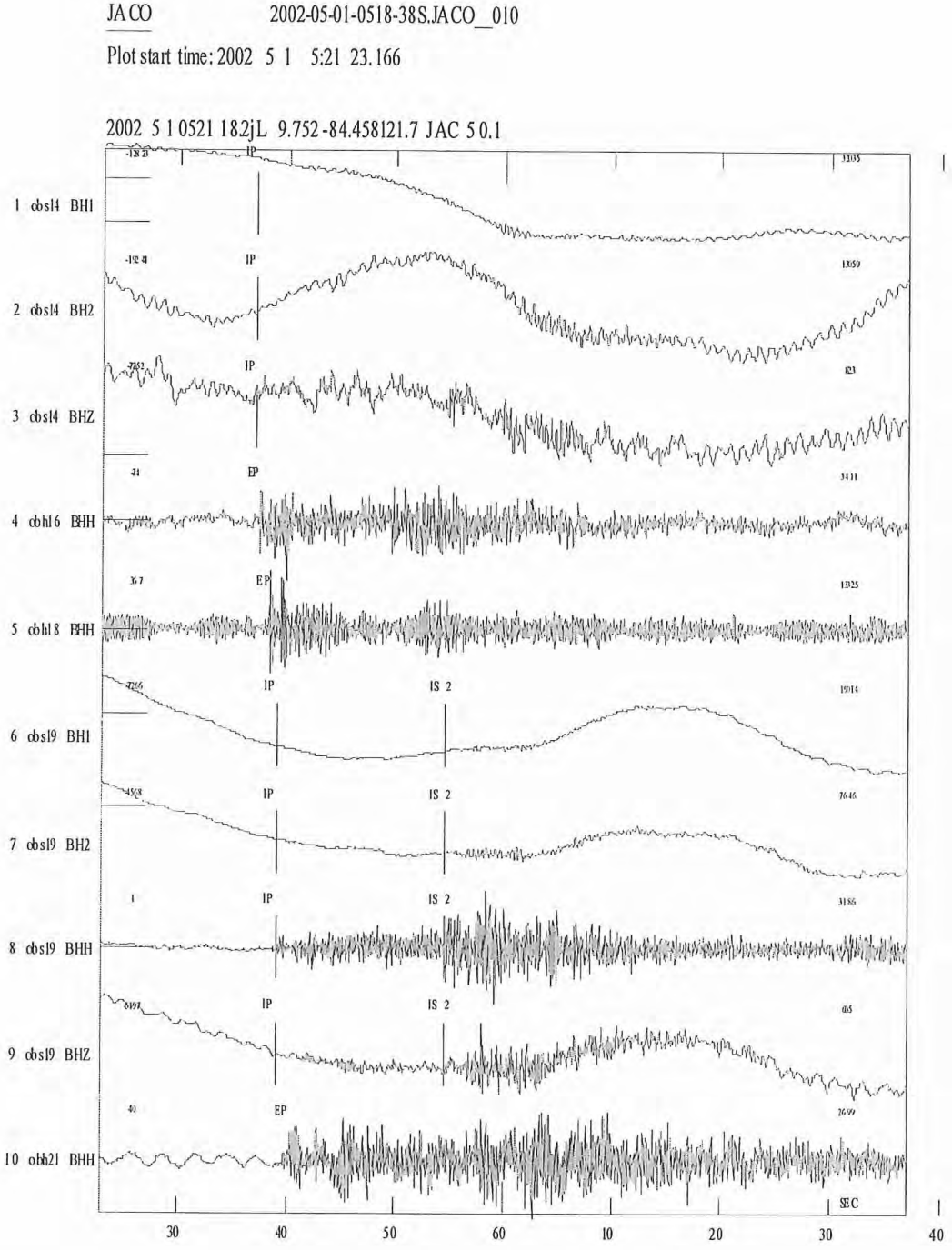


**Figure 6.6.5.4:** Earthquake from May 21, 2002 at 5:21 UTC from the subducting plate at a depth of about 122 km located at the north-western edge of the land stations network. All ocean bottom stations show up with good signals except obh15 and obh20 which have technical problems (see Table 6.6.5.1) and are not shown here. The seismometer channels can be easily recognized by their long-period signals, while the hydrophone channels yield only high frequent signals. Clear P and some S onsets have been observed, while obh18 shows up with a strong secondary onset one second after P, which maybe a depth phase.

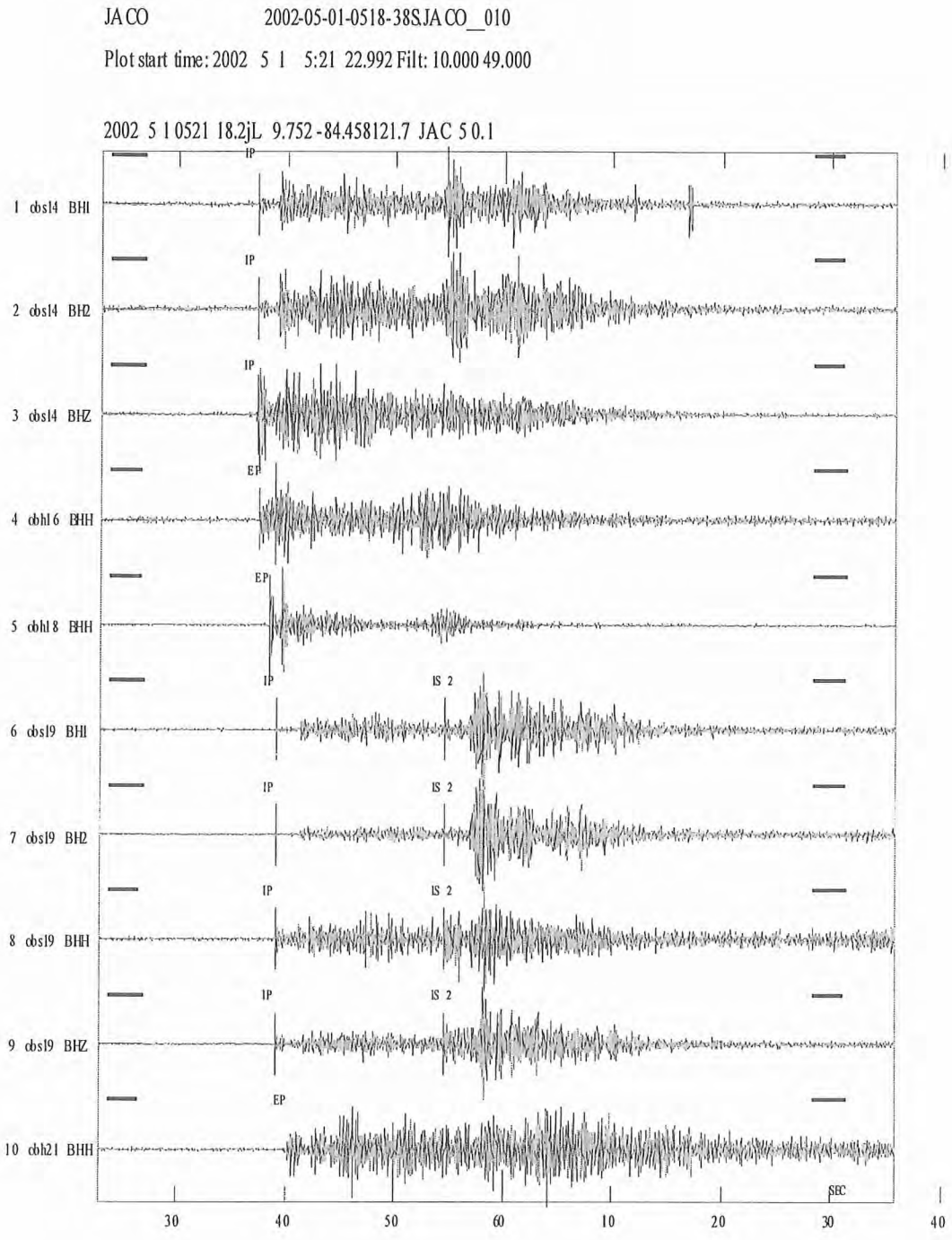


**Figure 6.6.5.5:** The same event from previous figure, but filtered by a 10 to 49 Hz bandpass filter. Now, all components show up with a clear first arrival and the S wave can be clearly seen on the seismometer channels, but also on some hydrophone channels.

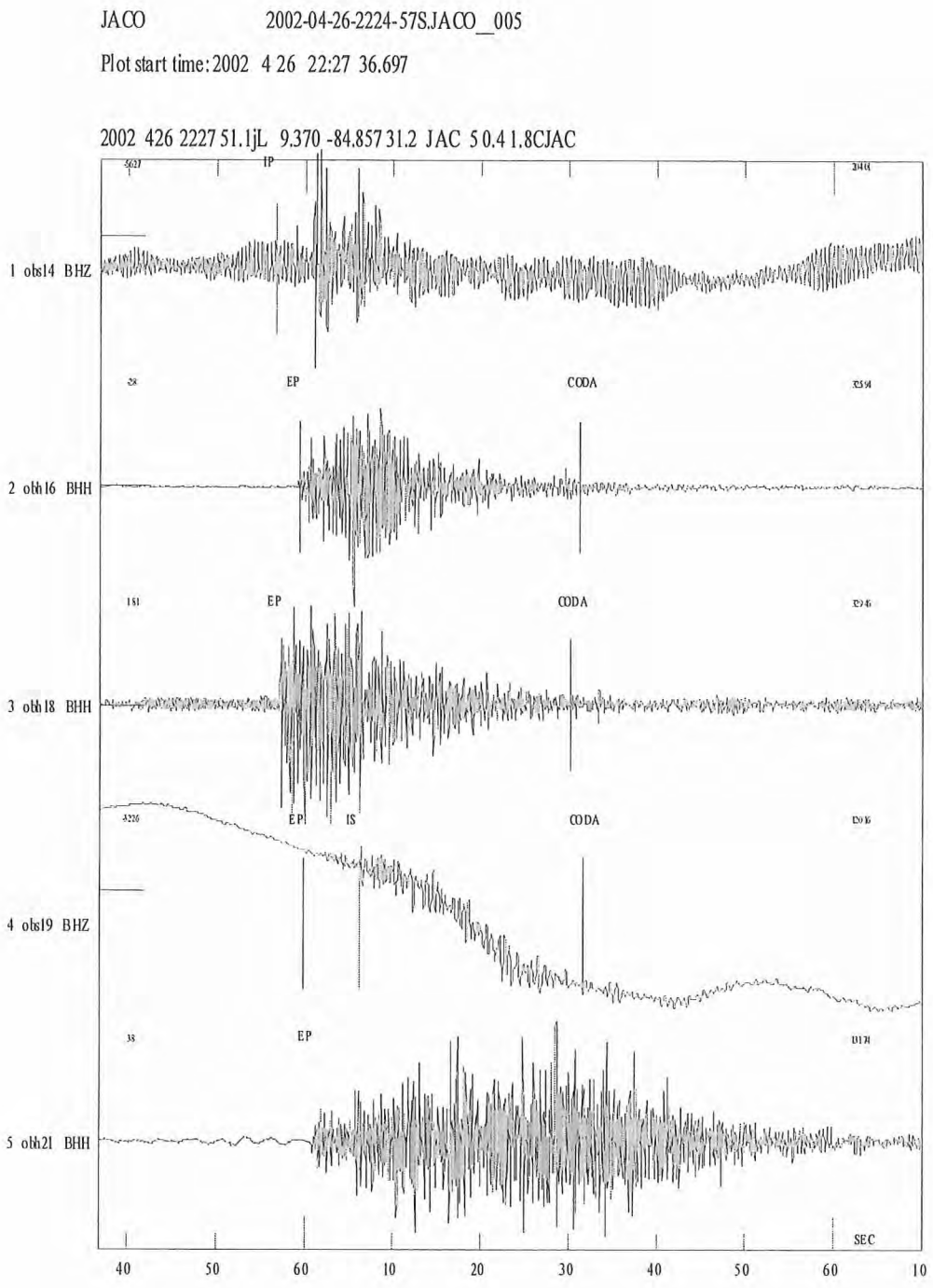


**Figure 6.6.5.6:** Swarm earthquake from April 26, 2002 at 22:27 UTC located where a large seamount has already entered the continental lithosphere. The focal depth of about 31 km is more than questionable, not only because only one S-pick could be made, but also because of the majority of the swarm events have shallow depths.

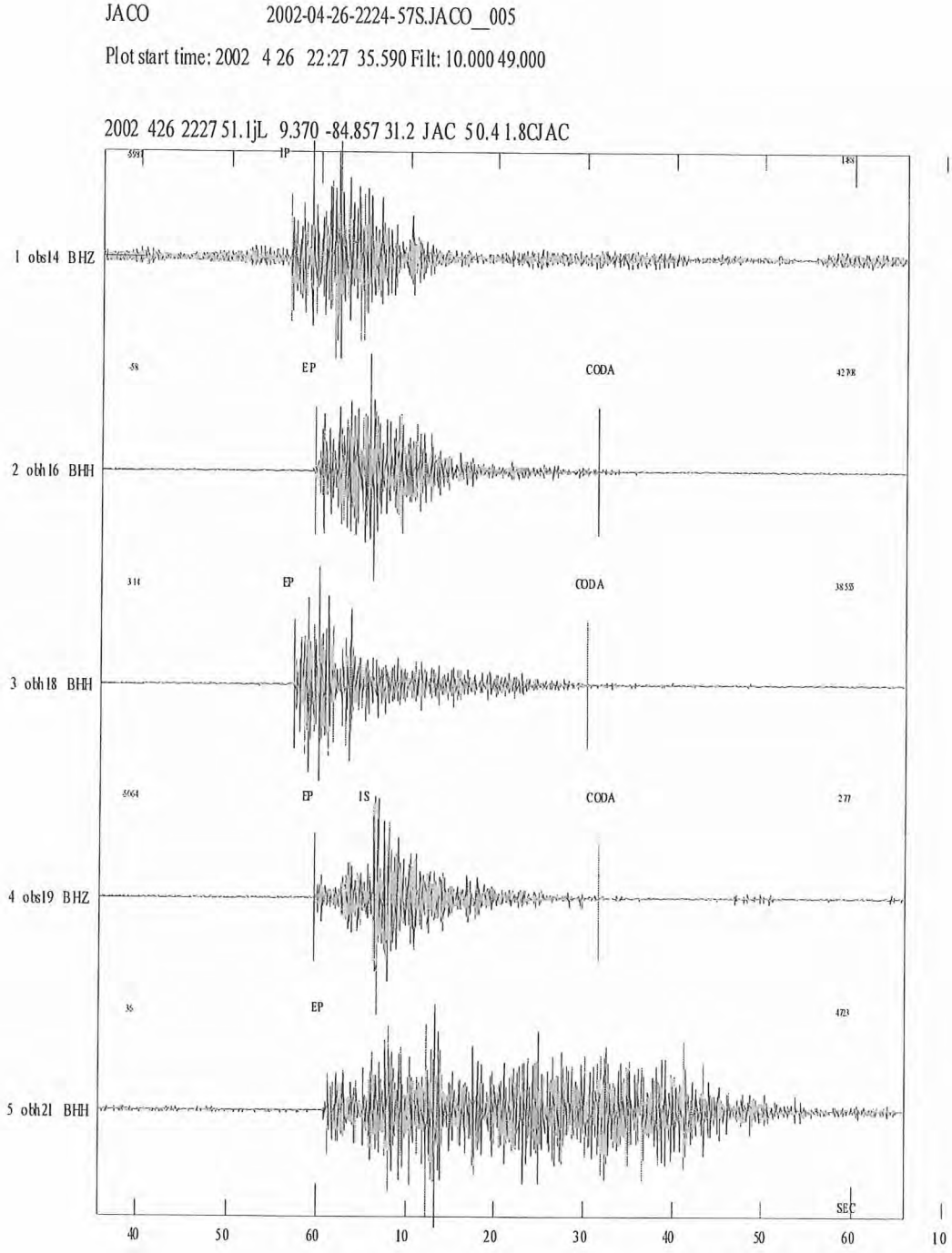


**Figure 6.6.5.7:** Event from previous figure, but filtered by a 10 to 49 Hz bandpass.

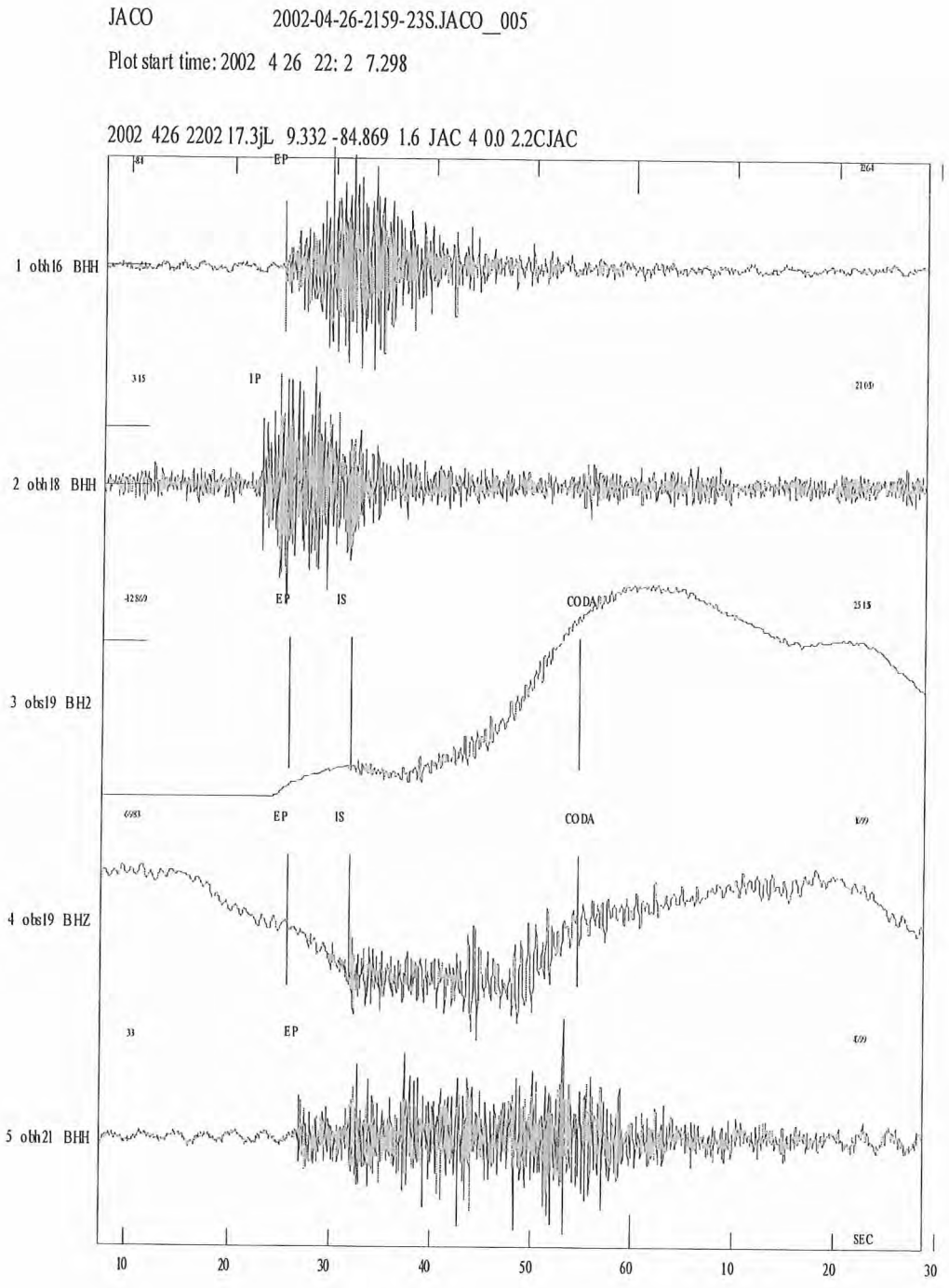


**Figure 6.6.5.8:** Another event from the earthquake swarm from April 26, 2002 at 22:02. Focal depth is about 2 km. Trace 3 from obs19 horizontal component demonstrate that it is sometimes possible to use corrupted seismograms, if the interesting part is not effected by distortion. Until 8 seconds before the P onset trace 3 was out of range, and recovered just in time for registering the earthquake.

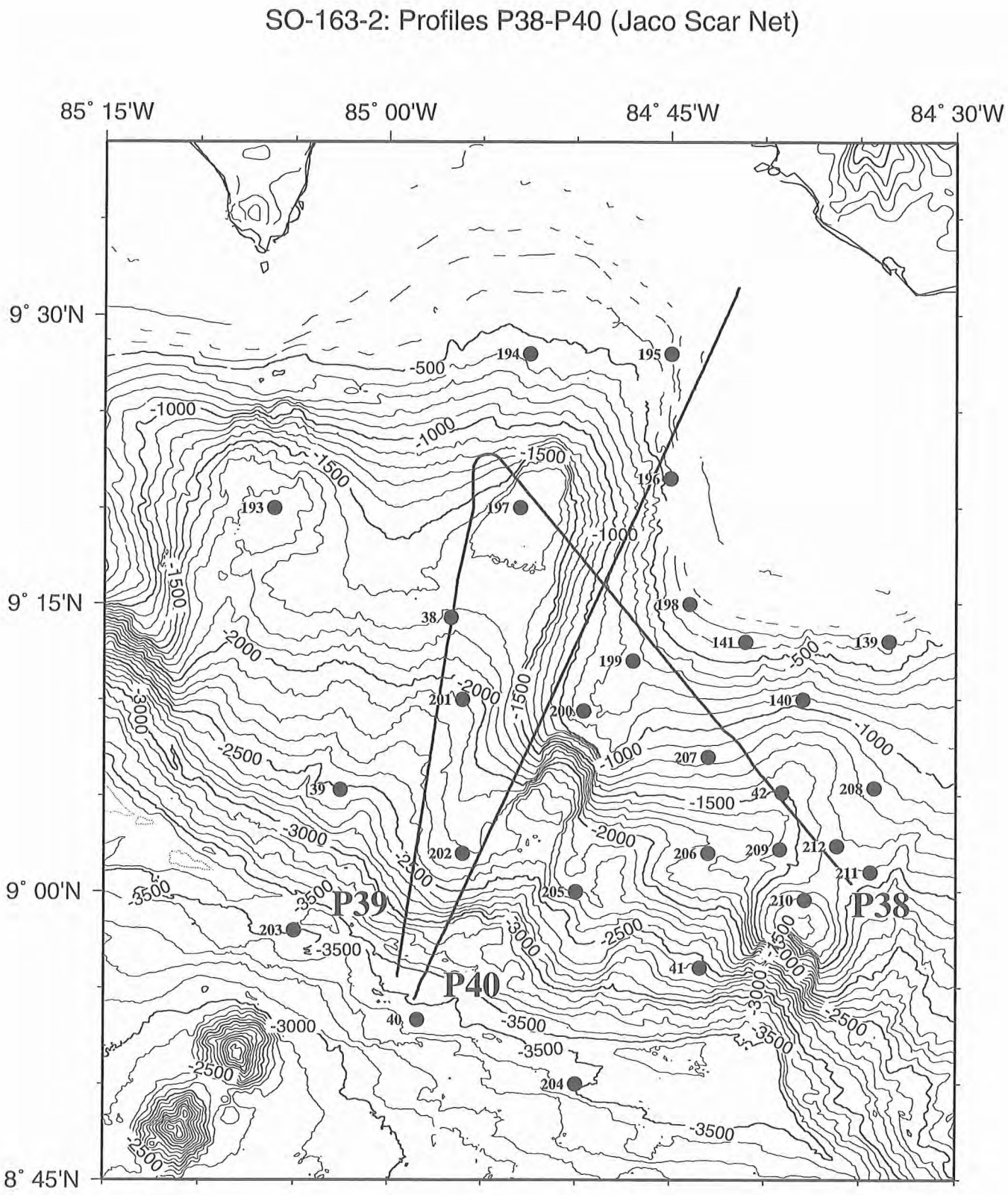


**Figure 6.6.5.9:** Location map of profiles P38-P40 with 100 m isolines and Jaco Scar Net stations.


**Figure 6.6.5.10:** Record section from str 938 (Streamer,ch2), Profile 38.

**Figure 6.6.5.11:** Record section from str 939 (Streamer,ch2), Profile 39.

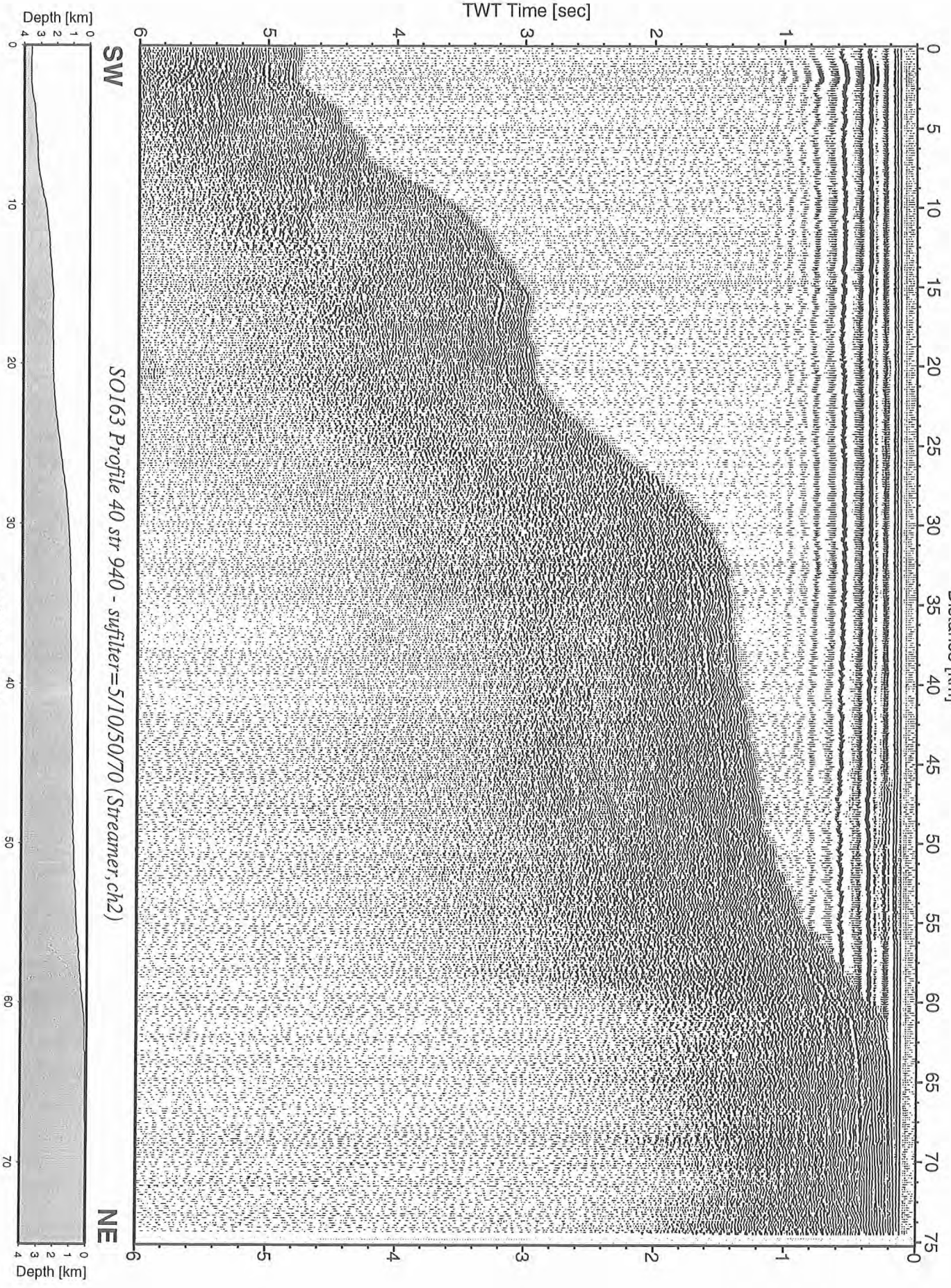


**Figure 6.6.5.12:** Record section from str 940 (Streamer,ch2), Profile 40.

**Figure 6.6.6.2:** Record section from obh 167 (HTI-Hydrophone), Profile 34.

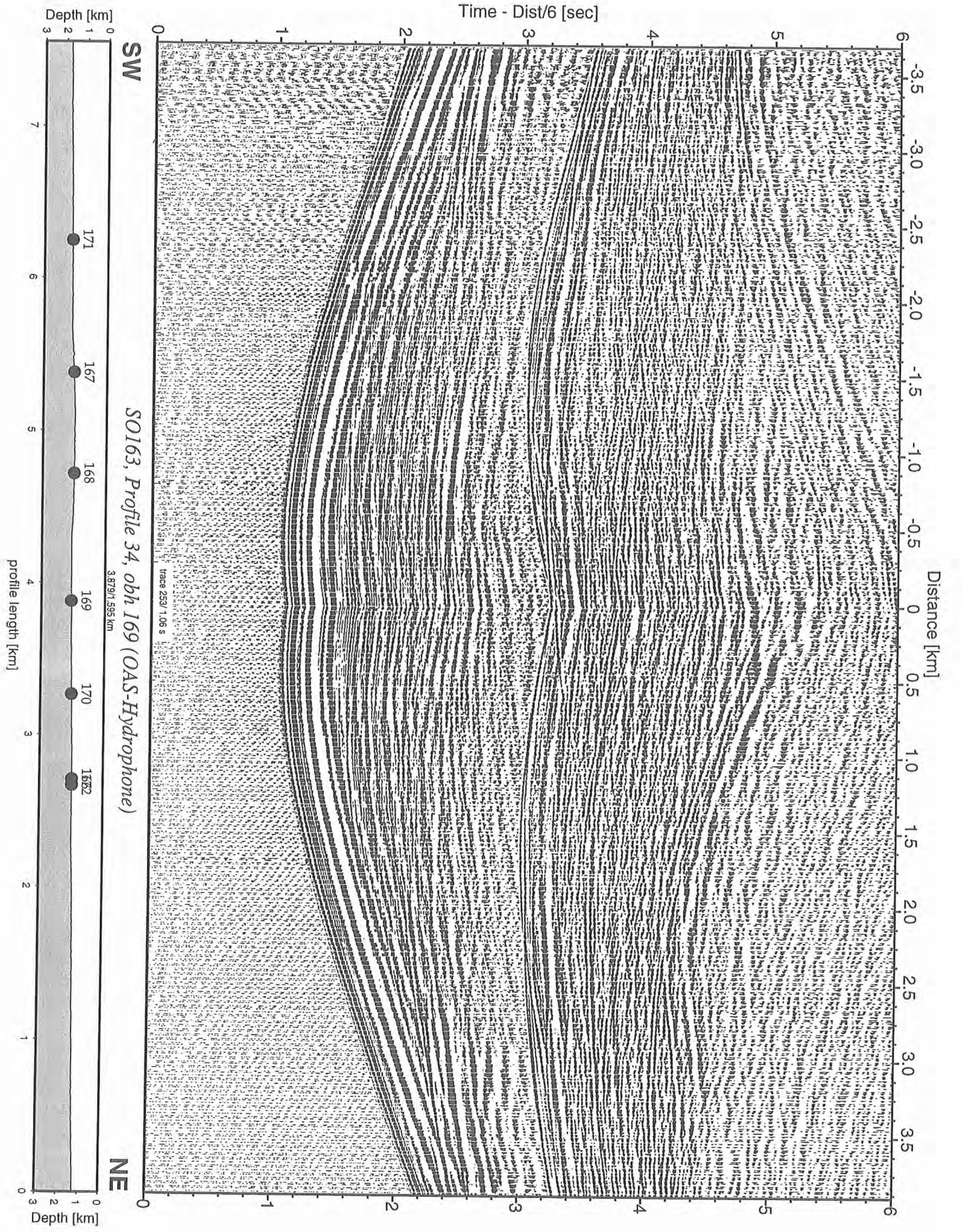


**Figure 6.6.6.3:** Record section from obh 169 (OAS-Hydrophone), Profile 34.

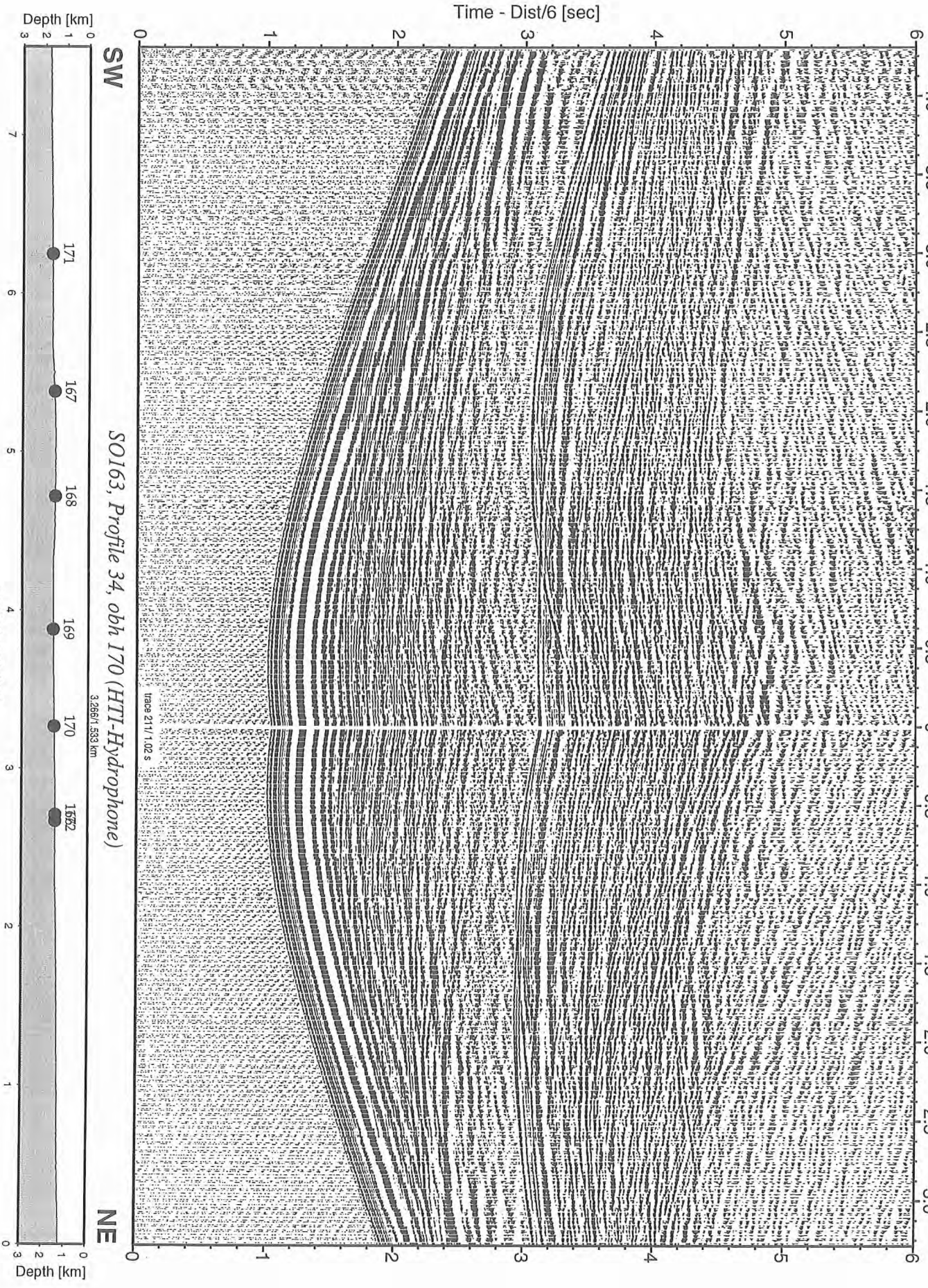


**Figure 6.6.6.4:** Record section from obh 170 (HTI-Hydrophone), Profile 34.

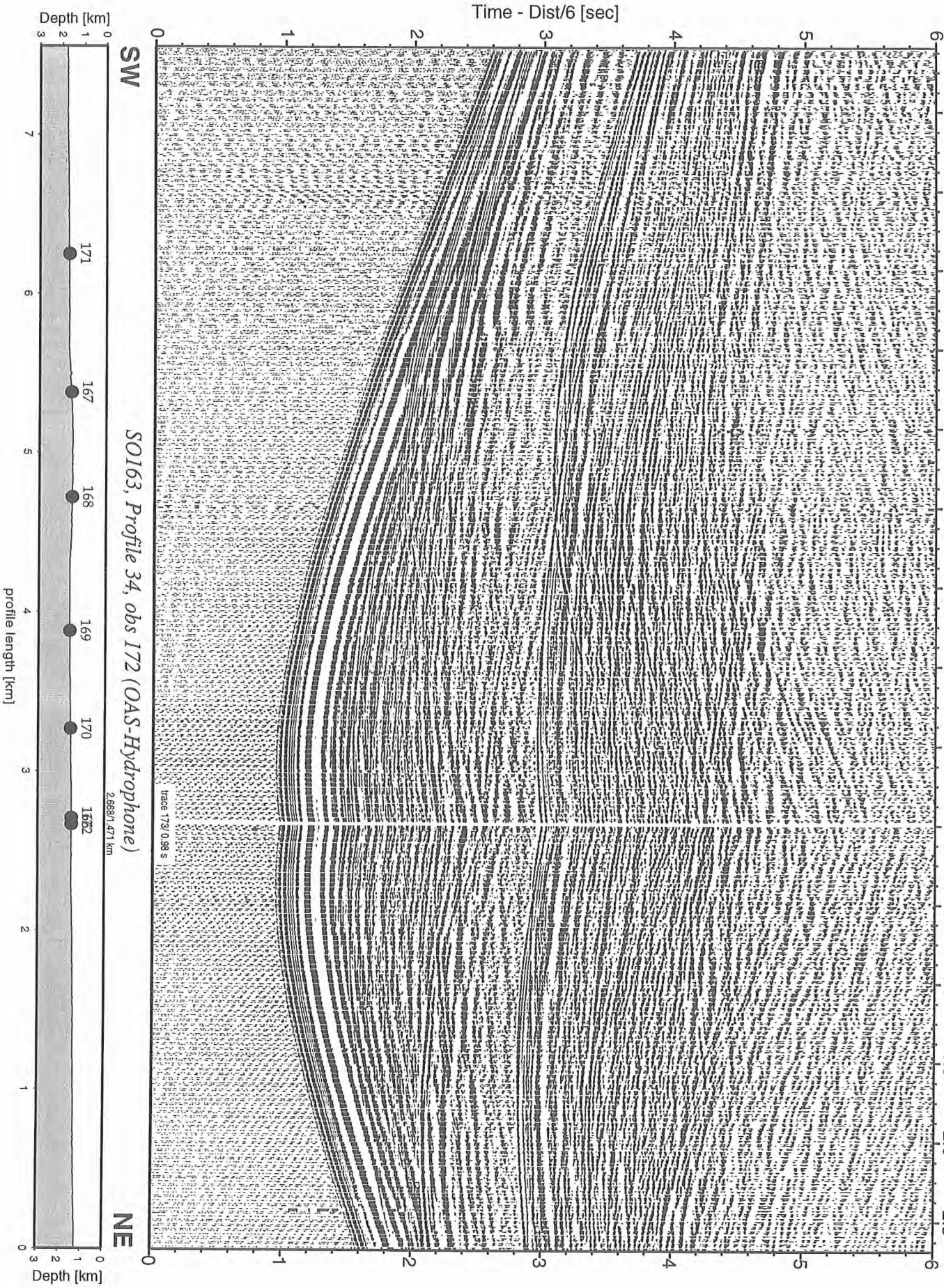


**Figure 6.6.6.5:** Record section from obs 172 (OAS-Hydrophone), Profile 34.

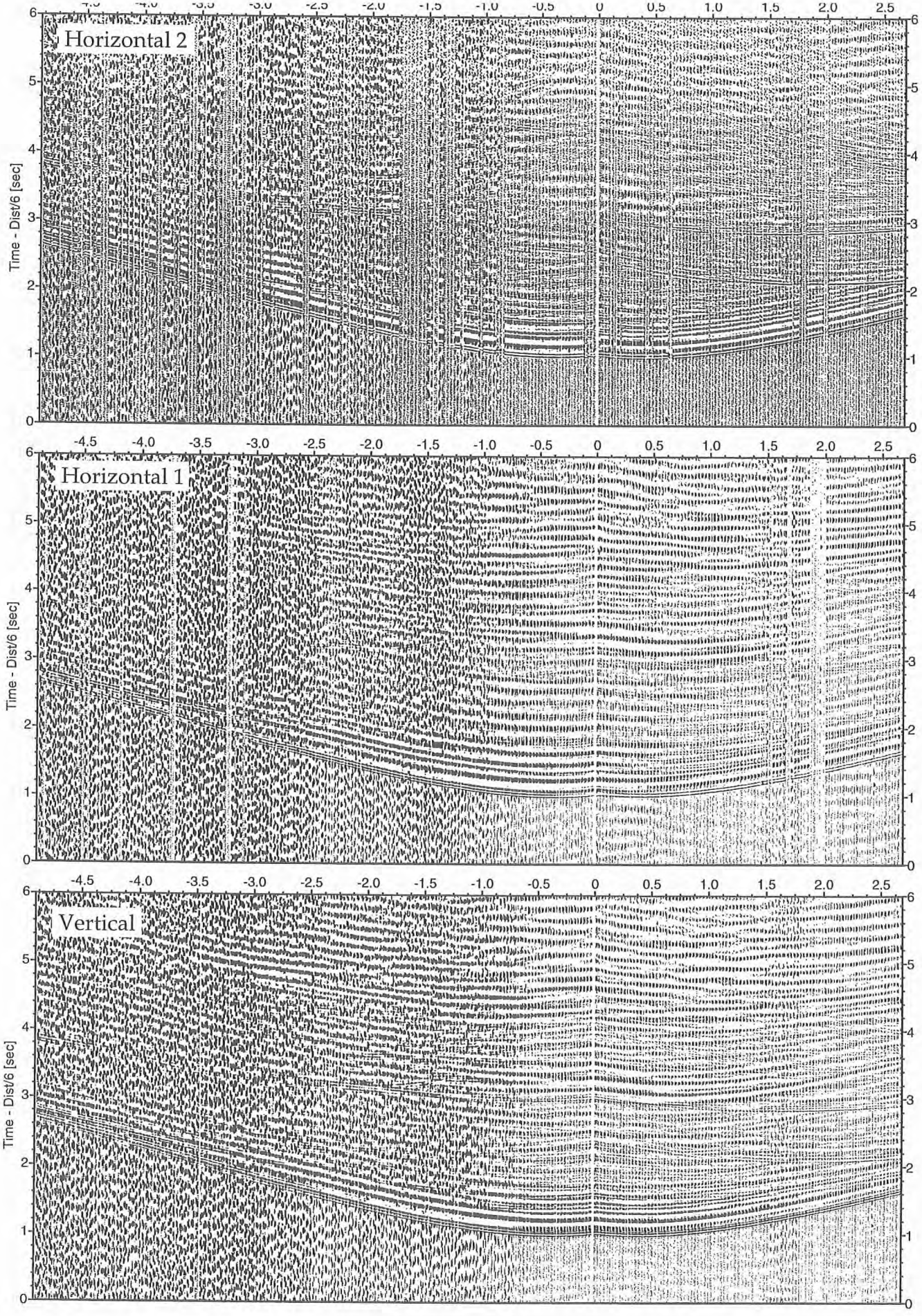


**Figure 6.6.6.6:** Record sections from obs 172 (PMD), SO163, Profile 34.

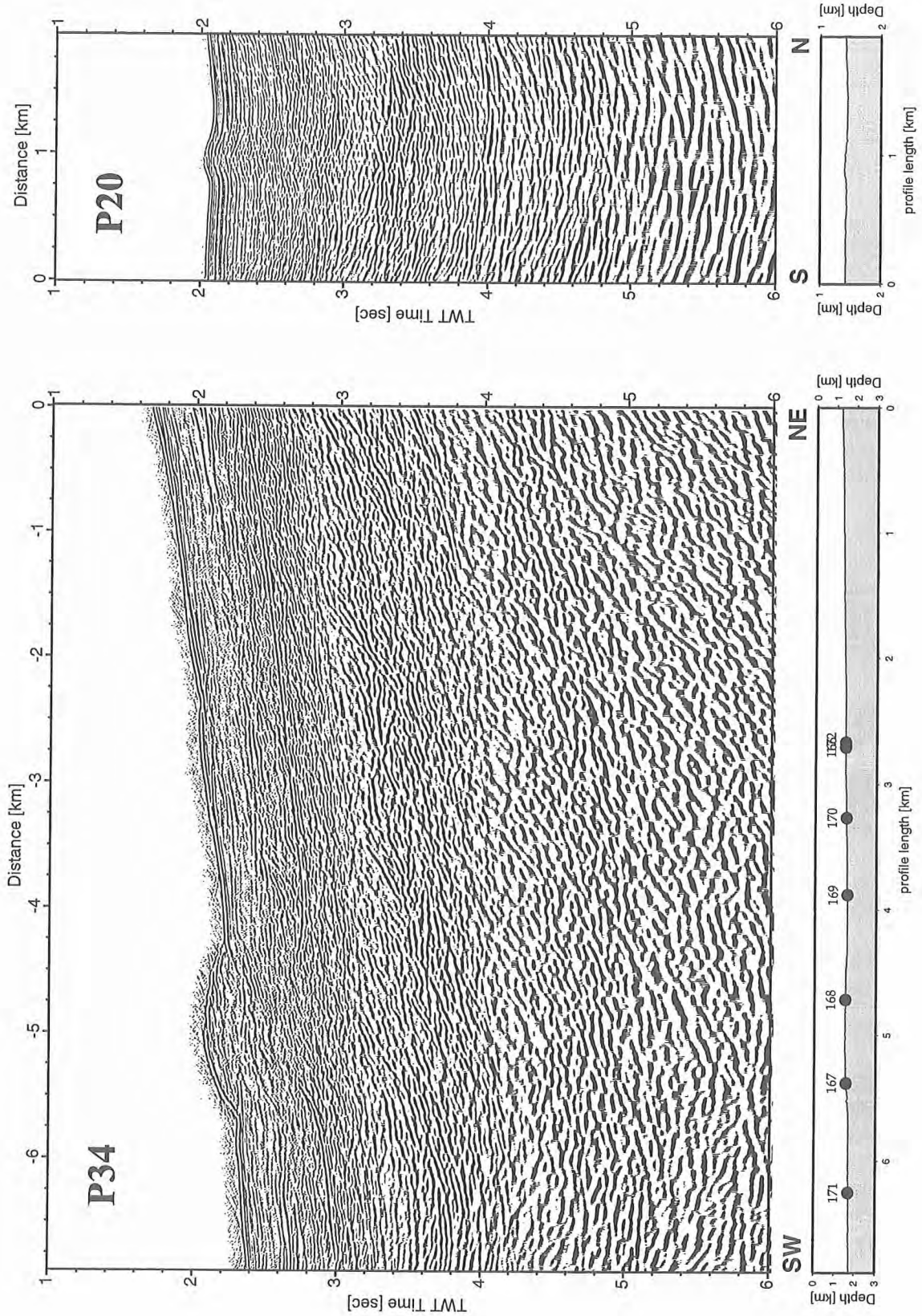


**Figure 6.6.6.7:** Post-stack time migration of profiles P20 and P34 across Mound Culebra and Mound Quepos.

## 6.7 Water column and upper sediment investigations

(G. Rehder, S. Grandel, S. Mau, and K. Stange)

### 6.7.1 Introduction

Water column program

An intensive sampling program was performed during SO 163/2 to investigate the methane and oxygen distribution within the water column. Methane is one of the key components cycled in the process of dewatering at active continental margins. It can be oxidized within the upper sediment, can provide the carbon and energy source for chemoautotrophic communities, or can be injected into the water column. All these processes have to be assessed to close the carbon budget at active seep sites. The methane injected into the water column will be oxidized on time scales from decades to days [Rehder et al., 1999; Valentine et al., 2001], strongly dependent on the surrounding and amount of methane available. Strong isotopic fractionation occurs during the oxidation process, which allows insight in the processes controlling the methane pathways.

Due to the relatively short lifetime and its generally low background in deep waters, the analysis of methane is ideally suited to locate currently active vent sites. Other than for the ionic constituents, methane can be transported both within the fluids in dissolved form, or by transport of free gas in case the pore waters become over-saturated. In the latter case, the transport is independent of the transport of other fluid components, and can lead to transfer to relatively shallow depth levels [Rehder et al., in press].

While today's ocean can be considered as a negligible source of methane to the atmosphere, its cycle, turnover times and transport pathways are still an important topic of marine research. Large excursions in the carbon isotopic signature of benthic and planctonic foraminifera have been suggested to be caused by gas hydrate destabilization [Dickens et al., 1995]. All models used to assess the importance of a large scale hydrate decomposition for ancient and future climate scenarios lack an understanding of the role of the ocean to mitigate the direct transfer of the gas to the atmosphere [Dickens et al., 2001]. Seepage from hydrate bearing sediments is thus the ideal setting to investigate the role of the ocean in what is now known as the "clathrate gun hypothesis".

Sediment investigations

Investigations of the geochemcial composition of porewaters provide information to investigate the forces and impacts driving redox-, and remineralization processes within the upper sediment column. During the SO 163/2 cruise, pore water composition of surface sediments was investigated at about ten locations to get a first insight into sediment diagenetic processes in the subduction zone off Costa Rica. Concentration and distribution of the parameters total alkalinity, ammonia, chloride and sulphide in the porewater were determined in surface sediments This allows to identify locations influenced by seepage and to assess the effect of methane formation and decomposition regarding sediment diagenetic processes.
Distinctive colonies of clams as well as precipitates of authigenic carbonates, resulting from biogeochemical turnover and interaction between fluids and ambient bottom water, are found at cold vent sites ([e.g. Suess et al., 1985, Suess and Whiticar, 1989, Henry et al., 1992, Torres et al., 1996, Suess and Bohrmann, 1997]. Bacterial mats have also been identified and can be indicative of subsurface gas hydrate pavement [Bohrmann et al., 1998]. Preliminary OFOS-track investigations executed during So163/1 were used to determine areas where active seepage could be expected. Sediment samples were collected at these sites, in addition to reference sites reflecting 'normal' off-shore and deep-sea situations at similar water depths. First results of the geochemical pore water studies executed during this cruise are reported.

## 6.7.2 Material and Methods

Water column sampling and analysis

The CTD unit as well as the 24 bottle water column carousel worked well throughout the cruise, with the exception of major problems with the performance of the oxygen sensor at the beginning of the cruise. After CTD station 10 (and using the fifth oxygen sensor), problems were resolved. At all stations, samples were taken for shipboard analysis of oxygen and methane, and 2 sets of 250ml water samples poisoned with 0.5ml of saturated HgCl were sampled into crim cap glass bottles sealed with a butyl rubber septum.

Oxygen was measured using the method developed by Winckler as described in Grasshoff et al. (1997). Usually, three Niskin bottles were sampled twice to control reproducibility of the measurements. The Seabird oxygen sensor worked well after CTD-station 10, but had been replaced several times before due to electronic noise or calibration inconsistencies. After CTD station 10, the absolute values of oxygen sensor and Winckler titration differed by less than 10 % (Fig. 6.7.2.1). However, both data sets will be further improved. The addition of the (oxygen containing) chemical reagents to the samples leads to a blind value which has not been substracted yet. The output of the oxygen sensor is calculated from the electrode current as well as the change in current over time to adjust for the response time of the instrument. During in situ oxygen monitoring, the slope $dC_{(ox)}/dt$ can be calculated only by looking backward in the recording data. The slope can be reprocessed with the SEASAT command DERIVE, which looks at the data before and after an individual point to derive the slope. Both data sets will be reprocessed shortly after the cruise and will be incorporated into the SFB 574 data base.

For $CH_4$ analysis aboard, a modification of the vacuum degassing method described by *Lammers and Suess* [1994] was used [Rehder et al., 1999]. 1600 ml of water were injected into pre-evacuated 2200 ml glass bottles, which leads to almost quantitative degassing. The gas phase was subsequently recompressed to atmospheric pressure and the $CH_4$ mole fraction of the extracted gas was determined by gas chromatography. A Shimadzu GC14A gas chromatograph equipped with a flame ionization detector was used in connection with a Shimadzu CR6A Integrator. Nitrogen was used as carrier gas, and separation was performed using a 4m 1/8' SS column packed with Porapack Q (50/80 mesh) run isothermally at 50°C. The total gas content of the sample was calculated from the measured dissolved oxygen concentration and assuming that $N_2$ and argon are 100% saturated relative to their atmospheric partial pressures [Weiss, 1970]. The dissolved methane concentration was calculated as the product of the mole fraction in the extracted gas phase and the amount of total gas (STP) in the sample. For calibration, mixtures of 1.936ppm ±0.003 ppm and 9.854 ±0.006 ppm in synthetic air (Deuste Steininger, calibrated against NOAA/CMDL standards at the Institute for Environmental Physics, Heidelberg) were used.

The 2 sets of 250ml water samples will be transported to Kiel at 4 °C after SO164. One set will be used to measure methane concentration with a standard purge and trap technique for intercomparison. The other will be used for the analysis of the stable carbon isotopic ratio of methane ($\delta^{13}C$) using the new MAT 253 Mass Spectrometer which will be delivered to GEOMAR in early summer.

Sediment investigations

Sediments were sampled using a minicorer (see section 5.8). The cores, usually containing 25cm of sediment, were sliced in segments of 1cm from 0-10cm, and in segments of 3cm below that level.

Pore waters were separated from the sediment by low-pressure squeezing (1-3 atm) using argon gas, executed in the ship's cold room at 4°C. The analyses performed on the pore waters of the different

cores and the analytical techniques used are listed in Table 1. Modifications of pore water analysis are necessary for samples with high sulphide concentrations.

Table 1: Techniques used for pore water analyses.

| Constituent | Method | Reference |
|---|---|---|
| | | |
| Alkalinity | Titration | Ivanenkov and Lyakhin [1978] |
| Ammonium | Spectrophotometry | Grasshoff et al. [1997] |
| Chloride | Mohr ($AgNO_3$) titration | Gieskes et al. [1991] |
| Hydrogen sulphide | Spectrophotometry | Grasshoff et al. [1997] |

Ammonia and sulphide
Concentrations of dissolved ammonia were determined using standard photometric procedures described in Grasshoff et al. [1997]. In order to remove the $H_2S$ in samples containing high concentrations of sulphide, a certain volume (1-5ml) was acidified with 65% suprapure HCl (10µl/ml sample), and then left open for 48 hours in the cold room.
The method for sulphide determination according to Grasshoff et al. [1997] has been adapted for pore water concentrations of $S^{2-}$ in the millimolar range. For reliable and reproducible results, an aliquot of pore water was diluted with appropriate amounts of oxygen-free artificial seawater, the sulphide was fixed by addition of zinc acetate gelatin solution immediately after pore-water recovery. After dilution, the sulphide concentration in the sample should be less than 50 µmol/l.

Titration of Cl
High concentrations of $H_2S$ (> 1mM) in the sample disturb the measurements. Therefore, these samples were pre-treated with a 1:1 dilution of 0.01 N suprapure $HNO_3$ and stored for 1-2 days, without lid, in a cool room. Subsequent titration with silver nitrate is standardized against IAPSO seawater or a 1:1 dilution of IAPSO seawater for samples containing sulphide.

Total alkalinity (TA)
Samples of the sediment pore water for total alkalinity measurements were analyzed by titration of 1 ml pore water (+ 4 ml MilliQ and 20µl indicator solution) with 0.02 N HCl in an special titration vessel according to Ivanenkov and Lyakhin [1978]. Titration was finished until a stable pink color occurs. During titration the sample is continuously degassed with argon to remove the generated $CO_2$ or $H_2S$. The acid was standardized using an IAPSO seawater solution.
This method is well suited for samples containing $H_2S$ and those with TA values largely exceeding 2.3 mM, because the $CO_2$ and $H_2S$ is removed during the titration by the continuous stream of argon. A mixture of methylene blue and methyl red was used as indicator.

Shore based laboratory analyses
Acidified subsamples (35µl suprapure HCl 30% + 2.5 ml sample) were prepared for ICP analyses of major cations ($Na^+$, $K^+$, $Li^+$, $Mg^{2+}$, $Ca^{2+}$, $Sr^{2+}$ and $Mn^{2+}$). Sulphate, DIC, $\delta^{18}O$ and $\delta^{13}C$ of $CO_2$ will be determined on selected sub-samples in the shore-based laboratories.

## 6.7.3 Preliminary results

### 6.7.3.1 Overview

Instrument deployment
A total of 24 CTD stations were deployed, of which 14 were performed with the mini corer attached underneath the CTD/rosette unit (Fig. 6.7.3.1.1 & Table 6.7.3.1.1). The investigations focussed on four key objectives. In order to understand the background distribution of methane within the water column, two hydrographic sections of about a 100 nm length were sampled in the northern and

southern part of the research area (see Fig. 6.7.3.1.1, CTD stations 1-6 and 15-20). The simultaneous deployment of the minicorer also allowed sampling of the upper sediment in areas not influenced by seepage phenomena. In addition, three areas, which appeared likely to be influenced by active seepage, were investigated. The choice of the locations was based on the results of the OFOS/CTD survey during SO144 [Bohrmann et al., 2002], and the detailed OFOS investigation during the first leg of SO 163 (see chapter by Sahling et al. in this cruise report). Five stations were dedicated to investigate the methane distribution and upper sediment pore water properties at Jaco Scarp. Four stations were used to monitor the methane distribution at Quepos Mound, a small scale mound which has been explored during SO 163/1 for the first time. Two stations were dedicated to investigate the water column methane distribution and the upper sediment layer at mound Culebra, a mound with a diameter of nearly 1nm and an elevation of more than 100m. During all of the stations at the geological structures, the ship's own SSBL transponder was attached at the cable about 40m above the CTD/rosette unit, which allowed exact positioning during the deployment of the mini corer and the water column sampling. The movement of the device at depths also gave valuable hints of the deep water current direction, which was very valuable for the choice of the following station locations.

### 6.7.3.2 Hydrographic Sections

There are a variety of scientific reasons that made it essential to map the methane distribution in the water column without focussing on potential seepage sites. One is that in order to quantify the excess methane in a plume caused by tectonic dewatering, one has to know the background concentration at that depth (or density) level. Very often, sharp concentration maxima are found at seepage sites, but there is also a relatively small enhancement of the $CH_4$ concentration in a broad layer, which might be of similar importance for the budget, but needs detailed knowledge of the background concentration to be even recognized. However, apart from defining the background for seepage investigations, the biogeochemical cycling of methane in the area is an interesting topic of marine research by its own. The geostrophic, seasonally wind enhanced upwelling west of Costa Rica and Nicaragua, known as the Costa Rica Dome [Fiedler et al., 2002], leads to enhanced biological production and a shoaling of the thermocline. Oxygen is completely depleted around the core of the oxygen minimum layer, and suboxic conditions are found nearshore at depths shallower than 100m. It has recently been shown for a section off Nicaragua that the anoxic conditions lead to methane production, generating one of the most far-reaching $CH_4$ plumes in the ocean [Sansone et al., in press]. The authors also showed that there is isotopic evidence for another, deeper $CH_4$ source on the shelf. In addition, upwelling has been shown to cause an enhanced flux of methane to the atmosphere, both due to enhanced in situ production [Bange et al., 1998] as well as due to the upwelling of water enriched in methane due to bottom sources [Rehder et al., in press].

The general distribution of methane and oxygen is illustrated in Fig. 6.7.3.2.1 by the profiles recorded at Station 18 at about 2500m water depth. A pronounced maximum in the methane concentration exists at about 400, centered around the oxygen depletion zone. A slight $CH_4$ oversaturation of the surface waters is driven by a narrow, sharp subsurface maximum, with concentrations up to 6x the saturation with the ambient atmosphere. Subsurface maxima are a common observation in low latitude surface waters [Karl and Tilbrook, 1994], and were shown to be generated by anoxic production within particles and fecal pellets. However, the feature is unusually pronounced in the research area. The extremely low oxygen content at shallow depth in combination with high surface production seems the most likely explanation for this finding.

Sections of the methane distribution within the upper several hundred meters along the northern and southern section are repreesented in Fig. 6.7.3.2.2. Methane saturation with respect to the ambient atmospheric partial pressure is plotted rather than concentrations to eliminate the effect of the temperature dependence of methane solubility [Wanninkhof, 1992]. The methane inventory seems to

diminish from the upper slope to the open ocean in the northern section (a). The southern section shows the highest subsurface concentrations towards the upper slope, while the maximum around the oxygen minimum shows no such trend. Both layers are slightly shifted to greater water depth towards the open ocean.

Sediment

Sediment cores were sampled at four stations, three of them located in the northern section (MUC-1, 2, 3) and one located in the southern Section (MUC-9) to get pore water data characterizing off-vent sites. The four stations are located in water depths similar to the sites, examined in the potential seepage areas with the aim to get information of the geochemical background situation in the area. Water depths of the investigated stations were 420m (MUC-9), 1340m (MUC-1), 2395m (MUC-3) and 3215m (MUC-2).

All cores were characterized by a dark, greenish colour. Differences were obvious in the texture. The cores of the northern section in water depths > 1300m consist mainly of silt and clay, whereas the major component of the core sampled in 400m water depth was sand, presumably due to the deposition of terrigenious material. The cores in the northern section showed many tubes from the surface down to a depth of 10cm, indicating high degree of bioturbation. MUC-9 was almost not bioturbated, the sediment contained a lot of small muscle shells (size 1-2cm) in depths > 7cm. All cores showed no visible indicators of seepage fauna.

First results of pore water analysis are shown in Fig.6.7.3.2.3. Concentrations of sulphide remains < 3 µmol/l in all cores throughout the investigated sediment column (the data of MUC-9 is not shown; concentrations were below the detection limit). Concentrations of chloride ranged between 525-570 mmol/L for MUC 1 and 2, and between 550 – 580 mmol/L for MUC 3 and 9. The profiles of the latter scatter to a lesser extent and are characterized by slightly higher $Cl^-$ concentrations near the surface and more or less constant values throughout the remaining sediment column. The scattering in the profiles of MUC 1 and 2 might be induced by analytical procedures. Besides these small differences and the scattering, all chloride profiles range within $Cl^-$ concentrations of the IAPSO seawater standard (557 mmol/L), and show no anomalies, as expected for non-vent sites.

Ammonia concentrations were in general < 200 µmol/L. At the deepest site (MUC-2), $NH_4^+$ concentrations remain more or less constant <10 µmol/L. At the other locations ammonia concentrations raise from 5 µmol/L in the bottom water to up to 40 µmol/L (MUC-9) and about. 150 µmol/l (MUC-1, MUC-3), respectively. These slight variations in the ammonia distribution might be caused by variations in bottom water oxygen concentrations and differences the content of organic matter.

Total alkalinity (TA) in the bottom water is about 2.6 mmol/L, concentrations increase up to 3 mmol/L in the cores 2 and 9, and up to 4 mmol/L at the stations located in 1400m and 2400m water depth. Lower TA values in the former stations are probably due to a lesser amount of degradable organic material at these sites, but further interpretation remain open until the analysis of organic carbon content etc. on land.

In summary all stations investigated in the northern and southern section are characterized by pore water chemistry as expected for a reference site not influenced by active seepage.

### 6.7.3.3. Jaco Scarp

Water column

The Jaco Scarp is created in consequence of the subduction of a seamount on the oceanic plate. This leads to a circular uplift with faulting at the upper plate (dome). Seawards, the process is associated with sedimentary landslides, leading to the formation of steep scarps. During expedition SO 144,

chemoautotrophic clam colonies had been observed at 1800 and 1900m depths, and a CTD cast revealed the highest concentrations of the entire water column program corresponding to this depths level. We reconfirmed the presence of a methane plume between 1700 and 1850m water depth with concentrations up to 270 nmol/L centered at 1780m at the station visited during SO 144 (their CTD station 2, here CTD/MUC 07 – (04). Thus, it was decided to map the $CH_4$ distribution along the slope of Jaco Scarp. CTD/MUC was deployed at a total of 5 stations within the Jaco Scarp area with the aim to map the extend of the plume as well as to look for indication of other vent sites within the Scarp Fig. (6.7.3.3.1).

Station CTD/MUC 08 – (05) was located at a position where the occurrence of bacterial mats and clams had been reported before [Bohrmann et al., 2002]. However, the station showed no evidence for seepage in the upper part of the slope (bottom depth 1400m]. The same proved to be true at the northern sill of Jaco Scarp (900m). Sample analysis of station CTD/MUC 21 – (11) at a water depth of 2255m, however, indicate a water column enriched in methane everywhere in the depth range between 1600 and 2100m, including a narrow layer with peak concentrations near 100 nmol/L at 1930 m depth. Both plumes can still be recognized at station CTD/MUC 24 – (14) further to the south. An overview of the location of the stations along the slope and the observed methane concentration pattern is given in Fig. 6.7.3.3.2.

While the aim of the sampling was to assure that the stations with greater water depths always cover the water masses which showed an enhanced methane budget at shallower stations, it is not sure that this has been achieved at station CTD/MUC 21 – (11). Water samples were taken up to a water depths of 1600m, while the plume found at station CTD/MUC 07 – (04) had its upper boundary at 1700m. However, it appears that we did not cover the density layer of the core of the plume at station CTD/MUC 07 – (04) (Fig. 6.7.3.3.3). The reason for this phenomenon is a very different density layering in these two stations (Fig. 6.7.3.3.4)., suggesting a downward sloping of the isopynical surface $\sigma_\Theta = 26.63$ of more than 200 m towards the northern wall of Jaco Scarp. This would be a very unusual finding which will need further investigation and check of data consistency. However, station CTD/MUC 24 – (14) was sampled with a detailed look at the density structure of the water column, and all density layers where plumes had been observed at the 2 shallower stations were sampled.

Sediment

Multiple cores at the subducting seamount of Jaco Scarp were sampled according to preliminary studies published by Bohrmann et al. (2002). Deployments were executed at the head of the seamount (MUC-6), the uplifted area over the scar (MUC-5) and within the slide structure (MUC-4, MUC-11), where vent fauna and carbonates had been observed during OFOS tracks. The instrument was deployed further down the slope (MUC –14) at the very end of the cruise. However, these measurements will not be finished for this report.

Figure 6.7.3.3.5 shows the results of the cores deriving from the deployments at 1400m (MUC-5) and 2200m (MUC-11). Texture and colour of all cores were similar to the ones found at the reference sites, and no vent-indicating fauna was visible. Concentration and distribution of the parameters sulphide, chloride, ammonia and total alkalinity correspond with the geochemical characteristics measured at the reference sites. The results suggest no active venting at the sampled locations. Further investigation in this area, especially by TV-guided instruments, will be necessary to get further insight into the regional distribution and scaling of the seepage activity and characteristics at Jaco Scarp, which is evident from the results of the OFOS surveys and water sampling program.

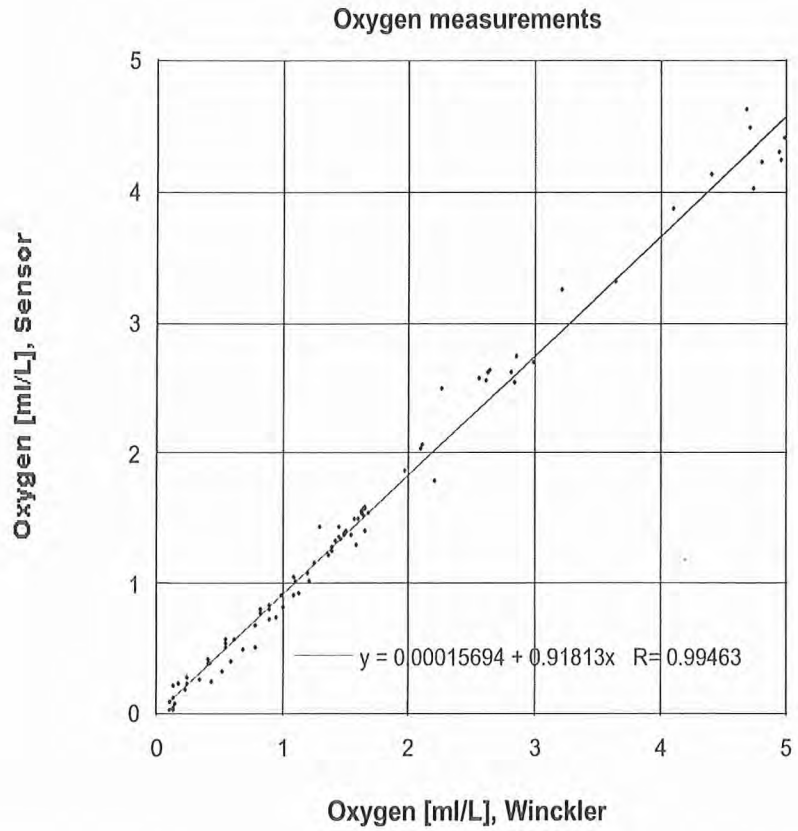


Fig 6.7.2.1 Results of the measurements of dissolved oxygen concentrations of stations 14, 17, 18, and 23 vs the output of the Beckmann oxygen sensor attached to the CTD unit.

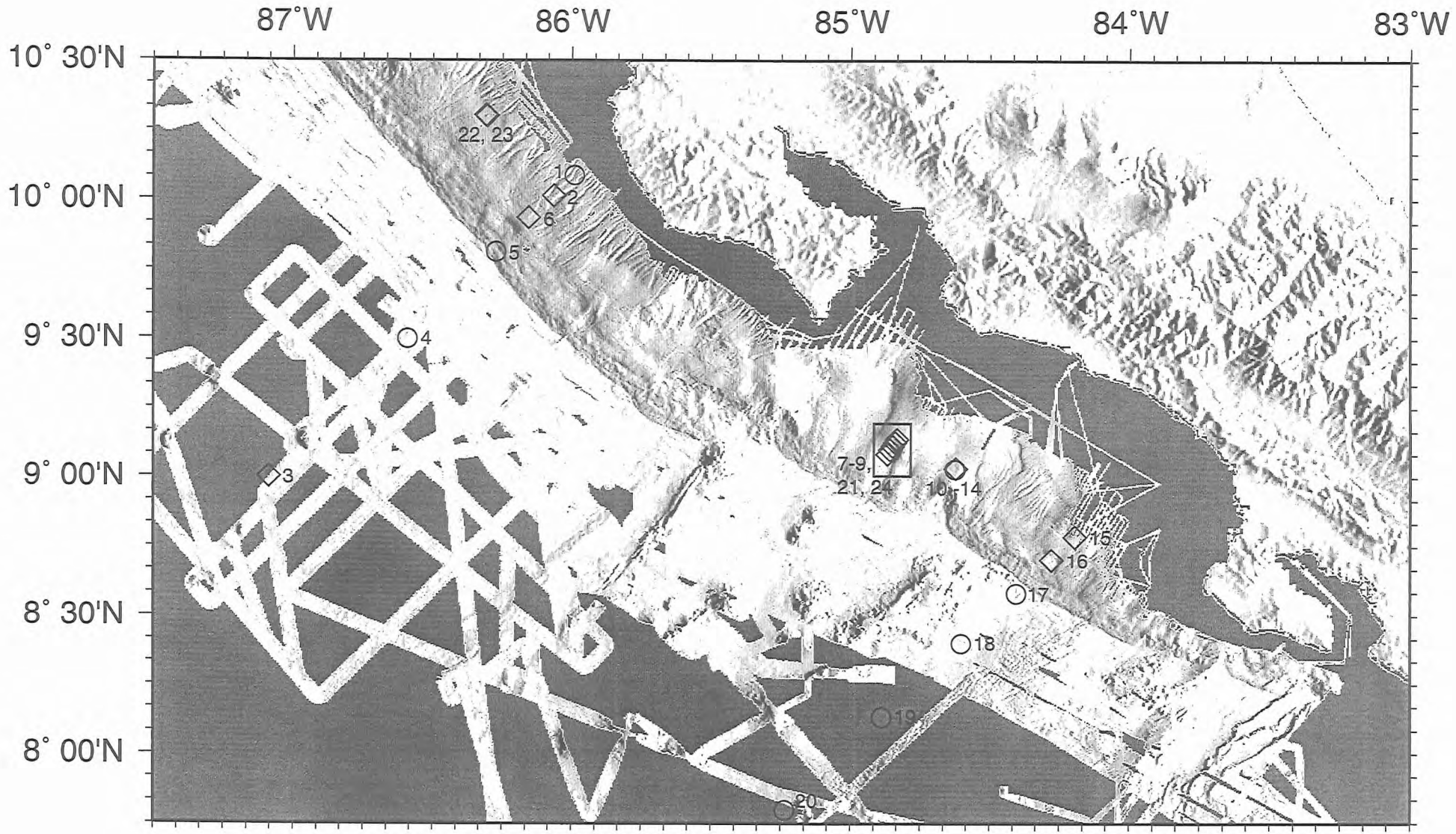


Fig. 6.7.3.1.1 Station locations of the CTD/MUC program during SO 163/2. CTD stations are indicated by circles, CTD/MUC stations by diamonds. Overlying symbols from investigations at small scale geological structures are shown in detail maps in the following chapters.

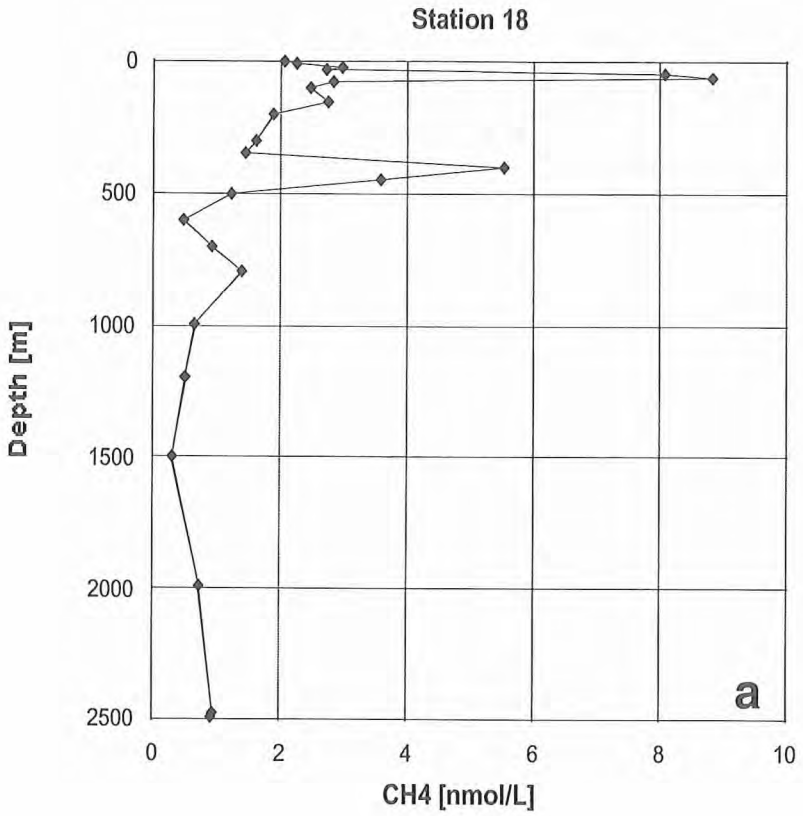


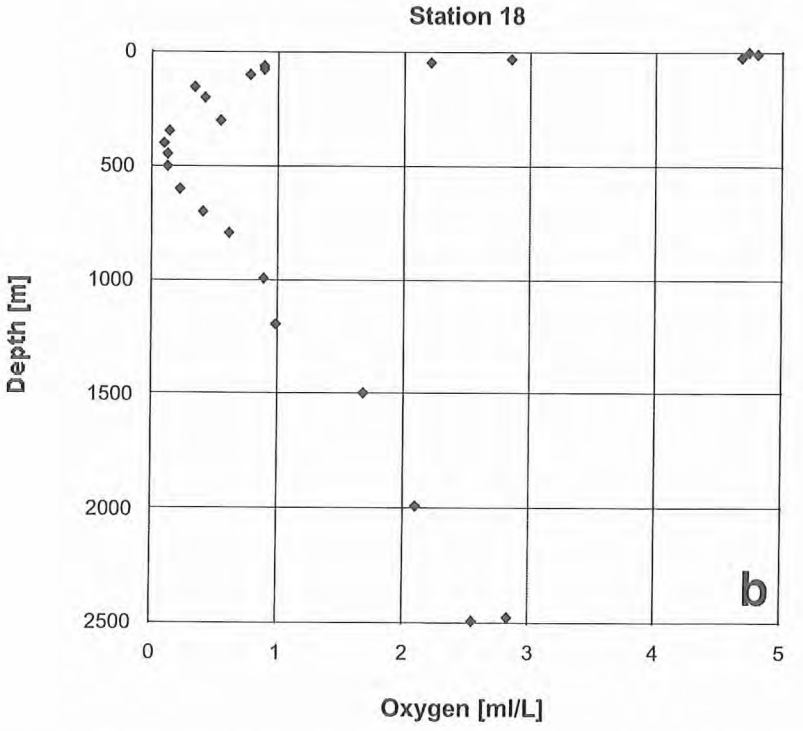


Fig. 6.7.3.2.1 Typical distribution of (a) methane and (b) oxygen within the research area (from station 18).

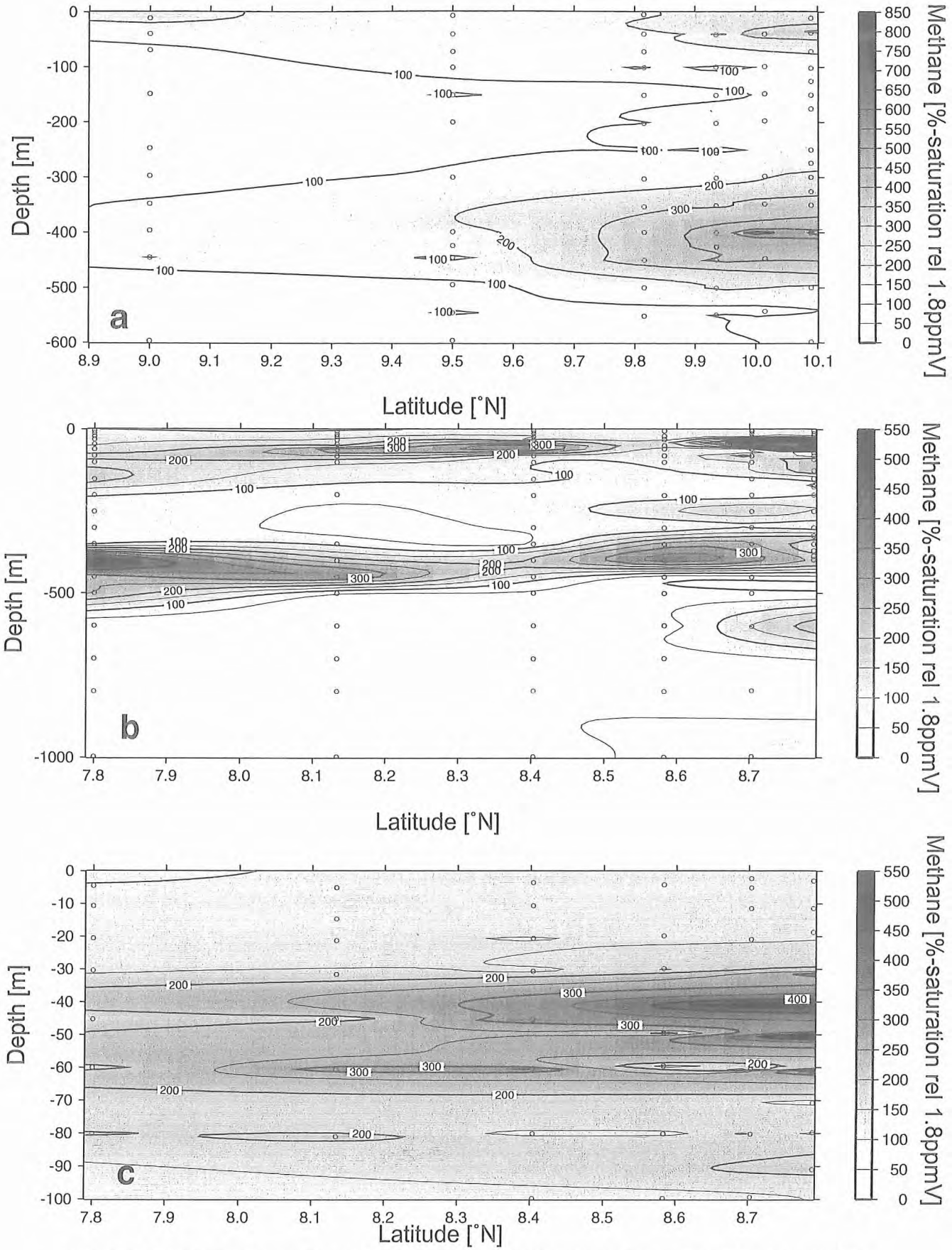


Fig. 6.7.3.2.2 Sections of methane saturation of waters along the 2 hydrographic sections: (a) Northern Transect (CTD stations 1-6); (b) Southern transect (CTD stations 15-20); (c) close-up or the upper 100m along the southern transect.

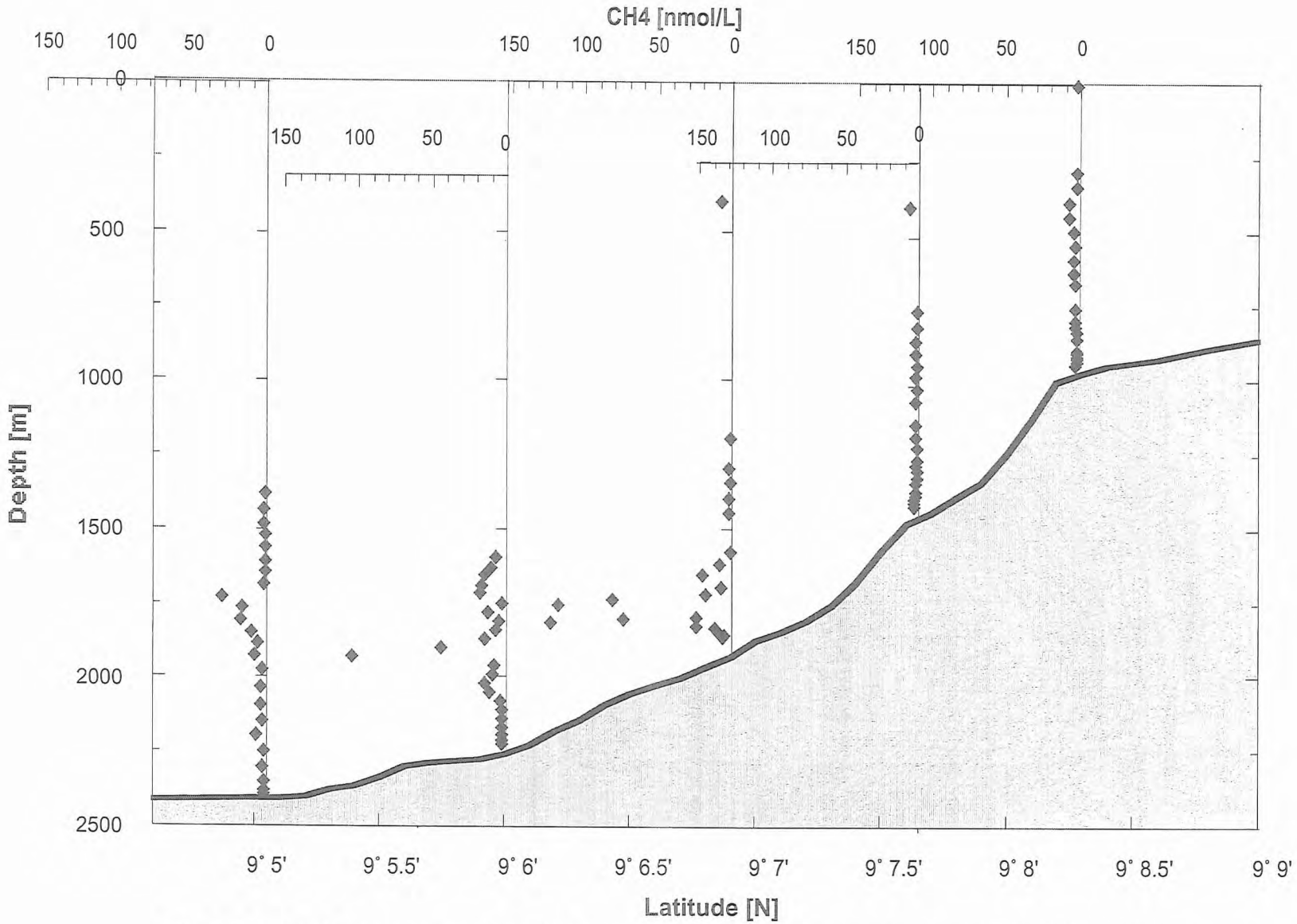


Fig. 6.7.3.3.2 Cross section of Jaco Scarp along the line defined by the CTD/MUC stations. The results of the dissolved methane analysis observed at the stations is presented.

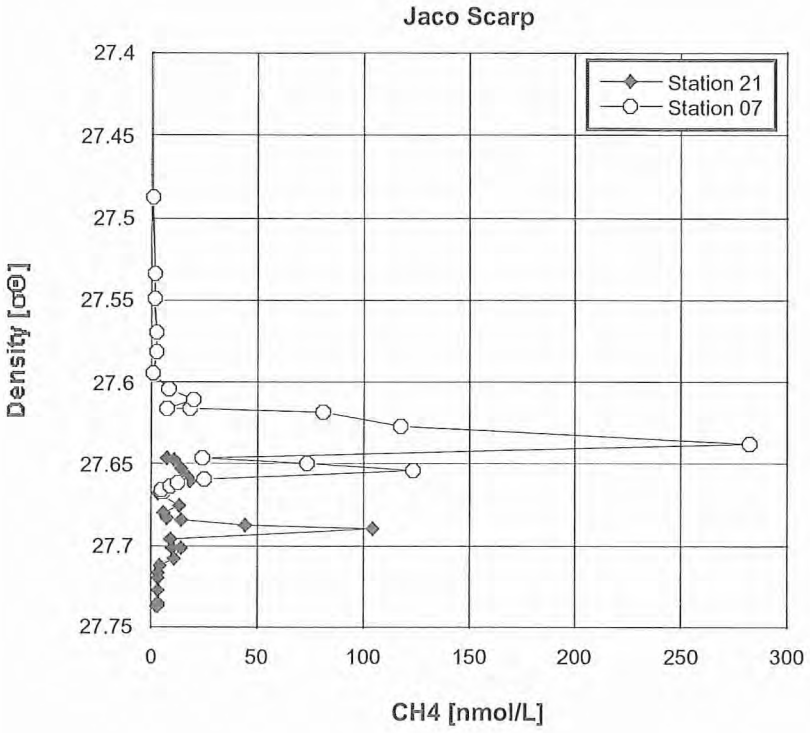


Fig. 6.7.3.3.3 Methane vs density (σΘ) at CTD stations 7 and 21.

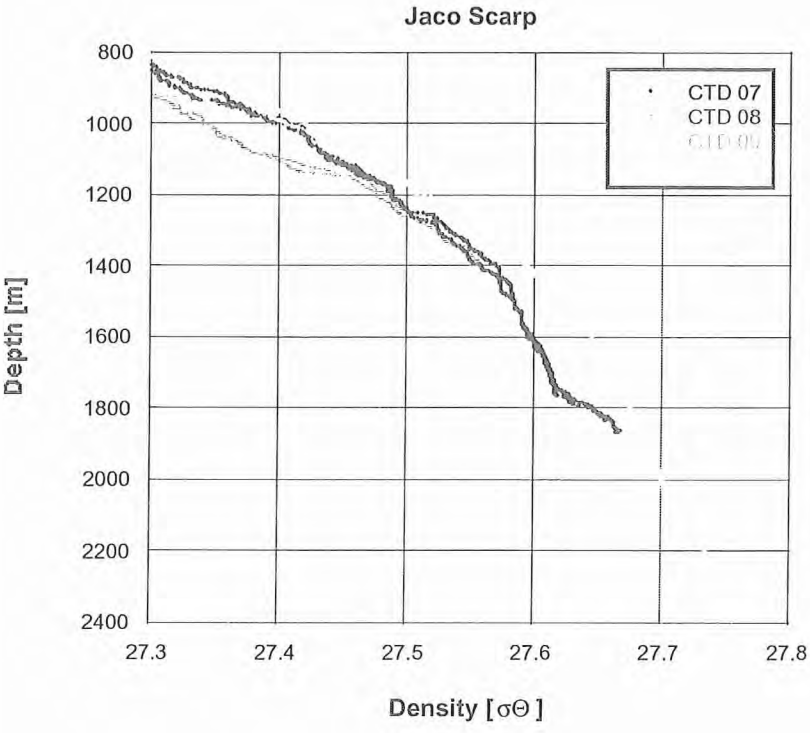


Fig. 6.7.3.3.4 Density (σΘ) vs depth for CTD stations 7-9 and 21.

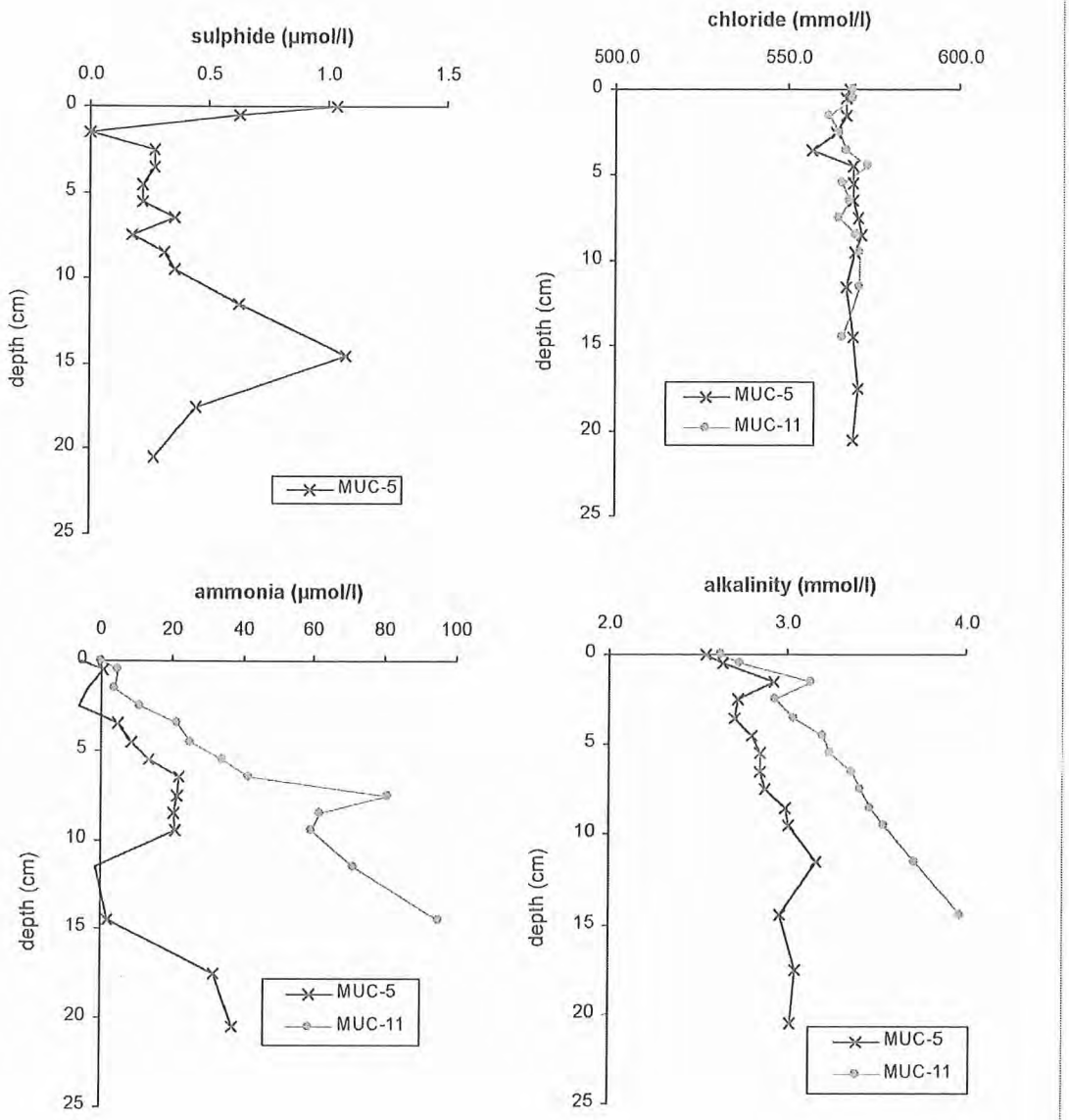


Fig. 6.7.3.3.5 Results of pore water analysis - Jaco Scarp stations.

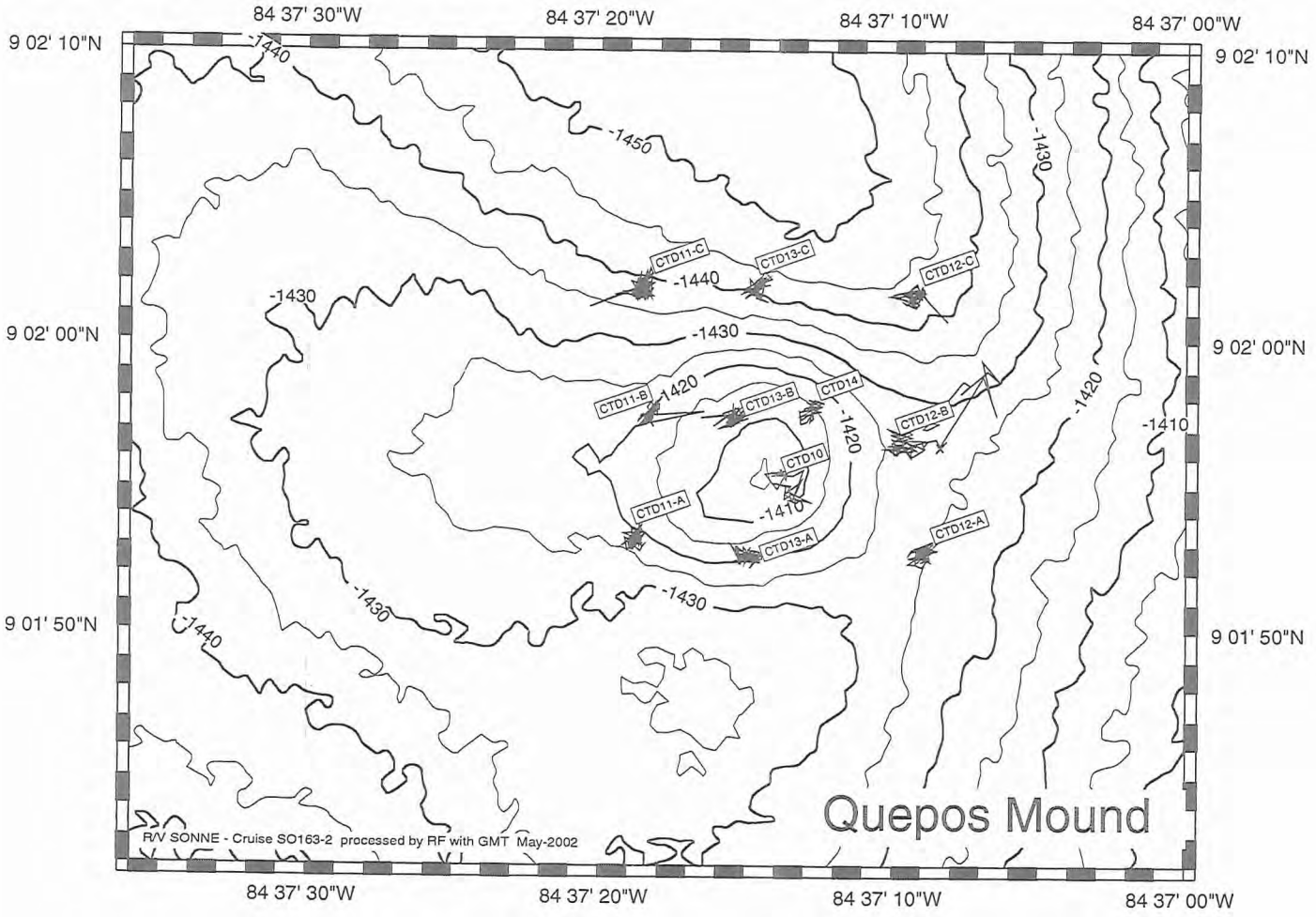


Fig 6.7.3.4.1: Bathymetric map of Quepos Mound with the positions of the SSBL (attached 40m above the CTD/rosette) during sampling.

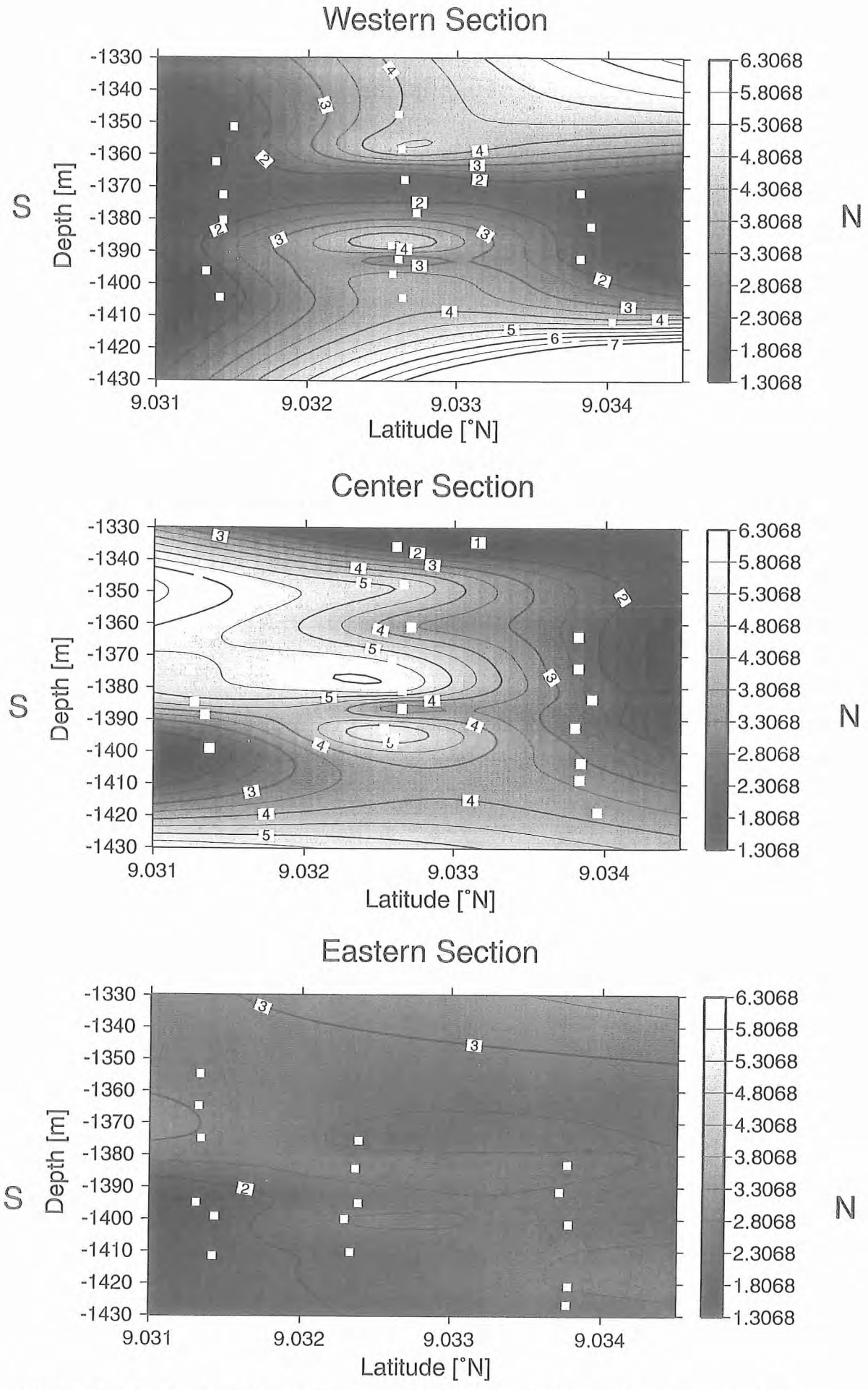


Fig 6.7.3.4.2: North-south trending cross-sections of the methane concentration in the lower water column with values given in nmol/L.

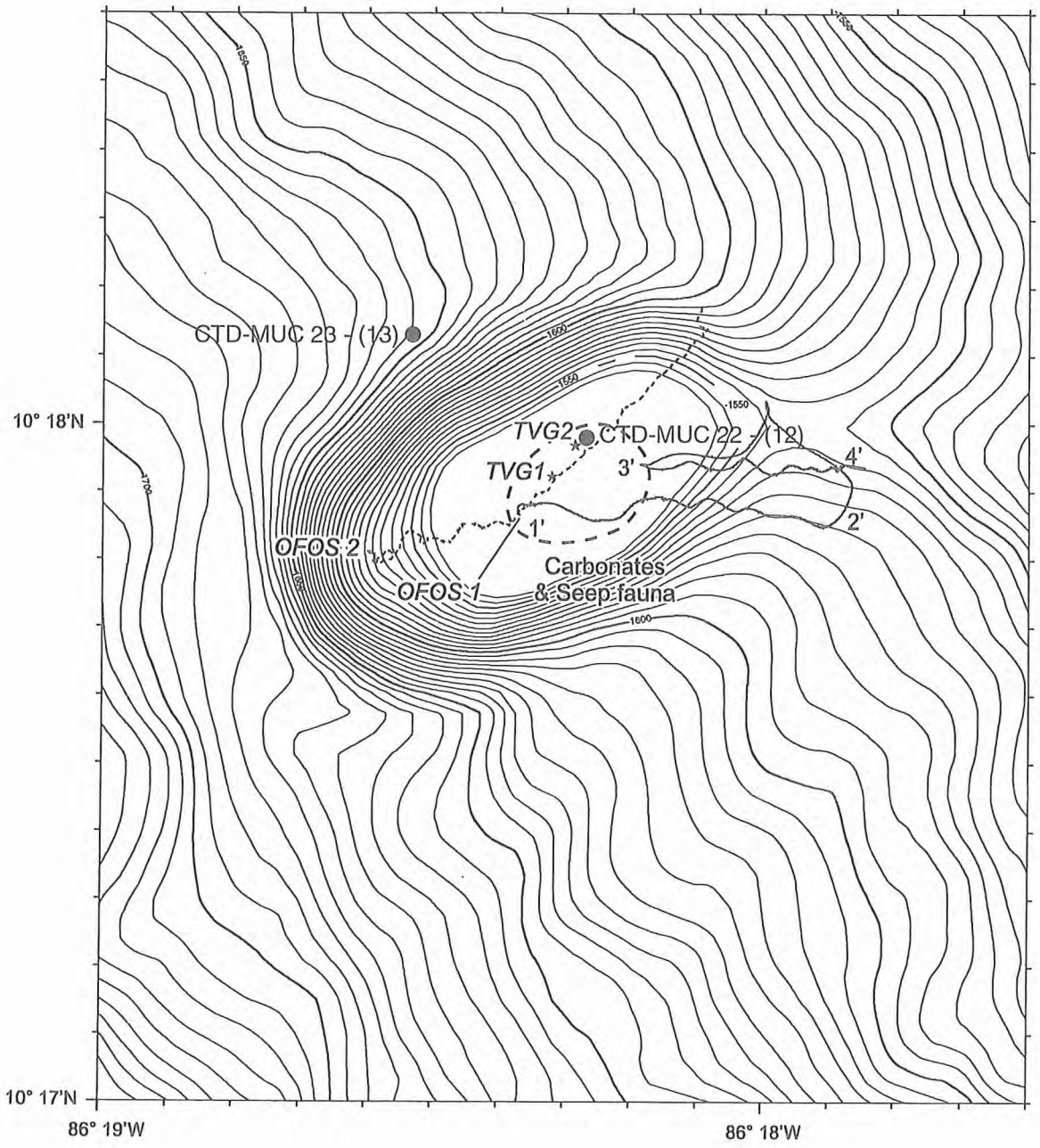


Fig 6.7.3.5.1 Bathymetric map of Mound Culebra. Indicated are the locations of the CTD/MUC deployment as well as the locations of TVG locations and OFOS surveys (SO163/1).

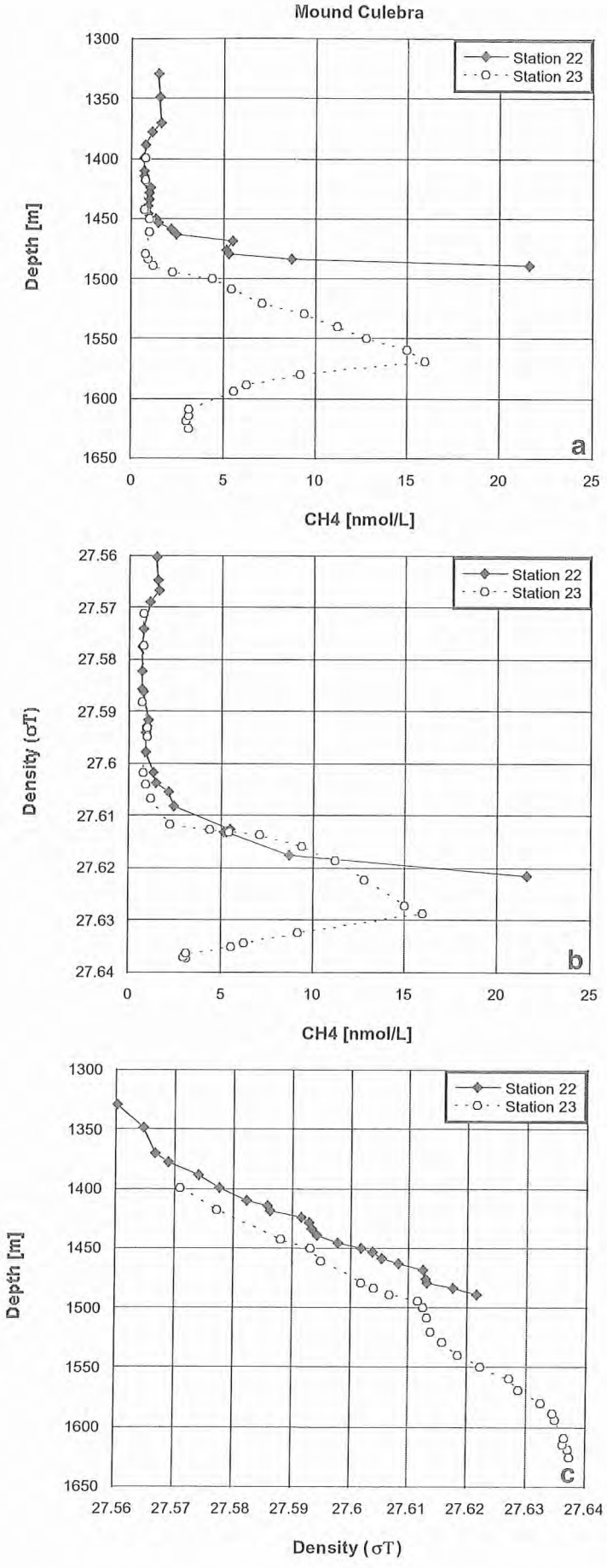


Fig 6.7.3.5.2 (a) Methane concentration vs depth, (b) methane concentration vs density, and density vs depth for stations 22 and 23 at Mound Culebra.

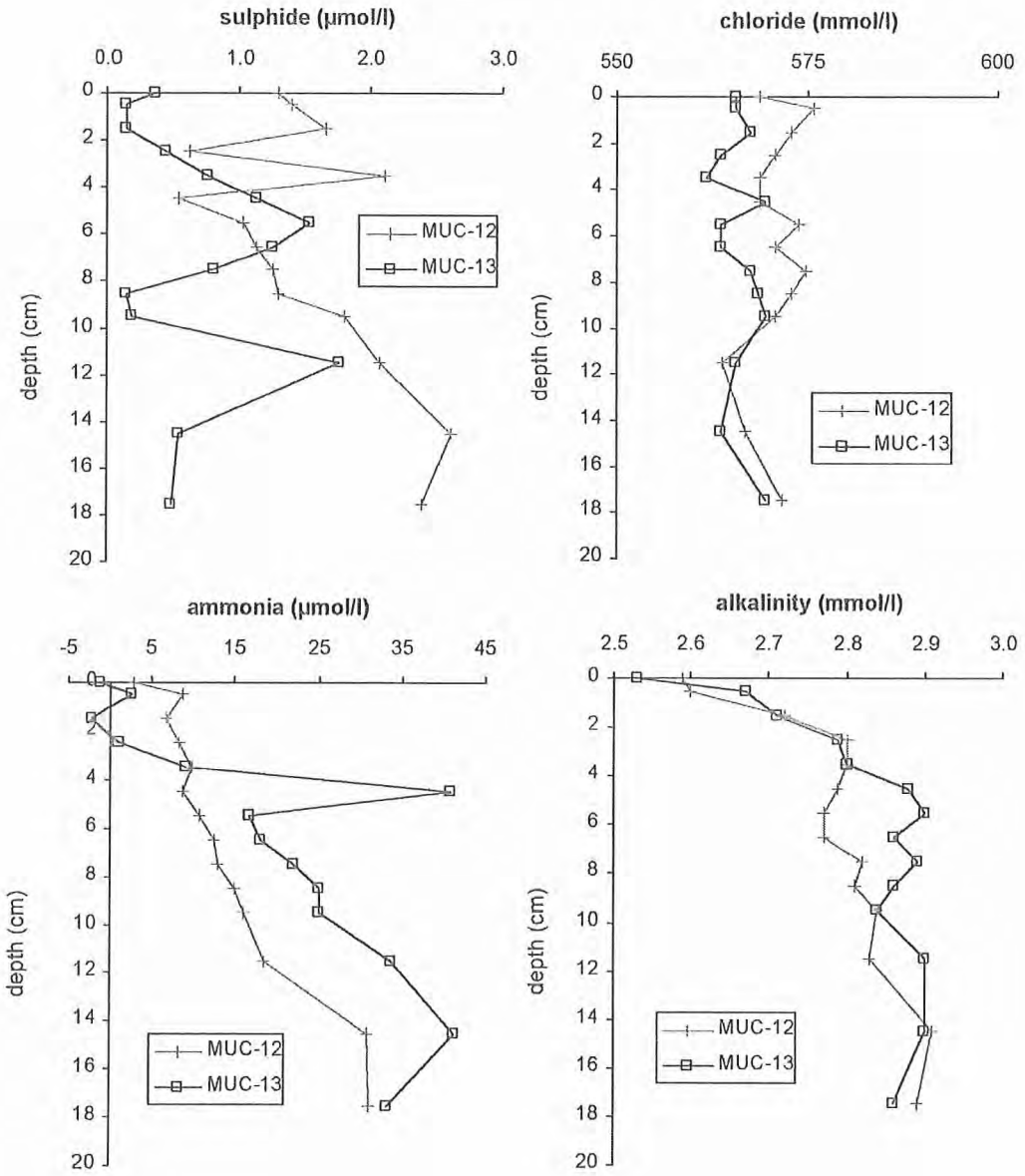


Fig 6.7.3.5.3 Results of pore water analysis from the Mound Culebra stations.

Duennebier, F.K., and Harris, D., 1990, Broad-band seismometers on the ocean floor. EOS, Trans. Am. Geophys. Union, 70, 1216.

Endrun, B. (2001): Eine Receiver Function-Studie mit den Dreikomponentenstationen des GERESS-Array, diploma-thesis, Ruhr-Universität Bochum

Fiedler, P. C. (2002). "The annual cycle and biological effects of the Costa Rica Dome." Deep-Sea Res. I 49: 321-338.

Fisher, D.M., T.W. Gardner, J.S. Marshall, P.B. Sak, and M. Protti, Effect of subducting sea-floor roughness on fore-arc kinematics, Pacific coast, Costa Rica, Geology, 26( 5), 467-470, 1998.

Flewellen, C., Millard N. and Rouse I. 1993. TOBI, a vehicle for deep ocean survey. Electronics and Communication Engineering Journal, April issue.

Flueh E R and Bialas J, 1996: A digital, high capacity ocean bottom recorder for seismic investigations; Int. Underwater Systems Design 18(3), 18-20.

Flüh, E. R., Kukowski, N. and Reichert, C. (Ed.) 1997, FS SONNE, Fahrtbericht/Cruise Report SO123: MAMUT (MAKRAN MURRAY TRAVERSE - Geophysik Plattentektonischer Extremfälle). Maskat - Maskat, 07.09 - 03.10.1997, GEOMAR Report 62, 292 pp.

Gieskes, J. M., Garno, T., and Brumsack, H. (1991). "Chemical methods for interstitial water analysis aboard Joides Resolution." Ocean Drilling Program, Texas A & M Univ.

Graefe, K., Exhumation and thermal evolution of the Cordillera de Talamanca (Costa Rica): Constraints from fission track analysis, 40 Ar-39 Ar, and 87 Rb-87 Sr chronology, Tübinger Geowissenschaftliche Arb., Ser. A, Vol. 39, 113 pp., 1998.

Grasshoff, K., Ehrhardt, M., and Kremling, K. (1997). "Methods of seawater analysis." Verlag Chemie. Gulf Publishing, Houston, TX, pp. 757-773

Hauff F., Hoernle K., Schmincke, H-U, and Werner, R., 1997, A mid Cretaceous origin for the Galapagos hotspot: Volcanological, Petrological, and Geochemical Evidence from Costa Rican Oceanic Crustal Segments: Geologische Rundschau 86, p. 141-155.

Hauff, F., 1998, Age and geochemical constraints on the origin of oceanic basement complexes in Costa Rica and the Caribbean large igneous province: Ph.D. thesis, University of Kiel.

Henry, P. et al. (1992). "Interpretation of temperature measurements from the Kaiko-Nankai cruise: Modeling of fluid flow in clam colonies." Earth Planet. Sci. Lett. 109, 355-371.

Hinz, K., Adam, J., Bargeloh, H.O., Bergmann, P., Bialas, J., Block, M., Dohmann, H., Eidam, J., Fabel, E., Flüh, E., Fritsch, J., Handke, J., Kewitsch, P., Kläschen, D., Leandro, G., Leon, L.B., Meyer, H., Mrazek, J., Popovici, A., Puskeppeleit, K., Schlumschinski, B., Schrader, U., Schreckenberger, B., Spranger, M., Stavenhagen, A., Steinmann, D., von Huene, R. and Walther, C., 1992: Bericht PAKOMAR 2 (Costa Rica), Bundesanstalt für Geowissenschaften und Rohstoffe, Hannover

Hinz, K., von Huene, R. Ranero, C.R. and the PAKOMAR Working Group (1996). Tectonic structure of the convergent Pacific margin offshore Costa Rica from multichannel seismic reflection data. Tectonics 15, 54-66.

Ivanenkov, V. N. and Lyakhin, Y. I. (1978). "Determination of total alkalinity in seawater". In: Bordovsky, O.K. and Ivenenkov, V. N. (eds.): Methods of hydrochemical investigations in the ocean, Nauka Publ. House, Moscow, 110-114 (in Russian).

Kahn L. M., Silver E. A., Orange D. L., Kochevar R., and McAdoo B. G. (1996) Surficial evidence of fluid expulsion from the Costa Rica accretionary prism. Geophysical Research Letters 23(8), 887-890.

Karl, D. M. and B. D. Tilbrook (1994). "Production and transport of methane in oceanic particulate organic matter." Nature 368: 732-734.

Kimura, G., Silver, E. and Blum, P. (1997): Proceedings of the Ocean Drilling Program, Initial Reports 170, College Station, Texas (Ocean Drilling Program)

Knickmeyer, E.T., 1996: Hochgenaues Differential-GPS, Proc. 11th Annual Meeting of the German Hydrographic Society, Glücksburg, 3.-5.6.

Lammers, S. and E. Suess (1994). "An improved head-space analysis method for methane in seawater." Mar. Chem. 47: 115-125.

Langseth M. G. and Silver E. A. (1996) The Nicoya convergent margin-a region of exceptionally low heat flow. Geophysical Research Letters 23(8), 891-894.

Lonsdale, P., and K.D. Klitgord, Structure and tectonic history of the eastern Panama Basin, Geol. Soc. Am. Bull., 89, 981-999, 1978.

Luegert, J.H., 1992, R1D One-Dimensional Seismic Travel Modeling: USGS Open File Report 43.

McAdoo B. G., Orange D. L., Silver E. A., McIntosh K. D., Abbott L., Galewsky J., Kahn L., and Protti M. (1996) Seafloor structural observations, Costa Rica accretionary prism. Geophysical Research Letters 23(8), 883-886.

McIntosh K, Silver E, Shipley T, 1993; Evidence and mechanisms for forearc extension at the accretionary Costa Rica convergent margin; Tectonics 12, 1380-1392

McGee, T.M., 2000: A single-channel seismic reflection method for quantifying lateral variations in BSR reflectivity, Marine Geology, 164, 29-35

Mienert J, Posewang J, Baumann M, 1998; Gas hydrate along the north eastern Atlantic margin: possibly hydrate-bound margin instabilities and possible release of methane. In: Gas hydrates: Relevance to world margin stability and climate change (ed. J-P Henriet and J Mienert), pp. 275-292.

Moore, G.F., and T.H. Shipley, Behavior of the decollement at the toe of the Middle America Trench, Geol. Rundsch., 77(1), 275-284, 1988.

Oldenburg, D.W., 1981: A comprehensive solution to the linear deconvolution problem, Geophysical Journal of the Royal Astronomic Society, 44, 413-431

Pecher, I.; Ranero, C. R.; von Huene, R.; Minshull, T. A. and Singh, S. C. The nature and distribution of bottom simulating reflectors at the Costa Rican convergent margin. Geophysical Journal International vol. 133, 219-229 (1998).

Pecher, I.A. (1995): Seismic studies of bottom simulating reflectors at the convergent margins offshore Peru and Costa Rica, Ph.D.-thesis, Christian-Albrechts-Universität zu Kiel.

Pecher, I.A., Ranero, C.R., von Huene, R., Minshull, T.A. and Singh, S.C. (1998): The nature and distribution of bottom simulating reflectors at the Costa Rican convergent margin, Geophysical Journal International, 133, 219-229

Ranero, C. R., von Huene, R. Subduction erosion along the Middle America convergent margin. Nature 404, 748-752 (2000).

Ranero, C. R.; von Huene, R.; Flueh, E., Duarte, M. and Baca, D. A cross section of the forearc Sandino Basin, Pacific Margin of Nicaragua. Tectonics vol.19, 335-357 (2000a).

Ranero, C.R., von Huene, R., Weinrebe, W., McIntosh, K., Reichert, C., Mass transfer and fluid flow paths related to subduction erosion at the Middle America convergent margin, Eos, 81, American Geophysical Union Fall Meeting (San Francisco). (2000b)

Rehder, G., P. G. Brewer, et al. (2001). "Enhanced lifetime of methane bubble streams within the deep ocean." Geophys. Res. Lett. in press.

Rehder, G., R. S. Keir, et al. (1999). "Methane in the northern Atlantic controlled by oxidation and atmospheric history." Geophys. Res. Lett. 26: 587-590.

Rehder, G., R. W. Collier, et al. (2002). "Enhanced marine methane emissions to the atmosphere caused by upwelling." Glob. Biogeochem. Cycl. 80, in press

Sansone, F. J., B. N. Popp, et al. (2002). "Highly elevated methane in the eastern tropical North Pacific and associated isotopically enriched fluxes to the atmosphere." Geophys. Res. Lett. in press.

Seeber, G., 1996: Stand und Einsatzmöglichkeiten von GPS - ein Überblick, Proc. 11th Annual Meeting of the German Hydrographic Society, Glücksburg, 3.-5.6.

Shipley, T.H. and Moore, G.F. (1986). Sediment accretion, subduction, and dewatering at the base of the trench slope off Costa Rice: a seismic reflection view of the décollement. J. Geophys. Res. 91, 2019-2028.

Shipley, T.H., K.D. McIntosh, E.A. Silver, and P.L. Stoffa, Three-dimensional seismic imaging of the Costa Rica accretionary prism: Structural Diversity in a Small Volume of the Lower Slope, J. Geophys. Res., 97/B4, 4439-4459, 1992.

Shipley, T.H., P.L. Stoffa, and D.F. Dean, Underthrust sediments, fluid migration paths, and mud volcanoes associated with the accretionary wedge off Costa Rica: Middle America Trench, J. Geophys. Res., 95/B6:, 8743-8752, 1990.

Silver E., Kastner M., Fisher A., Morris J., McIntosh K., and Saffer D. (2000) Fluid flow paths in the Middle America trench and Costa Rica margin. Geology 28(8), 679-682.

Sinton, C.W., Duncan, R.A., and Denyer, P., 1997, Nicoya Peninsula, Costa Rica: A Single Suite of Caribbean Oceanic Plateau Magmas: Journal of Geophysical Research, 102(B7), p. 15507-15520.

Sinton, C.W., Duncan, R.A., Storey, M., Lewis, J., Estrada, J.J., 1998, An oceanic flood basalt province within the Caribbean plate: Earth Planetary Science Letters, 155, p. 221-235.

Suess, E. and Bohrmann, G. (1997). RV Sonne Cruise Report SO110. GEOMAR.

Suess, et al. (1985). "Biological communities at vent sites along the subduction zone off Oregon." In: The Hydrothermal Vents of the Eastern Pacific: An Overview (ed. M. L. Jones), Vol.6, pp. 475-484, Bull. Biol. Soc., Wash.

Suess; E. and Whiticar, M. J. (1989). "Methane-derived $CO_2$ in pore fluids expelled from the Oregon subduction zone. Palaeo. Palaeo. Palaeo. 71, 119-136.

Tinivella, U. and Accaino, F. (2000): Compressional velocity structure and Poisson's ratio in marine sediments with gas hydrate and free gas by inversion of reflected and refracted seismic data (South Shetland Islands, Antarctica), Marine Geology, 164, 13-27

Tobin,H., Vannucchi, P. and Meschede,M. (2001). Structure, inferred mechanical properties, and implications for fluid transport in the décollement zone, Costa Rica convergent margin. Geology 29, 907-910.

Tolstoy, M., Constable, S., Orcutt, J., Staudigel, H., Wyatt, F.K., and Anderson G., 1998, Short and long baseline tiltmeter measurements on axial seamount, Juan de Fuca Ridge.

Torres, M., Bohrmann, G. and Suess, E. (1996). "Authigenic barites and fluxes of barium associated with fluid seeps in the Peru subduction Zone." Earth Planet. Sci. Lett. 144, 469-481.

Valentine, D. L., D. C. Blanton, et al. (2001). "Water column methane oxidation adjacent to an area of active hydrate dissociation, Eel River Basin." Geochim. Cosmochim. Acta 65: 2633-2640.

Vannucchi, P., Scholl, D., Meschede, M. & McDougall-Reed K. (2001).Tectonic erosion of the Pacific Margin of Costa Rica: combined implications from ODP Leg 170, seismic offshore data and regional geology of the Nicoya Peninsula. Tectonics, 20/5, pp. 649-668

von Huene, R. Ranero, C. R., Weinrebe, W. and Hinz, K. Quaternary convergent margin tectonics of Costa Rica, segmentation of the Cocos Plate, and Central American volcanism. Tectonics 19, 314-334 (2000).

von Huene, R., and E.R. Flueh, A review of marine geophysical studies along the Middle American Trench off Costa Rica and the problematic seaward terminus of continental crust, Profil 7, Stuttgart, 143-159, 1994.

von Huene, R., J. Bialas, E.R. Flueh, B. Cropp, T. Csernok, E. Fabel, J. Hoffmann, K. Emeis, P. Holler, G. Jeschke, C. Leandro M., I. Perez Fernandez, J. Chavarria S., A. Florez H., D. Escobedo Z., R. Leon, O. Barrios L., Morphotectonics of the Pacific convergent margin of Costa Rica, in Geologic and tectonic development of the Caribbean plate boundary in southern Central America, edited by P. Mann, Geol. Soc. Am. Special Paper 295, 291-308, 1995.

Walther, C. H.; Flueh, E.; Ranero, C. R., von Huene, R.; Strauch, W. An unusual crustal structure across the Pacific Margin of Nicaragua. Geophysical Journal International 141, 759-777 (2000).

Wanninkhof, R. (1992). "Relationship between wind speed and gas exchange over the ocean." J. Geophys. Res. 97: 7373-7382.

Weiss, R. F. (1970). "The So5lubility of Nitrogen, Oxygen and Argon in Water and Seawater." Deep-Sea-Res. 17: 721-735.

Werner, R., K. Hoernle, P. van den Bogaard, C.R. Ranero, R. von Huene, and D. Korich, Drowned 14 m.y. old Galapagos archipelago off the coast of Costa Rica: Implications for tectonic and evolutionary models, Geology, 27, 499-502, 1999.

Wyatt, F.K., Orcutt, J.A., Sasagawa, G., Staudigel, H., and Zimmer, P., 1996, Toward in situ monitoring of active submarine volcanoes: a progress report. In: Salisbury, G.P., Salisbury, A.C. (Eds), Fifth Circum-Pacific Energy and Mineral Resources Conference Transactions.

Ye, S., Bialas, J., Flüh, E.R., Stavenhagen, A., von Huene, R., Leandro, G. and Hinz, K. (1996): Crustal structure of the Middle American Trench off Costa Rica from wide-angle seismic data, Tectonics, 15, 1000-1021.

Yuan, X., Ni, J., Kind, R., Mechie, J. and Sandvol, E. (1997): Lithospheric and upper mantle structure of southern Tibet from a seismological passive source experiment, Journal of Geophysical Research, 102, 27491-27500.

## Appendix 9.1 Mapping profiles

| line number | date | time | position | | course | length | remarks |
|---|---|---|---|---|---|---|---|
| | | | | | | | |
| EM-01 | 15.03.02 | 10:50 | 07°31.91 N | 83°01.31 W | 298 | | |
| | | 14:09 | 07°45.00 N | 83°30.00 W | 296 | 22 | |
| | | 21:24 | 08°17.44 N | 84°55.81 W | 318 | 73 | |
| | 16.03.02 | 06:56 | 09°39.50 N | 85°51.57 W | | 111 | |
| | | | | | | | |
| EM-02 | 16.03.02 | 18:20 | 09°38.28 N | 85°53.91 W | | | |
| | | 20:09 | 09°50.02 N | 85°44.36 W | 322 | 15 | |
| | | 21:04 | 09°56.33 N | 85°49.19 W | 219 | 9 | |
| | | 21:15 | 09°55.40 N | 85°50.23 W | 144 | 1 | |
| | | 21:56 | 09°49.91 N | 85°46.39 W | 244 | 7 | |
| | | 22:07 | 09°49.06 N | 85°47.87 W | 327 | 2 | |
| | | 23:14 | 09°58.39 N | 85°53.91 W | 41 | 11 | |
| | | 23:44 | 10°00.98 N | 85°51.69 W | 306 | 4 | |
| | | 24:00 | 10°00.98 N | 85°51.69 W | | 4 | |
| | | | | | | | |
| EM-03 | 17.03.02 | 00:00 | 10°03.20 N | 85°54.60 W | | | |
| | | 00:35 | 10°08.07 N | 85°58.54 W | 292 | 6 | |
| | | 00:45 | 10°07.22 N | 85°59.72 W | 139 | 2 | |
| | | 01:23 | 10°02.41 N | 85°55.76 W | 216 | 6 | |
| | | 01:33 | 10°01.13 N | 85°56.75 W | 320 | 2 | |
| | | 02:32 | 10°08.53 N | 86°02.58 W | 233 | 10 | |
| | | 02:45 | 10°07.32 N | 86°04.70 W | 141 | 2 | |
| | | 03:46 | 09°59.36 N | 85°58.49 W | 234 | 10 | |
| | | 04:04 | 09°57.57 N | 86°00.86 W | 322 | 3 | |
| | | 05:12 | 10°06.38 N | 86°07.83 W | 47 | 11 | |
| | | 06:02 | 10°12.01 N | 86°01.80 W | 322 | 8 | |
| | | 08:21 | 10°28.10 N | 86°13.85 W | 50 | 20 | |
| | | 08:50 | 10°28.93 N | 86°12.81 W | 142 | 1 | |
| | | | | | | | |
| EM-04 | 17.03.02 | 09:36 | 10°41.92 N | 86°34.92 W | 21 | | |
| | | 10:29 | 10°45.91 N | 86°32.67 W | 270 | 4 | |
| | | 10:58 | 10°46.07 N | 86°35.79 W | 137 | 3 | |
| | | 12:45 | 10°38.75 N | 86°29.18 W | | 10 | |
| | | | | | | | |
| EM-05 | 17.03.02 | 13:23 | 10°37.32 N | 86°36.00 W | 324 | | |
| | | 15:10 | 10°45.94 N | 86°42.46 W | 90 | 11 | |
| | | 15:22 | 10°46.26 N | 86°41.54 W | 124 | 1 | |
| | | 16:13 | 10°42.43 N | 86°36.84 W | | 6 | |
| | | | | | | | |
| EM-06 | 22.03.02 | 23:11 | 10°19.09 N | 86°17.98 W | 25 | | |
| | 23.03.02 | 00:06 | 10°26.96 N | 86°13.98 W | 325 | 10 | |
| | | 00:28 | 10°30.00 N | 86°16.00 W | 312 | 4 | |
| | | 02:09 | 10°41.30 N | 86°28.50 W | 54 | 17 | |
| | | 02:22 | 10°41.82 N | 86°27.67 W | 131 | 2 | |
| | | 04:09 | 10°31.44 N | 86°15.00 W | 44 | 17 | |
| | | 04:21 | 10°32.85 N | 86°13.69 W | 306 | 2 | |
| | | 05:26 | 10°39.40 N | 86°22.50 W | 213 | 11 | |
| | | 05:36 | 10°38.83 N | 86°22.87 W | 128 | 1 | |
| | | 06:40 | 10°32.68 N | 86°15.08 W | 90 | 10 | |
| | | 06:45 | 10°32.49 N | 86°14.38 W | 156 | 1 | |
| | | 07:30 | 10°25.87 N | 86°11.37 W | 195 | 7 | |
| | | 09:33 | 10°05.91 N | 86°16.73 W | | 21 | |
| | | | | | | | |

| line number | date | time | position | | course | length | remarks |
|---|---|---|---|---|---|---|---|
| | | | | | | | |
| EM-07 | 25.03.02 | 12:31 | 09°20.70 N | 86°04.00 W | | | |
| | | 14:21 | 09°32.97 N | 85°50.20 W | 90 | 18 | |
| | | 15:15 | 09°32.00 N | 85°41.22 W | | 9 | |
| | | | | | | | |
| EM-08 | 29.03.02 | 06:44 | 10°00.98 N | 86°11.29 W | | | |
| | | 11:35 | 09°49.13 N | 86°41.88 W | | 32 | |
| | | | | | | | |
| EM-09 | 29.03.02 | 11:35 | 09°49.13 N | 86°41.88 W | | | |
| | | 12:00 | 09°48.01 N | 86°43.26 W | 134 | 2 | |
| | | 16:58 | 09°30.21 N | 86°24.68 W | 41 | 26 | |
| | | 17:15 | 09°31.18 N | 86°23.65 W | 314 | 4 | |
| | | 20:57 | 09°44.85 N | 86°37.63 W | | 19 | |
| | | | | | | | |
| EM-10 | 30.03.02 | 09:20 | 09°48.22 N | 86°41.97 W | | | |
| | | 12:34 | 10°20.13 N | 86°41.50 W | 140 | 27 | |
| | | 17:03 | 09°45.00 N | 86°12.00 W | 131 | 46 | |
| | | 20:27 | 09°21.11 N | 85°45.13 W | 90 | 36 | |
| | | 21:56 | 09°21.01 N | 85°29.86 W | | 15 | |
| | | | | | | | |
| EM-11 | 02.04.02 | 06:47 | 09°09.58 N | 85°41.42 W | | | |
| | | 08:51 | 09°06.10 N | 85°36.00 W | 56 | 14 | |
| | | 12:07 | 09°19.00 N | 85°36.00 W | | 14 | |
| | | | | | | | |
| EM-12 | 14.04.02 | 14:04 | 09°00.00 N | 84°23.00 W | 35 | | |
| | | 14:37 | 09°02.32 N | 84°22.05 W | 129 | | |
| | | 15:28 | 08:58.40 N | 84°17.20 W | | 11 | |
| | | | | | | | |
| EM-13 | 14.04.02 | 19:51 | 08°46.29 N | 84°14.65 W | 196 | | |
| | | 20:45 | 08°51.00 N | 84°22.10 W | | 11 | |
| | | | | | | | |
| EM-14 | 14.04.02 | 22:43 | 08°46.29 N | 84°14.65 W | 304 | | |
| | | 00:39 | 08°51.00 N | 84°22.10 W | | 11 | |
| | | | | | | | |
| EM-15 | 18.04.02 | 04:00 | 09°06.80 N | 84°51.90 W | 213 | | |
| | | 05:01 | 09°02.50 N | 84°54.78 W | 120 | 5 | |
| | | 05:37 | 09°01.01 N | 84°52.20 W | 34 | 3 | |
| | | 06:47 | 09°05.61 N | 84°48.98 W | 38 | 7 | |
| | | 07:09 | 09°06.92 N | 84°47.97 W | | 2 | |
| | | | | | | | |
| EM-16 | 18.04.02 | 14:11 | 09°01.45 N | 84°38.00 W | 288 | | |
| | | 15:22 | 09°04.52 N | 84°46.95 W | 61 | 10 | |
| | | 15:50 | 09°06.23 N | 84°43.96 W | 108 | 3 | |
| | | 19:00 | 09°00.00 N | 84°25.35 W | | 19 | |
| | | | | | | | |
| EM-17 | 18.04.02 | 19:26 | 09°01.56 N | 84°23.00 W | 288 | | |
| | | 21:45 | 09°07.55 N | 84°40.81 W | | 19 | |
| | | | | | | | |
| EM-18 | | 22:04 | 09°09.61 N | 84°40.62 W | | | |
| | 19.04.02 | 00:32 | 09°03.52 N | 84°23.00 W | 63 | 20 | |
| | | 00:40 | 09°03.67 N | 84°21.48 W | 288 | 1 | |
| | | 03:04 | 09°10.37 N | 84°40.00 W | | | |
| | | | | | | | |

## Appendix 9.2 TOBI profiles

| M-O Number | File Name | Time/ Day START | Time/ Day STOP | Comments / Run # |
|---|---|---|---|---|
| 830 | TOBIB.DAT | 1813/076 | 0523/077 | Run 1 curtailed due to cable short. Day number corrected. |
| 831 | TOBI.DAT<br>TOBIB.DAT<br>TOBIC.DAT | 2310/077<br>0334/078<br>0339/078 | 0329/078<br>0337/078<br>1526/078 | Run 2 Day number corrected<br><br>Day number correct |
| 832 | TOBI.DAT | 1526/078 | 0733/079 | |
| 833 | TOBI.DAT | 0733/079 | 2340/079 | |
| 834 | TOBI.DAT | 2340/079 | 1548/080 | |
| 835 | TOBI.DAT | 1548/080 | 0755/081 | |
| 836 | TOBI.DAT | 0755/081 | 1419/081 | End of run 2 |
| 837 | TOBI.DAT | 2120/082 | 1323/083 | Start of run 3 |
| 838 | TOBI.DAT | 1323/083 | 0535/084 | |
| 839 | TOBI.DAT | 0535/084 | 1558/084 | End of run 3 |
| 840 | TOBI.DAT | 0145/096 | 1752/096 | Start of run 4 |
| 841 | TOBI.DAT | 1752/096 | 1000/097 | |
| 842 | TOBI.DAT | 1000/097 | 0207/098 | |
| 843 | TOBI.DAT | 0207/098 | 1815/098 | |
| 844 | TOBI.DAT | 1815/098 | 1022/099 | |
| 845 | TOBI.DAT | 1022/099 | 0229/100 | |
| 846 | TOBI.DAT | 0229/100 | 1355/100 | End of run 4 |
| 847 | TOBI.DAT<br>TOBIA.DAT<br>TOBIB.DAT | 0052/102<br>0340/102<br>1016/102 | 0156/102<br>1014/102<br>1846/102 | Run 5<br>Start of run 6<br>Reboot logging |
| 848 | TOBI.DAT | 1846/102 | 1053/103 | |
| 849 | TOBI.DAT | 1053/103 | 2103/103 | End of run 6 |

## Appendix 9.3 DTS-1 profiles

| Deploy-ment | Average water depth | Track length | Mapped area | Time on sea-floor | Deployment | Recovering | Total |
|---|---|---|---|---|---|---|---|
| 1 | 1300-2400 | 141.0 km | 162.2 km² | 37 h | 1 h 40 | 2 h | 40 h 40 |
| 2 | 2500-3200 | 134.0 km | 145.0 km² | 44 h | 2 h 30 | 2 h 50 | 49 h 20 |
| 3 | 400-1900 | 172.4 km | 175.2 km² | 44 h | 35 min | 2h | 46 h 30 |
| 4 | 900-2000 | 120.4 km | 161.0 km² | 30 h | 2 h | 2 h | 34 h |
| 5 | 1300-1500 | 9.0 km | 1.8 km² | 2h | 55 min | 1h 05 | 4h |

| | | | at seafloor | | | | off seafloor / grab location | | | | |
|---|---|---|---|---|---|---|---|---|---|---|---|
| Station | Area | Date | Time | Lat | Long | Depth | Time | Lat | Long | Depth | Observation / recovery |
| **Mounds** | | | | | | | | | | | |
| OFOS 1 | Mound # 1 | 22.03.2002 | 17:41:48 | 10° 17.86 | 86° 18.37 | 1540 | 19:41:49 | 10° 18.01 | 86° 17.99 | 1570 | Carbonates, clams and pogonophorans, No SSBL Position |
| OFOS 2 | Mound # 1 | 22.03.2002 | 21:29:10 | 10° 17.84 | 86° 18.56 | 1510 | 23:21:10 | 10° 18.14 | 86° 18.07 | 1550 | Carbonates, clams and pogonophorans, SSBL 50 m above OFOS |
| TVG 1 | Mound # 1 | 23.03.2002 | 01:59:50 | 10° 17.88 | 86° 18.40 | 1500 | 02:07:00 | 10° 17.923 | 86° 18.32 | 1516 | 2 carbonate pieces on top of grab |
| TVG 2 | Mound # 1 | 23.03.2002 | 03:26:00 | 10° 17.93 | 86° 18.33 | 1490 | 03:36:00 | 10° 17.987 | 86° 18.29 | 1473 | Several carbonate pieces and clamshell fragments |
| OFOS 3 | Mound # 2-6 | 28.03.2002 | 00:10:30 | 9° 37.12 | 85° 46.53 | 1588 | 08:25:26 | 9° 35.95 | 85° 50.15 | 1989 | Crossed 4 mounts from NE to SW, some with carbonates, pogonophorans, clams; Camera B problems |
| OFOS 4 | Mound # 7, 8 | 18.03.2002 | 11:32:36 | 9° 42.53 | 85° 56.30 | 2203 | 15:17:14 | 9° 41.98 | 85° 56.90 | 2240 | Small aera with carbonates, pogonophorans and clams |
| OFOS 6 | Mound # 9 | 29.03.2002 | 05:01:30 | 10° 02.16 | 86° 11.80 | 2240 | 07:24:10 | 10° 01.56 | 86° 12.23 | 2342 | No seep indication |
| OFOS 7 | Mound # 10 | 29.03.2002 | 09:24:10 | 10° 00.73 | 86° 11.35 | 2305 | 11:36:10 | 10° 00.65 | 86° 11.50 | 2341 | Abundant vent indication; clams, pogonophorans, carbonate |
| OFOS 13 | "Bright Spot W of Parrita" | 05.04.2002 | 20:19:50 | 9° 59.70 | 84° 42.50 | | 23:35:00 | 8° 58.00 | 84° 41.65 | | Beside scattered clamshells no seep indications |
| OFOS 19 | Mound # 11, 12 | 14.04.2002 | 05:44:20 | 8° 54.94 | 84° 17.91 | 1023 | 08:14:32 | 8° 55.95 | 84° 18.83 | 1005 | Extensive carbonates, clams, mussels and pogonophorans |
| OFOS 21 | Mound # 12 | 14.04.2002 | 15:09:30 | 8° 55.94 | 84° 18.53 | 998 | 18:40:16 | 8° 55.73 | 84° 18.95 | 1013 | Extensive carbonates, clams, mussels and pogonophorans; Video on 16:32 |
| TVG 4 | Mound # 12 | 14.04.2002 | 22:29:35 | 8° 55.79 | 84° 18.74 | 1002 | 23:14:45 | 8° 55.81 | 84° 18.62 | 992 | Piece of outcropping carbonate |
| TVG 5 | Mound # 12 | 15.04.2002 | 00:16:50 | 8° 55.79 | 84° 18.75 | 1002 | 00:41:00 | 8° 55.80 | 84° 18.74 | 1005 | Complete seep ecosystem: Acharax, Bathymodiolus, Lamellibrachia, galatheid crabs and carbonates |
| OFOS 23 | Mound # 13 | 17.04.2002 | 05:12:40 | 9° 02.20 | 84° 37.24 | 1451 | 12:28:39 | 9° 01.78 | 84° 37.06 | 1403 | Most extensive field of carbonates, pogonophorans, bivalves |
| OFOS 24 | Mound # 13 | 17.04.2002 | 14:27:44 | 9° 01.95 | 84° 37.22 | 1406 | 16:41:50 | 9° 01.95 | 84° 37.13 | 1397 | Mapping most extensive seep area |
| TVG 8 | Mound # 13 | 18.04.2002 | 16:55:10 | 9° 01.96 | 84° 37.22 | 1408 | 17:06:40 | 9° 01.97 | 84° 37.22 | 1408 | Carbonates |
| TVG 9 | Mound # 13 | 18.04.2002 | 18:44:15 | 9° 01.96 | 84° 37.25 | 1408 | 18:47:35 | 9°0 1.96 | 84° 37.24 | 1408 | Vent fauna, carbonates |

| | | | at seafloor | | | | off seafloor / grab location | | | | |
|---|---|---|---|---|---|---|---|---|---|---|---|
| Station | Area | Date | Time | Lat | Long | Depth | Time | Lat | Long | Depth | Observation / recovery |
| **High heatflow area** | | | | | | | | | | | |
| OFOS 8 | Basement hight | 30.03.2002 | 04:43:17 | 9° 40.25 | 86° 33.76 | 3275 | 08:20:00 | 9° 41.01 | 86° 33.17 | 3267 | No indication for hydrothermal venting |
| OFOS 9 | Fault | 30.03.2002 | 10:58:04 | 9° 46.48 | 86° 40.78 | 3315 | 13:40:51 | 9° 46.89 | 86° 40.41 | 3346 | No indication for hydrothermal venting |
| **seamount scars** | | | | | | | | | | | |
| OFOS 5 | Scarp of fracture ridge trace | 28.03.2002 | 17:42:39 | 9° 36.31 | 85° 54.28 | 2194 | 23:00:40 | 9° 33.94 | 85° 56.53 | 3145 | very few seep indication or other geological structures |
| OFOS 10 | Rio Bongo Scarp | 02.04.2002 | 18:39:39 | 9° 18.86 | 85° 15.54 | 470 | 23:27:30 | 9° 19.16 | 85° 18.31 | 772 | Carbonated top, few vent fauna |
| OFOS 11 | Jaco Scarp | 03.04.2002 | 04:52:39 | 9° 10.43 | 84° 47.75 | 731 | 07:16:42 | 9° 10.40 | 84° 48.66 | 779 | Carbonates, bivalve shells |
| OFOS 12 | Jaco Scarp | 03.04.2002 | 09:03:40 | 9° 10.40 | 84° 50.34 | 928 | 13:15:33 | 9° 08.74 | 84° 48.69 | 865 | Chemoherm-like carbonates, vesicomyid clamfield |
| TVG 3 | Jaco Scarp | 05.04.2002 | 15:44:10 | 9° 10.42 | 84° 48.25 | 763 | 15:50:57 | 9° 10.43 | 84° 48.24 | 763 | Chemoherm-like carbonates, living solemyid bivalves, bivalve shells |
| OFOS 25 | Jaco Scarp | 18.04.2002 | 00:09:48 | 9° 11.60 | 84° 47.80 | 774 | 05:03:20 | 9° 10.78 | 84° 50.62 | 996 | No vent indication |
| OFOS 26 | Jaco Scarp | 18.04.2002 | 06:22:55 | 9° 08.24 | 84° 49.64 | 953 | 09:08:31 | 9° 09.14 | 84° 48.04 | 810 | No vent indication |
| TVG 7 | Jaco Scarp | 18.04.2002 | 14:01:32 | 9° 09.03 | 84° 49.18 | 834 | 14:32:00 | 9° 09.01 | 84° 49.13 | 824 | Carbonates |
| OFOS 15 | "Frontal collision" | 11.04.2002 | 00:02:00 | 8° 22.20 | 83° 47.684 | 1260 | 02:52:24 | 8° 21.182 | 83° 48.013 | 1633 | Steep morphology, beside clamshells no seep indication |
| OFOS 16 | "Small seamount scarp" | 11.04.2002 | 05:05:00 | 8° 26.48 | 83° 54.981 | 701 | 07:48:14 | 8° 25.893 | 83° 56.002 | 1095 | No vent indication |
| OFOS 22 | Parrita | 15.04.2002 | 09:15:58 | 8° 57.55 | 84° 36.51 | 1228 | 14:12:57 | 8° 55.17 | 84° 37.89 | 2338 | Beside scattered clamshells no seep indications |

| | | | at seafloor | | | | off seafloor / grab location | | | | |
|---|---|---|---|---|---|---|---|---|---|---|---|
| Station | Area | Date | Time | Lat | Long | Depth | Time | Lat | Long | Depth | Observation / recovery |
| **Accretionary wedge** | | | | | | | | | | | |
| OFOS 14 | "Creast of Cocos Ridge" | 10.04.2002 | 19:21:24 | 8° 15.572 | 83° 34.185 | 1710 | 20:41:58 | 8° 15.343 | 83° 34.803 | 1902 | No seep indication |
| OFOS 17 | "Seismic Line SO 81 #5" | 11.04.2002 | 12:34:30 | 8° 40.56 | 84° 18.35 | 2000 | 20:57:25 | 8° 35.93 | 84° 21.30 | 2500 | No seep indication |
| **Landslide** | | | | | | | | | | | |
| OFOS 18 | Quepos Lanslide | 13.04.2002 | 22:56:41 | 8° 51.87 | 84° 12.60 | 179 | 03:48:43 | 8° 49.50 | 84° 15.51 | 831 | Larg bacterial mats at headwall, few seep indications in slide mass |
| OFOS 20 | Quepos Lanslide | 14.04.2002 | 10:16:00 | 8° 50.30 | 84° 13.00 | 438 | 13:06:00 | 8° 48.61 | 84° 13.90 | 740 | Beside one bacterial mat no seep indication at slide mass |

| INST. | LAT (N) | LON (W) | DIST. TO | DEPTH | REL. | ANT. | REC. | SKEW | SENSOR | Other Sensors | REMARKS |
|---|---|---|---|---|---|---|---|---|---|---|---|
| | D:M | D:M | NEXT (nm) | (m) | CODE | CH. | NO. | (ms) | HYDRO | | |
| OBH 01 | 09:39.456 | 85:51.494 | 2,45 | 1866 | 3624 | C | 991249 | 131 | OAS 13 | | |
| OBH 02 | 09:40.605 | 85:53.698 | 2,45 | 1924 | 3669 | D | 991247 | 51 | OAS 02 | | |
| OBH 03 | 09:38.135 | 85:53.489 | 1,20 | 2068 | 3659 | C | 991256 | -62 | OAS 30 | | |
| OBH 04 | 09:38.849 | 85:52.508 | 1,11 | 1996 | 3674 | C | 991235 | 63 | DPG 93 | | |
| OBH 05 | 09:39.911 | 85:52.805 | 0,93 | 1940 | 039A+0355 | D | 000713 | 85 | DPG 92 | | |
| OBH 06 | 09:39.394 | 85:53.584 | 0,58 | 1871 | 6334 | A | 000708 | -235 | DPG 87 | | |
| OBH 07 | 09:39.930 | 85:53.109 | 0,65 | 1997 | 3609 | D | 991252 | -60 | OAS 22 | | |
| OBH 08 | 09:39.450 | 85:52.528 | 0,60 | 1964 | 0387+0355 | B | 991242 | -43 | DPG 75 | | |
| OBH 09 | 09:39.691 | 85:53.108 | 0,32 | 1951 | 3664 | D | 000707 | -133 | OAS 27 | | |
| OBH 10 | 09:39.461 | 85:52.905 | 1,03 | 1893 | 0386+0355 | C | 991237 | -79 | DPG 91 | | 50 m anchor rope |
| OBH 22 | 09:38.507 | 85:52.366 | 1,95 | 2116 | 3614 | C | 980901 | 15 | OAS 29 | | |
| OBH 23 | 09:40.222 | 85:53.495 | | 1931 | 03B6+0355 | A | 010703 | -1 | OAS 38 | | 550 m anchor rope |

| INST. | LAT (N) | LON (W) | Deployed | DEPTH | REL. | ANT. | REC. | SKEW | SENSOR | Other Sensors | REMARKS |
|---|---|---|---|---|---|---|---|---|---|---|---|
| | D:M | D:M | Recovered | (m) | CODE | CH. | REC. | (ms) | HYDRO. | | |
| OBS 14 | 09:19.985 | 84:52.996 | 22.04./ 09.05.02 | 1741 | 0399+0355 | C | 0706 | | OAS 34 | PMD 540 | power failure |
| OBH 15 | 09:14.661 | 84:36.046 | 22.04./ 09.05.02 | 114 | 0398+0355 | A | 0711 | -18 | DPG 95 | | |
| OBH 16 | 09:09.975 | 84:38.015 | 22.04./ 09.05.02 | 944 | 0397+0355 | C | 10405 | 5 | HTI 302 | | |
| OBT 17 | 09:09.405 | 84:49.577 | 22.04./ 28.04.02 | 824 | 03BC+0355 | C | 020303 | -26 | | TM 4948 | |
| OBH 18 | 09:09.397 | 84:49.588 | 23.04./ 09.05.02 | 827 | 4A44 | C | 010402 | 2976 | OAS 18 | | |
| OBS 19 | 08:59.996 | 84:50.055 | 23.04./ 09.05.02 | 2206 | 03B9+355 | C | 010401 | | OAS 31 | PMD 509 | Rec.end: 05.05.02 |
| OBH 20 | 08:50.006 | 84:49.996 | 23.04./ 09.05.02 | 3473 | 03B7+0355 | D | 991238 | -19 | HTI 602 | | |
| OBH 21 | 08:58.032 | 85:05.046 | 23.04./ 09.05.02 | 3602 | 03BB+0355 | C | 991243 | 20 | HTI 102 | | |
| OBH 38 | 09:14.271 | 84:56.637 | 28.04.02 | 1752 | 03BD+0355 | D | 000713 | | DPG 93 | | |
| OBH 39 | 09:05.280 | 85:02.560 | 28.04.02 | 2496 | 03B6+0355 | C | 991249 | | DPG 75 | | |
| OBH 40 | 08:53.328 | 84:58.432 | 28.04.02 | 3420 | 03B5+0355 | C | 991237 | | DPG 91 | | |
| OBH 41 | 08:56.043 | 84:43.428 | 28.04.02 | 2615 | 03B3+0355 | C | 991242 | | DPG 87 | | |
| OBH 42 | 09:05.173 | 84:39.092 | 28.04.02 | 1481 | 03B8+0355 | C | 991250 | | DPG 92 | | |
| OBH 139 | 09:13,023 | 84:33,508 | 12.05.02 | 379 | 03B7+0355 | C | 991247 | | OAS 02 | | |
| OBH 140 | 09:10,017 | 84:37,993 | 12.05.02 | 939 | 03BB+0355 | A | 10405 | | OAS 04 | | |
| OBH 141 | 09:13,016 | 84:41,022 | 12.05.02 | 351 | 03B9+0355 | A | 10402 | | OAS 29 | | |
| OBH 193 | 09:19,989 | 85:06,063 | 16.05.02 | 1880 | 3659 | C | 991238 | | HTI 502 | | |
| OBH 194 | 09:28,015 | 84:52,503 | 16.05.02 | 560 | 039A+0355 | D | 707 | | OAS 18 | | |
| OBH 195 | 09:28,001 | 84:44,997 | 16.05.02 | 324 | 0387+0355 | B | 991256 | | OAS 30 | | |
| OBH 196 | 09:21,531 | 84:45,034 | 16.05.02 | 413 | 3624 | C | 10401 | | HTI 302 | | |
| OBS 197 | 09:20,022 | 84:53,006 | 16.05.02 | 1745 | 03BA+0355 | C | 10404 | | HTI 702 | Owen 22 (4,5Hz) | |
| OBH 198 | 09:14,975 | 84:44,001 | 16.05.02 | 291 | 3674 | C | 991243 | | OAS 27 | | |
| OBH 199 | 09:12,016 | 84:46,990 | 16.05.02 | 734 | 03B1+0355 | D | 20303 | | HTI 802 | TM 4949 | |
| OBH 200 | 09:09,419 | 84:49,601 | 16.05.02 | 824 | 03B2+0355 | C | 20302 | | HTI 602 | TM 4948 | |
| OBS 201 | 09:10,013 | 84:56,020 | 16.05.02 | 2080 | 0397+0355 | D | 991252 | | OAS 31 | LG 01 (4,5 Hz) | |
| OBH 202 | 09:01992 | 84:56,010 | 17.05.02 | 2237 | 0386+0355 | D | 991236 | | HTI 102 | | |
| OBH 203 | 08:57,974 | 85:05,004 | 17.05.02 | 3561 | 3614 | D | 706 | | OAS 18 | | |
| OBH 204 | 08:50,000 | 84:49,995 | 17.05.02 | 3474 | 3629 | D | 991246 | | OAS 38 | | |
| OBH 205 | 08:59,985 | 84:49,996 | 17.05.02 | ??? | 3669 | B | 991241 | | HTI 902 | | |
| OBS 206 | 09:01,996 | 84:43,006 | 17.05.02 | 1726 | 03BC+0355 | D | 10403 | | OAS 46 | Owen 21 (4,5Hz) | |
| OBH 207 | 09:07,000 | 84:43,003 | 17.05.02 | 1159 | 3609 | C | 711 | | OAS 22 | | |
| OBH 208 | 09:05,376 | 84:34,248 | 17.05.02 | 1155 | 0399+0355 | D | 991248 | | HTI 202 | | |
| OBH 209 | 09:02,296 | 84:39,205 | 17.05.02 | 1615 | 3664 | A | 991244 | | OAS 75 | | |
| OBH 210 | 08:59,579 | 84:37,907 | 17.05.02 | 1202 | 03B4+0355 | D | 708 | | HTI 101 | | |
| OBH 211 | 09:01,004 | 84:34,461 | 17.05.02 | 1411 | 6334 | C | 616 | | OAS 09 | | |
| OBH 212 | 09:02,387 | 84:36,203 | 17.05.02 | 1326 | 4A44 | B | 971202 | | OAS 28 | | |

| INST. | LAT (N) | LON (W) | Dist. To | DEPTH | REL. | ANT. | REC. | SKEW | SENSOR | Other Sensors | REMARKS |
|---|---|---|---|---|---|---|---|---|---|---|---|
| | D:M | D:M | Next (nm) | (m) | CODE | CH. | REC. | (ms) | HYDRO. | | |
| OBS 24 | 09:15.938 | 85:37.412 | 0.11 | 2770 | 3614 | C | 98040 | -6 | OAS 75 | LG 01 (4,5Hz) | |
| OBS 25 | 09:16.017 | 85:37.308 | 0.11 | 2768 | 03BA+0355 | B | 991247 | 2 | HTI 702 | PMD 539 | |
| OBS 26 | 09:16.093 | 84:37.255 | 0.11 | 2770 | 03B4+0355 | C | 971202 | -6 | HTI 202 | Owen 02 (4,5Hz) | |
| OBH 27 | 09:16.182 | 85:37.195 | 0.12 | 2738 | 3624 | D | 010703 | -1 | OAS 13 | | |
| OBH 28 | 09:16.267 | 85:37.079 | 0.16 | 2736 | 3664 | C | 980403 | -2 | OAS 27 | | |
| OBH 29 | 09:16.407 | 85:37.026 | 0.16 | 2705 | 03B6+0355 | D | 010708 | 2 | OAS 38 | | |
| OBH 30 | 09:16.519 | 85:36.915 | 0.54 | 2654 | 3669 | C | 980901 | 17 | OAS 02 | | 500m anchor rope |
| OBS 31 | 09:16.948 | 85:36.558 | 0.11 | 2657 | 03B5+0355 | A | 000616 | -9 | OAS 46 | Owen 21 (4,5Hz) | |
| OBH 32 | 09:17.043 | 85:36.508 | 4.54 | 2628 | 3659 | D | 991256 | -2 | OAS 30 | | |
| OBH 33 | 09:20.606 | 85:33.705 | 0.11 | 2260 | 6334 | C | 000707 | -7 | OAS 29 | | |
| OBS 34 | 09:20.687 | 85:33.625 | 0.11 | 2257 | 03B2+0355 | C | 980402 | -5 | HTI 002 | Owen 22 (4,5Hz) | |
| OBH 35 | 09:20.785 | 85:33.567 | 4.60 | 2246 | 03BD+0355 | B | 991252 | -3 | HTI 802 | | |
| OBH 36 | 09:17.135 | 85:36.425 | 0.11 | 2626 | 03BD+0355 | B | 000614 | -1 | HTI 302 | | |
| OBH 37 | 09:17.183 | 85:36.328 | | 2607 | 3629 | D | 000610 | -2 | HTI 502 | | OBS-design 2002 |

| INST. | LAT (N) | LON (W) | DIST. TO | DEPTH | REL. | ANT. | REC. | SKEW | SENSOR | Other Sensors | REMARKS |
|---|---|---|---|---|---|---|---|---|---|---|---|
| | D:M | D:M | NEXT (nm) | (m) | CODE | CH. | NO. | (ms) | HYDRO | | |
| OBH 43 | 09:17.082 | 84:10.505 | 1.17 | 92 | 3659 | D | 707 | -6 | OAS 30 | | |
| OBH 44 | 09:16,119 | 84:11,232 | 1,49 | 105 | 3669 | C | 980403 | -2 | OAS 02 | | |
| OBH 45 | 09:14,911 | 84:12,091 | 1,71 | 122 | 0387+0355 | A | 010708 | 0 | OAS 38 | | |
| OBH 46 | 09:13,517 | 84:13,139 | 1,91 | 149 | 03B4+0355 | D | 971202 | -2 | HTI 202 | Owen 02 (4.5Hz) | |
| OBH 47 | 09:11,929 | 84:14,261 | 1,73 | 205 | 3629 | D | 610 | 3 | HTI 502 | Owen 11 (30Hz) | |
| OBH 48 | 09:10,597 | 84:15,290 | 1,97 | 360 | 03B2+0355 | C | 980402 | -4 | HTI 002 | Owen 22 (4.5Hz) | |
| OBH 49 | 09:08,993 | 84:16,479 | 1,14 | 459 | 3664 | C | 010404 | 2 | OAS 27 | | |
| OBH 50 | 09:08,041 | 84:17,154 | 1,93 | 480 | 0386+0355 | C | 980401 | -4 | OAS 46 | Owen 21 (4,5Hz) | |
| OBH 51 | 09:06,502 | 84:18,299 | 1,80 | 502 | 3624 | B | 991252 | -2 | OAS 13 | | |
| OBH 52 | 09:05,042 | 84:19,370 | 1,86 | 570 | 03BC+0355 | D | 000616 | -4 | HTI 102 | Owen 16 (30Hz) | |
| OBH 53 | 09:03,524 | 84:20,505 | 1,90 | 666 | 6334 | D | 991248 | -1 | OAS 29 | | |
| OBH 54 | 09:02,004 | 84:21,628 | 2,42 | 765 | 03BA+0355 | B | 00611 | -3 | HTI 702 | Owen 14 (30Hz) | |
| OBH 55 | 09:00,040 | 84:23,038 | 2,36 | 965 | 3609 | A | 980901 | 8 | HTI 902 | | |
| OBH 56 | 08:58,138 | 84:24,460 | 2,63 | 1192 | 039A+0355 | B | 991256 | -1 | OAS 22 | | |
| OBH 57 | 08:56,013 | 84:26,055 | 1,82 | 1579 | 3614 | D | 010703 | -1 | OAS 75 | LG 01 (4.5 Hz) | |
| OBH 58 | 08:54,525 | 84:27,135 | 1,86 | 1820 | 03B1+0355 | C | 991247 | 0 | HTI 402 | | |
| OBH 59 | 08:53,041 | 84:28,294 | | 1975 | 3674 | D | 00614 | -4 | HTI 802 | | |
| | | | | | | | | | OAS 09 | | |
| | | | | | | | | | OAS 04 | | |
| | | | | | | | | | OAS 14 | | |

| INST. | LAT (N) | LON (W) | DIST. TO | DEPTH | REL. | ANT. | REC. | SKEW | SENSORS | Other Sensors | REMARKS |
|---|---|---|---|---|---|---|---|---|---|---|---|
| | D:M | D:M | NEXT (nm) | (m) | CODE | CH. | NO. | (ms) | HYDRO. | | |
| OBH 62 | 09:06,999 | 84:33,540 | 1,85 | 1038 | 3659 | D | 980403 | -1 | OAS 30 | | |
| OBH 63 | 09:05,992 | 84:31,949 | 1,89 | 1008 | 3669 | C | 010708 | 1 | OAS 02 | | |
| OBH 64 | 09:04,977 | 84:30,407 | 1,86 | 2031 | 0387+0355 | C | 010404 | 2 | OAS 38 | | |
| OBS 65 | 09:03,974 | 84:28,774 | 1,83 | 1127 | 03B4+0355 | A | 010703 | -1 | HTI 202 | Owen 02 (4.5Hz) | |
| OBS 66 | 09:03,014 | 84:27,238 | 1,91 | 1181 | 3664 | D | 991248 | -1 | OAS 27 | | |
| OBH 67 | 09:02,014 | 84:25,604 | 1,82 | 1190 | 3624 | D | 000611 | -3 | OAS 13 | | |
| OBS 68 | 09:01,010 | 84:24,017 | 1,99 | 1155 | 03BA+0355 | B | 980402 | -3 | HTI 702 | Owen 14 (30 Hz) | |
| OBH 69 | 08:59,944 | 84:22,329 | 1,94 | 929 | 6334 | D | 980401 | -3 | OAS 29 | | |
| OBS 70 | 08:58,901 | 84:20,658 | 1,92 | 977 | 0386+0355 | C | 971202 | | OAS 46 | Owen 21 (4,5Hz) | no data |
| OBH 71 | 08:57,881 | 84:19,051 | 1,93 | 904 | 3609 | D | 991252 | -2 | HTI 902 | | |
| OBS 72 | 08:56,849 | 84:17,392 | 1,99 | 930 | 03BC+0355 | B | 000616 | -3 | HTI 101 | | |
| OBH 73 | 08:55,797 | 84:15,654 | 1,97 | 945 | 039A+0355 | B | 991256 | 0 | OAS 22 | | |
| OBS 74 | 08:54,703 | 84:13,982 | 2,11 | 789 | 3614 | D | 000610 | -2 | OAS 75 | | |
| OBH 75 | 08:53,637 | 84:12,190 | 2,50 | 272 | 3674 | D | 000614 | -1 | HTI 802 | | |
| | | | | | | | | | OAS 09 | | |
| | | | | | | | | | OAS 04 | | |
| | | | | | | | | | OAS 14 | | |

| INST. | LAT (N) | LON (W) | Dist. To | DEPTH | REL. | ANT. | REC. | SKEW | SENSOR | Other Sensors | REMARKS |
|---|---|---|---|---|---|---|---|---|---|---|---|
| | D:M | D:M | Next (nm) | (m) | CODE | CH. | REC. | (ms) | HYDRO. | | |
| OBH 76 | 09:03,698 | 84:32,899 | 1,53 | 1186 | 0387+0355 | D | 010708 | 0 | OAS 38 | | |
| OBH 77 | 09:02,900 | 84:31,593 | 1,51 | 1238 | 3664 | A | 980901 | 14 | OAS 27 | | not active |
| OBH 78 | 09:02,096 | 84:30,294 | 1,54 | 1273 | 3624 | B | 980403 | -2 | OAS 13 | | |
| OBH 79 | 09:01,254 | 84:28,970 | 1,47 | 1319 | 6334 | D | 991248 | -1 | OAS 29 | | |
| OBH 80 | 09:00,477 | 84:27,715 | 1,41 | 1337 | 3609 | C | 991252 | -4 | HTI 902 | | |
| OBS 81 | 08:59,741 | 84:26,508 | 1,49 | 1342 | 03BA+0355 | C | 000616 | -7 | HTI 702 | Owen 14 (30 Hz) | |
| OBS 82 | 08:58,933 | 84:25,208 | 1,53 | 1246 | 03BC+0355 | D | 971202 | -5 | HTI 101 | Owen 16 (30 Hz) | |
| OBS 83 | 08:58,111 | 84:23,913 | 1,51 | 1168 | 0386+0355 | D | 980402 | -5 | OAS 04 | Owen 21 (4,5 Hz) | |
| OBS 84 | 08:57,313 | 84:22,607 | 1,47 | 1117 | 03B4+0355 | D | 980401 | -5 | HTI 202 | Owen 02 (4,5 Hz) | |
| OBS 85 | 08:56,497 | 84:21,350 | 1,45 | 1092 | 3614 | C | 000611 | -3 | OAS 75 | LG 01 (4,5 Hz) | |
| OBH 86 | 08:55,718 | 84:20,107 | 1,52 | 1111 | 3629 | C | 000610 | -8 | HTI 502 | | OBS-design 2002 |
| OBH 87 | 08:54,903 | 84:18,785 | 1,49 | 1111 | 039A+0355 | D | 000707 | -5 | HTI 102 | | |
| OBH 88 | 08:53,555 | 84:16,626 | 1,07 | 1089 | 3659 | D | 991247 | 0 | OAS 30 | | |
| OBH 89 | 08:54,104 | 84:17,515 | 0,99 | 1062 | 3674 | B | 000614 | -6 | HTI 802 | | |
| | | | | | | | | | OAS 09 | | |
| | | | | | | | | | OAS 04 | | |
| | | | | | | | | | OAS 14 | | |
| OBH 90 | 08:53,017 | 84:15,767 | 2,50 | 960 | 3669 | B | 010404 | 3 | OAS 02 | | |
| OBH 92 | 09:14,922 | 84:15,185 | 1,46 | 150 | 0387+0355 | B | 010404 | 2 | OAS 38 | | |
| OBH 93 | 09:13,72 | 84:16,04 | 1,58 | 186 | 3664 | A | 010708 | 0 | OAS 27 | | |
| OBH 95 | 09:12,444 | 84:16,982 | 1,64 | 374 | 3629 | D | 000610 | -2 | OAS 18 | | |
| OBH 94 | 09:11,083 | 84:17,967 | 1,67 | 468 | 3624 | D | 980403 | -2 | OAS 13 | | |
| OBS 96 | 09:09,756 | 84:18,997 | 2,32 | 497 | 3614 | B | 000611 | -4 | OAS 75 | LG 01 (4,5 Hz) | |
| OBS 97 | 09:07,875 | 84:20,329 | 2,11 | 548 | 03B4+0355 | D | 971202 | -3 | HTI 202 | Owen 02 (4,5 Hz) | |
| OBS 98 | 09:06,187 | 84:21,581 | 2,31 | 649 | 03BA+0355 | C | 980401 | -4 | HTI 702 | Owen 14 (30 Hz) | |
| OBS 99 | 09:04,285 | 84:22,966 | 1,55 | 840 | 03BC+0355 | D | 000616 | -5 | HTI 101 | Owen 16 (30 Hz) | |
| OBS 100 | 09:03,013 | 84:23,927 | 1,51 | 1077 | 0386+0355 | D | 980402 | -4 | OAS 46 | Owen 21 (4,5 Hz) | |
| OBH 101 | 09:01,785 | 84:24,812 | 1,79 | 1157 | 6334 | D | 991247 | 0 | OAS 29 | | |
| OBH 102 | 09:00,351 | 84:25,876 | 1,70 | 1296 | 3609 | D | 980901 | +9 | HTI 902 | | |
| OBH 103 | 08:58,937 | 84:26,892 | 1,60 | 1429 | 039A+0355 | B | 000707 | -3 | OAS 22 | | |
| OBH 104 | 08:57,671 | 84:27,841 | 2,00 | 1614 | 3674 | C | 000614 | -5 | HTI 402 | | |
| | | | | | | | | | HTI 102 | | |
| | | | | | | | | | OAS 14 | | |
| | | | | | | | | | OAS 06 | | |
| OBH 105 | 08:56,043 | 84:29,050 | 2,13 | 1794 | 3659 | D | 991256 | -1 | OAS 30 | | |
| OBH 106 | 08:54,313 | 84:30,349 | | 1960 | 3669 | C | 991248 | -1 | OAS 02 | | |

| INST. | LAT (N) | LON (W) | Dist. To | DEPTH | REL. | ANT. | REC. | SKEW | SENSOR | Other Sensors | REMARKS |
|---|---|---|---|---|---|---|---|---|---|---|---|
| | D:M | D:M | Next (nm) | (m) | CODE | CH. | REC. | (ms) | HYDRO. | | |
| OBH 107 | 08:40.537 | 84:18.342 | 0,17 | 1837 | 0387+0355 | A | 980403 | -1 | OAS 38 | | 1000m anchor rope |
| OBH 108 | 08:40.290 | 84:18.499 | 0,18 | 1872 | 3664 | C | 010404 | 2 | OAS 27 | | |
| OBH 109 | 08:40.071 | 84:18.624 | 0,17 | 1938 | 3629 | D | 000610 | -5 | OAS 04 | | |
| OBH 110 | 08:39.925 | 84:18.717 | 0,20 | 1979 | 3624 | B | 010708 | 0 | OAS 13 | | |
| OBS 111 | 08:39.765 | 84:18.812 | 0,21 | 2043 | 3614 | B | 980401 | -2 | OAS 75 | Owen 18 (30 Hz) | |
| OBS 112 | 08:39.601 | 84:18.913 | 0,17 | 2107 | 03B4+0355 | C | 000611 | -2 | HTI 202 | Owen 02 (4.5 Hz) | |
| OBS 113 | 08:39.450 | 84:19.021 | 0,18 | 2127 | 03BA+0355 | C | 000616 | -4 | HTI 702 | Owen 22 (4.5 Hz) | |
| OBS 114 | 08:39.295 | 84:19.115 | 0,18 | 2162 | 03BC+0355 | D | 971202 | -2 | HTI 101 | Owen 16 (30 Hz) | |
| OBS 115 | 08:39.123 | 84:19.217 | 0,18 | 2204 | 0386+0355 | D | 980402 | -3 | OAS 46 | Owen 21 (4.5 Hz) | |
| OBH 116 | 08:39.003 | 84:19.294 | 0,17 | 2234 | 6334 | D | 991248 | -1 | OAS 29 | | |
| OBH 117 | 08:38.801 | 84:19.418 | 0,20 | 2294 | 3609 | C | 000707 | -2 | HTI 902 | | |
| OBH 118 | 08:38.644 | 84:19.516 | 0,20 | 2320 | 039A+0355 | D | 991247 | 0 | OAS 22 | | |
| OBH 119 | 08:38.504 | 84:19.605 | 0,25 | 2366 | 3674 | D | 000614 | -4 | HTI 402 | | |
| | | | | | | | | | HTI 002 | | |
| | | | | | | | | | OAS 14 | | |
| | | | | | | | | | OAS 06 | | |
| OBH 120 | 08:38.337 | 84:19.717 | 0,24 | 2385 | 3659 | B | 991256 | 0 | OAS 30 | | |
| OBH 121 | 08:38.203 | 84:19.809 | 5,40 | 2432 | 3669 | D | 980901 | 6 | OAS 02 | | 1000m anchor rope |
| OBH 122 | 08:34.808 | 84:17.358 | 0,85 | 2583 | 0397+0355 | C | 010708 | 0 | HTI 302 | | |
| OBS 123 | 08:35.249 | 84:18.047 | 0,79 | 2614 | 03B9+0355 | C | 991243 | 0 | OAS 31 | PMD 509 | |
| OBH 124 | 08:35.687 | 84:18.768 | 0,63 | 2635 | 039A+0355 | C | 010404 | 2 | OAS 22 | | |
| OBH 125 | 08:36.015 | 84:19.312 | 0,38 | 2617 | 3609 | D | 991248 | -1 | HTI 902 | | |
| OBS 126 | 08:36.183 | 84:19.657 | 0,55 | 2656 | 03BA+0355 | C | 980401 | -2 | HTI 702 | Owen 22 (4,5 Hz) | |
| OBH 127 | 08:36.469 | 84:20.154 | 0,62 | 2689 | 0398+0355 | D | 000711 | -1 | DPG 95 | | |
| OBS 128 | 08:36.827 | 84:20.664 | 0,75 | 2682 | 0386+0355 | C | 000611 | -2 | OAS 04 | Owen 21 (4,5 Hz) | |
| OBH 129 | 08:37.210 | 84:21.284 | 0,69 | 2702 | 6334 | B | 010402 | -1 | OAS 29 | | |
| OBH 130 | 08:37.528 | 84:21.888 | 0,65 | 2690 | 3624 | C | 000707 | -2 | OAS 03 | | |
| OBH 131 | 08:38.076 | 84:21.474 | 0,76 | 2573 | 4A44 | D | 000616 | -3 | OAS 18 | | |
| OBS 132 | 08:37.672 | 84:20.800 | 0,59 | 2594 | 03B4+0355 | C | 971202 | -1 | HTI 101 | Owen 02 (4,5 Hz) | |
| OBH 133 | 08:37.355 | 84:20.293 | 0,91 | 2617 | 03BB+0355 | A | 980402 | -1 | HTI 102 | | |
| OBH 134 | 08:36.897 | 84:19.506 | 0,83 | 2595 | 03B7+0355 | D | 010405 | 1 | OAS 08 | | |
| OBH 135 | 08:36.463 | 84:18.773 | 0,89 | 2519 | 3669 | C | 991247 | 0 | OAS 02 | | |
| OBS 136 | 08:35.948 | 84:17.956 | 0,88 | 2446 | 0399+0355 | D | 010401 | -1 | OAS 09 | PMD 540 | |
| OBH 137 | 8:35.521 | 84:17.260 | 2,49 | 2503 | 3659 | D | 980403 | 0 | OAS 30 | | |
| OBH 138 | 08:35.188 | 84:16.655 | | 2479 | 3674 | D | 000614 | -1 | HTI 002 | | |
| | | | | | | | | | HTI 402 | | |
| | | | | | | | | | OAS 14 | | |
| | | | | | | | | | OAS 34 | | |

| INST. | LAT (N) | LON (W) | DIST. TO | DEPTH | REL. | ANT. | REC. | SKEW | SENSOR | Other Sensors | REMARKS |
|---|---|---|---|---|---|---|---|---|---|---|---|
| | D:M | D:M | NEXT (nm) | (m) | CODE | CH. | REC. | (ms) | HYDRO. | | |
| OBH 142 | 10:20.969 | 86:07.899 | 1.08 | 207 | 3609 | B | 010404 | 1 | HTI 902 | | |
| OBH 143 | 10:20.262 | 86:08.681 | 1.08 | 302 | 3669 | D | 010708 | 1 | HTI 302 | | |
| OBH 144 | 10:19.542 | 86:09.433 | 1.08 | 401 | 0398+0355 | C | 000711 | -2 | DPG 95 | | |
| OBH 145 | 10:18.760 | 86:10.243 | 1.08 | 523 | 6334 | D | 000707 | -3 | OAS 22 | | |
| OBH 146 | 10:17.981 | 86:11.003 | 1.08 | 656 | 3659 | D | 991256 | | OAS 30 | | no data |
| OBH 147 | 10:17.209 | 86.11.792 | 1.08 | 804 | 3674 | D | 000614 | -4 | HTI 002 | | |
| | | | | | | | | | HTI 402 | | |
| | | | | | | | | | OAS 14 | | |
| | | | | | | | | | OAS 34 | | |
| OBH 148 | 10:16.465 | 86:12.560 | 1.08 | 927 | 03B2+0355 | C | 991248 | -2 | HTI 602 | | OBS frame |
| OBH 149 | 10:15.692 | 86:13.383 | 1.08 | 1033 | 03B1+0355 | D | 991252 | -5 | HTI 802 | | OBS frame |
| OBH 150 | 10:14.943 | 86:14.094 | 1.08 | 1153 | 3624 | D | 980901 | 10 | OAS 13 | | |
| OBH 151 | 10:14.161 | 86:14.923 | 1.08 | 1337 | 4A44 | C | 991238 | -1 | OAS 18 | | |
| OBS 152 | 10:13.402 | 86:15.681 | 1.08 | 1546 | 039A+0355 | D | 010401 | -5 | OAS 31 | PMD 509 | |
| OBS 153 | 10:12.652 | 86:16.504 | 1,08 | 1701 | 3629 | C | 000610 | -9 | HTI 502 | Owen 14 (30 Hz) | OBS-design 2002 |
| OBS 155 | 10:11.933 | 86:17.267 | 1,08 | 1878 | 0386+0355 | C | 971202 | -4 | OAS 04 | Owen 21 (4.5 Hz) | |
| OBS 157 | 10:11.149 | 86:18.016 | 1.08 | 2072 | 03BC+0355 | C | 980401 | -5 | HTI 202 | Owen 16 (30 Hz) | |
| OBS 158 | 10:10.347 | 86:18.767 | 1.08 | 2224 | 3614 | A | 000611 | -5 | OAS 75 | Owen 18 (30 Hz) | |
| OBS 159 | 10:09.599 | 86:19.572 | 1,08 | 2399 | 0399+0355 | B | 991243 | 0 | OAS 09 | PMD 540 | |
| OBH 160 | 10:08.843 | 86:20.330 | 1.08 | 2583 | 0397+0355 | D | 000706 | 5 | HTI 102 | | |
| OBH 161 | 10:08.120 | 86:21.173 | 1.08 | 2732 | 3664 | D | 980401 | -2 | OAS 27 | | 1000 m anchor rope |
| OBH 162 | 10:14.241 | 86:19.563 | 1.08 | 1919 | 3659 | B | 010404 | 1 | OAS 30 | | |
| OBS 154 | 10:13.430 | 86:18:820 | 1,08 | 1902 | 03B4+0355 | C | 000101 | -4 | HTI 101 | Owen 02 (4.5 Hz) | west of line P32 |
| OBH 163 | 10:12.709 | 86:18.055 | 1,08 | 1886 | 3674 | D | 000614 | -2 | HTI 002 | | |
| | | | | | | | | | HTI 402 | | |
| | | | | | | | | | OAS 14 | | |
| | | | | | | | | | OAS 34 | | |
| OBS 155 | 10:11.933 | 86:17.267 | 1,08 | 1878 | 0386+0355 | C | 971202 | -4 | OAS 04 | Owen 21 (4.5 Hz) | |
| OBH 164 | 10:11.137 | 86:16.530 | 1,08 | 1841 | 6334 | D | 010708 | 1 | OAS 22 | | |
| OBS 156 | 10:10.361 | 86:15.749 | 1,08 | 1906 | 03BA+0355 | D | 000616 | -9 | HTI 702 | Owen 22 (4.5 Hz) | east of line P32 |
| OBH 165 | 10:09.576 | 86:14.940 | | 1993 | 3669 | D | 000707 | -3 | HTI 302 | | |

| INST. | LAT (N) | LON (W) | DIST. TO | DEPTH | REL. | ANT. | REC. | SKEW | SENSOR | Other Sensors | REMARKS |
|---|---|---|---|---|---|---|---|---|---|---|---|
| | D:M | D:M | NEXT (nm) | (m) | CODE | CH. | REC. | (ms) | HYDRO. | | |
| OBS 171 | 10:18,867 | 86:17,649 | 0,40 | 1481 | 0398+0355 | D | 991248 | -1 | OAS 13 | Owen 02 (4,5Hz) | no data |
| OBH 167 | 10:17,691 | 86:18,496 | 0,44 | 1570 | 3669 | B | 991252 | 0 | HTI 302 | | |
| OBH 168 | 10:18,002 | 86:18,265 | 0,40 | 1525 | 6334 | D | 000711 | 0 | DPG 95 | | |
| OBH 169 | 10:18,348 | 86:18,001 | 0,43 | 1591 | 3664 | C | 991238 | 0 | OAS 27 | | |
| OBH 170 | 10:18,610 | 86:17,799 | 0,34 | 1533 | 0397+0355 | D | 010708 | 0 | HTI 102 | | |
| OBH 166 | 10:17,323 | 86:18,747 | 0,28 | 1686 | 03B4+0355 | A | 000708 | -1 | HTI 101 | | |
| OBS 172 | 10:18,873 | 86:17,603 | | 1470 | 039A+0355 | D | 991243 | 0 | OAS 31 | PMD 509 | |
| | | | | | | | | | | | |
| OBH 173 | 09:26.944 | 85:39.277 | 0.11 | 2389 | 0398+0355 | C | 980901 | 7 | OAS 01 | | 500m anchor rope |
| OBH 186 | 09:27.019 | 85:39.236 | 0.11 | 2375 | 0397+0355 | D | 991256 | -2 | HTI 102 | | |
| OBH 187 | 09:27.089 | 85:39.136 | 0.11 | 2351 | 3664 | A | 980403 | -1 | OAS 27 | | |
| OBS 176 | 09:27.171 | 85:39.072 | 0.11 | 2325 | 3614 | B | 000616 | -6 | OAS 75 | Owen 18 (30 Hz) | |
| OBS 177 | 09:27.266 | 85:38.998 | 0.11 | 2311 | 03BC+0355 | D | 000611 | -3 | HTI 202 | Owen 16 (30 Hz) | |
| OBH 178 | 09:27.331 | 85:38.930 | 0.24 | 2323 | 3669 | D | 991238 | -1 | HTI 302 | | |
| OBH 179 | 09:27.570 | 85:39.018 | 0.11 | 2332 | 3674 | C | 000614 | -5 | OAS 14 | | offline |
| | | | | | | | | | OAS 34 | | |
| | | | | | | | | | HTI 002 | | |
| | | | | | | | | | HTI 402 | | |
| OBS 180 | 09:27.498 | 85:38.932 | 0.11 | 2335 | 03B4+0355 | C | 991252 | -3 | HTI 101 | Owen 02 (4.5 Hz) | offline |
| OBH 181 | 09:27.420 | 85:38.856 | 0.11 | 2328 | 3659 | B | 991248 | -1 | OAS 30 | | |
| OBH 182 | 09:27.355 | 85:38.775 | 0.11 | 2323 | 4A44 | C | 010404 | 3 | OAS 18 | | offline |
| OBS 183 | 09:27.268 | 85:38.688 | 0.24 | 2322 | 0386+0355 | C | 971202 | -3 | OAS 46 | Owen 21 (4.5 Hz) | offline |
| OBS 175 | 09:27.490 | 85:38.780 | 0.11 | 2324 | 03BA+0355 | C | 980402 | -4 | HTI 702 | Owen 22 (4.5 Hz) | |
| OBS 185 | 09:27.557 | 85:38.685 | 0.11 | 2318 | 0399+0355 | D | 010703 | 0 | OAS 09 | LG 01 | |
| OBS 174 | 09:27.666 | 85:38.618 | 0.11 | 2319 | 039A+0355 | C | 991243 | 0 | OAS 31 | PMD 509 | |
| OBS 184 | 09:27.740 | 85:38.557 | 0.11 | 2304 | 3629 | D | 000610 | -7 | HTI 502 | Owen 14 (30 Hz) | OBS design 2002 |
| OBH 188 | 09:27.813 | 85:38.494 | 0.11 | 2307 | 3624 | D | 000706 | 3 | OAS 22 | | |
| OBH 189 | 09:27.903 | 85:38.403 | 0.11 | 2300 | 3609 | D | 010401 | -4 | HTI 902 | | |
| OBH 190 | 09:27.976 | 85:38.345 | 0.11 | 2281 | 0387+0355 | C | 980401 | -4 | OAS 38 | | |
| OBH 192 | 09:28.070 | 85:38.255 | 0.11 | 2283 | 03BA+0355 | D | 010708 | 0 | HTI 802 | | OBS-frame |

| Line | Shot Number | Date | Time UTC | Latitude N | Longitude W | Trigger interval [s] | Gun type | Remarks |
|---|---|---|---|---|---|---|---|---|
| P 1 | 1 | 23.04.02 | 14:05:38 | 09:40,960 | 85:53,952 | 30 | 32 L | at 9.4m depth |
| | 121 | 23.04.02 | 15:05:19 | 09:38,342 | 85:52,156 | | | |
| | | | | | | | | |
| P 2 | 1 | 23.04.02 | 15:20:41 | 09:38,342 | 85:52,156 | 30 | 32 L | at 7.5m depth |
| | 172 | 23.04.02 | 16:46:10 | 09:41,193 | 85:54,195 | | | |
| | | | | | | | | |
| P 3 | 1 | 23.04.02 | 17:03:15 | 09:42,097 | 85:54,87 | 30 | 32 L | at 5.5m depth |
| | 196 | 23.04.02 | 18:40:52 | 09:38,342 | 85:52,156 | | | |
| | | | | | | | | |
| P 4 | 1 | 23.04.02 | 18:56:20 | 09:37,655 | 85:51,681 | 30 | 32 L | at 3.5m depth |
| | 176 | 23.04.02 | 20:23:45 | 09:41,211 | 85:54,162 | | | |
| | | | | | | | | |
| P 5 | 1 | 23.04.02 | 20:37:45 | 09:41,950 | 85:54,682 | 30 | 32 L | at 12.5m depth |
| | 202 | 23.04.02 | 22:17:56 | 09:38,223 | 85:52,061 | | | |
| | | | | | | | | |
| P 6 | 1 | 23.04.02 | 22:28:40 | 09:37,758 | 85:51,755 | 30 | 32 L | at 14.5m depth |
| | 177 | 23.04.02 | 23:56:42 | 09:41,527 | 85:54,418 | | | |
| | | | | | | | | |
| P 9 | 1 | 26.04.02 | 00:10:47 | 09:39,630 | 85:18,776 | 60 | 32 L | |
| | 1224 | 26.04.02 | 20:33:00 | 08:33,563 | 86:10,591 | | | |
| | | | | | | | | |
| P 10 | 1 | 26.04.02 | 21:06:00 | 08:33,553 | 86:09,592 | 60 | G-Gun cluster | |
| | 895 | 27.04.02 | 12:00:46 | 09:34,740 | 85:22,500 | | | |
| | | | | | | | | |
| P 11 | 1 | 27.04.02 | 16:51:28 | 09:17,160 | 85:36,327 | 20 | sb+ps G-Gun | first shot both |
| | 40 | 27.04.02 | 17:04:29 | | | | | last shot both |
| | 41 | 27.04.02 | 17:04:49 | | | 20 | sb G-Gun | first shot sb |
| | 52 | 27.04.02 | 17:08:25 | | | | | last shot sb |
| | 53 | 27.04.02 | 17:08:45 | | | 20 | ps G-Gun | first shot ps |
| | 64 | 27.04.02 | 17:12:45 | | | | | last shot ps |
| | 65 | 27.04.02 | 17:13:05 | | | 20 | sb+ps G-Gun | first shot both |
| | 76 | 27.04.02 | 17:17:05 | | | | | last shot both |
| | 77 | 27.04.02 | 17:17:25 | | | 20 | sb G-Gun | first shot sb |
| | 88 | 27.04.02 | 17:21:25 | 09:15,674 | 85:37,646 | | | last shot sb |

| Line | Shot Number | Date | Time UTC | Latitude N | Longitude W | Trigger interval [s] | Gun type | Remarks |
|---|---|---|---|---|---|---|---|---|
| P 12 | 1 | 27.04.02 | 17:41:06 | 09:16,393 | 85:35,530 | 20 | sb+ps G-Gun | first shot both |
| | 72 | 27.04.02 | 18:04:45 | | | 20 | ps G-Gun | first shot ps |
| | 84 | 27.04.02 | 18:08:45 | | | 20 | sb G-Gun | first shot sb |
| | 96 | 27.04.02 | 18:12:45 | | | 20 | sb+ps G-Gun | first shot both |
| | 108 | 27.04.02 | 18:16:45 | | | 20 | ps G-Gun | first shot ps |
| | 120 | 27.04.02 | 18:20:45 | | | 20 | sb G-Gun | first shot sb |
| | 132 | 27.04.02 | 18:24:48 | 09:15,834 | 85:36,540 | 20 | sb+ps G-Gun | first shot both |
| | | | | | | | | |
| | | | | | | | | |
| P 13 | 1 | 27.04.02 | 18:37:25 | 09:15,413 | 85:35,875 | 20 | sb+ps G-Gun | first shot both |
| | 79 | 27.04.02 | 19:03:25 | | | 20 | ps G-Gun | first shot ps |
| | 91 | 27.04.02 | 19:07:25 | | | 20 | sb G-Gun | first shot sb |
| | 103 | 27.04.02 | 19:11:25 | | | 20 | sb+ps G-Gun | first shot both |
| | 115 | 27.04.02 | 19:15:25 | | | 20 | ps G-Gun | first shot ps |
| | 126 | 27.04.02 | 19:19:08 | 09:17,337 | 85:36,683 | | | last shot ps |
| | | | | | | | | |
| P 14 | 1 | 27.04.02 | 20:00:48 | 09:17,750 | 85:36, 044 | 20 | ps G-Gun+32 L | first shot ps+32 L |
| | 13 | 27.04.02 | 20:04:48 | | | 20 | sb G-Gun+32 L | first shot sb+32 L |
| | 25 | 27.04.02 | 20:08:48 | | | 20 | sb+ps G-Gun+32 L | first shot both+32 L |
| | 37 | 27.04.02 | 20:11:48 | | | 20 | ps G-Gun+32 L | first shot ps+32 L |
| | 49 | 27.04.02 | 20:16:48 | | | 20 | sb G-Gun+32 L | first shot sb+32 L |
| | 61 | 27.04.02 | 20:20:48 | | | 20 | sb+ps G-Gun+32 L | first shot both+32 L |
| | 73 | 27.04.02 | 20:24:48 | | | 20 | ps G-Gun+32 L | first shot ps+32 L |
| | 85 | 27.04.02 | 20:38:48 | | | 20 | sb G-Gun+32 L | first shot sb+32 L |
| | 97 | 27.04.02 | 20:32:48 | | | 20 | sb+ps G-Gun+32 L | first shot both+32 L |
| | 100 | 27.04.02 | 20:33:48 | | | 20 | ps+sb G-Gun+32 L | last shot both+32 L |
| | 108 | 27.04.02 | 20:36:28 | 09:15,831 | 85:37,421 | | | last shot profile |
| | | | | | | | | |
| P 15 | 1 | 29.04.02 | 17:46:48 | 08:44,004 | 84:34,871 | 30 | G-Gun cluster | |
| | 1304 | 30.04.02 | 04:44:00 | 09:17,417 | 84:10,404 | | | |
| | | | | | | | | |
| P 16 | 1 | 30.04.02 | 05:42:42 | 09:15,800 | 84:11,446 | 30 | sb G-Gun+32 L | first shot sb+32 L |
| | 147 | 30.04.02 | 06:55:31 | 09:11,951 | 84:14,242 | | | last shot sb+32 L |
| | 148 | 30.04.02 | 07:25:27 | 09:10,304 | 84:15,501 | 30 | 32 L | first shot 32 L |
| | 973 | 30.04.02 | 15:31:30 | 08:44,20 | 84:37,324 | | | last shot 32 L |

| Line | Shot Number | Date | Time UTC | Latitude N | Longitude W | Trigger interval [s] | Gun type | Remarks |
|---|---|---|---|---|---|---|---|---|
| P 17 | 1 | 02.05.02 | 13:36:58 | 08:51,360 | 84:08,571 | 30 | G-Gun cluster | |
| | 1092 | 02:05:02 | 22:42:27 | 09:08,358 | 84:35,869 | | | |
| | | | | | | | | |
| P 18 | 1 | 02.05.02 | 23:09:30 | 09:08,678 | 84:35,936 | 30 | 32 L | |
| | 1048 | 03.05.02 | 07:43:00 | 08:52,285 | 84:10,007 | | | |
| | | | | | | | | |
| P 19 | 1 | 04.05.02 | 03:07:08 | 08:52,346 | 84:14,907 | 10 | Prakla-array | |
| | 2443 | 04.05.02 | 09:54:00 | 09:05,044 | 84:35,040 | | | |
| | | | | | | | | |
| P 20 | 1 | 04.05.02 | 09:5315 | 09:02,320 | 84:37,254 | 10 | Prakla-array | first shot A |
| | 457 | 04.05.02 | 11:09:30 | 09:01,430 | 84:37,251 | | | last shot A |
| | 458 | 04.05.02 | 11:57:16 | 09:01,500 | 84:37,250 | | | first shot B |
| | 566 | 04.05.02 | 12:15:23 | 09:02,500 | 84:37,256 | | | last shot B |
| | | | | | | | | |
| P 21 | 1 | 04.05.02 | 13:10 | 09:05,100 | 84:35,290 | 30 | 32 L | |
| | 876 | 04.05.02 | 20:28 | 08:51,547 | 84:13,282 | | | |
| | | | | | | | | |
| | | | | | | | | |
| | | | | | | | | |
| P 22 | 1 | 04.05.02 | 21:08:18 | 08:51,631 | 84:13,614 | 30 | G-Gun cluster | |
| | 604 | 05.05.02 | 04:09:38 | 09:05,058 | 84:35,075 | | | |
| | | | | | | | | |
| P 23 | 1 | 05.05.02 | 04:58:11 | 09:05,056 | 84:35,001 | 30 | 32 L | |
| | 227 | 05.05.02 | 06:45:13 | 09:01,405 | 84:28,902 | | | stop |
| | 228 | 05.05.02 | 07:16:22 | 09:00,826 | 84:28,232 | 30 | G-Gun cluster | start again |
| | 816 | 05.05.02 | 12:10:08 | 08:51,620 | 84:13,524 | | | |
| | | | | | | | | |
| P 24 | 1 | 06.05.02 | 10:02:51 | 08:44,766 | 84:37,413 | 30 | G-Gun cluster | |
| | 1443 | 06.05.02 | 22:03:51 | 09:18,635 | 84:12,431 | | | |
| | | | | | | | | |
| P 25 | 1 | 06.05.02 | 22:36:21 | 09:18,475 | 84:12,365 | 30 | G-Gun cluster+32 L | |
| | 1610 | 07.05.02 | 12:00:50 | 08:45,471 | 84:36,618 | | | |
| | | | | | | | | |
| P 26 | 1 | 08.05.02 | 06:00:16 | 08:34,988 | 84:21,426 | 10 | Prakla -7 guns | |
| | 137 | 08.05.02 | 06:23:00 | 08:35,899 | 84:21,222 | | Prakla -6 guns | |
| | 1465 | 08.05.02 | 10:04:16 | 08:42,814 | 84:16,922 | | | |

| Line | Shot Number | Date | Time UTC | Latitude N | Longitude W | Trigger interval [s] | Gun type | Remarks |
|---|---|---|---|---|---|---|---|---|
| P 27 | 1 | 08.05.02 | 10:46:50 | 08:43,207 | 84:16,609 | 10 | G-Gun cluster | |
| | 1819 | 08.05.02 | 15:48:10 | 08:35,762 | 84:21,297 | | | |
| | | | | | | | | |
| P 28 | 1 | 08.05.02 | 15:48:20 | 08:35,762 | 84:21,297 | 20 | G-Gun cluster | |
| | 686 | 08.05.02 | 19:36:12 | 08:42,792 | 84:16,929 | | | |
| | | | | | | | | |
| | | | | | | | | |
| P 29 | 1 | 08.05.02 | 20:51:20 | 08:39,800 | 84:18,598 | 20 | 1 ps G-Gun | first shot 1ps |
| | | | 20:53:20 | | | | 2 ps G-Gun | first shot 2ps |
| | | | 20:55:20 | | | | 1 sb G-Gun | first shot 1sb |
| | | | 20:57:00 | | | | 2 sb G-Gun | first shot 2sb |
| | | | 20:58:40 | | | | 2 ps+2 sb G-Gun | first shot 2 ps+2 sb |
| | | | 21:00:20 | | | | 1 ps+1 sb G-Gun | first shot 1 ps+1 sb |
| | | | 21:02:00 | | | | 2 ps+1 sb G-Gun | first shot 2 ps+1 sb |
| | | | 21:03:40 | | | | 1 ps+2 sb G-Gun | first shot 1 ps+2 sb |
| | 40 | 08.05.02 | 21:04:08 | 08:39,478 | 84:19,148 | | | last shot profile |
| | | | | | | | | |
| P 30 | 1 | 11.05.02 | 07:05:04 | 08:33,576 | 84:14,000 | 20 | G-Gun cluster | |
| | 741 | 11.05.02 | 11:11:44 | 08:38,880 | 84:22,951 | | | |
| | | | | | | | | |
| P 31 | 1 | 11.05.02 | 11:31:04 | 08:38,171 | 84:22,985 | 20 | G-Gun cluster | |
| | 613 | 11.05.02 | 14:55:00 | 08:33,710 | 84:15,147 | | | |
| | | | | | | | | |
| P 32 | 1 | 13.05.02 | 00:33:17 | 09:41,677 | 86:48,186 | 60 | G-Gun cluster+32 L | |
| | 955 | 13.05.02 | 16:27:16 | 10:31,585 | 85:56,966 | | | |
| | | | | | | | | |
| P 33 | 1 | 13.05.02 | 23:12:45 | 10:07,772 | 86:13,176 | 10 | ps G-Gun | |
| | 320 | 14.05.02 | 01:50:15 | 10:16,171 | 86:21,501 | | | |
| | | | | | | | | |
| P 34 | 1 | 14.05.02 | 18:51:10 | 10:19,984 | 86:16,796 | 10 | sb G-Gun | |
| | 511 | 14.05.02 | 20:16:09 | 10:16,732 | 86:19,262 | | | |
| | | | | | | | | |
| P 35 | 1 | 15.05.02 | 18:14:35 | 09:31,018 | 85:42,630 | 60 | G-Gun cluster | |
| | 122 | 15.05.02 | 20:15:22 | 09:25,158 | 85:35,606 | | | |
| | | | | | | | | |
| P 36 | 1 | 15.05.02 | 20:16:22 | 09:25,158 | 85:35,606 | 60 | G-Gun cluster | |
| | 171 | 15.05.02 | 23:06:22 | 09:35,902 | 85:31,144 | | | |

| Line | Shot Number | Date | Time UTC | Latitude N | Longitude W | Trigger interval [s] | Gun type | Remarks |
|---|---|---|---|---|---|---|---|---|
| P 37 | 1 | 15.05.02 | 23:06:22 | 09:35,902 | 85:31,144 | 60 | G-Gun cluster | |
| | 678 | 16.05.02 | 10:24:21 | 08:59,333 | 86:04,947 | | | |
| | | | | | | | | |
| P 38 | 1 | 17.05.02 | 14:53:24 | 09:00,413 | 84:35,406 | 60 | G-Gun cluster | first shot G-Gun |
| | 22 | 17.05.02 | 15:14:25 | 09:00,968 | 84:35,884 | | G-Gun+32 L | first shot G-Gun+32 L |
| | 368 | 17.05.02 | 21:00:19 | 09:22,398 | 84:53,977 | | | |
| | | | | | | | | |
| P 39 | 1 | 17.05.02 | 21:41:19 | 09:21,168 | 84:55,528 | 60 | G-Gun cluster+32 L | |
| | 324 | 18.05.02 | 03:04:19 | 08:55,535 | 84:59,499 | | | |
| | | | | | | | | |
| P 40 | 1 | 18.05.02 | 03:30:19 | 08:54,384 | 84:58,616 | 60 | G-Gun cluster+32 L | |
| | 527 | 18.05.02 | 12:16:18 | 09:31,480 | 84:41,472 | | | |
| | | | | | | | | |

Appendix 9.7.1

# F.S. "S O N N E" Reise SO 163/1

| Eingesetzte Geräte | | Einsätze |
|---|---|---|
| OBH/ OBS | Ocean Bottom Hydrophones / Seismograph | 10 ausgelegt |
| TOBI | Towed Ocean Bottom Investigation Vehicle | |
| DTS | tiefgeschelepptes Sidescan Sonar | |
| PSD | POSIDONIO Transpondersystem zur Ortung des TOBI | |
| MAG | Magnetometer | |
| EM | SIMRAD-Fächerlot | |
| OFOS | Ocean Floor Observation System | 26 |
| GTV-A | Fernsehgreifer Typ A | 09 |

**Vermessen wurden :**

| | | |
|---|---|---|
| Mit EM | 897 | sml |
| Mit TOBI | 494 | sml |
| Mit DTS | 321 | sml |
| Mit OFOS | 052 | sml |
| Mit MAG | 612 | sml |

**Eingesetzte Winden :**

| *Winde* | *D/M* | *Typ* | *RF-Nr* | *SO 163/1 Einsatz* | *Gesamt Einsatz* | *SO 163/1 S`länge* | *Gesamt S`länge* | *Zust.* |
|---|---|---|---|---|---|---|---|---|
| W 1 | 18,2 | LWL | 812001 | 0000 h | 0000 h | 000000 m | 0000000 m | 1 |
| W 2 | 18,2 | LWL | 810001 | 0618 | 0942 | 093688 | 0199774 | 3 |
| W 4 | 11,0 | NSW | 819052 | 0000 | 0000 | 000000 | 0000000 | 1 |
| W 5 | 11,0 | NSW | 817164 | 0003 | 0228 | 002100 | 0194453 | 4 |
| W 6 | 18,2 | DRAKO | 814150 | 0002 | 2132 | 001750 | 1856443 | 3 |

| *Winde* | *SO 163/1 gefierte max.Länge* | *jemals gefierte max.Länge* | |
|---|---|---|---|
| W 1 | 0000 m | 0000 m | |
| W 2 | 7202 | 7202 | |
| W 4 | 0000 | 0000 | |
| W 5 | 2100 | 5200 | |
| W 6 | 1750 | 7900 | ( SL aktuell = 6456 m ) |

**Geräteverluste :**
Keine

**Abkürzungen im Stationsprotokoll:**

| | |
|---|---|
| z.W. | zu Wasser |
| a.D. | an Deck |
| Boko | Bodenkontakt |
| Bosi | Bodensicht |
| SL(max.) | (maximale)Seillänge |
| LT | Lottiefe nach Hydrosweep |
| W x | eingesetzte Winde |
| SM | Simrad- Multibeam-Lot |
| PS | Parasound |
| XPNDR | Transponder |

**Zeit : UTC – 05 Stunden**

**15.03.02**

Profil EM-01 v = 10,0 kn

| | | | |
|---|---|---|---|
| 1036 – 1050 | bringen Magnetometer aus | | |
| 1050 | Beginn Profil | 07 31,91 N 83 01,31 W | |
| | Kurs = 298 Grad | | |
| 1409 | ä.K. auf 296 Grad | 07 45,00 N 83 30,00 W | 22 sml |
| 2124 | ä.K. auf 318 Grad | 08 17,44 S 84 55,81 W | 73 sml |
| 2128 | stellen Uhren 20 Minuten zurück | | |
| 2400 | 08 37,84 N 84 54,78 W | | |

**16.03.02**

| | | | |
|---|---|---|---|
| 0003 | stellen Uhren 20 Minuten zurück | | |
| 0430 | stellen Uhren 20 Minuten zurück | | |
| 0656 | Ende Profil | 09 39,50 N 85 51,57 W | 111 sml |
| 0703 | Beginn Einholen Magnetometer | | |
| 0713 | Magnetometer a:D. | | |

**Bordzeit : UTC – 6 Stunden**

Releaser-Teststation W 6

| | | | |
|---|---|---|---|
| 0729 | Beginn Station | LT = 1857 m | 09 39,55 N 85 51,56 W |
| 0731 | 3 Releaser z.W. | | |
| 0825 | Slmax = 1750 m | LT = 1860 m | |
| 0825 – 0827 | Releasertest per Transducer | | |
| 0827 | Beginn hieven | | |
| 0904 | Releaser a.D./ Ende Station | | |

Auslegung OBH/S 1-10

| | | | |
|---|---|---|---|
| 0920 | OBH 1 z.W. | LT = 1866 m | 09 39,46 N 85 51,50 W |
| 0946 | OBH 2 z.W. | LT = 1924 m | 09 40,60 N 85 53,70 W |
| 1017 | OBH 3 z.W. | LT = 2065 m | 09 38,14 N 85 53,49 W |
| 1037 | OBH 4 z.W. | LT = 1997 m | 09 38,85 N 85 52,51 W |
| 1056 | OBH 5 z.W. | LT = 1940 m | 09 39,91 N 85 52,80 W |
| 1112 | OBH 6 z.W. | LT = 1980 m | 09 39,39 N 85 53,58 W |
| 1132 | OBH 7 z.W. | LT = 1999 m | 09 39,09 N 85 53,11 W |
| 1143 | OBH 8 z.W. | LT = 1970 m | 09 39,45 N 85 52,54 W |
| 1204 | OBH 9 z.W. | LT = 1963 m | 09 39,69 N 85 53,10 W |
| 1226 | OBH 10 z.W. | LT = 1893 m | 09 39,46 N 85 52,90 W |

Station 03 CTD W 5

| | | | |
|---|---|---|---|
| 1308 | Beginn Station | LT = 2093 m | 09 38,28 N 85 53,91 W |
| 1310 | CTD z.W. | | |
| 1322 | CTD a.D. | | |
| 1339 | CZD z.W. | LT = 2100 m | 09 38,39 N 85 53,87 W |
| 1414 | POSIDONIA-Transducer im Loschacht abgesenkt | | |
| 1418 | Slmax = 1900 m | LT =2069 m | 09 38,36 N 85 53,68 W |
| 1501 | CTD a.D. / Ende Station | | 09 38,06 N 85 53,47 W |

Kalibrierung POSIDONIA

| | | | |
|---|---|---|---|
| 1518 | OBH-K z.W. | LT = 2089 m | 09 38,31 85 53,89 W |
| 1700 | POSIDONIA ausgefallen | | |
| 1731 | OBH-K ausgelöst 1747 aufgetaucht 1757 a.D. 09 38,24 N 85 53,58 W | | |

Profile EM-02 und 03 v= 10,0 kn

| | |
|---|---|
| 1815 | Beginn Aussetzen Magnetometer |

| | | | |
|---|---|---|---|
| 1820 | Beginn EM 02 | 09 38,28 N 85 53,91 W | |
| 1826 | Magnetometer ausgesteckt | l = 250 m | |
| 2009 | ä.K. auf 322 Grad | 09 50,02 N 85 44,36 W | 15 sml |
| 2104 | ä.K. auf 219 | 09 56,33 N 85 49,19 W | 09 sml |
| 2115 | ä.K. auf 144 | 09 55,40 N 85 50,23 W | 01 sml |
| 2156 | ä.K. 244 | 09 49,91 N 85 46,39 W | 07 sml |
| 2207 | ä.K. 327 | 09 49,06 N 85 47,87 W | 02 sml |
| 2314 | ä.K. 041 | 09 58,39 N 85 53,91 W | 11 sml |
| 2344 | ä.K. 306 | 10 00,98 N 85 51,69 W | 04 sml |
| 2400 | Profilwechsel EM 02/03 | 10 03,20 N 85 54,60 W | 04 sml |
| **17.03.02** | | | |
| 0035 | ä.K. 292 | 10 08,07 N 85 58,54 w | 06 sml |
| 0045 | ä.K. 139 | 10 07,22 N 85 59,72 W | 02 sml |
| 0123 | ä.K. 216 | 10 02,41 N 85 55,76 W | 06 sml |
| 0133 | ä.K. 320 | 10 01,13 N 85 56,75 W | 02 sml |
| 0232 | ä.K. 233 | 10 08,53 N 86 02,58 W | 10 sml |
| 0245 | ä.K. 141 | 10 07,32 N 86 04,70 W | 02 sml |
| 0346 | ä.K. 234 | 09 59,36 N 85 58,49 W | 10 sml |
| 0404 | ä.K. 322 | 09 57,57 N 86 00,86 W | 03 sml |
| 0512 | ä.K. 047 | 10 06,38 N 86 07,83 W | 11 sml |
| 0602 | ä.K. 322 | 10 12,01 N 86 01,80 W | 08 sml |
| 0740 | v = 7,0 kn | | |
| 0807 | ä.K. 050 | 10 28,10 N 86 13,85 W | 20 sml |
| 0821 | ä.K. 142 | 10 28,93 N 86 12,81 W | 01 sml |
| 1050 | Ende Profil EM 03 | | |
| 1056 – 1106 | holen Magnetometer ein | | |

Profile TOBI 01 – xxv = 2,5 kn W 2

| | | | |
|---|---|---|---|
| 1135 | Beginn aussetzen TOBI | | |
| 1136 | TOBI z.W. | | |
| 1211 | Depressor z.W. Beginn Profil 01 | 10 12,15 N 86 02,54 W | |
| | Kurs = 318 Grad fieren bis SL = 100 m | | |
| 1229 | v = 2,5 kn | | |
| 1240 – 1248 | fieren auf SL = 202 m | | |
| 1256 | Magnetometer z.W. SL = 30 m | | |
| 1559 – 1604 | holen Magnetometer ein | | |
| 1800 | SL = 506 m | 10 22,75 N 86 13,63 W | |
| 2400 | SL = 326 m LT = 591 m | 10 34,76 N 86 24,55 W | |
| **18.03.02** | | | |
| 0047 | Abbruch Profil | 10 36,50 N 86 26,12 W | 35 sml |
| 0051 | hieven auf SL = 200 m | | |
| 0057 | ä.K. auf 300 Grad v = 2,0 kn warten auf Tageslicht | | |
| 0611 | hieven SL = 200 m LT = 990 m | 10 40,91 N 86 34,76 W | |
| 0622 | Depressor a.D. Check der Kabelverbiindung | | |
| 0710 | Beginn Einholen TOBI | | |
| 0808 | TOBI a.D. | | |

Profil EM-04 v = 6,0 kn

| | | | |
|---|---|---|---|
| 0936 | Beginn Profil Kurs = 21 Grad | 10 41,92 N 86 34,92 W | |
| 1029 | ä.K. 270 Grad | 10 45,91 N 86 32,67 W | 4 sml |
| 1058 | ä.K. 137 | 10 46,07 N 86 35,79 W | 3 sml |
| 1245 | Ende Profil | 10 38,75 N 86 29,18 W | 10 sml |

Profil EM-05 v = 6,0 kn

| | | |
|---|---|---|
| 1323 | Beginn Profil Kurs = 324 Grad | 10 37,32 N 86 36,00 W |
| 1329 | Magnetometer z.W. SL = 250 m | |

| | | | | |
|---|---|---|---|---|
| 1510 | ä.K. 090 | | 10 45,94 N 86 42,46 W | 11 sml |
| 1522 | ä.K. 124 | | 10 46,26 N 86 41,54 W | 01 sml |
| 1612 | Magnetometer a.D. | | | |
| 1613 | Ende Profil | | 10 42,43 N 86 36,84 W | 06 sml |

Profil TOBI 02 - xx W 2

| | | | | | |
|---|---|---|---|---|---|
| 1623 | Beginn Aussetzen | | | 10 42,48 N 86 37,01 W | |
| 1626 | TOBI z.W. | | | | |
| 1704 | Depressor z.W. | LT = 1036 m | | 10 42,68 N 86 36,41 W | |
| | Kurs 137 Grad | v = 2,5 kn fieren W 2 | | | |
| 1800 | Beginn Profil 2 | SL = 755 m | LT = 976 m | 10 41,60 N 86 34,60 W | |
| 2352 | | SL = 931 m | LT = 974 m | 10 32,02 N 86 24,00 W | |
| **19.03.02** | | | | | |
| 0243 | | SL = 1518m | LT = 1284 m | | |
| 0600 | | SL = 999 m | LT = 986 m | 10 18,52 N 86 13,51 W | |
| 0924 | Ende Profil 2 | SL = 610 m | LT = 914 m | 10 12,31 N 86 07,92 W | 39 sml |
| 0924 – 1947 | Schleife über Stb | | | | |
| 1047 | Beginn Profil 03 | SL = 794 m | LT = 1179 m | 10 10,68 N 86 09,98 W | |
| | Kurs = 318 Grad | v = 2,5 kn | | | |
| 1200 | | SL = 1631 m | LT = 1129 m | 10 13,02 N 86 12,09 W | |
| 1600 | | SL = 2255 m | LT = 1552 m | 10 20,59 N 86 18,92 W | |
| 2020 | | SL = 1712 m | LT = 1192 m | 10 28,85 N 86 26,34 W | |
| 2400 | | SL = 1713 m | LT = 1280 m | 10 35,51 N 86 32,36 W | |
| **20.03.02** | | | | | |
| 0234 | Ende Profil 03 | SL = 1713 m | LT = 1265 m | 10 40,20 N 86 36,60 W | 39 sml |
| 0234 – 0414 | Schleife über Bb | | | | |
| 0414 | Beginn Profil 04 | SL = 1342 m | LT = 1644 m | 10 38,81 N 86 38,90 W | |
| | Kurs = 138 Grad | v = 2,5 kn | | | |
| 0800 | | SL = 2472 m | LT = 1634 m | 10 31,85 N 86 32,63 W | |
| 1200 | | SL = 2697 m | LT = 1845 m | 10 24,34 N 86 25,87 W | |
| 1600 | | SL = 2788 m | LT = 1775 m | 10 16,89 N 86 19,19 W | |
| 2000 | | SL = 2178 m | LT = 1626 m | 10 09,34 N 86 12,39 W | |
| 2217 | Ende Profil 04 | SL = 2231 m | LT = 1544 m | 10 05,19 N 86 08,69 W | 40 sml |
| 2246 – 2400 | Schleife über Stb | | | | |
| **21.03.02** | | | | | |
| 0000 – 0028 | Fortsetzung Schleife | | | | |
| 0028 | Beginn Profil 05 | SL = 1672 m | LT = 1973 m | 10 03,50 N 86 10,77 W | |
| | Kurs = 318 Grad | v = 2,5 kn | | | |
| 0348 | | SL = 3673 m | LT = 2897 m | 10 09,60 N 86 16,32 W | |
| 0800 | | SL = 3223 m | LT = 2139 m | 10 17,15 N 86 23,21 W | |
| 1200 | | SL = 3718 m | LT = 2153 m | 10 24,49 N 86 29,79 W | |
| 1600 | | SL = 3416 m | LT = 1958 m | 10 32,00 N 86 36,61 W | |
| 1950 | Ende Profil 05 | SL = 3004 m | LT = 2166 m | 10 37,29 N 86 41,47 W | 45 sml |
| 2023 | | SL = 3004 m | LT = 2187 m | 10 38,78 N 86 42,37 W | |
| | Beginn Schleife über Bb | | | | |
| 2039 | Ende Schleife | | | 10 36,77 N 86 44,24 W | |
| 2053 | fieren mit 0,2 m/sec | | | | |
| 2107 | Beginn Profil 06 | SL = 3160 m | LT = 2499 m | 10 35,93 N 86 43,49 W | |
| 2200 | | SL = 4100 m | LT = 2477 m | 10 34,39 N 86 42,11 W | |
| 2400 | | SL = 3287 m | LT = 2413 m | 10 30,55 W 86 38,70 W | |
| **22.03.02** | | | | | |
| 0009 | Slmax = 4352 m | | | | |
| 0600 | Ende Profil 06 | SL = 4235 m | LT = 2694 m | 10 19,33 N 86 26,87 W | 22 sml |
| | beginnen hieven mit 0,5 m/sec | | | | |

0824 Depressor a.D.
0912 TOBI a.D.

OFOS-Profile 01-02 W 2

| | | | | |
|---|---|---|---|---|
| 1042 | stand by | | LT = 1515 m | 10 17,85 N 86 18,38 W |
| 1110 | OFOS z.W. | | | |
| 1141 | Bosi | SL = 1522 m | LT = 1509 m | 10 17,86 N 86 18,37 W |
| 1234 | | | | 10 17,88 N 86 17,88 W |
| 1342 | hieven ein | SL = 1534 m | LT = 1553 m | 10 17,94 N 86 17,83 W |
| 1421 | OFOS a.D. | | | |
| 1455 | OFOS z.W. | | LT = 1552 m | 10 17,78 N 86 18,52 W |
| 1529 | Bosi | SL = 1548 m | LT = 1554 m | 10 17,81 N 86 18,56 W |
| 1721 | hieven | SL = 1575 m | LT = 1598 m | 10 18,17 N 86 18,05 W |
| 1810 | OFOS a.D. / Ende Station | | | |

GTV 01-02 W 2

| | | | | |
|---|---|---|---|---|
| 1924 | Beginn Station 01 | | | |
| 1926 | GTV z.W. | | LT = 1531 m | 10 17,96 N 86 18,40 W |
| 1959 | Bosi | SL = 1520 m | LT = 1529 m | 10 17,93 N 86 18,35 W |
| 2007 | 1. Griff | SL = 1519 m | LT = 1523 m | 10 17,94 N 86 18,33 W |
| 2049 | GTV a.D. / Ende Station 1 | | | |
| 2055 | Beginn Station GTV-02 | | | |
| 2057 | GTV z.W. | | | |
| 2126 | Bosi | SL = 1504 m | LT = 1518 m | 10 17,93 N 86 18,33 W |
| 2134 | 1. Griff | SL = 1515 m | LT = 1520 m | 10 17,96 N 86 18,28 W |
| 2214 | GTV a.D. | | | |
| 2254 | Ende GTV-02 | | | |

Profil EM-06 v = 10,0 kn

| | | | |
|---|---|---|---|
| 2304 | Magnetometer z.W. | | |
| 2311 | Beginn Profil | 10 19,09 N 86 17,98 W | |
| | Kurs = 25 Grad | | |
| **23.03.02** | | | |
| 0006 | ä.K. 325 Grad | 10 26,96 N 86 13,98 W | 10 sml |
| 0028 | ä.K. 312 | 10 30,00 N 86 16,00 W | 04 sml |
| 0209 | ä.K. 054 | 10 41,30 N 86 28,50 w | 17 sml |
| 0222 | ä.K. 131 | 10 41,82 N 86 27,67 W | 02 sml |
| 0409 | ä.K. 044 | 10 31,44 N 86 15,00 W | 17 sml |
| 0421 | ä.K. 306 | 10 32,85 N 86 13,69 W | 02 sml |
| 0526 | ä.K. 213 | 10 39,40 N 86 22,50 W | 11 sml |
| 0536 | ä.K. 128 | 10 38,83 N 86 22,87 w | 01 sml |
| 0640 | ä.K. 090 | 10 32,68 N 86 15,08 w | 10 sml |
| 0645 | ä.K. 156 | 10 32,49 N 86 14,38 W | 01 sml |
| 0730 | ä.K. 195 | 10 25,87 N 86 11,37 W | 07 sml |
| 0933 | Ende Profil | 10 05,91 N 86 16,73 W | 21 sml |

Profil TOBI 07 W 2 v = 2,5 kn

| | | |
|---|---|---|
| 1346 | Beginn Aussetzen TOBI | 10 06,85 N 86 17,89 W |
| 1349 | TOBI z.W. | |
| 1416 | Depressor z.W. | 10 06,69 N 86 17,56 W |
| 1421 | KL = 157 m Störung, hieven ein | |
| 1435 | Depressor a.D. | |

| | | | | |
|---|---|---|---|---|
| 1519 | Depressor z.W. | LT = 2453 m | 10 06,02 N 86 16,71 W | |
| | Kurs = 138 Grad | fieren mit 0,5 m/sec | erhöhen auf 2,5 kn | |
| 1600 | KL = 1205 m | LT = 2379 m | 10 04,80 N 86 15,61 W | |
| 1955 | ä.K. 147 SL = 3847 m | LT = 2319 m | 09 57,41 N 86 09,01 W | 11 sml |
| 2400 | KL = 4245 m | LT = 2456 m | 09 48,81 N 86 03,44 W | |
| **24.03.02** | | | | |
| 0230 | ä.K. 123 SL = 4128 m | LT = 2469 m | 09 43,51 N 86 00,00 W | |
| 0938 | Ende Profil SL = 2474 m | LT = 2109 m | 09 33,57 N 85 44,90 W | 18 sml |

Profil TOBI 08-09 v = 2,5 kn W 2

| | | | | |
|---|---|---|---|---|
| 0938 – 1056 | Schleife über Bb | | | |
| 1130 | Beginn Profil SL = 2338 m | LT = 1590 m | 09 36,57 N 85 44,69 W | |
| 1200 | SL = 2338 m | LT = 1464 m | 09 37,24 N 85 45,67 W | |
| 1600 | SL = 2884 m | LT = 1918 m | 09 43,00 N 85 54,08 W | |
| 1700 | Ende Profil 08 SL = 3152 m | LT = 2081 m | 09 44,39 N 85 56,11 W | 14 sml |
| 1700 | Beginn Schleife über Stb | | | |
| 2052 | Beginn Profil 09 SL = 2087 m | LT = 1564 m | 09 44,93 N 85 50,53 W | |
| | Kurs = 206 Grad | | | |
| 2400 | SL = 2953 m | LT = 2181 m | 09 37,99 N 85 53,95 W | |
| **25.03.02** | | | | |
| 0116 | ä.K. 227 Grad SL = 3606 m | LT = 2742 m | 09 35,00 N 85 55,50 W | 11 sml |
| 0727 | Ende Profil 09 SL = 5964 m | LT = 3703 m | 09 25,58 N 86 05,70 W | 14 sml |
| | Beginn hieven | | | |
| 1005 | Depressor a.D. | 1040 Tobi a.D. | | |

Profil EM-07 v = 10,0 kn

| | | | |
|---|---|---|---|
| 1150 | Magnetometer z.W. SL = 250 m | | |
| 1231 | Beginn Profil | 09 20,70 N 86 04,00 W | |
| 1421 | ä.K. 90 | 09 32,97 N 85 50,20 W | 18 sml |
| 1515 | Ende Profil EM-07 | 09 32,00 N 85 41,22 W | 09 sml |
| 1529 | Magnetometer ein | | |

Kalibrierung POSIDONIA W 5

| | | | |
|---|---|---|---|
| 1550 | OBH-P z.W. | LT = 2052 m | 09 33,01 N 85 41,21 W |
| 1659 - 1728 | Transponder z.W. W 5 | | |
| 1748 | OBH ausgelöst | | |
| 1816 | OBH a.D. | | 09 33,00 N 85 41,34 W |
| 1827 | OBH-P z.W. | | 09 33,01 N 85 41,20 W |
| 1952 – 2127 | Achterfahrt um den OBH | | |
| 2146 | OBH ausgelöst | | |
| 2215 | OBH a.D. | | 09 33,06 N 85 41,24 W |

Profile DTS-01 bis xx v = 3,5 kn W 2

| | | | | |
|---|---|---|---|---|
| 2226 | Beginn Aussetzen Sidescan | | 09 33,26 N 85 41,48 W | |
| 2230 | Depressor z.W. , fieren W 2 mit 0,3 m/sec | | | |
| **26.03.02** | | | | |
| 0015 | Beginn Profil 01 SL = 3228 m | LT = 1726 m | 09 36,13 N 85 46,80 W | |
| | Kurs = 303 Grad | | | |
| 0408 | Ende Profil 01 SL = 4983 m | LT = 2196 m | 09 42,66 N 85 58,20 W | 13 sml |
| 0538 | Beginn Profil 02 SL = 3842 m | LT = 2383 m | 09 40,97 N 85 57,53 W | |
| 0932 | Ende Profil 02 SL = 4325 m | LT = 2158 m | 09 33,40 N 85 46,04 W | 13 sml |
| 0953 – 1045 | Schleife über Bb | | | |
| 1120 | Beginn Profil 03 SL = 3730 m | LT = 1802 m | 09 35,56 N 85 47,07 W | |
| 1523 | Ende Profil 03 SL = 5133 m | LT = 2286 m | 09 43,45 N 85 59,00 W | 13 sml |
| 1558 – 1645 | Schleife | | | |
| 1800 | Beginn Profil 04 SL = 5562 m | LT = 2524 m | 09 40,43 N 85 57,83 W | |

| | | | | | | |
|---|---|---|---|---|---|---|
| 2114 | Ende Profil 04 | SL = 4543 m | LT = 2007 m | 09 34,09 N | 85 48,2 W | 11 sml |
| 2212 – 2245 | Schleife | | | | | |
| 2342 | Beginn Profil 05 | SL = 4073 m | LT = 1874 m | 09 35,11 N | 85 47,52 W | |
| **27.03.02** | | | | | | |
| 0340 | Ende Profil 05 | SL = 5232 m | LT = 2406 m | 09 42,75 N | 85 59,25 W | 13 sml |
| 0429 – 0512 | Schleife | | | | | |
| 0639 | Beginn Profil 06 | SL = 4216 m | LT = 2170 m | 09 42,94 N | 85 56,01 W | |
| 0853 | Ende Profil 06 | SL = 3801 m | LT = 1781 m | 09 38,80 N | 85 49,60 W | 08 sml |
| 0853 – 1053 | Schleife | | | | | |
| 1117 | Beginn Profil 07 | SL = 2504 m | LT = 1715 m | 09 36,44 N | 85 40,95 W | |
| 1310 | Ende Profil 07 | SL = 4022 m | LT = 2217 m | 09 36,07 N | 85 52,56 W | 07 sml |
| | hieven ein | | | | | |
| 1454 | Depressor a.D. | | | | | |
| 1503 | Sidescan a.D. | | | | | |

OFOS 03 W 2

| | | | | | | |
|---|---|---|---|---|---|---|
| 1630 | Beginn Station | | LT = 1591 m | 09 37,37 N | 85 46,58 W | |
| 1635 | OFOS z.W. | | | | | |
| 1642 | SL = 210 m | Ausfall Datenstrecke, hieven ein | | | | |
| 1652 | OFOS a.D. | | | | | |
| 1721 | OFOS z.W. | | | | | |
| 1810 | Bosi | SL = 1595 m | LT = 1603 m | 09 37,08 N | 85 46,53 W | |
| | Kurs = 235 | v = 0,8 kn | | | | |
| 1930 | ä.K. 251 | SL = 1762 m | LT = 1760 m | 09 36,46 N | 85 47,37 W | 1,0 sml |
| 1958 | ä.K. 301 | SL = 1794 m | LT = 1742 m | 09 36,33 N | 85 47,81 W | 0,5 sml |
| 2133 | ä.K. 236 | SL = 1830 m | LT = 1832 m | 09 36,98 N | 85 48,51 W | 0,9 sml |
| 2339 | ä.K. 270 | SL = 1874 m | LT = 1905 m | 09 36,23 N | 85 49,35 W | 1,4 sml |
| **28.03.02** | | | | | | |
| 0118 | ä.K. 206 | SL = 1983 m | LT = 1973 m | 09 36,30 N | 85 49,89 W | 1,4 sml |
| 0154 | ä.K. 225 | SL = 1905 m | LT = 1904 m | 09 36,10 N | 85 50,00 W | 0,5 sml |
| 0225 | hieven | SL = 1991 m | LT = 2002 m | 09 35,92 N | 85 50,19 W | 1,5 sml |
| 0317 | OFOS a.D. | | | | | |
| 0320 | Ende Station | | | | | |

OFOS 04 W 2

| | | | | | | |
|---|---|---|---|---|---|---|
| 0420 | Beginn Station | | LT = 2222 m | 09 42,71 N | 85 56,40 W | |
| 0444 | OFOS z.W. | | | | | |
| 0532 | Bosi | SL = 2208 m | LT = 2214 m | 09 42,50 N | 85 56,29 W | |
| | Kurs = 231 Grad | v = 0,8 kn | | | | |
| 0705 | ä.K. 257 | SL = 2178 m | LT = 2238 m | 09 41,85 N | 85 56,98 W | 1,0 sml |
| 0755 | ä.K. 090 | SL = 2233 m | LT = 2256 m | 09 41,82 N | 85 57,38 W | 0,5 sml |
| 0902 | ä.K. 045 | SL = 2235 m | LT = 2258 m | 09 41,95 N | 85 56,89 W | 0,5 sml |
| 0918 | hieven | SL = 2303 m | LT = 2184 m | 09 42,17 N | 85 56,72 W | 0,3 sml |
| 1002 | OFOS a.D. | | | | | |
| 1012 | Ende Station | | | | | |

OFOS-05 W 2

| | | | | | | |
|---|---|---|---|---|---|---|
| 1102 | OFOS z.W. | | LT = 2208 m | 09 36,31 N | 85 54,29 W | |
| 1143 | Bosi | SL = 2200 m | LT = 2208 m | 09 36,29 N | 85 54,29 W | |
| | Kurs = 237 | v = 0,8 kn | | | | |
| 1316 | ä.K. 210 | SL = 2433 m | LT = 2433 m | 09 35,80 N | 85 55,10 W | 1,5 sml |
| 1608 | ä.K. 233 | SL = 3080 m | LT = 3067 m | 09 33,97 N | 85 56,14 W | 2,0 sml |
| 1700 | hieven ein | SL = 3250 m | LT = 3232 m | 09 33,53 N | 85 56,74 W | 0,6 sml |
| 1810 | OFOS a.D. | Ende Station | | | | |

OFOS-06 W 2

| | | | | | |
|---|---|---|---|---|---|
| 2043 | OFOS z.W. | LT = 2248 m | 10 02,25 N | 86 11,77 W | |
| 2123 – 2249 | Ausfall Spulgeschirr | | | | |
| 2302 | Bosi SL = 2243 m | LT = 2254 m | 10 02,18 N | 86 11,77 W | |
| | Kurs = 213 Grad v = 0,8 kn | | | | |
| **29.03.02** | | | | | |
| 0124 | hieven ein SL = 2354 m | LT = 2370 m | 10 01,43 N | 86 12,25 W | 1,0 sml |
| 0223 | OFOS a.D. | | | | |

OFOS-07 W 2

| | | | | | |
|---|---|---|---|---|---|
| 0240 | OFOS z.W. | LT = 2326 m | 10 00,86 N | 86 11,41 W | |
| 0324 | Bosi SL = 2312 m | LT = 2330 m | 10 00,71 N | 86 11,35 W | |
| | Kurs = 191 Grad v = 0,8 kn | | | | |
| 0432 | ä.K. 011 SL = 2319 m | LT = 2370 m | 10 00,22 N | 86 11,45 W | 0,5 sml |
| 0536 | hieven SL = 2350 m | LT = 2350 m | 10 00,66 N | 86 11,49 W | 0,5 sml |
| 0634 | OFOS a.D. | | | | |
| 0644 | Ende Station | | | | |

Profil EM-08 v = 8,0 kn

| | | | | | |
|---|---|---|---|---|---|
| 0644 | Beginn Profil | | 10 00,98 N | 86 11,29 W | |
| 1135 | Ende Profil 09 | | 09 49,13 N | 86 41,88 W | 32 sml |

Profil EM-09 v = 5,0 kn

| | | | | | |
|---|---|---|---|---|---|
| 1135 | Beginn Profil | | 09 49,13 N | 86 41,88 W | |
| 1200 | ä.K. 134 | | 09 48,01 N | 86 43,26 w | 02 sml |
| 1658 | ä.K. 041 | | 09 30,21 N | 86 24,68 W | 26 sml |
| 1715 | ä.K. 314 | | 09 31,18 N | 86 23,65 W | 04 sml |
| 2057 | Ende Profil | | 09 44,85 N | 86 37,63 W | 19 sml |

OFOS 08 und 09 W 2

| | | | | | |
|---|---|---|---|---|---|
| 2144 | Beginn Station | LT = 3304 m | 09 40,28 N | 86 33,81 W | |
| 2146 | OFOS z.W. | | | | |
| 2243 | Bosi SL = 3284 m | LT = 3302 m | 09 40,26 N | 86 33,78 W | |
| | Kurs = 312 Grad v = 1,0 kn | | | | |
| 2400 | SL = 3280 m | LT = 3311 m | 09 40,78 N | 86 34,25 W | |
| **30.03.02** | | | | | |
| 0014 | ä.K. 90 SL = 3292 m | LT = 3299 m | 09 40,74 N | 86 34,16 W | 1,0 sml |
| 0119 | ä.K. 45 SL = 3272 m | LT = 3286 m | 09 40,75 N | 86 33,52 W | 1,0 sml |
| 0220 | hieven SL = 3359 m | LT = 3311 m | 09 41,39 N | 86 32,89 W | 1,0 sml |
| 0342 | OFOS a.D. | | | | |
| 0344 | Ende Station | | | | |
| 0455 | OFOS z.W. | LT = 3342 m | 09 40,26 N | 86 40,84 W | |
| 0558 | Bosi SL = 3328 m | LT = 3348 m | 09 46,49 N | 86 40,80 W | |
| | Kurs = 45 Grad v = 1,0 kn | | | | |
| 0641 | hieven SL = 3380 m | LT = 3382 m | 09 47,01 N | 86 40,26 w | 1,0 sml |
| 0850 | OFOS a.D. Ende Station | | | | |

Profil EM-10 v = 10,0 kn

| | | | | | |
|---|---|---|---|---|---|
| 0858- 0905 | bringen Magmetometer aus | | | | |
| 0920 | Beginn Profil | LT = 3354 m | 09 48,22 N | 86 41,97 W | |
| | Kurs = 360 | | | | |
| 1234 | ä.K. 140 | LT = 43100 m | 10 20,13 N | 86 41,50 W | 27 sml |
| 1703 | ä.K. 131 | LT = 3373 m | 09 45,00 N | 86 12,00 W | 46 sml |
| 2027 | ä.K. 090 | | 09 21,11 N | 85 45,13 W | 36 sml |
| 2156 | Ende Profil | LT = 1650 m | 09 21,01 N | 85 29,86 W | 15 sml |
| 2212 | Magnetometer a.D. | | | | |

Kalibrierung POSIDONIA

| | | | | | |
|---|---|---|---|---|---|
| 2217 | Transducer im Lotschacht z.W. | | | | |
| 2238 | OBH-T z.W. | LT = 1656 m | 09 21,02 N | 85 30,03 W | |
| 2258 | Beginn Schleife | | | | |
| **31.03.02** | | | | | |
| 0030 | Ende Kalibrierung | | | | |
| 0041 | OBH ausgelöst | 0106 aufgetaucht | 0117 a.D. | 09 21,10 N | 85 30,14 W |

Profile DTS-08 bis 13 W 2 v = 3,5 kn

| | | | | | |
|---|---|---|---|---|---|
| 0224 | SideScanSonar z.W. | | | | |
| 0232 | Depressor z.W. | | | | |
| | Kurs = 294 Grad | v = 2,5 kn | fieren W 2 mit 0,5 m/sec | | |
| 0504 | Beginn Profil 08 | | 09 18,60 N | 85 33,95 W | |
| | Kurs = 290 Grad | v = 3,5 kn | SL = 5117 m | LT = 2668 m | |
| 0916 | Ende Profil 08 | | 09 23,79 N | 85 47,73 W | 17 sml |
| 1200 | Beginn Profil 09 | | 09 21,20 N | 83 45,80 W | |
| | Kurs = 110 Grad | v = 3,0 kn | SL = 6144 m | LT = 3142 m | |
| 1740 | Ende Profil 09 | | 09 15,33 N | 85 30,10 W | 17 sml |
| | | | SL = 3944 m | LT = 2718 m | |
| 1935 | Beginn Profil 10 | | 09 18,04 N | 85 34,12 W | |
| | Kurs = 290 | v = 3,0 kn | SL = 4551 m | LT = 2969 m | |
| **01.04.03** | | | | | |
| 0018 | Ende Profil 10 | | 09 23,50 N | 85 48,73 W | 15 sml |
| | | | SL = 6321 m | LT = 3272 m | |
| 0434 | Beginn Profil 11 | | 09 20,70 N | 85 46,05 W | |
| | Kurs = 110 | v = 3,0 kn | SL = 6809 m | LT = 3136 m | |
| 0930 | Ende Profil 11 | | 09 15,60 N | 85 32,54 W | 15 sml |
| | | | SL = 5840 m | LT = 2714 m | |
| 1147 | Beginn Profil 12 | | 09 17,48 N | 85 34,33 W | |
| | Kurs = 290 | v = 3,2 kn | SL = 4937 m | LT = 2676 m | |
| 1629 | Ende Profil 12 | | 09 22,87 N | 85 48,50 W | 18 sml |
| | | | SL = 6543 m | LT = 3294 m | |
| 2011 | Beginn Profil 13 | | 09 20,26 N | 85 46,45 W | |
| | Kurs = 111 Grad | v = 3,2 kn | SL = 6872 m | LT = 3199 m | |
| **02.04.02** | | | | | |
| 0058 | Ende Profil 13 | | 09 14,84 N | 85 32,26 W | 15 sml |
| | | | SL = 6323 m | LT = 2743 m | |
| 0059 | hieven mit 0,7 m/sec | | | | |
| 0340 | Depressor a.D. | | | | |
| 0348 | Sidescan a.D. | | | | |

Profil EM 13 v = 7,5 kn

| | | | |
|---|---|---|---|
| 0647 | Beginn Profil | 09 09,58 N | 85 41,42 W |
| 0851 | ä.K. 56 | 09 06,10 N | 85 36,00 W 14 sml |
| 1207 | Ende Profil | 09 19,00 N | 85 36,00 W 14 sml |

OFOS-10 W 2

| | | | | |
|---|---|---|---|---|
| 1215 | Beginn Station | LT = 504 m | 09 18,82 N | 85 15,39 W |
| 1221 | OFOS z.W. | | | |
| 1239 | Bosi SL = 472 m | LT = 483 m | 09 18,36 N | 85 15,50 W |
| | Kurs = 270 Grad v = 0,8 kn | | | |
| 1500 | hieven ein wegen Angelleinen | | | |
| 1515 | OFOS Wasseroberfäche, ok | | | |
| 1530 | Bosi SL = 544 m | LT = 549 m | 09 18,91 N | 85 17,03 W |
| | Kurs = 280 Grad v = 0,7 kn | | | |
| 1727 | hieven SL = 780 m | LT = 790 m | 09 19,18 N | 85 18,33 W 1 sml |

1752 OFOS a.D.

OFOS-11 W 2

2234 Beginn Station LT = 744 m09 10,42 N 84 50,89 W
2235 OFOS z.W.
2255 Bosi SL = 737 m LT = 743 m09 10,42 N 84 44,71 W
Kurs = 270 v = 0,5 kn

**03.04.02.**

0117 hieven SL = 773 m LT = 783 m09 10,39 N 84 48,70 W 1 sml
0133 OFOS a.D.

OFOS-12 W 2

0237 Beginn Station LT = 940 m09 10,47 N 84 50,35 W
0239 OFOS z.W.
0303 Bosi SL = 948 m LT = 919 m09 10,36 N 84 50,25 W
Kurs = 132 v = 0,6 kn
0715 hieven SL = 865 m LT = 871 m09 08,70 N 84 48,61 W 3 sml
0750 OFOS a.D.

DTS-Profile 14 bis 22

0908 LT =1089 m 09 08,00 N 84 41,77 W
0911 Sidescan z.W.
0915 Depressor z.W. fieren mit 0,3 m/s
0941 SL = 582 m fieren mit 0,5 m/s
1012 Beginn DTS-14 SL = 1390 m LT = 1055 m 09 08,01 N 84 45,02 W
Kurs = 270 Grad v = 3,5 kn
1336 Ende DTS-14 SL = 3426 m LT = 2200 m 09 08,00 N 84 56,70 W 12 sm
1522 Beginn DTS-15 SL = 4132 m LT = 1842 m 09 10,40 N 84 53,01 W
Kurs = 90 Grad v = 3,5 kn
1847 Ende DTS-15 SL = 1365 m LT = 760 m09 10,39 N 84 43,33 W 12 sm
2006 Beginn DTS-16 SL = 1325 m LT = 989 m09 08,61 N 84 45,02 W
Kurs = 270 v = 3,5 kn
2333 Ende DTS-16 SL = 3472 m LT = 2217 m 09 08,56 N 84 57,17 W 11 sm

**04.04.03**

0112 Beginn DTS-17 SL = 3863 m LT = 1921 m 09 11,00 N 84 55,00 W
Kurs = 90 v = 3,5 kn
0422 Ende DTS-17 SL = 1247 m LT = 684 m09 11,00 N 84 43,59 W 12 sm
0552 Beginn DTS-18 SL = 1130 m LT = 923 m09 09,20 N 84 45,00 w
Kurs = 270 v = 3,5 kn
0913 Ende DTS-18 SL = 3565 m LT = 2172 m 09 09,19 N 84 56,69 W 12 sm
1047 Beginn DTS-19 SL = 3471 m LT = 1880 m 09 11,59 N 84 55,06 W
1436 Ende DTS-19 SL = 682 m LT = 538 m09 11,60 N 84 41,81 W 13 sm
1600 Beginn DTS-20 SL = 1044 m LT = 861 m09 09,79 N 84 44,94 W
1923 Ende DTS-20 SL = 3569 m LT = 2144 m 09 09,79 N 84 56,74 W 12 sm
2053 Beginn DTS-21 SL = 3462 m LT = 1818 m 09 12,20 N 84 55,02 W

**05.04.02**

0037 Ende DTS-21 SL = 565 m LT = 480 m09 12,20 N 84 42,08 W 12 sm
0253 Beginn DTS-22 SL = 1094 m LT = 710 m09 12,40 N 84 46,70 W
Kurs = 206 Grad
0411 ä.K. 215 SL = 935 m LT = 835 m09 09,08 N 84 48,40 W
0613 Ende DTS-22 SL = 3457 m LT = 2376 m 09 04,38 N 84 51,77 W 10 sm
0746 Depressor a.D.
0754 Sidescan a.D.

GTV-03 W 2

0924 Beginn Station LT = 754 m09 10,28 N 84 48,27 W

| | | | | | |
|---|---|---|---|---|---|
| 0925 | GTV z.W. | | | | |
| 0944 | Bosi | SL = 754 m | LT = 763 m | 09 10,42 N 84 48,25 W | |
| 0951 | Griff | SL = 777 m | LT = 762 m | 09 10,44 N 84 48,25 W | |
| 0955 | hieven | | | | |
| 1013 | GTV a.D. | | | | |
| 1044 | Ende Station | | | | |

OFOS 13 W 2

| | | | | | |
|---|---|---|---|---|---|
| 1240 | Beginn Station | | LT = 1839 m | 08 59,87 N 84 42,22 W | |
| 1244 | OFOS z.W. | | | | |
| 1252 | SL = 291 m | Datenausfall hieven | | | |
| 1337 | OFOS z.W. | | LT = 1868 m | 08 59,73 N 84 42,57 W | |
| 1420 | Bosi | SL = 1862 m | LT = 1876 m | 08 59,69 N 84 42,51 W | |
| | Kurs = 156 | v = 0,9 kn | | | |
| 1700 | ä.K. 90 | SL = 2109 m | LT = 2099 m | 08 58,62 N 84 42,03 W | |
| 1735 | hieven | SL = 2033 m | LT = 1999 m | 08 58,63 N 84 41,61 W | 2 sm |
| 1827 | OFOS a.D. | | | | |

Profile TOBI 10 bis xx W 2

| | | | | | |
|---|---|---|---|---|---|
| 1909 | TOBI z.W. | | | 09 09.95 N 84 41,32 W | |
| 1939 | Depressor z.W. | | | 09 00,59 N 84 41,15 W | |
| | Kurs = 158 | v = 1,5 kn | | | |
| 2049 | v = 2,5 kn | | | | |
| 2400 | | SL = 5651 m | LT = 3064 m | 08 51,16 N 84 37,44 W | |
| **06.04.02** | | | | | |
| 0110 | v = 2,2 kn | | | | |
| 0251 | ä.K. 121 | SL = 5612 m | LT = 3391 m | 08 45,02 N 84 34,92 W | 18 sm |
| 0400 | | SL = 5721 m | LT = 3248 m | 08 43,65 N 84 32,78 W | |
| 0800 | | | | 08 36,68 N 84 21,34 W | |
| 1200 | | SL = 4280 m | LT = 2585 m | 08 34,38 N 84 17,63 W | |
| 1535 | v = 2,5 kn | | | | |
| 1600 | | SL = 3752 m | LT = 2391 m | 08 29,72 N 84 09,90 W | |
| 2000 | ä.K. 107 | SL = 3855 m | LT = 2216 m | 08 24,45 N 84 01,29 W | 39 sm |
| 2400 | | SL = 2891 m | LT = 83 51,51 W | 08 21,26 N 83 51,51 W | |
| **07.04.02** | | | | | |
| 0400 | | SL = 0770 m | LT = 1695 m | 08 18.13 N 83 41,81 W | |
| 0800 | | SL = 2790 m | LT = 1657 m | 08 14,91 N 83 31,82 W | |
| 1205 | Ende TOBI-10 | SL = 2614 m | LT = 1882 m | 08 11,85 N 85 22,39 W | 39 sm |
| 1410 | Beginn TOBI-11 | SL = 2366 m | LT = 1846 m | 08 14,80 N 83 22,50 W | |
| | Kurs = 287 | v = 2,5 kn | | | |
| 1800 | | SL = 1772 m | LT = 1464 m | 08 17,71 N 83 31,74 W | |
| 2400 | | SL = 1793 m | LT = 1180 m | 08 22,38 N 83 46,49 W | |

| | | | | | |
|---|---|---|---|---|---|
| **08.04.02** | | | | | |
| 0522 | ä.K. 301 | SL = 2009 m | LT = 1496 m | 08 26,50 N 83 59,40 W | 38 sml |
| 1200 | | SL = 3195 m | LT = 2145 m | 08 35,32 N 84 13,74 W | |
| 1800 | | SL = 3627 m | LT = 2316 m | 08 43,14 N 84 26,53 W | |
| 2109 | Ende Tobi-11 | SL = 3959 m | LT = 2574 m | 08 47,35 N 84 33,34 W | 39.5 sm |
| 2324 | Beginn TOBI-12 | SL = 3780 m | LT = 2378 m | 08 48,54 N 84 30,35 W | |
| **09.04.02** | | | | | |
| 0600 | | SL = 2693 m | LT = 1725 m | 08 39,88 N 84 16,16 W | |
| 1200 | | SL = 1006 m | LT = 1048 m | 08 31,81 N 84 02,94 W | |
| 1800 | | SL = 150 m | LT = 316 m | 08 26,08 N 83 48,03 W | |
| 2400 | | SL = 1228 m | LT = 1017 m | 08 21,41 N 83 33,98 W | |
| **10.04.02** | | | | | |

| | | | | | |
|---|---|---|---|---|---|
| 0700 | Ende TOBI-12 hieven ein | SL = 1300 m | LT = 1008 m | 08 16,25 N 83 17,25 W | 43 sm |
| 0800 | Depressor a.D. | | | | |
| 0823 | Tobi a.D. | | | | |

OFOS-14 W 2

| | | | | | |
|---|---|---|---|---|---|
| 1243 | OFOS z.W. | | LT = 1734 m | 08 15,56 N 83 34,11 W | |
| 1321 | Bosi | SL = 1722 m | LT = 1738 m | 08 15,60 N 83 34,22 W | |
| | Kurs = 248 Grad | v = 0,5 kn | | | |
| 1442 | hieven | SL = 1915 m | LT = 1922 m | 08 15,35 N 83 34,80 W | 1 sm |
| 1521 | OFOS a.D. / | Ende Station | | | |

OFOS-15 W 2

| | | | | | |
|---|---|---|---|---|---|
| 1725 | Beginn Station | | LT = 1528 m | 08 22,21 N 83 47,54 W | |
| 1727 | OFOS z.W. | | | | |
| 1800 | Bosi | SL = 1267 m | LT = 1288 m | 08 22,20 N 83 47,70 W | |
| | Kurs = 180 | v = 1,0 kn | | | |
| 1840 | ä.K. 143 | SL = 1435 m | LT = 1480 m | 08 21,66 N 83 47,69 W | |
| 1930 | stoppen auf | SL = 1505 m | LT = 1545 m | 08 21,19 N 83 47,40 W | |
| 1940 | Kurs = 270 | v = 0,5 kn | | | |
| 2052 | hieven ein | SL = 1624 m | LT = 1648 m | 08 21,18 N 83 48,10 W | 2 sm |
| 2127 | OFOS a.D. | Ende Station | | | |

OFOS-16 W 2

| | | | | | |
|---|---|---|---|---|---|
| 2248 | Beginn Station | | LT = 709 m | 08 26,48 N 83 55,00 W | |
| 2249 | OFOS z.W. | | | | |
| 2305 | Bosi | SL = 699 m | LT = 712 m | 08 26,49 N 83 54,99 W | |
| | Kurs = 258 | v = 0,7 kn | | | |
| **11.04.02** | | | | | |
| 0057 | ä.K. 180 | SL = 860 m | LT = 875 m | 08 26,31 N 83 56,00 W | |
| 0148 | hieven ein | SL = 1113 m | LT = 1150 m | 08 25,83 N 83 56,01 W | 2 sm |
| 0214 | OFOS a.D. | Ende Station | | | |

OFOS-17 W 2

| | | | | | |
|---|---|---|---|---|---|
| 0545 | Beginn Station | | LT = 1782 m | 08 40,63 N 84 18,20 W | |
| 0553 | OFOS z.W. | | | | |
| 0634 | Bosi | SL = 1797 m | LT = 1817 m | 08 40,60 N 84 18,32 W | |
| | Kurs = 212 | v = o,5 – 1,0 kn | | | |
| 1000 | | SL = 2345 m | LT = 2357 m | 08 38,51 N 84 19,63 W | |
| 1200 | | SL = 2578 m | LT = 2582 m | 08 37,28 N 84 20,39 W | |
| 1400 | | SL = 2806 m | LT = 2795 m | 08 36,23 N 84 21,06 W | |
| 1525 | Ende Bosi | SL = 2922 m | LT = 2863 m | 08 35,46 N 84 21,55 W | |
| 1527 | OFOS a.D. | Ende Station | | | |

TOBI-13 W 2

| | | | | | |
|---|---|---|---|---|---|
| 1820 | | | LT = 1895 m | 08 48,50 N 84 24,98 W | |
| 1823 | TOBI z.W. | | | | |
| 1851 | Depressor z.W. | | | 08 48,15 N 84 24,42 W | |
| 1930 | SL = 952 m | Datenausfall ; hieven ein | | | |
| 2002 | Depressor a.D. | | | | |
| 2032 | TOBI a.D. | | | 08 46,82 N 84 22,71 W | |
| 2116 | TOBI z.W. | | | | |
| 2138 | Depressor z.W. | | LT = 1890 m | 08 48,40 N 84 24,85 W | |
| | Kurs = 122 | v = 1,5 kn | | | |
| 2200 | | SL = 624 m | LT = 1889 m | 08 48,07 N 84 24,35 W | |
| 2241 | v = 2,5 kn | | | | |

2400 SL = 2670 m LT = 1602 m 08 45,65 N 84 20,55 W
**12.04.02**
0400 SL = 1399 m LT = 1062 m 08 40,26 N 84 12,08 W
0800 SL = 199 m LT = 533 m 08 34,79 N 84 03,55 W
0833 Ende TOBI-13 SL = 151 m LT = 465 m 08 33,97 N 84 02,26 W 27 sm
0833 – 0937 Schleife über Bb

TOBI-14 W 2
0937 Beginn Profil SL = 151 m LT = 366 m 08 35,63 N 84 01,20 W
Kurs = 304 v = 2,5 kn
1200 SL = 200 m LT = 492 m 08 39,22 N 84 06,54 W
1600 SL = 894 m LT = 991 m 08 44,67 N 84 14,67 W
1957 Ende Profil SL = 2085 m LT = 1613 m 08 50,25 N 84 22,96 W 25 sm

TOBI-15 W 2
2210 Beginn Profil SL = 1796 m LT = 1330 m 08 51,86 N 84 20,26 W
Kurs = 127 v = 2,5 kn
0221 Ende Profil SL = 325 m LT = 629 m 08 45,41 N 84 11,88 W 11 sm

TOBI-16 W 2
0333 Beginn Profil SL = 151 m LT = 335 m 08 47,30 N 84 10,70 W
Kurs = 311 v = 311
0943 Ende Profil SL = 1172 m LT = 1126 m 08 57,68 N 84 22,34 W 16 sm

TOBI-17 W 2
1108 Beginn Profil SL = 956 m LT = 863 m 08 59,27 N 84 20,69 W
Kurs = 133 v = 2,5 kn
1447 Ende Profil SL = 442 m LT = 625 m 08 52,97 N 84 13,97 W 09 sm
1510 Depressor a.D.
1537 TOBI a.D.

OFOS-18 W 2

1646 Beginn Station LT = 184 m 08 51,94 N 84 12,60 W
1647 OFOS z.W.
1653 Bosi SL = 178 m LT = 185 m 08 51,88 N 84 12.60 W
Kurs = 216 v = 0,8 kn
1814 ä.K. 227 SL = 397 m LT = 403 m 08 51,00 N 84 13,23 W 1,2
2048 ä.K. 292 SL = 702 m LT = 708 m 08 49,39 N 84 14,92 W 1,8
2134 ä.K. 180 SL = 828 m LT = 848 m 08 49,62 N 84 15,47 W 0,6
2155 hieven ein SL = 815 m LT = 808 m 08 49,39 N 84 15,50 W 0,4
2215 OFOS a.D.
2220 Ende OFOS 18

OFOS-19 W 2
2322 Beginn Station LT = 1036 m 08 54,98 N 84 17,82 W
2323 OFOS z.W.
2344 Bosi SL = 1024 m LT = 1037 m 08 54,94 N 84 17,93 W
Kurs = 318 v = 0,5 kn
**14.04.02**
0217 hieven ein SL = 1005 m LT = 1010 m 08 56,00 N 84 18,86 W 2
0240 OFOS a.D.
0242 Ende Station

OFOS-20 W 2
0352 Beginn Station LT = 429 m 08 50,40 N 84 12,98 W

| | | | | | |
|---|---|---|---|---|---|
| 0403 | OFOS z.W. | | | | |
| 0417 | Bosi | SL = 436 m | LT = 444 m | 08 50,30 N 84 12,99 W | |
| | Kurs = 223 | v = 0,7 kn | | | |
| 0600 | ä.K. 180 | SL = 641 m | LT = 651 m | 08 49,32 N 84 13,92 W | 1 |
| 0707 | hieven ein | SL = 721 m | LT = 774 m | 08 48,58 N 84 13,90 W | 1 |
| 0730 | OFOS a.D. / Ende Station | | | | |

OFOS-21 W 2

| | | | | | |
|---|---|---|---|---|---|
| 0849 | Beginn Station | | LT = 1004 m | 08 55,96 N 84 18,57 W | |
| 0851 | OFOS z.W. | | | | |
| 0910 | Bosi | SL = 1000 m | LT = 1005 m | 08 55,94 N 84 18,53 W | |
| | Kurs = 219 | v = 0,6 kn | | | |
| 0938 | ä.K. 042 | SL = 992 m | LT = 1013 m | 08 55,71 N 84 18,71 W | 0,4 |
| 1031 | div. Kurse | | | 08 55,90 N 84 18,55 W | 1,0 |
| 1249 | hieven ein | SL = 1015 m | LT = 1022 m | 08 55,69 N 84 19,00 W | 0,6 |
| 1313 | OFOS a.D. | | | | |
| 1214 | Ende Station | | | | |

Profil EM-12

| | | | | |
|---|---|---|---|---|
| 1404 | Beginn Profil | | 08 23,64 N 84 23,95 W | |
| | Kurs = 35 | | | |
| | ä.K. 20 | | 09 00,00 N 84 23,00 W | |
| 1437 | ä.K. 129 | | 09 02,32 N 84 22,05 W | |
| 1528 | Ende Profil | | 08 58,40 N 84 17,20 W | 11 sm |

GTV-04 und 05

| | | | | | |
|---|---|---|---|---|---|
| 1600 | Beginn Station | | LT = 1002 m | 08 55,81 N 84 18,73 W | |
| 1602 | GTV z.W. | | | | |
| 1630 | Bosi | SL = 996 m | LT = 1002 m | 08 55,80 N 84 18,74 W | |
| 1705 | 1. Griff | SL = 986 m | LT = 980 m | 08 55,81 N 84 18,62 W | |
| 1715 | 2. Griff | SL = 990 m | LT = 990 m | 08 55,81 N 84 18,62 W | |
| 1721 | hieven ein | | | | |
| 1746 | GTV a.D. | | | | |
| 1748 | Ende Station | | | | |
| 1751 | GTV z.W. | | | | |
| 1816 | Bosi | SL = 993 m | LT = 1002 m | 08 55,80 N 84 18,75 W | |
| 1841 | Griff | SL = 1001 m | LT = 999 m | 08 55,80 N 84 18,73 W | |
| 1844 | hieven ein | | | | |
| 1922 | GTV a.D. | | | | |
| 1930 | Ende Station | | | | |

Profil EM-13

| | | | | |
|---|---|---|---|---|
| 1951 | Beginn Profil | | 08 53,58 N 84 19,33 W | |
| | Kurs = 132 | v = 8 kn | | |
| 2045 | Ende Profil | | 08 49,02 N 84 16,41 W | 7 |

Station GTV-06 W 2

| | | | | | |
|---|---|---|---|---|---|
| 2112 | Beginn Station | | LT = 399 m | 08 51,23 N 84 13,11 W | |
| 2114 | GTV z.W. | | | | |
| 2124 | Bosi und Griff | SL = 391 m | LT = 399 m | 08 51,22 N 84 13,10 W | |
| 2126 | hieven ein | | | | |
| 2150 | GTV a.D. | | | | |
| 2213 | Ende Station | | | | |

Profil EM-14

| | | | | |
|---|---|---|---|---|
| 2243 | Beginn Profil | | 08 46,29 N 84 14,65 W | |
| | Kurs = 196 | v = 8 kn | | |

| | | | | | |
|---|---|---|---|---|---|
| 2330 | ä.K. 304 | | | 08 46,29 N 84 14,65 W | |
| 0039 | Ende Profil | | | 08 51,00 N 84 22,10 W | 11 |

OFOS-22 W 2

| | | | | | |
|---|---|---|---|---|---|
| 0244 | Beginn Station | | LT = 1242 m | 08 57,63 N 84 36,51 W | |
| 0248 | OFOS z.W. | | | | |
| 0316 | Bosi | SL = 1238 m | LT = 1240 m | 08 57,51 N 84 36,50 W | |
| | Kurs = 180 v = 0,8 kn | | | | |
| 0540 | ä.K. 235 | SL = 1610 m | LT = 1636 m | 08 55,85 N 84 36,49 W | 1,5 |
| 0755 | ä.K. 180 | SL = 2283 m | LT = 2339 m | 08 55,21 N 84 37,91 W | 1,4 |
| 0813 | hieven ein | SL = 2364 m | LT = 2373 m | 08 55,00 N 84 37,91 W | 0,2 |
| 0858 | OFOS a.D. / Ende Station | | | | |

Profile DTS 23 bis xx W 2

| | | | | | |
|---|---|---|---|---|---|
| 1104 | | | LT = 2234 m | 09 01,94 N 84 51,07 W | |
| 1108 | Sidescan z.W. | | | | |
| 1113 | Depressor z.W. | | | | |
| | Kurs = 108 v = 3,0 kn | | | | |
| 1200 | | SL = 1579 m | LT = 2187 m | 09 01,27 N 84 48,83 W | |
| 1303 | Beginn DTS-23 | SL = 4000 m | LT = 2029 m | 09 00,16 N 84 45,42 W | |
| | Kurs = 108 v = 3,5 kn | | | | |
| 1708 | Ende DTS-23 | SL = 4063 m | LT = 2047 m | 08 55,55 N 84 31,64 W | 14 |
| 1921 | Beginn DTS-24 | SL = 3344 m | LT = 1907 m | 08 57,72 N 84 32,40 W | |
| | Kurs = 288 v = 3,5 kn | | | | |
| 2332 | Ende DTS-24 | SL = 3851 m | LT = 2040 m | 09 02,37 n 84 46,43 W | 15 |
| **16.04.02** | | | | | |
| 0110 | Beginn DTS-25 | SL = 3568 m | LT = 1833 m | 09 00,70 N 84 45,23 W | |
| | Kurs = 108 v = 3,5 kn | | | | |
| 0542 | Ende DTS-25 | SL = 4028 m | LT = 1852 m | 08 55,94 N 84 30,91 W | 16 |
| 0735 | Beginn DTS-26 | SL = 3218 m | LT = 1848 m | 08 58,27 N 84 32,31 W | |
| | Kurs = 288 v = 3,5 kn | | | | |
| 1155 | Ende DTS-26 | SL = 3515 m | LT = 1977 m | 09 02,98 N 84 46,36 W | 15 |
| 1412 | Beginn DTS-27 | SL = 3858 m | LT = 1797 m | 09 01,28 N 84 45,04 W | |
| | Kurs = 108 v = 3,5 kn | | | | |
| 1842 | Ende DTS-27 | SL = 4168 m | LT = 1793 m | 08 56,46 N 84 30,55 W | 15 |
| | hieven ein | | | | |
| 2026 | Depressor a.D. | | | | |
| 2045 | Sidescan a.D. | | | | |

OFOS-23

| | | | | | |
|---|---|---|---|---|---|
| 2242 | Beginn Station | | LT = 1452 m | 09 02,19 N 84 37,22 W | |
| 2244 | OFOS z.W. | | | | |
| 2312 | Bosi | SL = 1436 m | LT = 1449 m | 09 02,20 N 84 37,24 W | |
| | Kurs = 180 v = 0,5 kn | | | | |
| 2400 | | SL = 1423 m | LT = 1432 m | 09 02,02 N 84 37,20 W | |
| **17.04.02** | | | | | |
| 0200 | | SL = 1412 m | LT = 1424 m | 09 01,97 N 84 37,32 W | |
| 0400 | | SL = 1397 m | LT = 1415 m | 09 01,91 N 84 37,21 W | |
| 0628 | hieven ein | SL = 1400 m | LT = 1403 m | 09 01,77 N 84 37,03 W | 4 |
| 0703 | OFOS a.D. / Ende Station | | | | |

OFOS-24

| | | | | | |
|---|---|---|---|---|---|
| 0758 | Beginn Station | | LT = 1416 m | 09 01,93 N 84 37,22 W | |
| 0800 | OFOS z.W. | | | | |
| 0828 | Bosi | SL = 1396 m | LT = 1407 m | 09 01,95 N 84 37,23 W | |
| | diverse Kurse ; v = 0,3 kn | | | | |

| | | | | | |
|---|---|---|---|---|---|
| 1042 | hieven | SL = 1400 m | LT = 1410 m | 09 01.82 N 84 37,06 W | 1 |
| 1113 | OFOS a.D / | Ende Station | | | |

Profil DTS-28 W 2

| | | | | | |
|---|---|---|---|---|---|
| 1208 | Sidescan z.W. | | LT = 1538 m | 08 59,78 N 84 31,87 W | |
| 1212 | Depressor z.W. | | | | |
| | Kurs = 292 | v = 2,5 kn | | | |
| 1300 | | SL = 1854 m | LT = 1480 m | 09 00,53 N 84 33,80 W | |
| 1400 | | SL = 2191 m | LT = 1363 m | 09 01,40 N 84 36,19 W | |
| 1506 | hieven ein | SL = 2209 m | LT = 1539 m | 09 02,48 N 84 38,72 W | 6 |
| 1604 | Depressor a.D. | | | | |
| 1620 | Sidescan a.D. | | | | |
| 1625 | POSIDONIA a.D. | | | | |

OFOS-25 W 2

| | | | | | |
|---|---|---|---|---|---|
| 1744 | OFOS z.W. | | LT = 774 m | 09 11,62 N 84 47,79 W | |
| 1810 | Bosi | SL = 769 m | LT = 774 m | 09 11,59 N 84 47,79 W | |
| | Kurs = 264 Grad | v = 0,7 kn | | | |
| 2140 | ä.K. 225 | | | 09 11,36 N 84 50,05 W | |
| 2302 | hieven ein | SL = 1018 m | LT = 999 m | 09 10,73 N 84 50,67 W | 4 |
| 2330 | OFOS a.D. / | Ende Station | | | |

OFOS-26 W 2

| | | | | | |
|---|---|---|---|---|---|
| 2355 | Beginn Station | | LT = 953 m | 09 08,25 N 84 49,65 W | |
| 2400 | OFOS z.W. | | | | |
| **18.04.02** | | | | | |
| 0023 | Bosi | SL = 946 m | LT = 954 m | 09 08,22 N 84 49,63 W | |
| | Kurs = 90 | v = 0,6 kn | | | |
| 0114 | ä.K. 50 | SL = 946 m | LT = 931 m | 09 08,25 N 84 49,10 W | |
| 0309 | hieven ein | SL = 812 m | LT = 810 m | 09 09,17 N 84 48,02 W | 2 |
| 0329 | OFOS a.D. | | | | |
| 0330 | Ende Station | | | | |

Profil EM-15 v = 5,0 kn

| | | | | |
|---|---|---|---|---|
| 0400 | Beginn Profil | Kurs = 213 | 09 06,80 N 84 51,90 W | |
| 0501 | ä.K. 120 | | 09 02,50 N 84 54,78 W | 5 |
| 0537 | ä.K. 034 | | 09 01,01 N 84 52,20 W | 3 |
| 0647 | ä.K. 038 | | 09 05,61 N 84 48,98 W | 7 |
| 0709 | Ende Profil | | 09 06,92 N 84 47,97 W | 2 |

Station GTV-07 W 2

| | | | | | |
|---|---|---|---|---|---|
| 0736 | Beginn Station | | LT = 851 m | 09 09,04 N 84 49,23 W | |
| 0739 | GTV z.W. | | | | |
| 0800 | Bosi | SL = 836 m | LT = 830 m | 09 09,04 N 84 49,18 W | |
| 0907 | Griff | SL = 828 m | LT = 825 m | 09 09,02 N 84 49,13 W | |
| 0907 | GTV a.D. | | | | |
| 0915 | Ende Station | | | | |

Station GTV-08 W 2

| | | | | |
|---|---|---|---|---|
| 1025 | Beginn Station | | LT = 1410 m | 09 01,97 N 84 37,21 W |
| 1027 | GZV z.W. | | | |
| 1055 | Bosi | SL = 1399 m | LT = 1404 m | 09 01,94 N 84 37,23 W |
| 1106 | Griff | SL = 1405 m | LT = 1408 m | 09 01,94 N 84 37,23 W |
| 1107 | hieven | | | |
| 1143 | GTV a.D. | | | |

Station GTV-09 W 2

| | | | | |
|---|---|---|---|---|
| 1218 | GTV z.W. | | LT = 1413 m | 09 01,97 N 84 37,24 W |
| 1244 | Bosi | SL = 1400 m | LT = 1409 m | 09 01,95 N 84 37,24 W |
| 1248 | Griff | SL = 1408 m | LT = 1409 m | 09 01,95 N 84 37,23 W |
| 1339 | GTV a.D. | | | |
| 1400 | Ende Station | | | |

Profil EM-16 v = 8,0 kn

| | | | | |
|---|---|---|---|---|
| 1411 | Beginn Profil | Kurs = 288 | 09 01,45 N 84 38,00 W | |
| 1522 | ä.K. 061 | | 09 04,52 N 84 46,95 W | 10 |
| 1550 | ä.K. 108 | | 09 06,23 N 84 43,96 W | 03 |
| 1900 | Ende Profiil | | 09 00,00 N 84 25,35 W | 19 |

Profil EM-17 v = 8,0 kn

| | | | | |
|---|---|---|---|---|
| 1926 | Beginn Profil EM-17 | Kurs = 288 | 09 01,56 N 84 23,00 W | |
| 2145 | Ende Profil EM-17 | | 09 07,55 N 84 40,81 W | 19 |
| 2204 | Beginn Profil EM-18 | | 09 09,61 N 84 40,62 W | |

**19.04.02**

| | | | |
|---|---|---|---|
| 0032 | ä.K. 063 | 09 03,52 N 84 23,00 W | 20 |
| 0040 | ä.K. 288 | 09 03,97 N 84 21,48 W | 1 |
| 0304 | Ende Profil EM-18 | 09 10,37 N 84 40,00 W | |
| | Ende der Auszeichnunge | | |

**Appendix 9.7.2**

## F.S. "S O N N E" Reise SO 163/2

| Eingesetzte Geräte | | | Einsätze |
|---|---|---|---|
| OBH/ OBS | Ocean Bottom Hydrophones / Seismograph | ( Ausgesetzt ) | : 196 |
| OBH/OBS | dto | ( Aufgenommen ) | : 177 |
| MAG | Magnetometer | | : 2 |
| CTD | CTD Rosette | | : 8 |
| CTD/MUC | CTD Rosette mit Multicorer | | : 16 |
| 32 Ltr Airgun, 250 m Streamer, aktiv, 4 Kanal | | | |
| G-Gun | | | |
| Prakla Airgun-Array | | | |
| DR | Kettensackdredge | | : 4 |

**Vermessen wurden :**

| | |
|---|---|
| Mit Magnetometer | 223 sm |
| Mit Seizmik | 826 sm |

**Eingesetzte Winden :**

| *Winde* | *D/M* | . | *Typ* | *RF-Nr* | *SO 163/2 Einsatz* | *Gesamt Einsatz* | *SO 163/2 S'länge* | *Gesamt S'länge* | *Zust.* |
|---|---|---|---|---|---|---|---|---|---|
| W 1 | 18,2 | | LWL | 812001 | 0000 h | 0000 h | 000000 m | 0000000 m | 1 |
| W 2 | 18,2 | | LWL | 810001 | 0000 | 0942 | 093688 | 0199774 | 3 |
| W 4 | 11,0 | | NSW | 819052 | 0000 | 0000 | 000000 | 0000000 | 1 |
| W 5 | 11,0 | | NSW | 817164 | 0041 | 0269 | 045177 | 0239630 | 4 |
| W 6 | 18,2 | | DRAKO | 814150 | 0016 | 2148 | 013641 | 1870084 | 6 |

( Die W6 wird mit einem neuen Draht in Balboa am 20.05.02 bestückt )

| *Winde* | *SO 163/2 gefierte max.Länge* | *jemals gefierte max.Länge* |
|---|---|---|
| W 1 | 0000 m | 0000 m |
| W 2 | 0000 | 7202 |
| W 4 | 0000 | 0000 |
| W 5 | 4197 | 5200 |
| W 6 | 3000 | 7900 |

**Geräteverluste** :
1 Kettensackdredge ( Bundeseigentum )

**Abkürzungen im Stationsprotokoll:**

| | |
|---|---|
| z.W. | zu Wasser |
| a.D. | an Deck |
| Boko | Bodenkontakt |
| Bosi | Bodensicht |
| SL(max.) | (maximale)Seillänge |
| LT | Lottiefe nach Hydrosweep |
| W x | eingesetzte Winde |
| SM | Simrad- Multibeam-Lot |
| PS | Parasound |
| XPNDR | Transponder |

**Zeit : UTC – 06 Stunden**

**22.04.02**

| | | | |
|---|---|---|---|
| 1310 | Beginn Aufzeichnungen mit SM | | 09-28.85N 84-51.00W |
| 1400 | OBS 14 z/W | LT = 1748 m | 09-19.99N 84-53.00W |
| 1535 | OBH 15 z/W | LT = 115 m | 09-14.66N 84-36.05W |
| 1608 | OBH 16 z/W | LT = 945 m | 09-09.98N 84-38.01W |

Teststation 01 Releaser W6

| | | | |
|---|---|---|---|
| 1755 | Arbeitskorb mit Releasern z/W | LT = 3317 m | 08-53.10N 84-47.93W |
| 1855 | Slmax 3000m | LT = 3346 m | 08-53.04N 84-48.00W |
| 1941 | Hieven | | |
| 2045 | Arbeitskorb a/D | | |
| 2234 | OBH 19 z/W | LT = 2205 m | 09-00.00N 84-50.05W |
| 2338 | OBH 18 z/W | LT = 825 m | 09-09.39N 84-49.60W |
| 2340 | OBH 17 z/W ^ | LT = 825 m | 09-09.39N 84-49.60W |

**23.04.02**

| | | | |
|---|---|---|---|
| 0121 | OBH 21 z/W | LT = 3603 m | 08-58.02N 85-05.02W |
| 0558 | OBH 22 z/W | LT = 2019 m | 09-38.58N 85-52.35W |
| 0659 | OBH 23 z/W | LT = 1932 m | 09-40.20N 85-53.45W |

Seizmik Profil 01

| | | |
|---|---|---|
| 0729 | Airgun z/W | |
| 0742 | Streamer ausgesteckt, L 300m | |
| 0804 | Beginn Profil; V 3.5Kn; Kurs 145° | 09-40.98N 85-53.97W |
| 0858 | Ende Profil, 3.2sm | 09-38.34N 85-52.15W |
| 0909 | Stb Airgun vorgehievt | |
| 0917 | Airgun z/W | |
| 0920 | Drehen über Stb | |

Seizmik Profil 02

| | | |
|---|---|---|
| 0953 | Beginn Profil, V 4 Kn; Kurs 325° | 09-38.34N 85-52.15W |
| 1043 | Ende Profil; 3.2 sm | 09-40.99N 85-55.98W |
| 1047 | Stb Airgun vorgehievt | |
| 1103 | Airgun z/W | |
| 1104 | Drehen über Stb | |

Seizmik Profil 03

| | | |
|---|---|---|
| 1142 | Beginn Profil; V 4Kn; Kurs 145° | 09-40.99N 85-55.98W |
| 1238 | Ende Profil; 3.2sm | 09-38.34N 85-52.15W |
| 1248 | Stb Airgun vorgehievt | |
| 1253 | Airgun z/W | |
| 1300 | Drehen über Stb | |

Seizmik Profil 04

| | | |
|---|---|---|
| 1335 | Beginn Profil; V 4 Kn; Kurs 325° | 09-38.34N 85-52.15W |
| 1420 | Ende Profil, 3.2sm | 09-40.99N 85-53.98W |
| 1428 | Stb Airgun vorgehievt | |
| 1435 | Airgun z/W | |
| 1438 | Drehen über Stb | |

Seizmik Profil 05

| | | | |
|---|---|---|---|
| 1519 | Beginn Profil; V 4Kn; Kurs 145° | | 09-40.99N 85-53.98W |
| 1615 | Ende Profil; 3.2sm | | 09-38.34N 85-52.15W |
| 1625 | Stb Airgun vorgehievt | | |
| 1630 | Airgun z/W | | |
| 1632 | Drehen über Stb | | |

Seizmik Profil 06

| | | | |
|---|---|---|---|
| 1705 | Beginn Profil; V 4Kn; Kurs 325° | | 09-38.34N 85-52.15W |
| 1748 | Ende Profil; 3.2sm | | 09-40.99N 85-53.98W |
| 1803 | Airgun a/D | | |
| 1820 | Streamer a/D | | |

OBH 06

| | | | |
|---|---|---|---|
| 1827 | Release Command | | |
| 1851 | OBH gesichtet; Release Command OBH 03 | | |
| 1904 | OBH a/D | LT = 1980 m | 09-39.37N 85-53.76W |

OBH 03

| | | | |
|---|---|---|---|
| 1917 | Weitere Release Commands | | |
| 1941 | OBH gesichtet | | |
| 1950 | OBH a/D | LT = 2078 m | 09-38.13N 85-53.66W |

Station CTD 01 W5

| | | | |
|---|---|---|---|
| 2213 | Beginn Station | LT = 757 m | 10-05.45N 85-59.32W |
| 2215 | CTD z/W | | |
| 2220 | CTD a/D ( Probleme Bodenmelder ) | | |
| 2228 | CTD z/W | | |
| 2248 | Boko, Slmax 731m | LT = 739 m | 10-05.40N 85-59.28W |
| 2330 | CTD a/D | | |
| 2332 | Ende Station | | |

**24.04.02**

Station CTD/MUC 02 W5

| | | | |
|---|---|---|---|
| 0030 | Beginn Station | LT = 1357 m | 10-00.84N 86-03.84W |
| 0121 | MUC z/W | | |
| 0135 | CTD z/W | | |
| 0210 | Boko Slmax 1334m | LT = 1345 m | 10-00.84N 86-03.83W |
| 0318 | CTD a/D | | |
| 0326 | MIC a/D | | |
| 0330 | Ende Station | | |

Profil MAG 01

| | | | |
|---|---|---|---|
| 0357 | MAG z/W | | 10-00.57N 86-06.68W |
| 0403 | MAG ausgesteckt; L 250m | | |
| 0420 | Beginn Profil; V 11Kn; Kurs 225° | | 10-00.00N 86-10.00W |
| 0956-1136 | Fahren div. Ausweichkurse ( Longline Fischerei ) | | |
| 1318 | Ende Profil; 91 smEinhieven MAG | | 09-02.56N 87-05.36W |
| 1330 | MAG a/D | | |

Station CTD/MUC 03 W5

| | | | |
|---|---|---|---|
| 1348 | Beginn Station | LT = 3191 m | 09-00.02N 87-03.15W |
| 1350 | MUC z/W | | |
| 1357 | CTD z/W | | |

| | | | |
|---|---|---|---|
| 1525 | Boko, Slmax 3181m | LT = 3195 m | 09-00.05N 87-05.04W |
| 1655 | CTD a/D | | |
| 1705 | MIC a/D | | |
| 1707 | Ende Station | | |

Test G-Guns

| | | | |
|---|---|---|---|
| 1717 | GI Guns z/W; V 2Kn | | 09-00.49N 87-04.86W |
| 1737 | GI Guns a/D | | |

Station CTD 04 W5

| | | | |
|---|---|---|---|
| 2110 | Beginn Station | LT = 3135 m | 09-30.00N 86-35.29W |
| 2112 | CTD z/W | | |
| 2120 | CTD a/D ( Techn. Probleme ) | | |
| 2149 | CTD z/W | | |
| 2236 | Slmax 2080m | LT = 3131 m | 09-30.00N 86-35.29W |
| 2338 | CTD a/D | | |
| 2346 | Ende Station | | |

Seizmik Profil 07

| | | |
|---|---|---|
| 0330 | G-Gun z/W | 09-42.52N 85-55.09W |
| 0407 | Beginn Profil; V 4Kn; Kurs 145° | |
| 0455 | Ende Profil; 3 sm | 09-38.34N 85-52.15W |
| 0505 | G-Gun a/D | |

Seizmik Profil 08

| | | |
|---|---|---|
| 0510 | G-Gun z/W | |
| 0515 | Beginn Profil; V 4Kn; Kurs 325° | 09-38.34N 85-52.15W |
| 0600 | Ende Profil; 3 sm | 09-40.98N 85-53.98W |
| 0611 | G-Gun a/D | |

OBH 02

| | | |
|---|---|---|
| 0615 | Release Command | |
| 0636 | OBH aufgetaucht | |
| 0644 | OBH a/D | 09-40.69N 85-53.85W |

OBH 23

| | | |
|---|---|---|
| 0627 | Release Command | |
| 0645 | OBH aufgetaucht | |
| 0654 | OBH a/D | 09-40.39N 85-53.90W |

OBH 09

| | | |
|---|---|---|
| 0647 | Release Command | |
| 0710 | OBH aufgetaucht | |
| 0715 | OBH a/D | 09-39.65N 85-53.25W |

OBH 05

| | | |
|---|---|---|
| 0702 | Release Command | |
| 0730 | OBH aufgetaucht | |
| 0733 | OBH a/D | 09-39.90N 85-52.87W |

OBH 07

| | | |
|---|---|---|
| 0715 | Release Command | |
| 0742 | OBH aufgetaucht | |
| 0747 | OBH a/D | 09-39.04N 85-53.25W |

| | | | |
|---|---|---|---|
| OBH 10 | | | |
| 0725 | Release Command | | |
| 0755 | OBH aufgetaucht | | |
| 0802 | OBH a/D | | 09-39.46N 85-53.20W |
| 0728 | Schlauchboot z/W ( Aufnahme der OBH's ) | | |
| OBH 08 | | | |
| 0733 | Release Command | | |
| 0810 | OBH aufgetaucht | | |
| 0815 | OBH a/D | | 09-39.46N 85-52.83W |
| OBH 04 | | | |
| 0747 | Release Command | | |
| 0817 | OBH aufgetaucht | | |
| 0831 | OBH a/D | | 09-38.92N 85-53.03W |
| OBH 22 | | | |
| 0800 | Release Command | | |
| 0828 | OBH aufgetaucht | | |
| 0841 | OBH a/D | | 09-38.85N 85-53.09W |
| 0845 | Schlauchboot z/W | | |
| OBH 01 | | | |
| 0840 | Release Command | | |
| 0903 | OBH aufgetaucht | | |
| 0914 | OBH a/D | | 09-39.48N 85-51.74W |
| 0918 | Schlauchboot a/D | | |
| 1202 | OBS 24 z/W | LT = 2771 m | 09-15.92N 85-37.40W |
| 1225 | OBS 25 z/W | LT = 2769 m | 09-16.00N 85-37.31W |
| 1248 | OBH 26 z/W | LT = 2756 m | 09-16.08N 85-37.25W |
| 1303 | OBH 27 z/W | LT = 2756 m | 09-16.18N 85-37.17W |
| 1315 | OBH 28 z/W | LT = 2739 m | 09-16.27N 85-37.08W |
| 1327 | OBH 29 z/W | LT = 2703 m | 09-16.40N 85-37.00W |
| 1351 | OBH 30 z/W | LT = 2665 m | 09-16.52N 85-36.91W |
| 1417 | OBH 31 z/W | LT = 2658 m | 09-16.94N 85-36.56W |
| 1431 | OBH 32 z/W | LT = 2630 m | 09-17.03N 85-36.50W |
| 1505 | OBH 33 z/W | LT = 2263 m | 09-20.60N 85-33.68W |
| 1516 | OBH 34 z/W | LT = 2249 m | 09-20.69N 85-33.61W |
| 1529 | OBH 35 z/W | LT = 2247 m | 09-20.78N 85-33.55W |
| Seizmik/Mag Profil 09 | | | |
| 1801 | Airgun z/W | | |
| 1825 | Streamer ausgesteckt L 350m<br>Beginn Profil; V 4Kn; Kurs 218° | | 09-38.50N 85-16.30W |
| **26.04.02** | | | |
| 1240 | MAG ausgesteckt; L 250m | | |
| 1430 | Ende Profil 84sm | | 08-33.63N 86-10.44W |

| | | | |
|---|---|---|---|
| 1442 | Airgun a/D | | |

Seizmik/MAG Profil 10

| | | | |
|---|---|---|---|
| 1456 | G-Gun z/W; Stb Seite | | |
| 1504 | G-Gun z/W; Bb Seite | | |
| 1506 | Beginn Profil; V 4 Kn; Kurs 38° | | 08-33.53N 86-09.60W |

**27.04.02**

| | | | |
|---|---|---|---|
| 0040 | MAG a/D | | |
| 0600 | Ende Profil 76 sm | | 09-34.66N 85-22.64W |
| 0606 | Stb G-Gun a/D | | |
| 0610 | Bb G-Gun a/D | | |
| 0622 | Streamer a/D | | |

OBH 35

| | | | |
|---|---|---|---|
| 0748 | Release Command | | |
| 0811 | Div. Release Commands | | |
| 0835 | OBH geortet | | |
| 0847 | OBH a/D | | 09-21.22N 85-33.87W |

OBH 34

| | | | |
|---|---|---|---|
| 0749 | Release Command | | |
| 0815 | OBH geortet | | |
| 0832 | OBH a/D | | 09-21.24N 85-34.20W |

OBH 33

| | | | |
|---|---|---|---|
| 0749 | Release Command | | |
| 0815 | OBH geortet | | |
| 0827 | OBH a/D | | 09-21.08N 85-34.13W |
| 0822 | Schlauchboot z/W | | |
| 0850 | Schlauchboot a/D | | |
| 0935 | OBH 36 z/W | LT = 2613 m | 09-17.13N 85-36.42W |

Schwimmtest OBH ( Neu )

| | | | |
|---|---|---|---|
| 0954 | OBH z/W | | 09-17.09N 85-36.41W |
| 0956 | Ende Schwimmtest | | |
| 1026 | OBH z/W | LT = 2612 m | 09-17.18N 85-36.33W |

Seizmik Profil 11

| | | | |
|---|---|---|---|
| 1048 | G-Gun , Bb/Stb-Seeite z/W | | |
| | Beginn Profil; V 4Kn; Kurs 217° | | 09-17.30N 85-36.29W |
| 1100 | Streamer z/W, L350m | | |
| 1117 | Ende Profil 2 sm | | 09-15.85N 85-37.40W |

Seizmik Profil 12

| | | | |
|---|---|---|---|
| 1131 | Stb Airgun vorgehievt | | |
| 1137 | Stb Airgun z/W | | |
| 1203 | Beginn Profil; V 4Kn, Kurs 129° | | 09-16.77N 85-37.65W |
| 1223 | Ende Profil 2 sm | | 09-15.86N 85-36.54W |

| | | |
|---|---|---|
| 1229 | Bb Airgun a/D | |
| Seizmik Profil 13 | | |
| 1235 | Bb Airgun z/W | |
| 1305 | Beginn Profil; V 4Kn; Kurs 309° | 09-16.77N 85-35.97W |
| 1322 | Ende Profil; 2 sm | 09-17.47N 85-36.84W |
| Seizmik Profil 14 | | |
| 1337 | 32 Ltr Airgun z/W | |
| 1405 | Beginn Profil; V 4Kn; Kurs 218° | 09-17.40N 85-36.19W |
| 1435 | Ende Profil ; 2 sm | 09-15.85N 85-37.40W |
| 1447 | Airgun a/D | |
| 1451 | G-Gun Stb Seite a/D | |
| 1454 | G-Gun Bb Seite a/D | |
| 1504 | Streamer a/D | |
| OBS 24 | | |
| 1510 | Release Command | |
| 1548 | OBS gesichtet | |
| 1606 | OBS a/D | 09-16.55N 85-37.48W |
| OBS 25 | | |
| 1515 | Release Command | |
| 1550 | OBS gesichtet | |
| 1610 | OBS a/D | 09-16.55N 85-37.48W |
| OBS 26 | | |
| 1517 | Release Command | |
| 1555 | OBS gsichtet | |
| 1618 | OBS a/D | 09-16.86N 85-37.46W |
| OBH 27 | | |
| 1518 | Release Command | |
| 1556 | OBH gesichtet | |
| 1627 | OBH a/D | 09-16.65N 85-37.70W |
| OBH 28 | | |
| 1519 | Release Command | |
| 1610 | OBH gesichtet | |
| 1637 | OBH a/D | 09-16.77N 85-37.78W |
| OBH 29 | | |
| 1519 | Release Command | |
| 1620 | OBH gesichtet | |
| 1700 | OBH a/D | 09-17,77N 85-37.74W |
| 1600 | Schlauchboot z/W | |
| OBH 30 | | |
| 1610 | Release Command | |
| 1640 | OBH gesichtet | |
| 1722 | OBH a/D | 09-17.57N 85-37.47W |
| OBS 31 | | |

| | | | |
|---|---|---|---|
| 1624 | Release Command | | |
| 1650 | OBS gesichtet | | |
| 1731 | OBS a/D | | 09-18.07N 85-37.09W |

OBH 32

| | | | |
|---|---|---|---|
| 1640 | Release Command | | |
| 1730 | OBH gesichtet | | |
| 1801 | OBH a/D | | 09-17.86N 85-37.00W |

OBH 36

| | | | |
|---|---|---|---|
| 1646 | Release Command | | |
| 1730 | OBH gesichtet | | |
| 1801 | OBH a/D | | 09-17.86N 85-37.00W |
| 1700 | Schlauchboot a/D | | |
| 1735 | Schlauchboot z/W | | |
| 1822 | Schlauchboot a/D | | |

OBH 37

| | | | |
|---|---|---|---|
| 1750 | Release Command | | |
| 1844 | OBH gesichtet | | |
| 1853 | OBH a/D | | 09-17.79N 85-36.65W |

Station CTD 05 W5

| | | | |
|---|---|---|---|
| 2328 | Beginn Station | LT = 4227 m | 09-48.88N 86-16.23W |
| 2329 | CTD z/W | | |

**28.04.02**

| | | | |
|---|---|---|---|
| 0054 | Ausfall Winde | | |
| 0115 | Winde ok ( Sicherung ) | | |
| 0118 | Slmax 4197m | LT = 4228 m | 09-48.90N 86-16.23W |
| 0322 | CTD a/D | | |
| 0325 | Ende Station | | |

Station CTD/MUC 06 W5

| | | | |
|---|---|---|---|
| 0435 | Beginn Station | LT = 2403 m | 09-56.10N 86-09.00W |
| 0447 | MUC z/W | | |
| 0500 | CTD z/W | | |
| 0551 | Boko Slmax 2406m | LT = 2408 m | 09-56.10N 86-09.00W |
| 0704 | CTD a/D | | |
| 0715 | MUC a/D | | |
| 0716 | Ende Statiopn | | |

OBH 17

| | | | |
|---|---|---|---|
| 1515 | Release Command | | |
| 1523 | OBH gesichtet | | |
| 1535 | OBH a/D | | 09-09.55N 84-49.51W |
| 1627 | OBH 38 z/W | LT = 1745 m | 09-14.27N 84-56.65W |
| 1730 | OBH 39 z/W | LT = 2495 m | 09-05.26N 85-02.56W |
| 1848 | OBH 40 z/w | LT = 3420 m | 08-53.33N 84-58.43W |

| | | | |
|---|---|---|---|
| 2001 | OBH 41 z/W | LT = 2614 m | 08-56.04N 84-43.43W |
| 2058 | OBH 42 z/W | LT = 1485 m | 09-05.17N 84-39.09W |

Station CTD/MUC 07 W5

| | | | |
|---|---|---|---|
| 2216 | Beginn Station | LT = 1888 m | 09-06.91N 84-50.87W |
| 2218 | MUC z/W | | |
| 2225 | CTD z/W | | |
| 2315 | Boko; Slmax 1871m | LT = 1906 m | 09-06.91N 84-50.86W |

**29.04.02**

| | | | |
|---|---|---|---|
| 0033 | CTD a/D | | |
| 0042 | MUC a/D | | |
| 0043 | Ende Station | | |
| 0428 | OBH 43 z/W | LT = 93 m | 09-17.09N 84-10.52W |
| 0443 | OBH 44 z/W | LT = 105 m | 09-16.12N 84-11.22W |
| 0500 | OBH 45 z/W | LT = 120 m | 09-14.92N 84-12.10W |
| 0517 | OBH 46 z/W | LT = 148 m | 09-13.52N 84-13.14W |
| 0538 | OBH 47 z/W | LT = 205 m | 09-11.96N 84-14.26W |
| 0600 | OBS 48 z/W | LT = 360 m | 09-10.59N 84-15.29W |
| 0618 | OBH 49 z/W | LT = 459 m | 09-08.99N 84-16.48W |
| 0639 | OBS 50 z/W | LT = 480 m | 09-08.04N 84-17.15W |
| 0700 | OBH 51 z/W | LT = 502 m | 09-06.50N 84-18.30W |
| 0720 | OBS 52 z/W | LT = 567 m | 09-05.05N 84-19.37W |
| 0737 | OBH 53 z/W | LT = 666 m | 09-03.54N 84-20.50W |
| 0755 | OBS 54 z/W | LT = 763 m | 09-02.02N 84-21.61W |
| 0824 | OBH 55 z/W | LT = 966 m | 09-00.04N 84-23.03W |
| 0847 | OBH 56 z/W | LT = 1192 m | 08-58.14N 84-24.46W |
| 0916 | OBH 57 z/W | LT = 1578 m | 08-56.01N 84-26.05W |
| 0938 | OBH 58 z/W | LT = 1819 m | 08-54.52N 84-27.14W |
| 1000 | OBH 59 z/W | LT = 1975 m | 08-53.04N 84-28.30W |

Seizmik Profil 15

| | | |
|---|---|---|
| 1127 | G-Gun Bb Seite z/W | |
| 1134 | G-Gun Stb Seite z/W | |
| 1134 | Streamer z/W L 350m | |
| 1156 | Beginn Profil; V 4Kn; Kurs 036° | 08-44.56N 84-34.48W |
| 2240 | Ende Profil 43sm | 09-17.09N 84-10.56W |

Seizmik Profil 16

| | | |
|---|---|---|
| 2250 | G-Gun Bb Seite vorgehievt | |
| 2255 | G-Gun Bb Seite z/W | |
| 2301 | G-Gun Stb Seite vorgehievt | |
| 2309 | G-Gun Stb Seite z/W | |
| 2323 | Beginn Profil; V 4Kn; Kurs 216° | 09-16.81N 84-10.74W |
| 2329 | 32 Ltr. Airgun z/W | |
| 2345 | G-Gun Bb Seite eingeholt | |

**30.04.02**

| | | |
|---|---|---|
| 0113 | G-Gun Stb Seite a/D | |
| 0928 | Ende Profil 40 sm | 08-44.26N 84-34.69W |
| 0914 | Sreamer a/D | |
| 0938 | Airgun a/D | |

| | | | |
|---|---|---|---|
| OBH 59 | | | |
| 1027 | Release Command | | |
| 1052 | OBH gesichtet | | |
| 1102 | OBH a/D | 08-52.99N | 84-28.17W |
| OBH 58 | | | |
| 1050 | Release Command | | |
| 1113 | OBH gesichtet | | |
| 1126 | OBH 58 a/D | 08-54.59N | 84-26.99W |
| OBS 57 | | | |
| 1115 | Release Command | | |
| 1135 | OBH gesichtet | | |
| 1155 | OBS a/D | 08-55.98N | 84-25.89W |
| OBS 56 | | | |
| 1145 | Release Commmand | | |
| 1210 | OBS aufgetaucht | | |
| 1224 | OBH a/D | 08-58.13N | 84-24.53W |
| OBH 55 | | | |
| 1224 | Release Command | | |
| 1242 | OBH gesichtet | | |
| 1253 | OBH a/D | 09-00.04N | 84-23.08W |
| OBS 54 | | | |
| 1254 | Release Command | | |
| 1308 | OBH gesichtet | | |
| 1320 | OBS a/D | 09-02.05N | 84-21.66W |
| OBH 53 | | | |
| 1322 | Release Command | | |
| 1330 | OBH gesichtet | | |
| 1344 | OBH a/D | 09-03.59N | 84-20.55W |
| OBS 52 | | | |
| 1350 | Release Command | | |
| 1357 | OBS gesichtet | | |
| 1413 | OBS 52 a/D | 09-05.14N | 84-19.39W |
| OBH 51 | | | |
| 1415 | Release Command | | |
| 1425 | OBH gesichtet | | |
| 1436 | OBH a/D | 09-06.60N | 84-18.30W |
| OBS 50 | | | |
| 1441 | Release Command | | |
| 1448 | OBS gesichtet | | |
| 1500 | OBS a/D | 09-08.11N | 84-17.17W |
| OBH 49 | | | |
| 1502 | Release Command | | |
| 1510 | OBH gesichtet | | |
| 1524 | OBH a/D | 09-08.97N | 84-16.48W |

Test G-Gun

| | | |
|---|---|---|
| 1530 | G-Gun z/W | 09-08.97N 84-16.48W |
| 1535 | G-Gun a/D | |

OBS 48

| | | |
|---|---|---|
| 1542 | Release Command | |
| 1550 | OBS gesichtet | |
| 1604 | OBS a/D | 09-10.61N 84-15.29W |

OBS 47

| | | |
|---|---|---|
| 1605 | Release Command; keine Anzeige, daß steigt; div. Ortungsversuche | |
| 1704 | Div. Simrad Profile über Pos. OBS | |

OBH 46

| | | |
|---|---|---|
| 1142 | Release Command | |
| 1650 | OBH gesichtet | |
| 1704 | OBH a/D | 09-13.46N 84-13.22W |

1. Bergungsversuch OBS 47 W6

| | | |
|---|---|---|
| 1755 | Beginn Versuch; DR z/W LT = 203 m | 09-12.03N 84-14.36W |
| 1756-1809 | Setzen SL 80m alle 30m ein Eisenbahnstück bis SL 200 | |
| 1811 | Boko; SL 235m; Beginn Vollkreisfahren um Pos. OBS ; Abstand 0.15sm V 0.8Kn; Fieren 0.5msec | |
| 1910 | Erreichen Aussetzpunkt; Vollkreis gefahren; SL 2178m Fahren in NE#L Richtung | |
| 1930 | Stoppen Winde Slmax 2637 m | 09-12.25N 84-14.27W |
| 1931 | Beginn Hieven, 0.8m/sec | |
| 1945 | Draht aus Seilrolle Schiebebalken gesprungen: SL 2038m | |
| 2024 | Draht klariert | |
| 2134 | DR a/D | |

2. Bergungsversuch OBS 47 W6

| | | |
|---|---|---|
| 2139 | Beginn Versuch; DR z/W LT = 203 m | 09-12.02N 84-14.36W |
| 2143-2154 | Setzen SL 80m alle 30m ein Eisenbahnstück | |
| 2155 | Boko; SL 235m; Beginn Vollkreisfahren um Pos. OBS ; Abstand 0.15sm; V 0.8Kn; Fieren 0.8m/sec | |
| 2217 | Verringern Vollkreis um OBS auf 0.05sm | 09-11.90N 84-14.21W |
| 2214 | Fahren div. Ausweichkurse wegen Fischerei | |
| 2230 | Erreichen Aussetzpos.; drehen über Stb auf 135° | |
| 2249 | Seillänge 1800m; Stoppen Winde; V 0.8Kn | |
| 2256 | Stoppen Schiff; Hieven mit 0.6m/sec | |
| 2354 | DR a/D | |

**01.05.02**

OBH 45

| | | |
|---|---|---|
| 0017 | Release Command | |
| 0020 | OBH gesichtet | |
| 0034 | OBH a/D | 09-14.98N 84-12.16W |

OBH 44

| | | |
|---|---|---|
| 0046 | Release Command | |
| 0048 | OBH gesichtet | |
| 0100 | OBH a/D | 09-16.13N 84-11.27W |

OBH 43

| | | | |
|---|---|---|---|
| 0112 | Release Command | | |
| 0114 | OBH gesichtet | | |
| 0125 | OBH a/D | | 09-17.08N 84-10.61W |

Station CTD/MUC 08 W5

| | | | |
|---|---|---|---|
| 0450 | Beginn Station | LT = 1417 m | 09-07.68N 84-50.35W |
| 0523 | MUC z/W | | |
| 0530 | CTD z/W | | |
| 0535 | XPNDR z/W | | |
| 0613 | Boko; SImax 1407m | LT = 1439 m | 09-07.68N 84-50.33W |
| 0717 | XPNDR a/D | | |
| 0721 | CTD a/D | | |
| 0730 | MUC a/D | | |
| 0731 | Ende Station | | |

Station CTD/MUC 09 W5

| | | | |
|---|---|---|---|
| 0919 | Beginn Station | LT = 967 m | 09-08.30N 84-49.93W |
| 0922 | MUC z/W | | |
| 0929 | CTD z/W | | |
| 0936 | XPNDR z/W | | |
| 0954 | Boko; SImax 948m | LT = 967 m | 09-08.30N 84-49.93W |
| 1037 | XPNDR a/D | | |
| 1048 | CTD a/D | | |
| 1055 | MUC a/D | | |
| 1056 | Ende Station | | |

3. Bergungsversuch OBS 47 W6

| | | | |
|---|---|---|---|
| 1405 | Beginn Versuch; DR z/W | LT = 203 m | 09-11.86N 84-14.22W |
| 1407-1414 | Setzen alle SL 20m von DR z/W je ein Eisenbahnst5ück | | |
| 1420 | Boko; SL 239m; fahren in W'l Richtung S'l an Pos. OBS vorbei | | |
| 1430 | Beginn Vollkreis zu fahren V 0.8Kn; Fieren 0.4m/sec; Abstand Pos. OBS 0.11s | | 09-12.01N 84-14.38W |
| 1453 | Verringern Vollkreis auf 0.05sm | | |
| 1500 | Div. Ausweichen wegen Fischerei | | |
| 1525 | Vollkreis abgefahren SL 1530m; fahren in Richtung NE | | |
| 1535 | Seillänge 1807m; Stoppen Fieren; V 0.8KN | | |
| 1615 | Stoppen Schiff; Beginn Hieven 0.6m/sec; | | |
| 1625 | OBS geortet; Tension auf 5.5 to; dann Entlastun | | |
| 1630 | OBS gesichtet | | |
| 1651 | Drahtende a/D; verloren : 1 Kettensackdredge; 811m Draht; 5 Eisenbahnstücke | | |

OBS 47

| | | | |
|---|---|---|---|
| 1630 | OBS gesichtet | | |
| 1710 | OBS a/D | | 09-12.24N 84-13.77W |
| 2048 | OBT 60 z/W | LT = 1839 m | 08-36.01N 84-35.77W |
| 2056 | OBT 61 z/W | LT = 1840 m | 08-36.00N 84-35.49W |

Station CTD/MUC 10 W5

| | | | |
|---|---|---|---|
| 2306 | Beginn Station | LT = 1411 m | 09-01.96N 84-57.22W |
| 2351 | MUC z/W | | |
| 2400 | CTD z/W | | |

**02.05.02**

| | | | |
|---|---|---|---|
| 0006 | XPNDR z/W | | |
| 0035 | Boko, Slmax 1390m | LT = 1406 m | 09-01.93N 84-37.24W |
| 0135 | XPNDR a/D | | |
| 0140 | CTD a/D | | |
| 0150 | MUC a/D | | |
| | | | |
| 0226 | OBH 62 z/W | LT = 1035 m | 09-06.99N 84-33.56W |
| 0244 | OBH 63 z/W | LT = 1009 m | 09-05.98N 84-31.98W |
| 0301 | OBH 64 z/W | LT = 1031 m | 09-04.97N 84-30.40W |
| 0318 | OBS 65 z/W | LT = 1128 m | 09-03.98N 84-28.79W |
| 0335 | OBH 66 z/W | LT = 1173 m | 09-03.01N 84-27.23W |
| 0353 | OBH 67 z7W | LT = 1191 m | 09-02.01N 84-25.59W |
| 0410 | OBS 68 z/W | LT = 1157 m | 09-01.01N 84-24.03W |
| 0427 | OBH 69 z/W | LT = 929 m | 09-59.95N 84-22.35W |
| 0512 | OBS 70 z/W | LT = 980 m | 08-58.91N 84-20.67W |
| 0530 | OBH 71 z/W | LT = 904 m | 08-57.88N 84-19.05W |
| 0547 | OBS 72 z/W | LT = 930 m | 08-56.85N 84-17.40W |
| 0604 | OBH 73 z/W | LT = 944 m | 08-55.79N 84-15.65W |
| 0632 | OBS 74 z/W | LT = 792 m | 08-54.70N 84-13.98W |
| 0648 | OBH 75 z/W | LT = 274 m | 08-53.64N 84-12.20W |

Seizmik Profil 17

| | | |
|---|---|---|
| 0725 | G-Gun Bb Seite z/W | |
| 0729 | G-Gun Stb Seite z/W | |
| 0738 | Streamer z/W, L 350m | |
| 0751 | Beginn Profil, V 3.5Kn; Kurs 302° | 08-51.83N 84-07.33W |
| 1640 | Ende Profil 30sm, | 09-08.33N 84-35.72W |

Seizmik Profil 18

| | | |
|---|---|---|
| 1648 | G-Gun Stb Seite a/D | |
| 1652 | G-Gun Bb Seite a/D | |
| 1706 | 32 Ltr Airgun z/W | |
| 1710 | Beginn Profil; V 3.5Kn; Kurs 122° | 09-08.65N 84-35.91W |

**03.05.02**

| | | |
|---|---|---|
| 0142 | Ende Profil 30sm | |
| 0151 | Airgun a/D | |
| 0200 | Streamer a/D | |

OBH 75

| | | |
|---|---|---|
| 0223 | Release Command | |
| 0226 | OBH gesichtet | |
| 0239 | OBH a/D | 08-53.58N 84-12.24W |

OBS 74

| | | |
|---|---|---|
| 0248 | Release Command | |
| 0304 | OBS gesichtet | |
| 0312 | OBS a/D | 08-54.60N 84-13.95W |

OBH 73

| | | |
|---|---|---|
| 0315 | Release Command | |
| 0328 | OBH gesichtet | |

| | | | |
|---|---|---|---|
| 0337 | OBH a/D | 08-55.77N | 84-15.63W |
| OBS 72 | | | |
| 0339 | Release Command | | |
| 0351 | OBS gesichtet | | |
| 0400 | OBS a/D | 08-56.87N | 84-17.29W |
| OBH 71 | | | |
| 0402 | Release Command | | |
| 0414 | OBH gesichtet | | |
| 0426 | OBH a/D | 08-57.95N | 84-18.99W |
| OBS 70 | | | |
| 0427 | Release Command | | |
| 0440 | OBS gesichtet | | |
| 0452 | OBS a/D | 08-58.95N | 84-20.56W |
| OBH 69 | | | |
| 0452 | Release Command | | |
| 0503 | OBH gesichtet | | |
| 0517 | OBH a/D | 08-59.97N | 84-22.20W |
| OBS 68 | | | |
| 0518 | Release Command | | |
| 0535 | OBH gesichtet | | |
| 0544 | OBS a/D | 09-01.01N | 84-23.99W |
| OBH 67 | | | |
| 0545 | Release Command | | |
| 0558 | OBH gesichtet | | |
| 0606 | OBH a/D | 09-02.09N | 84-25.61W |
| OBH 66 | | | |
| 0606 | Release Command | | |
| 0621 | OBH gesichtet | | |
| 0627 | OBH a/D | 09-03.10N | 84-27.23W |
| OBS 65 | | | |
| 0627 | Release Command | | |
| 0638 | OBH gesichtet | | |
| 0647 | OBH a/D | 09-04.02N | 84-28.77W |
| OBH 64 | | | |
| 0650 | Release Command | | |
| 0700 | OBH gesichtet | | |
| 0706 | OBH a/D | 09-04.99N | 84-30.42W |
| OBH 63 | | | |
| 0708 | Release Command | | |
| 0719 | OBH gesichtet | | |
| 0725 | OBH a/D | 09-06.02N | 84-31.96W |
| OBH 62 | | | |
| 0725 | Release Command | | |
| 0737 | OBH gesichtet | | |

| | | | |
|---|---|---|---|
| 0744 | OBH a/D | | 09-07.01N 84-33.59W |

Station CTD 11 W5

| | | | |
|---|---|---|---|
| 0930 | Beginn Station | LT = 1428 m | 09-01.87N 84-37.32W |
| 0936 | CTD z/W | | |
| 0943 | SL 40 XPNDR z/W | | |
| 1021 | Slmax 1408m | LT = 1429 m | 09-01.87N 84-37.32W |
| 1033 | SL 1354 m, verholen 0.08sm N'l | | |
| 1059 | Slmax 1409m | LT = 1419 m | 09-01.95N 84-37.31W |
| 1111 | SL 1350m verholen 0.07sm N'l | | |
| 1132 | Slmax 1421m | LT = 1433 m | 09-02.02n ($-§/:§"w |
| 1220 | XPNDR a/D | | |
| 1230 | CTD a/D | | |
| 1232 | Ende Station | | |

Station CTD 12 W5

| | | | |
|---|---|---|---|
| 1230 | Beginn Station | LT = 1428 m | 09-02.02N 84-37.32W |
| 1333 | CTD z/W | | |
| 1339 | XPNDR z/W SL 40m | | |
| 1415 | Slmax 1415m | LT = 1426 m | 09-02.02N 84-37.32W |
| 1425 | SL 1357m verholen 0.08sm N'l | | |
| 1450 | Slmax 1410m | LT = 1417 m | 09-01.95N 84-37.17W |
| 1510 | SL 1301m verholen 0.07sm N'l | | |
| 1535 | Slmax 1435m | LT = 1441 m | 09-02.02N 84-37.17W |
| 1620 | XPNDR a/D | | |
| 1625 | CTD a/D | | |
| 1625 | Ende Station | | |

| | | | |
|---|---|---|---|
| 1658 | OBH 76 z/W | LT = 1186 m | 09-03.69N 84-32.88W |
| 1713 | OBH 77 z/W | LT = 1244 m | 09-02.89N 84-31.58W |
| 1727 | OBH 78 z/W | LT = 1273 m | 09-02.08N 84-30.28W |
| 1742 | OBH 79 z/W | LT = 1315 m | 09-01.25N 84-28.96W |
| 1754 | OBH 80 z/W | LT = 1340 m | 09-00.46N 84-27.70W |
| 1807 | OBS 81 z/W | LT = 1340 m | 08-59.74N 84-26.51W |
| 1822 | OBH 82 z/W | LT = 1242 m | 08-58.93N 84-25.19W |
| 1833 | OBS 83 z7W | LT = 1172 m | 08-58.11N 84-23.92W |
| 1851 | OBS 84 z/W | LT = 1117 m | 08-57.31N 84-22.60W |
| 1905 | OBS 85 z/W | LT = 1099 m | 08-56.50N 84-21.36W |
| 1918 | OBS 86 z/W | LT = 1118 m | 08-55.72N 84-20.12W |
| 1933 | OBH 87 z/W | LT = 1117 m | 08-54.91N 84-18.81W |
| 1947 | OBH 88 z/W | LT = 1077 m | 08-54.11N 84-17.51W |
| 1959 | OBH 89 z/W | LT = 1089 m | 08-53.56N 84-16.62W |
| 2011 | OBH 90 z/W | LT = 958 m | 08-53.01N 84-15.77W |

Seizmik Profil 19

| | | |
|---|---|---|
| 2026 | Streamer z/W L 350m | |
| 2106 | Prakla Airgun z/W Bb Seite | |
| 2113 | Beginn Profil, V 3.5Kn, Kurs 302° | 08-52.58N 84-15.14W |

**04.05.02**

| | | |
|---|---|---|
| 0354 | Ende Profil 23 sm | |

Seizmik Profil 20

| | | |
|---|---|---|
| 0453 | Beginn Profil, V 3.5<Kn, Kurs 180° | 09-02.50N 84-37.25W |

| | | |
|---|---|---|
| 0509 | Ende Profil 1 sm | |
| Seizmik Profil 20B | | |
| 0600 | Beginn Profil, V 3.5Kn, Kurs 360° | 09-01.50N 84-37.25W |
| 0616 | Ende Profil 1sm ; Prakla Airgun Array a/D | 09-02.57N 84-37.25W |
| Seizmik Profil 21 | | |
| 0703 | 32 Ltr Airgun Stb Seite z/W | |
| 0724 | Beginn Profil, V 3.5Kn, Kurs 122° | 09-04.80N 84-34.62W |
| 1426 | Ende Profil 34sm | |
| 1436 | Airgun a/D, drehen über Stb | |
| 1450 | G-Gun Bb Seite z/W | |
| 1455 | G-Gun Stb Seite z/W | |
| Seizmik Profil 22 | | |
| 1502 | Beginn Profil, V 3.5Kn, Kurs 302° | 08-51.68N 84-13.63W |
| 2209 | Ende Profil 25sm | 09-05.03N 84-35.00W |
| 2215 | G-Gun Bb Seite a/D | |
| 2218 | G-Gun Stb Seite a/D, drehen über Stb | |
| 2254 | 32 Ltr Airgun z/W | |
| Seizmik Profil 23 | | |
| 2255 | Beginn Profil, V 3.5Kn; Kurs 122° | 09-05.10N 85-35.09W |
| **05.05.02** | | |
| 0100 | G-Gun Bb Seite z/W | |
| 0103 | G-Gun Stb Seite z/W | |
| 0108 | Airgun a/D | |
| 0607 | Ende Profil 25sm | 08-51.70N 84-13.66W |
| 0612 | G-Gun Bb Seite a/D | |
| 0620 | G-Gun Stb Seite a/D | |
| 0629 | Streamer a/D | |
| OBH 90 | | |
| 0656 | Release Command | |
| 0707 | OBH gesichtet | |
| 0712 | OBH a/D | 08-53.04N 84-15.78W |
| OBH 88 | | |
| 0707 | Release Command | |
| 0750 | OBH gesichtet | |
| 0759 | OBH a/D | 08-54.33N 84-17.37W |
| OBH 89 | | |
| 0727 | Release Command | |
| 0744 | OBH gesichtet | |
| 0747 | OBH a/D | 08-53.61N 84-16.62W |
| OBH 87 | | |
| 0800 | Release Command | |
| 0816 | OBH gesichtet | |
| 0827 | OBH a/D | 08-54.96N 84-18.72W |
| OBH 86 | | |
| 0801 | Release Command | |

| | | |
|---|---|---|
| 0834 | OBH gesichtet | |
| 0848 | OBH a/D | 08-55.86N 84-19.99W |
| | | |
| OBH 85 | | |
| 0845 | Release Command | |
| 0901 | OBH gesichtet | |
| 0910 | OBH a/D | 08-56.57N 84-21.35W |
| | | |
| OBS 84 | | |
| 0905 | Release Command | |
| 0919 | OBH gesichtet | |
| 0937 | OBH a/D | 08-57.40N 84-22.64W |
| | | |
| OBH 83 | | |
| 0920 | Release Command | |
| 0945 | OBH gesichtet | |
| 0956 | OBS a/D | 08-58.21N 84-23.92W |
| | | |
| OBS 82 | | |
| 0948 | Release Command | |
| 1007 | OBS gesichtet | |
| 1016 | OBS a/D | 08-58.99N 84-25.20W |
| | | |
| OBS 81 | | |
| 1016 | Release Command | |
| 1032 | OBS gesichtet | |
| 1037 | OBS a/D | 08-59.78N 84-26.52W |
| | | |
| OBH 80 | | |
| 1032 | Release Command | |
| 1055 | OBH gesichtet | |
| 1057 | OBH a/D | 09-00.51N 84-27.69W |
| | | |
| OBH 79 | | |
| 1055 | Release Command | |
| 1106 | OBH gesichtet | |
| 1115 | OBH a/D | 09-01.32N 84-28.97W |
| | | |
| OBH 78 | | |
| 1109 | Release Command | |
| 1125 | OBH gesichtet | |
| 1131 | OBH a/D | 09-02.08N 84-30.30W |
| | | |
| OBH 77 | | |
| 1125 | Release Command | |
| 1145 | OBH geischte | |
| 1151 | OBH a/D | 09-02.90N 84-31.64W |
| | | |
| OBH 76 | | |
| 1145 | Release Command | |
| 1200 | OBH gesichtet | |
| 1228 | OBH a/D | 09-03.66N 84-32.96W |

Station CTD 13 W5

| | | | |
|---|---|---|---|
| 1308 | Beginn Station | LT = 1419 m | 09-01.87N 84-37.25W |
| 1310 | CTD z/W | | |
| 1318 | XPND z/W SL 40m | | |
| 1347 | Slmax 1403m | LT = 1418 m | 09-01.87N 84-37.25W |
| 1400 | SL 1328m, verholen 0.08sm N'l | | |
| 1423 | Slmax 1401m | LT = 1412 m | 09-01.95N 84-37.26W |
| 1433 | SL 1339m, verholen 0.07sm N'l | | |
| 1455 | Slmax 1423m | LT = 1431 m | 09-02.02N 84-37.25W |
| 1535 | XPNDR a/D | | |
| 1540 | CTD a/D | | |
| 1541 | Ende Station | | |

Station CTD/MUC 14 W5

| | | | |
|---|---|---|---|
| 1645 | Beginn Station | LT = 1402 m | 09-01.95N 84-37.22W |
| 1650 | MUC z/W | | |
| 1700 | CTD z/W; SL 10m über MUC | | |
| 1708 | XPNDR z/W | | |
| 1733 | Boko, Slmax 1397m | LT = 1403 m | 09-01.95N 84-37.22W |
| 1817 | XPNDR a/D | | |
| 1829 | CTD a/D | | |
| 1830 | Ende Station | | |

Test OBS 2002

| | | | |
|---|---|---|---|
| 2117 | Beginn Test | LT = 62 m | 09-22.11N 84-13.50W |
| 2121 | OBS z/W ( Fangleine und Transducer ) | | |
| 2123 | Release Command OBS | | |
| 2138 | OBS a/D | | |
| 2149 | Ende Test | | |

| | | | |
|---|---|---|---|
| 2242 | OBH 92 z/W | LT = 151 m | 09-14.92N 84-15.18W |
| 2257 | OBH 93 z/W | LT = 186 m | 09-13.72N 84-16.04W |
| 2312 | OBH 94 z/W | LT = 374 m | 09-12.44N 84-16.99W |
| 2325 | OBH 95 z/W ^ | LT = 467 m | 09-11.08N 84-17.96W |
| 2341 | OBS 96 z/W | LT = 497 m | 09-09.74N 84-19.03W |
| 2400 | OBS 97 z/W | LT = 554 m | 09-07.85N 84-20.34W |

**06.05.02**

| | | | |
|---|---|---|---|
| 0019 | OBS 98 z/W | LT = 651 m | 09-06.15N 84-21.61W |
| 0038 | OBS 99 z/W | LT = 847 m | 09-04.27N 84-22.97W |
| 0054 | OBS 100 z/W | LT = 1082 m | 09-03.01N 84-23.93W |
| 0108 | OBH 101 z/W | LT = 1160 m | 09-01.77N 84-24.83W |
| 0124 | OBH 102 z/W | LT = 1297 m | 09-00.34N 84-25.88W |
| 0138 | OBH 103 z/W | LT = 1423 m | 08-58.95N 84-26.88W |
| 0152 | OBH 104 z/W | LT = 1614 m | 08-57.66N 84-27.85W |
| 0210 | OBH 105 z/W | LT = 1789 m | 08-56.04N 84-29.05W |
| 0227 | OBH 106 z/W | LT = 1961 m | 08-54.31N 84-30.33W |

Seizmik Profil 24

| | | |
|---|---|---|
| 0345 | Streamer z/W; L 350m | |
| 0355 | G-Gun Bb Seite z/W | |
| 0359 | G-Gun Stb Seite z7W | |
| 0420 | Beginn Profil, V 3.5Kn, Kurs 36° | 08-45.56N 84-36.77W |
| 1600 | Ende Profil, 41sm; drehen über Stb | |

Seizmik Profil 25

| | | |
|---|---|---|
| 1630 | 32 Ltr Airgun z/W | |
| 1635 | Beginn Profil, V 3.5Kn; Kurs 216° | 09-18.44N 84-12.45W |

**07.05.02**

| | | |
|---|---|---|
| 0600 | Ende Profil 41sm | 08-45.56N 84-36.77W |
| 0610 | Airgun a/D | |
| 0615 | G-Gun Stb Seite a/D | |
| 0620 | G-Gun Bb Seite a/D | |
| 0626 | Streamer a/D | |

OBH 106

| | | |
|---|---|---|
| 0716 | Release Command | |
| 0736 | OBH gesichtet | |
| 0745 | OBH a/D | 08-54.28N 84-30.28W |

OBH 105

| | | |
|---|---|---|
| 0736 | Release Command | |
| 0801 | OBH gesichtet | |
| 0812 | OBH a7d | 08-56.02N 84-28.99E |

OBH 104

| | | |
|---|---|---|
| 0801 | Release Command | |
| 0827 | OBH gesichtet | |
| 0836 | OBH a/D | 08-57.70N 84-27.85W |

OBH 103

| | | |
|---|---|---|
| 0828 | Release Command | |
| 0850 | OBH gesichtet | |
| 0858 | OBH a/D | 08-58.94N 84-26.91W |

OBH 102

| | | |
|---|---|---|
| 0850 | Release Command | |
| 0911 | OBH gesichtet | |
| 0919 | OBH a/D | 09-00.39N 84-25.92W |

OBH 101

| | | |
|---|---|---|
| 0910 | Release Command | |
| 0930 | OBH gesichtet | |
| 0942 | OBH a/D | 09-01.84N 84-24.84W |

OBS 100

| | | |
|---|---|---|
| 0935 | Release Command | |
| 0951 | OBS gesichtet | |
| 1003 | OBS a/D | 09-03.11N 84-23.90W |

OBS 99

| | | |
|---|---|---|
| 0955 | Relaese Command | |
| 1014 | OBS gesichtet | |
| 1023 | OBS a/D | 09-04.42N 84-22.97W |

OBS 98

| | | |
|---|---|---|
| 1030 | Release Command | |
| 1041 | OBS gesichtet | |

| | | | |
|---|---|---|---|
| 1048 | OBS a/D | | 09-06.17N 84-21.55W |
| OBS 97 | | | |
| 1055 | Release Command | | |
| 1106 | OBS gesichtet | | |
| 1113 | OBS a/D | | 09-07.95N 84-20.29W |
| OBS 96 | | | |
| 1122 | Release Command | | |
| 1130 | OBS gesichtet | | |
| 1136 | OBS a/D | | 09-07.75N 84-18.98W |
| OBH 94 | | | |
| 1143 | Release Command | | |
| 1151 | OBH aufgetaucht | | |
| 1159 | OBH a/D | | 09-11.12N 84-17.99W |
| OBH 95 | | | |
| 1206 | Release Command | | |
| 1213 | OBH gesichtet | | |
| 1222 | OBH a/D | | 09-12.42N 84-17.01W |
| OBH 93 | | | |
| 1233 | Release Command | | |
| 1237 | OBH gesichtet | | |
| 1247 | OBH a/D | | 09-13.77N 84-16.07W |
| OBH 92 | | | |
| 1255 | Release Command | | |
| 1258 | OBH gesichtet | | |
| 1309 | OBH a/D | | 09-14.96N 84-15.19W |
| Station CTD/MUC 15 W5 | | | |
| 1550 | Beginn Station | LT = 420 m | 08-47.24N 84-11.60W |
| 1555 | MUC z/W | | |
| 1603 | CTD z/W SL 20m | | |
| 1623 | Boko, Slmax 401m | LT = 421 m | 08-47.23N 84-11.62W |
| 1700 | CTD a/D | | |
| 1707 | MUC a/D | | |
| 1710 | Ende Station | | |
| Station CTD/MUC 16 W5 | | | |
| 1800 | Beginn Station | LT = 1474 m | 08-42.20N 84-16.70W |
| 1835 | Muc z/W | | |
| 1841 | CTD z/W SL 20m | | |
| 1913 | Boko, Slmax 1449m | LT = 1466 m | 08-42.20N 84-16.71W |
| 2008 | CTD a/D | | |
| 2016 | MUC a/D | | |
| 2025 | Ende Station | | |
| 2107 | OBH 107 z/W ( 1000m Seil ) | LT = 1839 m | 08-40.51N 84-18.32W |
| 2114 | OBH 108 z/W | LT = 1865 m | 08-40.31N 84-18.48W |
| 2122 | OBH 109 z/W | LT = 1011 m | 08-40.08N 84-18.61W |
| 2127 | OBH 110 z/W | LT = 1963 m | 08-39.93N 84-18.71W |

| | | | |
|---|---|---|---|
| 2133 | OBS 111 z/W | LT = 2042 m | 08-39.76N 84-18.81W |
| 2141 | OBS 112 z/W | LT = 2098 m | 08-39.61N 84-18.91W |
| 2146 | OBS 113 z/W | LT = 2127 m | 08-39.45N 84-19.02W |
| 2152 | OBS 114 z/W | LT = 2168 m | 08-39.30N 84-19.11W |
| 2205 | OBS 115 z/W | LT = 2198 m | 08-39.14N 84-19.19W |
| 2211 | OBH 116 z/W | LT = 2228 m | 08-38.99N 84-19.29W |
| 2217 | OBH 117 z/W | LT = 2272 m | 08-38.82N 84-19.41W |
| 2222 | OBH 118 z/W | LT = 2304 m | 08-38.64N 84-19.51W |
| 2226 | OBH 119 z/W | LT = 2353 m | 08-38.50N 84-19.60W |
| 2232 | OBH 120 z/W | LT = 2385 m | 08-38.35N 84-19.71W |
| 2301 | OBH 121 z/W ( 1000m Seil ) | LT = 2425 m | 08-38.21N 84-19.80W |

Seizmik Profil 26

| | | |
|---|---|---|
| 2337 | Streamer z/W, L 350m | |
| 2400 | Beginn Profil, V 2.0Kn, Kurs 32°; Pr. Airgun Array z/W | 08-35.27N 84-21.68W |

**08.05.02**

| | | |
|---|---|---|
| 0403 | Ende Profil, 9sm | 08-42.80N 84-16.92W |
| 0420 | Airgun Array a/D | |
| 0440 | G-Gun Bb Seite z/W | |
| 0442 | G-Gun Stb Seite z/W | |

Seizmik Profil 27

| | | |
|---|---|---|
| 0445 | Beginn Profil, V 2Kn, Kurs 212° | 08-43.27N 84-16.55W |
| 0911 | Ende Profil 9 sm | 08-35.89N 84-21.24W |

Seizmik Profil 28

| | | |
|---|---|---|
| 0950 | Beginn Profil, V 2.0Kn, Kurs 32° | 08-35.89N 84-21.24W |
| 1335 | Ende Profil 9sm, | 08-42.80N 84-16.92W |

Kalibrierungsprofil 29

| | | |
|---|---|---|
| 1455 | Beginn Profil, V 3.0Kn; div. Kurse | 08-39.17N 84-18.81W |
| 1505 | Ende Profil 5sm | 08-39.55N 84-19.24W |
| 1515 | G-Gun Bb Seite a/D | |
| 1516 | G-Gun Stb Seite a/D | |
| 1525 | Srteamer a/D | |

OBH 107

| | | |
|---|---|---|
| 1650 | Release Command, Schlauchboot z/W ( Aufnahme OBH/S ) | |
| 1700 | OBH gesichtet | |
| 1706 | OBH a/D | 08-40.59N 84-18.19W |

OBH 108

| | | |
|---|---|---|
| 1652 | Release Command | |
| 1717 | OBH gesichtet | |
| 1723 | OBH a/D | 08-40.35N 84-18.34W |

OBH 109

| | | |
|---|---|---|
| 1700 | Release Command | |
| 1717 | OBH gesichtet | |
| 1730 | OBH a/D | 08-40.35N 84-18.34W |

OBH 110

| | | |
|---|---|---|
| 1706 | Release Command | |

| | | | |
|---|---|---|---|
| 1732 | OBH gesichtet | | |
| 1741 | OBH a/D | 08-39.98N | 84-18.49W |
| OBH 111 | | | |
| 1718 | Release Command | | |
| 1759 | OBH gesichtet | | |
| 1800 | OBH a/D | 08-39.85N | 84-18.62W |
| OBH 112 | | | |
| 1733 | Release Command | | |
| 1800 | OBH gesichtet | | |
| 1818 | OBH a/D; Schlauchboot a/D ( Riß in Stb Kammer ) | 08-39.75N | 84-18.57W |
| OBS 113 | | | |
| 1743 | Release Command | | |
| 1819 | OBS gesichtet | | |
| 1834 | OBS a/D | 08-39.51N | 84-18.86W |
| OBS 114 | | | |
| 1750 | Release Command | | |
| 1823 | OBS gesichtet | | |
| 1844 | OBSa/D | 08-39.52N | 84-18.71W |
| OBS 115 | | | |
| 1805 | Release Command | | |
| 1830 | OBS gesichtet | | |
| 1857 | OBS a/D | 08-39.32N | 84-18.79W |
| OBH 116 | | | |
| 1819 | Release Command | | |
| 1846 | OBH gesichtet | | |
| 1903 | OBH a/D | 08-39.14N | 84-18.95W |
| OBH 117 | | | |
| 1855 | Release Command | | |
| 1924 | OBH gesichtet | | |
| 1932 | OBH a/D | 08-38.83N | 84-19.27W |
| OBH 118 | | | |
| 1906 | Release Command | | |
| 1940 | OBH gesichtet | | |
| 1944 | OBH a/D | 08-38.63N | 84-19.41W |
| OBH 119 | | | |
| 1919 | Release Command | | |
| 1947 | OBH gesichtet | | |
| 1952 | OBH a/D | 08-38.48N | 84-19.51W |
| OBH 120 | | | |
| 1933 | Release Command | | |
| 2007 | OBH gesichtet | | |
| 2011 | OBH a/D | 08-38.34N | 84-19.58W |

OBH 121

| | | | |
|---|---|---|---|
| 1952 | Release Command | | |
| 2011 | OBH aufgetaucht | | |
| 2020 | OBH a/D | | 08-38.21N 84-19.65W |

Station CTD 17 W5

| | | | |
|---|---|---|---|
| 2057 | Beginn Station | LT = 2833 m | 08-34.99N 84-24.18W |
| 2109 | CTD z/W | | |
| 2211 | Slmax 2810m | LT = 2835 m | 08-35.00N 84-24.20W |

**09.05.02**

| | | | |
|---|---|---|---|
| 0040 | CTD a/D | | |
| 0041 | Ende Station | | |

Station CTD 18 W5

| | | | |
|---|---|---|---|
| 0210 | Beginn Station | LT = 2515 m | 08-24.20N 84-35.95W |
| 0213 | CTD z/W | | |
| 0314 | Slmax 2497m | LT = 2515 m | 08-24.20N 84-36.00W |
| 0435 | CTD a/D | | |
| 0436 | Ende Station | | |

OBT 60

| | | | |
|---|---|---|---|
| 0535 | Release Command | | |
| 0552 | OBT gesichtet | | |
| 0602 | OBT a/D | | 08-36.03N 84-35.37W |

OBT 61

| | | | |
|---|---|---|---|
| 0545 | Release Command | | |
| 0602 | OBT gesichtet | | |
| 0613 | OBT a/D | | 08-35.98N 84-35.41W |

OBH 20

| | | | |
|---|---|---|---|
| 0749 | Release Command | | |
| 0818 | OBH gesichtet | | |
| 0828 | OBH a/D | | 08-49.92N 84-49.79W |

OBH 21

| | | | |
|---|---|---|---|
| 0946 | Release Command | | |
| 1023 | OBH gesichtet | | |
| 1035 | OBH a/D | | 08-58.09N 85-05.02W |

OBS 19

| | | | |
|---|---|---|---|
| 1223 | Release Command | | |
| 1308 | OBS gesichtet | | |
| 1316 | OBS a/D | | 09-19.99N 84-53.12W |

OBH 18

| | | | |
|---|---|---|---|
| 1410 | Release Command | | |
| 1421 | OBH gesichtet | | |
| 1431 | OBH a/D | | 09-09.40N 84-49.60W |

OBH 15

| | | | |
|---|---|---|---|
| 1545 | Release Command | | |
| 1547 | OBH gesichtet | | |
| 1555 | OBH a/D | | 09-14.64N 84-36.11W |

OBH 16

| | | | |
|---|---|---|---|
| 1620 | Release Command | | |
| 1630 | OBH gesichtet | | |
| 1639 | OBH a/D | | 09-10.01N 84-38.10W |

OBS 19

| | | | |
|---|---|---|---|
| 1740 | Release Command | | |
| 1826 | OBS gesichtet | | |
| 1845 | OBS a/D | | 09-00.06N 84-50.19W |

Profilfahrt mit Simrad

| | | | |
|---|---|---|---|
| 1845 | Beginn Profil, V 11Kn, Kurs div | | 09-00.06N 84-50.19W |

**10.05.02**

| | | | |
|---|---|---|---|
| 0718 | Ende Profil 135sm | | 08-07.87N 84-52.98W |

Station CTD 19 W5

| | | | |
|---|---|---|---|
| 0738 | Beginn Station | LT = 2573 m | 08-07.98N 84-53.20W |
| 0755 | CTD z/W | | |
| 0851 | Slmax 2564m | LT = 2579 m | 08-07.99N 84-53.24W |
| 1010 | CTD a/D | | |
| 1011 | Ende Station | | |

Station CTD 20 W5

| | | | |
|---|---|---|---|
| 1235 | Beginn Station | LT = 2467 m | 07-47.96N 85-13.97W |
| 1236 | CTD z/W | | |
| 1328 | Slmax 2470m | LT = 2481 m | 07-47.99N 85-13.99W |
| 1450 | CTD a/D | | |
| 1452 | Ende Station | | |

| | | | |
|---|---|---|---|
| 2109 | OBH 122 z/W | LT = 2581 m | 08-34.80N 84-17.37W |
| 2131 | OBS 123 z/W | LT = 2624 m | 08-35.25N 84-18.05W |
| 2146 | OBH 124 z/W | LT = 2630 m | 08-35.68N 84-18.77W |
| 2156 | OBH 125 z/W | LT = 2618 m | 08-36.00N 84-19.31W |
| 2202 | OBS 126 z/W | LT = 2647 m | 08-36.18N 84-19.64W |
| 2212 | OBH 127 z/W | LT = 2689 m | 08-36.45N 84-20.15W |
| 2221 | OBS 128 z/W | LT = 2686 m | 08-36.83N 84-20.66W |
| 2232 | OBH 129 z/W | LT = 2718 m | 08-37.21N 84-21.28W |
| 2242 | OBH 130 z/W | LT = 2688 m | 08-37.53N 84-21.89W |
| 2253 | OBH 131 z/W | LT = 2571 m | 08-38.07N 84-21.48W |
| 2304 | OBS 132 z/W | LT = 2589 m | 08-37.69N 84-20.83W |
| 2312 | OBH 133 z/W | LT = 2620 m | 08-37.37N 84-20.31W |
| 2325 | OBH 134 z/W | LT = 2603 m | 08-36.90N 84-19.52W |
| 2335 | OBH 135 z/W | LT = 2526 m | 08-36.46N 84-18.78W |
| 2350 | OBS 136 z/W | LT = 2446 m | 08-35.96N 84-17.99W |

**11.05.02**

| | | | |
|---|---|---|---|
| 0003 | OBH 137 z/W | LT = 2501 m | 08-35.53N 84-17.26W |
| 0014 | OBH 138 z/W | LT = 2485 m | 08-35.17N 84-16.64W |

Seizmik Profil 30

| | | | |
|---|---|---|---|
| 0048 | Streamer z/W L350m | | |
| 0101 | G-Gun Bb Seite z/W | | |

| | | | |
|---|---|---|---|
| 0104 | G-Gun Stb Seite z/W | | |
| 0134 | Beginn Profil, V 2.5Kn, Kurs 301° | 08-34.26N | 84-15.12W |
| 0508 | Ende Profil 9sm | | |

Seizmik Profil 31

| | | | |
|---|---|---|---|
| 0525 | Beginn Profil, V 2.5Kn; Kurs 121° | 08-38.38N | 84-33.22W |
| 0853 | Ende Profil 9sm | 08-33.70N | 84-15.47W |
| 0902 | G-Gun Bb Seite a/D | | |
| 0907 | G-Gun Stb Seite a/D | | |
| 0915 | Streamer a/D | | |

OBH 138

| | | | |
|---|---|---|---|
| 0924 | Release Command | | |
| 0950 | OBH gesichtet | | |
| 1000 | OBH a/D | 08-35.18N | 84-16.55W |

OBH 137

| | | | |
|---|---|---|---|
| 0924 | Release Command | | |
| 1008 | OBH gesichtet | | |
| 1017 | OBH a/D | 08-35.58N | 84-17.19W |

OBS 136

| | | | |
|---|---|---|---|
| 0932 | Release Command | | |
| 1024 | OBS gesichtet | | |
| 1033 | OBS a/D | 08-36.00N | 84-17.71W |

OBH 135

| | | | |
|---|---|---|---|
| 1023 | Release Command | | |
| 1053 | OBH gesichtet | | |
| 1057 | OBH a/D | 08-36.42N | 84-18.66W |

OBH 134

| | | | |
|---|---|---|---|
| 1024 | Release Command | | |
| 1103 | OBH gesichtet | | |
| 1111 | OBH a/D | 08-36.92N | 84-19.35W |

OBH 133

| | | | |
|---|---|---|---|
| 1036 | Release Command | | |
| 1116 | OBH gesichtet | | |
| 1124 | OBH a/D | 08-37.35N | 84-20.02W |

OBS 132

| | | | |
|---|---|---|---|
| 1102 | Release Command | | |
| 1134 | OBS gesichtet | | |
| 1139 | OBS a/D | 08-37.67N | 84-20.69W |

OBH 131

| | | | |
|---|---|---|---|
| 1141 | Release Command | | |
| 1210 | OBH gesichtet | | |
| 1225 | OBH a/D | 08-38.04N | 84-21.33W |

OBH 130

| | | | |
|---|---|---|---|
| 1145 | Release Command | | |

| | | | |
|---|---|---|---|
| 1200 | OBH gesichtet | | |
| 1239 | OBH a/D | | 08-37.53N 84-21.65W |
| OBH 129 | | | |
| 1145 | Release Command | | |
| 1246 | OBH gesichtet | | |
| 1302 | OBH a/D | | 08-37.32N 84-20.87W |
| OBS 128 | | | |
| 1238 | Release Command | | |
| 1315 | OBS gesichtet | | |
| 1324 | OBS a/D | | 08-36.79N 84-20.46W |
| OBH 127 | | | |
| 1249 | Release Command | | |
| 1330 | OBH gesichtet | | |
| 1343 | OBH a/D | | 08-36.50N 84-20.00W |
| OBS 126 | | | |
| 1315 | Release Command | | |
| 1358 | OBS gesichtet | | |
| 1405 | OBS a/D | | 08-36.17N 84-19.52W |
| OBH 125 | | | |
| 1334 | Release Command | | |
| 1410 | OBH gesichtet | | |
| 1424 | OBH a/D | | 08-36.16N 84-19.20W |
| OBH 124 | | | |
| 1353 | Release Command | | |
| 1432 | OBH gesichtet | | |
| 1443 | OBH a/D | | 08-35.82N 84-18.65W |
| OBS 123 | | | |
| 1430 | Release Command | | |
| 1520 | OBS gesichtet | | |
| 1536 | OBS a/D | | 08-35.58N 84-18.12W |
| OBH 122 | | | |
| 1435 | Release Command | | |
| 1505 | OBH gesichtet | | |
| 1515 | OBH a/D | | 08-34.91N 84-17.31W |
| 1848 | OBH 139 z/W | LT = 380 m | 09-13.02N 84-33.50W |
| Test OBS 2002 | | | |
| 1918 | OBS z7W | LT = 96 m | 09-15.72N 84-32.78W |
| 1923 | Hydrophon z/W | | |
| 1929 | Release Command | | |
| 1931 | OBS aufgetaucht | | |
| 1936 | Ende Station, OBS a/D | | |
| 2026 | OBH 140 z/W | LT = 934 m | 09-10.00N 84-38.00W |
| 2057 | OBH 141 z/W | LT = 352 m | 09-13.01N 84-41.02W |

Station CTD/MUC 21 W5

| | | | |
|---|---|---|---|
| 2205 | Beginn Station | LT = 2252 m | 09-06.03N 84-51.40W |
| 2210 | MUC z/W | | |
| 2217 | CTD z/W | | |
| 2220 | XPNDR z/W SL 50m | | |
| 2312 | Boko, Slmax 2240m | LT = 2256 m | 09-06.03N 84-51.40W |

**12.05.02**

| | | | |
|---|---|---|---|
| 0033 | XPNDR a/D | | |
| 0040 | CTD a/D | | |
| 0045 | MUC a/D | | |
| 0046 | Ende Station | | |
| 0843 | OBH 142 z/W | LT = 207 m | 10-20.98N 86-07.91W |
| 0858 | OBH 143 z/W | LT = 302 m | 10-20.25N 86-08.68W |
| 0917 | OBH 144 z/W | LT = 401 m | 10-19.55N 86-09.44W |
| 0933 | OBH 145 z/W | LT = 525 m | 10-18.76N 86-10.25W |
| 0951 | OBH 146 z/W | LT = 657 m | 10-17.99N 86-11.01W |
| 1009 | OBH 147 z/W | LT = 795 m | 10-17.23N 86-11.78W |
| 1022 | OBH 148 z/W | LT = 932 m | 10-16.46N 86-12.57W |
| 1037 | OBH 149 z/W | LT = 1031 m | 10-15.69N 86-13.38W |
| 1050 | OBH 150 z/W | LT = 1157 m | 10-14.92N 86-14.11W |
| 1102 | OBH 151 z/W | LT = 1330 m | 10-14.17N 86-14.91W |
| 1129 | OBS 152 z/W | LT = 1541 m | 10-13.42N 86-15.68W |
| 1142 | OBS 153 z/W | LT = 1697 m | 10-12.66N 86-16.50W |
| 1201 | OBS 154 z/W | LT = 1902 m | 10-13.43N 86-18.82W |
| 1223 | OBS 155 z/W | LT = 1874 m | 10-11.89N 86-17.23W |
| 1250 | OBS 156 z/W | LT = 1897 m | 10.10.35N 86-15.74W |
| 1312 | OBS 157 z/W | LT = 2074 m | 10-11.13N 86-18.01W |
| 1326 | OBS 158 z/W | LT = 2226 m | 10-10.34N 86-18.78W |
| 1350 | OBS 159 z/W | LT = 2393 m | 10-09.59N 86-19.58W |
| 1406 | OBH 160 z/W | LT = 2583 m | 10-08.84N 86-20.34W |
| 1449 | OBH 161 z/W (Ankers. 1000m) | LT = 2731 m | 10-08.10N 86-21.14W |

Seizmik Profil 32

| | | |
|---|---|---|
| 1800 | Streamer z/W L 350m | |
| 1815 | G-Gun Bb Seite z/W | |
| 1821 | G-Gun Stb Seite z/W | |
| 1832 | 32 Ltr Airgun Stb Seite z/W | |
| 1835 | Beginn Profil, V 4.5Kn, Kurs 045° | 09-41.74N 86-48.12W |

**13.05.02**

| | | |
|---|---|---|
| 1015 | Ende Profil 70sm | 10-31.30N 85-57.25W |
| 1030 | Streamer a/D | |
| 1035 | G-Gun Bb Seite a/D | |
| 1049 | Airgun a/D | |
| 1045 | G-Gun Stb Seite a/D | |

OBH 142

| | | |
|---|---|---|
| 1200 | Release Command | |
| 1215 | OBH gesichtet | |
| 1223 | OBH a/D | 10-21.17N 86-08.06W |

| | | | |
|---|---|---|---|
| OBH 143 | | | |
| 1230 | Release Command | | |
| 1235 | OBH gesichtet | | |
| 1242 | OBH a/D | | 10-20.39N 86-08.83W |
| OBH 144 | | | |
| 1250 | Release Command | | |
| 1257 | OBH gesichtet | | |
| 1304 | OBH a/D | | 10-19.74N 86-09.63W |
| OBH 145 | | | |
| 1310 | Release Command | | |
| 1316 | OBH gesichtet | | |
| 1324 | OBH a/D | | 10-18.99N 86-10.55W |
| OBH 146 | | | |
| 1330 | Release Command | | |
| 1338 | OBH gesichtet | | |
| 1347 | OBH a/D | | 10-18.23N 86-11.33W |
| OBH 147 | | | |
| 1354 | Release Command | | |
| 1404 | OBH gesichtet | | |
| 1415 | OBH a/D | | 10-17.54N 86-12.21W |
| 1505 | OBH 162 z/W | LT = 1919 m | 10-14.25N 86-19.59W |
| 1530 | OBH 163 z/W | LT = 1892 m | 10-12.70N 86-18.07W |
| 1555 | OBH 164 z/W | LT = 1845 m | 10-11.14N 86-16.53W |
| 1616 | OBH 165 z/W | LT = 1992 m | 10-09.57N 86-14.95W |
| Seizmik Profil 33 | | | |
| 1653 | Streamer z/W L350m | | |
| 1704 | G-Gun Bb Seite z/W | | |
| 1708 | G-Gun Stb Seite | | |
| 1721 | Beginn Profil, V 4.5Kn, Kurs 315° | | 10-08.26N 86-13.68W |
| 1941 | Ende Profil 10sm | | 10-15.74N 86-21.10W |
| 1949 | Streamer a/D | | |
| 1959 | G-Gun Bb Seite a/D | | |
| 2000 | G-Gun Stb Seite a/D | | |
| Station CTD/MUC 22 | W5 | | |
| 2043 | Beginn Station | LT = 1521 m | 10-17.99N 85-18.29W |
| 2047 | MUC z/W | | |
| 2055 | CTD z/W | | |
| 2200 | Boko, SImax 1497m | LT = 1519 m | 10-17.99N 86-18.28W |
| 2246 | CTD a/D | | |
| 2251 | MUC a/D | | |
| 2255 | Ende Station | | |
| OBH 148 | | | |
| 2326 | Release Command | | |
| 2332 | OBH gesichtet | | |
| 2346 | OBH a/D | | 10-16.84N 86-12.98W |

| | | | |
|---|---|---|---|
| OBH 149 | | | |
| 2346 | Release Command | | |
| 2350 | OBH gesichtet | | |
| **14.05.02** | | | |
| 0015 | OBH a/D | 10-16.08N | 86-14.18W |
| OBH 150 | | | |
| 0022 | Release Command | | |
| 0037 | OBH gesichtet | | |
| 0054 | OBH a/D | 10-15.25N | 86-14.61W |
| OBH 151 | | | |
| 0040 | Release Command | | |
| 0102 | OBH gesichtet | | |
| 0117 | OBH a/D | 10-14.59N | 86-15.58W |
| OBS 152 | | | |
| 0103 | Release Command | | |
| 0135 | OBS gesichtet | | |
| 0150 | OBS a/D | 10-13.75N | 86-16.40W |
| OBS 153 | | | |
| 0136 | Release Command | | |
| 0218 | OBS gesichtet | | |
| 0235 | OBS a/D | 10-13.12N | 86-17.40W |
| OBS 154 | | | |
| 0218 | Release Command | | |
| 0245 | OBS gesichtet | | |
| 0330 | OBS a/D | 10-14.23N | 86-20.22W |
| OBH 162 | | | |
| 0300 | Release Command | | |
| 0330 | OBH gesichtet | | |
| 0345 | OBH a/D | 10-14.69N | 86-20.46W |
| OBH 163 | | | |
| 0333 | Release Command | | |
| 0400 | OBH gesichtet | | |
| 0425 | OBH a/D | 10-13.31N | 86-19.13W |
| OBS 155 | | | |
| 0400 | Release Command | | |
| 0425 | OBS gesichtet | | |
| 0450 | OBS a/D | 10-12.72N | 86-18.44W |
| OBS 157 | | | |
| 0435 | Release Command | | |
| 0502 | OBS gesichtet | | |
| 0516 | OBS a/D | 10-11.61N | 86-18.70W |
| OBS 158 | | | |
| 0502 | Release Command | | |
| 0550 | OBS gesichtet | | |

| | | | |
|---|---|---|---|
| 0612 | OBS a/D | | 10-11.28N 86-19.82W |
| OBS 159 | | | |
| 0530 | Release Command | | |
| 0629 | OBS gesichtet | | |
| 0648 | OBS a/D | | 10-10.63N 86-20.94W |
| OBH 160 | | | |
| 0612 | Release Command | | |
| 0650 | OBH gesichtet | | |
| 0713 | OBH a/D | | 10-09.70N 86-21.64W |
| OBH 161 | | | |
| 0653 | Release Command | | |
| 0723 | OBH gesichtet | | |
| 0743 | OBH a/D | | 10-08.72N 86-22.33W |
| OBH 164 | | | |
| 0819 | Release Command | | |
| 0848 | OBH gesichtet | | |
| 0855 | OBH a/D | | 10-11.54N 86-17.34W |
| OBS 156 | | | |
| 0850 | Release Command | | |
| 0930 | OBS gesichtet | | |
| 0945 | OBS a/D | | 10-11.54N 86-17.34W |
| OBH 165 | | | |
| 0933 | Release Command | | |
| 0959 | OBH gesichtet | | |
| 1015 | OBH a/D | | 10-11.54N 86-17.34W |
| 1106 | OBS 166 z/W | LT = 1689 m | 10-17.32N 86-18.76W |
| 1116 | OBH 167 z/W | LT = 1571 m | 10-17.69N 86-18.50W |
| 1125 | OBH 168 z/W | LT = 1517 m | 10-17.99N 86-18.27W |
| 1135 | OBH 169 z/W | LT = 1605 m | 10-18.33N 86-18.00W |
| 1145 | OBH 170 z/W | LT = 1538 m | 10-18.61N 86-17.80W |
| 1157 | OBH 171 z/W | LT = 1481 m | 10-18.87N 86-17.65W |
| 1202 | OBS 172 z/W | LT = 1480 m | 10-18.86N 86-17.60W |
| Seizmik Profil 34 | | | |
| 1230 | Streamer z/W | | |
| 1239 | G-Gun Bb Seite z/W | | |
| 1250 | Beginn Profil, V 3.0Kn, Kurs 216° | | 10-20.00N 86-16.79W |
| 1405 | Ende Profil 4sm | | 10-17.03N 86-19.00W |
| 1415 | Streamer a/D | | |
| 1420 | G-Gun Bb Seite a/D | | |
| OBH 166 | | | |
| 1429 | Release Command | | |
| 1449 | OBH gesichtet | | |
| 1456 | OBH a/D | | 10-17.55N 86-19.14W |
| OBH 167 | | | |

| | | | |
|---|---|---|---|
| 1450 | Release Command | | |
| 1510 | OBH gesichtet | | |
| 1518 | OBH a/D | | 10-17.85N 86-18.84W |

OBH 168

| | | | |
|---|---|---|---|
| 1511 | Release Command | | |
| 1532 | OBH gesichtet | | |
| 1540 | OBH a/D | | 10-18.18N 86-18.64W |

OBH 169

| | | | |
|---|---|---|---|
| 1526 | Release Command | | |
| 1550 | OBH gesichtet | | |
| 1600 | OBH a/D | | 10-18.53N 86-18.40W |

OBH 170

| | | | |
|---|---|---|---|
| 1545 | Release Command | | |
| 1605 | OBH gesichtet | | |
| 1614 | OBH a/D | | 10-18.85N 86-18.30W |

OBH 171

| | | | |
|---|---|---|---|
| 1600 | Release Command | | |
| 1618 | OBH gesichtet | | |
| 1632 | OBH a/D | | 10-19.17N 86-18.30W |

OBS 172

| | | | |
|---|---|---|---|
| 1608 | Release Command | | |
| 1637 | OBS gesichtet | | |
| 1648 | OBS a/D | | 10-19.19N 86-18.10W |

Station DR 01 W6

| | | | |
|---|---|---|---|
| 1720 | Beginn Station | LT = 1583 m | 10-17.71N 86-18.53W |
| 1725 | DR z/W | | |
| 1831 | Boko; SL 2194m | LT = 1503 m | 10-17.87N 86-18.32W |
| 1831 | Slmax 2194 m | LT = 1504 m | 10-17.94N 86-18.27W |
| 1939 | DR a/D | | |
| 1940 | Ende Station | | |

Station DR 02

| | | | |
|---|---|---|---|
| 1942 | Beginn Station | LT = 1588 m | 10-18.00N 86-18.34W |
| 1943 | DR z/W | | |
| 2005 | Boko, SL 1602m | LT = 1593 m | 10-17.99N 86-18.53W |
| 2033 | Slmax 2203m | LT = 1522 m | 10-17.83N 86-18.23W |
| 2136 | DR a/D | | |
| 2137 | Ende Station | | |

Station CTD/MUC 23 W5

| | | | |
|---|---|---|---|
| 2150 | Beginn Station | LT = 1514 m | 10-18.02N 86-18.30W |
| 2200 | MUC z/W | | |
| 2206 | CTD z/W | | |
| 2242 | Boko, Slmax 1633m | LT = 1657 m | 10-18.14N 86-18.54W |
| 2335 | CTD a/D | | |
| 2342 | MUC a/D | | |
| 2345 | Ende Station | | |

**15.05.02**

Profil 205 Hydroakustik

| | | | |
|---|---|---|---|
| 0315 | Beginn Profil, V 5.0Kn, Kurs 222° | | 09-41.02N 86-09.64W |
| 0418 | Ende Profil 5sm | | 09-36.96N 86-13.27W |
| 0754 | OBH 173 z/W (Ankers.500m) | LT = 2384 m | 09-26.95N 85-39.30W |
| 0800 | OBH 174 z/W | LT = 2375 m | 09-27.01N 85-39.23W |
| 0809 | OBH 175 z/W | LT = 2348 m | 09-27.08N 85-39.13W |
| 0819 | OBH 176 z/W | LT = 2326 m | 09-27.17N 85-39.07W |
| 0827 | OBH 177 z/W^ | LT = 2324 m | 09-27.27N 85-39.00W |
| 0836 | OBH 178 z/W | LT = 2323 m | 09-27.30N 85-38.94W |
| 0848 | OBH 179 z/W | LT = 2332 m | 09-27.33N 85-39.01W |
| 0854 | OBH 180 z/W | LT = 2326 m | 09-27.50N 85-38.94W |
| 0902 | OBH 181 z/W | LT = 2330 m | 09-27.42N 85-38.86W |
| 0908 | OBH 182 z/W | LT = 2323 m | 09-27.35N 85-38.77W |
| 0915 | OBH 183 z/W | LT = 2327 m | 09-27.26N 85-38.68W |
| 0926 | OBH 184 z/W | LT = 2325 m | 09-27.49N 85-38.77W |
| 0950 | OBS 185 z/W | LT = 2317 m | 09-27.56N 85-38.68W |
| 1011 | OBS 186 z/W | LT = 2304 m | 09-27.66N 85-38.61W |
| 1042 | OBS 187 z/W | LT = 2304 m | 09-27.74N 85-38.56W |
| 1048 | OBH 188 z/W | LT = 2301 m | 09-27.81N 85-38.49W |
| 1055 | OBH 189 z/W | LT = 2307 m | 09-27.90N 85-38.40W |
| 1100 | OBH 190 z/W | LT = 2285 m | 09-27.98N 85-38.35W |
| 1107 | OBS 191 z/W | LT = 2283 m | 09-28.07N 85-38.25W |
| 1113 | OBH 192 z/W | LT = 2281 m | 09-28.12N 85-38.18W |

Seizmik Profil 35

| | | |
|---|---|---|
| 1155 | Streamer z/W | |
| 1205 | G-Gun Bb Seite z/W | |
| 1208 | G-Gun Stb Seite z/W | |
| 1240 | Beginn Profil, V 4.5Kn, Kurs 132° | 09-29.64N 85-41.24W |
| 1408 | Ende Profil 7sm | 09-25.21N 85-36.45W |

Seizmik Profil 36

| | | |
|---|---|---|
| 1408 | Beginn Profil, V 4.5Kn, Kurs 026° | 09-25.21N 85-36.45W |
| 1642 | Ende Profil 10sm | 09-34.58N 85-30.64W |

Seizmik Profil 37

| | | |
|---|---|---|
| 1718 | Beginn Profil, 4.5Kn, Kurs 223° | 09-35.31N 85-31.57W |

**16.05.02**

| | | |
|---|---|---|
| 0415 | Ende Profil 48sm | 08-59.72N 86-04.75W |
| 0417 | Streamer a/D | |
| 0430 | G-Gun Bb Seite a/D | |
| 0438 | G-Gun Stb Seite a/D | |

OBH 173

| | | |
|---|---|---|
| 0717 | Release Command | |
| 0740 | OBH gesichtet | |
| 0754 | OBH a/D | 09-27.09N 85-39.58W |

OBH 186

| | | |
|---|---|---|
| 0725 | Release Command | |
| 0758 | OBH gesichtet | |
| 0804 | OBH a/D | 09-27.17N 85-39.56W |

| | | | |
|---|---|---|---|
| OBH 187 | | | |
| 0735 | Release Command | | |
| 0813 | OBH gesichtet | | |
| 0822 | OBH a/D | 09-27.28N | 85-39.55W |
| OBH 176 | | | |
| 0810 | Release Command | | |
| 0820 | OBH gesichtet | | |
| 0830 | OBH a/D | 09-27.40N | 85-39.53W |
| OBS 177 | | | |
| 0736 | Release Command | | |
| 0833 | OBS gesichtet | | |
| 0841 | OBS a/D | 09-27.55N | 85-39.56W |
| OBH 178 | | | |
| 0824 | Release Command | | |
| 0903 | OBH gesichtet | | |
| 0909 | OBH a/D | 09-27.57N | 85-39.31W |
| OBS 180 | | | |
| 0852 | Release Command | | |
| 0920 | OBS gesichtet | | |
| 026 | OBS a/D | 09-27.69N | 85-39.16W |
| OBH 181 | | | |
| 0907 | Release Command | | |
| 0935 | OBH gesichtet | | |
| 0941 | OBH a/D | 09-27.54N | 85-39.08W |
| OBH 182 | | | |
| 0924 | Release Command | | |
| 0950 | OBH gesichtet | | |
| 0958 | OBH a/D | 09-27.53N | 85-39.04W |
| OBS 183 | | | |
| 0928 | Release Command | | |
| 1001 | OBS gesichtet | | |
| 1011 | OBS a/D | 09-27.53N | 85-39.08W |
| OBH 179 | | | |
| 0955 | Release Command | | |
| 1023 | OBH gesichtet | | |
| 1031 | OBH a/D | 09-27.80N | 85-39.27W |
| OBS 175 | | | |
| 1011 | Release Command | | |
| 1048 | OBS gesichtet | | |
| 1103 | OBS a/D | 09-27.80N | 85-39.17W |
| OBS 185 | | | |
| 1034 | Release Command | | |
| 1111 | OBS gesichtet | | |
| 1119 | OBS a/D | 09-27.80N | 85-38.83W |

| | | | |
|---|---|---|---|
| OBS 174 | | | |
| 1034 | Release Command | | |
| 1119 | OBS gesichtet | | |
| 1127 | OBS a/D | | 09-27.89N 85-38.79W |
| OBS 184 | | | |
| 1051 | Release Command | | |
| 1145 | OBS gesichtet | | |
| 1200 | OBS a/D | | 09-28.13N 85-39.60W |
| OBH 188 | | | |
| 1119 | Release Command | | |
| 1142 | OBH gesichtet | | |
| 1218 | OBH a/D | | 09-28.46N 85-39.33W |
| OBH 189 | | | |
| 1127 | Release Command | | |
| 1200 | OBH gesichtet | | |
| 1238 | OBH a/D | | 09-28.71N 85-39.34W |
| OBH 190 | | | |
| 1141 | Release Command | | |
| 1200 | OBH gesichtet | | |
| 1255 | OBH a/D | | 09-28.94N 85-39.49W |
| OBH 191 | | | |
| 1245 | Release Command | | |
| 1325 | OBH gesichtet | | |
| 1350 | OBH a/D | | 09-28.78N 85-38.66W |
| OBH 192 | | | |
| 1245 | Release Command | | |
| 1320 | OBH gesichtet | | |
| 1335 | OBH a/D | | 09-28.26N 85-38.66W |
| 1655 | OBH 193 z/W | LT = 1879 m | 09-19.99N 85-06.02W |
| 1825 | OBH 194 z/W | LT = 567 m | 09-28.02N 84-52.40W |
| 1911 | OBH 195 z/W | LT = 323 m | 09-28.00N 84-45.00W |
| 2002 | OBH 196 z/W | LT = 414 m | 09-21.53N 84-45.03W |
| 2049 | OBS 197 z/W | LT = 1739 m | 09-20.02N 84-53.00W |
| 2153 | OBH 198 z/W | LT = 289 m | 09-14.99N 84-44.01W |
| 2223 | OBT 199 z/W | LT = 733 m | 09-12.01N 84-46.99W |
| 2251 | OBT 200 z/W | LT 823 m | 09-09.42N 84-49.60W |
| 2333 | OBS 201 z/W | LT = 2079 m | 09-10.01N 84-56.01W |
| **17.05.02** | | | |
| 0022 | OBH 202 z/W | LT = 2230 m | 09-02.00N 84-56.01W |
| 0116 | OBH 203 z/W | LT = 3535 m | 08-57.99N 85-04.99W |
| 0246 | OBH 204 z/W | LT = 3472 m | 08-50.00N 84-50.00W |
| 0343 | OBH 205 z/W | LT = 2207 m | 09-00.00N 84-50.00W |
| 0426 | OBS 206 z/W | LT = 1727 m | 09-02.00N 84-43.00W |
| 0503 | OBH 207 z/W | LT = 1168 m | 09-07.00N 84-43.00W |
| 0600 | OBS 208 z/W | LT = 1155 m | 09-05.37N 84-34.24W |

| | | | |
|---|---|---|---|
| 0639 | OBH 209 z/W | LT = 1613 m | 09-02.29N 84-39.18W |
| 0703 | OBH 210 z/W | LT = 1207 m | 08-59.58N 84-37.91W |
| 0730 | OBH 211 z/W | LT = 1412 m | 09-01.00N 84-34.46W |
| 0754 | OBH 212 z/W | LT = 1327 m | 09-02.38N 84-36.20W |

Seizmik Profil 38

| | | |
|---|---|---|
| 0838 | Streamer z/W, L350m | |
| 0840 | G-Gun Bb Seite z/W | |
| 0845 | G-Gun Stb Seite z/W | |
| | Beginn Profil, V 4.5Kn, Kurs 320° | 09-00.31N 84-35.34W |
| 0906 | 32 Ltr Airgun z/W | |
| 1500 | Ende Profil 29sm | 09-22.49N 84-54.05W |

Seizmik Profil 39

| | | |
|---|---|---|
| 1528 | Beginn Profil, V 4.5Kn; Kurs 320° | 09-21.94N 84-55.51W |
| 2115 | Ende Profil 29sm | |

Seizmik Profil 40

| | | |
|---|---|---|
| 2138 | Beginn Profil V 4.5Kn, Kurs 025° | 08-55.02N 84-58.33W |

**18.05.02**

| | | |
|---|---|---|
| 0600 | Ende Profil 40sm | 09-31.10N 84-41.55W |
| 0619 | Streamer a/D | |
| 0630 | Airgun a/D | |
| 0634 | G-Gun Bb Seite a/D | |
| 0638 | G-Gun Stb Seite a/D | |

Station CTD/MUC 24

| | | | |
|---|---|---|---|
| 0925 | Beginn Station | LT = 2413 m | 09-05.02N 84-51.96W |
| 0930 | MUC z/W | | |
| 0935 | CTD z/W | | |
| 0939 | XPNDR z/W | | |
| 1024 | Boko, Slmax 2395m | LT = 2412 m | 09-05.02N 84-51.94W |
| 1150 | XPNDR a/D | | |
| 1154 | CTD a/D | | |
| 1200 | MUC a/D; Ende Station | | |

Profil MAG 04

| | | |
|---|---|---|
| 1530 | MAG z/W | |
| 1606 | Beginn Profil, V 11.0Kn, Kurs 120° | 08-20.00N 84-55.00W |

19.05.02

| | | |
|---|---|---|
| 0416 | Ende Profil, 132sm | 07-12.50N 83-00.00W |
| 0430 | MAG a/D | |

## Appendix 9.8

# Press Clippings

REPUBLICA: Lunes 22 de abril, 2002
). 14A.

Barco científico realiza estudios geológicos y sismológicos en aguas ticas

# Valioso equipo previene amenaza sísmica

## Estudios ayudan a instituciones como el ICE para diseñar obras de ingeniería

**RODRIGO DIAZ LORIA**
La República

Un grupo de expertos alemanes y un millonario equipo científico previenen al país de eventuales desastres naturales, al hacer diversos estudios geológicos, sismológicos, vulcanológicos y biológicos en aguas territoriales.

En este momento se encuentra en el país el RV Sonne, una de las dos embarcaciones alemanas que desarrollan una serie de investigaciones en la zona desde 1991. Desde entonces se han efectuado estudios de vulcanología submarina y terrestre, sobre sismología y tectónica, así como peligros por maremotos y biología marina, además se inició la confección de un mapa de relieve combinado.

Para estas investigaciones, el barco laboratorio cuenta con varias grúas, sismómetros o estaciones sismológicas (con un costo de $700 mil cada una), hidrófonos, una cámara especial para hacer el barrido fotográfico de las profundidades (cuyo costo supera los $500 mil), un sofisticado equipo de cómputo y demás equipo científico. El barco cuenta con el sistema GPS, de posicionamiento global y un sonar que le permite hasta detectar otras embarcaciones cercanas.

Su tripulación es de 55 personas, entre personal técnico, náutico y científico.

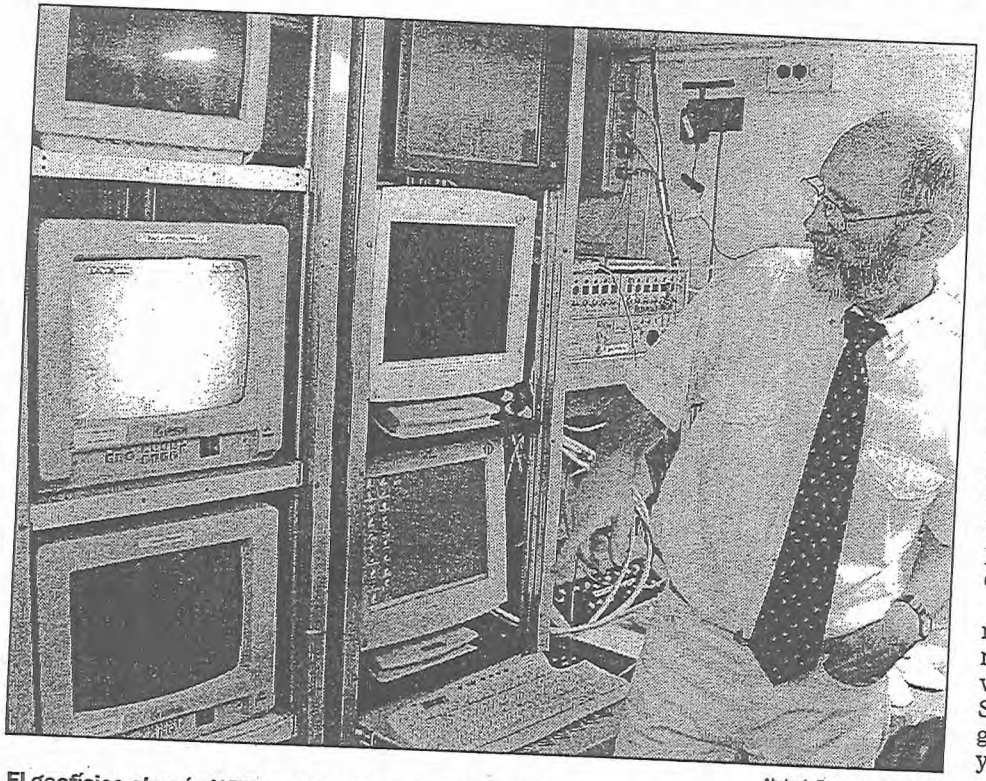

Abelardo Fonseca/La República

**El geofísico alemán Willhem Weinrebe explicó las técnicas que utilizan para estudiar el fondo marino.**

"Se han reconocido 89 volcanes, hay más de 1.000 toneladas de roca que son estudiadas en Alemania, y hay estudios muy importantes sobre la sismicidad terrestre", precisó el ingeniero Guillermo Alvarado, del Instituto Costarricense de Electricidad (ICE).

En un recorrido por la embarcación, el geofísico alemán Willhem Weinrebe, mostró los principales avances que se han hecho y explicó las relaciones que pueden existir en el cambio climático y su relación con una serie de fumarolas que se forman entre las placas. También se estudian la fauna y flora marina que rodean dichos focos volcánicos.

Este año desarrolla un proyecto de investigación de la zona de subducción o de contacto de las placas Cocos y ribe, frente a las costas del Pacífico tarricense, y la relación que esto p tener con los cambios climáticos y desastres naturales. Además se c nuará con las labores de mapeo de l perficie bajo las aguas.

El presupuesto de esta invest ción es de $5 millones, financiados el gobierno de Alemania, con el au cio de la Universidad Christian brecht en Kiel y su Instituto de Inve gaciones Geomar.

En nuestro país, ICE brinda su ap te en investigaciones en tierra que cen los especialistas. Precisamente, ta institución es una de las más ben ciadas con el proyecto, debido a la ap cación de sus investigaciones en proyectos geotérmicos e hidroeléct cos que construye.

"Esta información ha sido fund mental para el diseño y todo lo que t ne que ver con seguridad operativa varias obras importantes como Boruc Savegre, Brujos y Pirrís", expresó el i geniero Salvador López, director de pr yectos del ICE.

López reconoció que si no fuera p el apoyo de los alemanes, el país no te dría posibilidad de contar con una i formación precisa sobre las fuentes sí micas más importantes.

Para estas investigaciones, el Inst tuto Geomar también cuenta con otr barco, que hace estudios similares e otras partes del mundo.

El Sonne permanecerá en nuestr país hasta finales de agosto y posterior mente continuará estudios en Panam y Suramérica.

Científicos alemanes

# Estudian amenaza sísmica

*A través de un proyecto conjunto con la Universidad de Kiel, la UCR y el ICE, el barco alemán Sonne estudia causas de los desastres naturales, como los sismos que afectan a toda Centroamérica.*

**FABIOLA POMAREDA G.**
redactora
fpomareda@hotmail.com

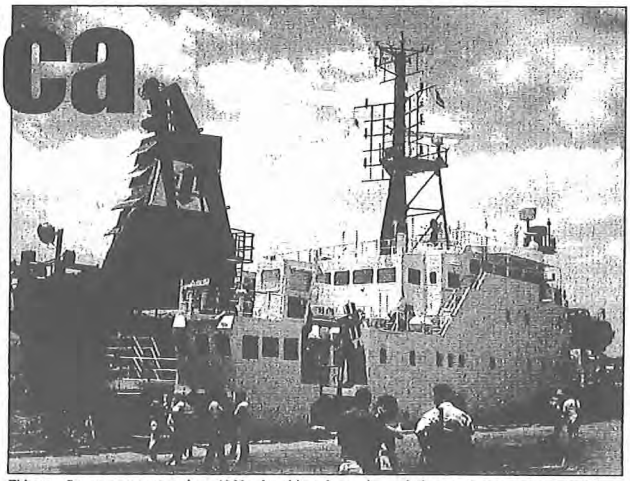

*El barco Sonne se construyó en 1969 y ha sido reformado paulatinamente a un barco científico.*

EN EL "SONNE" no falta el sol, porque el nombre con que bautizaron a este barco significa eso mismo en alemán. Los científicos que viajan en la embarcación, que proviene de la Universidad de Kiel, en Alemania, se encuentran frente a Puerto Caldera, en Puntarenas, realizando investigaciones geológicas, sismológicas y vulcanológicas.

No es la primera vez que visita el país, pero este año los investigadores iniciaron el proyecto "Volátiles y fluidos en zonas de subducción: retroalimentación del clima y mecanismo disparador de desastres naturales", que desarrolla en conjunto con el Instituto Costarricense de Electricidad (ICE) y la Universidad de Costa Rica (UCR).

El objetivo del proyecto es estudiar las zonas donde se unen las placas Coco y Caribe, frente a las costas del Pacífico de Costa Rica y Nicaragua, donde circulan fluidos y materias volátiles. Estos procesos están relacionados con el clima en la Tierra, la evolución geoquímica de la hidrosfera y la atmósfera y con las causas de los desastres naturales.

Para emprender esta investigación cuentan con un presupuesto de alrededor de $5 millones, financiados por el Gobierno de Alemania y el Instituto de Investigaciones Geomar, de la Universidad de Kiel. El acuerdo duraría cinco años y eventualmente puede ser renovado.

## TEMA DE PRIORIDAD

En una visita realizada el pasado 20 de abril al barco, los encargados explicaron los aportes del estudio. Participaron Andrés Papenhagen, capitán del Sonne; Guillermo Ruiz, presidente del Instituto Costarricense de Puertos del Pacífico y el embajador de Alemania, Friedrich Gröning.

También los acompañaron Pablo Cob, presidente del ICE y Guillermo Alvarado, coordinador del Area de Amenazas y Auscultación Sismovolcánica del ICE y profesor de geología en la UCR.

Como recordó el capitán Papanhagen, desde 1991 el ICE y la UCR participan en estudios similares, que han generado datos relevantes para elaborar estudios geológicos y de amenaza sísmica, para los proyectos de generación eléctrica y la infraestructura del ICE.

El embajador alemán planteó preguntas críticas con respecto a los fines de las investigaciones científicas que se realizan en el ámbito global, por ejemplo: ¿se fijan en la investigación científica las prioridades correctas o nos dejamos llevar por determinadas modas?

"Ciertamente estudiar las amenazas que causan problemas climatológicos o desastres naturales, como en este proyecto, debe ser una prioridad. No es un lujo, son temas que nos conciernen a todos y que son vitales para la supervivencia de muchos seres humanos."

## ESCUCHAR A LA TIERRA

En esta etapa de la investigación se han generado datos muy detallados y también se destacó el aporte de la Escuela Centroamericana de Geología, de la UCR.

Guillermo Alvarado dijo que, por ejemplo, hay rocas que se son estudiadas en Alemania para determinar cómo se formaron y cuál es la relación que tienen en la incidencia de los sismos. Agregó que la UCR ha aportado con la participación de geólogos en los estudios.

El ICE, por su parte, está involucrado por los proyectos hidroeléctricos y geotérmicos que se ubican cerca de volcanes activos. Consiste en instalar 15 estaciones sismológicas en la tierra, y 25 en el mar, para entender por qué se generan sismos y cómo se pueden prevenir.

"Se trata de determinar cuándo y en qué zona esperar un fuerte movimiento sísmico,".

En el Sonne, construido en 1969, viajan 25 científicos y 30 personas que forman la tripulación. Uno de los investigadores, el biólogo Heibo Sahling, junto con Germán Leandro, que colabora con el ICE, guiaron el recorrido a través del barco.

Los sismómetros del fondo oceánico -en forma de grandes boyas- son los instrumentos que conforman las estaciones por instalar y son capaces de detectar las fricciones de la tierra. El movimiento del fondo marino se registra en un sensor y luego se transmiten las señales acústicas a computadores en el centro de información.

Además, se cuenta con un sistema "multibeam", que consiste en cien sonares ubicados en el casco del barco, que barren el fondo oceánico y envían ondas que son interpretadas con un software especial. Este sirve para mostrar la estructura del suelo del mar.

Los investigadores pueden usar una cámara filmadora gigante, que pesa aproximadamente 1 tonelada métrica y costó unos $200.000, según Sahling. Esta rueda por el fondo oceánico, se maneja desde el barco y permite ubicar organismos vivientes, como bivalvos y gusanos que se acumulan entre las placas tectónicas.

Meteor es el otro barco que llegará al país en setiembre, según dijo su capitán, Michael Berkenheger. ❑

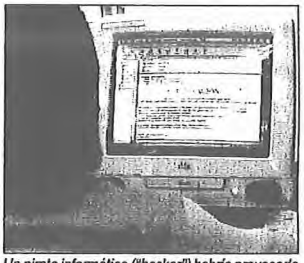

*Un pirata informático ("hacker") habría provocado daños en los programas de correo electrónico.*

# Cariari sufre averías

**EDUARDO RAMÍREZ FLORES**
redactor
erflores@carlari.ucr.ac.cr

EL SERVIDOR DE CORREO electrónico "Cariari" de la Universidad de Costa Rica (UCR), ha sufrido desde el 18 de abril averías que lo han mantenido prácticamente fuera de servicio y con ello se han visto afectados sus casi 6.000 usuarios.

Problemas originados aparentemente en los programas ("software") que se utilizan para prestar el servicio de correo, impiden desde la fecha mencionada enviar mensajes; no obstante los usuarios sí los reciben.

Según el encargado en el Centro de Informática de administrar el servidor -Bernal Calderón-, al pasado 26 de abril no sabían con precisión la causa del problema, aunque sospechan que podrían ser culpa de un pirata informático ("hacker") que alteró los programas.

Esta es la primera vez -comentó- que un "hacker" habría entrado a la plataforma mediante la cual se opera el correo electrónico de la UCR.

A los obstáculos citados -agregó Calderón-, se suma el saturamiento en el uso de ese servidor, al tener en algunos momentos de 200 a 300 usuarios simultáneos, lo cual bloquea la salida de mensajes hacia servidores externos.

Para corregir los daños, el Centro de Informática contrató a un asesor especializado en el programa Linux y a partir del 29 de abril comenzarían a instalar un paquete con nuevos "software", incluido un cambio de la versión del sistema operativo, lo cual le dará mayor velocidad al servicio.

Calderón aseguró que hacer estos cambios es más práctico y rápido que tratar de detectar lo que provoca la caída del servidor.

Dejó abierta la posibilidad de que puedan restablecer el correo electrónico en los primeros días de la semana; en caso contrario, a más tardar el 2 de mayo lo tendrían listo.

De última hora (martes 28), mediante un correo electrónico a los usuarios, el director del Centro de Informática -Guillermo Loría- avisó que los problemas los resolvieron el viernes 26.

Asimismo, informó que entre el sábado 4 y domingo 5 de mayo interrumpirían periódicamente el servicio, con el fin de trasladar los archivos de cada usuario a un nuevo servidor. ❑

# Pescando Terremotos

ILLERMO CUBILLOS
RA NUESTRO AGRO

El RV Sonne ancló en Puerto Caldera. Su ulación, compuesta por científicos alema- s y algunos costarricenses, visita por segun- vez costas centroamericanas, desde Nicara- a hasta Panamá.

Pero no son los atunes, los pargos o los ca- rones el motivo de su interés. Son los terre- otos a los que pretenden "pescar" antes de e ocurran.

El Gobierno alemán donó $5 millones pa- desarrollar esta investigación, en la que par- ipan la Universidad de Costa Rica y el Ins- uto Costarricense de Electricidad (ICE).

El presidente ejecutivo del ICE, Ing. Pablo ob, indicó que para esta institución es impor- nte este tipo de investigaciones, pues es un ctor de consideración a la hora de desarrollar oyectos como plantas hidroeléctricas y geo- rmicas.

En general, Centroamérica es propensa a frir con regularidad este tipo de fenómenos turales. La gran actividad volcánica y el cons- nte choque de las placas Cocos y Caribe man- nen vibrando estas tierras a un ritmo más erte que la salsa, el merengue o la cumbia.

"Lo cierto es que existe una cordillera vol- nica en las profundidades marinas —asegu- el ingeniero geólogo Guillermo Alvarado, la Universidad de Costa Rica—. Se han re- istrado más de 100 bajo las aguas del Pacífi- o costarricense, y de ellos más de 80 se en- uentran activos".

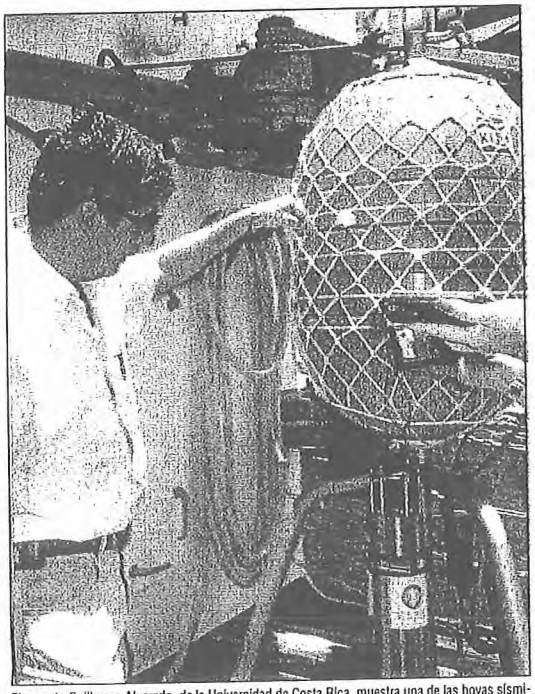

El experto Guillermo Alvarado, de la Universidad de Costa Rica, muestra una de las boyas sísmi- cas que se han distribuido en diversos sectores del Golfo de Nicoya, en el marco de las investi- gaciones que se realizan en cooperación con el gobierno alemán. (Leví Vega M.-Nuestro Agro)

El capitán del Sonne dio a conocer algunas propiedades de la nave y otros detalles sobre su operación y versatilidad. A su lado, la periodista de la embajada alemana, Betina Susin, tra- ductora que ya ha hecho anteriormente la travesía de la investigación. (Leví Vega M.-Nues- tro Agro)

## Subducción

La palabra puede parecer familiar, pero no ene nada que ver con la seducción. Se refiere ás bien al movimiento por el que una placa asa por debajo de otra, avanzando constante- iente.

En nuestro caso, la placa Caribe es sub- uccionada por la Cocos. Este movimiento ento y en la mayoría de los casos imperceptible arrastra tras de sí todo cuanto en ella se en- uentre.

Pero, ¿qué pasa si también es subducciona- do un volcán? Esta es precisamente una de las interrogantes que los científicos alemanes y costarricenses buscan evacuar.

Y aún más allá. La investigación trata de determinar si estas zonas de subducción pueden ser la causa de los cambios climáticos, la evolución geoquímica de la hidrosfera y la atmósfera y, por supuesto, los desastres naturales.

Laboran dentro de las investigaciones científicos encabezados por los geólogos alemanes, los Drs. Hans-Ulrich Schmincke, Kaj Hoernle, Folmar Hauff, Reinhard Werner, y por el geólogo costarricense, Dr. Guillermo Alvarado de la UCR.

## La investigación

El RV Sonne está equipado con el instrumental tecnológico más moderno. Mediante él se extraen muestras del fondo del mar, para lo cual se sumergen a profundidades que superan los 2 mil metros. Toneladas de rocas son extraídas y estudiadas para determinar su edad.

Además, una cámara especialmente diseñada contra la presión hace tomas de suelo marino, registrando así no solo información geológica, sino también biológica.

De paso se elaboran planos que permiten un mejor reconocimiento y caracterización de los lechos marinos.

En esta oportunidad la meta es colocar al menos unas 50 estaciones sismológicas, la mitad en tierra y el resto en el mar, que permitirán el monitoreo total de cualquier movimiento telúrico.

Consultado el embajador Alemán Friederick Gröneng sobre el interés de su gobierno en realizar esa investigación en nuestras aguas, indicó que una de las principales razones son las características geológicas de la región, y en segundo lugar, la estabilidad político-social de Costa Rica.

El presidente ejecutivo del INCOP, don Guillermo Ruiz, formó parte de la comitiva invitada a conocer el Sonne, en el puerto de Caldera. (Leví Vega M.-Nuestro Agro)

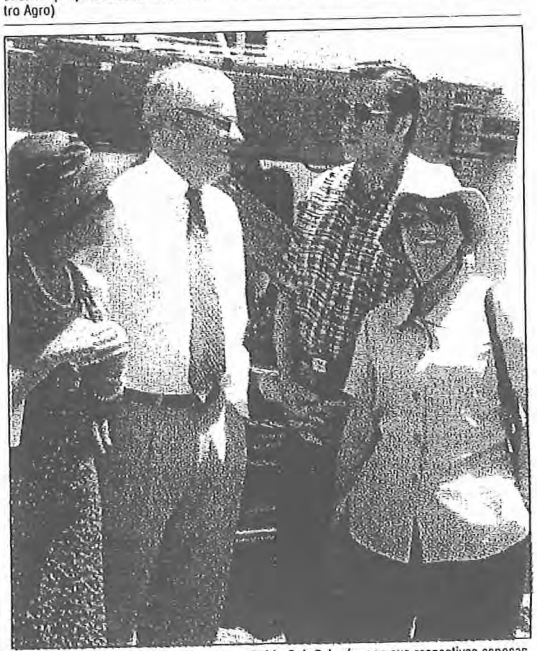

El embajador Friederick Gröneng y el Ing. Pablo Cob Saborío, con sus respectivas esposas, Sra. de Gröneng y Roxana de Cob, recorrieron el barco para conocer las maravillas que en el mismo hay. (Leví Vega M.-Nuestro Agro)

**Editor:** Leví Vega M. Periodista Colegiado Nº 071

**Colaborador:** Guillermo Cubillos

**Diseño:** Dep. Arte La República

**Escaneo:** Fabián Araya y Wálter Ballestero

# GEOMAR REPORTS

1 GEOMAR FORSCHUNGSZENTRUM FÜR MARINE GEOWISSENSCHFTEN DER CHRISTIAN-ALBRECHTS-UNIVERSITÄT ZU KIEL. BERICHT FÜR DIE JAHRE 1987 UND 1988. 1989. 71 + 6 pp. In German

2 GEOMAR FORSCHUNGSZENTRUM FÜR MARINE GEOWISSENSCHAFTEN DER CHRISTIAN-ALBRECHTS-UNIVERSITÄT ZU KIEL. JAHRESBERICHT/ANNUAL REPORT 1989. 1990. 96 pp. In German and English

3 GEOMAR FORSCHUNGSZENTRUM FÜR MARINE GEOWISSENSCHAFTEN DER CHRISTIAN-ALBRECHTS-UNIVERSITÄT ZU KIEL. JAHRESBERICHT/ANNUAL REPORT 1990. 1991. 212 pp. In German and English

4 ROBERT F. SPIELHAGEN
DIE EISDRIFT IN DER FRAMSTRASSE WÄHREND DER LETZTEN 200.000 JAHRE. 1991. 133 pp.
In German with English summary

5 THOMAS C. W. WOLF
PALÄO-OZEANOGRAPHISCH-KLIMATISCHE ENTWICKLUNG DES NÖRDLICHEN NORDATLANTIKS SEIT DEM SPÄTEN NEOGEN (ODP LEGS 105 UND 104, DSDP LEG 81). 1991. 92 pp. In German with English summary

6 SEISMIC STUDIES OF LATERALLY HETEROGENOUS STRUCTURES – INTERPRETATION AND MODELLING OF SEISMIC DATA. Ed. by ERNST R. FLUEH
Commission on Controlled Source Seismology (CCSS), Proceedings of the 8th Workshop Meeting, held at Kiel – Fellhorst (Germany), August 27-31, 1990. 1991. 359 pp. In English

7 JENS MATTHIESSEN
DINOFLAGELLATEN-ZYSTEN IM SPÄQUARTÄR DES EUROPÄISCHEN NORDMEERES: PALÖKOLOGIE UND PALÄO-OZEANOGRAPHIE. 1991. 104 pp. In German with English summary. Out of print

8 DIRK NÜRNGERG
HAUPT- UND SPURENELEMENTE IN FORAMINIFERENGEHÄUSEN – HINWEISE AUF KLIMATISCHE UND OZEANOGRAPHISCHE ÄNDERUNGEN IM NÖRDLICHEN NORDATLANTIK WÄHREND DES SPÄTQUARTÄRS. 1991. 117 pp. In German with English summary. Out of print

9 KLAS S. LACKSCHEWITZ
SEDIMENTATIONSPROZESSE AM AKTIVEN MITTELOZEANISCHEN KOLBEINSEY RÜCKEN (NÖRDLICH VON ISLAND). 1991. 133 pp. In German with English summary. Out of print

10 UWE PAGELS
SEDIMENTOLOGISCHE UNTERSUCHUNGEN UND BESTIMMUNG DER KARBONATLÖSUNG IN SPÄTQUARTÄREN SEDIMENTEN DES ÖSTLICHEN ARKTISCHEN OZEANS. 1991. 106 pp.
In German with English summary

11 FS POSEIDON. EXPEDITION 175 (9.10.-1.11.1990)
175/1:OSTGRÖNLÄNDISCHER KONTINENTALRAND (65°N)
175/2: SEDIMENTATION AM KOLBEINSEYRÜCKEN (NÖRDLICH VON ISLAND).
Hrsg. von J. MIENERT und H.-J. WALLRABE-ADAMS. 1992. 56 pp. + app. In German with some English chapters

12 GEOMAR FORSCHUNGSZENTRUM FÜR MARINE GEOWISSENSCHAFTEN DER CHRISTIAN-ALBRECHTS-UNIVERSITÄT ZU KIEL. JAHRESBERICHT/ANNUAL REPORT 1991. 1992. 152 pp. In German and English.
Out of print

13 SABINE E. I. KÖHLER
SPÄTQUARTÄRE PALÄO-OZEANOGRAPHISCHE ENTWICKLUNG DES NORDPOLARMEERES UND EUROPÄISCHEN NORDMEERES ANHAND VON SAUERSTOFF- UND KOHLENSTOFF-ISOTOPENVERHÄLTNISSEN DER PLANKTISCHEN FORAMINIFERE Neogloboquadrina pachyderma (sin.).
1992. 104 pp. In German with English summary

14 FS SONNE. FAHRTBERICHT SO78 PERUVENT: BALBOA, PANAMA - BALBOA, PANAMA, 28.2.1992-16.4.1992
Hrsg. von ERWIN SUESS. 1992. 120 pp. In German with some English chapters. Out of print

15 FOURTH INTERNATIONAL CONFERENCE ON PALEOCEANOGRAPHY (ICP IV): SHORT- AND LONG-TERM GLOBAL CHANGE: RECORDS AND MODELLING. 21-25 SEPTEMBER 1992, KIEL/GERMANY.
PROGRAM & ABSTRACTS. 1992. 351 pp. In English

16 MICHAELA KUBISCH
DIE EISDRIFT IM ARKTISCHEN OZEAN WÄHREND DER LETZTEN 250.000 JAHRE. 1992. 100 pp.
In German with English summary

17 PERSISCHER GOLF: UMWELTGEFÄHRDUNG, SCHADENSERKENNUNG, SCHADENSBEWERTUNG AM BEISPIEL DES MEERRESBODENS; ERKENNEN EINER ÖKOSYSTEMVERÄNDERUNG NACH ÖLEINTRÄGEN.
Schlußbericht zu den beiden BMFT-Forschungsvorhaben 03F0055 A + B. 1993. 108 pp. In German with English summary

18 TEKTONISCHE ENTWÄSSERUNG AN KONVERGENTEN PLATTENRÄNDERN / DEWATERING AT CONTINENTAL MARGINS. Hrsg. von/ed. by ERWIN SUESS. 1993. 196 + 32 + 68 + 16 + 22 + 38 + 4 + 19 pp.
Some chapters in English, some in German

19 THOMAS DICKMANN
DAS KONZEPT DER POLARISATIONSMETHODE UND SEINE ANWENDUNGEN AUF DAS SEIMISCHE VEKTORWELLENFELD IM WEITWINKELBEREICH. 1993. 121 pp. In German with English summary

20 GEOMAR FORSCHUNGSZENTRUM FÜR MARINE GEOWISSENSCHAFTEN DER CHRISTIAN-ALBRECHTS-UNIVERSITÄT ZU KIEL. JAHRESBERICHT/ANNUAL REPORT 1992. 1993. 139 pp. In German and English

21 KAI UWE SCHMIDT
PALYNOMORPHE IM NEOGENEN NORDATLANTIK - HINWEISE ZUR PALÄO-OZEANOGRAPHIE UND PALÄOKLIMATOLOGIE. 1993. 104 + 7 + 41 pp. In German with English summary

22 UWE JÜRGEN GRÜTZMACHER
DIE VERÄNDERUNGEN DER PALÄOGEOGRAPHISCHEN VERBREITUNG VON *Bolboforma* - EIN BEITRAG ZUR REKONSTRUKTION UND DEFINITION VON WASSERMASSEN IM TERTÄR. 1993. 104 pp.
In German with English summary

23 RV PROFESSOR LOGACHEV. Research Cruise 09 (August 30 - September 17, 1993): SEDIMENT DISTRIBUTION ON THE REYKJANES RIDGE NEAR 59°N. Ed. by H.-J. WALLRABE-ADAMS & K.S. LACKSCHEWITZ. 1993. 66 + 30 pp.
In English

24 ANDREAS DETTMER
DIATOMEEN-TAPHOZÖNOSEN ALS ANZEIGER PALÄO-OZEANOGRAPHISCHER ENTWICKLUNGEN IM PLIOZÄNEN UND QUARTÄREN NORDATLANTIK. 1993. 113 + 10 + 25 pp. In German with English summary

25 GEOMAR FORSCHUNGSZENTRUM FÜR MARINE GEOWISSENSCHAFTEN DER CHRISTIAN-ALBRECHTS-UNIVERSITÄT ZU KIEL. JAHRESBERICHT/ANNUAL REPORT 1993. 1994. 69 pp. In German and English

26 JÖRG BIALAS
SEISMISCHE MESSUNGEN UND WEITERE GEOPHYSIKALISCHE UNTERSUCHUNGEN AM SÜD-SHETLAND TRENCH UND IN DER BRANSFIELD STRASSE - ANTARKTISCHE HALBINSEL. 1994. 113 pp.
In German with English summary

27 JANET MARGARET SUMNER
THE TRANSPORT AND DEPOSITIONAL MECHANISM OF HIGH GRADE MIXED-MAGMA IGNIMBRITE TL, GRAN CANARIA: THE MORPHOLOGY OF A LAVA-LIKE FLOW. 1994. 224 pp. In English with German summary. Out of print

28 GEOMAR LITHOTHEK. Ed. by JÜRGEN MIENERT. 1994. 12 pp + app. In English. Out of print

29 FS SONNE. FAHRTBERICHT SO 97 KODIAK-VENT: KODIAK - DUTCH HARBOR - TOKYO - SINGAPUR, 27.7.- 19.9.1994. Hrsg. von ERWIN SUESS. 1994. Some chapters in English, some in German. Out of print

30 CRUISE REPORTS:
RV LIVONIA CRUISE 92, KIEL-KIEL, 21.8.-17.9.1992: GLORIA STUDIES OF THE EAST GREENLAND CONTINENTAL MARGIN BETWEEN 70°AND 80°N
RV POSEIDON PO200/10, LISBON-BREST-BREMERHAVEN, 7.-23.8.1993: EUROPEAN NORTH ATLANTIC MARGIN: SEDIMENT PATHWAYS, PROCESSES AND FLUXES
RV AKADEMIK ALEKSANDR KARPINSKIY, KIEL-TROMSÖ, 5.-25.7.1994: GAS HYDRATES ON THE NORTHERN EUROPEAN CONTINENTAL MARGIN
Edited by JÜRGEN MIENERT. 1994. 186 pp.
In English; report of RV AKADEMIK ALEKSANDR KARPINSKIY cruise in English and Russian

31 MARTIN WEINELT
BECKENENTWICKLUNG DES NÖRDLICHEN WIKING-GRABENS IM KÄNOZOIKUM - VERSENKUNGSGESCHICHTE, SEQUENZSTRATIGRAPHIE, SEDIMENTZUSAMMENSETZUNG. 1994. 85 pp.
In German with English summary

32 GEORG A. HEISS
CORAL REEFS IN THE RED SEA: GROWTH, PRODUCTION AND STABLE ISOTOPES. 1994. 141 pp.
In English with German summary

33 JENS A. HÖLEMANN
AKKUMULATION VON AUTOCHTHONEM UND ALLOCHTHONEM ORGANISCHEM MATERIAL IN DEN KÄNOZOISCHEN SEDIMENTEN DER NORWEGISCHEN SEE (ODP LEG 104). 1994. 78 pp.
In German with English summary

34 CHRISTIAN HASS
SEDIMENTOLOGISCHE UND MIKROPALÄONTOLOGISCHE UNTERSUCHUNGEN ZUR ENTWICKLUNG DES SKAGERRAKS (NE NORDSEE) IM SPÄTHOLOZÄN. 1994. 115 pp. In German with English summary

35 BRITTA JÜNGER
TIEFENWASSERERNEUERUNG IN DER GRÖNLANDSEE WÄHREND DER LETZTEN 340.000 JAHRE / DEEP WATER RENEWAL IN THE GREENLAND SEA DURING THE PAST 340,000 YEARS. 1994. 6 + 109 pp.
In German with English summary

36 JÖRG KUNERT
UNTERSUCHUJNGEN ZU MASSEN- UND FLUIDTRANSPORT ANHAND DER BEARBEITUNG REFLEXIONSSEISMISCHER DATEN AUS DER KODIAK-SUBDUKTIONSZONE, ALASKA. 1995. 129 pp.
In German with English summary

37 CHARLOTTE M. KRAWCZYK
DETACHMENT TECTONICS DURING CONTINENTAL RIFTING OFF THE WEST IBERIA MARGIN: SEISMIC REFLECTION AND DRILLING CONSTRAINTS.1995. 133 pp. In English with German summary

38 CHRISTINE CAROLINE NÜRNBERG
BARIUMFLUSS UND SEDIMENTATION IM SÜDLICHEN SÜDATLANTIK - HINWEISE AUF PRODUKTIVITÄTSÄNDERUNGEN IM QUARTÄR. 1995. 6 + 108 pp. In German with English summary

39 JÜRGEN FRÜHN
TEKTONIK UND ENTWÄSSERUNG DES AKTIVEN KONTINENTALRANDES SÜDÖSTLICH DER KENAI-HALBINSEL, ALASKA. 1995. 93 pp. In German with English summary

40 GEOMAR FORSCHUNGSZENTRUM FÜR MARINE GEOWISSENSCHAFTEN DER CHRISTIAN-ALBRECHTS-UNIVERSITÄT ZU KIEL. JAHRESBERICHT/ANNUAL REPORT 1994. 1995. 125 pp. In German and English.
Out of print

41 FS SONNE. FAHRTBERICHT / CRUISE REPORT SO 103 CONDOR 1 B: VALPARAISO-VALPARAISO, 2-21.7.1995. Hrsg. von ERNST R. FLUEH. 1995. 140 pp. Some chapters in German, some in English

42 RV PROFESSOR BOGOROV CRUISE 37: CRUISE REPORT "POSETIV": VLADIVOSTOK-VLADIVOSTOK, September 23 - October 22, 1994. Edited by CHRISTOPH GAEDICKE, BORIS BARANOV, and EVGENY LELIKOV. 1995. 49 + 33 pp.
In English

43 CHRISTOPH GAEDICKE
DEFORMATION VON SEDIMENTEN IM NANKAI-AKKRETIONSKEIL, JAPAN. BILANZIERUNG TEKTONISCHER VORGÄNGE ANHAND VON SEISMISCHEN PROFILEN UND ERGEBNISSEN DER ODP-BOHRUNG 808. II + 89 pp.
In German with English summary

44 MARTIN ANTONOW
SEDIMENTATIONSMUSTER UM DEN VESTERIS SEAMOUNT (ZENTRALE GRÖNLANDSEE) IN DEN LETZTEN 250.000 JAHREN. 1995. 121 pp. In German with English summary

45 INTERNATIONAL CONGRESS: CORING FOR GLOBAL CHANGE - ICGC '95. KIEL, 28 - 30 June, 1995.
Edited by JÜRGEN MIENERT and GEROLD WEFER. 1996. 83 pp. In English

46 JENS GRÜTZNER
ZUR PHYSIKALISCHEN ENTWICKLUNG VON DIAGENETISCHEN HORIZONTEN IN DEN SEDIMENTBECKEN DES ATLANTIKS. 1995. 96 pp. In German with English summary

47 INGO A. PECHER
SEISMIC STUDIES OF BOTTOM SIMULATING REFLECTORS AT THE CONVERGENT MARGINS OFFSHORE PERU AND COSTA RICA. 1996. 159 pp. In English with German summary

48 XIN SU
DEVELOPMENT OF LATE TERTIARY AND QUATERNARY COCCOLITH ASSEMBLAGES IN THE NORTHEAST ATLANTIC. 1996. 120 pp. +7 pl. In English with German summary

49 FS SONNE - FAHRTBERICHT/CRUISE REPORT SO108 ORWELL: SAN FRANCISCO - ASTORIA, 14.4. - 23.5.1996
Edited by ERNST R. FLUEH and MICHAEL A. FISHER. 1996. 252 pp. + app. In English with German summary

50 GEOMAR FORSCHUNGSZENTRUM FÜR MARINE GEOWISSENSCHAFTEN DER CHRISTIAN-ALBRECHTS-UNIVERSITÄT ZU KIEL. JAHRESBERICHT/ANNUAL REPORT 1995. 1996. 93 pp. In German and English

51 THOMAS FUNCK
STRUCTURE OF THE VOLCANIC APRON NORTH OF GRAN CANARIA DEDUCED FOM REFLECTION SEISMIC, BATHYMETRIC AND BOREHOLE DATA. 1996.VI, 144 pp. In English with German summary

52 PETER BRUNS
GEOCHEMISCHE UND SEDIMENTOLOGISCHE UNTERSUCHUNGEN ÜBER DAS SEDIMENTATIONSVERHALTEN IM BEREICH BIOSTRATIGRAPHISCHER DISKONTINUITÄTEN IM NEOGEN DES NORDATLANTIK, ODP LEG 104, SITES 642B UND 643A. 1996. V, 73 pp. In German with Engllish summary

53 CHRISTIANE C. WAGNER
COLD SEEPS AN KONVERGENTEN PLATTENRÄNDERN VOR OREGON UND PERU: BIOGEOCHEMISCHE BESTANDSAUFNAHME. 1996. 108, XXXVI pp. In German with English summary

54 FRAUKE KLINGELHÖFER
MODEL CALCULATIONS ON THE SPREADING OF SUBMARINE LAVA FLOWS. 1996. 98 pp.
In English with German summary

55 HANS-JÜRGEN HOFFMANN
OBJEKTORIENTIERTE ANALYSE UND MIGRATION DIFFRAKTIERTER WELLENFELDER UNTER VERWENDUNG DER STRAHLENMETHODE UND DER EDGE-WAVE-THEORIE. 1996. XXI, 153 pp. In German with English summary

56 DIRK KLÄSCHEN
STRAHLENSEISMISCHE MODELLIERUNG UNTER BERÜCKSICHTGUNG VON MEHRFACHDIFFRAKTIONEN MIT HILFE DER EDGE-WAVES: THEORIE UND ANWENDUNGSBEISPIELE 1996. X, 159 pp.
In German with English summary

57 NICOLE BIEBOW
DINOFLAGELLATENZYSTEN ALS INIKATOREN DER SPÄT- UND POSTGLAZIALEN ENTWICKLUNG DES AUFTRIEBSGESCHEHENS VOR PERU. 1996. IV, 100, 17, 14 (7 pl.) pp. In German with English summary

58 RV SONNE. CRUISE REPORT SO109: HYDROTRACE ASTORIA-VICTORIA-ASTORIA-VICTORIA. MAY 23 - JULY 8, 1996. Ed. by PETER HERZIG, ERWIN SUESS, and PETER LINKE. 1997. 249 pp. In English

59 RV SONNE. CRUISE REPORT SO110: SO - RO (SONNE - ROPOS). VICTORIA-KODIAK-VICTORIA. JULY 9 - AUGUST 19, 1996. Ed. by ERWIN SUESS and GERHARD BOHRMANN. 1997. 181 pp. In English

60 RV AKADEMIK M. A. LAVRENTYEV CRUISE 27. CRUISE REPORT: GREGORY. VLADIVOSTOK-PUSAN-OKHOTSK SEA-PUSAN-VLADIVOSTOK. SEPTEMBER 7 - OCTOBER 12, 1996.
Ed. by DIRK NÜRNBERG, BORIS BARANOV, and BORIS KARP.1997. 143 pp. In English

61 GEOMAR FORSCHUNGSZENTRUM FÜR MARINE GEOWISSENSCHAFTEN DER CHRISTIAN-ALBRECHTS-UNIVERSITÄT ZU KIEL. JAHRESBERICHT / ANNUAL REPORT 1996. 1997. 169 pp.
In German and English

62 FS SONNE. FAHRTBERICHT/CRUISE REPORT SO123: MAMUT (MAKRAN MURRAY TRAVERSE - GEOPHYSIK PLATTENTEKTONISCHER EXTREMFÄLLE). Maskat - Maskat, 07.09 - 03.10.1997. Ed. by ERNST R. FLUEH, NINA KUKOWSKI, and CHRISTIAN REICHERT. 1997. 292 pp. In English with German summary

63 RAINER ZAHN
NORTH ATLANTIC THERMOHALINE CIRCULATION DURING THE LAST GLACIAL PERIOD: EVIDENCE FOR COUPLING BETWEEN MELTWATER EVENTS AND CONVECTIVE INSTABILITY. 1997. 133 pp. In English

64 FS SONNE. FAHRTBERICHT/CRUISE REPORT SO112 HIRESBAT (HIGH RESOLUTION BATHYMETRY). Victoria, B.C., Canada - Apra Harbor, Guam. 17.09 - 08.10.1996. Hrsg. von WILHELM WEINREBE. 1997. 90 pp.
Some chapters in German, some in English

65 NIELS NØRGAARD-PEDERSEN
LATE QUATERNARY ARCTIC OCEAN SEDIMENT RECORDS: SURFACE OCEAN CONDITIONS AND PROVENANCE OF ICE-RAFTED DEBRIS. 1997. 115 pp. In English with German summary

66 THOMAS NÄHR
AUTHIGENER KLINOPTILOLITH IN MARINEN SEDIMENTEN - MINERALCHEMIE, GENESE UND MÖGLICHE ANWENDUNG ALS GEOTHERMOMETER. 1997. 119, 43 pp. In German with English summary

67 MATTIAS KREUTZ
STOFFTRANSPORT DURCH DIE BODENGRENZSCHICHT: REGIONALISIERUNG UND BILANZIERUNG FÜR DEN NORDATLANTIK UND DAS EUROPÄISCHE NORDMEER. 1998. IV, 166 pp. In German with English summary

68 AMIT GULATI
BENTHIC PRIMARY PRODUCTION IN TWO DIFFERENT SEDIMENT TYPES OF THE KIEL FJORD (WESTERN BALTIC SEA). 1998. 139 pp. In English with German summary

69 RÜDIGER SCHACHT
DIE SPÄT- UND POSTGLAZIALE ENTWICKLUNG DER WOOD- UND LIEFDEFJORDREGION NORDSPITZBERGENS. 1999. 123 pp. + app. In German with English summary

70 GEOMAR FORSCHUNGSZENTRUM FÜR MARINE GEOWISSENSCHAFTEN DER CHRISTIAN-ALBRECHTS-UNIVERSITÄT ZU KIEL. JAHRESBERICHT/ANNUAL REPORT 1997. 1998. 155 pp. In German and English

71 FS SONNE. FAHRTBERICHT/CRUISE REPORT SO118 BIGSET (BIOGEOCHEMICAL TRANSPORT OF MATTER AND ENERGY IN THE DEEP SEA). MUSCAT (OMAN) - MUSCAT (OMAN). 31.03.-11.05.1997. Ed. by OLAF PFANNKUCHE and CHRISTINE UTECHT. 1998. 188 pp. In English

72 FS SONNE. FAHRTBERICHT/CRUISE REPORT SO131 SINUS (SEISMIC INVESTIGATIONS AT THE NINETY EAST RIDGE OBSERVATORY USING SONNE AND JOIDES RESOLUTION DURING ODP LEG 179). KARACHI - SINGAPORE. 04.05-16.06.1998. Ed. by ERNST R. FLUEH and CHRISTIAN REICHERT. 1998. 337 pp. In English

73 THOMAS RICHTER
SEDIMENTARY FLUXES AT THE MID-ATLANTIC RIDGE: SEDIMENT SOURCES, ACCUMULATION RATES, AND GEOCHEMICAL CHARACTERISATION. 1998. IV, 173 + 29 pp. In English with German summary

74 BARBARA MARIA SPRINGER
MODIFIKATION DES BODENNAHEN STRÖMUNGSREGIMES UND DIE DEPOSITION VON SUSPENDIERTEM MATERIAL DURCH MAKROFAUNA. 1999. 112 pp. In German

75 SABINE JÄHMLICH
UNTERSUCHUNGEN ZUR PARTIKELDYNAMIK IN DER BODENGRENZSCHICHT DER MECKLENBURGER BUCHT. 1999. 139 pp. In German

76 WOLFRAM W. BRENNER
GRUNDLAGEN UND ANWENDUNGSMÖGLICHKEITEN DER MIKRO-ABSORPTIONSPHOTOMETRIE FÜR ORGANISCH-WANDIGE MIKROFOSSILIEN. 1999. 141 pp. In German with English summary

77 SUSAN KINSEY
TERTIARY BENTHIC FORAMINIFERAL BIOSTRATIGRAPHY AND PALAEOECOLOGY OF THE HALTEN TERRACE, NORWAY. 1999. VI, 145 pp. In English with German summary

78 HEIDI DOOSE
REKONSTRUKTION HYDROGRAPHISCHER VERHÄLTNISSE IM CALIFORNIENSTROM UND IM EUROPÄISCHEN MITTELMEER ZUR BILDUNGSZEIT ORGANISCH KOHLENSTOFFREICHER SEDIMENTE. 1999. IV, 111 pp. + app. In German with English summary

79 CLAUDIA WILLAMOWSKI
VERTEILUNGSMUSTER VON SPURENMETALLEN IM GLAZIALEN NORDATLANTIK: REKONSTRUKTION DER NÄHRSTOFFBILANZ ANHAND VON CADMIUMKONZENTRATIONEN IN KALKSCHALIGEN FORAMINIFEREN.
1999. 86, XXI pp. In German with English summary

80 FS SONNE. FAHRTBERICHT/CRUISE REPORT SO129. BIGSET (BIOGEOCHEMICAL TRANSPORT OF MATTER AND ENERGY IN THE DEEP SEA). PORT SULTAN QUABOOS - DUBAI. JANUARY 30 - MARCH 9, 1998. Ed. by OLAF PFANNKUCHE and CHRISTINE UTECHT. 1999. 107 pp. In English

81 FS SONNE. FAHRTBERICHT/CRUISE REPORT SO138. GINCO-2 (GEOSCIENTIFIC INVESTIGATIONS ON THE ACTIVE CONVERGENCE ZONE BETWEEN THE EAST EURASIAN AND AUSTRALIAN PLATES ALONG INDONESIA). JAKARTA - JAKARTA. 29.12.1998 - 28.01.1999. Ed. by ERNST R. FLUEH, BERND SCHRECKENBERGER, and JÖRG BIALAS. 1999. 333 pp. In English

82 CRUISE REPORTS: KOMEX I and II (KURILE OKHOTSK SEA MARINE EXPERIMENT)
RV PROFESSOR GAGARINSKY CRUISE 22
RV AKADEMIK M. A. LAVRENTYEV CRUISE 28
VLADIVOSTOK - PUSAN - OKHOTSK SEA - PUSAN - VLADIVOSTOK. 7 JULY - 12 SEPTEMBER 1998.
Ed. by NICOLE BIEBOW and EDNA HÜTTEN. 1999. 188, 89 pp. In English

83 GREGOR REHDER
QUELLEN UND SENKEN MARINEN METHANS ZWISCHEN SCHELF UND OFFENEM OZEAN. REGIONALE VARIABILITÄT UND STEUERNDE PARAMETER DER METHANVERTEILUNG UND DER AUSTAUSCH MIT DER ATMOSPHÄRE. 1999. 161, 20 pp. In German with English summary

84 SVEN-OLIVER FRANZ
PLIOZÄNE ZEITREIHEN ZUR REKONSTRUKTION DER TIEFENWASSERZIRKULATION UND DER SILIZIKLASTISCHEN AMAZONASFRACHT IM ÄQUATORIALEN WESTATLANTIK
(CEARA SCHWELLE, ODP LEG 154). 1999. 183 pp. In German with English summary

85 SYLKE HLAWATSCH
Mn-Fe-AKKUMULATE ALS INDIKATOR FÜR SCHAD- UND NÄHRSTOFFFLÜSSE IN DER WESTLICHEN OSTSEE. 1999. 132 pp. In German with English summary

86 BETTINA GEHRKE
ZUSAMMENSETZUNG UND VERTEILUNG DER LITHOGENEN FEINFRAKTION IN SPÄTQUARTÄREN SEDIMENTEN DES MITTELATLANTISCHEN REYKJANES RÜCKENS (59°N) - TONMINERALE ALS INDIKATOREN FÜR LIEFERGEBIETE, TRANSPORTMECHANISMEN UND ABLAGERUNGSPROZESSE. 1999. 102 pp.
In German with English summary

87 JENS GREINERT
REZENTE SUBMARINE MINERALBILDUNGEN: ABBILD GEOCHEMISCHER PROZESSE AN AKTIVEN FLUIDAUSTRITTSSTELLEN IM ALEUTEN- UND CASCADIA-AKKRETIONSKOMPLEX. 1999. 196, XX pp.
In German with English summary

88 CRUISE REPORTS: KOMEX V and VI (KURILE OKHOTSK SEA MARINE EXPERIMENT)
RV PROFESSOR GAGARINSKY CRUISE 26
MV MARSHAL GELOVANY CRUISE 1
VLADIVOSTOK - PUSAN - OKHOTSK SEA - PUSAN - VLADIVOSTOK. 30 JULY - 5 SEPTEMBER, 1999.
Ed. by NICOLE BIEBOW, THOMAS LÜDMANN, BORIS KARP, and RUSLAN KULINICH. 2000. 296 pp. In English

89 FS SONNE. FAHRTBERICHT/CRUISE REPORT SO136. TASQWA (QUATERNARY VARIABILITY OF WATER MASSES IN THE SOUTHERN TASMAN SEA AND THE SOUTHERN OCEAN, SW PACIFIC SECTOR). WELLINGTON - HOBART. OCTOBER 16 - NOVEMBER 12, 1998. Ed. by JÖRN THIEDE, STEFAN NEES et al. 1999. 78, 106 pp. In English

90 FS SONNE. FAHRTBERICHT/CRUISE REPORT SO142. HULA (INTERDISCIPLINARY INVESTIGATIONS ON THE TIMING OF THE HAWAII-EMPEROR BEND AND THE ORIGIN OF LITHOSPHERIC ANOMALIES ALONG THE MUSICIAN SEAMOUNT CHAIN. MIDWAY - HONOLULU. MAY 30 - JUNE 28, 1999. Ed. by ERNST R. FLUEH, JOHN O'CONNOR, JASON PHIPPS MORGAN, and JOCHEN WAGNER. 1999. 224 pp. In English

91 J. HAUSCHILD, T. GINDLER, D. RISTOW, A. BERHORST, C. BÖNNEMANN, K. HINZ
DFG-FORSCHUNGSPROJEKT *"KRUSTENSPLITTER"*. 3D-MAKRO-GESCHWINDIGKEITSBESTIMMUNGEN UND 3D-TIEFENMIGRATION DES SEISMISCHEN 3D-COSTA-RICA-DATENSATZES. 1999. 85 pp.
In German with English summary

92 FS AKADEMIK MSTISLAV KELDYSH. Fahrtbericht Reise Nr. 40: Norwegisch-Grönländische See, 27.6.-29.7.1998. Hrsg. von J. MIENERT, A. OMLIN, T. GÖLZ, D. LUKAS, J. POSEWANG. 1999. 65, 7 pp. In German

93 FS SONNE. FAHRTBERICHT/CRUISE REPORT SO143 TECFLUX. Ed. by GERHARD BOHRMANN, PETER LINKE, ERWIN SUESS, and OLAF PFANNKUCHE. 2000. 243 pp. In English

94 FS SONNE. FAHRTBERICHT/CRUISE REPORT SO144-1&2. PAGANINI (PANAMA BASIN AND GALAPAGOS "PLUME" - NEW INVESTIGATIONS OF INTRAPLATE MAGMATISM). SAN DIEGO - CALDERA. SEPTEMBER 7 - NOVEMBER 7, 1999. Ed. by JÖRG BIALAS, ERNST R. FLUEH, and GERHARD BOHRMANN. 1999. 437 pp. + app.
In English

95 CHRISTIAN MATTHIAS HÜLS
MILLENNIAL-SCALE SST VARIABILITY AS INFERRED FROM PLANKTONIC FORAMINIFERAL CENSUS COUNTS IN THE WESTERN SUBTROPICAL ATLANTIC. 2000. 81 pp. + app. In English with German summary

96 FS SONNE. FAHRTBERICHT/CRUISE REPORT SO146-1&2. GEOPECO (GEOPHYSICAL EXPERIMENTS AT THE PERUVIAN CONTINENTAL MARGIN - INVESTIGATIONS OF TECTONICS, MECHANICS, GASHYDRATES, AND FLUID TRANSPORT). ARICA - TALCAHUANO. MARCH 1 - MAY 4, 2000. Ed. by JÖRG BIALAS and NINA KUKOWSKI. 2000. 508 pp. In English

97 GEOMAR FORSCHUNGSZENTRUM FÜR MARINE GEOWISSENSCHAFTEN DER CHRISTIAN-ALBRECHTS-UNIVERSITÄT ZU KIEL. JAHRESBERICHT/ANNUAL REPORT 1998/1999. 2000. 261 pp. In German and English

98 RV SONNE. CRUISE REPORT SO148. TECFLUX-II-2000 (TECTONICALLY-INDUCED MATERIAL FLUXES. VICTORIA - VICTORIA - VICTORIA. 20.07.-15.08.2000. Ed. by PETER LINKE and ERWIN SUESS. 122 pp. In English

99 GEOMAR FORSCHUNGSZENTRUM FÜR MARINE GEOWISSENSCHAFTEN DER CHRISTIAN-ALBRECHTS-UNIVERSITÄT ZU KIEL. JAHRESBERICHT/ANNUAL REPORT 2000. 2001. 180 pp. In German and English

100 FS POSEIDON. FAHRTBERICHT/CRUISE REPORT POS 260 BIGSET (BIOGEOCHEMICAL TRANSPORT OF MATTER AND ENERGY IN THE DEEP SEA). LEIXOES/OPORTO (PORTUGAL) - GALWAY (IRELAND) - CORK (IRELAND). 26.04.-23.06.2000. Ed. by OLAF PFANNKUCHE and CHRISTINE UTECHT. 2001. 67 pp. In English

101 FS SONNE. FAHRTBERICHT/CRUISE REPORT SO159. SALIERI (SOUTH AMERICAN LITHOSPHERIC TRANSECTS ACROSS VOLCANIC RIDGES). GUAYAQUIL - GUAYAQUIL. AUGUST 21 - SEPTEMBER 17, 2001.
Ed. by ERNST R. FLÜH, JÖRG BIALAS, and PHILIPPE CHARVIS. 2001. 256 pp. In English

102 FS SONNE. FAHRTBERICHT/CRUISE REPORT SO161-1&4. SPOC (SUBDUCTION PROCESSES OFF CHILE). ANTOFAGASTA - VALPARAISO. OCTOBER 9 - OCTOBER 15, 2001 &
VALPARAISO - VALPARAISO. NOVEMBER 30 - DECEMBER 23, 2001.
Ed. by ERNST R. FLÜH, HEIDRUN KOPP, and BERND SCHRECKENBERGER. 2002. 383 pp. In English

103 FS SONNE. FAHRTBERICHT/CRUISE REPORT SO162. INGGAS TEST (INTEGRATED GEOPHYSICAL CHARACTERISATION AND QUANTIFICATION OF GAS HYDRATES - INSTRUMENT TEST CRUISE).
VALPARAISO - BALBOA. FEBRUARY 21 - MARCH 12, 2002.
Ed. by TIMOTHY JOHN RESTON and JÖRG BIALAS. 2002. In English

104 FS SONNE. FAHRTBERICHT/CRUISE REPORT SO158. MEGAPRINT (MULTIDISCIPLINARY EXAMINATION OF GALÁPAGOS PLUME RIDGE INTERACTION). ISLA DE PASCUA - GUAYAQUIL. JULY15 - AUGUST 20, 2001.
Ed. by REINHARD WERNER. 2002. 53 pp + app. In English

105 CRUISE REPORT: KOMEX (KURILE OKHOTSK SEA MARINE EXPERIMENT)
RV PROFESSOR GAGARINSKY CRUISE 32. SERENADE. SEISMO-STRATIGRAPHIC RESEARCH OFF NORTHERN SAKHALIN AND IN THE DERUGIN BASIN. VLADIVOSTOK - PUSAN - SEA OF OKHOTSK - PUSAN - VLADIVOSTOK.
AUGUST 31 - SEPTEMBER 29, 2001.
Ed. by THOMAS LÜDMANN, BORIS BARANOV, and BORIS KARP. 2002. 42 pp. In English

106 FS SONNE. FAHRTBERICHT/CRUISE REPORT SO163. SUBDUCTION I. MULTI-SYSTEM ANALYSIS OF FLUID RECYCLING AND GEODYNAMICS AT THE CONTINENTAL MARGIN OFF COSTA RICA.
SO163-1. BALBOA- CALDERA. MARCH 13 - APRIL 20, 2002
SO163-2. CALDERA - BALBOA. APRIL 20 - MAY 21, 2002
Ed. by WILLI WEINREBE and ERNST R. FLÜH. 2002. In English